eman ta zabal zazu

Universidad del País Vasco

Euskal Herriko Unibertsitatea

CALCIUM EFFECT ON DYNAMICS AND STABILITY OF KV7.2 CHANNEL

DOCTORAL THESIS LEIOA, 2020

EIDER NUÑEZ VIADERO

Dr. Alvaro Villarroel
Dr. Oscar Millet

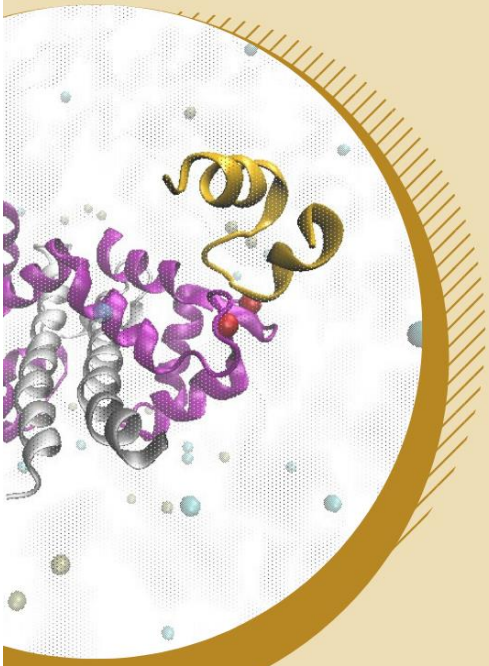

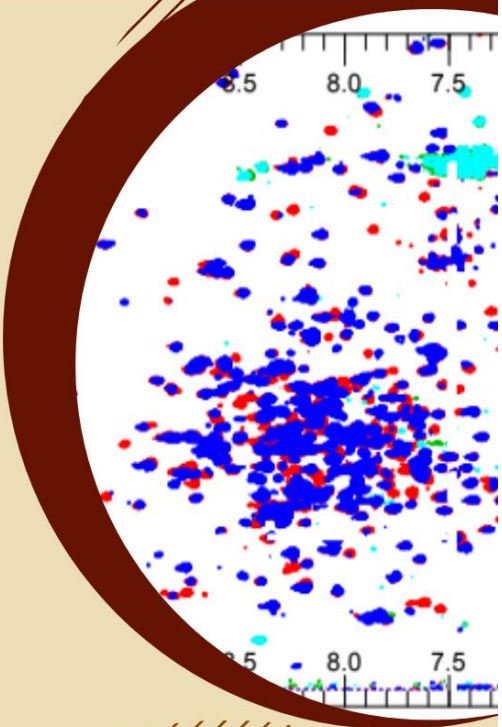

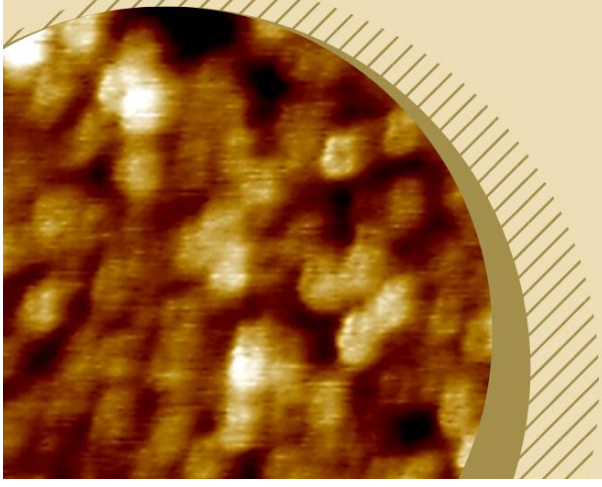

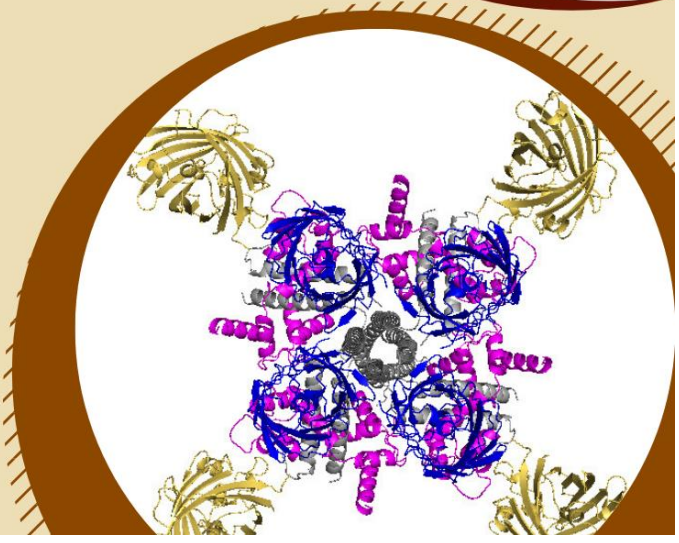

eman ta zabal zazu
Universidad del País Vasco
Euskal Herriko Unibertsitatea

Tesis Doctoral

Calcium effect on dynamics and stability of K_V7.2 channel.

Memoria presentada por

Eider Nuñez Viadero

dirigida por

Dr. Alvaro Villarroel

Dr. Oscar Millet

para optar al título de

Doctora por la Universidad del País Vasco (UPV/EHU)

Instituto Biofisika (UPV/EHU, CSIC)

Departamento de Bioquímica y Biología Molecular

Facultad de Ciencia y Tecnología

Universidad del País Vasco/Euskal Herriko Unibertsitatea
(UPV/EHU)

Amamari

Izarren hautsa egun batean bilakatu zen bizigai
Hauts hartatikan uste gabean noizpait ginaden gu ernai.

.

Gizonen lana jakintza dugu:
ezagutuz aldatzea,
naturarekin bat izan eta
harremanetan sartzea.
eta indarrak ongi errotuz,
gure sustraiak lurrari lotuz,
bertatikan irautea:
ezaren gudaz baietza sortuz
ukazioa legetzat hartuz
beti aurrera joatea

AKNOWLEMENTS

Como no podía ser de otra forma, empezaré por agradecer a Alvaro el haberme dado la oportunidad de formar parte de su grupo. Alvaro, los que nos conocen saben que no hemos tenido la típica relación de director-doctorando, y es que realmente, has sido más que un director para mí, has sido mi mentor. Gracias por guiarme, no solamente en el desarrollo de esta tesis, también en mi formación como investigadora. Me has dado libertad para tomar decisiones, me has hecho reflexionar y pensar las cosas más de dos veces. Me has dejado aprender de mis errores, sin reprocharme un "te lo dije" después. Has sabido estimularme los días en los que no encontraba inspiración y me has apoyado cuando lo he necesitado. Gracias por enseñarme a ver la ciencia con dedicación, pasión y creatividad. Lo dije cuando empecé está tesis y lo repito ahora: no podía haber tenido un director mejor.

Quiero agradecer también a las *Calmodulinas, (*AKA *Villarroelianas):* Aran, Karol, Cova, Janire y Alejandra. Me habéis acompañado estos cuatro años y hay parte de cada una en esta tesis. Ha sido un camino largo y duro en el que, algunas veces, la fijación por lograr tus objetivos te hace olvidar la importancia del contacto humano. Mil gracias por vuestra generosidad y apoyo, teneros cerca ha sido esencial. Todas vosotras habéis compartido conmigo conocimientos y experiencias de tipo profesional y personal que han sido de gran valor. Es un lujo contar con amigas como compañeras de grupo.

También quiero dar las gracias a Oscar y a Ganeko del CIC-Biogune, por haberme ayudado y facilitado los medios para desarrollar todos los experimentos de NMR, por asesorarme y guiarme en una técnica en la que estaba realmente perdida. No hay duda de que vuestra participación ha enriquecido el trabajo.

I don't forget Arin and FM4 group in Marseille. Thank you for welcoming me as one of the group, for making me feel at home. Thanks for the support, the guidelines, and the advice, I will be indebted to you forever.

A Itsas y a Laura, por compartir conmigo los "*ires y venires*" durante esta etapa de mi vida, en el plano personal y el profesional. Por escuchar mis ensayos antes de un seminario, o la presentación de un poster en un congreso. Por esas cañas un viernes por la noche con debates multidisciplinares intentando arreglar el mundo, o al menos, hacerlo un *poquito* mejor. Podéis estar orgullosas, no conozco a nadie con un expediente tan alejado de la fisiología que sepa tanto de la Calmodulina y los canales iónicos.

Y por último a aita y ama. Por haber creído siempre en mí, incluso cuando yo misma no lo hacía. Si una cosa tengo clara, es que no hubiera llegado hasta aquí sin vuestro apoyo, maite zaituztet.

INDEX

1. INTRODUCTION

1.1. ION-CHANNELS

Each cell is enclosed by a membrane, which consist of a double layer of phospholipids. This membrane holds the essential cellular components together and separates them from the external environment. Because of the tight packing of lipid molecules, the bilayer forms a hydrophobic flat sheet which acts as a barrier to the diffusion of small charged molecules and ions such as Na^+, K^+, Ca^{2+} or Cl^-. Ion channels form pores that facilitate the flow of these ions across membranes, either plasma membranes or the membranes of intracellular organelles (such as nucleus, mitochondria, endoplasmic reticulum, Golgi apparatus and so on).

The result of this evolution is the diversity of genes that code for ion channels. More than 200 ion channel genes have now been discovered, a number that could not have been anticipated from early studies of ion channel function (Purves et al., 2001). Diversity is achieved by different mechanisms, including the existence of multiple genes for the pore-forming α subunits, alternative splicing of the messenger RNA transcribed, formation of heterotetramers containing different α subunits, and modulation of channel properties by auxiliary subunits that may themselves comprise a large and diverse family of proteins. Small conformational changes in the channel induce a transition from the closed to the open state, allowing up to 10 million ions per second to flow into or out of the cell. Usually, ion channels are classified according to a specific type of ion that passes the channel; however, some are less selective. Moreover, potassium channels can be additionally classified into voltage-dependent, calcium-dependent, sodium-dependent, two-pore, and inward rectifier channels. Emerging evidence shows that many human diseases are associated with dysfunction of individual classes of ion channels (Levitan et al., 2015).

Ion channels allow for the passive diffusion of ions, determined by a favourable electrochemical gradient, set up and maintained by ATP-driven ionic transporters that actively pump ions across the membrane. When an ion channel opens, the ions rapidly diffuse through the channel pore, generating a flow of current and changing the membrane potential. Ion channels are found in the membranes of all cells, where they fulfil several essential functions. These include controlling the resting membrane potential, shaping electrical signals in excitable cells and gating the flow of messenger Ca^{2+} ions (Hille, 2001).

Many ion channels (e.g., K, Na, Ca, HCN and TRP channels) share several structural similarities. These channels are thought to have evolved from a common ancestor and have been classified together as the “voltage-gated-like” (VGL) ion channel family (see Yu *et al.*, 2005). Other ion channels, however, such as Cl channels, aquaporins and connexins, have completely different structural properties, having evolved quite separately.

1.2. MEMBRANE POTENTIAL

In every cell, particularly in excitable ones, there is a difference between the steady transmembrane potential, called resting membrane potential, being the inside of the cell more negative with respect to the outside. Depending on the ion-pumps, transporters, and exchangers

(remarkably Na^+/K^+ pump) that are located in the plasma membrane, each cell type will have a different resting potential. In neurons, their value is ~-70 mV.

In the cytoplasm there is a high concentration of negatively charged proteins that cannot cross the plasma membrane and K^+ ions, while outside the cell are the same functions of Na^+, Cl^- and Ca^{2+}. The difference in concentration on the two sides of the membrane creates concentration gradients. Pumps, exchangers and transporters are responsible for the maintenance of these gradients. The most important of these, the Na^+/K^+ pump, pumps, expending energy in the form of ATP, Na^+ outside and K^+, against its gradients. In particular, the involved proteins ensure different concentrations of the ions across the membrane, ultimately shaping the net charge between both sides of the membrane.

When the membrane potential reaches the electrochemical equilibrium for a certain ion, the net flux for this ion stops. Under these conditions, the **Nernst equation** can be applied to calculate the resting potential for a given ion. This equation takes into account both the voltage and the concentration gradients across the membrane. If we keep in mind that the membrane potential is influenced by more than one ion, it is better to use **Goldman-Hogkin-Katz equation** which contemplates all multi-ionic scenarios. Actually, this equation is used nowadays to estimate the theoretical resting potential in any kind of cell. The membrane potential of excitable cells does not remain steady. In the plasma membrane excitable cells have inserted voltage-gated channels that are responsible of triggering the **action potential** (AP) (Figure 1.1).

1.2.1. Action Potential

Succeeding changes in the membrane's permeability to Na^+ and K^+ generate action potentials. The action potential is an **all-or-none event** that has a threshold for initiation. When a signal arrives, the cell can be depolarized; and if this depolarization reaches the threshold, an action potential is fired, with the rapid and subsequent opening of voltage-gated Na^+ channels.

In the absence of input, most neurons have a stable potential across the entire membrane, which is often around negative 60 millivolts. Without any input, the resting potential will just stay right there. But excitatory or inhibitory inputs, which usually come in through the dendrites, but less often can come into the soma or the axon itself, will cause changes to the resting potential that we call graded potentials. These may be either a depolarization, also called an excitatory potential, or a hyperpolarization, also called an inhibitory potential. They are called excitatory or inhibitory because they involve movement to the membrane potential, closer to or farther away from this threshold potential, which is often around -50 mV. These graded potentials decay with both time and distance, so that as a polarization from an excitatory input spreads along the membrane, the size of the graded potential gets smaller, and the same occurs with the hyperpolarization caused by an inhibitory input. If summation of all **the excitatory and inhibitory potentials surpass the threshold value,** which is often around -50 mV, usually an **action potential will be started reaching the trigger zone** (the AIS) and conducted all the way down the axon of neurons. Neurons can transmit information over a wide range of distances, which may be one meter or more.

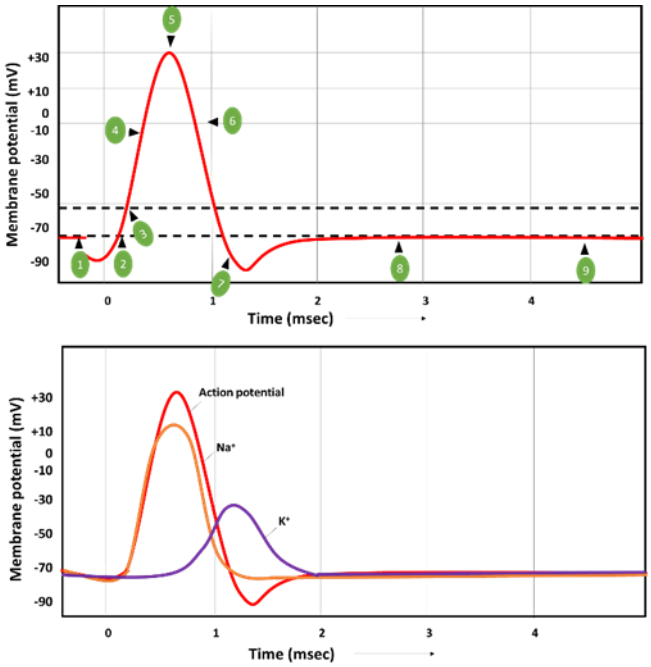

Figure 1.1. Ideal representation of action potential with its different phases. **(1)** Resting membrane potential (without any stimulus). **(2)** Cell suffers a depolarizing stimulus. **(3)** If incoming stimulus overcomes the threshold, voltage sensing Na_V channels open. **(4)** Na^+ inward flow depolarizes the cell. **(5)** Rapid influx of Na^+ causes plasma membrane polarity reversion. Therefore, Na^+ ion channels rapidly inactive and slower K^+ channels open. **(6)** Na^+ ions cannot longer enter the neuron and they are transported out of the cell by active sodium and potassium pumps. **(7)** K^+ channels remain activated. There is an outward flow of K^+ ions. In this case, plasma membrane suffers a hyperpolarization, which creates a brake to new depolarizing stimulus. **(8)** K_V channels close. **(9)** After a while, the electrochemical gradient returns to the resting state. Adapted from Human Physiology, an integrated approach, third edition, 2003.

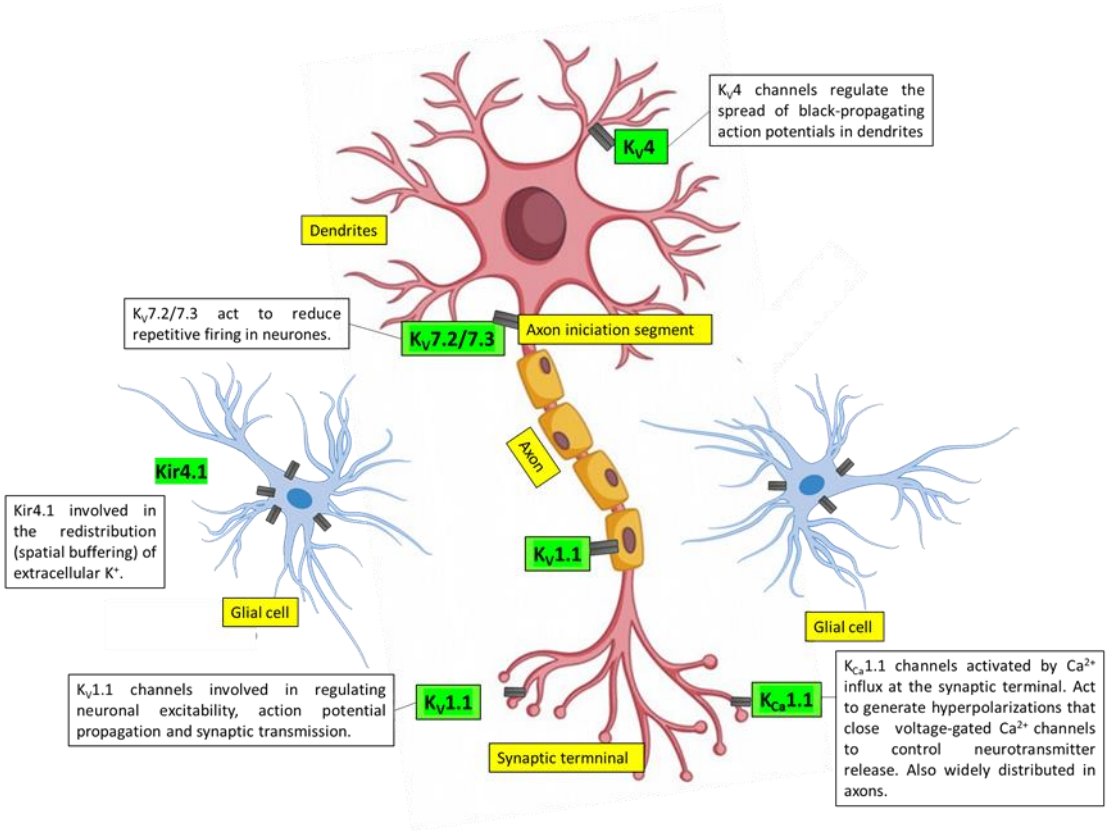

Figure 1.2. Differential localization of K^+ channel subtypes in neurons. $K_V1.1$-containing channels are expressed in the axon and presynaptic terminal, where they regulate neuronal excitability, action potential propagation, and synaptic transmission. $K_V4.3$-containing channels are expressed in dendrites and are involved in regulating the spread of back-propagating action potentials in the dendritic tree. $K_V7.2/7.3$ channels, which form the M-current, are expressed in the axon initial segment and are active at subthreshold membrane potentials where most voltage-gated K^+ channels are closed (also in the node of Ranvier). They act to dampen excitability and repetitive firing in neurons. $K_{Ca}1.1$-containing channels are expressed in the presynaptic terminal, where they localize with voltage-gated Ca^{2+} channels. They are activated by the Ca^{2+} influx that occurs in response to action potential–induced terminal depolarization and act to terminate the action potential and generate after-hyperpolarizations that close Ca^{2+} channels and reduce neuronal excitability. Kir4.1-containing channels are expressed in glial cells, where they are potentially involved in the redistribution of K^+. Adapted from Humphries & Dart, 2015.

The expression in central neurons of multiple types of potassium channels in particular confers the ability to fire with a variety of patterns over a broad range of frequencies. But how do the many channel types present in a particular neuron work together to determine its firing properties? This issue has been addressed primarily by computer modeling using Hodgkin–Huxley-like equations, extended by the addition of many conductances, with equations for each conductance based on experimental analysis of voltage and time dependence (Connor and Stevens, 1971b; Huguenard and McCormick, 1992, 1994; Johnston and Wu, 1995; Locke and Nerbonne, 1997b). As we can observe in Figure 1.2. **voltage-gated potassium channels play a major role in neuronal action potential (AP) repolarization and repetitive firing** (Connor and Stevens, 1971; Hille, 1992;Hodgkin and Huxley, 1952; Kolb, 1990; Rudy, 1988; Schwindt et al., 1988). A delayed rectifier K^+ current (I_K) was described first by Hodgkin and Huxley (1952) and found to be

responsible for AP repolarization in squid giant axons. However, the slow activation and inactivation properties of this current raised questions about its function in repolarization of more rapid mammalian neuronal APs. Subsequently, it was proposed that a transient K^+ current (I_A) contributed to neuronal repolarization and repetitive firing (Connor and Stevens 1971a,b; Hagiwara et al. 1961; Neher 1971; Schwindt et al. 1988; Storm 1987). The channels responsible for I_A (K_A channel) begin to activate below the threshold for AP generation and inactivate rapidly. Since these initial descriptions, a variety of transient K^+ currents with a wide range of voltage-dependent activation and inactivation have been recorded in a variety of neurons (Albert and Nerbonne 1995;Gestrelius and Grampp 1983; Kasai et al. 1986; Quandt 1988; Penner et al. 1986; Rudy 1988; Solaro et al. 1995; Spain et al. 1991; Stansfeld et al. 1986).

1.3. Voltage-Dependent Ion Channels

In humans there are more than 200 genes described that encode for ion channels, and more than a half are regulated by voltage, either inhibiting or activating them. Some evolved from a common ancestor, and they have varied their sequence allowing efficient functional specialization. Actually, K_V, Ca_V and Na_V channels are members of a phylogenetically related superfamily (Gutman et al., 2005). It has been suggested that the common ancestor of all voltage-gated ion channels could be the 2TM K_V, because it has the simplest structure and also the most divergent group of channels (Figure 1.3). A classical voltage-dependent ion channel is structured in multimers, composed by the assembly of four or even more α-subunits that can be identical or different. They arrange to form the selective pore for one type of ion. Every monomer has at least two transmembrane (TM) helices crossed over in the lipid bilayer, which composes the pore-forming domain. The rest of transmembrane domains or intra- or extra-cellular termini, completes the regulatory domain and will differ depending on the channel type.

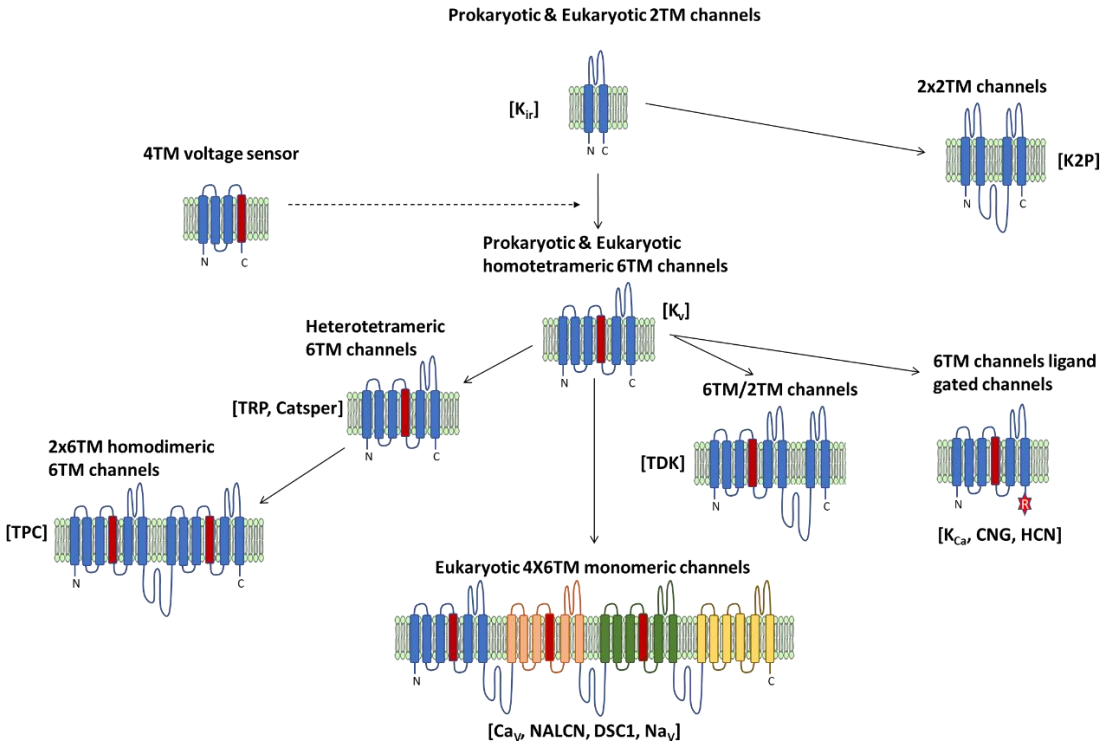

Figure 1.3. Scheme of the proposed evolutionary relationships between members of the voltage-gated ion channel family. The inwardly rectifying K^+ channels (Kir) represent the simplest structural motif in the ion channel superfamily in eukaryotes; their 2TM structure is highly representative of the pore domain found in many ancestral prokaryotic and eukaryotic channels. In the majority of eukaryotic channels, the 2TM motif has been augmented by 4 additional TM segments comprising a voltage-sensing domain (similar to that in the proton channel Hv1). Thus K_V channels (and prokaryotic Navs) are homo-tetrameric assemblies of 6TM subunits. It is currently thought that the single-domain 6TM K_V channels underwent two rounds of internal gene duplication leading to multi-domain Navs and Cavs, which resulted in superior kinetics and modulation of channel activation, inactivation, and recovery from inactivation. Two-repeat 6TM homodimeric channels, which may be an evolutionary intermediate, exist in the two-pore channel (TPC) family of Ca^{2+}-permeable channels (Adapted from Amey et al., 2015).

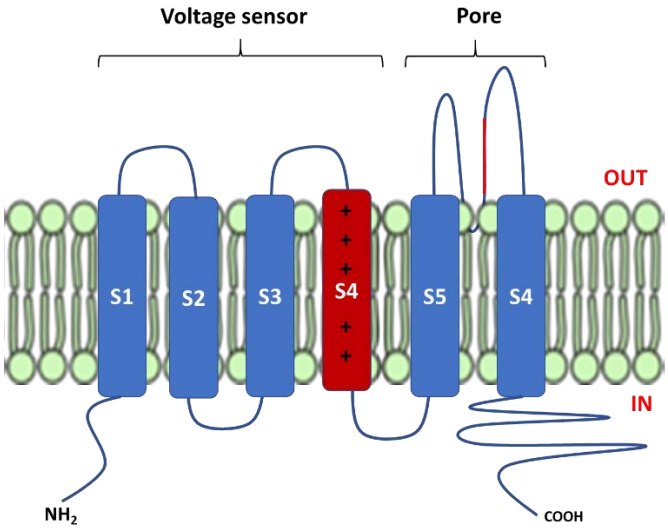

Figure 1.4. General architecture of a voltage-gated ion channel. Each subunit is made of six transmembranal helix (S1-S6) with intracellular N- and C-termini. S1-S4 forms the voltage sensor part of the channel whereas S5-S6 composes the selective pore. The amino acids in between S5 and S6 (red line) are responsible for the selectivity.

A classical voltage-dependent ion channel shares equivalent architecture. Every single subunit has six hydrophobic segments which are inserted in the plasma membrane forming the pore (Figure 1.4). Moreover, segments **S1-S4** are responsible for the **voltage sensing**, especially the fourth segment which has several amino acids with positive charge (Long et al., 2005). They have **intracellular carboxyl and amino moieties,** which often are important for the channels regulation as they comprise the **intracellular interaction site for ligands**. In fact, usually these kinds of ion channels are expressed in association with one or more auxiliary subunits which modulate and increase their functional properties.

1.3.1. Voltage Gated Potassium Channels (VGPC)

After the first *shaker* potassium channel was described in *Drosophila melanogaster* in the eighties, as much as 90 genes encoding for K^+ channels have been discovered until now, almost ten times than for Na^+ or Ca^{2+} channels. Moreover, 50 % of them depend on the membrane voltage to operate properly (Bradding & Wulff, 2013). According to the International Union of Basic and Clinical Pharmacology (www.iuphar.org), VGPCs are classified in twelve families (K_V1-12) (Figure 1.5) where it is noticeable that two main clusters are discerned: the first group includes K_V1 to K_V9 channels, in which K_V7 channels are separated rapidly; the second group goes from K_V10 to K_V12. However, even considering that the number of VGPC genes are low, the functional diversity of this family grows exponentially when taking into account what happens *in vivo*:

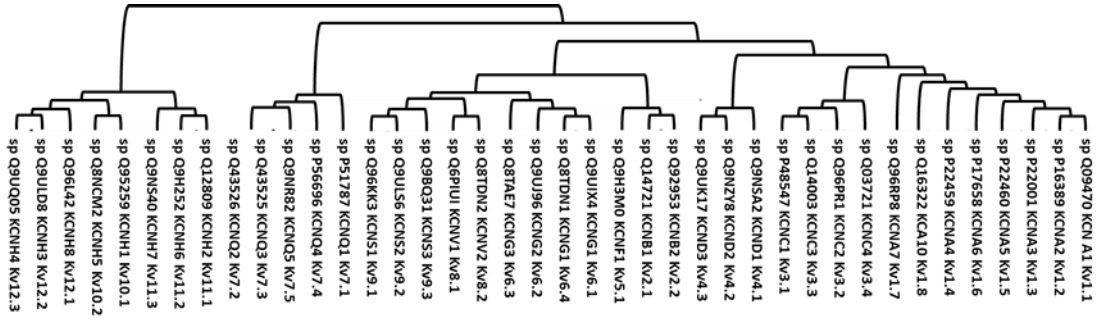

Figure 1.5. Maximum likelihood tree of human K_V channels. The amino acid sequence of each were obtained using their accession number displayed below in www.uniprot.org database.

Open K^+ channels keep the membrane potential closer to the potassium equilibrium potential, maintaining away from the threshold for firing an action potential. Accordingly, in excitable cells, K^+ channels fix the resting potential, short the action potential, finish high activity periods, regulate the intervals during recurrent firing and reduce the effectivity of excitatory inputs when they are open (Hille, 2001).

As discussed below, K_V architecture is typically arranged by a tetramer of 4 replicas of alpha subunits arranged as a ring (MacKinnon, 1991). Contrary to Na^+ and Ca^{2+} channels, which are formed by a unique protein that is, indeed, four repeats of the same pattern (Catteral, 2000). Na_V, Ca_V and K_V units share the topology of six transmembrane domains. Hence, four copies of K_V tetramerize to form a structure analogous to Na^+ and Ca^{2+} channels.

1.3.1.1. Classification of alpha subunits

According to the International Union of Pharmacology (IUPHAR), K_V are classified into 12 families (K_V1-12), with several isoforms in each. Although alpha subunits of K_V can be divided based on different principles, they are normally classified according to the **function** by which they were initially identified (Hille, 2001; Gutman et al., 2005).

• Delayed rectifier (IDR): channels that allow a sustained K^+ efflux with a delay after membrane depolarization. The outflow of potassium ions repolarizes the membrane rapidly. The influx of Na^+ ions to the cell increases the membrane potential and causes the aperture of these channels, which repolarizes the membrane. This repolarization restrains the prolongation of the nerve impulse and takes part in the regulation of repetitive firing of the neuron. In addition, these channels slowly inactivate or do not inactivate at all. This group contains channels from K_V1 (KCNA, *Shakers*), K_V2 (KCNB, *Shabs*), K_V3 (KCNC, *Shaws*), K_V7 (KCNQ) and $K_V10.1$ (KCNH1, eag1) families.

• A-type (IA): channels that also generate an outward K^+ current following a depolarization of the membrane. In contrast to delayed rectifiers, A-type channels open by depolarization following hyperpolarization. It helps neurons to fire repetitively at low frequencies because, usually, this hyperpolarization increases the interval between action potentials. This group includes channels of K_V1 ($K_V1.4$), K_V3 ($K_V3.3$ and $K_V3.4$) and all the members of K_V4 (KCND, *Shals*).

• Modifier/silencer: proteins that, despite having similar sequences and structures to other categories, they are not able to produce ion currents by themselves. Beyond this, they heterotetramerize with members of K_V2 family, modifying or suppressing their activity. This category includes members of K_V5 (KCNF), K_V6 (KCNG), K_V8 (KCNV) and K_V9 (KCNS).

• Other: Other channels do not suit into any category mentioned above or so far has not been widely studied to be classified. This is the case of channels such as $K_V10.2$, which has been classified sometimes as outward-rectifying; $K_V11.2$ and $K_V11.3$, relative of inwardly-rectifying $K_V11.1$; and K_V12, considered as slowly activating.

1.3.1.2. Transmembrane domains of VGPCS

The pore-forming domain is one of the main characteristic features, shared by all potassium channels. To form a functional pore, it is necessary to assemble four pore-forming domains together. As this is a common characteristic, the **two TM K^+ channels named KcsA can represent this pore perfectly.** In fact, almost all the information about the pore structure relays on the work done by the Nobel Awardee Roderick MacKinnon on KcsA channels (Doyle et al., 1998) (PDB: 1K4C). This structural information has been essential to understand how a potassium channel is selective for K^+ ions in among the rest of ions (10000:1 K^+ to Na^+ ions); how the transport of such a large quantity of ions is realized (10^7 ions channel-1 s-1) (Sansom et al., 2002) and how channel gating may originate.

1.3.1.2.1. Selectivity filter and conductivity

The mechanism of the selectivity filter is shown in Figure 1.6. When K^+-ion is close to the pore, it is electrostatically bound to water molecules. These intermolecular bonds would be broken up for this ion to cross the pore of the channel, and energetically this is an inconvenient (around 75 kcal/mol) (Thompson et al., 2009). However, channel has assembled some amino acids next to the pore domain with their carboxyl group are located facing to the outside, which are capable of displace the bounds with water, causing the ion desolvation. When the ion has crossed the membrane, it rehydrates again.

The amino acid sequence, which fulfils the selectivity filter for KcsA, is located in the P-loop and submits the consensus sequence TVGYG. It is noteworthy that the GYG triplet is highly conserved between all potassium channels. Their carbonyl groups have their oxygen atoms exposed to the inner part of the pore (Figure 1.6). The selectivity filter contains four sites for interaction with the hydrated K^+ ion, two of them accommodated to interact with two water molecules whereas the other two interacts with two ions and they alternate between them. When a third ion gets to the outside part of the pore, it produces new electrostatic interactions that destabilize preceding ions supporting their cross through the membrane.

In addition, the negative charges of the carbonyl groups would repeal the anions, making impossible for them to pass through the channel. On the other hand, other cations that are not K^+, could pass through the pore, however due to their size differences, they do not match the carboxyl groups as well as the K^+ ions do, making the through of those cation energetically unfavourable. How is it possible, though, that the ion **conductivity** process takes places so rapidly? MacKinnon and colleges affirm that only two K^+ ions can go by simultaneously through the filter. Labelling the ions from the top to the bottom from 1 to 7, it is thought that only pair or odd configurations can be achieved (MacKinnon, 2003). Shifting from the first to the second configuration is energetically allowed through a mechanism where top dehydrated-ions' hydration favours dehydration of bottom ions. In addition, K^+ ions stabilize the open conformation of the selective filter, favouring K^+ conduction

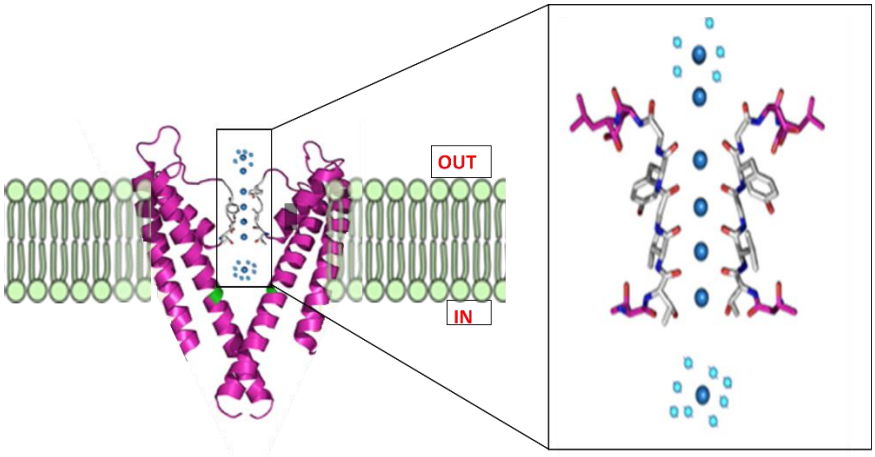

Figure 1.6. Structure of KcsA. (Right) Representation of two of the four monomers forming the channel. In green has been highlighted the glycine 99 which takes the function of the gating-hinge. In white TVGYG selective filter is coloured. Dark-blue spheres are K^+ ions and cyan spheres are H_2O molecules and have been placed there to empathise the hydration of ions. (Left) Selective filter of the channel. The TVGYG motif of the P-loop appears in white. Lateral chains of these amino acids are able to create polar contacts with water molecules and K^+ ions. (PDB: 1K4C)

1.3.1.2.2. Voltage-sensor domain

Action potentials generated by nerve cells depend on several types of voltage-gated channels. Voltage-sensing domains (VSDs) are four-helical bundle domains, called **S1–S4**, which are highly

conserved. They respond to changes in membrane potential, coupling changes in transmembrane electrical potential to conformational changes that regulate ion conductance through a central channel. In general, the S4 segment is formed with **4–8 basic amino acids** (mostly arginines), fulfilling the requirements of a voltage sensor. The basis for structural and electrical changes in S4 that give rise to voltage dependence is key to understanding the response of voltage-gated ion channels to changes in membrane potential. Structural data is compatible with the model where amino acids in the S4 suffering a rotation and a displacement, changing subsequently of conformation helix S6 and finally resulting in the opening of the channel (Bezanilla et al., 2000; Aggarwal & MacKinnon *1996*).

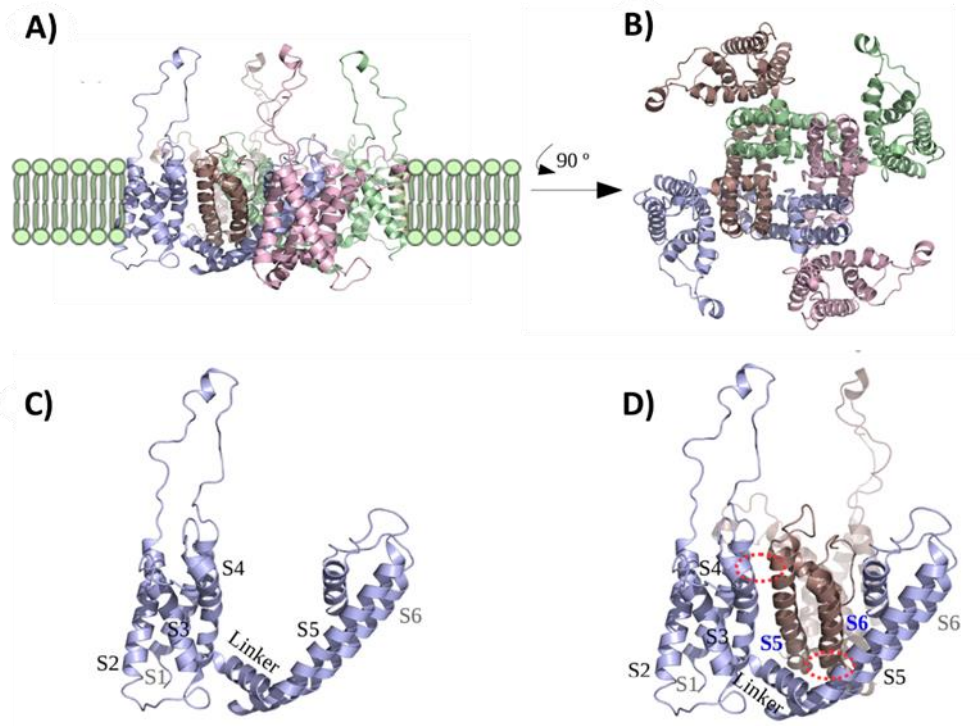

Figure 1.7. Structure of K_V1.2. **(A)** Lateral view of the tetramer. Every subunit is represented in different colour. Only transmembrane domains are shown. **(B)** Upper view of the channel where a central pore is visible. All selective filters are looking towards the inner part of the pore. **(C)** Structure of a single subunr region (S1-S4) and the pore forming region (S5 and S6). **(D)** Intermolecular contact regions surrounded in red circles. By these contacts voltage-dependent gating occurs in the channel. This regulation is among all the subunits. (PDB:3LUT).

1.3.1.2.3. Intracellular Domains

The first high resolution structure of the intracellular domains from K_V7 voltage-gated potassium channels was resolved recently (Sun & MacKinnon, 2017), where The $KCNQ1_{EM}$/CaM complex structure was determined to an overall resolution of 3.7 Å with C4 symmetry imposed.

Considering all available information, clustering of K_V channels in two main groups has been proposed (Barros et al., 2012):

1) K_V channels with the tetramerization domain in the N-terminal (K_V1-K_V4)

2) K_V channels with the tetramerization domain in the C-terminal domain (K_V7 and K_V10-K_V12).

Several parts of the N-terminus have been resolved and are referred here: T1 domain of Shaker (PDB: 1A68) (Kreusch et al., 1998), K_V1.2 (PDB: 1QDW) (Minor et al., 2000), K_V4.3 (PDB:1S1G) (Scannevin et al., 2004), K_V4.3 with KchIp1 (PDB: 2I2R) (Pioletti et al., 2006), K_V1.3 (PDB: 4BGC) (Kremer et al., 2013). Distal N-terminus activation structures of K_V3.4 (PDB: 1ZTO) (Antz et al., 1997), K_V1.4 (PDB: 1KN7) (Wissmann et al., 2003). PAS domain of K_Vv11.1 (PDB: 1BYW) (Morais Cabral et al., 1998), (PDB: 2LOW) (Ng et al., 2011), (PDB: 4HQA &4HP9) (Adaixo et al., 2013).

Some of the C-termini have been resolved too. Coiled coil segment of K_V7.4 (PDB: 2OVC (Howard et al., 2007), K_V7.1 (PDB: 3BJ4) (Wiener et al., 2008). K_V7.1 channel's helix B in complex with holo-CaM (PDB: 4GOW) (Q. Xu et al., 2013) K_V7.1 channel's helices A and B in complex with CaM (PDB: 4UMO & 4V0C) (Sachyani et al., 2014) and more recently, the $KCNQ1_{EM}$ structure (Sun & MacKinnon, 2017) with 4 intracellular helices (*h*A-*h*D). The cytosolic *h*A and *h*B helices, which are connected to the S6 transmembrane helix, are sandwiched between the N- and C-lobes of CaM. *h*C and *h*D form two long helical bundles that facilitate tetramerization of the channel. In contrast to a previous SAXS study carried out in the absence of the transmembrane domain (Sachyani et al., 2014), which identified flexibility in a location proximal to *h*C, they observe flexibility distal to the *h*C helix. This flexibility produced disorder in the position of the D helix and therefore a higher resolution map could be achieved by masking out the *h*D bundle during single-particle reconstruction.

Even when considering the large divergence among the intracellular domains, a general structural model of K_V channels can be devised (Figure 1.8). The **T1 tetramerization domain** of K_V1-K_V4 channels, which is also called NAB, is located in the N-terminal. Moreover K_V1.5 channels have a tandem of two **SH3 binding domains** whereas a secondary inactivation domain is always present in K_V1.4 channels. The N-type inactivation-prevention domain (**NIP**) of K_V1.6 channels is also represented as it protects potassium channels against rapid inactivation. Finally, in the very beginning of the N-terminus the ball-like structure is located, responsible of the N-type inactivation, which is correlated to **PAS domain** of eag-like channels. In the C-terminal domain a C-linker/cNBD regions of the K_V related HCN and CNG channels can be found. The localization and C-terminal activation (**CTA**) domains correspond to K_V2.1. Finally, a postsynaptic density protein-binding domain (**PSD-95**) is located in the most distal part of the C-terminus which are present in some K_V1 channels. However, a more detailed view of K_V7 channels and the implications of the model in M-current density regulation will be discussed later on.

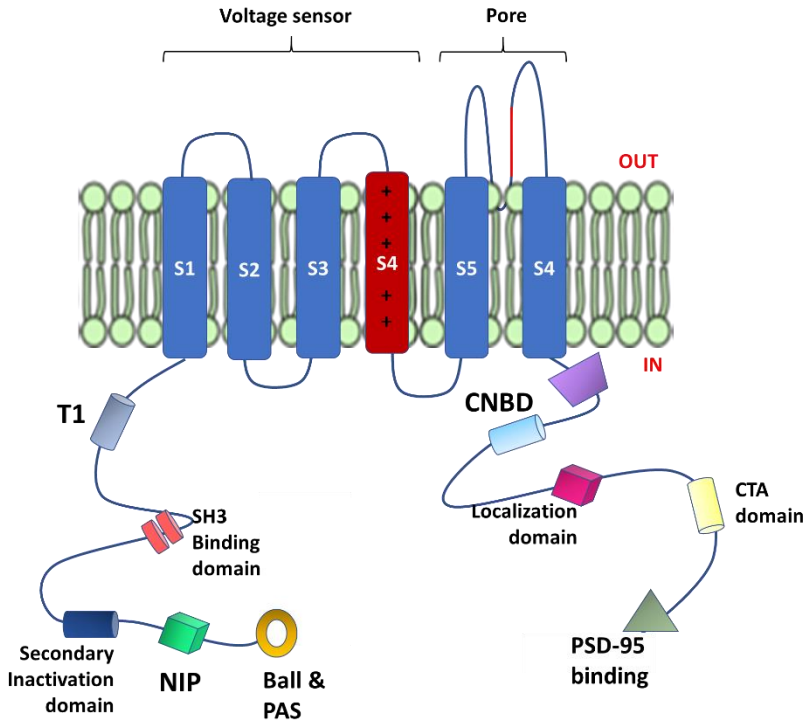

Figure 1.8. Schematic representation of the intracellular domain of K_V channels. Different regions and domains have been highlighted. In the N-terminal, T1, tetramerization domain of K_V1-K_V4 channels, SH3 binding domain from $K_V1.5$; Secondary inactivation domain, from $K_V1.4$; NIP,N-type inactivation-prevention domain from $K_V1.6$; Ball-like structure and PAS domain from eag-like channels. In the C-terminal, C-linker/cNBD regions from K_V related HCN and CNG channels; Localization and CTA (C-terminal activation) domains from $K_V2.1$; and PSD-95, post-synaptic density protein binding domain from some K_V1 channels.

1.3.1.3. Gating

The mechanism of ion channel voltage gating has been debated since Hodgkin and Huxley find out that the crux of nerve conduction is ion flow across cellular membranes (Hodgkin & Huxley, 1952). Up to three decades later voltage-sensing domains (VSDs) were identified as controlling the activity of voltage-gated K^+, Na^+, and Ca^{2+} channels (Noda et al., 1985; Tempel et al., 1987; Nelson et al., 1999), shifting these proteins between activated and deactivated states in response to changes in transmembrane voltage (Bezanilla et al., 2000). Since then, different mechanistic models have been proposed to describe how arginine and lysine gating-charge residues on S4 transmembrane domain associate with the electric field to gate ion channel conduction (Aggarwal & MacKinnon, 1996; Long et al., 2007).

These are the two main mechanisms proposed for VGPC's gating:

- In the case of KcsA, three key hydrophobic residues have been detected in the end of the second transmembrane domain: V, T and A. Their hydrophobic moieties are located around the entry of the pore and block the pass of ions. When the pore has to open, these residues change their configuration thanks to a glycine that serves as a *hinge* (Figure 1.6.). However, this glycine is not present in all channels, but other conserved amino acid sequences can also act as a hinge, such as, PxP, where P is proline and X is any

amino acid. In K_V channels, this mechanism also permits the direct interaction between the sixth helix of the pore-forming domain and the voltage sensor domain (Figure 1.7.D). Therefore, the voltage sensor domain transfers the signal allosterically towards the pore domain (Long et al., 2005).

- **N-inactivation:** also known as "ball-and-chain" mechanism, has a specific region in the N-terminus of the channel that is able to be inserted in the inner part of the pore when this is opened ultimately blocking the channel. Other regulatory subunits such as K_V β can mimic the "ball" region when this is not present in the channel. N-type inactivation, however, is slower and it seems to occur due to the movement of the residues located in the selectivity filter (Batulan et al., 2010). Apparently, this method is sensitive to the extracellular K^+ concentrations, which means that this could regulate an excess of K^+ ions.

1.3.1.4. Fundamental Models of Activation of K_V Channels

All K_V channels share a similar mechanism of activation. They can be present in three functional states: quiescent state (closed conformation) ↔ activated state (open conformation) ↔ inactivated state

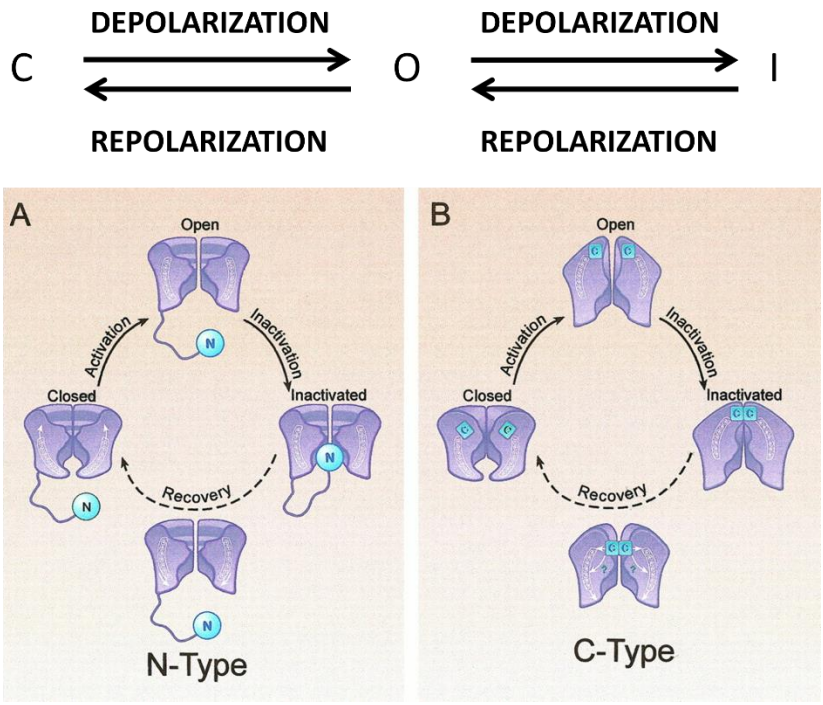

Figure 1.9. Scheme of the conformational transitions in K_V channels: C – closed channel; O – open channel; I – inactivated channel. B. N-type inactivation. The inactivation peptide enters the pore and physically blocks the transfer of ions after the activation of the channel. C. C-type inactivation. The selectivity filter acts as the second gate and closes, preventing the penetration of ions. The channels completely return to the closed conformation when the potential drops to the resting potential level. (Modified from Grizel et al., 2014)

- A sliding-helix model (SHM) *(Cattetall, 2010)*

This mechanism is explained as an **electromechanical coupling** in which outward movement of gating charges in the S4 transmembrane segments catalyzed by sequential formation of ion pairs pulls the S4-S5 linker, bends the S6 segment, and opens the pore (Catterall, 2010). Based on thermodynamic and structural information proposed that the arginine residues in the S4 segments form ion pairs with negatively charged amino acid residues in the neighboring S1, S2, and/or S3 segments. Thus, the residues in the S4 segment which are positively charged are attracted by the electrostatic force of the negative inter membrane potential. After depolarization this electrostatic force is softened and the S4 segments move outward along a spiral path such that each positively charged amino acid residue in the S4 segment makes a series of ion pairs with negative charges (Catterall, 2010).

- A paddle model *(Jiang et al., 2003)*

This is a completely different activation model that was described after resolving the crystal structure of the bacterial channel KvAP (Jiang et al., 2003). There, S3-S4 helices are located next to the intracellular surface of the membrane and perpendicular to the pore axis. This model was inmediatelly discarded by those in the ion channel field but gained popularity due to the prestige of its proponent. The basic tenants of the model are not substaned by evidence. However, it is a good example on how the prestige of a proponent can distort science, bypassing strict scrutiny by peers in vanity journals.

Two segments (S3a and S3b) which are connected by the S3 loop form S3 helix. The S3b segment and N-terminal part of the S4 helix are oriented in antiparallel strictly opposite each other, and they form **a hydrophobic helix-loop-helix** structure linked to the pore domain by the flexible loop of the S3 helix and S4-S5 linker. The S3b-S4 region was termed the “paddle” (Jiang et al., 2003), because of the structure adopted.

Accordingly, when the channel is closed the positively charged paddles of the channel are situated near the intracellular surface of the membrane, thanks to a large electrical field, while the membrane resting potential is negative. Upon depolarization, the paddles move together towards the external side, pulling along the S4-S5 linker that in turn pulls the S5 helix away from the pore axis, opening the pore (Jiang et al., 2003).

- Advanced SHM model *(Durell* et al., 2004*)*

It was proposed based on the data of the sequence of the *Shaker* channel and the crystal structure of the KvAP channel (Jiang et al., 2003). Relative to the paddle model this also suggests that the movement from open to close conformation involves three steps: first S4 moves by ~13.5 Å along the axis and rotates by 180^{o}. Simultaneously, the positively charged S4 segments remain in the polar environment interacting with the negatively charged residues of S1-S3 helices, other polar atoms, negatively charged lipid heads, and water.

- Transport model (TM) *(Chanda et al., 2005)*

This model suggested that **S4 moves** during channel activation, inclining by 45°, but simultaneously moving perpendicularly to the membrane surface. Arg on S4 move from the cavity on the intracellular side to the cavity on the outer side of the membrane. This movement of the S4 helix blends rotation and tilt, being the helix always in the polar environment. Here, S4 is compared to a transporter that has its binding site changing between the inner and outer sides in each cycle. This mechanism allows the transfer of a large amount of charge through the electric field without movement of S4 through the membrane.

- Model of coordinated movement of helices (CMH) *(Pathak et al., 2007)*

This model suggests that the **S4 pivots by ~180° clockwise** (on the extracellular side), during depolarization, rising by 6-8 Å and changing its inclination from 65° to 35°. The tilt of the S4 helix promotes the inclination of the intracellular half of S5. This counterclockwise movement (on the extracellular membrane side) enables S4-S5 linkers and S6 helices (in all subunits) to move together and to open the intracellular gate.

- A consensus model (CM) *(Vargas et al., 2011)*

This model was developed by Vargas *et al*. (2011) based on an improved CMH model (Pathak et al., 2007). They used data on the basic interactions between the amino acid residues of the VSD domain helices in the closed channel.

- A model of charge transfer (MCT)

It is also of interest to understand how different compounds or toxins are able to modulate the gating properties of the channels. For a long time it has been known that some animals such as spiders, snakes, scorpion among others have a large variety of toxins that affect the neural system of other animals in which humans are included (Strong et al., 1990). Originally, it was thought that some of these toxins were specially affecting ion-channels. This idea was supported by physiological studies, but more recent studies where KcsA was analysed in presence of kaliotoxin (a scorpion toxin) by solid-state NMR revealed some structural rearrangements that can explain the blockage of channels (Lange et al., 2006). In 2013, the group of MacKinnon published a structure of a K_V1.2-2.1 chimera in complex with the scorpion toxin Charybdotoxin (PDB: 4JTA) (Banerjee et al., 2013). The toxin is plugging the ion conduction pathway of the pore rather than changing the channel structure *per se*. Despite the discrepancy with the solid-state NMR data, there is no evidence for a unique way in which toxins act on channels and therefore both mechanisms are plausible.

1.3.2. Other voltage-gated ion channels

This doctoral thesis is focused on K_V7 channels. However, for the sake of completeness, we are going to briefly describe some other voltage-gated ion channel families:

1.3.2.1. Ca_V channels: a group of voltage-gated ion channels found in the membrane of excitable cells (*e.g.*, muscle, glial cells, neurons, etc.) with selectivity for the calcium ion Ca^{2+}. These channels also are barely permeable to sodium ions. They are involved in many physiological

processes such as muscular contraction and relaxation, intracellular signalling, heart beating, and secretion of neurotransmitters and hormones.The pore-forming unit of all known Ca^{2+} channels is expressed as a single protein composed of four repeated domains that are expressed as separate proteins and then assembled. Voltage-gated calcium channels are formed as a complex of several different subunits: α_1, $\alpha_2\delta$, β_{1-4}, and γ. The α_1 subunit forms the pore and the voltage sensor while the associated subunits have several functions including modulation of gating. It is arranged in four homologous motifs (I-IV), each of which owns six transmembrane segments. Some of them have associated an intracellular β subunit and a transmembranal α_2 β subunit. Ca^{2+} channels show high structural and functional diversity as it is patent in the case of heart contraction, where 3 subfamilies are described to take part in the process: Cav1 (type L), Cav2 (type P/Q, N and R) and Cav3 (type T).

1.3.2.2. Na_V channels: Voltage-gated sodium channels are responsible for action potential initiation and propagation in excitable cells, including nerve, muscle, and neuroendocrine cell types. Although these channels have extreme selectivity towards Na^+ ion, they have structural similitude with Ca^{2+} channels. There are 11 genes that encode for Na+ channels' α subunits in humans. Furthermore, they are also responsible for many physiological processes; the most studied one is the generation and propagation of the action potential.

Following channels are not exactly voltage-dependent, but they show large homology with the voltage-gated ion channels.

1.3.2.3. Channels activated by cyclic-nucleotides (CNG): CNG family also shares the same structural characteristics with other voltage gated ion-channels. They are opened by the direct binding of cyclic nucleotides, cAMP and cGMP. They are nonselective cation channels that are found in the membranes of various tissue and cell types and are significant in sensory transduction as well as cellular development. They are indispensable for the olfactory and visual perception. Although their activity shows truly little voltage dependence, CNG channels belong to the superfamily of voltage-gated ion channels. However, they only activate when their ligands are bound to their intracellular carboxyl terminus (cAMP or cGMP). Like their cousins the voltage-gated K^+ channels, CNG channels form heterotetrameric complexes consisting of two or three different types of subunits.

1.3.2.4. SK channels: SK channels contribute to the after-hyperpolarization following an action potential and mediate the intrinsic excitability of many excitable cells (Adelman et al., 2012), modulate the activation of immune responses (Feske, 2015), and contribute to the regulation of vascular tone (Wulff, 2013). These 6TM channels share ~40% residue conservation with voltage-activated K^+ channels. Although the S4 segment contains three positively charged Arg residues, opening of SK channels is insensitive to transmembrane voltage (Hirschberg, 1998). CaM is constitutively bound through the C-lobe to the distal part of helix A that follows transmembrane S6. This interaction alters the geometry of the C-lobe E-F hands, such that one or both are incapable of binding Ca^{2+} (Lee and MacKinnon, 2018; Schumacher et al., 2001). Besides its role in Ca^{2+} signaling, calmodulin (CaM) is critical for surface expression and tetramerization (Joiner et al., 2001; Lee et al., 2003).

1.3.2.5. EAG channels: EAG1 potassium channel belongs to the KCNH or ether-a-go-go family of voltage-gated K^+ channels and have roles in cardiac repolarization, neuronal excitability

(Bauer and Schwarz, 2018; Pardo and Stuhmer, 2014) , and tumorogenesis (Pardo et al., 1999). This family of channels has an unusually long cytosolic loop joining S2 and S3. The cytoplasmic regions connected to the N- and C-termini comprises over 70% of the amino acid sequence. It includes a PAS domain (Per-ARNT-Sim) on the N terminus that is preceded by a sequence of 25-27 amino acids known as the PAS-cap. The C-terminus, attached to the pore through the C-linker domain, contains a region with homology to cyclic-nucleotide binding domains (CNBHD) that does not bind cyclic nucleotides, followed by a coiled coil C-terminal tetramerization domain (Jenke et al., 2003). These channels are functional when the cytoplasmic region is removed, saving the distal C-terminal coiled coil tetramerization domain (Whicher and MacKinnon, 2019), or when combining split subunits, N-terminus/VSD on one side + PD/C-terminus on the other (Lorinczi et al., 2015), highlighting the modular design. Furthermore, functional channels are generated when the split point is located at the S2-S3 intracellular loop or at the S3-S4 extracellular linker (de la Pena et al., 2018). Because split PD on its own is non-conducting even when carrying a mutation in S6 that generates constitutive active channels in the full-length or in the split VSD/PD configuration, it appears that PD needs to associate with VSD to adopt a configuration compatible with ion permeation (Tomczak et al., 2017).

1.3.2.6. Transient Receptor Potential (TRP): TRPV5 and TRPV6 are close homologs (~75% sequence identity) that belong to the transient receptor (TRP) family of ion channels, but contrary to other family members, they are not thermosensitive or activated by ligands. Both are expressed in epithelial cells, TRPV5 mainly in the kidney and placenta, whereas TRPV6 in intestine. They are characterized by a high selectivity for Ca^{2+} over monovalent cations (100 times higher) and play critical roles for Ca^{2+} homeostasis (Alaimo and Rubert, 2019; Nijenhuis et al., 2005; Nilius et al., 2001). TRPV5/6 channels are composed of four subunits, each containing a 4TM domain, reminiscent of a VSD but insensitive to voltage (ViSD), a PD domain in a swapped configuration, with intracellular amino and carboxi termini, resembling 6TM potassium channels. A defining feature is the presence at the N-terminus of a number of repeating ankyrin domains having a canonical helix-loop-helix fold. The high Ca^{2+} selectivity is determined by a single aspartate residue (TRPV5-D542, TRPV6-D541) in the reentrant loop at the pore (Saotome et al., 2018). These channels are tightly regulated by PIP_2 and CaM, which stimulate and inhibit activity, respectively. CaM participates in a negative feedback mechanism that inhibits channel activity, preventing excessive Ca^{2+} influx (de et al., 2011; Lambers et al., 2004). Small changes in intracellular Ca^{2+} have a major effect on Ca^{2+} entry via these channels because half maximal inhibition is observed at about 90 nM (Nilius et al., 2001).

1.4. M-CURRENT AND K_V7 CHANNELS

The M channel-mediated current, M-current or I_M, was first described by Brown and Adams in 1980 in bullfrog sympathetic ganglion neurons (Brown et al., 1980). It was termed as "*M-current*" because at the early stages of the investigation it was only known that **muscarine** was able to suppress it (Figure 1.9). It is a K^+, voltage- and time-dependent, non-inactivating current, which activates near the threshold for action potential initiation. The activation of the M-current is **slow**, not participating in the repolarization of the cell, but it **can exert a profound dampening**

effect on repetitive or burst-firing and on the general excitability of neurons. That is why when the M-current is suppressed, there is an increase in neuronal excitability.

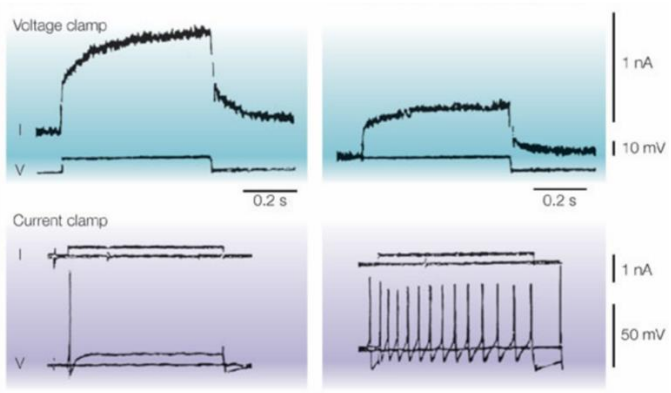

Figure 1.10. Neuronal response to a stimulus in absence and in presence of muscarine. Left: After depolarizing the neuron from the resting potential to -40 mV produces the M-current where only a single spike appears. Right: when $K_V7.2$ and $K_V7.3$ are closed due to the muscarinic effect, M-current is suppressed and therefore a depolarizing stimulus can generate a train of action potentials. Adapted from Delmas & Brown, 2005).

In fact, the M-current constitutes for many cells the principal potassium current in the sub-threshold area of the membrane potential, preventing the excitability and the trigger of repetitive *AP*s. Moreover, this current never inactivates, so it influences the firing rate.

Until 1998 there was not enough evidence to support that the $K_V7.2$ and $K_V7.3$ heterotetramers are the molecular components responsible for the current (Wang et al., 1998), and that mutations on these subunits are responsible for diseases such as BFNC (Biervert et al., 1998; Cooper et al., 2000; Delmas & Brown, 2005). In addition, both channels express mainly in the hippocampus, neocortex and cerebellar cortex. Within the neuron, $K_V7.2$ and $K_V7.3$ channels (encoded by KCNQ2 and KCNQ3 genes respectively) gather in the soma, dendrites, in the initial segment of the axon and finally in the *Ranvier nodes* where the *AP* regenerates in myelinated nerves where present a specific regionalized distribution. In these regions, KCNQ2 and KCNQ3 are co-expressed and co-assembled (Cooper et al., 2000), and thus both subunits are thought to fully function when they are assembled as a heterotetramer, because KCNQ2/KCNQ3 heteromeric channels generate 15-fold larger current than homomeric channels (Wang et al., 2000; Schroeder et al., 2000).

The high presence of both channels in these cells highlights the key-role of the I_M in the regulation of neuronal excitability. However, it has also been demonstrated that although M-currents are mostly produced by $K_V7.2$ and $K_V7.3$, homomers of $K_V7.2$ and $K_V7.5$ could generate M-currents *in vivo* (Schwarz et al., 2006), while in cellular models like HEK293T and CHO any K_V7 could generate it (Shapiro et al., 2000).

1.4.1. Structure

K_V7 family members share the typical structure of six transmembrane domains of voltage dependent potassium selective channels **(TM/S1-6).** S1-S4 segments form the voltage sensing region, especially the arginine rich, and so positively charged, S4, S5, S6 and the loop between them form the pore, with the typical feature GYG which confers the selectivity to potassium. Both,

the amino (N-) and carboxy (C-) terminal domains are located intracellularly. As in many other ion-channels, four subunits must assemble in a tetramer to form the functional pore.

Even if most K_V channels tetramerize at the N-terminus via a tetramerization domain (T1), K_V7 channels lack this domain, but they have at the helix-D of the C- terminus (Maljevic et al., 2003). It must be said that the C-terminus of K_V7 channels is particularly long and regulates the assembly, trafficking, and gating of the channel (Haitin et al., 2008; Barros et al., 2012).

1.4.2. K_V7 FAMILY MEMBERS

1.4.2.1. $K_V7.1$

The gene encoding for $K_V7.1$ protein, KCNQ1, was the first family member to be cloned and it was identified on chromosome 11p15.5 by using a positional cloning approach in families with long QT syndrome type 1 (Wang et al., 1996). Particularly, $K_V7.1$ is the only member of the family that cannot form heterotetramers with other K_V7 members. However, it co-assembles with the auxiliary subunit KCNE1, also known as *mink* or *IsK*, to generate the cardiac **I_{Ks} current**, which is an essential component for **cardiac cell repolarization** (Barhanin et al., 1996; Sanguinetti et al., 1996). $K_V7.1$/KCNE1 also express in the inner ear, thyroid gland, lung, gastrointestinal tract, the small intestine, pancreas, forebrain neuronal networks and brain stem nuclei, ovaries and the proximal and distal tubule of nephron, highlighting the influence of these channels in many cellular functions (Jespersen et al., 2005).

Long QT syndrome (LQTS) is a disorder of the heart´s electrical activity, which affects cell repolarization. Often provokes strong suppression of WT currents and lead the patients to arrhythmias and cardiac sudden death (Maljevic et al., 2010).

In addition, two different syndromes have been related with mutations in KCNQ1: autosomal dominant Romano-Ward and the recessive Jervell and Lange-Nielsen syndrome. In the later one, the affected individual besides the cardiac deficiency, suffer congenital deafness as well (Wang et al., 1996).

1.4.2.2. $K_V7.2$ and $K_V7.3$

Genes encoding for $K_V7.2$ and $K_V7.3$ channels, KCNQ2 and KCNQ3, were identified by using two different approaches. Firstly, human brain cDNA library was screened based on a KCNQ1-derived sequence (Yang et al., 1998) and secondly, positional cloning was explored in families with **Beningn familial neonatal convulsions (BFNC)** (Biervert et al., 1998; Schroeder et al., 1998). As we mention in the section of **M-current**, $K_V7.2$ and $K_V7.3$ are present in different **brain** regions and can form both homo and heterotetramers. They underlie the neuronal M-current and mutations in these proteins have been related to a series of diseases such as neonatal seizures, Rolandic epilepsy (Neubauer et al., 2008), epileptic encephalopathy (Weckhuysen et al., 2012) and autism (Gilling et al., 2013).

1.4.2.3. $K_V7.4$

Human retina cDNA library was screening based on KCNQ3 partial cDNA and KCNQ4 gene was identified. **DFNA2**, which is an inherited nonsyndromic hearing loss was also identified to co-segregate with this gene (Jentsch et al., 2000). Small expression level was found in the brain,

mainly in the nuclei and paths of the central auditory pathway (Kharkovets et al., 2000), but it is highly expressed in the **cochlea**, which is a part of the inner ear (Kubisch et al., 1999). DFNA2 mutations show a loss of function either by a haploinsufficiency mechanism or by a dominant negative effect (Maljevic et al., 2010). Finally, $K_V7.4$ can form heterotetramers with $K_V7.3$ and yield M-type currents (Kubisch et al., 1999).

1.4.2.4. $K_V7.5$

KCNQ5 was the last member to be cloned and it is less characterized than the others are, even though it has a noteworthy homology to KCNQ3 (Schroeder et al., 2000). It is expressed principally in the **brain** and in the **skeletal muscle**, being regulated during myoblast proliferation (Lerche et al., 2000). Lower levels of $K_V7.5$ have been found in colon, lungs and uterus. As it can be inhibited by muscarinic receptors, and as it is expressed mostly in the central nervous system, this member could me included within **the M-channel family**. Actually, they can also form heteromultimers with $K_V7.2$ and $K_V7.3$ channels expressed in the central nervous system and peripheral ganglions. The assembly with Kv7.3 amplifies the current and provokes small changes on the activation kinetics. It has also been demonstrated that $K_V7.5$ can interact with KCNE peptides (KCNE1, KCNE3), increasing the diversity of K^+ currents (Roura-Ferrer et al., 2009). Loss-of-function and gain-of-function *KCNQ5* mutations, associated with increased excitability and decreased repolarization reserve, lead to pathophysiology (Lehman et al., 2017).

1.4.3. Regulation of the M-Current in $K_V7.2$ and $K_V7.3$

The carboxyl-terminal is extensive (320-560 amino acids), varying its length in the following order: $K_V7.5 > K_V7.2 > K_V7.3 > K_V7.4 > K_V7.1$. This contrasts to the short intracellular amino end of other channels (~100 amino acids). Although no crystal structure of the whole C-terminus has been obtained yet, secondary structure predicting programs have revealed that different α-helix, coiled coil, and basic amino acids clusters are present. C-terminal becomes a place where channel trafficking and assembling is controlled in as much as other accessory molecules interact and modulate it, turning the region as a “multi-modular domain” (Sachyani et al., 2014). Sun and MacKinnonm recently resolved the structure of full KCNQ1 in complex with CaM (Sun and MacKinnon, 2017) were the he cytosolic *h*A and *h*B helices, which are connected to the S6 transmembrane helix, are sandwiched between the N- and C-lobes of CaM. *h*C and *h*D form two long helical bundles that facilitate tetramerization of the channel (Figure 1.11).

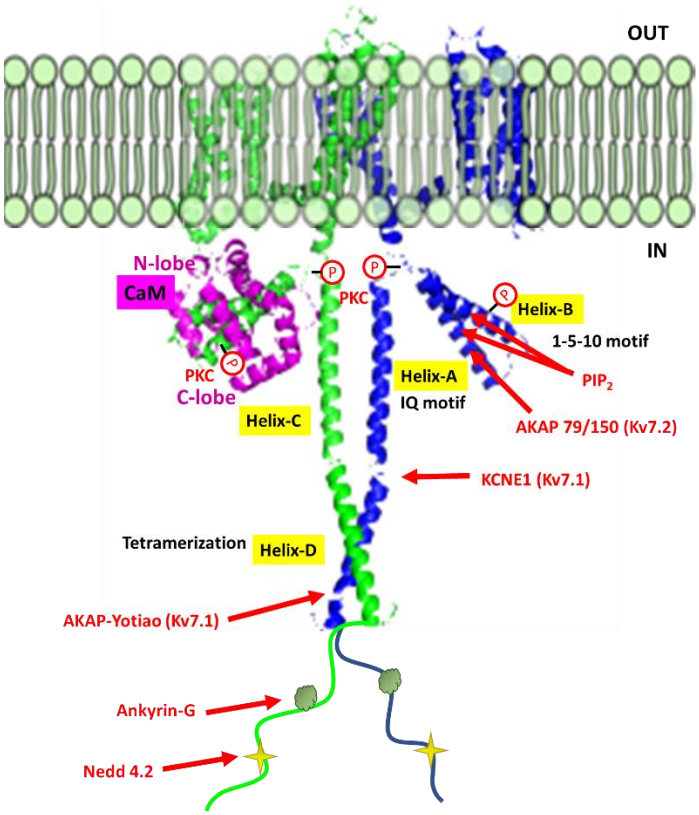

Figure 1.11. Scheme of the C-terminus of K_V7 channels. Two of the four subunits are represented (in green and blue). A and B helix have conserved interaction domain for CaM (in magenta). Also PIP_2 interaction sites may exist in these helices. AKAP-yotiao in K_V7.1, AKAP79/150 in K_V7.2, Ankyrin-G in K_V7.2/3 and Nedd 4.2 in K_V7.1-3 also interact with K_V channels. Several phosphorylation sites have been reported too. Helix C may undergo dimerization whereas helix D forms coiled coil structure as have been seen in crystal structures.

1.4.3.1. Helices A and B

Helix A is located just after the sixth transmembrane segment, which corresponds to aminoacids from V320 to Y372 in the case of K_V7.2. Following this helix; there is a linker of almost 130 amino acids separating the second helix B, which encompasses amino acids from T501 to E529. Recently was resolved the structure of this particular region for K_V7.2 channels (Bernardo-Seisdedos et al., 2018) by NMR.

In 2002 it was demonstrated that CaM is a binding protein of all the members of K_V7 family. Two different biding domains have been described: 1) In helix A, the IQ motif (**IQ**xxx**R**xxxx**R**) and 2) in helix B, two overlapping 1-5-10 motifs (**L**xxx**I**xxxx**V** and **M**xxx**V**xxxx**F**) (Table 1.2). In the resolved structure of K_V7.2 has been shown that helix *h*A is bound to the C-lobe of CaM, whereas helix *h*B is making contact with the N-lobe. This result is largely consistent with the crystallographic structures of the CaM/K_V7.1-*h*AB and CaM/K_V7.3-*h*A/K_V7.2-*h*B complexes reported by Hirsch and coworkers (2014) and with the cryo-EM structure of KCNQ1 reported by Sun and MacKinnon (2017).

	HELIX A	HELIX B
Kv7.1	A A S L **I Q** T A W **R** C Y A A E N P D S	E H **H** R A T I K V I R R M Q Y F V A K K K F Q Q A R K
Kv7.2	A A G L **I Q** S A W **R** F Y A T N L S R T	P G L K V S I R A V C **V** M R F L V S K R K F K E S L R
Kv7.3	A A E L **I Q** A A W **R** Y Y A T N P N R I	P T L K A A I R A V R I L Q F R L Y K K K F K E T L R
Kv7.4	A A N L **I Q** S A W **R** L Y S T D M S R A	P T L K A A I R S I R I L K F L V A K R K F K E T L R
Kv7.5	A A N L **I Q** C V W **R** S Y A A D E K S V	P P L K T V I R A I R I M K F H V A K R K F K E T L R
	x x x x **I Q** x x x **R** x x x x **R** x x x x	x x **L** x x x I x x x x **V** x x
		x x x **M** x x x **V** x x x x **F** x x x
	IQ MOTIF	1-5-10

Table 1.1. Sequence alignment of helices A and B of K_V7 channels. In bold there are highlighted conserved amino acids compiling CaM binding motifs.

1.4.3.2. PIP_2

Among K_V channels, KCNQ1-5 (K_V7.1-7.5) channels are regulated by several intracellular signaling molecules, including phosphatidylinositol 4,5- bisphosphate (PIP_2), which is present in the inner leaflet of the cell plasma membrane at only modest abundance.

When the membrane phosphatidylinositol is phosphorylated at positions 3, 4 and/or 5 of the inositol group, seven different phosphoinositides can be produced. All of them are classified as minority lipids and it is considered that each one is expressed in the membrane of one organelle, keeping an asymmetrical arrangement across the cell. However, they can be interconverted due to the action of kinases and phosphatases (Hille et al., 2014).

The most significant phosphoinositide present in the plasma membrane is phosphatidylinositol-4,5-biphosphate (PIP_2).

Phosphatidylinositol-4,5-bisphosphate (PIP_2) **is required to stabilize the K_V7 channel open state** by increasing the coupling between the voltage sensor domain and the pore region, thereby preventing current rundown (Gamper & Shapiro, 2007). PIP_2 interaction site in K_V7.2-4 channels has been mapped in the linker connecting helices A and B (Hernandez et al., 2008). However, another study indicated that this linker is not required for PIP_2 regulation of K_V7.2 (Aivar et al., 2012). In K_V7.1 channels, where PIP_2 is also necessary for maintaining activity, clusters of basic residues potentially forming PIP_2 interaction sites, has been identified specifically at the S2-S3 and S4-S5 intracellular linkers as well as in the C-terminus (Choveau et al., 2012; Eckey et al., 2014; Thomas et al., 2011).

Recently, has been described a competition of PIP_2 and the calcified CaM N-lobe to a previously unidentified site in K_V7.1 helix B (Tobelaim et al., 2017). They show that residues K526 and K527 in K_V7.1 helix B form a critical site where CaM competes with PIP_2 to stabilize the I_{KS} channel open state. Apparently, PIP_2 and Ca^{2+}-CaM perform the same function on I_{KS} channel gating by producing a left-shift in the voltage dependence of activation. The LQT mutant K526E revealed a severely impaired channel function with a right-shift in the voltage dependence of activation, a reduced current density and insensitivity to gating modulation by Ca^{2+}-CaM. Furthermore, these residues have been conserved in helix B of K_V7.2 and K_V7.3 subunits suggesting that PIP_2-CaM interactions occurring in helix B could be very important for modulating channel activity in a K_V7 subtype-dependent fashion (Tobelaim et al., 2017). Recently has been demonstrated that PIP2 occupies a site on KCNQ1 within the inner membrane leaflet, which triggers a large conformational change that leads to dilation of the pore's gate (Sun and MacKinnon, 2019). It is likely that this mechanism of PIP_2 activation is conserved among K_V7 channels.

1.4.3.3. Muscarinic and angiotensin II AT1 regulation

After acetylcholine activation of M1 muscarinic receptors, coupled to Gq/11, PLC activates and cleaves PIP_2 to generate diacylglycerol (DAG) and inositol-3-phosphate (IP_3). Subsequently, DAG activates PKC and IP_3 releases Ca^{2+} from intracellular stores. Those two pathways have been studied for long time in order to identify the second messenger responsible for muscarinic inhibition of M current. Finally, it was demonstrated that PIP_2 depletion itself is responsible for inhibition. Firstly, the activation of PLC hydrolyses PIP_2 inhibiting K_V7 channels and the administration of soluble PIP_2 analogues restores the function (Zhang et al., 2003; Li et al., 2005; Hernandez et al., 2008). Secondly, the PIP_2 dephosphorylation by a voltage-sensing (VSP) or by chemically- or photo-recruitable lipid-5-phosphatase, which does not generate any second messenger that could hide the response, provokes K_V7 channels inhibition (Suh et al., 2006b; Murata et al., 2007; Kruse et al., 2012). Finally, after PIP_2 depletion, the time course of PIP_2 resynthesis at the plasma membrane is proportional to K_V7 current recovery (Falkenburger et al., 2010a; Falkenburger et al., 2013).

In addition, it has been shown that muscarinic stimulation can deplete more than the 75 % of PIP_2 found in neuroblastoma cells within 30-60 s (Xu et al., 2003). Simultaneously time current the translocation of the fluorescent PIP2-binding domain into cytosol when PIP_2 is depleted, show a good correlation with muscarinic inhibition (Winks et al., 2005). Angiotensin II AT1 activation also depletes PIP_2 (Zaika et al., 2006).

K_V7 isoforms present different affinity for PIP_2. The EC_{50} values comprise from 3 µM to hundreds of micromolar, having intermediate values for $K_V7.2/3$ channel. These values explain why at resting conditions, the open probability (P_O) of $K_V7.3$, which displays a high-affinity for PIP_2, is almost one; however, membrane PIP_2 levels are too low for $K_V7.2$, which present small PIP_2 affinity, and a P_O of 0.15-0.17. Considering that at different neuronal loci M current channels are formed by different subunits (homomeric or heteromeric), these differences in PIP_2 affinity could explain the different grades of inhibition in response to different neurotransmitters (Delmas et al., 2005).

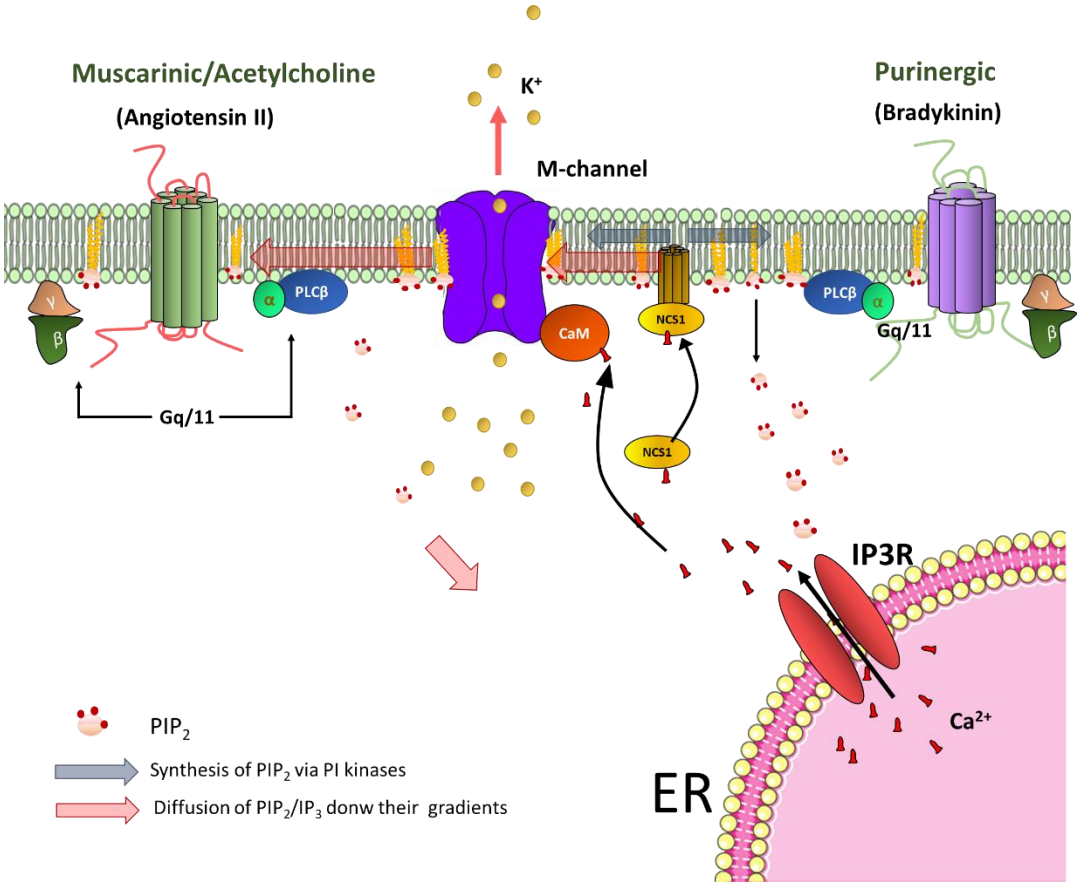

Figure 1.12. M-current inhibition in sympathetic neurons. On the left muscarinic acetylcholine and AT2 angiotensin II receptors are represented. Even if PLC activation creates IP_3 there is not activation of Ca^{2+} signalling as the receptors are situated far from the ER. Nevertheless, PIP_2 depletion causes M channels inhibition. On the right bradykinin B2 and purinergic P2Y6 receptors are represented. Both colocalize spatially with ER creating Ca^{2+} signals. The increase of Ca^{2+} binds to NCS1 and CaM. Adapted from Hernandez et al., 2008.

1.4.3.4. Calcium and Bradykinin/Purinergic inhibition

In resting conditions [Ca^{2+}] is keep up at ~0.1 µM. After PIP_2 hydrolysis, **IP_3** translocate to the cytoplasm and liberates Ca^{2+} from intracellular stores. Several experiments show that Ca^{2+} has a direct effect in K_V7 currents. In inside-out excided patches from sympathetic neurons, Ca^{2+} demonstrates an IC_{50} of ~100 nM, barely above of the resting Ca^{2+} concentration of ~70-80 nM (Selyanko et al., 1996). As M1 receptors, bradykinin receptors and purinergic P2Y (Filippov et al., 1998) are also coupled to Gq/11 proteins, allowing the activation of PLC, which generates DAG and IP_3 from the hydrolysis of PIP_2. In contrast to the muscarinic regulation, **bradykinin inhibition can be prevented by buffering intracellular Ca^{2+}** (Cruzblanca et al., 1998).

In both muscarinic and bradykinin inhibition activate the same PLC, but the mediator is different. The rapid Ca^{2+} increase after bradykinin addition can activate PIP_2 resynthesis, through the activation of neuronal Ca^{2+} sensor protein (NCS1) which ultimately activates PI4K (Santagata et al., 2001), preventing PIP_2 depletion from the membrane. Nevertheless, muscarinic inhibition is

not able to generate such a transient increment in Ca^{2+} in the submembrane region and thus it cannot restore membrane PIP_2 levels rapidly.

1.4.3.5. AKAP79/150 and PKC

The second product generated by PIP_2 hydrolysis is **DAG**. This second messenger activates the phosphorylation route of protein kinase C (PKC) in the period of muscarinic $K_V7.2$ channel inhibition (Hoshi et al., 2010). AKAP79/150 binds in the region between residues 321 and 499 of $K_V7.2$ (Cooper et al., 2000; Hoshi et al., 2003) and is used as a scaffold by PKC, from where it can phosphorylate different targets in helix B or C.

Although PKC was initially described as an M channel modulator (Higashida et al., 1986), for many years its effect has not been clear. Succeeding experiments in which PCK was activated with Phorbol esters did not observe any M-current suppression (Marrion, 1997). It has been suggested that PKC anchoring to a kinase anchoring protein AKAP79 can affect the susceptibility of PKC to modulators such as staurosporine (Hoshi et al., 2010). This could explain why some PKC modulators do not show any effect on K_V7 channels.

It has been demonstrated that the response to PKC phosphorylation of Kir2.3 channels relies on available PIP_2 levels (Keselman et al., 2007). In a similar way, it was shown that in $K_V7.2$ channels, PKC phosphorylation suppresses M current depending on the endogenous PIP_2 levels (Kosenko et al., 2012). In the same study, they affirm that PKC phosphorylation reduces the affinity for PIP_2 and that PIP_2 depletion and the reduction in affinity act synergistically.

1.4.3.6. Helices C and D

Even though helices A and B hold the CaM binding domain and motifs for other auxiliary proteins, they are not able to tetramerize by themselves. A Subunit interaction domain (SID) has been identified in the helices C and D and it is related with the exclusive assembling of different K_V7 subunits. Albeit it has been studied in detail, the molecular mechanisms that determine the K_V7 subunit assembly it is still poorly understood.

The helix C is more conserved than helix D in all K_V7 channels. This region is delimited from M537 to V561 residues in $K_V7.2$, and it is required for the assembling of homomers and heteromers. Helix D (R594-R619), it is more variable region that can explain the restricted association between all the K_V7 subunits. The crystal structure of helix D (available for $K_V7.1$ and $K_V7.4$ channels) show a **four stranded parallel coiled coil** as well as a self-assembling capacity (Howard et al., 2007; Sun & MacKinnon, 2017). In contrast to a previous SAXS study carried out in the absence of the transmembrane domain (Sachyani et al., 2014), which identified flexibility in a location proximal to HC, in the cryo-EM structure is observed flexibility distal to the HC helix (Sun & MacKinnon, 2017). Because this flexibility produced disorder in the position of the HD helix, they achieved a higher-resolution map by masking out the HD bundle during single-particle reconstruction.

1.4.3.7. Distal extreme

It has been described that $K_V7.2/3$ channels possess a binding motif for ***ankyrin-G*** (motif C3, ~ 10 amino acids) at this region. Owing the interaction of the channel with this large adaptor K_V7 is retained at the axon initial segments and Ranvier Nodes, because ankyrin-G binds to cytoskeletal actin. Thus, it is believed that *ankyrin-G* is required for the regulation of M channels'

concentration in these neuronal localizations. For K_V7.1-3, has been described that also interact with the ubiquitine ligase *Nedd4-2*. This interaction decreases ion flux in complexes KCNQ1/KCNE1, KCNQ2/KCNQ3 and KCNQ3/KCNQ5 (Miranda et al., 2013).

1.5. CHANNELOPATHIES

Due to the widespread tissue distribution and the pivotal roles played by ion channels it is not surprising that mutations in genes encoding ion channel subunits, or their interacting proteins, cause inherited ion channelopathies. These diseases can be common to very rare disorders and their severity can be mild, disabling, or life threatening. Despite this, ion channels are the primary target of only about 5% of the commercial drugs suggesting their potential in drug discovery.

The discovery of missense mutations in genes encoding for K_V channels has underscored the wide function diversity channels. Mutations may affect protein expression, trafficking, protein folding or regulation but not very often the ion channel function *per se.* As VGPCs are responsible of pumping positive charges out of the cell, a malfunction often causes cellular hyperexcitability. In Table 1.2 some examples of channelopathies are reported.

Protein	Gene	Disease
Kv1.1	KCNA1	Episodic ataxia myokymia
Kv7.1	KCNQ1	Autosomal-dominant long -QT-syndrome with deafness
		Autosomal-dominant long-QT-syndrome
Kv7.2	KCNQ2	Benign familial neonatal convulsions (BFNC), also with myokymia
Kv7.3	KCNQ3	Benign familial neonatal convulsions (BFNC)
Kv7.4	KCNQ4	Autosomal-dominant deafness
KCNH2	KCNH2	Long-QT syndrome
Kir1.1	KCNJ1	Batter syndrome
Kir2.1	KCNJ2	Long-QT syndrome with dysmorphic features
Kir6.2	KCNJ11	Persistent hyperinsulinaemic hypoglycaemia of infancy diabetes mellitus
SUR1	SUR1	Persistent hyperinsulinamic hypoglycaemia of infancy
SUR2	SUR2	Dilated cardiomyopathy
KCNE1	KCNE1	Autosomal-dominant long-QT syndrome with deafness
		Autosomal-dominant long-QT-syndrome
KCNE2	KCNE2	Long-QT syndrome
KCNE3	KCNE3	Hypokalaemic periodic paralysis

Table 1.2. Potassium channels and human diseases. Table of the protein causing the disease, the gene, which encodes the protein, and finally the caused disease.

It is important to emphasize that, among all VGPC families, the larger number of channelopathies are found in the K_V7 family. In fact, each member of the K_V7 family is related with at least one disease. Regarding KCNQ2 and KCNQ3, they were linked to the clinical phenotype of BFNC (Maljevic et al., 2008). As time went on, other different phenotypes have been associated, such as peripheral nerve hyperexcitability (PNH), myokymia or Rolandic epilepsy. Finally, KCNQ2 mutations have been also related to Ohtahara Syndrome, an early infantile epileptic encephalopathy, also called early infantile epileptic encephalopathy (EIEE).

1.5.1. Clinical and Pathological Features of Benign Familiar Neonatal Seizure (BFNS)

BFNC starts typically before the fifth day of life (Rett et al., 1964) and consists of generalized focal seizures, which have transient expression. Seizures remit spontaneously after weeks to months. It has an autosomal dominant inheritance, with around 85 % of penetrance. About 15 % of patients may have recurring seizures later in life (Maljevic et al., 2008).

Sometimes, patients with mental retardation and difficult to treat epilepsies have been described. A recent study of BFNC families reported that some individuals display more severe clinical features (Soldovieri et al., 2014). While other affected members of the family only suffered from benign neonatal seizures, these individuals display delayed psychomotor development, intellectual disability, or other neurological features. The phenotype of these affected patients is now described as KCNQ2-related encephalopathies.

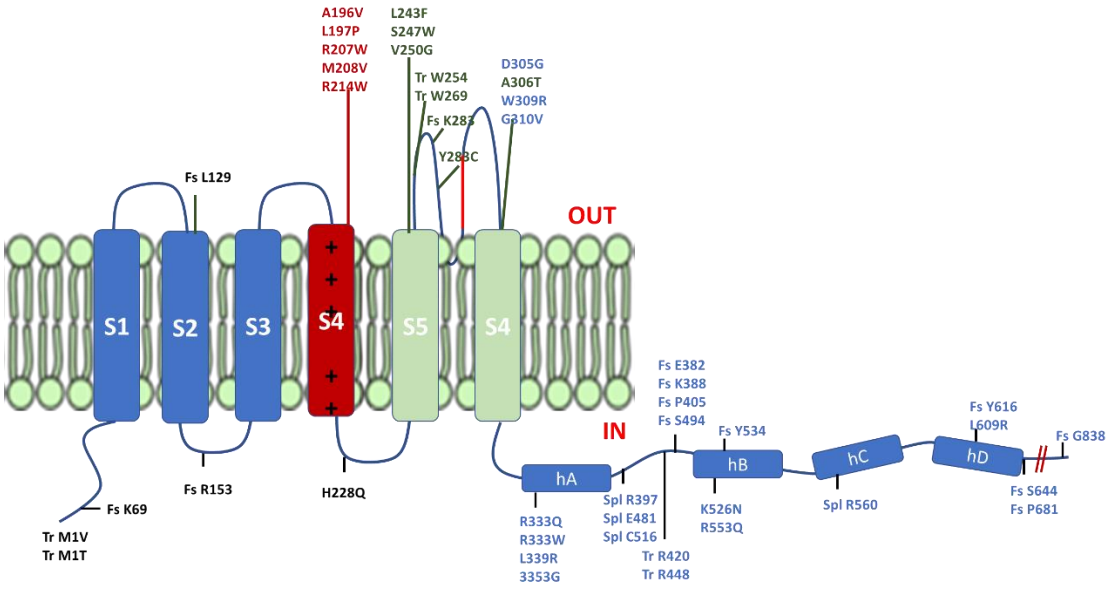

Figure 1.13. Localization of BFNC-linked mutations. *Fs* frame shift mutation; *Spl*, alternative splicing variants; *Tr*, truncation. In purple and italic $K_V7.3$ related mutations are shown.

Most of $K_V7.2$ and $K_V7.3$ mutations have been studied in heterologous systems and the most common result is a reduction in the K^+ current, although sometimes there is a complete loss of

function (Jentsch et al., 2000; Lerche et al., 1999; Maljevic et al., 2010). Coexpression of WT K_V7.2 or K_V7.3 with a mutant subunit, in a 2:1:1 ratio, resembling the patients situation with one of the four alleles mutated, revealed that a mere 20-25 % reduction in current is sufficient to cause seizures (Schroeder et al., 1998). Families with more severe phenotype also display a mild reduction of K_V7.2/3 current, suggesting other factors may be implicated in the final outcome of the disease (Steinlein et al., 2007).

While more than 130 described BFNC causing mutations in K_V7.2 are present at different parts of the protein including the cytoplasmic C-terminus, the pore region (S5-S6), voltage sensor (S4) and S1-S2 region, in K_V7.3 only six mutations have been reported to cause BFNS, five of which are located in the pore, while the last one is in the S6 (Soldovieri et al., 2014).

As has been described, C-terminal domain has different regions for binding regulatory proteins, as well as tetramerization domains. Mutations here could affect the functionality of the channel by affecting tetramerization and/or the surface expression (Etxebarria et al., 2008; Schwake et al., 2000). Alternatively, mutations in the pore domain probably alter the conductance of the channel through a haploinsufficiency mechanism. Mutations in S1-S2 and S4 have been related with changes in channel gating.

However, there is not a molecular explanation to support the disappearance of the seizures by themselves. Some scientist, based on the up-regulation found in rodent brain in the first postnatal weeks, have suggest that the expression pattern in K_V7.2/3 changes during the development of the new-born (Geiger et al., 2006; Maljevic et al., 2008; Weber at al., 2006). Consequently, the expression of a mutant subunit would result in a reduction of the current, which is not enough for the normal function of the cells at the first stage of the development. Nevertheless, in adulthood, as other K^+ channels are also up regulated, increasing the total K^+ conductance, they can compensate the mutation. The suggested excitatory action of GABA in the newborn brain could worsen this effect as far as the inhibitory GABA system is properly developed (Okada et al., 2003).

1.5.2. Clinical and Pathological Features of Early Infantile Epileptic Encephalopathy (EIEE)

In this case, seizures begin before age 3 months. Babies typically show severe developmental challenges and abnormal neurological examination, even before seizures start. Actually, motor and cognitive problems can get progressively worse as seizures increase. Ohtahara syndrome can affect both boys and girls.

Many seizure types may occur, but tonic seizures (stiffening of the arms or legs) are seen most often.

These seizures last only seconds and can occur alone or in clusters. They may affect one side of the body more prominently. They are seen both when the baby is awake and sleeping. Other seizure types that may also occur in Ohtahara syndrome include focal (start in one area of the brain), atonic, myoclonic or generalized tonic-clonic seizures. Infants with Ohtahara syndrome may also develop infantile spasms.

Most cases of Ohtahara syndrome are due to brain malformation or certain gene mutations. Metabolic causes are less likely. In some cases, no clear cause is found.

Brain malformations may be diffuse (affecting both sides of the brain) or focal (affecting only one area or side).

Some genes that have been associated with Ohtahara syndrome include KCNQ2, ARX, CDKL5, SLC25A22, STXBP1… among others.

1.5.3. KCNQ3 and Autism

Mutations in KCNQ3, the other responsible of M-current as we will see below, are related with autism spectrum disorders (Gilling et al., 2013). Recently have been described the novel electroclinical phenotype in 11 patients with 4 different heterozygous mutations in KCNQ3 that do not present with seizures in the neonatal period. Instead, within the first 2 years of life, they demonstrate global NDD and autism spectrum disorder (ASD) or autistic features. For 6 of 9 (67%) recorded between 1.5 and 6 years of age, spikes became near-continuous during sleep, raising concerns for epileptic encephalopathy (Tristan et al., 2019).

In KCNQ2 patients, in addition to the general cognitive and developmental disabilities affecting nearly all of those, many children also display repetitive movements, poor eye contact, self-harm, sensitivity to sound, or other symptoms associated with autism.

1.6. The importance of Calcium

Calcium ion (Ca^{2+}) is one of the most important intracellular messengers in cells. Either in prokaryotes or in eukaryotes, this ion is used in order to regulate different activities such as gene expression, cell growth, development, migration, survival and death. Actually, Ca^{2+} **influences nearly every aspect of cellular life**. The reason why this is so is that to adapt to changing environments, cells must signal, and signaling requires messengers whose concentration varies with time. In response to an extracellular stimulus, the concentration of cytosolic free calcium ions increases from its resting level of around **100 nM to in the region of 1 µM.** The mechanisms by which this phenomenon involve the participation of voltage-dependent, receptor-dependent, calcium-dependent and TRP channels that open their pores allowing Ca^{2+} influx in favor of the electrochemical gradient. Besides, endoplasmic reticulum (ER) and sarcoplasmic reticulum (SR) also liberate calcium when other type of second messengers such as IP3 or ryanodine stimulates them.

Filling this role, Ca^{2+}, either with phosphate ions, have come to rule signaling. Actually, cells invest much of their energy to affect changes in Ca^{2+} concentration. Unlike complex molecules, Ca^{2+} cannot be chemically altered. Thus, to exert control over Ca^{2+}, cells must chelate, compartmentalize, or extrude it. Hundreds of cellular proteins have been adapted to bind Ca^{2+} over a million-fold range of affinities (nM to mM), in some cases simply to buffer or lower Ca^{2+} levels, and in other to trigger cellular processes. The local nature of Ca^{2+} signaling is intimately tied to this large range of affinities.

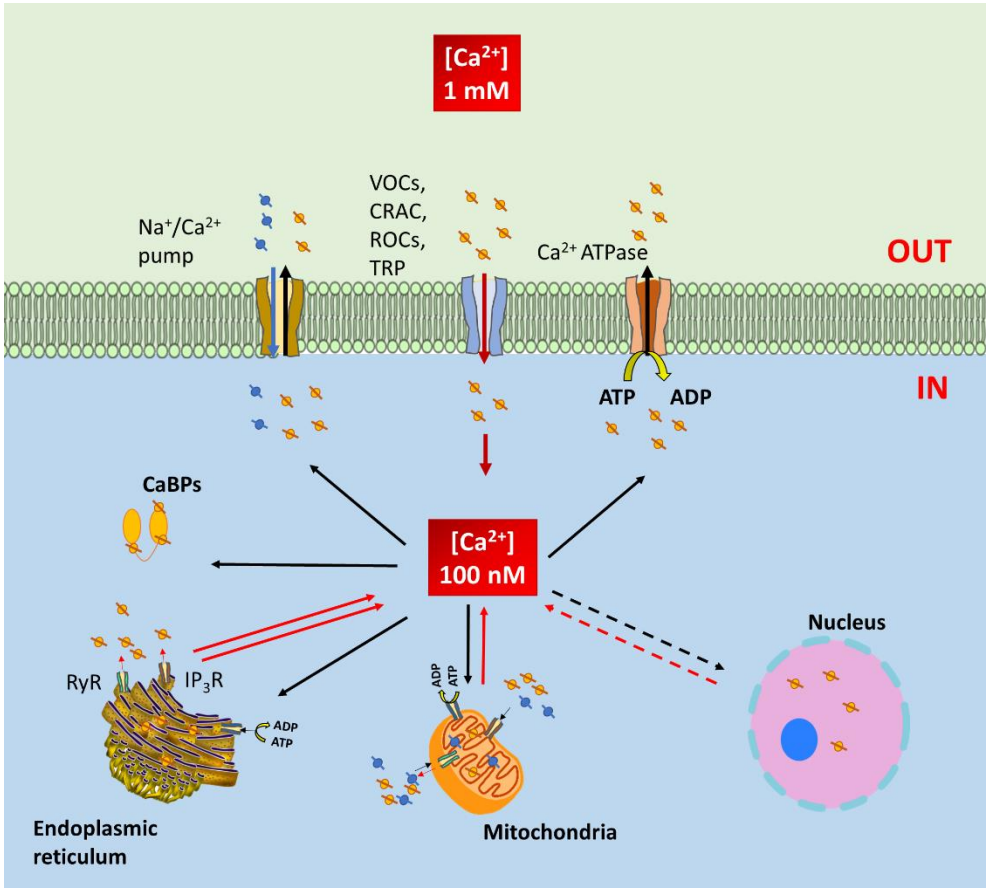

Figure 1.14. Calcium homeostasis in cells. After a stimulus, Ca^{2+} concentration rapidly rises when Ca2+ channels such as Voltage-Operated Channels (VOCs). Receptor-Operated Channels (ROCs), Calcium Release-Activated Channels (CRACs) or Transient Receptor Potential Channels (TRP) open. Moreover, more Ca^{2+} could be released to the cytoplasm through the activation of inositol 1,4,5-triphosphate receptors (IP_3P) or Ryanodine receptors (RyR). At resting conditions, intracellular Ca^{2+} levels are maintained at < µM levels thanks to Ca^{2+}-ATPases and Na^+/Ca^{2+} exchangers located in plasma membrane, endo/sarcoplasmatic reticulum and mitochondria. Nuclear pores are opened every time and can contribute to buffering Ca^{2+} levels.

1.6.1. E-F Hand Calcium-Binding Protein Family

Proteins capable to bind Ca^{2+} reversibly and specifically constitute this proteins family. The E-F hand motif is the most common calcium-binding motif found in proteins, as we will discuss in more detail in chapter 3.

This kind of calcium binding proteins (CaBPs) is found usually in the cytoplasm or inside the endoplasmic reticulum. In some cases, Ca^{2+} can directly regulate the function of a CaBPs such as PKCs, PI3K, PLCs, calpain or calcineurin, this last one is estimulated by CaM. Even so, CaBPs have frequently the role of a mediator in which they can sense Ca^{2+} concentration and communicate the signal to their targets.

Taking into the account all the calcium fluctuations that a single neuron may suffer, E-F hand protein family has evolved to detect a wide range of calcium levels, which include Ca^{2+} affinities from kD 10^{-9} to 10^{-5}. In addition, the number of E-F hands in CaBPs also vary from one protein to another (four in CaM, five in calpains and six in calbindin) even the length of the helices E and F.

1.6.2. The structure of Calmodulin and Calmodulin Binding Domains

The professional protein chelator of Ca^{2+} is the EF-hand domain (named after E and F regions of parvalbumin) (Nakayama and Kretsinger, 1994) which is present in hundreds of proteins. Helix-turn-helix motifs are common in proteins ranging from channel voltage sensor "paddles" to DNA-binding proteins. In E-F hand helix-turn-helix motifs, negatively charged oxygen atoms cradle Ca^{2+} within a ~12 amino acid loop between two orthogonal α-helices.
A single E-F hand is composed of an N-terminal helix (helix E) followed by a small coil and a C-terminal helix (helix F). The structure has a peculiar similarity to a hand in which the pointer finger represents helix F, the thumb helix E and the remaining fingers the loop for Ca^{2+} binding (more information acout E-F hands in chapter 6).
Even if all these proteins are able to bind calcium, the mechanisms by which they react may be different. The affinities of E-F hand domains for Ca^{2+} vary ~100,000-fold depending on a variety of factors ranging from critical amino acids in the Ca^{2+} binding loop to sidechain packing in the protein core. A group of CaBPs (parvalbumin, careticulin, calbindin, etc) does not suffer a conformational change after Ca^{2+} binding and they are more related to a buffering function rather than a signalling function. The second group are considered as “real calcium sensors” which decodes calcium signalling into structural changes upon Ca^{2+} binding: First, Ca^{2+} binds to CaBP opening its structural conformation exposing an interaction site for a target protein, and second, CaBP binds target protein changing its structure again. However, as we will see not all the CaBP proteins need Ca^{2+} to interact which their targets.
Besides CaM, among all these CaBPs two main groups are important for neuronal function.
- **Synaptotagmins:** These transmembrane proteins are associated with synaptic and secretory vesicles. They are composed of two C2 domains which are able to bind up to 3 Ca^{2+} ions with a relatively low affinity (Kd > 10 µM). This binding process requires coordination by the protein and the membrane lipids.
- **Neuronal Calcium Sensors (NCS):** These are related to CaM. They have four EF-hands but not all of them are functional. Unlike CaM, they have a compact conformation when they are binding Ca^{2+} and open conformation when they are not. They also have some motifs that allow membrane association which is regulated by Ca^{2+} binding.

Calmodulin (CaM) is the most studied Ca^{2+} sensor protein, probably because its evolutionary importance in Ca^{2+} signaling. It has been changed only slightly over 1.5 billion years of evolution and furthermore, it is transcribed from three separate chromosomes in humans (Abzhanov et al., 2006). Is a very soluble, thermostable, and small acidic protein (pI ~ 4) of 148 residues (first methionine is not numbered) which is ubiquitously expressed in all the cells.
The mechanism by which CaM sense Ca^{2+} is by a highly extended helix-turn-helix E-F-hand (Grabarek, 2006; Kawasaki & Kretsinger, 1994). As a prototypical E-F hand protein, calmodulin

(CaM) contains four Ca^{2+} binding EF-hand motifs: E-F (1) and E-F (2) associated to its N-domain, and E-F (3) and E-F (4) associated to its C-domain. The two domains are tethered through a flexible intervening sequence, known as the linker (Babu et al. 1988). That´s why CaM is shaped like a dumbbell (Meador et al., 1992).
The EF hands of CaM have distinct affinities for Ca^{2+}, and their binding affinities are often altered by interaction with target proteins. Binding of Ca^{2+} is associated with a large change in conformation and exposure of hydrophobic surfaces within each domain, which triggers calmodulins's Ca^{2+} sensor activity (binding to its targets). Hydrophobic residues, usually containing methionine, wrap around amphipathic regions of targets proteins.

1.6.3. The Role of Calmodulin in Calcium Signaling

CaM is involved in many cellular processes in which it senses calcium levels within the cell and relays calcium signals on its targets. Among all these roles CaM has been shown to be involved in inflammatory processes, immune response, smooth muscle contraction, cell division and proliferation, gene expression, hormones secretion, neurotransmitters secretion, short-term and long-term memory, and apoptosis.

When Ca^{2+} binds to CaM, the shape of the calmodulin domains change, triggering their ability to relieve protein autoinhibition, remodel active sites, and dimerize proteins. Hundreds of proteins contain calmodulin recruitment sites characterized by interspersed basic and bulky hydrophobic amino acid bracketed by aromatic residues.

CaM is involved in a large number of cellular processes in which it senses calcium levels within the cell and relays calcium signals on its targets, including inflammatory processes, immune response, smooth muscle contraction, cell division and proliferation, gene expression, hormones secretion, neurotransmitters secretion, short-term and long-term memory and apoptosis. Moreover, CaM directly interacts and regulates (**activating or inhibiting**) many proteins such as enzymes, cytoskeleton, transporters, receptors, and ion channels (Figure 1.15) (Table 1.3). It is also involved, directly and indirectly, in modulation of several ion channels, including Na^{+}, K^{+}, L-type Ca^{2+}, and RyR2 channels.

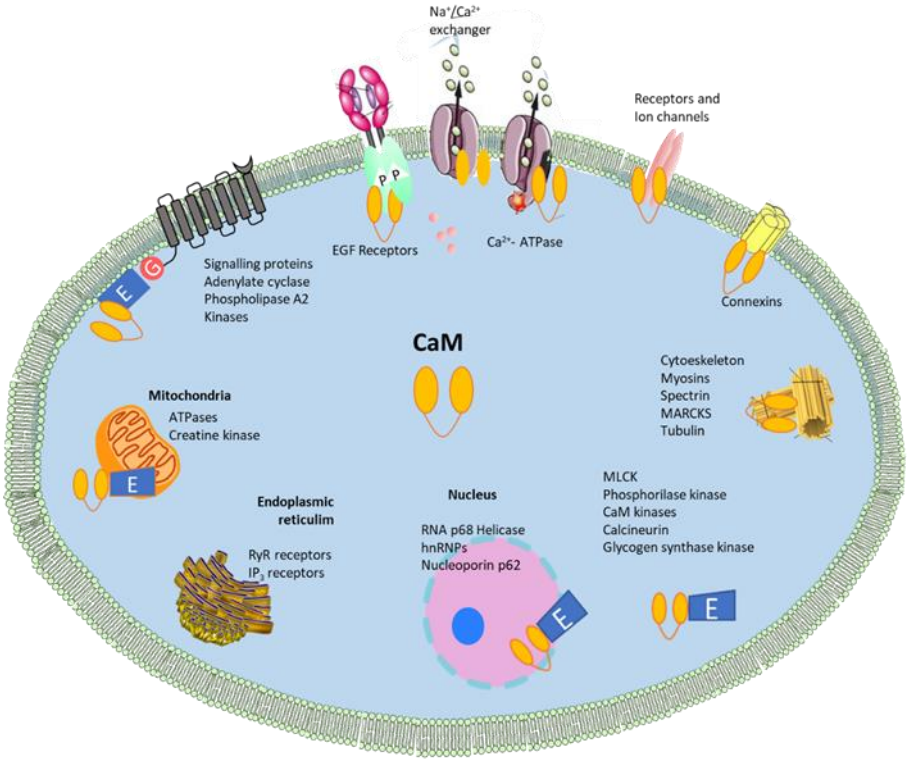

Figure 1.15. Net of proteins regulated by CaM. Different cellular processes are regulated by CaM.

Type	Proteins
Kinases	Myosin light-chain kinases (MLCKs)
	Ca^{2+}-CaM dependent protein kinases (CaMKs)
	Phosphorylase kinases
	Phosphofructokinases
	G-protein coupled receptor kinases s(GRKs)
	NAD+ kinases
	Glycogen synthase kinases
Other enzymes	Calcineurins
	Adenylate cyclases
	Glutamate descarboxylases
	Nitric oxide synthases (NOS)
	Phosphodiesterase
Transporters	Ca^{2+}-ATPases
	Na^{+}/Ca^{2+} exchangers
Reticular receptors	Inositol 1,4,5-triphosphate receptors (IP_3P)
	Ryanodine receptors (RyR)
Ion channels and receptors	Small conductance calcium-activated potassium channels (SK, IK)
	Cyclic nucleotide gated channels (CNGs)
	Transient receptor potential channels (TRPs)
	NMDA receptors
	Ca_V channels (L, P/Q, R)
	Na_V channels
	K_V channels
	Epidermal growth factor receptor (EGFR)
	Connexins (GAP junctions)
CaM reservoir proteins	Neuromodulin
	Neurogranin
	Regulator of calmodulin signalling (RCS)
Genes expression systems	RNA helicase p68
	Heterogeneous nuclear ribonucleoproteins (hnRNPs)
	Nucleoporin p62
	Caldesmon, Spectrin. Syntrophin, Dystrophin, PEP-19
Cytoeskeleton and other proteins	MAP2, Adducin, Marck, Tubulin, Myosin, Actinin, etc.

Table 1.3. Examples of proteins regulated by CaM .

1.6.3.1. K_V7:CaM Complex

In 2002, it was demonstrated that CaM is a binding protein of K_V7 channels (Yus-Nájera et al., 2002). K_V7 channels have two different CaM binding domains: one located in helix A (*h*A) and the other in helix B (*h*B) (Yus-Nájera et al., 2002), and there are separated by approximately 135 residues (Figure 1.15). Even if another helix between *h*A and *h*B in $K_V7.2$ ("TW helix") has been described that could also assist in CaM binding (Gomis-Perez et al., 2015), it has not been demonstrated yet.

CaM is also essential in the generation of functional M-current ($K_V7.2/K_V7.3$) in heterologous cells (Gamper and Shapiro, 2003) and in neurons (Shahidullah et al., 2005). It is also believed to mediate the Ca^{2+}-dependent inhibition (Selyanko and Brown, 1996) of $K_V7.2/7.3$ heterotetramers by bradykinin or UTP in sympathetic neurons (Gamper and Shapiro, 2003). Also, it has been demonstrated that **CaM influences channel gating in a K_V7 subunit-specific manner, suppressing $K_V7.2$, $K_V7.4$ and $K_V7.5$ currents but stimulating $K_V7.1$ and IKS channels ($K_V7.1$ + KCNE1) activity** (Gamper and Shapiro, 2003). CaM binding to $K_V7.1$ is also required for appropriate folding of the C-terminus and it is also necessary for correct channel trafficking to the plasma membrane (Shamgar et al., 2005).

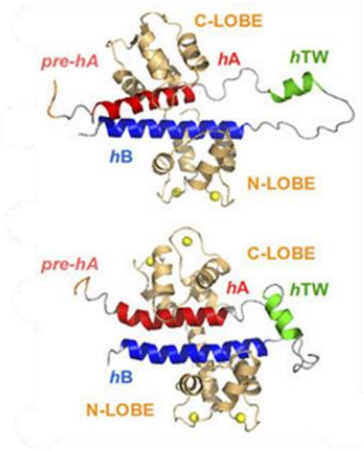

Figure 1.16. A ribbon representation of the intCaM/$K_V7.2$-*h*AB or holoCaM/$K_V7.2$*h*AB complex shows the structural elements: CaM protein (orange); the prehelix A(pre-*h*A), which connects segment 6 of the pore with the rest of the intracellular C terminus of the $K_V7.2$ channel (purple); helix *h*A (red); helix *h*TW (green); and helix *h*B (blue). Ca^{2+} ions are represented as spheres. The same color code is used for the ribbon representations of the apoCaM/$K_V7.2$-*h*AB complex. From Bernardo-Seisdedos et al., 2018.

Mutants that were deficient in CaM binding were unable to generate measurable currents (Saimi and Kung, 2002), as occurs in small conductance Ca^{2+}-activated K^+ channels (SK) (Xia et al., 1999). That is why CaM was defined as an integral subunit constitutively tethered to the C-terminal region of $K_V7.2/3$ channels. However, this model has been questioned, since $K_V7.2$ *h*B (Gomez-Posada et al., 2011) or $K_V7.4$ *h*A mutated channels (Sihn et al., 2016) that do not bind CaM, can still reach the plasma membrane and be functional. In brief, apparently, **the constitutive tethering of CaM is not an absolute requirement for M-channel function**. In 2007, a **crucial role of CaM** in $K_V7.2$ channels **trafficking** was shown. We found that mutations in *h*A and *h*B underlying benign familiar neonatal convulsions (BFNC), an autosomal dominant form of neonatal epilepsy, weakened CaM binding, leading to reduced currents as a consequence of an endoplasmic reticulum (ER) retention of $K_V7.2$ subunits. Due to this retention, a reduced number of channels reached the plasma membrane (Etxeberria et al., 2008).

Furthermore, we confirmed the critical role played by CaM in the intracellular transport of $K_V7.2$ proteins, proposing a model in which CaM needs to adopt an "active" conformation to promote the exit from the ER (Alaimo et al., 2009). Subsequently, this was also observed in hippocampal

neurons where CaM regulates the trafficking and the enrichment of $K_V7.2/K_V7.3$ channels at the axonal surface (Liu et al., 2014).

The CaM binding domain is composed by two sites, referred to as *h*A and *h*B, which adopt an alpha helical configuration (Wiener et al., 2008) and that the binding of CaM can take place on the same or on different subunits of the tetrameric channel (Sachyani et al., 2014). Additionally, CaM can bind individually *h*A or *h*B, both in the presence or absence of Ca^{2+} (Alaimo et al., 2013). We found that *h*A of $K_V7.2$ presents a notable preference for the C-lobe, while *h*B binds more favorably to the N-lobe of CaM (Alaimo et al., 2014) (Figure 1.15). In addition, this arrangement is also observed on the crystallographic complexes of CaM with $K_V7.1$ (Sachyani et al., 2014), $K_V7.4$, $K_V7.5$ (Chang et al., 2018) and a chimera between *h*A of $K_V7.3$ and *h*B of $K_V7.2$ (Strulovich et al., 2016). As described below, this arrangement is also evident in the nuclear magnetic resonance (NMR) $K_V7.2$*h*AB-CaM complex (Bernardo-Seisdedos et al., 2018) and in the cryo-EM structure of $K_V7.1$ (Sun and MacKinnon, 2017).

1.6.4. Structural plasticity of CaM

CaM is formed by two mostly globular domains that are most likely produced *via* a sequential double-gene duplication event. Each domain (N- and C-terminal; also called the N-lobe and the C-lobe), has two Ca^{2+} binding E-F hand motifs. Both lobes are connected by a very flexible linker, which confers structural plasticity. Moreover, this linker provides for each lobe almost a full autonomy to fold, to bind Ca^{2+} or to interact with target proteins. This plasticity on its structure confers to CaM the capability to interact with many proteins. It has been suggested that this structural plasticity is a result of many CaM target sites being intrinsically disordered and folding upon the binding of CaM, which itself undergoes a disorder-to-order transition (Radivojac et al., 2006; Wall et al., 1997)

Besides, the structures of both lobes are modestly different: The N-lobe has a very compact conformation while the C-lobe has a semi-open conformation where some hydrophobic residues are exposed to the solvent. This may assist the CaM binding to the target in the absence of calcium as it occurs in SK2, neurogranin, Ca_V and Na_V channels. In the presence of Ca^{2+}, apo-CaM undergoes a large structural rearrangement upon Ca^{2+} binding, changing its conformation from closed to opened (Holo-CaM). Accordingly, the hydrophobic residues that were previously hidden will be completely exposed to the solvent. In addition, the linker between lobes that was disordered before will form a big α-helix connecting E-F (2) and E-F (3) hands (Figure 1.17).

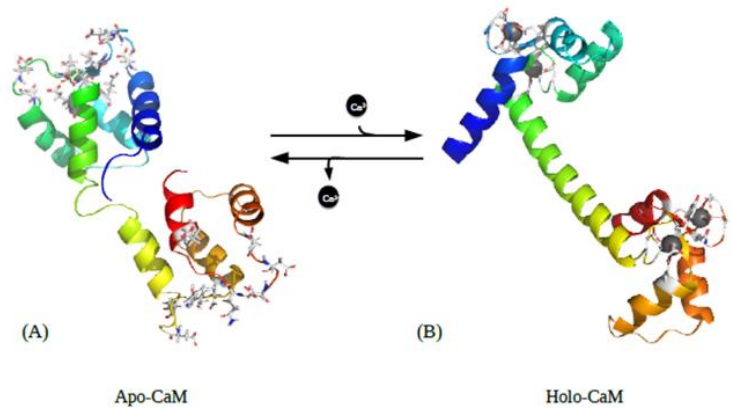

Figure 1.17. CaM structure rearrangement based on Ca^{2+}. (A) Apo-CaM (B) Holo-CaM. The N-lobe and the C-lobe of CaM are connected by a flexible linker, which is not structured in absence of Ca^{2+} and is structured in presence of it. In grey side chain atoms have been highlighted from the residues forming the E-F hands.

1.6.4.1. Calmodulin target recognition

As we mentioned before CaM acts as a calcium sensor for many target proteins translating the Ca^{2+} signal into a cellular process. Usually, its targets are formed by 16-30 amino acids containing basic and hydrophobic residues (Figure 1.18).

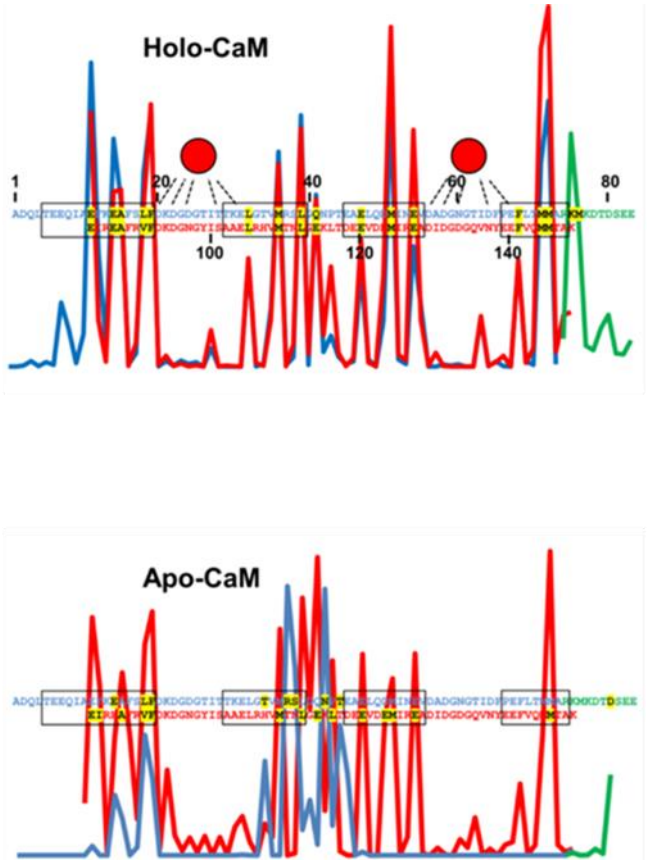

Figure 1.18. Interaction preference of each CaM residue with amino acids from target peptides. Aerial and side view of contact surface area (z-axis) 3D plots of different target residues (y-axis) in contact with each of vertebrate apo-CaM or holo-CaM residues (x-axis). The Ca^{2+} binding loops are indicated by the red spheres, and the CaM α-helices are boxed on top of the plot. Taken from Villarroel et al., 2014.

In general, they adopt an amphipathic helical structure but some of them have disordered structure in solution. However, once they interact with CaM often tends to adopt also the α-helical configuration. Additionally, CaM recognized its targets by some residues termed "hot

spots" which often results in hydrophobic pockets where Van der Waals and other kind of interactions occur (Figure 1.19).

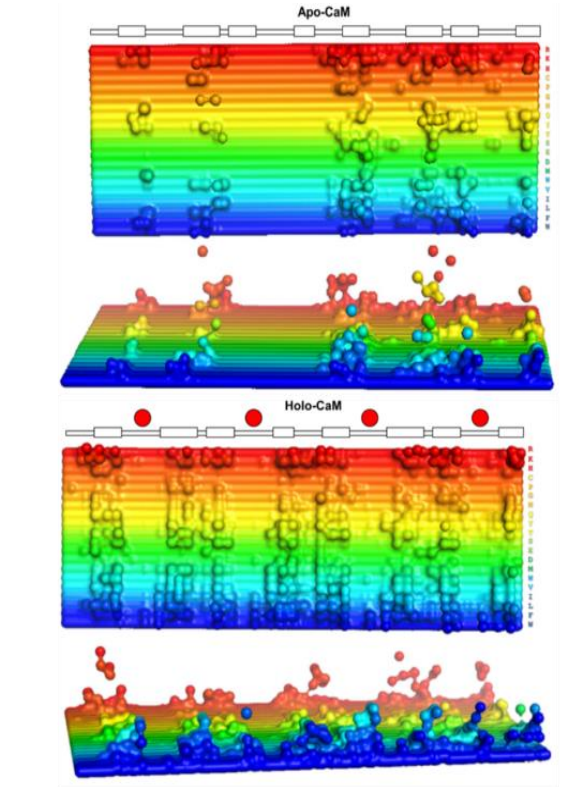

Figure 1.19. CaM´s averaged contact Surface with targets. It defines eight "hot spots" that corresponds to the eight α-helices of CaM represented as boxes. Plot of the weighted averaged CSU of the residues of holo-CaM and apo-CaM with targets. In red: C-lobe residues, blue: N-lobe residues. Ca^{2+} is represented by the red spheres, indicating the binding residues by broken lines. The main residues interacting with the target are shaded grey. The boxes indicate CaM α-helices. Two residues of the flexible inter-lobe linker (Lys75 and Met76) providing significant contributions to target binding are shown by the green line. The two inter-hand linkers also provide significant contribution through Gln41 (N-lobe) and Glu114 (C-lobe).

CaM can act as inhibitor or activator of its target protein and has been shown to regulate proteins with opposite functions (e.g. kinases and phosphatases). As there is a high variety of binding motifs for CaM it is not easy to classify them completely. However, most of them could be divided in two groups: Binding in holo-configuration and binding in apo-configuration:

- **Ca^{2+} dependent binding**

CaM's targets usually are small helices of 20 residues approximately where basic and hydrophobic amino acids are prevalent. Often, two hydrophobic residues called "anchors" are required for CaM binding and identification because these two anchoring residues interact with the hydrophobic pockets of one of the two lobes of CaM. The way in which these motifs have been classified is by numbering the amino acids between these hydrophobic residues. Some examples are illustrated in Table 1.4.

Although there are exceptions, the **most of Ca^{2+} dependent target binding consists of two conformational changes** (Figure 1.20). First, apo-CaM binds calcium ions, which provokes a conformational change from apo-CaM to holo-CaM conformation. Then, as the hydrophobic residues of CaM are exposed it is capable to recognize target's binding motives. Thereafter, CaM is exposed to the target and wraps it. Additionally, in some target type this wrapping effect may cause the target folding to a α-helix.

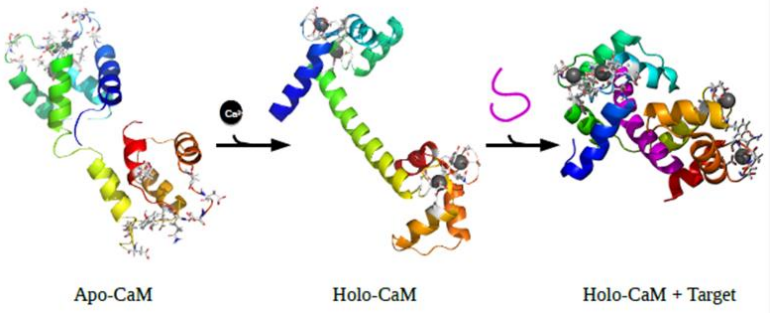

Figure 1.20. CaM complexing in presence of calcium with its target. Apo-CaM (PDB: 1CFC) binds Ca^{2+} ions which provokes a conformational change (PDB:3CLN). Hydrophobic residues are exposed, and target recognition occurs (PDB:2JZI).

- **Ca^{2+} independent binding**

Many targets that bind to CaM in the absence of Ca^{2+} have the **IQ motif.** Unlike to the previous group, IQ motif is further conserved, containing the following sequence: IQxxxBGxxxBxxX, where B means basic amino acid (Lys or Arg) and X is a hydrophobic residue (Phe, Ile, Leu, Val, Trp or Tyr) (Table 1.4). Target proteins owing the IQ motif tend to interact with the apo form of CaM, although in some cases it can also bind in holo-form.

There is less information about complexes with apo-CaM. The mechanisms by which Ca^{2+} signalling happens is less intuitive as the previous one thus set off many hypotheses of how this allowing the interaction with its target (Figure 1.21). After this interaction, the affinity of the C-lobe for Ca^{2+} often rise resulting in a protein-protein complex stabilization after Ca^{2+} binding. Furthermore, the N-lobe, is still free to bind Ca^{2+} or even another target. It is plausible to change the conformation upon Ca^{2+} binding, exposing hydrophobic residues to engage other targets.

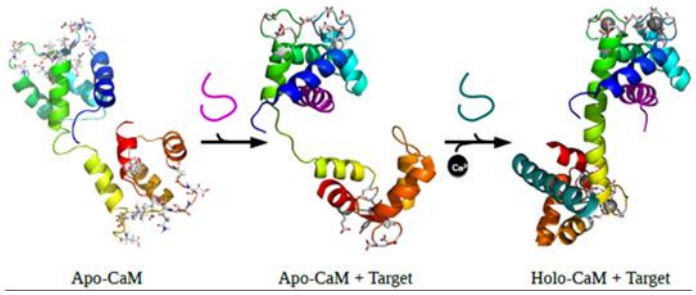

Figure 1.21. CaM complexing in absence of calcium with its target. Apo-CaM (PDB: 1CFC) binds a target protein (SK2) which provokes a minor conformational change (PDB: 1G4Y). However, after Ca^{2+} binding a drastic conformational change appends, by which second target is able to binds (PDB:3SJQ). In this last structure a dimer is formed which has not been represented.

Motif name	Motif sequence	Known targets
1-5-8-14	(FILVW)xxx(FAILVW)xx(FAILVW)xxxxx(FILVW)	Sodium calcium exchanger
1-8-14	(FILVW)xxxxxx(FAILVW)xxxxx(FILVW)	Neuronal nitric oxide synthase
1-8-14 basic	(RK)(RK)(RK)(FILVW)xxxxxx(FAILVW)xxxxx(FILVW)	Myosin light chain kinase
1-14	(FILVW)xxxxxxxxxxxx(FILVW)	Ryanodine receptor 1
1-5-10	xxx(FILVW)xxxx(FAILVW)xxxx(FILVW)	Heat shock protein 90
1-5-10 basic	(RK)(RK)(RK)(FAILVW)xxxx(FILV)xxxx(FILVW)	CaM dependent kinase II
1-10	(FILVW)xxxxxxxx(FILVW)	Inositol triphosphate 3 kinase
1-16	(FILVW)xxxxxxxxxxxxxx(FILVW)	CaM dependent kinase kinase
IQ	(FILV)Qxxx(RK)Gxxx(RK)xx(FILVWY)	L-type calcium channel
IQ-like	(FILV)Qxxx(RK)xxxxxxxx	Voltage-gated sodium channel

Table 1.4. Overall motif for CaM recognition. (Modified from Ishida & Vogel, 2006).

1.6.5. CaM and Disease

In vertebrates, humans included, there are three CaM genes in the genome (CALM1-3) which codify for identical CaM proteins. Considering that along evolution the amino acid sequence has kept invariable for vertebrates, we could assume that mutations in CaM would lead into a cellular malfunction and most likely to cell death. However, it is remarkable that in the last years up to ten CaM mutations have been related to arrhythmogenic human diseases (Urrutia et al., 2019) (Figure 1.22) termed Calmodulinopathies. Recently, has been analysed the sequence of 74 subjects, with a variant in the *CALM1* (n=36), *CALM2* (n=23), or *CALM3* (n=15) genes (Crotti et al., 2019). Interestingly, 86.5% (n=68) were symptomatic and the 10-year cumulative mortality was 27%. The two prevalent phenotypes are **long QT syndrome** (LQTS; *CALM*-LQTS, n=36, 49%) and **catecholaminergic polymorphic ventricular tachycardia** (CPVT; *CALM*-CPVT, n=21, 28%). *CALM*-LQTS patients have extremely prolonged QTc intervals (594±73 ms), high prevalence (78%) of life-threatening arrhythmias with median age at onset of 1.5 years and poor response to therapies. Other *CALM*-related phenotypes are idiopathic ventricular fibrillation (IVF, n=7), sudden unexplained death (SUD, n=4), overlapping features of CPVT/LQTS (n=3), and predominant neurological phenotype (n=1) (Crotti et al., 2019).

It is noteworthy that the 80% of the mutations are in the C-lobe, concretely in E-F (3) and E-F (4).

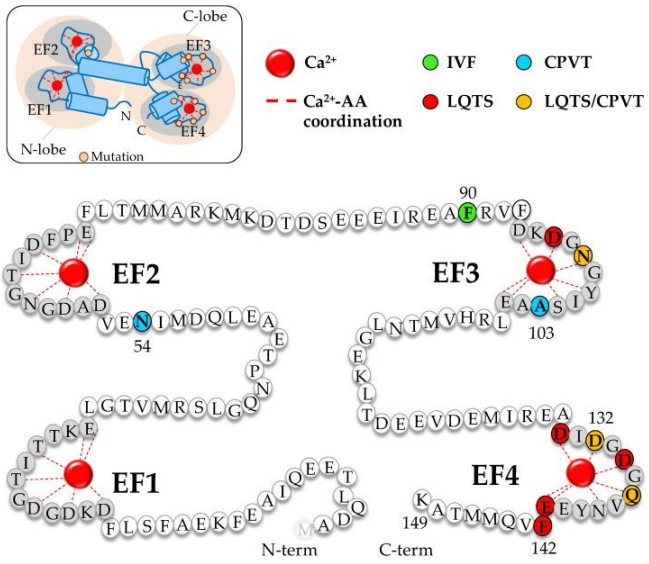

Figure 1.22. Location of the different mutations in calmodulinopathies. Top left panel: schematic representation of the structure of CaM showing Ca^{2+} coordination and mutations found in calmodulinopathies. The grey areas highlight the EF-hands shown in the main panel. Disease-associated residues are colored in green (IVF: idiopathic ventricular fibrillation), blue (CPVT: catecholaminergic polymorphic ventricular tachycardia), red (LQTS: long QT syndrome) and orange (both: LQTS/BrS) in the CaM sequence. The Ca^{2+}-binding loop of each EF-hand is emphasized with a grey background. Urrutia et al., 2019.

2. OBJECTIVES

The aims of the doctoral thesis are:

1. To get insights on the role of the linker between A and B helices of the C-terminal of K_V7 channels in calmodulin/calcium regulation.

2. To examine the influence of tetrameric formation on calmodulin binding.

3. To analyse the influence of tetrameric formation in calcium induced structural changes.

4. To investigate the contribution of each E-F hand on calcium signal transduction.

5. To address the functional significance of the interaction between the S2-S3 and EF3 loops on calcium dependent orientation of helices A and B.

3. ROLE OF THE LINKER BETWEEN HELIX A AND B OF THE C-TERMINAL OF K_V7 CHANNELS IN CALCIUM REGULATION

3.1. INTRODUCTION

3.1.1. Composition and function of the linker between *h*A and *h*B

Unfortunatelly, the linker between *h*A and *h*B of the C-terminal **is lacking in all structures resolved** (Sachyani et al., 2014; Sun & MacKinnon, 2017; Bernardo-Seisdedos et al., 2018).

3.1.1.1. TW helix

Gomis-Perez and coworkers demonstrated the existence of a site located in the inter-helical region between segments A and B of the K_V7.2 terminus that influences CaM-dependent regulation. Analysis of the relationship between the maximal D-CaM fluorescence and apparent binding affinity suggested that mutations at this site affect intramolecular rearrangements of the CaM–K_V7.2 complex. Functional examination by whole cell recording revealed that this site is **not essential for function by itself**. Rather, this site assists in maintaining the stability of an active CaM–K_V7.2 configuration and became crucial when the interactions of CaM with helix B or helix A were impaired (Gomis-Perez et al., 2015). Mutations that disrupt CaM binding within the TW site, helix B or helix A yield functional channels, whereas no function was observed when the TW site and helix A, or the TW site and helix B were mutated simultaneously (Gomis-Perez et al., 2015).

In addition, the TW site presents a **remarkable similarity with the C-lobe TRS of SK2 channels** In the SK2–CaM complex the C-lobe is found embracing the TW motif, in a disposition very similar to that seen in other complexes with an IQ motif (Villarroel et al., 2014). Interestingly, the structure of the SK2 CaM-binding domain on its own in solution (without CaM) contains a distorted helical region that includes the core sequence TWLIY, whereas the rest of the molecule lacks stable overall folding (Wissmann et al., 2002). However, given that the TW region of K_V7.2 channels is dispensable, it seems unlikely that it plays an important role in the initial steps of Kv7.2 target recognition.
The K_V7.1–CaM structure presents a typical IQ-motif–apoCaM engagement with the C-lobe, whereas the N-lobe is found anchoring helix B (Sachyani et al., 2014; Sun & MacKinnon, 2017). Has been suggested that beyond contacting both CaM lobes, the **TW site also participates on a contact network with helix B**. The structural information suggests that, after the initial CaM docking, there is a critical reorganization, during which the TW site helps pull helix B towards helix A (Gomis-Perez et al., 2015).

3.1.1.2. PIP_2 Binding Domain

Phosphatidylinositol 4,5-bisphosphate (PIP_2) in the plasma membrane **regulates the function** of many ion channels, including M-type (KCNQ, K_V7) K^+ channels; even so, the molecular mechanisms implicated are still poorly understood.
The *h*A–*h*B helix linker has been identified as a **primary site of PIP_2 action** for both KCNQ2 and KCNQ3 (Hernández et al., 2008). Particularly, a “cationic cluster” (K452, R459 and R461 in KCNQ2) in the linker between the A & B helices (A-B linker) of KCNQ2 and KCNQ3, which was

suggested to form electrostatic bonds with the phosphate head groups of PIP_2 molecules (Hernández et al., 2008). Exchange of the C terminus downstream of the beginning of the helix A-B linker inverted most of the divergence, suggesting that the prime site of PIP_2 action is on the linker, although a minor part (approximately threefold apparent affinity) remained (Hernandez et al., 2018).

Interestingly, a comparison between all of PIP_2 binding domains reveals very limited sequence homology (10–30%), but they share a key structural characteristic: a cluster of basic residues, which were proposed to be oriented to the inner membrane surface, produce an electrostatically polarized protein structure which suggest could favour interactions with phosphoinositides (Hernandez et al., 2008). The analysis reveals a conserved sequence motif for PIP_2 binding to PH domains, which is **[R/K]–X_{3-11}–[R/K]–X–[R/K]–[R/K]**, where X is any amino acid (Harlan et al., 1994). The *h*A-*h*B linker of K_V7 channels also presents a similar motif, **[K452]-[S/P]-X4-[D/N]-[R459/K]-X-[R461]-[F/A]-[R463]** (the basic residues of $K_V7.2$ are numbered), suggesting conserved structural mechanisms. In support of this conclusion, the solved structures of the phosphoinositide-binding modules share the motif of a **seven-stranded β-barrel structure**, closed off by an α-helix (Ferguson et al., 2000; Lemmon, 2003), with the "lip" of the barrel interacting with the lipid (Hernandez et al., 2008).

In the model of $K_V7.2$ structure, the PIP_2-binding domain is also a seven-stranded β-barrel, bounded by the A and B helices, with the suggested PIP_2-binding domain on the loop between strands β4 and β5. It is predicted that a core of three basic residues (R459, R461, and R463) on that loop forms hydrogen bonds mainly with the phosphates of the PIP_2 head group. The model predicts that mutations of these residues strongly alter the structural conformation of the loop and the GPMI-P_2 binding. Actually, the functional data shows profoundly altered PIP_2-apparent affinity. The data and modelling suggest a similar structural mechanism to also underlie PIP_2 interactions with $K_V7.3$, and perhaps for the other M-type channels as well (Hernandez et al., 2008).

3.2. OBJECTIVES

The objective of this chapter is to investigate the role of the linker between A and B helices of the C-terminal of K_V7 channels in CaM / Calcium regulation.

3.3. RESULTS

3.2.1. Differences in Ca^{2+} sensitivity between $K_V7.1$ and $K_V7.2$

Once we demonstrated that FRET was a technique suitable for measuring conformational changes caused by Ca^{2+}(shown in materials and methods), we compared the conformational change between $K_V7.1$ and $K_V7.2$. We observed different sensitivity for Ca^{2+} in the case of $K_V7.1$, where the FRET ratio was reduced 3 times compared to $K_V7.2$, being both in saturating concentrations of Ca^{2+} (500 µM). This means, that the conformational rearrangement upon Ca^{2+} binding might be different in each isoform. Nonetheless, the initial FRET index, which is in apo-state, was similar for both isoforms, 1.68 and 1.71 for $K_V7.1$ and $K_V7.2$ respectively (Figure 3.1), meaning that the structure of the apo-complex could be similar in both isoforms.

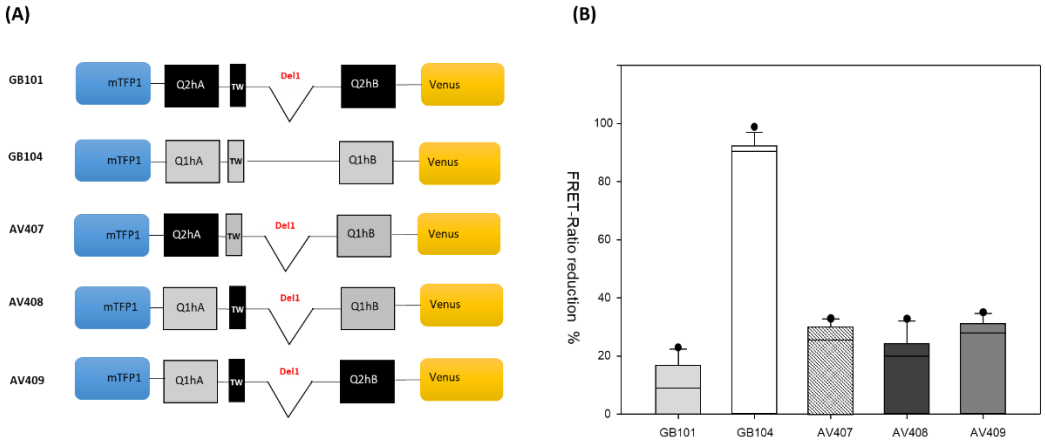

Figure 3.1. Ca^{2+} effect in $K_V7.1$, $K_V7.2$ and chimeras. A) Schematic representation of each construction. B) Percentage of FRET-ratio reduction as a function of Ca^{2+} (500 µM) in 500 nM of Q2*h*AB Del Y372-T501 (GB101), Q1*h*A*h*B (GB104), and three different chimeras AV407 mTFP1-Q2*h*A-Q1TW*hB*-pVenus, Q1*h*AdelQ2hB AV408-mTFP1-Q1*h*A-Q2TW-Q1*h*B-pVenus, AV409 mTFP1-Q1*h*A-TW-Q2*h*B-pVenus.

To try to find which region of $K_V7.1$ was responsible for conferring greater sensitivity to Ca^{2+}, different chimeras were created, where different regions of both isoforms were combined. These chimeras were co-transformed with CaM-pOKD4 and purified as previously described. Then, the Ca^{2+} effect was analyzed by FRET as mentioned above. However, none of them replicated the effect observed in $K_V7.1$, maintaining a modest reduction in FRET-Ratio as a function of Ca^{2+} as the one observed in $K_V7.2$ (Figure 3.1). The construction that maintains the TW and the B helix of Q1 (Q2*hA*-Q1*TW-hB*, AV407) is the one with the greatest reduction in the FRET-Ratio, however it is very far from that presented by $K_V7.1$, getting the half of the effect (12.9%). Followed by Q1*hA*-Q2*TW-hB* (AV409) with 12.5% and 10.2% for Q1*h*A-Q2*TW*-Q1*h*B (AV408).

The role of the linker was tested next, because there was a correlation between it being present and a large dynamic FRET change (Q1), vs Q2-Del6, with a smaller FRET change. To address the role of the linker, two constructions were tested, the $K_V7.2$ with the complete linker and the $K_V7.1$ without it (ΔY347-H478) (Figure 3.2 and 3.3). The results show that restoring the linker between helices A and B to $K_V7.2$, the effect of Ca^{2+} seen in $K_V7.1$ was replicated (a 30.5% reduction in the FRET-Ratio) (Figure 3.2), and linker removal in $K_V7.1$ reduced the changes in FRET to 9.4% of the construct with the linker.

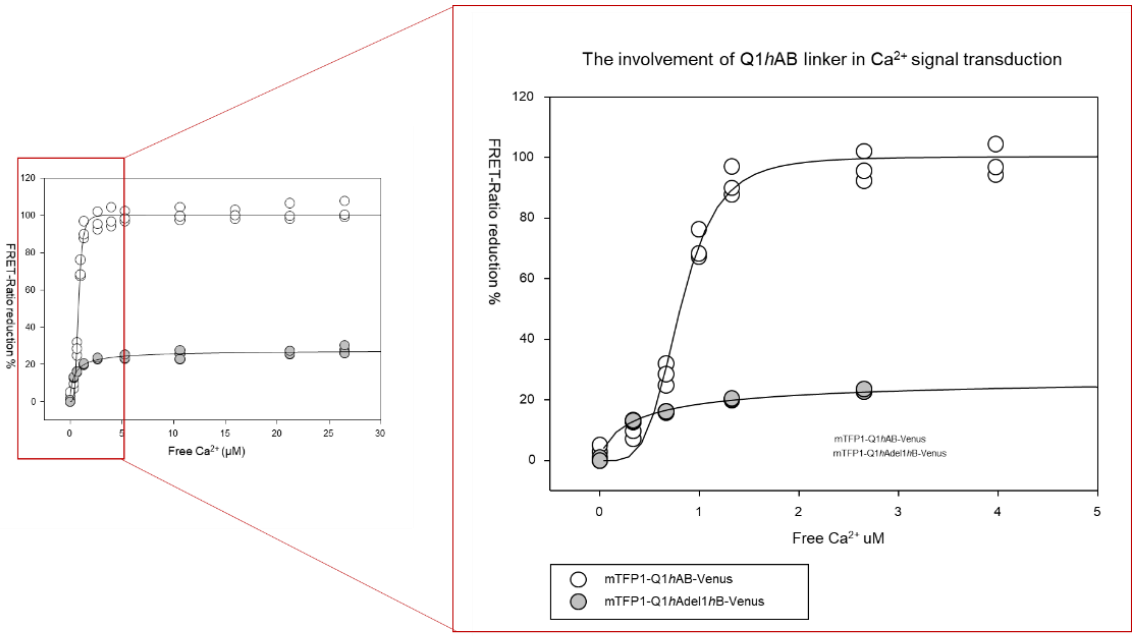

Construction	Max.expected	Ec50 (µM)	RSQR
Q1*h*AB	100.3 ± 9.8	0.81 ± 0.02	0.99
Q1*h*Adel1*h*B	27.8 ± 7.7	0.41 ± 0.04	0.98

Figure 3.2. The involvement of Q1*h*AB Linker in Ca^{2+} signal transduction. Graphic on the left shows the percentage of FRET-Index reduction vs. Ca^{2+} concentration. Titration until 25 µM free Ca^{2+} of 500 nM mTFP1-Q1*h*AB-Venus:CaM is represented in white spheres and in gray for 500 nM mTFP1-Q1*h*Adel1*h*B-Venus. On the right amplification of the same graphic in the range between 1-5 µM. The lines are the result of fitting the Hill-equation to the data. Below the parameters of these fittings are shown. Each plot represents the average of at least 3 independent experiments.

In absolute values, the FRET ratio in apo-state is similar in both, the presence and in absence of the *h*AB linker (1.70), implying that presumably the structure adopted by the complex is very similar. However, the complex (500 nM) was saturated with calcium (500 µM), the FRET ratio is much lower in the presence of the linker (1.55 for *Del1* and 1.19 for construction with the complete linker) (Figure 3.3).

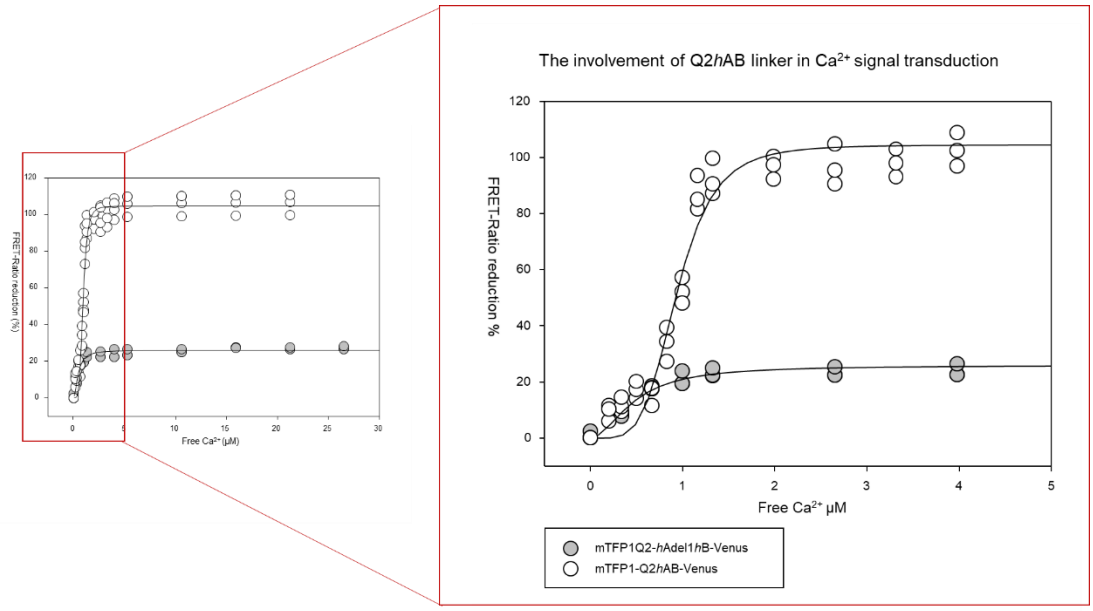

Construction	Max.expected	Ec50 (µM)	RSQR
Q2*h*AB	104.5 ± 5.9	0.94 ± 0.02	0.97
Q2*h*Adel1*h*B	25.9 ± 4.2	0.47 ± 0.03	0.96

Figure 3.3. The involvement of Q2*h*AB Linker in Ca^{2+} signal transduction. Graphic on the left shows the % of FRET-Index reduction vs. Ca^{2+} concentration. Titration until 25 µM free Ca^{2+} of 500 nM mTFP1-Q2*h*AB-Venus:CaM is represented in white spheres and in gray for 500 nM mTFP1-Q2*h*Adel1*h*B-Venus. On the right amplification of the same graphic in the range between 1-5 µM. The lines are the result of fitting the Hill-equation to the data. Below the parameters of these fittings are shown. Each plot represents the average of at least 3 independent experiments.

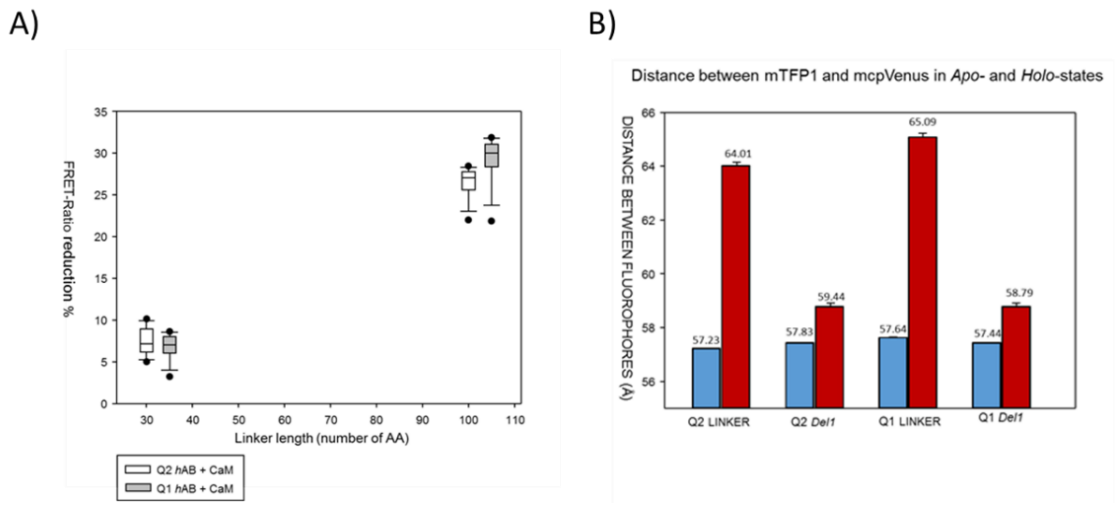

Figure 3.4. The role of the linker in Ca^{2+} driven conformational change. (A) The graphic shows FRET-index reduction upon Ca^{2+} binding vs. length of that linker (in number of aa). **(B)** Distance between fluorophores of different construction in absence (blue column) and in presence of Ca^{2+} (red column). Above of each columns the statistical average is shown. Each plot represents the average of at least 6 independent experiments.

The Ca^{2+} sensitivity increased in the presence of linker with a Kd ~0.5 nm (~0.9 nM), in both $K_V7.1$ and $K_V7.2$ (Figure 3.4).

One of the reasons that could explain this difference in calcium driven conformational change is that the absence of the linker restricts the relative movement of helices A and B. To test this idea, we attempted to increase the flexibility between the two helices with three different approaches: a.- replacing the linker by a poly-Q sequence, b.- introducing flexible GSG linkers, c.- eliminating the physical union between helices A and B. Approaches (a) and (c) did not yield meaningful data, because the constructs were instable and aggregated (Supplemental 2). The GGSSG linker showed a minimal reduction in FRET after binding to Ca^{2+}, comparable to that observed with *Del*1. Therefore, we conclude that the lack of flexibility is not the reason for the differences observed in the conformational change with and without linker.

3.1.2. Linker Deletions

Since the linker between helices A and B of the C-terminal domain of K_V7 channels is very long and poorly studied, the next step was to try to identify the exact region involved in signaling by Ca^{2+}. For this, different deletions were made in the linker and the conformational change as a function of Ca^{2+} was analyzed by FRET as described above

3.1.2.1. Deletions in the N-terminal of the *h*AB Linker

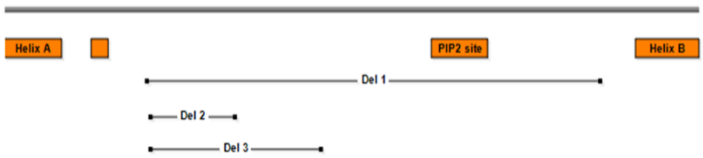

Figure 3.5. Schematic representation of Del1, Del2 and Del3 deletion in *h*AB linker.

The first deletions were made at the N-terminal end of the linker between the helices A and B, behind the TW helix. In this case, Ca^{2+} titrations were also made, as described above, to analyze the affinity of the complex for Ca^{2+} (Figure 3.6). The *Del2* (Δ I375-P400) has a deletion of 25 aa while the *Del3* (ΔI375-A424) has a deletion of 50 aa. In both cases the calcium effect replicates that seen in the complex with the complete linker (109% ± 7.3 for Del2 and 97% ± 9.2 for Del3). There were not notable differences in calcium affinity in either of the two deletions. 980 nM for construction with the complete linker, 494 nM for Del2 and 341 for Del3. We assume again that these differences may occur by mistake in pipetting, buffer composition, temperature, or pH, since the experiments were performed in different days.

We observed that the sequence of the linker deleted, which is right behind the TW helix, is poorly conserved among members of K_V7 family (Figure 3.7). In addition, some isoforms of K_V7, such as

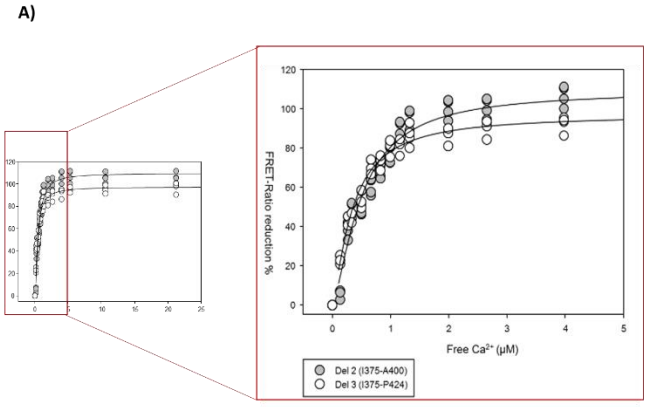

Construction	Max.expected	Ec50 (µM)	RSQR
Del2 (I375ΔA400)	109.4 ± 7.3	0.5 ± 0.02	0.97
Del3 (I375ΔP424)	97.18 ± 9.2	0.34 ± 0.03	0.98

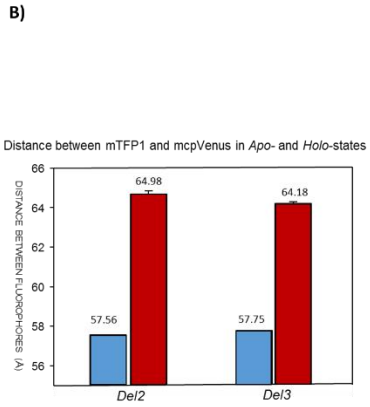

Figure 3.6. The involvement of Q2*h*AB Linker in Ca^{2+} signal transduction. (A) Graphic on the left shows the % of FRET-Index reduction vs. Ca^{2+} concentration. Titration until 25 µM free Ca^{2+} of 500 nM mTFP1-Q2*h*ADel2*h*B-Venus:CaM is represented in gray spheres and in white for 500 nM mTFP1-Q2*h*Adel3*h*B-Venus. On the right amplification of the same graphic in the range between 1-5 µM. The lines are the result of fitting the Hill-equation to the data. Below the parameters of these fittings are shown. (B) Distance between fluorophores of different construction in absence (blue column) and in presence of Ca^{2+} (red column). Above of each columns the statistical average is shown. Each plot represents the average of at least 6 independent experiments.

K_V7.1, K_V7.3 and K_V7.5, naturally lack parts of this region of the linker, which leads us to suggest that it does not have a relevant function in the regulation of the channel.

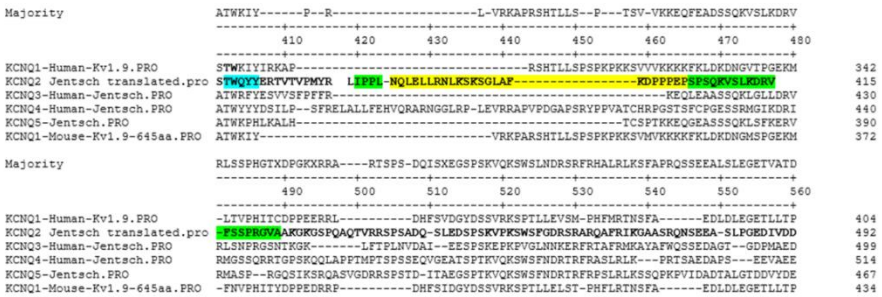

Figure 3.7. Sequence alignment of the linker between helices A and B of K_V7 isoforms. The fraction deleted in Del2 (I375-P400) is highlighted in yellow, and the fraction deleted in Del3 (I375-A424) in green, apart from the fraction of Del2 that is also deleted.

3.1.2.2. Deletions from the C-terminal: Del 4, Del 5 and Del 6

Analyzing the sequence, the most reasonable candidate is the PIP_2 binding site. This makes sense since *Del2* and *Del3* linkers conserve this region, while *Del1* eliminates it. This would explain the difference in the distance between fluorophores after calcium binding, and the impossibility of replicating with the artificial linkers the effect observed with the natural linker.

The data indicated that the reason did not reside in the length of the linker, but in the removal of a domain involved in the Ca^{2+} signaling, which is present in the linker and eliminated in *Del1*. Observing the most conserved regions in the *h*AB linker sequence, the PIP_2 binding domain was proposed as a potential candidate taking part in the calcium signaling by CaM, although without ruling out the possible collaboration of other regions.

To further investigate this domain as a responsible of a larger separation between helices A and B in the holo-complex, three new linkers were designed with deletions at the C-terminal end, where the PIP_2 binding site is located (Figure 3.8). The *Del3* was used as parental, which we had previously shown that it is able to replicate the effect observed with the complete linker.

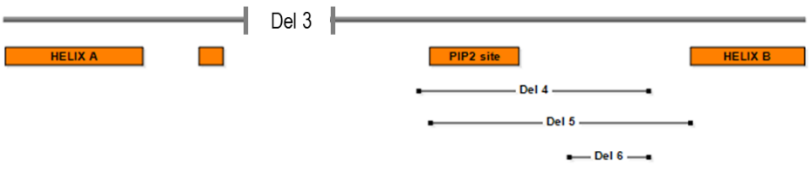

Figure 3.8. Schematic representation of Del4, Del5 and Del6 deletion using *h*ADel3*h*B construction as parental.

In the *Del4* (ΔI375-P424, ΔG453-E4506) and *Del5* (ΔI375-P424, ΔE451-E498) the proposed PIP_2 binding site is eliminated. In *Del6* (ΔI375-P424, ΔE481-E498,) (Figure 3.8) only 18 amino acids located between the PIP_2 binding site and helix B are eliminated.

Surprisingly, none of the new constructions was able to replicate the effect of their parental, *Del3*, obtaining in all cases a reduction in the FRET Ratio similar to that observed in *Del1* (11.6%, 14.15% and 12.52% for *Del4*, *Del5* and *Del6* respectively) (Figure 3.9). Again, the distance between the fluorophores in apo-state is as the one observed with the complete linker, presumably, because the structure adopts the same conformation. However, once CaM binds Ca^{2+}, the estimated separation between the fluorophores is around 2 Å in all deletions; 3 times lower than the observed with the Linker, *Del2* and *Del3*. If we compare with *Del1*, the distance is something higher, 1 Å approximately, being modestly larger for *Del5*.

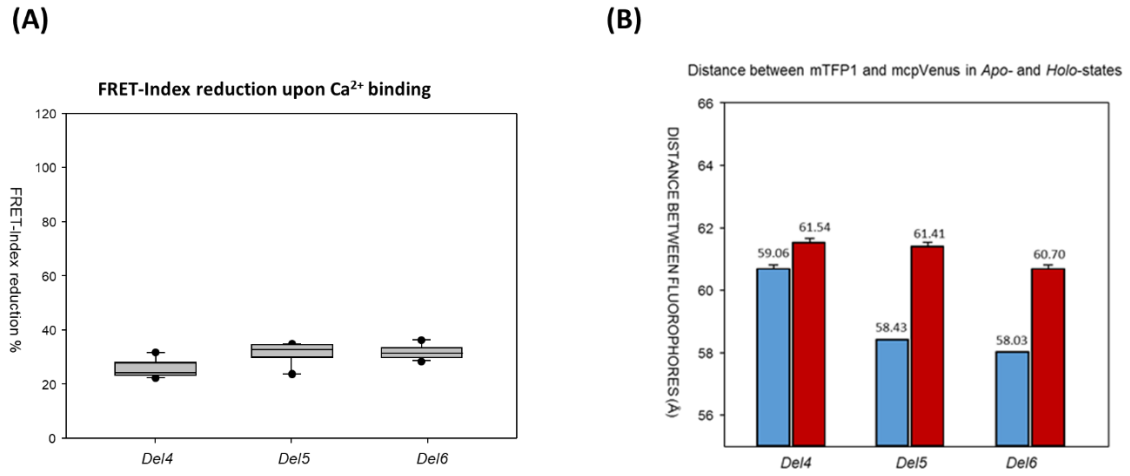

Figure 3.9. Increasing flexibility of the construction (A) The graphic shows FRET-index reduction upon Ca^{2+} binding in different constructions: light gray box for Del4, white for Del5 and dark gray for Del6 construction. **(B)** Distance between fluorophores of different construction in absence (blue column) and in presence of Ca^{2+} (red column). Above of each columns the statistical average is shown. Each plot represents the average of at least 6 independent experiments.

3.4. DISCUSSION

The calcium and CaM regulation of the $K_V7.2$ potassium channel is a complex process in which a multitude of factors are involved and on which there are many unknowns. It is known that the union of Ca^{2+} to CaM associated with the $K_V7.2$ channel entails a conformational change of its N- and C-lobes, which in turn causes a reorientation of the helices A and B of $K_V7.2$. It has been suggested that this change is transmitted to the transmembrane domain, closing the channel, and inhibiting the M current (Bernardo-Seisdedos et al. 2018). This process can be followed by changes in fluorescence resonance energy transfer (FRET), which allow us to estimate the distance between donor and acceptor fluorophores. Thus, by placing a donor fluorophore prior to helix A and an acceptor fluorophore subsequent to helix B, it can be seen

how, after binding of Ca^{2+} there is reorientation of helices A and B, which increases the distance between them. We observed that upon Ca^{2+} binding the distance between fluorophores is greater in the case of the construction with the complete linker. Consequently, the transmission of energy from the donor fluorophore to the acceptor is reduced. In other words, **helices A and B seem to be more separated** in the construction with the complete linker. Thus, we can assume that **the structural conformational change is larger than that described** in Bernardo-Seisdedos article (Bernardo-Seisdedos et al., 2018). There, a structural rearrangement of the CaMBD in KCNQ2 channels with *Del*1 was described, where the N-lobe/helix B complex remains almost unchanged, whereas the initial part of helix A bents by about 18˚ concomitant to a torsion of the C-lobe around the helix A axis.

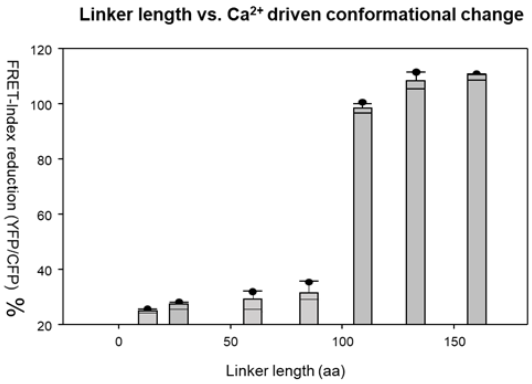

Figure 3.10. FRET change as a function of the number of aminoacids. Graphic shows the estimated distance between fluorophores vs. the numer of aa composing the linker between helices A and B.

After verifying that linker length and composition exert a surprisingly influence on the conformational change as a function of Ca^{2+} on $K_V7.2h$AB, we analyse different deletions yo clarify which region of the linker participates in calcium signaling.

In this regulation, the 157 amino acid linker between helices A and B becomes vital, whose role in conformational change is unknown. In preliminary tests with the natural linker (157 aa) and with deletions of 127 amino acids (*Del1*), it was seen how as the length of the connector decreased, reorientation was increasingly affected, for both $K_V7.2h$AB:CaM and Kv7.1*h*AB:CaM. However, this effect was not noticeable for deletion of 25 amino acid (*Del2*), nor for 50 (*Del3*) in $K_V7.2h$AB:CaM (Figure 3.10). Thus, we though that it would be possible that a specific region of the linker intervened in the Ca^{2+} signaling. According with that, the **PIP_2 binding site was proposed as a potential factor involved in the process**. In line with these results, in this work a series of deletions were designed from *Del3*, in which the reorientation mediated by CaM and Ca^{2+} was still produced. We deleted the proposed site of attachment to PIP_2 (K449-K469) (Hernández et al., 2008) in Del4 (ΔG453-E4506) and *Del5* (ΔE451-E498), and other sections located after this site in Del6 (ΔE481-E498) which is close to helix B. If this were involved in the process, at least in a unique way, the interruption of the process in *Del4* and *Del5* would be expected and a fully conformational change in the case of *Del6*. However, this was not the case. We observed that the **reorientation of the A and B helices mediated by Ca^{2+} and CaM decreases also in *Del*6, where 18 amino acids close to helix B and outside the PIP_2 binding site are deleted**, contradicting the initial hypothesis. Accordingly, the smaller deletion tested that reduced the structural changes was *Del6,* indicating that the molecular

determinant to allow **the full manifestation of the relative helix A/B movement upon calcification, is located between amino acids E481-E498**, which is poorly conserved among K_V7 family members. The highest homology is with $K_V7.4$, where it is 39 % (Figure 3.11), which also presents homology with other isoforms, especially with $K_V7.3$. $K_V7.1$ is the one with less homology compared to the other isoforms.

(A)

KCNQ1	E	D	L	D	L	E	G	E	T	L	L	T	P	I	T	H	-	-	-
KCNQ2	E	A	-	S	L	P	G	E	D	I	V	D	D	K	S	C	P	C	E
KCNQ3	D	A	G	T	-	-	G	D	P	M	A	E	D	R	G	Y	G	N	D
KCNQ4	D	A	P	S	-	-	-	E	E	V	A	E	E	K	S	Y	Q	C	E
KCNQ5	A	D	T	A	L	G	T	D	D	V	Y	D	E	K	G	C	Q	C	D

(B)

ISOFORM	HOMOLOGY WITH Q2	HOMO. OTHER ISOFORMS
KCNQ1	(4/18) 22%	(1/18) 6%
KCNQ3	(3/18) 17%	(7/18) 39%
KCNQ4	(7/18) 39%	(7/18) 39%
KCNQ5	(6/18) 33%	(7/18) 39%

Figure 3.11. Sequence alignment of the linker between helices A and B of K_V7 isoforms. (A) Del6 sequence alignment, in red coincidences with KCNQ2 are shown, in green coincidence with other isoforms. **(B)** Table summarizing the homology of the refion between KCNQ isoforms.

Although many pathological mutations map in critical regions of $K_V7.2$ channels, no epilepsy causing mutation has been described in this region.

In future studies, a more thorough analysis of this region should be carried out, combined with electrophysiological analysis. **Other techniques such as nuclear magnetic resonance (NMR) could be used, in order to analyze the possible molecular interactions of this region** with potential ligands, although the large construction size represents a considerable challenge for the application of this technique. The linker could be divided into peptides of 20 aa, where the first 10 aa overlap with the last 10 aa of the previous peptide. Through a simple HSQC experiment with the *h*AB:CaM labeled complex and adding each peptide separately, the linker region that participates in signaling could be identified by chemical shifts, reducing it to up to 10 aa.

3.5. MATERIALS AND METHODS

3.5.1. Molecular Biology

3.5.1.1 PCR Technique

The polymerase chain reaction (PCR) is a biochemical technique to amplify DNA in several orders of magnitude, generating thousands to millions of copies of a particular DNA sequence. Moreover, different mutations can be introduced in the target DNA fragment by this technique. The amplification process is based on a set of cycles of heating and cooling of the reaction to ensure DNA melting and enzymatic replication of the DNA (T100tm Thermal Cycler, Bio-Rad). Different kinds of PCR reactions were assayed:

1. SIMPLE PCR: to amplify sequences in cassettes not longer than 700 bp which allows the addition of new restriction on the edges. The polymerase used was the Expand High Fidelity

polymerase (Ref.: 03300242001, Roche) because it introduces deoxiadenosines in the 3 termini, which facilitates the insertion in the EasyT cloning vector.
2. QUICK CHANGE: useful to mutate residues located in the inner part of a fragment that is flanked by restriction sites. First, two simple PCR reactions using the PfTurbo polymerase (Ref.: 600250, Agilent) are done. Each PCR corresponds to half of the fragment where the mutations are wanted to be introduced. The primers from each PCR are specifically designed to hybridize between them at least in one extreme. Next step is to make a third PCR with the Expand polymerase to amplify the whole fragment with the deoxiadenosines at the extremes.
Primers were designed and synthesized by IDT (Integrated DNA Technologies).

3.5.1.2. Del 1, Del 2 and Del 3

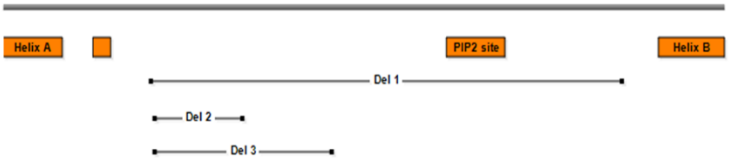

Figure 3.12. Schematic representation of Del1 (L373-T501), Del2 (I375-P400) and Del3 (I375-A424) of K_V7.2*h*AB.

Del1 (L373-T501) was produced by inserting restriction sites for BamHI and XhoI at position 373 and 501 respectively.
Del2 (I375-P400) and Del3 (I375-A424) were produced by PCR using the KOD plus kit (Toyobo). The reaction mixture, with a final volume of 25 µl, is shown in Table 2.

DNA (100 ng/ µL)	KOD plus Buffer (10x)	dNTPs (2 mM)	$MgSO_4$ (25 mM)	Primer (10 µM)	KOD plus (1U/µL)	H_2O
1 µL	2.5 µL	2.5 µL	1 µL	0.75 µL	0.75 µL	16.5 µL

Table 3.2. KOD+ PCR reaction mixture protocol.

For KOD+ enzyme (Toyobo) the design of the primer is critical for obtaining good results. Mutation sites should be designed only at the 5' terminal end of primers. Specific sites should be designed at the 3' region of the primers.
We use three primers for Del 2 and Del3, the inverse being common for both constructs (A846: 5´-GTTACCGTTCCGATGTACCGTCTG-3´), and the backwards different: for Del 2 A847: 5´-CCGCCGGAACCGTCTCCGTCTCAG-3´; and for Del3 A848: 5´-GCTAAAGGTAAAGGTTCTCCGCAT-3´.
The parental DNA in both cases was the construction GB105 (mTFP1-*h*AB-mcpVenus, the construction with the complete linker).
Once the samples were prepared for the PCR, they were introduced into a T100 thermocycler (Bio-Rad) following the protocol shown in Table 3.

Pre-denatural	Denaturalization	Hybridisation	Extension	Cycles
94 °C, 2 min	94 °C, 15 sec	55 °C, 30 sec	68 °C, 6 min	25

Table 3.3. KOD+ PCR protocol for DNA amplification.

Once the PCR products were obtained, the remaining parental DNA was digested by adding 1 µl of the DpnI restriction endonuclease (included in the kit). Finally, since the PCR products are linear molecules, the DNA was recirculated using T4 ligase (Table 4) and its T4 buffer (335 mM Tris-HCl, 33 mM MgCl2, 5 mM DTT and 84 mM (NH4) 2SO4, pH 8.8).

3.5.1.3. Del 4-9

3.5.1.3.1. Mutagenesis for M1 and M2

The last six deletions (Del4, Del5 and Del6) were produced from deletions in Del3. The method chosen to carry out the deletions consisted of introducing restriction sites for the EcoRI and SmaI enzymes at different position of the connector, to carry out the digestions between the artificially introduced points and the already present in the channel sequence. We introduced punctual mutations in three specific regions of the linker (Figure 3.3). From them, two digestions were carried out, one with the EcoRI enzyme and one with the SmaI enzyme, to get final constructions present in Figure 3.4.

Figure 3.13. Schematic representation of the construction used as parental for Del4, Del5 and Del6. Del3 construction was used as parental where were inserted new restriction sites are represented as orange box: Eco RI and SmaI before and after proposed site for PIP_2 binding.

These new restrictions sites were introduced with the PCR kit Quick 'QuickChange II Site-Directed Mutagenesis' (Agilent Technologies) and the T100 thermal cycler (Bio Rad). To get these mutant constructs we used a couple of primers for each. In this case, each pair of primers binds to the same sequence but in opposite strands of the plasmid, and also contains the cutting sequence for EcoRI (5 'G / AATTC 3') and SmaI (5 'CCC / GGG 3'), which produce cohesive and blunt ends, respectively. For M1 and M2 constructions, were used the following primers (for simplicity reasons only the primers that bind to the template strand), sequence, 5'-GACTCTCCGTCTGAATTCCCGGGATCTTGGTCTTTC-3' for M1 and 5'-CGTCAGAACTCTGAATTCCCGGGTCTGCCGGGTGAA-3 'for M2. Mix of reaction used, with a final volume of 20 µL, is shown in the Table.3.4

PFU Buffer 10x	DNA (100 ng/µL)	Primers (10 µM)	dNTPs (2.5 mM)	PFU Polimerase (2.5 U/µL)	H_2O
2 µL	0.5 µL	1 µL	2 µL	0.4 µL	13.1 µL

Table 3.4. Reaction mixture protocol for PFU DNA-polymerse enzyme.

As we used *Del3* as parental, all constructions contain the mTFP1 fluorophore (mTFP) at the N-terminal end, the helix A (*h*A), linker (with different length), helix B (*h*B), and mcpVenus173 (Venus) at the C-terminal end.
After the fulfilment of the PCR, the parental DNA (methylated and hemimethylated) was digested with 1 µL of the restriction enzyme DpnI (37 ºC/12 h), whose target sequence is 5 'GmA / TC 3', where adenine is methylated, to remove parental DNA and avoid false positive colonies. Finally, the PCR product was transformed in competent BSJ bacteria (see protocol below).

3.5.1.4. Bacterial transformation

Previously ligated vector and fragment are transformed in competent *E. coli* BSJ strain. This allows the insertion of a foreign DNA into the bacteria, so the cell is used as a host to amplify the plasmid in order to obtain large quantity of plasmid copies. Three main mechanisms are used to transform bacteria: electroporation, chemical transformation, and heat shock. For cloning and DNA expression we normally use heat shock transformation. When heating bacteria for 45 seconds in the presence of the ligated plasmid and subsequently cooling them in ice, small pores are created in the bacterial wall, making DNA uptake easier. Afterwards, to help bacterial cells to recover from the shock, they are briefly incubated with non-selective growth media for around 40 min, spin down, get rid of the excess of supernatant, resuspended and finally, the cells are seeded into LB agar plates with the specific antibiotic (Protocol P.4).

Protocol P.1: Heat shock transformation
- Thaw one vial (or more) of cells.
- In a Eppendorf of 1.5 ml add 50 µl of competent cells
- Add 5 µl of Ligation or 1 µl of a miniprep (1 µg/µl)
- Keep on ice for 20 mins.
- Place them in a thermoblock at 42 ºC for 45 secs.
- Place them back on ice for 5 mins.
- Add 500 µl of LB without antibiotics.
- Take it to the shaker at 37 ºC for 40-60 mins.
- Spin down the cells for 5 mins at 2500 g.

- Pour out 450 µl of the supernatant.
- Resuspend the pellet and seed a Petry dish with the corresponding antibiotic.
- Incubate the plates inverted at 37 ºC until colonies have grown (6 – 12 h)
- Plates can be stored at 4 ºC for weeks.

3.5.1.5. DNA extraction and quantification

To obtain small amounts of DNA (minipreps), each colony is grown in 3 ml of LB medium with the appropriate selective antibiotic at 37 °C and 220 rpm O/N. An aliquot of 2 ml of the culture is transferred to a 2 ml Eppendorf tube and spin at maximum speed for one minute to pellet cells. This pellet is then resuspended in TE 1 X (TE 10 X: 100 mM Tris-HCl pH 8, 10 mM EDTA), and then lysed with SDS/NaOH (0.2 M NaOH/ 1 % SDS). SDS denatures membranes and proteins while NaOH ensures a pH that denatures DNA. In less than a minute lysis time, cold neutralization buffer (3 M potassium acetate, 5 M acetic acid) is added and mixed immediately. This step neutralizes the mixture, allowing plasmid DNA to re-anneal. Next, to separate lipids from proteins, a solution made of phenol/chloroform (25:24) is added. The aqueous phase is removed and transferred to a new microcentrifuge tube. By adding isopropyl alcohol and centrifuging at maximum speed the DNA is precipitated and subsequently, rinsed with 70 % ethanol and resuspended in TE 1 X with RNAse to degrade the RNA. With this procedure between 1 and 2 µg/µl of DNA are obtained.

Protocol P.2: DNA extraction protocol
- Pick a colony and let it grow O/N in 3 ml of LB with antibiotics.
- Next day transfer 2 ml of culture to 2 ml Eppendorf and spin it to pellet the cells.
- Discard supernatant and respuspend the pellet in 150 µl of TE 1X.
- Add 150 µl NaOH/SDS lysis buffer. Mix gently inverting the tube 5-6 times.
- Add 150 µl of neutralizing buffer and mix.
- Add 80 µl of phenol/chloroform.
- Spin at maximum speed for 5 mins.
- Extract around 400 l of the upper phase and place it in other eppendorf.
- Add 200 µl of isopropyl alcohol to the new eppendorf.
- Spin at maximum speed for 5 mins.
- Get rid of the isopropyl alcohol and wash the pellet with 70 % EtOH.
- Get rid of EtOH and dry the pellet.
- Dissolve the plasmid in 30 µl of TE+RNAse buffer.

3.5.1.6. Sequence validation

In order to verify that the new restriction sites were present, the extracted DNA was digested with the Bgl I and Eco RI enzymes (Thermo Fischer) according to the protocol in Table 3.5, with a total reaction volume of 20 µL. The reaction mixtures were incubated at 37 ° C (optimal activity temperature of both enzymes) for 3 hours and subsequently underwent electrophoresis in 1.5% agarose gels in TBE buffer (45mM Tris-borate, 1 mM EDTA, pH 8), with a voltage of 120 V for 45 minutes. The samples were loaded together with 2 µL of loading buffer (50% glycerol, 0.2 M EDTA, 0.05% bromophenol blue, pH 8), and 20 µL of Phage DNA λ digested with BstEII (Thermo Fischer) was used as ladder.
Additionally, if the size of the bands after digestion was correct, the DNA was sent to Secugen to be sequenced to confirm that there had been no other mutations during the PCR.

3.5.1.7. Digestions

Once the constructions with the new restriction sites for EcoRI and SmaI were obtained, digestions were carried out to obtain the deleted mutants. Thus, from M1, Del4 and Del5 were obtained by digered with EcoRI and SmaI respectively, and from M2, Del6 was achieved after EcoRI disgestion. Reaction mixtures were prepared with the components shown in Table 3.5 and incubated at 37 °C, in the case of digestions with EcoRI, and at 30 °C, in the case of digestions with SmaI, for 12 hours.

DNA (100 ng/µL)	EcoRI/SmaI Buf.x10	EcoRI/SmaI (10U/µl)	H_2O
1 µl	2 µL	0.5 µL	16.5 µL

Table 3.5. Reaction-mixture protocol for DNA digestion with restriction enzymes.

3.5.1.8. Purification of DNA from agarose gels

Before recirculating the plasmid, it was necessary to migrate the digested products in a 1.5% agarose gel in TBE buffer (120 V / 40 minutes) to separate the digested fragment from the vector and thus be able to extract the second one. The DNA purification of the vector from the agarose gel was carried out by the GeneJET Gel Extraction kit (Thermo Fischer).

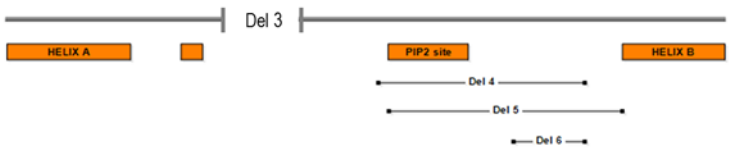

Figure 3.14. Schematic representation of Del4 (I375-A424), Del5 (I375-A424) and Del6 (I375-A424) of $K_V7.2hAB$.

3.5.1.9. Ligations

Once the agarose gel bands were purified, they were recirculated by means of T4 ligase in the presence of their T4 buffer (335 mM Tris-HCl, 33 mM MgCl2, 5 mM DTT, 84 mM (NH4) 2SO4,

pH 8.8). The reaction mixtures were prepared with the volumes of Table 3.6 and incubated at room temperature for 3 hours.

DNA (100 ng/µL)	T4 DNA ligase Buffer	T4 DNA ligase	MQ H_20
7.5 µL	1 µL	0.5 µL	1 µL

Table 3.6. Reaction mixture for DNA ligation with T4 DNA ligase.

The protocol follows with first transformation in BSJ bacteria, followed by DNA extraction and finally sequentiation as described above.

3.5.2. Protein expression and purification

3.4.2.1. Bacterial co-transformation

Bacterial co-expression has been used to simultaneously express CaM with a set of constructs for the C-terminus of K_V7.2 channels (but not in tandem as tested before). In order to do so, CaM was cloned in the pOKD4 vector while the rest of K_V7.2 constructs were cloned in the pProEX-HTc vector. Once the protein genes are cloned in the co-expression compatible vectors, they are co-transformed by electroporation. The machine employed is the ECM630 (BTX A division of Genetronics) and the following values are set:

V = 2500 V

R = 0.200 Ω

Capacitance = 0.025 µF

First, at the bottom of a pre-chilled electroporation cuvette, 0.5 µl of each plasmid are added. Next, 50 µl of electrocompetent BL21(DE3) bacteria are added and the sample is gently mixed, distributing the volume on the bottom to maximize the surface. Once the cuvette is adjusted in the holder or electroporation cell, a pulse of 5.9 µs is sent and immediately 1 ml of LB is added (without antibiotics). Bacteria are then incubated for recovery no longer than 40 min at 37 °C. Afterwards, bacteria are centrifuged for 1 min at maximum speed, the supernatant (about 950 µl) is discarded and the bacterial pellet is resuspended in the remaining LB to be plated in a Petri with the appropriate antibiotics (ampicillin and/or kanamycin in this case).

Protocol P.3: Co- transformation
Thaw one vial (or more) of electrocompetent cells.
In pre-chilled electroporation cuvette add 0.5 µl of each plasmid from a miniprep (1 µg/µl)
Add 50 µl of BL21(DE3) electrocompetent cells and mix and spread gently.
Configure electroporation machine as V =2500 V, R = 0.2 Ω and Capacitance = 0025 µF
Adjust the cuvette in the holder and send the pulse (around 5.9 µs).
Add 1 ml of LB without antibiotics.

Take it to the shaker at 37 ºC for 40 mins.
Spin down the cells for 1 min at maximum speed.
Pour out 950 µl of the supernatant.
Resuspend the pellet and seed a Petry dish with the corresponding double antibiotics.
Incubate the plates inverted at 37 ºC until colonies have grown (6 – 12 h)
Plates can be stored at 4 ºC for weeks.

3.5.2.2. Bacteria growth and induction

Four colonies were chopped for each of the plates and placed in 13 mL tubes with ventilation, with 3 mL of LB medium and 3 µL of the corresponding antibiotics. These cultures could grow for 12 hours at 37 ° C and with stirring until saturated cultures were achieved. After 12 hours, 1: 100 dilutions of the cultures were made, introducing 100 µL of them into a 50 mL Falcon tube (Sarstedt) with 10 mL of LB medium and 10 µL of ampicillin and kanamycin, the latter only in the cases of cotransformed bacteria. These new cultures were incubated at 37 ° C in an orbital incubator to achieve an optical density at 600 nm of 0.6-0.8, measured with the Jenway 6300 spectrophotometer (ICT SL). At this point, the cultures were induced with 0.5µL of IPTG / mL of culture, but not before saving 1 mL of each non-induced culture for later loading in the electrophoresis gel. After 3 hours of induction, the cultures were centrifuged (5,500 rpm / 10 minutes) in the 5430r centrifuge (Eppendorf), to then remove the supernatant and resuspend the bacteria in the small volume not discarded. This volume was then introduced into eppendorf tubes that were centrifuged (7,500 rpm / 5 minutes) in the MiniSpin centrifuge, to finally remove the supernatant.

3.5.2.3. Lysis and electrophoresis

Continuing with the protocol, and always keeping the samples on ice, the bacteria were resuspended in 500 µL of enriched lysis buffer (120 mM KCl, 50 mM Hepes, 5 mM NaCl, 5 mM EGTA, 1mM PMSF, protease inhibitors without
EDTA, 10 µg lysozyme, 500 µM DTT, pH 7.4). DTT is used as a reducing agent that prevents the formation of intra and intermolecular disulfide bonds. The lysis of the bacteria was then carried out with the Soniprep 150 (MSE) ultrasonic blaster in 3 cycles of 10 seconds of activity and 5 seconds of rest. Subsequently, the samples were centrifuged (14,500 rpm / 10 minutes) in the MiniSpin centrifuge; the supernatant was transferred to a new eppendorf tube (soluble protein fraction) and the precipitate was resuspended in 500 µL buffer (non-soluble protein fraction). Both fractions, the soluble and the non-soluble, together with the fraction
Soluble non-induced aliquot culture and molecular weight marker (PageRuler Unstained Protein Ladder, Thermo Fisher) were subjected to electrophoresis in 12% polyacrylamide gels with sodium dodecyl sulfate (SDS), that is, under pseudonative conditions. The samples were prepared as follows:
20 µL of each fraction was mixed with 5 µL of rupture buffer (62.5 mM Tris-

HCl, 20% glycerol, 2% SDS, 5% DTT, 0.05% bromophenol blue, pH 6.8) and of this volume 15 µL were loaded on the polyacrylamide gel in electrophoresis buffer (25 mM Tris, 192 mM glycine, 0.1% SDS, pH 8.3).
Once the electrophoresis was finished, the gels were observed in the Versadoc 4000 (Bio Rad) imaging system, where the construction fluorophores (at 488 nm for mTFP1 and 555 nm for mcpVenus173) were excited to observe their fluorescence, and then the gels were stained with Coomassie Blue R-250 (BioRad). Thus, the bacterial colony with the highest level of soluble protein expression with CaM was chosen to purify each construct.

3.5.2.4. Protein purification

Frozen bacterial pellets were thawed in ice and afterwards resuspended with 40 ml of *Lysis Buffer* (120 mM KCl, 20 mM KX(PO4) pH 7, 1 mM PMSF, 2 mM Imidazole and 1 tablet of Protease inhibitor without EDTA). Subsequently, it was passes through the **Emulsiflex** thrice, and followed by centrifugation in a JA25.50 rotor at 25000 g for 30 min at 4 °C. The rescued supernatant was filtered with 0.22 µm filter before running the AKTA. First, AKTA tubes were washed with degassed ddH2O and afterwards the column **HiTrap Talon Crude** 5 ml (GE Healthcare, Ref: 28-9537-67), was connected to the AKTA with slow flow to remove the air bubbles. Ethanol from the columns was washed out with 5 column volumes (CVs) of ddH2O at a flow of 5 ml/min. Equilibration of the column with 10 CVs of *Wash Buffer* (120 mM KCl, 20 mM KX(PO_4) pH 7) at 5 ml/min flow was followed by injection of the sample at 1 ml/min up to 50 ml. Fractions every 5 ml were collected. Next, the column was washed with different combinations of *Wash Buffer* and *Elution Buffer* (120 mM KCl, 20 mM KX(PO4) pH 6, 300 mM Imidazole): W0 = 10 CV of buffer A (0 mM imidazole) - 2 ml/min; W1 = 4 CV of 3 % mixture (9 mM imidazole) 2 ml/min; W2 = 8 CV of 6 % mixture (18 mM imidazole) 2 ml/min; and W3 = 4 CV of 8 % mixture (24 mM imidazole) 2 ml/min. Finally, the complex was eluted with a gradient from 30 to 300 mM of imidazole in 8 CVs at 2 ml/min flow. 1 ml fractions were collected and these with high 280 nm absorbance were picked. A 12 % acrylamide SDS-PAGE was run to check the presence of the protein in the fractions. To regenerate the column, apply 10 CVs of 20 mM MES pH 5.0, afterwards 10 CVs of ddH2O and finally 10 CVs of EtOh 20 %. All the positive fractions were pooled together and **dialysed** against 1 litre of *Running Buffer* (120 mM KCl, 20 mM KX(PO_4) pH 6 and 5 mM EGTA) O/N at 4 oC in dialysis tubing cellulose membrane (Sigma-Aldrich, Ref: D927-100FT). Protein complex was concentrated until 10 to 13 ml using Amicon Ultra-15 centrifugal units with a 3kDa cut-off in a fixed angle rotor at 3500 g.
A second purification step was done by **gel filtration**. First AKTA tubes were washed with degassed ddH2O. Afterwards, before connecting the Superdex 200 pg 26/60 (GE Healthcare, Ref.: 28-9893-36) column to the AKTA. An aliquot of 13 ml of dialysed and 0.22 µm filtered sample was injected.
Protein concentration was measured using the absorbance at 525 nm (mcpVenus).

3.5.3. Spectroscopy

3.5.3.1 Dynamic Light Scattering

Dynamic Light Scattering (DLS) was used to analyze the quality of the protein complex. Light scattering is a physical phenomenon in which light waves suffer a splitting in different frequencies

when they go through a specific material. It is very powerful tool to analyze the diffusion behaviour of macromolecules in solution. The way in which this dispersion happens is highly dependent on the structure of the material and, in solution; it enables the calculation of the hydrodynamic-radii of the particles. Dynamic Light Scattering (DLS), or photon correlation spectroscopy, allows us to obtain the size distribution profile of different particles within a dissolution and to estimate the percentage of every single species present in sample.

To determine the heterogeneity of the purified proteins, samples' dispersions were evaluated by Dynamic Light Scattering using a Zetasizer spectrometer (Malvern Instruments). All measurements were done using a sample aliquot of 80 µl. The prismatic plastic cuvette was incised by a 5 mW and 633 nm He-Ne laser beam. Scattered light was detected by a photomultiplier located at 173 degrees. Digital analysis of the data gives rise to the size distribution based on the particle's volume. The correlation function and the polydispersity allow determining the protein size and the possible aggregates.

3.5.3.2. Fluorescence Spectroscopy

3.5.3.2.1. Fluorescence resonance energy transfer (FRET)-based biosensors

Since the discovery of the fluorescence protein in 1992, fluorescence-based biosensors have become crucial to monitor and identify cellular physiology, molecular dynamics, and molecular interactions (Periasamy, 2001). Förster or fluorescent resonance energy transfer (FRET) is a process based on the radiation-less transfer of energy from a “donor” fluorophore to an “acceptor” fluorophore. FRET assays can translate a near-field interaction into a far-field signal, being, until now, a unique optical tool to analyze biological phenomena with higher resolution than standard optical microscopy (Roy et al. 2008; Moerner and Fromm 2003). FRET amplifies microscopic conformational changes by emitting light, which can be measured by a sensor (Ha et al. 1996).

Based on the physics of molecular proximity, FRET enable energy transfer only when the distance between the fluorophores are between 1–10 nanometers (nm) one of each other. Once it is excited the donor fluorophore it emits a virtual photon, which is absorbed by an acceptor fluorophore through nonradiative dipole–dipole coupling (Merchant et al. 2007; Kapanidis and Weiss 2002).

FRET can be used to analyse the interaction between biomolecules and is the basis for so-termed biosensors. Biosensors are designed to report on chemical states and can be used to measure concentrations of ions or small molecules, phosphorylation of peptides or the nucleotide loading state of a protein (Mehta & Zhang, 2011). The completion of FRET based biosensors depends on their brightness and dynamic range. These attributes are subject to the characteristics of the employed fluorescent proteins (Goedhart et al., 2007). Both FRET efficiency and brightness are determinated by the extinction coefficient and quantum yield and thus a general recommendation is to use the brightest fluorescent proteins available (Scott & Hoppe, 2015). For FRET imaging in living cells, several other parameters should be considered including maturation, photostability, oligomeric state and sensitivity to environmental changes (Scott & Hoppe, 2015).

The donor and the acceptor fluorophores can be placed in different ways. For example, one fluorophore can be bound to a substrate whereas the other could be attached to its binding

site, and once they are bound, the fluorophores would be in close enough distance to transfer energy (Joo et al. 2007). In another way, as is in our case, both fluorophores are attached to the same protein and, due to a change in the environment, the protein alter its conformation and initiate FRET (Kajihara et al. 2006).

However, our FRET biosensor is designed with fluorophores attached to a molecule at close positions to continually engage in FRET; after calcium addition, will be a conformational change that provokes a separation between fluorophores and decreasing the FRET efficiency.

3.5.3.2.2. FRET to Measure Distance

The FRET-efficiency hinges on the overlap of the donor and acceptor spectra and the orientation of the dipole moments of the donor and acceptor (Ansbacher et al. 2012). FRET efficiency is also dependent on the distance R_0 between the donor and acceptor. The relationship between FRET efficiency and R_0 is elucidated by the following equation:

$E=1/[1+(R/R_0)6]$

where R_0 is the Förster's radius, or the distance between the fluorophores at which $E=50$ %, and where $R_0=8.79\times10-5\times[n-4\times Q\times\kappa2\times J(\lambda)]$

R_0 is in Angstrom, n is the refractive index of medium in the range of overlap, Q is the quantum yield of the donor in the absence of acceptor, and $J(\lambda)$ is the spectral overlap. $\kappa2$ is the orientation factor of the two dipoles. $\kappa2=[\cos\vartheta T-3\cos\vartheta A\cos\vartheta D]$, where ϑT is the angle between donor (D) and acceptor (A) moments. The dynamic value of $\kappa2$ is commonly 2/3 for freely rotating donor and acceptor fluorophores (Jares-Erijman and Jovin 2003; Hoppe et al. 2002).

3.5.3.2.3. Donor and Acceptor Fluorophores

Generally, the donor and acceptor fluorophores should have different characteristics, especially in emission. Thus, FRET can be detected either by monitoring the fluorescence readout of the acceptor or by acceptor quenching. Both cases result in a reduction of donor fluorescence. FRET donor fluorophores are always fluorescent. Upon excitation, the electrons of the donor fluorophore jump from their ground state to a higher energy level. When they go back to the ground state, they emit a particle of light called photon. In FRET assays, the photon instead of being emitted, it is rather absorbed by the acceptor, exciting its electrons and provoking the acceptor to emit a photon (Meyer and Teruel, 2003). FRET quenchers were created to prevent fluorescence depletion between donor and acceptor. Without the presence of a quencher, the excited dye emits light while returns to the ground state. When there is a quencher present, the excited fluorophore can return to the ground state without emits light, but transferring its energy to the quencher, whereas leading the quencher to its excited state.

3.5.3.2.4. Considerations in the design of FRET Biosensors

a. Donor fluorophore emission range

The first factor to take care for is the donor emission range, that is, how much energy is emitted from an excited donor, and the acceptor excitation range, in other words, how much energy is required to excite an acceptor. They must coincide by at least 30 % (Lovell et al. 2009). Thus, there are a restricted number of fluorophore-couples. This can limit the use this process on specific sensitive cellular mechanisms.

The most used FRET-pair in living cells has been cyan fluorescent protein (CFP)- and yellow fluorescent protein (YFP). However other FRET-pairs such as, CFP and dsRED, BFP and GFP, GFP (or YFP) and dsRED, Cy3 and Cy5, Alexa488 and Alexa555, Alexa488 and Cy3, and FITC and rhodamine have been also widely used (Wiedenmann et al. 2009).

b. Auto-fluorescence

It should also be considered a phenomenon called auto-fluorescence since it could interfere with the FRET data. Auto-fluorescence is the fluorescence of natural occurring substances that when are excited by light photons, they release photons (Sturmey et al. 2006). This radiation masks the specific fluorescence of the FRET-couple, because sensors, in addition to the radiation produced by themselves, will measure it. Thus, it will produce significant error when trying to monitor cellular activity. The most auto-fluorescencing biological structures are mitochondria and lysosomes; the most commonly observed auto-fluorescencing molecules are NADPH and flavins; and generally, proteins containing an increased amount of the amino acids tryptophan, tyrosine and phenylalanine show some degree of autofluorescence.

c. Fluorescence- Lifetime

Another inconvenience of using fluorophores is that they have a short fluorescence lifetime. Thus, once they are excited, they remain excited for a noticeably short time. Due to the short time to measure fluorophore emissions, auto-fluorescence takes up more percentage of the recorded emissions over time (Davydov et al. 2008; Fernando et al. 2006).

d. Altering the structure

It is important to note that FRET fluorophores must have proper excitation and emission spectra but in addition, they should not affect the three-dimensional structure of the molecule(s) to which they are attached.

e. Analyte Concentration

Other important factor regarding to the detection of FRET includes analyte concentration (Long et al. 2012). Only molecules that interact with one another will achieve FRET. If there is a large concentration of donor and acceptor molecules, but without any interaction, the amount of FRET occurring would be low. Here, whereas the donor and the acceptor fluorophores should be easy to detect alone, the effective FRET activity may not be enough to detect (Kwak et al. 2010).

f. Maturation

The maturation is a crucial factor for effective brightness of a fluorescent protein and for efficient FRET (Miyawaki, 2011). The maturation efficiency is the fraction of produced protein that results in a correctly folded protein with a functional, fluorescent chromophore. On paper, the maturation of a fluorescent protein approximates 100%. If a protein does not fold correctly or forms an incorrect chromophore, the FRET pair will be lacking a functional donor or acceptor and this will avoid FRET, thus reducing the amount of functional FRET pairs and decreasing the dynamic range (Scott & Hoppe, 2015).

Designing FRET experiments has limitations. The most obvious limitation of current FRET models is the necessity of a close physical proximity between donor and acceptor probes for FRET to even occur. Depending on the assay design, close proximity will either be established or removed during the assay, resulting in a change in signaling that can be measured. Additionally, appropriate donor and acceptor pairs need to have enough spectral overlap for efficient energy transfer to take place or have enough of a difference in spectrums to be visually distinguishable from one another. The choice of filters for fluorescent wavelength selection is also critical, as the excitation filter for the donor
must be able to selectively excite the donor while minimizing excitation of the acceptor. Furthermore, the insertion of biosensors into live cells has had an efficiency rating of around 20–30 % (Komatsua et al. 2011).

3.5.3.2.5. mTFP1 and mcpVenus FRET-pair

An essential requirement for FRET is the clear spectral overlap between the donor emission and the acceptor absorption spectra (Periasamy & Day, 2005). Even though there are many different fluorophore-pairs satisfying this condition, the most common FRET pair currently is the combination of the *Aequorea*-based cyan FP (CFP) and yellow FP (YFP) (Zhang et al., 2003). They have been subject of many modifications, both CFP and YFP, to improve their utility in FRET-based assays. For example, Nagai and co-workers developed a brighter YFP called Venus that has maturation that is more efficient and reduced pH and halide sensitivity (Nagai et al., 2002). Additionally, Rizzo et al. demonstrated that substitutions on the solvent-exposed surface of CFP stabilized its excited state and generated a protein with a higher quantum yield termed Cerulean (Rizzo et al., 2004). Several studies have validated that these Cerulean and Venus variants are between the most efficient of the FRET pairs available (Koushik et al., 2006). However, it has still several limitations to the use of this popular FP pair in FRET-based imaging with laser scanning microscope (LSM) systems (Day & Booker, 2008).
Day and Booker, a decade ago, characterized new FPs that might overcome some of these limitations (Day & Booker, 2008). They found that mTFP has advantages over Cerulean as a FRET donor for Venus. It has increased brightness comparing with Cerulean, improving the detection of proteins that are difficult to express in cells, or that need to be produced at low levels in cells. Additionally, the higher photostability and improved spectral overlap with acceptor proteins, such as Venus or newer generation orange FPs (Shaner et al., 2005) make mTFP an ultimate donor fluorophore for FRET measurements (Day & Booker, 2008). However, they did not observe the expected enhanced efficiency predicted by the increased R_0. Finally, the probabiltity of dimer formation with the *Aequorea* fluorophore variants is reduced because the mTFP has been created from a protein originating in a different species. Regarding this, Cerulean and mTFP share about 41% sequence homology, but there is little homology in the carboxyl terminal dimer interface identified for the *Aequorea* FPs (Zacharias et al., 2002).
Even if the interactions between the FPs themselves is an undesired effect for almost all FRET experiments, it can be an advantage in assays that use FRET-based biosensor probes. These probes have a sensor domain that directly links the donor and acceptor FPs, allowing conformational changes in the sensor domain to be detected by changes in the emission ratio (Giepmans et al., 2006). Another study sought to improve the dynamic range of the FRET

sensor probes by using the directed coevolution of both CFP and YFP (Nguyen & Daugherty, 2002). This approach yielded sensor probes with substantially enhanced FRET signals, even though the evolved FPs had similar spectral characteristics and slightly decreased quantum yields when compared to the original FPs. This apparent contradiction was resolved when it was shown that the enhanced FRET signals resulted from mutations that promoted the stabilization of an intramolecular complex formed by the linked FPs (Ohashi et al., 2007).

FP	Peak Absorption	Peak Emission	Quantum Yield	Extinction Coefficient [a]	Intrinsic Brightness [b]
mTFP1	462	492	0.85	64	54
Venus	515	528	0.57	92.2	53

a. (x 10^{-3}) (M^{-1} cm^{-1})

Table 3.7. Spectral characteristics of mTFP1 and Venus.

As it is described above, fluorescence characteristics of a molecule depends on the electronic and vibrational states in which its energy levels are. First, fluorophores are excited at its specific wavelength, absorbing a photon and changing the relaxed electronic state to an excited state. Between other relaxation mechanisms, one mode to recover their basal energetic state is by colliding with other molecules and emitting their energy as fluorescence. The released photons will have different energies and, thus, different frequencies depending on the biochemical environment. Therefore, the structural effect of a fluorescent tag in a protein could be ascertained by analysing the different frequencies of the emitting light and their relative intensities in the spectrometer: when there is a structural change, the chemical environment of the target fluorophore in the labelled protein may change, modifying the emission spectra.

3.5.3.3. Fluorescence measurements

A. Sample Preparation

The protein concentration was determined by measuring the absorbance of mcpVenus173 (mTFP1 could also have been used, but it will be overestimated, since a portion of mcpVenus it is also absorved) at 515 nm and using the Lambert-Beer law (Equation 1):

$$Abs = \varepsilon \cdot C \cdot L$$

C is the concentration (M), Ɛ is the molar extinction coefficient (92,200 L / (mol · cm) for mcpVenus173) and L is the optical path (1 cm). Samples were prepared with 0.5 µM protein in fluorescence buffer and free Ca^{2+} in a concentration range from 0 to 10 µM (physiological range). The buffer contained EGTA (chelating agent), so the calculations made to prepare the samples took into account that the total [Ca^{2+}] was not equal to the free [Ca^{2+}]. The addition of Ca^{2+} could induce the formation of aggregates, whereby the samples were centrifuged (20,000 g / 10 minutes) and transferred to new Eppendorf tubes.

B. FRET measurements

The fluorescence emission spectrum was obtained with an Aminco Bowman Series 2 fluorescence spectrophotometer (SLM Aminco) in a final volume of 100 µl (using quartz cuvette) at 25 °C. The

excitation wavelength was 340 nm, and emissions were registered from 400 to 660 nm. For the titration experiments, increasing concentrations of Ca^{2+} were added to sample containing Q2*h*AB-CaM in fluorescence buffer (50 mM K-Hepes (pH 7.4), 120 mM KCl, 5 mM NaCl, 5 mM EGTA). This mode sought to see the changes in the FRET as a result of the reorientation of the A and B propellers, the result of the union of Ca^{2+} to CaM and the reorganization of its lobes. The energy transfer by FRET was determined as the ratio between the emission at 490-495 nm of mTFP1 and the emission at 525-530 nm of mcpVenus173.

The emission spectrum of mcpVenus173 between 525 and 570 nm also was collected, exciting at 515 nm, with the aim of ensuring that the fluorescence emission did not decrease due to the decrease in pH at increasing concentrations of Ca^{2+}.

C. SK2 CONTROL

We used SK2 as a reporter to validate that FRET technique within cyan and yellow couple is useful to analyse a conformational change in a protein complex. CaM binding domain of SK2 protein was cloned behind Citrine fluorescent protein (Citrine-SK2) in a pProEx Ht-C vector. It was co-transformed with mTFP1-CaM.

We show that the FRET-ratio increment two times before adding Ca^{2+} (free Ca^{2+} 1 mM). This means, that once CaM binds to Ca^{2+} ions, the N-terminal of SK2-CaM BD gets closer to the N-lobe of CaM.

K_V7.2-CaM BD was cloned flanked by mTFP1 and mcpVenus fluorophores and co-transformed with CaM. In this case, using the same procedure, Ca^{2+} binding to CaM provokes a little reduction in the FRET-ratio, very likely because of a subtle conformational where *h*A and *h*B separate.

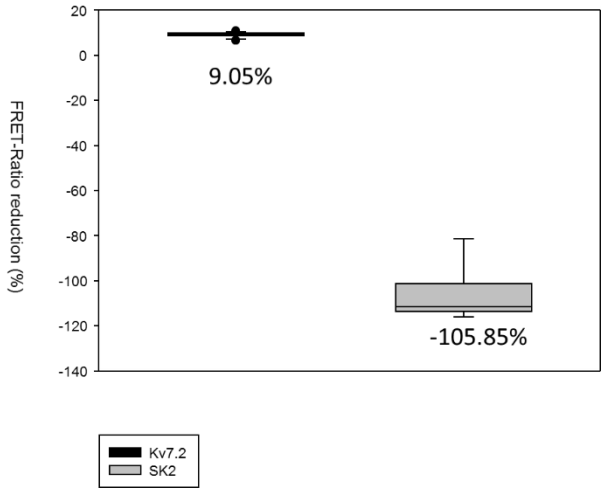

Figure 3.15. FRET-Ratio reduction upon Ca^{2+} binding in K_V7.2 and SK2 channels. Box of the percentage of FRET-Ratio reduction upon adding Ca^{2+} at saturating concentrations (500 µM). (n ≥ 3).

D. Calcium Titration

By combining these buffers we achieved different free Ca^{2+} levels in each sample:
A. BUFFER EGTA: 120 mM KCl, 50 mM HEPES Ph7.4, 5 mM EGTA, 5 mM NaCl
B. BUFFER Ca^{2+}: 120 mM KCl, 50 mM HEPES Ph7.4, 5 mM EGTA, 5 mM NaCl, 25 mM $CaCl_2$
Both buffers pH should be adjusted to pH 7.4 before using.

We employed MaxChelator (Annex V.) to estimate how much Buffer Ca^{2+} we should add to get a certain concentration of free Ca^{2+}. This is a program for determining the free metal concentration in the presence of chelators or total metal given a desired free concentration https://web.stanford.edu/~cpatton/CaEGTA-TS.htm

Considering that V_{total} = 500 µL, we add B. Fluorescence Ø Ca^{2+} up to 500 µL. We used the volumes of the Table 3.7 in our titrations: Assuming that the protein complex *stock* is at 20 µM.

SAMPLE PREPARATION FOR CALCIUM TITRATION					
Experiment condition↓	MaxChelator estimation ↓	C_{final} ↓	Sample Preparation		
			$V_{i1} = C_f \cdot V_f / C_i$	$V_{i2} = C_f \cdot V_f / C_i$	V3=Vf-V1-V2
Free Ca^{2+} (µM)	Total Ca^{2+} (M)	Total Ca^{2+} (mM)	Ca^{2+} Buffer (µL)	Protein (µL)	BF Ø EGTA (µL)
0	0	0,00	0,00	12,50	487,50
0,25	0,00297299	2,97	74,32	12,50	413,18
0,5	0,00372913	3,73	93,23	12,50	394,27
0,75	0,00407468	4,07	101,87	12,50	385,63
1	0,00427272	4,27	106,82	12,50	380,68
1,5	0,00449121	4,49	112,28	12,50	375,22
2	0,00460926	4,61	115,23	12,50	372,27
2,5	0,00468329	4,68	117,08	12,50	370,42
3	0,00468329	4,68	117,08	12,50	370,42
3,5	0,00477126	4,77	119,28	12,50	368,22
4	0,0047996	4,80	119,99	12,50	367,51
8	0,00490366	4,90	122,59	12,50	364,91
…	…		0,00	12,50	487,50

Table 3.8. Sample preparation for calcium titration of FRET-sensor protein complexes.

Then, the free Ca^{2+} levels were corrected with the error that had been previously estimated by Fura-2 (Supplemental 1).

3.5.4. Development of the FRET experiment simulator

The first step is the selection of two compatible fluorescent probes for resonance energy transfer (FRET) experiments. Then the Excitation and emission spectra of each probe in ASCII format and the data were transferred to an Excel calculation. The subsequent treatment of the data is based on basic theoretical aspects of spectroscopy. fluorescence, in such a way that mathematical operations that describe the path of the light from when it is emitted by an excitation lamp until it is absorbed by the detector.

First, a function is described that simulates the number of photons emitted by excitation (f(x)=f) with arbitrary scale and multiplied by the emission spectrum of the lamp corresponding (SExL), in this case we choose a Xenon lamp. From this moment, all calculations are given in terms of

energy, for which each corresponding value is divided by its length wave, resulting in the emission energy (EmL) (Eq.1).

$$\frac{[f(x)=f]*SEx_L}{\lambda} = Em_L \qquad (1)$$

The fluorescent probe that acts as a donor, absorbs the energy coming directly from the lamp (ExL) and each fluorophore absorbs the proportional part corresponding to its absorption spectrum (SAD) (Eq. 2).

$$Em_L * SAb_D = EAb_D \qquad (2)$$

To calculate the donor emission energy (EmD), was considered the area under the spectrum curve at all wavelengths (Eq. 3a) and subsequently was multiplied by its emission spectrum (SEmD) (Eq. 3b)

$$\int_{\lambda_0}^{\lambda_1} EAb_D \qquad (3a)$$

$$\int_{\lambda_0}^{\lambda_1} EAb_D * SEm_D = Em_D \qquad (3b)$$

Always looking for energy conservation, the total amount of absorbed energy is equalized with the total amount of energy emitted by the donor (Eq.4). In this way the emission energy was obtained of the preserved donor (EmD *).

$$\frac{(Em_D * \sum_{n=1}^{\lambda} Ab_D)}{\sum_{n=1}^{\lambda} Em_D} = Em_D^* \qquad (4)$$

The actual emission from the donor probe (Em_D^0) was then calculated, since, despite the conservation of energy, fluorophores are unable to emit all the energy they absorb due to a small lost as heat (Eq. 5).

$$Em_D^* * Q_D = Em_D^0 \qquad (5)$$

The data treatment was carried out identically for the acceptor, but in duplicate since it was taking into account that it is capable of absorbing as much energy that the lamp emits directly as the energy emitted by the donor. Once all the spectra of the system have been calculated and verified that the Energy is conserved in all cases, transfer parameters were added. At FRET there is an exponential relationship between the distance at which fluorophores are found and the efficiency of the energy transfer (Eq. 6), where R is the distance between the fluorophores and R0 the Föster distance for each pair of fluorophores.

$$E = \frac{1}{1 + (\frac{R}{R_0})^6} \qquad (6)$$

To check the efficiency of the simulation system, several controls were carried out and the calculations with tests previously carried out in the laboratory, confirming that using this simulator we can calculate the distance at which two fluorophores are found based on the spectra obtained experimentally and vice versa. The probes and all their intrinsic properties were obtained from the ThermoFisher Scientific website.

4. STABILITY AND CALCIUM EFFECT IN THE TETRAMER

4.1. INTRODUCTION

4.1.1. Coiled coils in K_V7

Coiled coils are bundles of intertwined α-helices, a conformation that is one of the most widespread and versatile protein-protein interactions found in nature. These structures are found in a subset of tetrameric ion channels, and there is much evidence that they determine the stability and selectivity of multimerization. The subunit responsible for the I_{Ks} current, $K_V7.1$ (KCNQ1), does not coassemble with other K_V7 subunits. In contrast, **Kv7.3 (KCNQ3) can form heterotetramers with all subunits except with $K_V7.1$** (Schwake et al., 2000). The other family members, $K_V7.2$ (KCNQ2), $K_V7.4$ (KCNQ4), and $K_V7.5$ (KCNQ5), can form functional homotetramers and functional heterotetramers with $K_V7.3$. Different combinations of K_V7 subunits display different biophysical properties that produce functional diversity (Hadley et al., 2000; Kubisch et al., 1999; Schwake et al., 2000; Selyanko et al., 2000; Wang et al., 1998). **It is thought that since helix D shows significant sequence difference among K_V7 channel subtypes, this domain could be a primary determinant of assembly specificity** (Maljevic *et al.* 2003; Schwake *et al.* 2003, 2006). K_V7 potassium channels lack the T1 domain, which is the responsible of tetramerization of K_V1 channels, but they have two coiled coil domains in the C-terminal (Jenke et al., 2003; Schwake et al., 2006), helices C and D. It was first demonstrated for $K_V7.1$ that deleting of helix D prevents channel tetramerization and alters function (Schmitt et al., 2000; Wiener et al., 2008). In the case of $K_V7.2/3$, deleting of helix D does not completely abolish function, but there is an important reduction. As for other K_V7 channels, $K_V7.2$ helix D can also be replaced by an artificial tetrameric domain (Schwake et al., 2006).

4.1.2. CaM and coiled coil domains

In addition to coiled coil domains, many channels contain separate calmodulin (CaM) binding domains, including SK, IK, TRP, K_V7 (KCNQ) and CNG channels. Similar to SK channels, trafficking of KCNQ channels to the membrane requires CaM (Etxebarria et al., 2008), and current density is affected by CaM availability: increases, decreases, or no effects upon CaM overexpression have been reported (Gamper et al., 2005; Shamgar et al., 2006; Etxebarria et al., 2008). Since the CaMBD has a notorious aggregation tendency when produced in bacteria in the absence of CaM, it is thought that CaM is a constitutive auxiliary subunit of KCNQ channels. Nevertheless, some mutant channels compromised for CaM binding are fully functional, suggesting that KCNQ constitutive CaM binding, or resident CaM, is not a strict requirement for function (Gomez-Posada et al., 2011; Sihn et al., 2016), and that CaM may exit and return to the channel under some circumstances.

Another feature of K_V7 channels is the absolute requirement of PIP_2 binding to be functional (Delmas & Brown, 2005; Li et al., 2005; Suh et al., 2006) and mounting evidence reveals that sensitivity to PIP_2 is modulated by CaM binding (Gomis-Perez et al., 2017). Recent findings indicate that the function of helix D goes beyond providing a physical platform for channel assembly. Accordingly, the relationship between the coiled coil and CaM binding domains has been examined recently in $K_V7.2$ channels, suggesting that the stability of the helix D coiled coil affects CaM binding and that it results in altered PIP_2 sensitivity (Alberdi et al., 2015).

The influence of CaM binding on assembly/tetramerization domain (CD module) of the K_V7.2 subunit was studied previously in our group. Toward that aim, we constructed chimeric proteins between the monomeric single transmembrane protein Tac and the K_V7.2 AB CaM-binding domain, and we expressed them in HEK293T cells (Etxebarria et al., 2008). A GFP tag was incorporated at the C-terminus that allowed the complexes to be pulled-down using anti-GFP antibodies. The signal from the pulled-down material by CaM, revealed with anti-CaM antibodies, was compared between the chimeras that incorporated the ABΔ2 and ABΔ2-CD modules. Furthermore, in a third chimera the CD module was replaced with an artificial, unrelated amino acid sequence (Tet) that adopts a tetrameric coiled coil configuration (Zerangue et al., 2000). We observed a **dramatic increase in the CaM signal when chimeras that incorporated either the natural or the artificial tetramerization signal** were pulled-down (Figure 4.1). Thus, it was concluded that coiled coil formation distal to the binding domain favours CaM engagement.

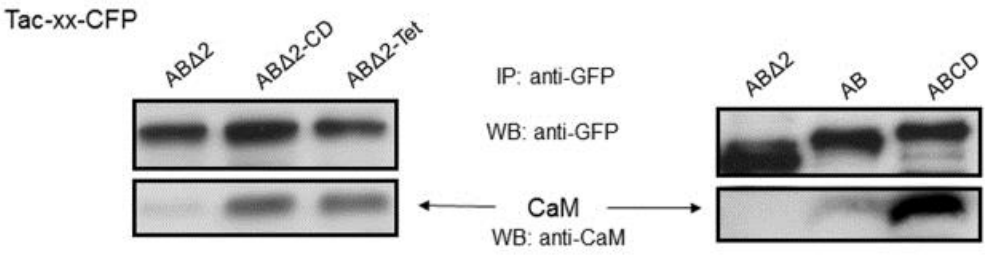

Figure 4.1. The presence of a tetramerization domain favors calmodulin binding to a membrane protein. Tac-K_V7.2-CFP chimeras extracted from HEK293T cells were immunoprecipitated using anti-GFP antibodies, separated by SDS-PAGE, transferred to membranes (WB), and probed with anti-GFP and anti-CaM antibodies (n≥ 3). The bottom panel in (Right) was obtained after a longer exposure than the top panel.

At the same time, Sachayini and co-workers, based on SAXS experiments, described helix C and D as modules that appear to be approximately coaxial, with the connecting linker in a fairly extended conformation with rather limited flexibility (Sachyani et al., 2014). In support of this model, the complete structure of *Xenopus* KCNQ1 has been recently resolved by Cryo-EM were *h*C and *h*D form two long helical bundles that facilitate tetramerization of the channel (Sun and MacKinnon, 2017). Complementing a previous SAXS study carried out in the absence of the transmembrane domain (Sachyani et al., 2014), which identified flexibility in a location proximal to hC, the cryo-EM images revealed flexibility distal to the hC helix (Sun and MacKinnon, 2017).

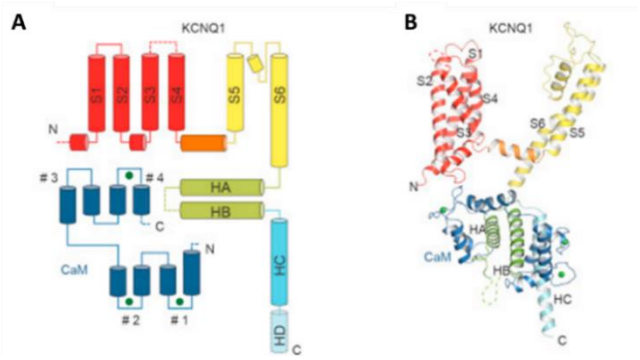

Figure 4.2. Domain Organization of KCNQ1$_{EM}$ (A) Domain organization of one subunit. Helix D, which is masked out in 3D reconstruction, is indicated by cylinder with dashed outlines. The EF hands of CaM are labelled as #1–#4 from the N-terminal to C-terminal end. The first two EF-hand regions form the N-lobe, and the other two form the C-lobe. Green spheres represent calcium ions.
(B) Model of one subunit with domains colored as in (A). (From Sun & MacKinnon, 2017) PDB: 5VMS.

4.1.3. *Cis*- and *Trans*-binding

Some years ago, it was suggested that CaM could embrace helices A and B from the same subunit (*cis*-binding) or from two adjacent subunits (*trans*-binding) (Alaimo et al., 2013). Apparently, bringing together AB modules from adjacent subunits, the distal assembly domain favours *trans*-binding. Indeed, the atomic structure of K_V7.1/CaM complex has been trapped bridging two CaM-binding domains, although results obtained using concatenated constructs suggest that CaM preferentially binds to K_V7.1 channel in *cis* configuration. By contrast, there are functional indications for the adoption of *trans*-binding in K_V7.2 channels. K_V7.2 channels that carry a mutation in helix A or helix B, each of which disrupts CaM binding individually are non-functional. Remarkably, when subunits carrying a mutation in helix A are co-expressed with subunits mutated in helix B, the resulting channel is functional, highlighting the relevance of CaM *trans*-binding (Alaimo et al, 2013).

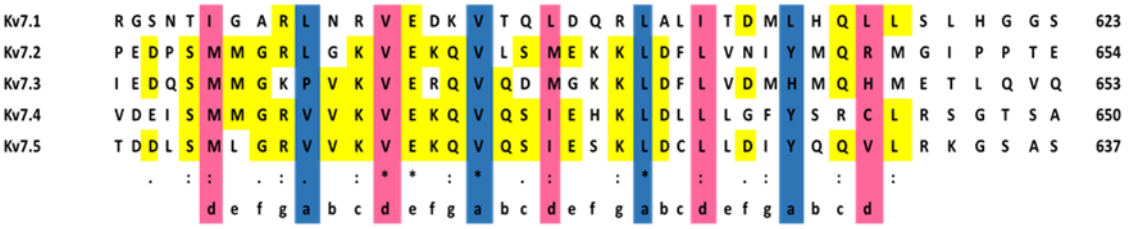

Figure 4.3. 1-9 K_V7 helix D sequence alignment. Yellow highlighting and symbols below alignments indicate sequence conservation (asterisk, identical residues; colon, conservative substitution; period, weakly conservative substitution). In the Tail region, the positions of the coiled coil heptad repeat (abcdefg) are indicated below the alignment. Coiled coil residues occupying hydrophobic ‘‘a’’ and ‘‘d’’ positions are denoted by blue and pink, respectively. Adapted from

4.2. OBJECTIVES

The main objectives of this chapter are to analyse the interchange between subunits in a tetramer and the contribution of helix D in CaM binding configuration (*cis* and *trans*). In addition, how Ca^{2+} affect the stability of the tetramers was addressed.

4.3. RESULTS

4.3.1. Complementation assay: *Trans*-binding configuration of CaM is affected by helix-D coiled coil.

We first evaluated binding properties of D-CaM to proteins devoid of mutations. Figure 4.4.A shows the time-course of the increase in D-CaM fluorescence after adding the CaM binding AB module, as well as the time-course after adding the ABCD module that included the CD assembly region. After less than 2 min the signal approached the full response in both cases.

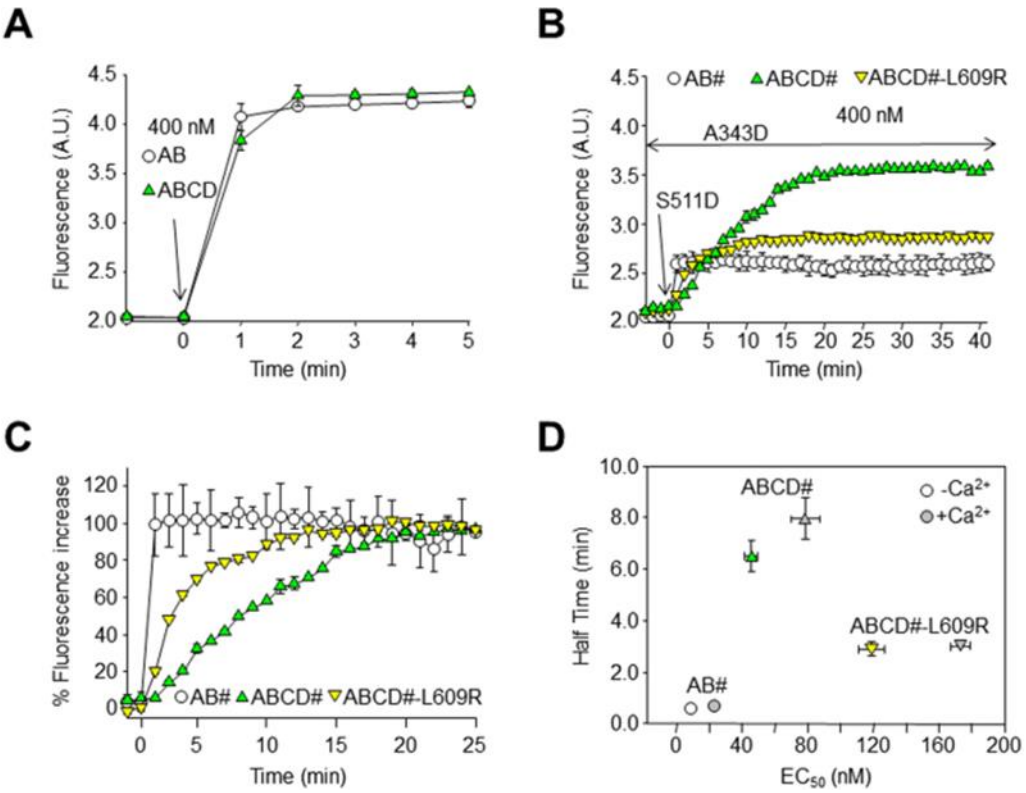

Figure 4.4. The time-course of *trans*-binding is affected by the helix D coiled coil. (**A**) Time-course of the increase in D-CaM (12.5 nM) fluorescence upon binding to AB and to ABCD (400 nM). Each point represents the average of 4 experiments. The maximal increase in fluorescence was reached in less than 2 min. (**B**) Comparison of the time-course of the increase in D-CaM fluorescence in the continued presence of the helix A A343D mutant (400 nM), and upon addition of the S511D helix B mutant (400 nM), for proteins devoid of the CD module (AB#, open circles), ABCD# (green upward triangles), and ABCD#-L609R (yellow downward triangles). The hash (#) denotes an equal mixture of helix A and helix B mutants. This set-up was designed to trap *trans*-binding. Each trace represents the average of 3 experiments. (**C**) Normalized time-course from the data displayed in (**B**). (**D**) Plot of the half-time to reach the maximal D-CaM fluorescence emission *vs* the apparent affinity for AB#, ABCD# and ABCD#-L609R.

After that, we analysed, by a complementation assay, the acquisition of *trans*-binding configuration, using mutants unable to bind CaM in helix A (A343D) and in helix B (S511D) respectively. Combining these mutant K_V7.2 CaM binding domains, we devised an assay to follow the adoption of the *trans*-binding mode *in vitro*, which involves monitoring D-CaM fluorescence while sequentially adding the mutant proteins. For simplicity, an equimolar mixture of the AB-A343D (helix A mutant) and the AB-S511D (helix B mutant) is denoted AB#, while ABCD# stands for an equimolar mixture of ABCD-A343D and ABCD-S511D. Please note that the concentrations refer to each mutated protein and thus, 100 nM of AB# is the result of mixing 100 nM of AB-A343D and 100 nM of AB-S511D. Consequently, the number of WT helices A and B should remain the same at a given concentration of AB and AB#, and consequently, the number of CaM binding sites is expected to be the same.

Thus, the increase in fluorescence might occur once D-CaM binds to helix B of A343D and to helix A of S343D. First, helix A A343D mutant was added to D-CaM, and there were no significant changes in fluorescence emission (Figure 4.5 AB#). Remarkably, the subsequent addition of the helix B S511D mutant resulted in an increase in fluorescence within 1 min, a time-course that was beyond the resolution of our experimental set up. Thus, the **acquisition of the *trans* configuration in solution took less than 1 min** in the absence of the assembly domain (Figure 4.5.B,C, *circles*).

We next tested the **influence of helices CD on the time-course of the acquisition of *trans*-binding**, using a mutation that impede tetramerization, L609R. Figure 4.4. B and C (upward triangles) show that the presence of helices CD produced several changes in the profile of the response. First, the magnitude of the increase in fluorescence was larger and second, the time-course for *trans*-binding was slower. The extent of the fluorescent increase was indistinguishable at 25 °C and 37 °C, whereas the time-course was faster at 37 °C. The time to reach the half-maximal signal was 9.2±0.3 and 12.0±0.4 min at 37 °C and 25 °C, respectively when the concentration tested was 400 nM.

The impact of Ca^{2+} was also analysed in a complementation assay with mutant ABCD proteins, indicating that **Ca^{2+} significantly reduced the rate of the increase in D-CaM fluorescence** (Figure 4.4. B and C). The Ca^{2+}-dependency of the rate of *trans* binding was clear at every protein concentration tested. Additionally, the apparent binding affinity was lower in the presence of Ca^{2+} for all the constructs tested (Yus-Najera et al., 2002; Bonache et al., 2014; Alaimo et al., 2017).

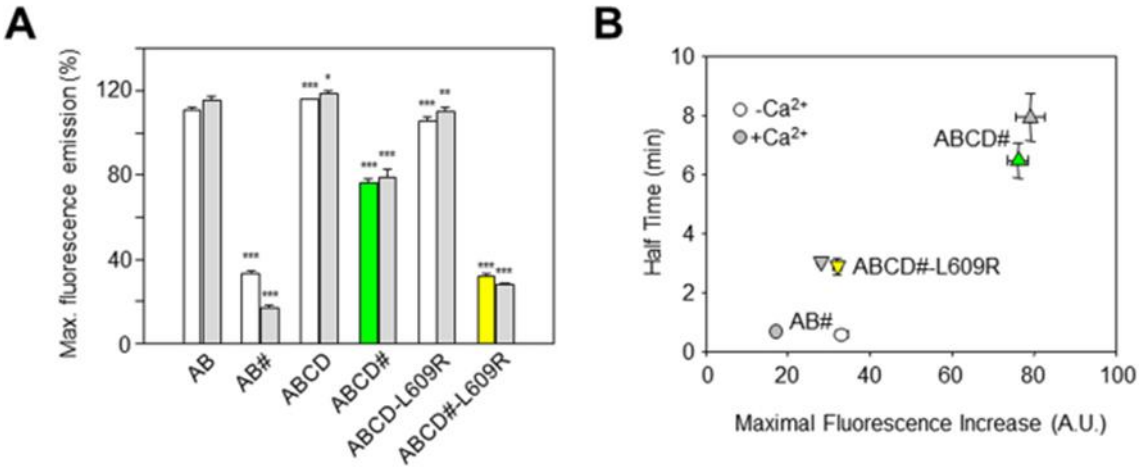

Figure 4.5. Summary of the maximal D-CaM fluorescence emission. (**A**) Maximal increases in D-CaM fluorescence emission induced by saturating concentrations of the indicated proteins. The data were collected in the presence (gray bars) or absence of Ca^{2+} (white; and in yellow and green bars for ABCD≠ and ABCD≠-L609R to stand out these results) (n≥3). Asterisks indicate significantly different values versus AB: *p<0.05; **p<0.01; ***p<0.001. (**B**) Plot of the time to reach the half-maximal D-CaM fluorescence versus the maximal increase in fluorescence. The symbol # indicates an equimolar mixture of the A343D and S511D mutants.

Finally, the **maximal increase in fluorescence was reduced in the complementation assay** (AB *vs* AB#, ABCD *vs* ABCD#, ABCD-L609R *vs* ABCD#-L609R; Figure 4.5.A), which was partially related to the kinetics of the increase in D-CaM fluorescence (Figure 4.5.B). Precluding *cis*-binding mode caused a reduction of about 25% in the maximal D-CaM fluorescence, as revealed by comparing ABCD and ABCD# (Figure 4.5). Except for AB#, the magnitude of this reduction was not affected by Ca^{2+} and it was larger (>65% reduction) when the tetramerization domain was absent (AB *vs* AB#) or when there was a mutation that was expected to preclude helix D coiled coil formation (ABCD *vs* ABCD#-L609R).

4.3.2. Subunit exchange between FP-ABCD/CaM tetrameric complexes is affected by calcium.

Results with GST-AB and functional complementation of mutant hA and hB indicate the formation of a *trans* configuration. To assess how helix D-mediated tetramerization affects exchange and to gain further insight into the relationship between CaM binding and tetramerization of the wt ABCD domain, the interchange between tetrameric assemblies was monitored by FRET. Two versions of the ABCD domain tagged at the N-terminus were produced in the presence of CaM, one tagged with a cyan fluorescent protein, (the CFP turquoise2 variant), and another tagged with a yellow FP (the YFP citrine variant) (Figure 4.7). It was previously shown that these proteins behave as tetramers with 4:4 ABCD/CaM stoichiometry.

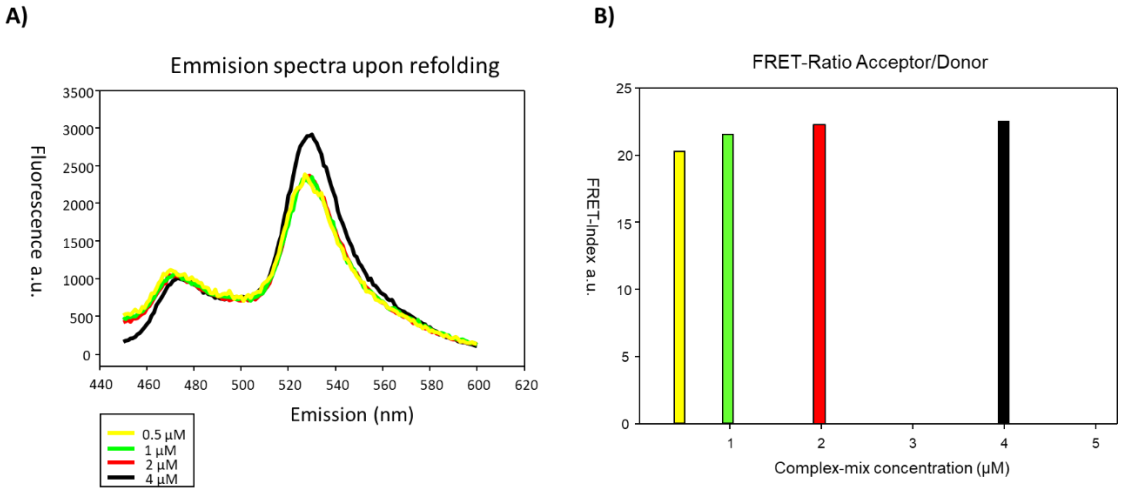

Figure 4.6. Unfolding with UREA and refolding. (A) CFP-hABCD and YFP-hABCD tetramers were mixed at equimolar concentrations (0.5, 1, 2 and 4 µM) and unfolded adding 6M urea. After dialysed in Fluorescence Buffer, and purified by Gel Filtration, samples were diluted or concentrated to 500 nM and emission spectra of each sample was measured exciting at 433 nm. **(B)** FRET-Index of different sample-concentration, after the refolding.

First, to estimate **the maximum FRET index**, we hypothesised that urea-denatured proteins will assemble randomly after removal of urea to promote refolding of the proteins. Therefore, we proceeded to denature the tetramers by adding 6M urea. We did the experiment at different concentrations of protein-mix: 0.5, 1, 2 and 4 µM, to analyse how the concentration of the sample could affect the maximum-FRET obtained.

After the unfolding with urea, samples were dialyzed against fluorescence buffer in order to get rid of the urea. After performing Gel Filtration with a Superdex 200 26/60, to eliminate multimers and monomers and keep the sample corresponding to the tetramer, the FRET index was measured, as described above.

The FRET-index (YFP/CFP) was similar in all concentrations tested: 2.1 ± 0.02 for 0.5 µM, 2.1 ± 0.05 for 1 µM, 2.2 ± 0.08 for 2.5 µM and 2.2 ±0.1 for 4 µM. Thus, the effect of the sample concentration on the maximum-FRET-index obtained is negligible in the range tested.

Note that according to the binomial distribution the tetramers refolded after denaturalization with urea are expected to be distributed in different compositions: (1) 3/8 formed by two CFP-hABCD and two YFP-hABCD subunits, (2) ¼ composed by three YFP and one CFP-hABCD, (3) ¼ composed by three CFP- and one YFP-hABCD, and (4) 1/16 will be entire tetramers of YFP-hABCD and (5) 1/16 will be CFP-hABCD subuinits.

After obtaining an approximation of the FRET that we can achieve after a 100% exchange, we carried out the experiment incubating the tetramers at equimolar concentrations of 0.5, 1, 2.5 and 4 µM (Figure 4.9). Thus, both tetramers were mixed, and the emission was measured for 45 min. There was a time dependent increase in the 530 nm emission of the acceptor upon excitation at 436 nm, suggesting that **exchange between subunits of tetrameric complexes was taking place.** The development of FRET over time in an equimolar mixture of the CFP-ABCD/CaM complex

(donor) and the YFP-ABCD/CaM complex (acceptor) is shown in Figure 4.8 The time to reach the half maximal FRET index was 12.2 ± 1.6 min for a 500 nM mixture. Assuming that the exchange between the ABCD domains is the rate-limiting step, the complementation and FRET assays, comparing between the rates obtained under both paradigms (complementation assay and subunits exchange) would seem to be feasible.

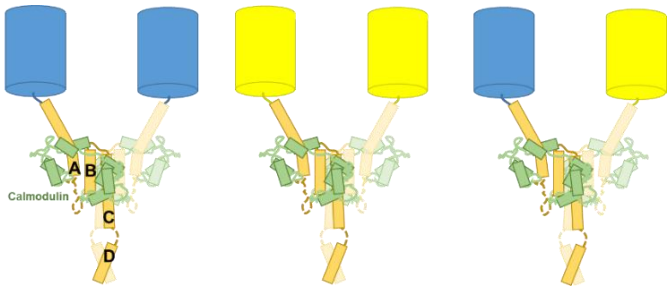

Figure 4.7. Cartoon representing the experiment: the CFP-ABCD/CaM complex was mixed with YFP-ABCD/CaM, resulting in an exchange of proteins that led to the development of FRET. Only two subunits of the tetrameric complexes are drawn for clarity.

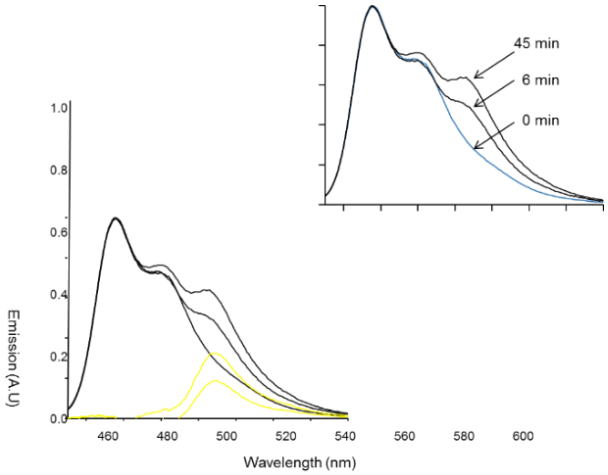

Figure 4.8. Emission spectra of an equimolar mixture at 2.5 µM. Normalized emission spectra of a mixture of 2.5 µM CFP-ABCD/CaM and 2.5 µM YFP-ABCD/CaM at different times. The yellow traces are the results of subtracting the normalized CFP (blue).

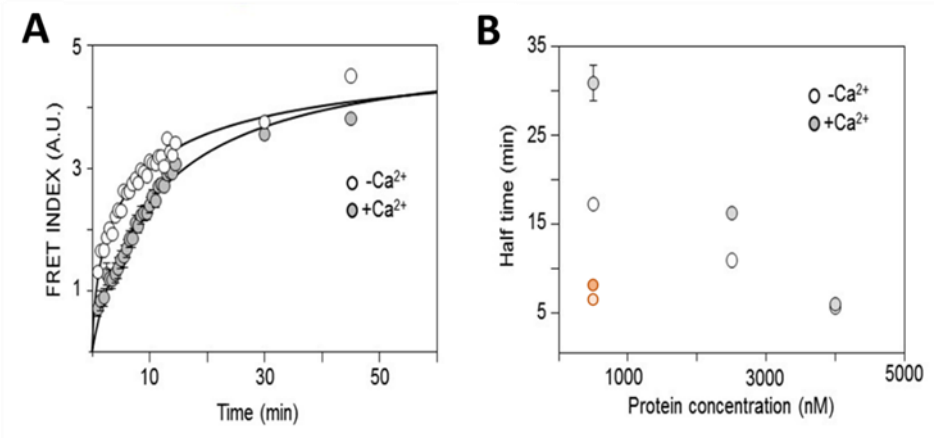

Figure 4.9. (**A**) Time course of the increase in the FRET index from a 2.5 µM CFP-ABCD/CaM and 2.5 µM YFP-ABCD/CaM mixture in the presence (gray circles) and absence (white circles) of Ca^{2+}. Each trace represents the average of 3 experiments. (**B**) Relationship between the time to reach the half-maximal increase in the FRET index and the protein concentration in the presence (gray circles) and absence of Ca^{2+} (white circles). In orange are represented the values of the complementation assay (Figure 4.4). Each point represents the average of 3 or more experiments.

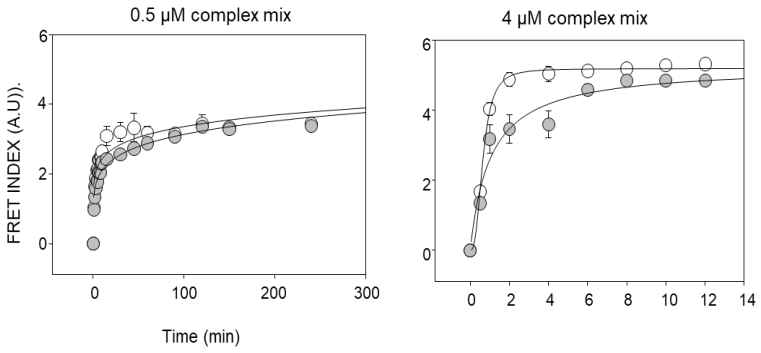

Figure 4.10. Time course of the increase in the FRET index from a 0.5 µM mixture (left) and 4 µM mixture (right) in the presence (gray circles) and absence (white circles) of Ca^{2}Each trace represents the average of 4 experiments.

The time-course of FRET development was **sensitive to Ca^{2+},** in presence of this cation, the EC_{50} is reached at later times compared to the sample without calcium: 17.2 ± 0.8 min. in absence and 30.8 ± 2.1 min. in presence of Ca^{2+} (Figure 4.9, half time with and without Ca^{2+}). Thus, the interchange between subunits was slower in presence of this cation, suggesting that the tetramers are **more stable** in this condition. This is similar to the results obtained in the complementation assay to monitor *trans*-binding (Figure 4.5), where it was demonstrated that the ABCD/CaM complexes were more stable in the presence of a physiologically relevant Ca^{2+} concentration, probably through the binding of this cation to CaM.

However, the FRET values obtained after 45 min incubation were strikingly low. In the Time-course experiment at 4 µM, after 45 min incubation, the FRET-ratio was 0.8 ± 0.04 in absence of

Ca^{2+} and 0.7 ± 0.05 in presence. This is notably lower that the maximum estimated after unfolding and refolding of the tetramers, were FRET Index exceeds 2.2 (Figure 4.6). This means that the exchange between subunits is slow-paced, and after 45 min incubation, only few subunits were exchanged.

The effect of the Ca^{2+} on the stability of the tetramers is particularly remarkable, considering that helix D and the AB CaM-binding domain lie more than 20 Å apart according to cryo-EM images, with no evidence of direct physical interactions between helix D and either CaM or the AB domain (Sun & MacKinnon, 2017).

4.3.3. The time-course of CaM exchange between FP-AB/CaM-FP complexes. The interchange is not carried out either in the absence or in the presence of a Ca^{2+}.

There is some controversy regarding the dynamic of CaM binding. In one view, CaM is regarded as a structural element of the channel, whereas in another view CaM is coming in a out of the channel. In order to understand better the relationship between CaM and CaM binding domains of $K_V7.2$ channels, the interchange between CaM was monitored by FRET. The AB domain was tagged at the N-terminus with cyan (the mTFP1 variant), and two versions of the AB:CaM complex were produced and purified: one with WT CaM (label free) and another tagged with CaM-YFP (the YFP Venus variant) fluorescent protein.

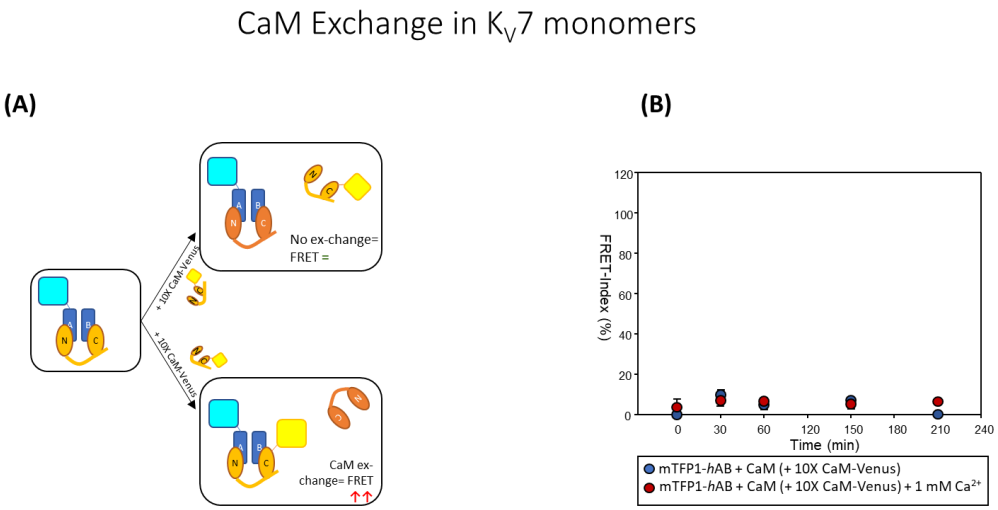

Figure 4.11. CaM exchange in $K_V7.2$ monomers. (A) Cartoon representing the experiment: the CFP-ABCD/CaM complex was mixed with CaM-YFP, to analyse if there is an exchange of proteins that led to the development of FRET. **(B)** Time course of the FRET-ratio in mTFP-Q2*h*AB:CaM (500 nM) complex upon the addition of 5 µM CaM-Venus. Blue circles represent the sample in absence of Ca^{2+} and red ones in presence of 1 mM free Ca^{2+}. The data represent the means ± SEM from 4 independent experiments.

The mTFP-*h*AB:CaM complex was mixed with CaM-Venus at 10 times higher concentration, 500 nM and 5 µM respectively. After mixing both proteins, we quantified the transfer of energy, by

exciting mTFP1 (458 nm) and measuring the emission from 470 to 570 nm. If there is an exchange between CaM we would see a development in FRET. The development of FRET over time (3 hours) in a mixture of the CFP-*h*AB/CaM complex (donor) and 10 timers more CaM-YFP complex (acceptor) is shown in Figure 4.11. The FRET-Index did not vary during incubation time. We assume that there is **no exchange between CaMs**, neither in the presence nor in the absence of Ca^{2+}. Similarly, when we mixed the complex mTFP1-Q2hAB:CaM-YFP with 10 times CaM, we did not see a reduction in FRET after 3 hours of incubation, as it was expected if there was an exchange between CaMs (Figure 4.12). In this case, the FRET ratio is lower in presence of Ca^{2+}, but it is because of the conformation of the complex and not due to an exchange between CaMs, as it is described in the first chapter.

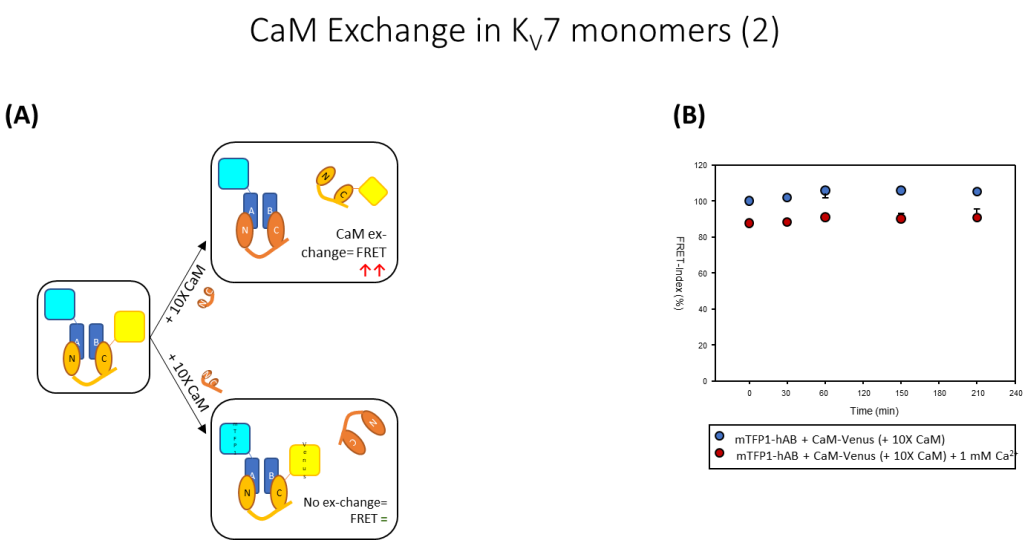

Figure 4.12. CaM exchange in $K_V7.2$ monomers (2). **(A)** Cartoon representing the experiment: the CFP-ABCD/CaM-YFP complex was mixed with CaM, to analyse if there is an exchange of proteins that leds to a reduction of FRET. **(B)** Time course of the FRET-ratio in mTFP-Q2*h*AB:CaM-Venus (500 nM) complex upon the addition of 5 µM CaM. Blue circles represent the sample in absence of Ca^{2+} and red ones in presence of 1 mM free Ca^{2+}. The data represent the means ± SEM from 4 independent experiments.

4.4. DISCUSSION

Here, we investigated the contribution of helix D in CaM binding. Previously, the presence of helix D had been shown to promote CaM binding in $K_V7.2$ channels, probably because of coiled coil structure (Figure 4.1). This is particularly remarkable, considering that helix D and the AB CaM-binding domain lie more than 20 Å apart according to cryo-EM images, with no evidence of direct physical interactions between helix D and either CaM or the AB domain (Sun & MacKinnon, 2017).

In this chapter we present evidence supporting the notion that the coiled coil formed by helix D distal to the AB CaM-binding module indirectly favors *trans*-binding of CaM to $K_V7.2$, and that CaM binding stabilizes the tetrameric C-terminal assembly. Remarkably, it appears that the tetrameric assembly is sensitive to Ca^{2+}, becoming more stable in the presence of this cation.

Thus, our data reveal an important reciprocal crosstalk between CaM-binding and the subunit-recognition domains of K_V7 channels. We introduced the **coiled coil disrupting L609R mutation** in Q2*h*ABCD protein. This protein could be subjected to binding analyses using D-CaM, a dansylated derivate that reports conformational changes of CaM as an increase in fluorescence emission upon binding to a target protein (Alaimo et al., 2013). Interestingly, comparing with WT ABCD, **the time to reach maximal fluorescence and the magnitude of the maximal change were reduced.** In addition, the apparent **binding affinity was lower** compared to ABCD# (equimolar mixture of a helix A mutant and an helix B mutant) (Ec50 = 45.5 ± 3.8 nM). Thus, the changes in apparent affinity failed to explain the differences in kinetics. There were no significant changes in D-CaM fluorescence emission upon addition of the helix B S511D mutant (Alaimo et al., 2013).
When comparing data obtained with ABCD and ABCD#, it should be considered that ABCD# could adopt either a configuration displaying the same number of CaM binding sites as ABCD or only half the binding sites. If both binding modes were present in equal proportions, the maximal fluorescence for ABCD# should be about 75%, not far from the value observed. **The simplest explanation is that the absence of helix D or its disruption by the L609R mutation reduced the stability of AB-CaM* in the *trans*-binding mode.**

To gain further insights into the relationship between CaM binding and tetramerization of the WT ABCD domain, the interchange between tetrameric assemblies was monitored by FRET. We produced two versions of the ABCD domain tagged at the N-terminus with cyan (the CFP turquoise2 variant) or yellow (the YFP citrine variant) fluorescent proteins and were mixed in equimolar concentration. These conditions do not distinguish the CaM binding mode and indeed, they could support both *cis*- and *trans*-CaM binding. After mixing both proteins, there was a time dependent increase in the 530 nm emission of the acceptor upon excitation at 436 nm, suggesting that **exchange between subunits of tetrameric complexes was taking place**. The time to reach the half maximal FRET index was 12.2 ± 1.6 min for a 500 nM mixture. Assuming that the exchange between the ABCD domains is the rate-limiting step for both the complementation and FRET assays, comparing between the rates obtained under both paradigms would seem to be feasible. The time to reach the half maximal FRET at 500 nM was about twice that for ABCD# proteins at 400 nM. When the donor and acceptor concentration was raised 5-fold (2.5 µM), the time to reach half maximal FRET was reduced to 6.9 ± 0.2 min, comparable to the 6.5 ± 0.1 min half-time observed in the *trans*-binding assay at 400 nM (Alaimo et al., 2017). Thus, the introduction of mutations into the CaM binding site led to a faster exchange (in the complementation assay), meaning that those mutations perturbed the stability of the tetrameric assembly.
In addition, here, the time-course of FRET development was sensitive to Ca^{2+}, taking longer to reach the half-maximal value in the presence of this cation (Figure 4.9). This is similar to the response in conditions designed to monitor *trans*-binding (Figure 4.5), indicating that the **ABCD/CaM complexes were more stable in the presence of Ca^{2+}.**
Our data shows that exchange between ABCD domains does occur in solution, yet how the transmembrane region of the channel, absent in the isolated domains, influences the exchange and flexibility of the assembly domain remains unclear.

Finally, to study how the interchange between $K_V7.2$ subunit and CaM occurs we made other FRET experiment. To examine the stability of the complex, free CaM was added. We incubated at room temperature and emission fluorescence was recorded every 30 min. However, changes in

FRET were not observed, nor in absence neither in presence of Ca^{2+} (1 mM), suggesting that **there is not an exchange between CaM in this complex** in this time frame. This means that even if an exchange between subunit can occur, CaM remains bound to the channel by at least one of the two lobes, presumably the interaction between the helix B and N-lobe, for which it has described greater affinity (Alaimo et al., 2014).

How can we explain the switch between *cis* and *trans* binding in the tetramer, and at the same time the lack of exchange of CaM?

We should consider that the switch between *cis* and *trans* binding in the tetramer does not necessarily imply an exchange of CaM molecules. It is possible that one CaM lobe remains bound to one helix (most likely, helix B and the N-lobe), whereas the other lobe (e.g. the C-lobe) binds to the complementary helix (e.g. helix A) of alternating subunits.

Nevertheless, the functional results suggest that the *trans* configuration would be a minority.

Besides, our data reveals that helix D-dependent coiled coil formation stabilizes the interaction between CaM and helices A and B (Figure 4.5). The tetrameric structure of $K_V7.1$ resolved by Sun & MacKinnon reveals interactions between Helix C and CaM C-lobe (Sun & MacKinnon, 2017), which could contribute to a more solid structure. This stabilization may arise in part from the geometric configuration, by helix D promoting the formation of a more compact AB/CaM ring under the pore, which in turn could allow CaM to engage helices A and B in different modes of binding, such as the *trans*-binding configuration. At the same time, CaM influences the stability of the tetrameric helix D coiled coil, conferring Ca^{2+}-dependency to the assembly of the C-terminal domain. The results are consistent with a model that involves active reciprocal coupling between the A-B module and the tetramer formed by helices D, CaM and Ca^{2+} thereby influencing the dynamic behaviour of the helix D coiled coil.

The results presented here are also able to explain the role of CaM and the calmodulation mechanism associated with the Ca^{2+}- gating of the $K_V7.2$ channel. As we have mentioned before, the $K_V7.2$-*h*AB complex subunit cannot be purified in the absence of CaM due to aggregation followed by precipitation. Moreover, CaM's affinity for the channel is so high that the complex cannot be dissociated by any of the *in vitro* conditions we have tested. Likely, this is also the case *in vivo,* due to the high intracellular concentration of CaM (10^{-6} - 10^{-5} M) (Ching & Mean, 2000). All together, these results suggest that **CaM associated to $K_V7.2$ may become consubstantial to the channel's integrity once both molecules interact**. This situation is similar to the homologous channel $K_V7.1$ where a constitutive binding role was hypothesized (Sachyani et al., *2014)* and to other proteins like phosphorylase kinase (Ching & Mean, 2000). However, this model has been questioned since $K_V7.2$ channels, carrying a *h*B mutation, S511D (Gomez-Posada et al., 2011) that impede CaM binding, are functional. The preservation of function could be due to the adoption of *trans* CaM binding, which is favored when one of the CaM binding sites is mutated, as we have demonstrated. Note that, the S511D mutation is phosphomimetic. Phosphorylation of this site, could, somehow weakens the CaM-binding favoring *trans*-binding.

4.5. MATERIALS AND METHODS

4.5.1. Recombinant protein production

Protein expression and purification protocols for K_V7.2 helices AB and the helices ABCD fused to GST (GST-AB and GST-ABCD), the deletions and mutants (as indicated in the figures). Proteins were checked for purity by Coomassie brilliant blue staining of 10 or 15% SDS-PAGE gels. In order to exclude the presence of aggregates, the oligomerization state of the purified proteins was examined by dynamic light scattering (DLS) using a Zetasizer Nano instrument (Malvern Instruments Ltd.). Samples were filtered through 0.22 µm membrane filters (Millipore) and centrifuged at 13,000 g for 10 min. Samples placed onto single use plastic cuvettes were maintained at a fixed temperature of 25 °C. The protein concentration was 1 mg/ml and the buffer used was Tris-HCl 20 mM, NaCl 100 mM [pH 7.5]. Measurements were made at an angle θ = 90° to the incident beam and the data were collected every 60 s. The correlation functions were analyzed to obtain the distributions of the decay rates and hence, the apparent diffusion coefficients, and ultimately the distributions of the hydrodynamic radius of the scattering particles in solution were obtained via a Stokes-Einstein equation. Finally, the monodispersity or polydispersity of the solutions was assessed, and the molecular weights of the predominant species were calculated.

4.5.2. Fluorometric measurements using dansyl-CaM

Dansyl-CaM production

- CaM purification

From the Petry dish, 10 ml of LB were inoculated with cells from a single colony O/N at 37 oC in presence of the appropriate antibiotics. Next day, a 1:50 dilution was performed into a 1 L of LB media with antibiotics. Bacteria were grown until OD600 reached 1. Afterwards, IPTG was added into a final concentration of 0.4 mM. Protein expression was done at 37 ^{o}C for 6 h. Cells were harvested by centrifuging at 5300 g for 15 min. SN was discarded. Cells were resuspended in 50 ml of *lysis buffer* (50 mM Tris-HCl pH 7.5, 2 mM EDTA and 0.2 mM PMSF).

Cell lysis was carried out by 3 passes through French press machine (Avestin, Emulsiflex-C5) Lysated sample was submitted to 3 cycles of freezing and defrosting using dry ice with EtOH and a water bath at 37 °C. Due to the reversible thermostability of CaM, this process does not affect CaM integrity. Sample was centrifuged at 25000 g for 30 min. SN was later heated at 70 °C for 10 min. Sample was centrifuged again at 25000 g for 30 min. The SN was directly poured into 10 ml of Phenyl-Sepharose resin which was previously pre-equilibrated with 10 CV of e*quilibrium buffer* (50 mM Tris-HCl pH 7.5, 5 mM CaCl2, 0.1 M NaCl). The flow-through was again loaded into the column. The second flow-through was stored and a first wash was done using 20 CVs of *wash buffer* (50 Mm Tris-HCl pH 7.5, 0.1 mM CaCl2, 0.1 M NaCl). The column was washed again with 10 CVs of *high salt buffer* (50 Mm Tris • HCl pH 7.5, 0.1 mM CaCl2, 0.5 M NaCl). Finally, the protein was eluted using *elution buffer* (50 mM Tris-HCl pH 7.5, 1 mM EGTA). During the purification, aliquots were saved from each step, that were used for SDS-PAGE gel analysis (with Coomassie staining). The interest fractions were selected, dialysed using dialysis cellulose membrane (Sigma-Aldrich, Ref.: D927-100FT) against ddH2O. Protein was then concentrated using Amicon Ultra-15

centrifugal filter units with a 3 kDa cutoff (Sigma-Aldrich, Ref.: Z677094-24EA) and protein concentration was measured using NanoDrop 3300 (ThermoScientific, Ref.: ND-3300).

- CaM dansylation

CaM was diluted to 1 mg/ml in 10 mM Tris-HCl (pH 8.5) and 2 mM of $CaCl_2$ buffer. Dansyl chloride (2.17 mg/ml dissolved in acetone) (Sigma-Aldrich, Ref.: 39220) was added to a final concentration of 100 µM. Incubation was done in the dark and at room temperature for 2 h vortexing every 20 min. The dansyl excess was eliminated using a 1 ml G-25 sepharose column (Sigma-Aldrich, Ref.: G25150).

Fluorescent dansylated CaM (D-CaM, 5-(dimethylamino)naphtalene-1-sulfonyl-calmodulin) was prepared using recombinant CaM and dansyl chloride, as described previously (Alaimo et al., 2013). Prior to the experiments, D-CaM and other proteins were dialyzed for 48 h against 2 L of the Fluorescence buffer containing Tris-HCl 25 mM [pH 7.4], KCl 120 mM, NaCl 5 mM, $MgCl_2$ 2 mM, EGTA 10 mM, changing the buffer every 12 h. Steady-state fluorescence measurements were obtained at 25 °C on an Aminco Bowman series 2 (SLM Aminco) fluorescence spectrophotometer in a final volume of 100 µl (using quartz cuvettes). Time course experiments were performed at 25 °C and 37 °C, with excitation at 340 nm and emissions recorded from 400 to 660 nm (titration experiments) or at 500 nm (time trace). Slit widths were set at 4 nm for excitation and 4 nm for emission.

Titration experiments were performed by adding increasing concentrations of each fusion protein to a cuvette containing D-CaM (12.5 nM) in Fluorescence buffer. Experiments were also performed in the presence of an excess of free Ca^{2+} (3.9 µM) by adding 9.63 mM Ca^{2+} to the Fluorescence buffer. The free Ca^{2+} concentration was determined using Fura-2 (Invitrogen), following the manufacturer's instructions.

For the time course experiments, the dansyl emission of D-CaM (at 500 nm) was measured as a function of time (min). In these experiments, a mutated protein (400 nM) was added to a stirred cuvette containing D-CaM (12.5 nM) in Fluorescence buffer (in the presence or absence of Ca^{2+}) and after two minutes, another mutant (400 nM) was added. Finally, the experiments involving GST-AB wt and GST-ABCD wt were conducted by adding 400 nM of these proteins to D-CaM (12.5 nM).

Fluorescence enhancement was plotted against the protein concentration to generate the concentration-response curves, or in the case of the time course experiments, it was plotted against time (min) to obtain the time-response curves. The parameters of the Hill equation were fitted to the data by curvilinear regression, enabling the apparent affinity (EC_{50} or concentration that gives half-maximal change in the intensity of the fluorescence emission) or the t_{50} (half-time or time that gives half-maximal change in the intensity of fluorescence emission). The data are shown as the average of 3 or more independent experiments.

4.5.3. FRET

Fluorescence resonance energy transfer (FRET) measurement is relatively easy to set up, yet is a powerful method; it can visualize substrate binding and dissociation as well as intramolecular structural changes within a single molecule in real time.

FRET techniques have been widely used for measuring the dynamics of biomolecules because of its high sensitivity as a nanoscale distance sensor. Between two closely located fluorescent molecules, energy in an excited donor fluorescent probe is resonantly transferred to an adjacent acceptor fluorescent probe, thereby decreasing the donor's fluorescence intensity, and increasing the acceptor's fluorescence intensity. The efficiency of this energy transfer is inversely proportional to the sixth power of the distance between the two fluorescent molecules. Accordingly, FRET is an extremely sensitive measurement system for detecting changes in the distance between two fluorescent probes, particularly around what is called the Förster distance, namely, a distance that yields a FRET efficiency of 0.5 (4–7 nm for a pair of typical fluorescent probes) (Lakowicz 2006). As such, FRET measurement is ideally suited for detecting changes in the distance between domains or subunits within a protein or nucleic acids during conformational changes. Moreover, based on the ratio of fluorescence intensities of two fluorescent molecules, it can achieve high signal-to-noise ratio in measurements of binding and dissociation reactions compared with measurements involving a single fluorescent molecule. These advantages have made FRET an extensively used technique for researching the dynamics of biomolecules.

More information about this technique is brought up in chapter 3.

4.5.4. mTurquoise2 and mCitrine as FRET-pair

The fluorescent mTurquoise2 (donor) and mCitrine (acceptor) proteins were fused to the N-terminal of K_V7.2-ABCD (residues 310-653) and cloned into a pProEX-HTc plasmid (Invitrogen) that introduces a 6xHis N-terminal tag. CaM was cloned into the co-expression compatible plasmid pOKD4 and both plasmids were co-transformed by electroporation in BL21(DE3) cells (Novagen) as described above. Cells were grown at 37 °C in 1 L of LB medium containing ampicillin and kanamycin until an A600 = 0.6–0.8 was reached. The expression of the fusion proteins was induced with 0.3 mM of IPTG O/N at 20 °C. The cells were then harvested by centrifugation at 9,000 g for 9 min and re-suspended in 25 ml of Buffer A (KCl 120 mM, K-HEPES 50 mM [pH 7.4], imidazole 20 mM, DTT 500 µM, PMSF 1 mM, protease inhibitor EDTA free: Roche, Ref. 04693132001). After lysis by sonication (15 s ON, 15 s OFF, 10 cycles), the slurry was centrifuged at 25,000 g for 30 min, and the supernatant was filtered (0.20 µm) and transferred to a clean tube. The complex was affinity purified from the supernatant using a His-Trap-talon column and equilibrated with FRET buffer (KCl 120 mM, Hepes 50 mM, NaCl 5 mM, EGTA 5 mM). The fractions containing soluble monomeric C-terminal proteins were identified by SDS-PAGE. Size-exclusion chromatography was performed using Superdex 200 pg 26/60 column (GE Healthcare, ref. 28–9893) pre-equilibrated with KCl 120 mM, HEPES 50 mM [pH 7.4], NaCl 5 mM and EGTA 5 mM. Fractions containing the protein complex were concentrated using Amicon Ultra-15 centrifugal filter units with a 3 kDa cut-off (Sigma-Aldrich).

All FRET experiments were carried out on an Aminco Bowman series 2 (SLM Aminco) luminescence fluorimeter, using quartz cuvettes (light width 3 mm, 0.1 mL volume). The Ca^{2+} concentration was calculated using Maxchelator Ca-EGTA calculator v1.3 (maxchelator.stanford.edu/CaEGTA-TS.htm). The samples were centrifuged at 14,000 g for 10 min to remove any aggregates formed. Each sample was excited at 433 nm (4 nm slit) and the emission spectra was collected from 450 to 600 nm (4 nm slit). The emission spectra was

normalized to the peak emission at 476 nm. The normalized emission spectrum of turquoise2-ABCD was subtracted from each normalized spectrum resulting in the isolation of the normalized emission spectra from the acceptor. A FRET index was obtained as the integral from 524 to 538 nm of the normalized acceptor emission.

4.5.5. Statistics

The data are expressed as the mean±SEM and significant differences between the data ($p<0.05$) were evaluated with the Student's t-test: ***, significance at $p<0.001$, **$p<0.01$, and *$p<0.05$.

5. CONFORMATIONAL CHANGE AS A FUNCTION OF CALCIUM IN K_V7.2 TETRAMERS

5.1. INTRODUCTION

As we mention in the introduction, M-current takes its name because activation of muscarinic receptors suppressed a K^+ conductance in sympathetic neurons causing an increase in excitability. It was soon found that the second messenger cascade invariably involved activation of phospholipase C, with the associated production of IP_3 and release of Ca^{2+} from intracellular stores. Therefore, Ca^{2+} became a suspect, and some early work pointed at this second messenger as the main culprit for current inhibition. However, more than 20 years after the discovery of the M-current, the "mystery second messenger" was finally revealed (Suh & Hille, 2002). It turned out to be PIP_2, which is a co-factor absolutely required for KCNQ channel function. When PIP_2 levels drop, the VSD disengages from the PD, and the channel cannot be opened in response to voltage changes (Zaydman & Cui, 2014).

The effect of Ca^{2+} on M-current is complex. Modest increases enhance the current in sympathetic neurons, and suppression is seen at higher concentration (Marrion et al., 1991). M-channel activity is reversibly suppressed by Ca^{2+} in excised inside-out patches of sympathetic neurons, indicating that kinases or phosphatases are not mediating the effect (Selyanko & Brown, 1996). The rise of intracellular Ca^{2+} and CaM stimulation due to activation of the phospholipase C cascade in *Xenopus* oocytes expressing KCNQ2/3 heteromers causes an enhancement of the M-current, whereas Eag1 currents are completely suppressed (Gomez-Posada et al., 2011). Thus, Ca^{2+} can cause both **inhibition and potentiation** of neuronal KCNQ currents. In contrast, only potentiation of the cardiac IKs or KCNQ1 currents has been described (Tobelaim et al., 2017). It is generally assumed that CaM is directly involved in Ca^{2+}-dependent regulation of KCNQ channels, although only indirect evidences are available.

As we have mentioned in the general introduction, KCNQ channels present a VSD swapped 6TM architecture, with a long C-terminal tail that harbors five alpha helices (Sun & MacKinnon, 2017). They adopt an antiparallel fork configuration and tend to run under the VSD. A/B has been trapped at about 45˚ to the membrane in KCNQ1 channels, leaving room so CaM can be positioned between the AB fork and the VSD (Figure 5.1). Helix TW (or post-helix A), named this way due to the similarity to the SK2 C-lobe docking helix sequence, is located after helix A in a long and poorly conserved linker (Gomis-Perez et al., 2015). There is a sharp turn following helix B, so helix C goes perpendicular to the membrane forming a loose bundle between the four subunits, in line with the tendency of helix C to form weak dimers *in vitro* (Wiener et al., 2008). A flexible sequence with no conservation among KCNQ subunits follows to link with helix D that forms a coiled coil tetramer, a feature also observed in Eag1 and SK channels (Jenke at al., 2003). The global architecture is notably like that of SK channels, with the CaM C-lobe also engaging helix A almost with the same orientation, even at the lateral chain level (Zhou et al., 2001). However, the C-lobe lands into the proximal part close to the gate in KCNQ channels, the helix A/B fork is much shorter, and helices A and B are connected by a much longer flexible loop. Departing from the S-shaped CaM structures seen in other channels, CaM adopts a more compact C-shaped configuration, embracing the A/B fork, where helix A pairs with the C-lobe and helix B marry the N-lobe (Alaimo et al., 2014).

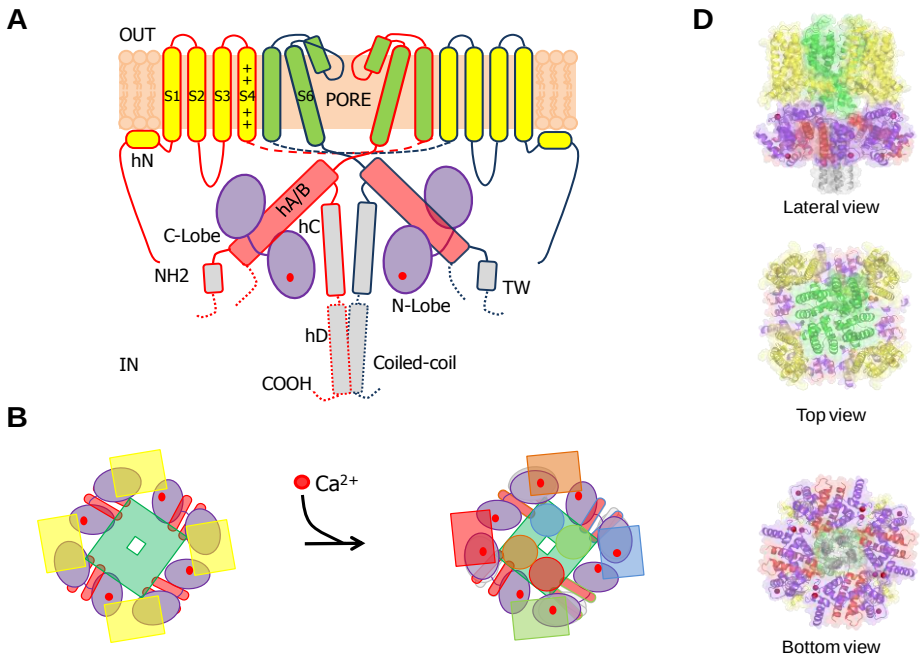

Figure 5.1. Representation of a KCNQ channel. A. Transmembrane regions are in yellow for the VSD, green for the PD and CaM is in purple. The cytosolic helix parallel to the membrane before S1 is labeled as hN. Helices A and B, colored in red, are at ~45˚ to the membrane under the VSD from the same of subunit. The border is colored red or blue to identify each subunit. To account for swapping, the VSD and PD of two different subunits are represented continuously. The presumed position of the tetrameric coiled coil is indicated with dashed lines. B. Realistic representation of the channel view from the top using the same color scheme as in A. Helices A and B are represented in red. On the right, upon Ca^{2+} loading (red dots) there is a small movement of helix A. Each subunit has a different color in this cartoon. D. Structures visualized using then PDB coordinates (5VMS), rendered with Pymol 1.30 using the same color scheme as in panel A. (From Nuñez et al., 2019)

The structure of the full-channel with Ca^{2+}-loaded CaM, resolved in 2017 by cryoEM, was captured in a configuration in which S4 is in the up position, but the VSD is disengaged from the PD. It has been assumed that this non-functional configuration represents the end stage adopted when plasma membrane PIP_2 levels drop (Sun & MacKinnon, 2017). In the cryo-EM particles and derived structures, four compact domains can be identified: the VSD, the PD, the CaMBD, and the distal tetrameric helix D coiled coil. However, the long linker between helix A and B is not seen in the atomistic model, and therefore it is not known if helices A and B come from the same or different subunits. The PD is in a closed configuration, very similar to that of other closed structures of potassium channels.

5.1.1. Calmodulin may act directly upon the S6 gate of KCNQ channels

Several structures of the isolated KCNQ CaMBD have been solved (PDBs: KCNQ1: 4V0C, 4UMO; KCNQ2: 6FEG, 6FEH; KCNQ2/3 chimera: 5J03; KCNQ4: 6B8L, 6B8M, 6B8N, 6B8P, 6N5W; KCNQ5: 6B8Q). All of them show a similar overall architecture with helix A engaging the C-lobe, and helix B docking into the N-lobe, matching the preferences for binding underscored in vitro (Alaimo et al., 2014). The first complex was crystallized without adding Ca^{2+}, but the N-lobe sites

where occupied, suggesting that the affinity for Ca^{2+} in the N-lobe increases when it is complexed with helix B of KCNQ channels, surpassing that of the C-lobe (Sachyani et al., 2014).

5.1.2. Current models of Ca^{2+} effect

Although the channel structure has recently been resolved (Sun & MacKinnon, 2017; 2019), there is still controversy over the conformational change as a function of Ca^{2+} in K_V7 channels.

A. Bernardo-Seisdedos et al., 2018. In this work the Calcium responsive domain (helices A and B) of $K_V7.2$ in complex with CaM were resolved in absence and in presence of Ca^{2+}, by NMR. Structural rearrangements of the CaMBD in KCNQ2 channels produced by Ca^{2+} show that the N-lobe/helix B complex remains almost unchanged, whereas the initial part of helix A bents by about **18° concomitant to a torsion of the C-lobe around the helix A axis.** This proximal helix A segment is attached to S6, close to the bundle crossing (Figure 5.2). It is very suggestive that the movement caused by Ca^{2+} is poised to affect the expansion of the S6 bundle crossing seen in a model for the KCNQ2 activated state (Gourgy-Hacohen et al., 2014).

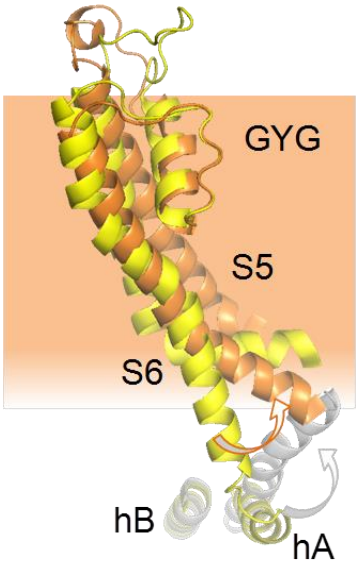

Figure 5.2. Possible direct gating transmitted from helix A to S6 in KCNQ2 channels. Comparison of the movement of S6 from a model (orange, Gourgy-Hacohen et al., 2014) of KCNQ2 opening with the position of helix A upon C-lobe Ca^{2+} loading (grey, PDB 6FEH). (From Nuñez et al., 2019)

B. Tobelaim et al., 2017 (Bernard Attali lab.). Protein pulldown, molecular docking, molecular dynamics simulations and patch-clamp recordings indicate that CaM embraces helices A and B with the apo C lobe and calcified N lobe, respectively. They suggest that at steady state, N-lobe is calcified and only the apo form of CaM C lobe can interact with $K_V7.1$ helix A. But in the presence of high Ca^{2+}, the calcified CaM **C lobe dissociates** from helix A, and CaM remains bound to the channel by the N-lobe to helix B.

C. Chang et al., 2018 and Xu et al., 2013 (Daniel Minor lab.). X-ray crystallographic analysis of $K_V7.4$ and $K_V7.5$ combined with small-angle X-ray scattering, biochemical, and functional studies, establish a regulatory mechanism for K_V7 CaM modulation. They confirmed observations first made by Attali and Hirsch (Tobelaim et al., 2017): the overall increase in volume of the CaMBD complexes caused by Ca^{2+} *in vitro vitro,* which arises from changes in the A-domain. They proposed that this volume increase could be due to **detachment of the C-lobe** from helix A or even helix A unwinding

(Figure 5.3). Therefore, this is an extension of Attali's model, adding to the proposed de-attachment of the C-lobe two new elements: unwinding of helix A and shutting of the gate, and biding of holo-C-lobe just upstream of helix B.

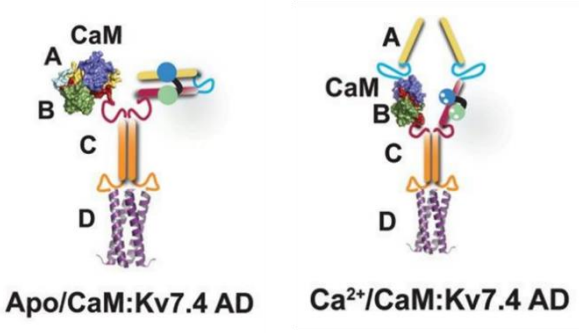

Figure 5.3. Calcium driven conformational change of K_V7 channels proposed by Chang et al., 2018. On the left $K_V7.4$ in absence of Ca^{2+}, showing a more compact structure. On the right, upon Ca^{2+} binding, where helix A releases from CaM (From Chang et al., 2018).

D. Archer et al., 2019. (Mark Shapiro's group): They proposed "**lobe-switching model**" for CaM regulation K_V7 channels. ITC, X-ray crystallography and HSQC techniques were to investigate the interactions between CaM and the A and B helices of the $K_V7.4$ subunit. They suggest that in response to increased Ca^{2+}, CaM undergoes lobe switching that imposes a dramatic mutually induced conformational fit to both the proximal C terminus of KCNQ4 channels and CaM, likely underlying Ca^{2+}-dependent regulation of KCNQ gating (Figure 5.4).

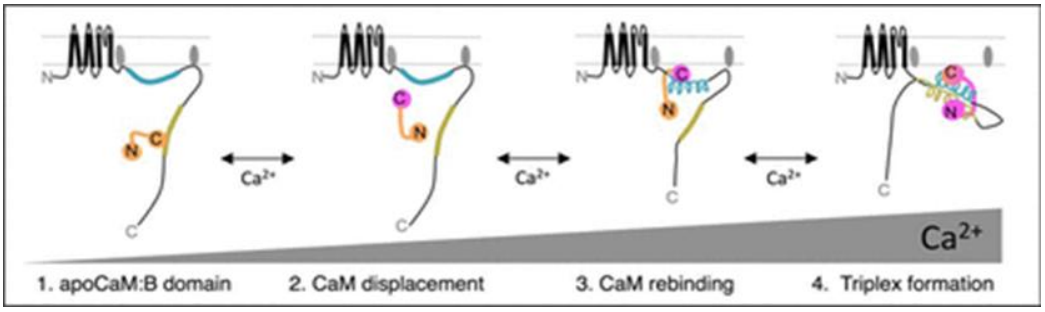

Figure 5.4. Proposed "lobe-switching model" for CaM regulation of neuronal KCNQ channels. 1. under very low (<10 nM) cytosolic $[Ca^{2+}]$ (a physiological state that we cannot determine), apoCaM is prebound to the B domain. Under such conditions, the A and B domains are likely disordered, not in a helical conformation. *2*, when $[Ca^{2+}]_i$ is in the range of that in cytoplasm in neurons at rest, Ca^{2+} first binds the EF-hands of the C-lobe, displacing CaM from the B domain. *3*, upon a rise in $[Ca^{2+}]$ in the proximity of the channel, the Ca^{2+}-bound C-lobe binds to the A domain with a K_d of ~400 nM, inducing an α-helical conformation to the A domain. *4*, in the final step, under a strong $[Ca^{2+}]$ signal (such as strong stimulation of certain $G_{q/11}$-coupled receptors), the EF-hands of the N-lobe become occupied by Ca^{2+} ions, enhancing its affinity for the B domain, inducing it into a helical formation, retaining C-lobe binding to the A domain (still a helix) (From Archer et al., 2019).

5.2. OBJECTIVES

A combination of techniques by different groups have been used to tackle the signal transduction mechanism used by CaM to regulate K_V7 channels. Every technique has its own limitations, in particular, most structural techniques can fail to detect flexible regions.

Furthermore, as we have shown in the previous chapter, helix D would be playing an important role in CaM binding.

Taking this into account, we proceeded to analyze the structural rearrangement driven by Ca^{2+}, in tetramers, adding the C and D helices to the constructions, which oversee mediating the tetramerization in these channels. To that, in addition to using FRET and NMR experiments, we also use HS-AFM, which allows us to obtain dynamics information in real time, in buffers that simulate the interior of the cell.

5.3. RESULTS

5.3.1. HS-AFM to analyse dynamics in the tetramer

Ca^{2+} titration in *h*ABCD:CaM tetramers bound to Streptavidin-Biotin 2D crystals:

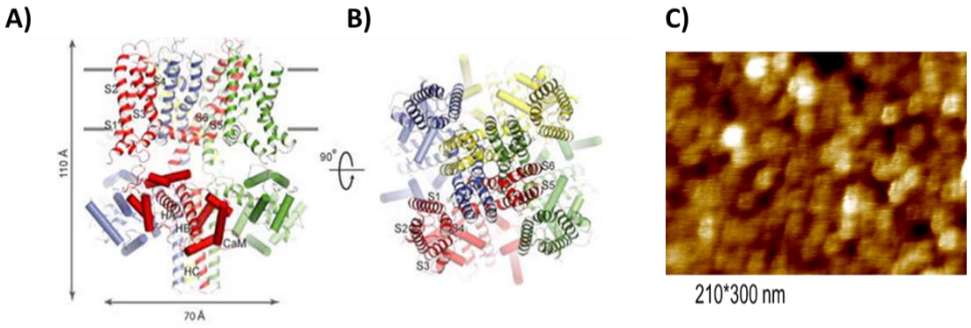

Figure 5.5. Ca^{2+} loaded complex of $K_V7.2$ tetramers, visualized by HS-AFM. (A-B) Side view and top view of the $KCNQ1_{EM}$/CaM complex. Each protomer is shown in a different color, and CaM is represented as cylinders. The S1-S6 and *h*A-*h*C are labelled (From Sun & MacKinnon, 2017). **(C)** Top view of KCNQ2 *h*ABCD/CaM complex recorded by HS-AFM.

Since it was challenging to fix the protein directly in the mica sheet (see supplemental 3) we used the strategy of Biotin-Streptavidin 2D crystals to immobilize the complex.

The protein was incubated in Biotin-Streptavidin crystals for 15 minutes.

Since the instrument is equipped with a small cantilever (Nanoworld 0.6) with resonant frequency of 1.5 MHz in water and spring constant of 0.6 N/m and a fast scanner with resonant frequency of 100–170 kHz in the Z-direction, we would have a resolution of 2–3 nm in the lateral direction (sub-molecular resolution for proteins) and ~1.5 nm in the vertical direction.

First, the tetramers are imaged in absence of calcium, for two minutes. Afterwards, titration was done by adding Calcium Buffer (120 mM KCl, 50 mM HEPES, 5 mM NaCl, 5 mM EGTA, 140 mM $CaCl_2$) sluggishly to the sample with a micropipette, to prevent disruption of the imaging process.

In the sample-chamber there were 100 µL of protein-buffer (120 mM KCl, 50 mM HEPES, 5 mM NaCl, 5 mM EGTA). As the sample chamber holds as much 130 µL, calcium Buffer was added in two injections of 5 µL. With the first injection, free Ca^{2+} reached 2 mM and 7 mM with the second, according to Maxchelator calculations (https://somapp.ucdmc.ucdavis.edu/pharmacology/bers/maxchelator/CaEGTA-TS.htm).

The image was recorded from the beginning to the end of the experiments, which was 5 min after the first Ca^{2+} injection.

Since HS-AFM produces large data sets of image sequences that are affected by a number of instrument-specific peculiarities (such as drift of the piezoelectric elements, contrast discontinuities along the fast- and slow-scan axes, feedback parameters, etc.) the image needed to be corrected in order to fix these instrument-specific hitches before any analysis is performed. In this case, we analysed the images using MATLAB following the protocol described by Zuttion and coworkers (Zuttion et al., 2018).
A marked change in the surface topography and 2D-crystal packing **was not observed**. Note, despite the fact that the transition in the 2D-crystal is significantly slowed down (~150s), and each image is taken at $1 s^{-1}$, each molecule in these frames (scanned by ~15 scan lines, where the full image contains 300 scan lines and thus the line acquisition speed is 3.3ms) existed for ~50ms in these images (Figure 5.5).

5.3.2. Conformational change analysed by FRET, comparation between monomer (Q2*h*AB:CaM) and tetramer (Q2*h*ABCD:CaM)

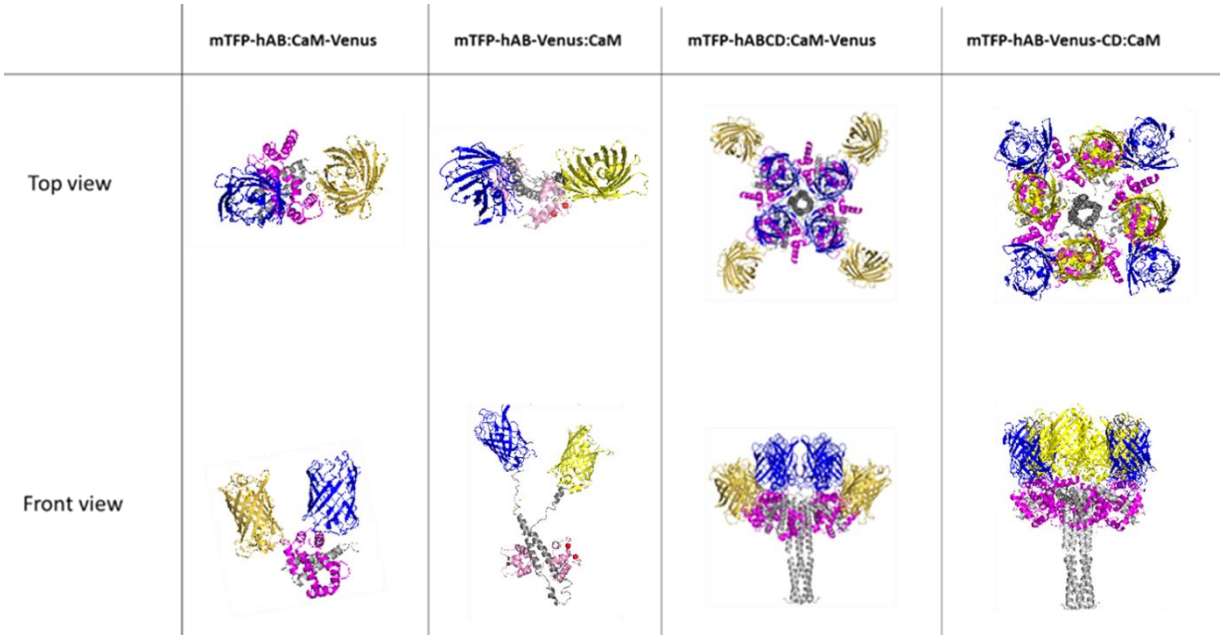

Figure 5.6. Schematic representation of FRET-complexes used in Ca^{2+} titrations, from top and front views. mTFP is represented in blue, Venus in yellow, CaM in purple and C-terminal of $K_V7.2$ in grey.

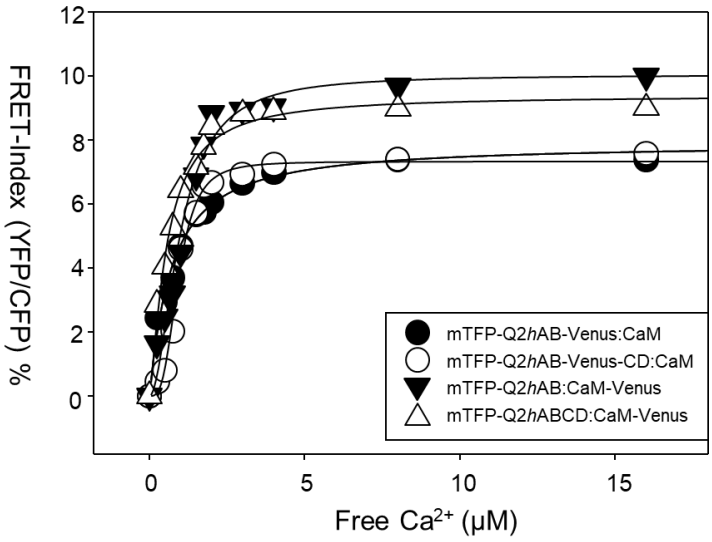

FRET-COMPLEX	Affinity E_c50 (nM)	RSQR
mTFP-Q2hAB-Venus:CaM	989 ± 75	0.98
mTFP-Q2hAB:CaM-Venus	695 ± 64	0.99
mTFP-Q2hAB-Venus:CaM	661 ± 40	0.99
mTFP-Q2hABCD:CaM-Venus	934 ± 34	0.99

Figure 5.7. FRET reduction ratios relative to the maximum excitation (Δ 491-5 nm) and emission peaks (Δ 525-9 nm). Ca^{2+} addition induces noticeable conformational changes (similar in magnitude) in the monomeric version (CaM/K_V7.2-*h*AB) or the tetrameric version (CaM/K_V7.2-*h*ABCD). A) Calcium titration in different FRET-sensor complexes. Ca^{2+} addition induces similar conformational changes in monomer (CaM/K_V7.2-*h*AB) and tetramer (CaM/K_V7.2-*h*ABCD), in both strategies. Additionally, the affinity for Ca^{2+} is also maintained at remarkably close values. Each plot represents the average of at least 3 independent experiments. B) Table summarizing the most important data from Ca^{2+} tritations of each strategy.

Ca^{2+} affinity for the C-lobe in CaM/K_V7.2-*h*AB has been determined by FRET: when two independent fluorophores are attached to K_V7.2-*h*AB, the abovementioned Ca^{2+}-gated conformational rearrangement produces a change in the FRET intensity (Figure 5.7). The FRET intensity as a function of the free Ca^{2+} concentration (as determined by fura-2, supplemental 1) provides an apparent affinity constant of 0.98 ± 0.07 µM for mTFP-*h*AB:CaM-Venus and 0.69 ± 0.06 µM for mTFP-*h*AB-Venus:CaM, consistent with other determinations in similar constructs (Alaimo et al., 2014). Similarly, the same assay done with tetramers show very close affinity values: 0.66 ± 0.04 µM in the case of mTFP-Q2*h*AB-Venus:CaM and 0.93 ± 0.03 µM for mTFP-*h*ABCD:CaM-Venus. Note, that FRET is overly sensitive technique, and the data we have obtained corresponds to a very slight movement. Calcium driven conformational change causes a FRET-Ratio reduction around 10% in the mTFP-*h*AB-Venus:CaM and mTFP-*h*AB-Venus:CaM complexes.

In the case of the mTFP-*h*AB: CaM-Venus constructs and its respective mTFP-*h*ABCD: CaM-Venus tetramer, although the **affinity is very similar** to that observed previously (0.95 ± 0.06 µM for mTFP-*h*ABCD/CaM-Venus and 0.75 ± 0.05 µM for mTFP-*h*AB-Venus-CD/CaM), **the reduction in FRET was even lower**, regarding to a smaller conformational change, as we expected. I that the

reduction observed in FRET-index could be **due to a small change in the orientation of the C-lobe**, and not due to a disruption between C-lobe of CaM and helix A, as other authors suggested (Chang et al., 2018, Archer et al., 2019).

5.3.3 $^{1}H,^{15}N$-TROSY-HSQC of the CaM/K_V7.2-*h*ABCD

To validate whether the observed changes are also present in a tetrameric architecture, we looked for Ca^{2+}-dependent conformational changes in a channel moiety that includes the regions responsible for tetramerization (helices *h*C and *h*D of the cytosolic C-lobe of K_V7.2).

NMR experiments provided further evidence that the Ca^{2+} dependent conformational changes are also present in the tetrameric complex. Needless to say, that homonuclear experiments suffer from spectral overlap, and thus render investigations of complex systems involving larger proteins such the case is challenging or unfeasible. The $^{1}H,^{15}N$–transverse relaxation optimized spectroscopy (TROSY)–heteronuclear single quantum spectroscopy (HSQC) of the CaM/K_V7.2-*h*ABCD (Figure 5.8) shows only a few peaks corresponding to residues from flexible regions, in good agreement with the spectrum of a tetrameric structure of more than 140 kDa.

The $^{1}H,^{15}N$-TROSY-HSQC of the CaM/K_V7.2-*h*ABCD (Figure 5.8) shows only a few peaks corresponding to residues from flexible regions, in good agreement with the spectrum of a tetrameric structure of more than 120 kDa. The methyl-TROSY spectroscopy (Wiesner & Sprangers, 2015) constitutes a proper alternative, suitable to study biomolecules with MW beyond 100 kDa. Consistently, the ^{13}C-δ-Ile methyl group HMQC spectrum of intCaM/K_V7.2-*h*ABCD displays the vast majority of residues. Despite the signal overlap, the superposition of intCaM/K_V7.2-*h*ABCD and intCaM/K_V7.2-*h*AB spectra (Figure 5.9) allows the assignment of the *hAB* δ-Ile residues in intCaM/K_V7.2-*h*ABCD. Noticeably, the spectrum for holoCaM/K_V7.2-*h*ABCD shows **the same Ca^{2+}-induced chemical shift perturbation** than holoCaM/K_V7.2-*h*AB (Figure 5.9), indicating that the ion dependent conformational changes are maintained in the tetrameric complex.

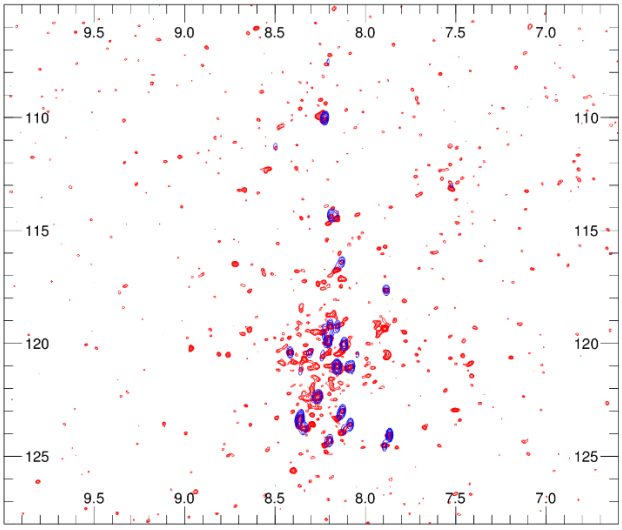

Figure 5.8. ^{15}N-HSQC spectra of Q2*h*ABCD:CaM protein complex. ^{1}H-^{15}N correlation of all amide groups are shown. In blue at the beginning of the experiment and in red at the end.

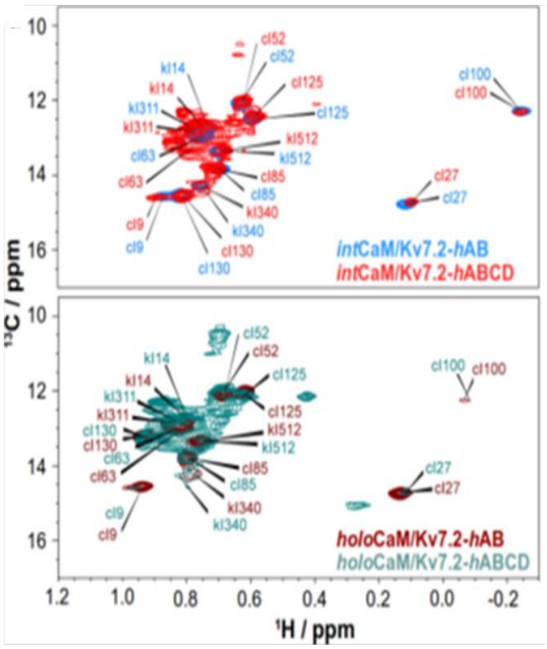

Figure 5.9. Conformational changes are also observed in tetrameric channel constructs. ^{13}C-δ-Ile region of the methyl-TROSY spectrum for intermediated CaM (only the N-lobe is Ca^{2+} loaded), *int*CaM/K_V7.2-*h*AB (blue, top), *apo*CaM/K_V7.2-*h*ABCD (red, top), *holo*CaM/K_V7.2-*h*AB (brown, bottom) and *holo*CaM/K_V7.2-*h*ABCD (green, bottom). The monomeric complex (CaM/K_V7.2-*h*AB) and the tetrameric assembly (CaM/K_V7.2-*h*ABCD) experience the same conformational changes triggered by Ca^{2+}. The assignment of the methyl peaks in *apo*CaM/K_V7.2-*h*AB was achieved by a combination of multiple 3D experiments, while the same peaks in *apo*CaM/Kv7.2-*h*ABCD are estimated by spectra overlap.

5.4. DISCUSSION

The conformational change of the complex after calcium binding was monitored by FRET, NMR and atomic force microscopy. To that purpose, two FRET sensors were created: mTFP1-*h*AB:CaM-Venus and mTFP1-*h*ABCD:CaM-Venus. While the first one creates monomers, the second one forms tetramers, since the helix D adopts coiled coil structure. Figure 5.7 shows how FRET analysis is sensitive to the conformational change occurring in the transition between *apo*CaM/K_V7.2-*h*AB and *holo*CaM/K_V7.2-*h*AB, when we analyse the movement between helices A and B (mTFP-*h*AB-Venus:CaM). The magnitude of such change is maintained in the K_V7.2-*h*ABCD:CaM complex (mTFP-*h*AB-Venus-BC:CaM). This result coincides with the model proposed by Bernardo-Seisdedos et al. (2018) where ion binding to the C-lobe produces a 17.9° rotation of the EF hands, displacing a segment of CaM (helices *h*5 and *h*8). This is allosterically transmitted to the channel moiety by modifying the orientation of helices *h*A and *h*B, with the subsequent conformational change that is allosterically transmitted up to the *pre-h*A element and likely to the trans-membrane region, ultimately resulting in the closing of the channel (Bernardo-Seisdedos et al., 2018).

Similarly, when the donor (mTFP1) is attached to the N-terminal of helix-A and the acceptor (mVenus) to C-lobe of CaM, Ca^{2+} binding provokes almost the same reduction in the ratio acceptor/donor (FRET-index YFP/CFP is reduced from 1.54 to 1.41). However, in the resolved structure by NMR, C-lobe remains bound to helix A also in holo-CaM/Q2hAB. If the C-lobe of CaM remains attached to the helix A both in the absence and in the presence of calcium, **how is a reduction in the FRET ratio explained after Ca^{2+} binding in this second complex?** Although there is no separation between helix A and C-lobe, a change in the orientation of fluorophores can occur, possibly caused by a turn in lobe C of the CaM, as we observed by NMR. If upon Ca^{2+} binding a dissociation between the C-lobe and the A-helix occurs, as it is suggested by other authors

(Tobelaim et al., 2017; Chang et al., 2018), we would observe a loss of FRET-index. Therefore, our results suggest that **C-lobe and helix A are held together after binding to Ca^{2+}.**

To analyse the conformational change as a function of Ca^{2+} in the tetramer by NMR we made a TROSY experiment. Since the tetramer in complex with CaM (Q2*h*ABCD DelY372-T501/CaM) has more than 140 KDa. Despite the signal overlap, the superposition of intCaM/K_V7.2-hABCD and intCaM/K_V7.2-hAB spectra (Figure 5.9) allows the assignment of the hAB δ-Ile residues in intCaM/K_V7.2-hABCD. Noticeably, **the spectrum for holoCaM/K_V7.2-hABCD shows the same Ca^{2+}-induced chemical shift perturbations as holoCaM/Kv7.2-hAB** (Figure 5.9), indicating that the ion-dependent **conformational changes are maintained in the tetrameric complex.**

It is necessary to state that neither by FRET nor by NMR we were able to see what occurs in the orientation of helices C and D.
In order to analyze the conformational change driven by calcium in K_V7.2 tetramers, we use HS-AFM. This technique allows the simultaneous assessment of structure and dynamics of single protein molecules in action. To immobilize Q2hABCD/CaM we use the Biotin-Streptavidin technique, as it is described in methods. The complex was visualized every-time during titration, starting at 0 and reaching 7 mM free Ca^{2+} (supplemental video 1).
We got a high-resolution image of the complex with calcium where it can detect isolated tetramers. After the image correction it is clearly observed **their square shape from a top-view upon Ca^{2+} addition, and a hole in the middle, presumably the pore.** This image matches with the cryo-EM structure of holo-CaM/K_V7.2 (Sun & MacKinnon, 2017) (Figure 5.5) both in size and in shape. In this structure, cytosolic A and B helices, which are connected to the S6 transmembrane helix, are sandwiched between the N- and C-lobes of CaM, in both apo- and holo-complex. During titration, no structural changes were observed. Taking into account that the resolution limit of the HS-AFM used is 10 Å, it is concluded that the conformational changes in the tetramer should be less than 10 Å, as we had seen by NMR and FRET (Bernardo-Seisdedos et al, 2018).

As we mention above, it has been long hypothesized that Ca^{2+} regulation is also driven by conformational changes derived from the interaction between Ca^{2+} and CaM. Several works have suggested that CaM's conformational change could be the mechanical switch required to open/close the pore depending on the Ca^{2+} levels (Tobelaim et al., 2017; Sun & MacKinnon, 2017; Bernardo-Seisdedos et al., 2018; Chang et al, 2018). Tobelaim and Chang´s models propose that loading of the CaM C-lobe releases the interactions with the A-helix. Chang et al additionally suggest that, consequently, the helix-A becomes disordered. They suggest that the C-lobe constitutes the moving part, whereas the N-lobe remains in place on the B-helix. This was also previously proposed (Xu et al., 2013). Similarly, Shapiro's group suggested recently a different model related to Ca^{2+}-dependent regulation of KCNQ gating (Archer et al., 2019). In response to increased Ca^{2+}, CaM undergoes lobe switching that imposes a dramatic mutually induced conformational fit. However, with our results obtained by HS-AFM, NMR and FRET, we were not able to see such transition between the open and closed state, nor an important conformational change as a function of Ca^{2+}. In this chapter, we provided extensive experimental evidence that **even such conformational change driven by Ca^{2+} does indeed occur, it is very slight.** We also assumed that the conformational change of helices A and B in complex with CaM is the same, both in the tetramer and the monomer. That is, the C-lobe of the CaM undergoes the same 17°

rotation after binding to Ca^{2+}, causing the same separation between helices. **Tetramerization does not change the signaling by Ca^{2+} in the channel.**

5.5. MATERIALS AND METHODS

5.5.1. FRET

A CaM mutant, unable to bind Ca^{2+} (CaM1234, D21A, D57A, D94A and D130A) was also cloned into a pOKD4 and cotransformed with mTFP1-K_V7.2*h*AB-Venus-YFP.

Additionally, mTFP1-K_V7.2*h*AB (residues 316-532) with the deletion ΔR374-K493 [Δ6L] and K_V7.2*h*ABCD (residues 316-845) with the deletion ΔR374-K493 [Δ6L] were cloned into pProEx Ht-C with CaM-Venus in pokD4 vector.

Recombinant protein expression and purification were done as described in Chaper 3.

A. Fluoresecence assay

Ca^{2+} titrations were done as described in Chapter 3, using the same buffers and instrument.

5.5.2. NMR

Nuclear magnetic resonance has proven the capacity to generate high resolution models of biomolecules, including proteins and nucleic acids. Nevertheless, this technique has molecular size limitations so as to get structural models, specially when dealing with proteins that are bigger than 20 kDa, as we will see later. Moreover, proteins above 12 KDa have to incorporate the appropriate isotope labelling to avoid signal overlapping. Al together, these limitations could explain why only 9 % of the structures in PDB have been obtained using this method.

The physics of NMR spectroscopy are briefly described. Once a nucleus is placed inside a strong magnetic field, it alters the energy levels for the atomic nuclei that have a magnetic spin. Then, when tehy are irradiated by a radiofrequency that matches the energy level splitting, the interaction between the radiation and the matter is maximal (resonance condition). When the irradiation finishes, the stimulated atomic nuclei return to its basal state (relaxation). This free induction decay process is recorded and results in the NMR spectrum after Fourier transform.

NMR is a very versatile technique that can provide multiple information depending on the measured observable. From these, the spatial (measuring distance) and the scalar (through bonds) observables are considered restraints that contain topological and structural information of the biomolecule. These restrains are then used to build up a structural model which reproduces the location of each atom in the space. The closest parameter to measure the accuracy of the model is express by the root-mean-square deviation (RMSD) of the atomic coordinates.

5.5.2.1. 15N-HSQC Spectrum and Interpretation

Heteronuclear Single-Quantum Coherence (HSQC) spectrum is, by far, the most used experiment in protein NMR. In fact, this NMR experiment is refereed as the “fingerprint” of the protein and a quality control method to be passed before further structural analysis of proteins.

This spectrum shows a signal for each covalently bonded 1H-15N group (J-coupling): every backbone amide protons (except for Pro) and every NH groups in tryptophans should be represented by a peak, and every side chain amide groups of each Asn and Gln residues should also show a pair of peaks. Accordingly, this spectrum provides very valuable information (Figure 5.10):

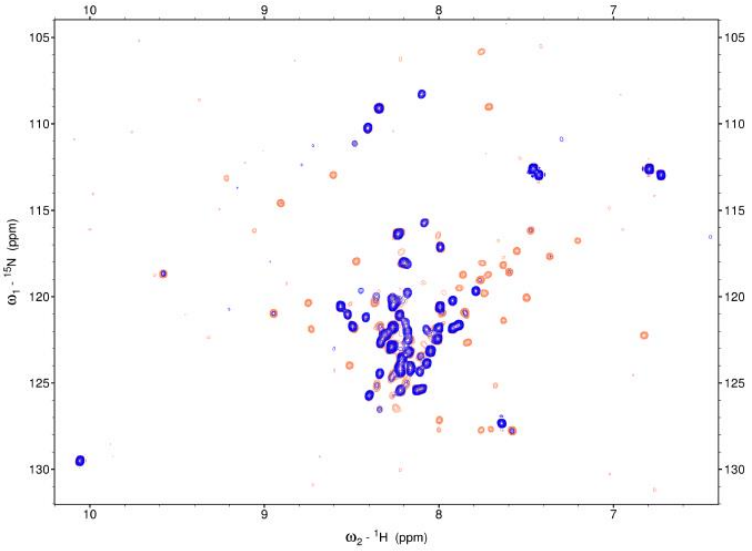

Figure 5.10. ^{15}N-HSQC spectra pf COX17 protein. ^{1}H-^{15}N correlation of all amide groups are shown. In blue the unfolded state and in orange the folded state of the protein in the presence and absence of DTT.

5.5.2.2. Methyl TROSY Spectroscopy to Study Large Biomolecular Complexes

In its inception, NMR studies of unlabeled proteins were done with ^{1}H homonuclear experiments, limiting the size to systems of less than 10 kDa. Year after, with the development of heteronuclear experiments on proteins uniformly labeled with ^{15}N and ^{13}C isotopes the size limitation was pushed to around 25 kDa (Fesik et al., 1989).Yet, larger proteins typically have faster relaxation rates, which results in broader peaks in the spectrum, tend to overlap. This is the case for the tetramer of the complete C-terminal of K_V7.2 channel, that has 140 kDa. Protein deuteration had long been known to enhance resolution and sensitivity of the NMR experiments by reducing the number of possible spin relaxation pathways. Deuterium labelling slows down spin–spin and spin–lattice relaxation resulting in sharper peaks and better signals. Furthermore, Together with ^{15}N and ^{13}C isotope labeling, deuteration opened up the utility of NMR spectroscopy to proteins of up to 50 kDa (Garret et al., 1997).

Later, the introduction of transverse relaxation optimized spectroscopy (TROSY) was revolutionary development in protein NMR spectroscopy, enabling structure determination of proteins as large as 80 kDa (Tugarinov et al., 2005).

Nonetheless, the size and complexity of the proteins are often too pronounced to enable recording of useful ^{1}H-^{15}N-based spectra for exceptionally large macromolecular assemblies, resulting in spectra difficult to analyse. An alternative is the application of isotopically labelled methyl groups [$^{13}CH_3$] in a fully deuterated background, in concert with the corresponding methyl TROSY spectra, this resulted in a successful approach for studying high molecular weight complexes.

To analyse if the conformational change driven by calcium observed in the monomer (Bernardo-Seisdedos et al., 2018) was also present in the tetramer we labelled the methyl-groups of *h*ABCD:CaM complex, in order to overlap with the spectra of the monomer *h*AB:CaM.

This strategy takes advantage from the excellent relaxation properties of methyl groups (Tugarinov et al., 2003). Methyl groups usually are situated in the hydrophobic cavity of proteins and along binding surfaces (Janin et al, 1988), being helpful reporters of structural integrity, conformational changes, dynamics, and interactions.

5.5.2.3. NMR Sample Preparation.

5.5.2.3.1. Expression (Labelling strategy for the entire complex)

Protocol 3.2: M9 media preparation
- Prepare a 10X M9 stock:
60 g Na_2HPO_4
30 g KH_2PO_4
5 g NaCl
- Dilute to desired volume with ddH2O to 1X.
* For 50 % D_2O media dilute 10X stock to 2X with ddH_2O)
- Autoclave previous liquids.
- For 1 litre of media add (everything sterile!)
* For 50 % D_2O media add now corresponding volume to reach 1X M9 and filter with 0.22 µM
1 g $^{14}NH_4Cl$ or 1 g $^{15}NH_4Cl$
3 g ^{12}C-Glucose or 2 g ^{13}C-Glucose
1 mM $MgSO_4$
0.1 mM $CaCl_2$
1 mg/ml Thiamine
1 mg/ml Biotin
- Add corresponding antibiotics
- Inoculate the cultures with the desired amount of bacteria

CaM and His-Q2*h*ABCD with deletion ΔY372_T501 (GB114) were cotransformed by electroporation as previously described. From the Petry dish, 10 ml of LB media with antibiotics were inoculated O/N at 37 °C. Next day, two different dilutions were prepared: 1) a 1:200 dilution to fresh 10 ml sterile Falcon in order to do a rapid solubility and expression test, and 2) a 0.2 µl

were inoculated in another fresh 10 ml sterile Falcon. After checking protein expression, in the evening new dilutions were done using different bacterial volumes (5, 10, 25 and 50 µl) into 4 Erlenmeyers with 200 ml of 14N-12C-M9 media (Protocol 3.2)

Next day, OD_{600} was measured from each Erlenmeyer and calculated to adjust the next culture to a starting OD_{600} 0.05-0.1. The given volume was collected and centrifuged at 2000 g for 30 mins at RT. SN was discarded and bacterial pellet was resuspended into the M9 labelled media. Bacteria were growth at 37 °C until the OD_{600} reached 0.5, when we added 70 mg of each labelled Isoketovalerate (Iso*) and Methionine (Met*). Then temperature was reduced to 25 °C. When OD_{600} reached 0.7, protein expression was induced with 0.5 mM IPTG for 12 h. The following day, bacteria were centrifuged in a JLA 8.1 rotor at 4 °C with 5000 g for 30 mins. SN was discarded and P was resuspended with pre-chilled *Wash Buffer* (120 mM KCl + 20 Mm K_X(PO4) pH 7). If needed, bacteria were once again centrifuged at 5000 g at 4 °C in a Falcon. SN was discarded and the bacterial pellet was frozen with liquid N_2 and stored in the freezer until purification.

5.5.2.3.2. Protein purification of the entire protein

Frozen bacterial pellets were thawed in ice and afterwards resuspended with 40 ml of *Lysis Buffer* (120 mM KCl, 20 mM K_X(PO4) pH 7, 1 mM PMSF, 2 mM Imidazole and 1 tablet of Protease inhibitor without EDTA). Subsequently, it was passes through the **Emulsiflex** thrice, and followed by centrifugation in a JA25.50 rotor at 25000 g for 30 min at 4 °C. The rescued supernatant was filtered with 0.22 µm filter before running the AKTA.

First, AKTA tubes were washed with degassed ddH2O and afterwards the column **HiTrap Talon Crude** 5 ml (GE Healthcare, Ref: 28-9537-67), was connected to the AKTA with slow flow to remove the air bubbles. Ethanol from the columns was washed out with 5 column volumes (CVs) of ddH2O at a flow of 5 ml/min. Equilibration of the column with 10 CVs of *Wash Buffer* (120 mM KCl, 20 mM KX(PO4) pH 7) at 5 ml/min flow was followed by injection of the sample at 1 ml/min up to 50 ml. Fractions every 5 ml were collected. Next, the column was washed with different combinations of *Wash Buffer* and *Elution Buffer* (120 mM KCl, 20 mM K_X(PO4) pH 6, 300 mM Imidazole): W0 = 10 CV of buffer A (0 mM imidazole) - 2 ml/min; W1 = 4 CV of 3 % mixture (9 mM imidazole) 2 ml/min; W2 = 8 CV of 6 % mixture (18 mM imidazole) 2 ml/min; and W3 = 4 CV of 8 % mixture (24 mM imidazole) 2 ml/min. Finally, the complex was eluted with a gradient from 30 to 300 mM of imidazole in 8 CVs at 2 ml/min flow. 1 ml fractions were collected and these with high 280 nm absorbance were picked. A 12 % acrylamide SDS-PAGE was run to check the presence of the protein in the fractions. To regenerate the column, apply 10 CVs of 20 mM MES pH 5.0, afterwards 10 CVs of ddH2O and finally 10 CVs of EtOh 20 %. All the positive fractions were pooled together and **dialysed 2 times to remove Ca^{2+} ions, first** against 1 litre of *APO1 SOLUTION* (120 mM KCl, 50 mM MES pH 6.5 and 5 mM EGTA) O/N at 4 °C in dialysis tubing cellulose membrane (Sigma-Aldrich, Ref: D927-100FT). Then, the dyalisis membrane was moved to *APO 2 SOLUTION* (120 mM KCl, 50 mM MES pH 6 and 5 mM EGTA), for 5 h, and finally, the sample was dialyzed against *Running Buffer* (120 mM KCl, 50 mM MES pH 6). Protein complex was concentrated until 10 to 13 ml using Amicon Ultra-15 centrifugal units with a 3 kDa cut-off in a fixed angle rotor at 3500 g.

A second purification step was done by **gel filtration**. First AKTA tubes were washed with degassed ddH2O. Afterwards, before connecting the Superdex 200 pg 26/60 (GE Healthcare, Ref.: 28-9893-

36) column to the AKTA. An aliquot of 13 ml of dialysed and 0.22 µm filtered sample was injected. Positive fractions were pooled together, and the protein was concentrated using a to 1 ml with a 3 kDa cut-off Amicon ultra-15 concentrator in a fixed angle rotor at 3500 g. When reached this point 5 % of D_2O was added to the sample as well as a NaN_3 and PIC to a final concentration of 3 µM and 1 µM respectively. Protein concentration was measured using NanoDrop and concentrated protein was transferred to a 5 mm NMR tube.

The CaM:K_V7.2-*h*ABCD protein complex was concentrated up to 50 µM for structure determination.

Accompanying the protein, the final sample should contain between 5 and 10 % of D_2O in order to adjust the "lock". Higher amounts of D_2O may jeopardize the observation of labile proton exchanges. Moreover, some other additives such as DTT, DMSO, or PIC are advisable to avoid protein aggregation. Besides, the use of 2 to 10 µM of NaN_3 (Sodium Azide) prevents microorganisms growth.

5.5.2.3.3. NMR Spectroscopy.

NMR data were were acquired on an 800 MHz Bruker Avance III spectrometer equipped with a TCI cryoprobe. All the spectra were processed using Topsping 3.2 (BRUKER) and they were analysed with Sparky (T. D. Goddard and D. G. Kneller, University of California) and NMRPipe (Delaglio et al., 1995).

Sample preparation for NMR

For calcium titration

Protein final concentration in a 450-500 µl sample SHOULD AT LEAST be at 50 µM!

1. Measure protein concentration from the Gel Filtration.

2. Concentrate the protein if possible to make it more manageable.

3. Prepare the final samples in parallel

Sample Name	Protein Concentration	Calcium concentration	D2O (5%)	Azida+PIC	Buffer	Final Volume
0 Equivalents	50 M (? ul)	0 uM (? ul)	24 ul	0.5 + 0.5 ul	(? ul)	480 ul
20 Eq	50 uM (? ul)	100 uM (? ul)	24 ul	0.5 + 0.5 ul	(? ul)	480 ul

5.5.3. HS-AFM

Finally, to investigate the conformational changes and dynamics associated with Ca^{2+} binding we used high-speed atomic force microscopy (HS-AFM) in real time, during my stay in Marseille, in collaboration with the AFM-Lab of INSERM-Aix Marseille University. HS-AFM, which can monitor the same molecule under different conditions in real time, is ideal for investigating this process.

Here, we show that conformational change, as a function of Ca^{2+} is not associated with large and extensive variation of the structure.

The atomic force microscopy (AFM) is a powerful tool to visualize proteins in an aqueous solution with demonstrated resolution on the order of fractions of a nanometer, more than 1000 times better than the optical diffraction limit. AFM can be used to form an image of the three-dimensional shape (topography) of a sample surface at a high resolution, thus has rapidly emerged as an effective structural analysis tool.

To acquire a topographic image, a sharp tip attached to the free end of a flexible cantilever put into contact with the sample and scanned over it. The sample is raster scanned along an x-y grid and its profile height is recorded over the selected scan area.

The feedback loop controls the height between the cantilever and the sample and allows for adjusting the applied force preventing the damage of fragile biological structures. As a result, a 3D profilometric image of the sample surface is obtained, in which each pixel represents an x-y position on the sample, and the color represents the recorded signal.

To study biological dynamic processes AFM presents some limitations, such as the framrate in which an image is obtained. It takes one image every few minutes and most dynamic processes of biological molecules that take place in its majority at subsecond time scales. The introduction of the high-speed atomic force microscopy (HS-AFM) in 2001 unravelled the visualization of biological molecule dynamics. The technical development of the HS-AFM was performed by the laboratory of Toshio Ando in the University of Kanazawa, Japan.

The imaging rate of the current HS-AFM has reached 15–25 frames per second (fps) for a scan range of ~240×240 nm^2 with 100 scan lines. By further reducing the scan range, the imaging rate can exceed 50 fps. The operating principle of the HS-AFM is based on the miniaturization of the moving components of the AFM (cantilever and scanner) to increase their velocity by 1000 times (small cantilevers applies less force during its scans) in the interest of achieving reaction speeds of tens of microseconds. Furthermore, the gain in speed does not suppose a lost in performance.

The protocol here described is adapted for any Ando-type HS-AFM setup “SS-NEX”, commercialized by the Research Institute of Biomolecule Metrology (RIBM), Japan, which was used for the experiment in the AFM-Lab of Aix Marseille University and it is fully described in the Nanoscale Imaging: Methods and Protocols (Zuttion et al., 2018).

5.5.3.1. The Hardware

A picture of the HS-AFM hardware of “SS-NEX” HS-AFM is presented in Fig. 1, where the cantilever is mounted up-facing in a cantilever holder that comes with a pool of 110 µL while the sample is mounted on top of the scanner facing down. In general, imaging experiments are performed in tapping mode where the tip is oscillated at constant amplitude. For that, the cantilever is excited at its resonance frequency with the help of a miniaturized piezoelectric actuator. The sample can move in the XY-plane and in the Z vertical direction thanks to three small multilayer piezoelectric actuators. The Z-piezo the one displaced at the highest frequency (nominal resonance frequency ~600 kHz and ~150 kHz once glued on the scanner). The deflection of the cantilever is monitored by an optical system. A laser beam with a 20_ optical microscope objective is focused on the

backside of the cantilever and the reflected beam tracked with a 15 MHz bandwidth photodiode which sends the signal to a Lock-In amplifier (Fourier Analyzer).

The signal goes to the Proportional Integral Derivative (PID) controller which compares the amplitude readout with the value settled by the operator (set point amplitude, A) to feed the adjustment of the clearance distance between the sample stage and the HS-AFM probe by the feedback loop.

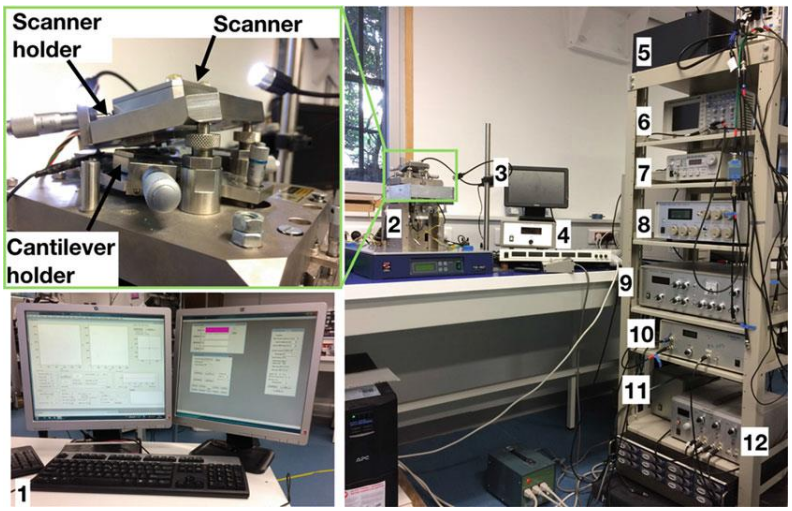

Figure 5.11. The hardware of the HS-AFM used. The description if each component is in the main text.

Image treatment

There are different hardware available to analyse the images obtained by the HS-AFM. These are the most commonly used:

1. Image processing software supplied with AFM instrument.

2. MATLAB (MathWorks, USA). This is a proprietary programming language specifically designed for simple and efficient matrix manipulation, data plotting and algorithm implementation.

3. ImageJ (NIH). This is a free, Java-based image processing platform (https://imagej.nih.gov/ij/). Although not specifically designed for AFM image treatment, several user-written plugins exist to efficiently tackle several of the procedures.

5.5.3.2. Biotin-Streptavidin complex to fix the K_V7.2 C-terminal to the Mica

The affinity of streptavidin for biotin is the strongest noncovalent biological interaction known, with a dissociation constant (K_d) in the femtomolar range. Each streptavidin monomer can bind one biotin molecule, allowing a streptavidin tetramer to bind four biotins (Figure 5.12). In addition, this interaction is highly specific and rapid on-rate. It is resistant to changes in temperature or pH and can support the presence of organic solvents and denaturing agents.

Figure 5.12. Schematic representation of Streptavidin-Biotin complex.

5.5.3.2.1. Strep-tag insertion

The strep-tag consists in eight amino acids (Trp-Ser-His-Pro-Gln-Phe-Glu-Lys) which was inserted in the plasmid GB116 by PCR by using 5´GATTACGATATCCCAtggagccacccgcagttcgaaaagACGACCGAAAACCTG3´as fordward and 5´CAGGTTTTCGGTCGTcttttcgaactgcgggtggctccaTGGGATATCGTAATC 3´as backward to insert the strep-tag in the N-terminal of GB116. It was done by quick-change mutagenesis as described before.

The construct was co-transformed with CaM_PokD4 by electroporation as previously described. From the Petry dish, 10 ml of LB media with antibiotics were inoculated O/N at 37 °C. Next day, a dilution was prepared (1:200 dilution) to fresh 10 ml sterile Falcon in order to do a rapid solubility and expression test. After checking protein expression, in the evening new 1:2000 dilution was done into 10 ml of LB media and grow again O/N at 37 °C.

Next day, the 10 ml were dissolved in 2 L and incubated at 37 until OD 600 reached 0.6-0.7. Then temperature was reduced to 20 °C. Protein expression was induced with 0.5 mM IPTG for 12 h.

The following day, bacteria were centrifuged in a JLA 9.1 rotor at 4 °C with 9000 g for 9 mins. SN was discarded and P was resuspended with pre-chilled *Wash Buffer* (120 mM KCl + 50 mM K-Hepes pH 7.4). If needed, bacteria were once again centrifuged at 5000 g at 4 oC in a Falcon. SN was discarded and the bacterial pellet was frozen with liquid N2 and stored in the freezer until purification.

5.5.3.2.2. Protein purification

Frozen bacterial pellets were thawed in ice and afterwards resuspended with 40 ml of *Lysis Buffer* (120 mM KCl, 50 mM K-Hepes pH 7.4, 1 mM PMSF, 2 mM Imidazole and 1 tablet of Protease inhibitor without EDTA). Subsequently, it was passes through the **Emulsiflex** thrice, and followed by centrifugation in a JA25.50 rotor at 25000 g for 30 min at 4 °C. The rescued supernatant was filtered with 0.2 µm filter before running the AKTA.

First, AKTA tubes were washed with degassed ddH2O and afterwards the column **HiTrap Talon Crude** 5 ml (GE Healthcare, Ref: 28-9537-67), was connected to the AKTA with slow flow to remove the air bubbles. Ethanol from the columns was washed out with 5 column volumes (CVs) of ddH2O at a flow of 5 ml/min. Equilibration of the column with 10 CVs of *Wash Buffer* (120 mM KCl, 50 mM K-Hepes pH 7.4) at 5 ml/min flow was followed by injection of the sample at 1 ml/min up to 50 ml. Fractions every 5 ml were collected.

Next, the column was washed with different combinations of *Wash Buffer* and *Elution Buffer* (120 mM KCl, 50 mM K-Hepes pH 7.4 and 300 mM Imidazole): W0 = 10 CV of buffer A (0 mM imidazole) - 2 ml/min; W1 = 4 CV of 3 % mixture (9 mM imidazole) 2 ml/min; W2 = 8 CV of 6 % mixture (18 mM imidazole) 2 ml/min; and W3 = 4 CV of 8 % mixture (24 mM imidazole) 2 ml/min. Finally, the complex was eluted with a gradient from 30 to 300 mM of imidazole in 8 CVs at 2 ml/min flow. 1 ml fractions were collected and these with high 280 nm absorbance were picked. A 12 % acrylamide SDS-PAGE was run to check the presence of the protein in the fractions. To regenerate the column apply 10 CVs of 20 mM MES pH 5.0, afterwards 10 CVs of ddH2O and finally 10 CVs of EtOh 20 %.

All the positive fractions were pooled together and EGTA was added till reach a final concentration of 100 mM). Then there were **dialysed** against 2 litre of *Running Buffer* (120 mM KCl, 50 mM K-Hepes pH 7.4, 5 mM NaCl and 5 mM EGTA) O/N at 4 °C in dialysis tubing cellulose membrane (Sigma-Aldrich, Ref: D927-100FT). Protein complex was concentrated until 10 to 13 ml using Amicon Ultra-15 centrifugal units with a 3kDa cut-off in a fixed angle rotor at 3500 g. Positive fractions were pooled together and the protein was concentrated using a to 1 ml with a 3 kDa cut-off Amicon ultra-15 concentrator in a fixed angle rotor at 3500 g.

Then the proteins were lyophilized to be transported to Marseille.

A second purification step was done by **gel filtration**. First AKTA tubes were washed with degassed ddH2O. Afterwards, before connecting the superdex 75 increase 10/300 (GE Healthcare, Ref.: 17-5174-01) column to the AKTA. An aliquot of lyophilized protein was resuspended in 1 ml and 0.22 µm filtered before injected.

5.5.3.2.3. Preparation of streptavidin 2D crystals

Streptavidin 2D crystals were formed on supported biotin-containing lipid bilayers. Briefly, a supported biotin-containing lipid bilayer was first obtained by applying 2 µl of biotin (0.2 mg/ml) in the surface of the Mica and incubated for 30 minutes. The lipid compositions were dioleoylphosphatidylcholine, dioleoylphosphatidylserine, and 1,2-dioleoyl-*sn*-glycero-3-phosphoethanolamine-*N*-(cap biotinyl) (biotinylated lipid) at 7:2:1 (w/w). After washing out the excess lipids with a crystallization buffer solution, a 0.1–0.2 mg/ml streptavidin solution was placed on the biotinylated lipid bilayer and incubated at room temperature in a sealed container. The crystallization buffers used was 10 mM HEPES, 150 mM NaCl, and 2 mM $CaCl_2$ (pH 7.4). After the incubation for at least 2 h, the excess streptavidin was washed out with the buffer solution used for crystallization. Finally, 2D crystals were incubated with our protein complex (strep-Q2*h*ABCD:CaM) (Figure 5.13)

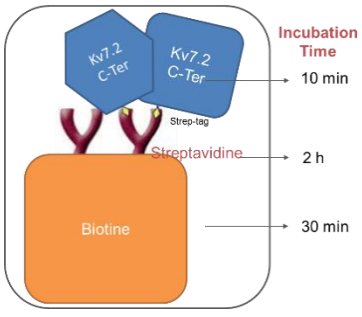

Figure 5.13. Incubation Time to create Biotine-Streptavidin 2D crystals bound to recombinant protein complex.

2 µl of biotin (0.2 mg/ml) were added in the surface of the Mica and incubated for 30 minutes. Then it was washed 20 times with a non-absorbent buffer. Subsequently, 0.5 µL of Streptavidin (0.5 mg/ml) and incubated for 2 hours, in order to create 2 D crystals (Figure 5.14).

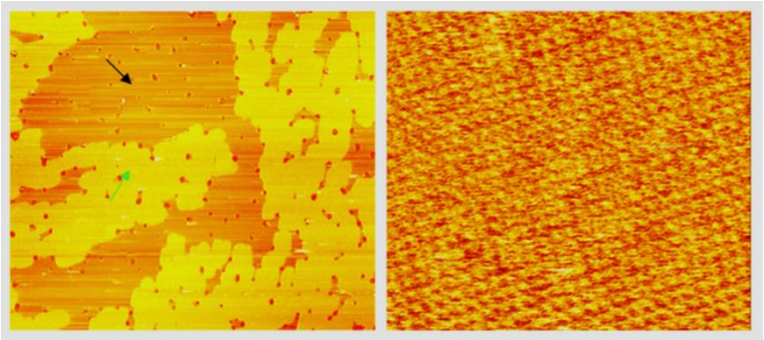

Figure 5.14 Streptavidin crystals grow in Biotin monolayer. (Right) Black arrow marks biotin layer and green arrow streptavidin crystals 500*500nm scan area. **(Left)** Streptavidin crystal 150*150 nm scan area.

The step by step of image adquisition is described in Supplemental 3.

6. The 3rd E-F Hand of Calmodulin Switches Calcium signals in K_V7 CDR

6.1. INTRODUCTION

In 1978, Brehm and Eckert described for the first time the Ca^{2+}-mediated inhibition of a voltage gated ion channel in *Paramecium* (Brehm & Eckert, 1978). These channels are equipped with a **special Ca^{2+}-sensitive toolkit**, which they use to exquisitely manipulate their own Ca^{2+} influx, and thereby adjust the many effector responses that lie downstream of Ca^{2+} entry. Nevertheless, the molecular mechanism underlying this Ca^{2+}-dependent regulation of an ion channel remained obscure until the '90s when it was suggested that CaM could mediate the regulation of Ca^{2+}-dependent Na^+- and K^+-channels in *Paramecium* (Kink et al., 1990; Saimi & Kung, 1994). Since then, over 40 years later, several studies have demonstrated that **CaM plays a pivotal role** in the modulation of ion channels and receptors, such as Ca^{2+}-activated K^+ channels (Xia et al., 1998), N-methyl-D-aspartate (NMDA) glutamate receptors (Ehlers et al., 1996), cyclic nucleotide-gated ion channels (Liu et al., 1994), transient receptor potential (TRP) channels (Phillips et al., 1992), voltage-gated Ca^{2+}-, Na^+- or K^+-channels (Zühlke et al., 1999; Peterson et al., 1999; Mori et al., 2000; Yus-Najera et al., 2002; Wen & Levitan, 2002) and many others (Saimi & Kung, 2002).

6.1.1. The specificity of E-F Hands

As its name suggests, calmodulin is a CALcium MODULated proteIN. CaM is formed by two similar globular domains, the N- and C-lobes linked by a very flexible sequence. Each lobe is composed of two E-F hands which are responsible for binding of up to four Ca^{2+} ions. CaM targets are usually amphipathic helical regions rich in hydrophobic and basic residues. CaM lobes can be in **an open, semi-open or closed configuration** depending on Ca^{2+} occupancy (Figure 6.1).

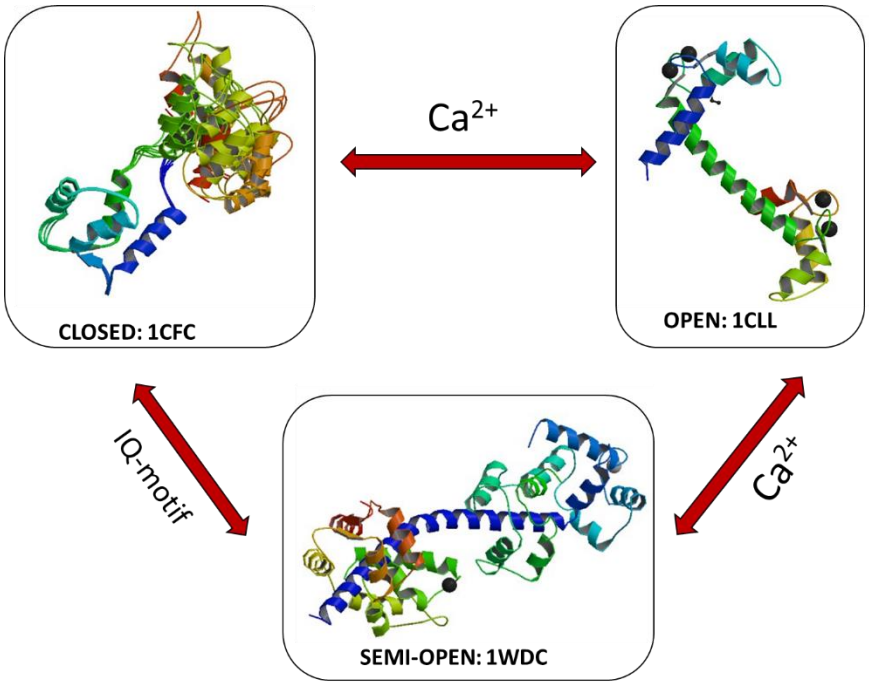

Figure 6.1. Three conformations of E-F hand domains: ribbon representations of apo and calcium-loaded calmodulin N-terminal domain and the C-terminal domain of myosin essential light chain are used to illustrate three of the known conformations of EF-hand domains. On the top left, apo CaM-N (pdb code=1CFC) is in the closed conformation. On the top right, calcium-loaded CaM-N (PDB=1CLL) is in the closed conformation. On the bottom, the C-terminal domain of myosin (pdb code=1WDC) is in the semi-open conformation. (Upson et al, 1989).

In addition, the abundance of methionine residues confers another level of **plasticity** at the amino acid level. These characteristics enable CaM to bind to more than 300 targets with little sequence similarity. Both lobes are connected by a flexible linker which confers structural **flexibility** and adaptable binding surfaces. Thus, CaM is able to interact with a large number of proteins and it is involved in many cellular pathways.

As mentioned above, CaM has four fully operative EF-hands which are composed by the amino acid segments 20-31 E-F (1), 56-67 E-F (2) in the N-lobe and 93-104 E-F (3) and 129-140 E-F (4) in the C-lobe (Figure 6.2).

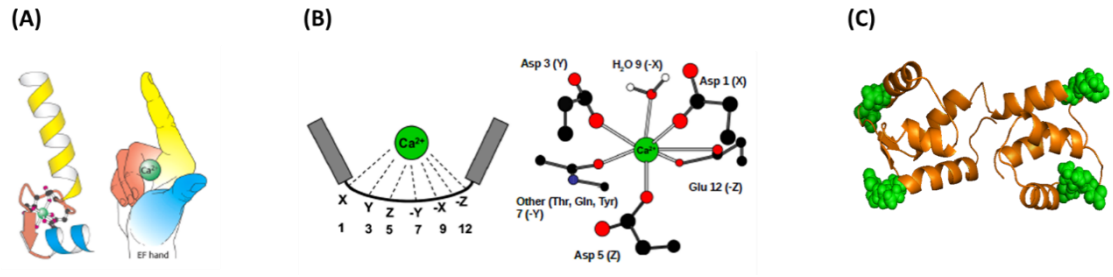

Figure 6.2. (A) Representation of the origin of the terminology "EF-Hand". **(B)** Overall Ca^{2+} binding motif corresponding to an EF-Hand. The characters (X, Y, Z,...) and numbers correspond to relative positions in the EF loop. (Pictures provided by Dr. Alessandro Alaimo). **(C)** Schematic representation of CaM, where E-F hands are represented in green spheres.

This canonical sequence is composed of 12 amino acids, which start with an Asp residue and ends with a Glu residue. The oxygen atoms of half of the canonical amino acids take part in Ca^{2+} binding (residues 1-3-5-7-9 and 12). In fact, due to a minor amino acidic differences between the lobes of CaM, **C-lobe has a higher affinity for Ca^{2+} than the N-lobe** (Kd ~ 0.2 µM and ~2 µM respectively) in solution (Alaimo et al., 2014).

The ample array of ionic conditions and CaM concentrations described in the literature results in different estimations for Ca^{2+} binding affinity, with reported Kd values ranging between 0.3 and 5 µM. Under near-physiological intracellular ionic conditions, the Kd is about 1 µM, a value that allows CaM to respond to intracellular Ca^{2+} oscillations. Nonetheless, this affinity varies when CaM is complexed with its targets.

In general, **CaM affinity for Ca^{2+} is higher when complexed with a target although the opposite effect has also been described**. Some reported values for the Ca^{2+} affinity of target-bound CaM are lower than 50 nM. This would suggest that at resting cell conditions, in which Ca^{2+} concentration is around 100 nM, the CaM/target complex may be saturated with Ca^{2+}. Reciprocally, the affinity of many targets for CaM increases when it is loaded with Ca^{2+}.
It has been revealed that mutating either E-F(1) or E-F(2), in the N-lobe of CaM, reduces the apparent Ca^{2+} sensitivity of the SK channels, shifting the dose-response curve to the right, while the double mutant, E-F(1,2) completely abolished channel activity (Keen et al., 1999). In striking contrast, mutating either of the C-lobe E-F hand motifs, E-F(3) or E-F(4), or both E-F(3,4), had no effect on Ca^{2+} gating (Keen et al., 1999). The interpretation of these experiments was that the N-lobe is the effector for the Ca^{2+} signal, a hypothesis fully in agreement with cryo-EM images of SK4 obtained with and without calcium (Lee & MacKinnon, 2018).

In **$Ca_V2.1$ channels**, the lobes of CaM produce opposing effects: the C-lobe of CaM triggers a kinetically rapid Ca^{2+}-dependent facilitation (CDF), whereas the N-lobe provokes a slower Ca^{2+}-dependent inactivation (CDI), (DeMaria et al., 2001; Lee et al., 2003). $Ca_V2.2$ and $Ca_V2.3$ channels manifest CDI triggered mainly by the N-lobe of CaM (Liang et al., 2003). These channels have different mechanism **for spatial Ca^{2+} selectivity under physiological conditions**, and the Ca^{2+} signal is the sum of two distinct components, the local and the global calcium. First, Ca^{2+} inflow during channel openings produces a 'local signal' component comprising brief yet intense local spikes of

amplitude Ca_{spike} ~100 µM. These spikes are tightly synchronized with openings of the host channel, and localized to the nanodomain (Neher, 1998; Sherman et al., 1990). Second, accumulation of Ca^{2+} from distant sources (e.g., other Ca^{2+} channels) generates a 'global signal' component consisting of a far smaller (~5 µM) global pedestal, which is spatially widespread. In the Ca_V1-2 family of Ca^{2+} channels, regulation triggered by the C-lobe of CaM exploits channel proximity and responds almost maximally to the local Ca^{2+} signal alone (Liang et al., 2003). CDI produces a strong decay of Ca^{2+} current during sustained voltage activation whether Ca^{2+} is buffered at physiological levels, or much more strongly. Since high Ca^{2+} buffering eliminates the global pedestal while hardly affecting local spikes (Neher, 1998), the sparing of CDI under this condition indicates that the local signal alone is sufficient. By contrast, N-lobe mediated regulation of all Ca_V2 channels somehow prefers the diminutive global pedestal over the far larger local spikes (Tadross et al., 2008). This spatial selectivity has sense for a calcium source, such as TRP, Ca_V or Ryonidine. However, in a potassium channels such as K_V7, this does not occur.

For K_V7 channels, there is controversy even for which CaM-lobe transmits the Ca^{2+} signal. Both hypotheses have been proposed, some suggesting that Ca^{2+} signal is transmitted by the N-lobe (Archer et al., 2019), and others arguing it is through the C-lobe (Tobelaim et al., 2015; Bernardo-Seisdedos et al., 2018; Chang et al., 2018). It would be very helpful if there were structures resolved in the absence and in the presence of calcium from the same isoforms, but to date only this information is available for $K_V7.2$. For $K_V7.1$, only structures in the presence of Ca^{2+} have been resolved (Sachyani et al., 2014; Sun & MacKinnon, 2017;), in $K_V7.2$ we resolved in presence and absence, but only the Calcium Responsive Domain was resolved (*h*AB of the C-terminal) (Bernardo-Seisdedos et al., 2018), for $K_V7.4$ the only resolved structure is in the absence of Ca^{2+} (Chang et al., 2018).

Actually, in those **resolved structures of K_V7 family most characteristic differences between the $K_V7.3/7.2$, $K_V7.4$ and the $K_V7.1$ *h*AB domain complexes occur in the occupancy of Ca^{2+} in the different E-F hands.** In the Apo/CaM:$K_V7.4$ *h*AB domain complex are empty (Chang et al., 2018), but N-lobe adopts Ca^{2+} loaded configuration. In the CaM:$K_V7.1$*h*AB domain complex crystal structure, the N-lobe E-F hands contain calcium ions whereas the C-lobe E-F hands lack bound divalents (Sachyani et al., 2014). In the cryo-EM structure, no density for a Ca^{2+} ion was observed in the E-F(3), even at the high Ca^{2+} concentration (5 mM) under which the structure was determined. Neither in the last structure published (Archer, 2019) where helices A and B of $K_V7.4$ are resolved in complex with CaM by X-ray crystallography. In that structure, E-F (3) and E-F (4) are empty, despite the complex was formed in a buffer containing an excess of Ca^{2+} (2 mM). This Ca^{2+}/N-lobe matches with the structure for the 1 mM $CaCl_2$ soaks of the Apo/CaM:$K_V7.4$*h*AB domain complex (Chang et al., 2018). The CaM:Q3*h*A/Q2*h*B chimera complex structure (Strulovich et al., 2016) has calcium ions in all four calmodulin E-F hands. Nevertheless the overall lobe conformations match open conformations seen in the Apo/CaM:$K_V7.4$ complex.

Although the resolved structures of the different isoforms are not very clarifying over which CaM lobe transmits the calcium signal, functional studies of $K_V7.1$:CaM suggested a critical role for E-F (3) (Chang & Minor, 2018).

6.2. OBJECTIVES

Here, we aim to obtain insights into the differential role of each E-F hand of CaM in calcium signal transmission of K_V7 channels. To that goal, we characterize the contributions of the different E-F hands in Ca^{2+} signalling. For this aim, the helix AB from $K_V7.2$ FRET-biosensor was co-expressed with different CaM mutants (CaMwt, CaM4, CaM124, CaM3, CaM123, and CaM1234) which surgically prevent Ca^{2+} binding to different E-F hands.

6.3. RESULTS

6.3.1. E-F (3) MEDIATES Ca^{2+} SIGNAL TRANSDUCTION IN $K_V7.2$ CHANNELS

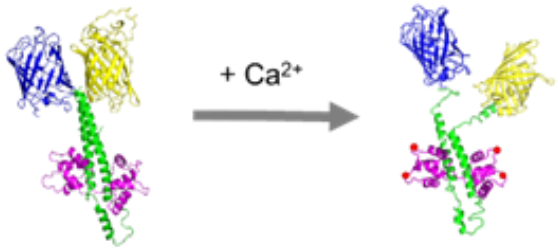

Figure 6.3. Atomic representation of the biosensor with mTFP1 (blue) fused to helix A, and Venus (yellow) fused the helix C. Upon calcification (red circles) of the C-lobe, the relative orientation of helices A and B changes, resulting in separation of mTFP1 and Venus, which leads to a reduction in FRET.

We used the FRET biosensor described before (Chapter-3) were the CRD (Calcium Responsive Domain) of K_V7 channel is flanked by a donor and acceptor fluorophores (mTFP1-hAB-Venus) (Figure 6.3). This protein was coexpressed with different CaM, which are mutated in specific E-F hands precluding Ca^{2+} binding (CaM3, CaM4, CaM123, CaM124, CaM1234). Proteins were purified by His-Trap and Gel Filtration as described in the methods section. Then they were mixed at 500 nM with different buffers, one with 5 mM EGTA, and the other with 1 mM free Ca^{2+}. Samples are excited at a 458 nm wavelength, and the ratio of fluorescence intensity of the mcpVenus channel (FRET) versus fluorescence intensity of the mTFP channel (CFP), YFP/CFP, is used to represent the level of FRET. Here, the "dynamic range" of the FRET biosensor is the theoretical range of YFP/CFP in the biosensor.

In practical use, the change of the structure of the molecule is monitored by the change of YFP/CFP after stimulation. This "gain" of the FRET signal is the relative increase or decrease in YFP/CFP after stimulation and is expressed as a percentage of the YFP/CFP value before stimulation.

The FRET-index (YFP/CFP) is reduced from 1.75 to 1.25 in the case of the biosensor co-transformed with CaM WT in presence of 10 µM free Ca^{2+} (Figure 6.4); and it is represented as the 100% to be compared with the mutant CaMs. FRET-index decreases from 1.71 to 1.27, which corresponds to a 90% in the case of CaM 4, almost 80% (from 1.75 to 1.31) in the case of CaM 124, FRET-index in complex with CaM 3, remains very similar upon Ca^{2+} addition, going from 1.68 to 1.55, which is a 32%, and from 1.74 to 1.66 in the case of CaM123, just a 13%. With CaM1234, as we expected, the FRET-index remains stable.

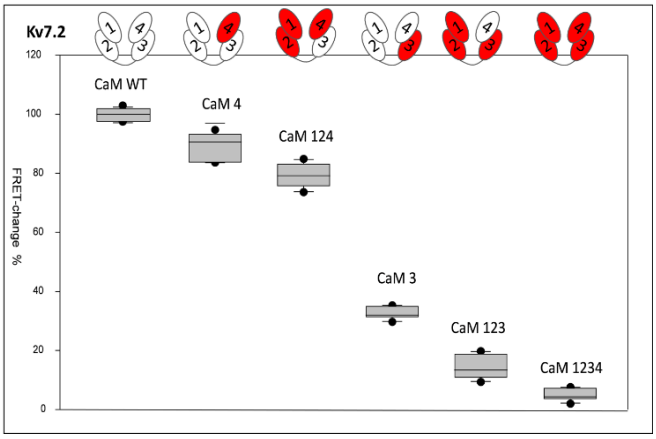

Figure 6.4. Reduction of FRET-index (%) from the purified complex of K_V7.2 co-expressed with CaM, CaM4, CaM124, CaM3 and CaM123, in presence of Ca^{2+}. The FRET reduction is maintained in 90% with CaM4, in 79% with CaM124, in 32% with CaM3, 13% with CaM123 and almost completely removed in CaM1234 (4%). Each plot represents the average of at least 6 independent experiments.

6.3.2. THE CALCIUM SIGNAL MACHINERY IS CONSERVED AMONG K_V7 MEMBERS

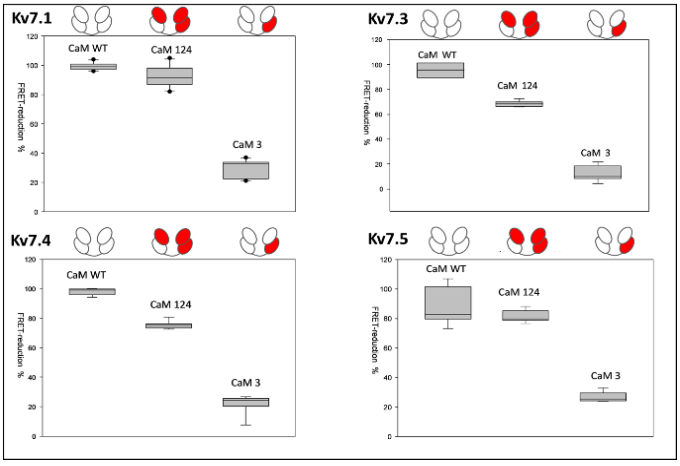

Figure 6.5. E-F (3) also mediates the Ca^{2+} signal transduction in other members of K_V7 family. Reduction of FRET-index (%) index from the purified complex of different isoforms of K_V7 co-expressed with CaM, CaM124 and CaM3, after Ca^{2+} addition (Free Ca^{2+} 1 mM). Each plot represents the average of at least 6 independent experiments.

In the other members of the K_V7 family, the behaviour is similar. We have demonstrated that precluding binding to E-F (3) results in insignificant FRET changes in the presence of Ca^{2+} (Figure 6.5) in K_V7.1, K_V7.3 K_V7 *h*AB helices, but somehow it is also modulated by the E-F (4), in a small proportion. While the mutations in the E-F hands of the N-lobe of the CaM (E-F (1) and E-F (2)) do not affect the conformational change triggered by the binding of Ca^{2+}.

In the case of K_V7.1, the FRET reduction is maintained in 91 % with CaM124 and reduced to 33% in the case of CaM3. For K_V7.3 the FRET-ratio reduces to 65% in the case of CaM124 and down to 10% in the case of CaM3. Similarly, in K_V7.4 CaM124 reduces the FRET-change to 65% and CaM3 to 24%. Regarding K_V7.5, CaM124 maintains the reduction as a function of Ca^{2+} in an 80%, and with CaM3 come down to 25%.

6.4. DISCUSSION

FRET experiments provide evidence that the conformational changes provoked by calcium are due, **mainly, to the binding of Ca^{2+} to the E-F (3)** hand of CaM. FRET has remained relatively stable

after addition of Ca^{2+} to Q2*h*AB complexed with CaM 3. **E-F (4) also has an effect on the Ca^{2+} signal transduction, even though in smaller magnitude**. While no change in the FRET signal can be detected when using a CaM mutant unable to bind Ca^{2+} (CaM[1234]). Based on the FRET-index we estimate that the calcium signal transduction depends at ~70% on E-F (3) hand, while E-F (4) is responsible of ~30%. However, we should remind that the relation between the FRET-index and the distance is not linear, rather exponential, and when converting these numbers into distances the contribution of one hand and the other could be different.

Our preliminary data, along with the high-resolution structures obtained suggest the following model: First, under resting cellular conditions (100 nM Ca^{2+}), the N-lobe is engaged with helix B and loaded with Ca^{2+}, whereas the C-lobe is engaged with helix B with empty E-F hands (Figure 5.3). When, as a result of neuronal activity, or activation of Gq-coupled receptors, such as the bradykinin receptor, intracellular levels of Ca^{2+} raise close to the channels above 1 µM, both E-F(3) and E-F(4) become loaded, but it is the occupancy of E-F(3) that triggers the reorientation and separation of helices A and B. The loading of E-F (4) plays only a marginal role, as revealed by our FRET studies. It is important to note that calcium binding is not independent for each E-F hand, especially in the E-F hands that are part of the same lobe. The union of calcium to one hand, affects the other, and vice versa (Strynadka et al., 1989).

The mechanisms supporting different Ca^{2+} selectivity has been described for other K^+-channels regulated by CaM, e.g. it is led by N-lobe for SK channels (Lee & MacKinnon, 2018), and by the C-lobe for Eag1 (Lorinczi et al. 2016). This can be explained as emergent behaviours of a system in which a lobe of apoCaM must ephemerally separate from a pre-association site before binding Ca^{2+}, and where a Ca^{2+}-bound lobe of CaM must associate with a channel effector site to mediate regulation (Tadross et al., 2008).

It is noteworthy that the data revealed here, is of a **level of discrimination between the contribution of each E-F hand never previously reported** in the calcium signalling of K^+ channels or any other protein. Preceding works had been limited to analyse the contribution of each lobe separately, without differentiating between the E-F hands that are part of each lobe.

As we comment in the 2nd chapter, NMR experiments demonstrated that Ca^{2+} association with CaM produces a 17.9° rotation of the E-F hands, which also pulls helices *h*8 and *h*5 of CaM, located at C-lobe, and helix *h*A of K_V7.2.

From the functional point of view, the key step is the transition from intCaM/K_V7.2-*h*AB to holoCaM/K_V7.2-*h*AB: ion binding to the E-F (3) concertedly displaces a segment of CaM (helices h5 and h8), which is allosterically transmitted to the channel moiety by modifying the orientation of helices hA and hB (Bernardo-Seisdedos et al., 2018). It is assumed that this conformational change is mechanically transmitted to the intramembranous region of the channel through a change in orientation of the pre-hA element, gating the closing of the channel, and ultimately resulting in the M-current depletion.

The experiment was repeated with the **different isoforms of K_V7**, analyzing the effect of calcium with CaM WT, CaM3 and CaM124, and we observed that **the response to Ca^{2+} qualitatively has the same profile**. The Calcium sensor responds in the same way in all isoforms, where precluding Ca^{2+} binding to hand E-F (3) significantly reduces the conformational change caused by Ca^{2+}, while with CaM 124, where only hand 3 is capable to bind Ca^{2+}, the response remains similar to that observed in the WT CaM.

In K_V7.1 the effect of each E-F hand is as clear as in K_V7.3. While CaM124 mimic the effect Of CaM WT, in K_V7.1:CaM3 only a third of the total effect is reproduced (33.1%). However, in previous

works, Ca^{2+}-insensitive CaM mutants shifted the K_V7.1 response in the depolarizing direction, opposing channel activation (Chang et al., 2018), in contrast with K_V7.2-K_V7.5. However, these results differ from the results obtained previously were K_V7.1/KCNE-expressing cells suppressed current density (Sachyani et al., 2014), and the lack of effect of BAPTA on K_V7.1 activation (Tobelaim et al., 2017). These differences could be due to different experimental techniques in cell recordings: the whole-cell configuration, where there is a dilution in the cytosol (Sachyani et al., 2014; Tobelaim et al., 2017) instead of the perforated-patch configuration (Chang et al., 2018). In addition, the way in which CaM is incorporated into the channel complex could cause these dissimilarities.

Our results match perfectly with functional studies done by Chang and co-workers (Chang et al., 2018). They measured K_V7.4 activity in presence of CaM or CaM mutants that disabled the calcium binding ability of the N-lobe (CaM12), the C-lobe (CaM34), or both (CaM1234) (Keen et al., 1999). Electrophysiological recordings revealed that co-expression of CaM1234 accelerated the fast component of K_V7.4 channel activation, sparing deactivation and produced a large (>35 mV) leftward shift in the voltage dependence of activation. Sihn and co-workers previously (Sihn et al., 2016) obtained similar results. In the experiments done with K_V7.2 co-expressed with CaM1234 produced lower but also pronounced leftward shift in the voltage (~25 mV) (Gomis-Perez et al., 2017). This comes along with our results, where CaM1234 it is insensitive to Ca^{2+}, the titration did not provoke a conformational change as a function of Ca^{2+}.

In the same way they show that co-expression with CaM34 mimic the effects of CaM1234 on both activation rate and activation voltage dependency (Sihn et al., 2016). However, CaM12 caused only modest perturbations to channel biophysical properties, producing only a slightly faster activation rate and a small activation curve leftward shift.

Furthermore, the single mutant CaM3 causes effects similar to CaM34 on both the activation rate and the voltage dependence of activation, whereas CaM4 caused milder effect. These results are consistent with the possibility that Apo/E-F (3) contacts the S2/S3 linker from the voltage sensor domain (Sun and MacKinnon, 2017). Similarly, the FRET reduction in K_V7.4:CaM 124 (67%) is close to the FRET-ratio reduction that occurs in K_V7.4:CaMwt (100%). However, when the E-F (3) is mutated, the conformational change is smaller and the FRET-ratio reduce just a %22 in K_V7.4:CaM3, comparing with K_V7:CaM wt.

In the same way, the effects of CaM1234 on K_V7.2 (Gomis-Perez et al., 2017), K_V7.3 (Gomis-Perez et al., 2017), and K_V7.4 (Chang et al., 2018) and K_V7.5 (Chang et al., 2018) demonstrate a unified mechanism for these channels, where Apo/CaM facilitates activation of the neuronal K_V7.2–K_V7.5 isoforms, whereas Ca^{2+}/CaM exerts an inhibitory effect.

Taken together available data further indicate that **CaM E-F (3) acts as a Ca^{2+}-dependent switch that controls channel activity in K_V7 family, while E-F (4) has a modulatory role**. Considering the degree of dependence between E-F hands of the same lobe, the results obtained with CaM3 surprised us. How can calcium binding to one hand affect calcium signalling so drastically? In addition, an interaction with the loop between the S2/S3 transmembrane with this E-F hand has been described which. Is the specificity of hand 3 and its interaction with S2/S3 an evolutionary mechanism developed in these channels for calcium signaling?

We analyze this question in the next chapter.

6.5. MATERIALS AND METHODS

6.5.1. Recombinant protein production

The expression of the cytosolic moiety of K_V7.2 covering helices hA and hB results in an insoluble protein. To alleviate this problem the fragment was coexpressed with CaM. To avoid aggregation DTT was added to all buffers in a 1mM concentration and renovated every 12 hours.
The fluorescent mTFP1 (donor) was fused to the N-terminal of K_V7.2-AB and mcpVenus (acceptor) to the C-terminal. This recombinant protein was cloned into a pProEX-HTc plasmid (Invitrogen) that introduces a 6xHis N-terminal tag. CaM, CaM3, CaM4, CaM123 and CaM124 were cloned into the co-expression compatible plasmid pOKD4 and both plasmids were co-transformed by electroporation in BL21(DE3) cells (Novagen).
Cells were grown at 37°C in 1L of LB medium containing ampicillin and kanamycin until an A_{600}=0.6–0.8 was reached. The expression of the fusion proteins was induced with 0.3mM of IPTG O/N at 25°C. The cells were then harvested by centrifugation at 9,000g for 9min and re-suspended in 25ml of Buffer A (KCl 120mM, K-HEPES 50mM [pH 7.4], imidazole 20mM, DTT 500µM, PMSF 1mM, protease inhibitor EDTA free: Roche, Ref. 04693132001). After lysis by sonication (10 s ON, 20s OFF, 20 cycles at 60% amplitude), the slurry was centrifuged at 25,000g for 30min, and the supernatant was filtered (0.20 µm) and transferred to a clean tube. The complex was affinity purified from the supernatant using a His-Trap-talon column and equilibrated with FRET buffer (KCl 120mM, Hepes 50mM, NaCl 5mM, EGTA 5mM, 1 mM DTT). The fractions containing soluble monomeric C-terminal proteins were identified by SDS-PAGE. Size-exclusion chromatography was performed using Superdex 200pg 26/60 column (GE Healthcare, ref. 28–9893) pre-equilibrated with KCl 120mM, HEPES 50mM [pH 7.4], NaCl 5mM,EGTA 5mM, 1 mM DTT. Fractions containing the protein complex were concentrated using Amicon Ultra-15 centrifugal filter units with a 3 kDa cut-off (Sigma-Aldrich).

FRET Experiments

FRET measurements were done as described in Chapter 3.

7. S2/S3 loop has a role on channel gating

7.1. INTRODUCTION

7.1.1. The role of S2/S3 loop

The PIP_2 free cryo-EM structure of Xenopus KCNQ1, which shares 78% sequence of identity with human KCNQ1, was resolved recently at overall 3.7 Å resolution (Sun & MacKinnon, 2017). The structure showed that CaM contacts KCNQ1-EM through two separate interfaces. One of these was identified previously in crystal structures of cytoplasmic domains (Sachyani et al., 2014).

In this contact, the A-B helices of KCNQ1-EM insert into the middle of a clamshell-like structure formed by the N- and C-lobes of CaM (Sun and MacKinnon, 2017). The structure of the CaM/AB complex is very similar in the cryo-EM and crystal structures, with an RMSD of 0.82 Å. However, they observed a difference in the density of the 4th EF hand that was absent in the crystal structure (PDB code: 4V0C).

Figure 7.1. Schematic representation of a subunit of K_V7.1 channel in complex with CaM. CaM is represented in purple, Ca^{2+} ions as red spheres, C-terminal in blue, transmembrane domains are represented in yellow, and in orange S2/S3 loop, which was synthesized as peptide for experiments. PDB: 5VMS.

This density is consistent with the presence of a Ca^{2+} ion. The **second contact is formed between the S2/S3 loop of the voltage sensor (part of the transmembrane channel) and the 3rd EF hand of CaM** (Figure 7.1). This second contact region was not observed in crystal structures because these did not contain the transmembrane channel.

It is noteworthy to mention than Sun & MacKinnon resolved recently a second structure of K_V7.1:CaM in presence of PIP_2 were the interaction between CaM and S2/S3 loop is not observed (Sun & MacKinnon, 2019). When engaged to PIP_2 and KCNE3 there are large conformational changes, as well as dilation of the pore's gate. It is known that conductivity of the pore is largely regulated by the signalling lipid PIP_2: the gate can only open in the presence of this lipid. Since PIP_2 likely acts by coupling the voltage sensor domain to the pore domain of KCNQ1, in the absence of PIP_2, the voltage sensors move, but are uncoupled from the pore, which does not

open (Zaydman et al., 2013). The structure shows that the binding of PIP_2 causes a rotation of the CaM binding domain of almost 180 degrees. In addition, there are a series of movements that, when also engaged to KCNE3, conclude with the dilation of the pore gate to a "near-open" state. It is noteworthy that PIP_2 binding site involves the S2-S3 loop, and also S0 and the S4-S5 linker of KCNQ1 (Figure 7.2), maybe preventing the interaction with CaM. For other known PIP2 sites, however, no lipid occupancy was detected, indicating that caution should be exerted when interpreting cryo-EM images.

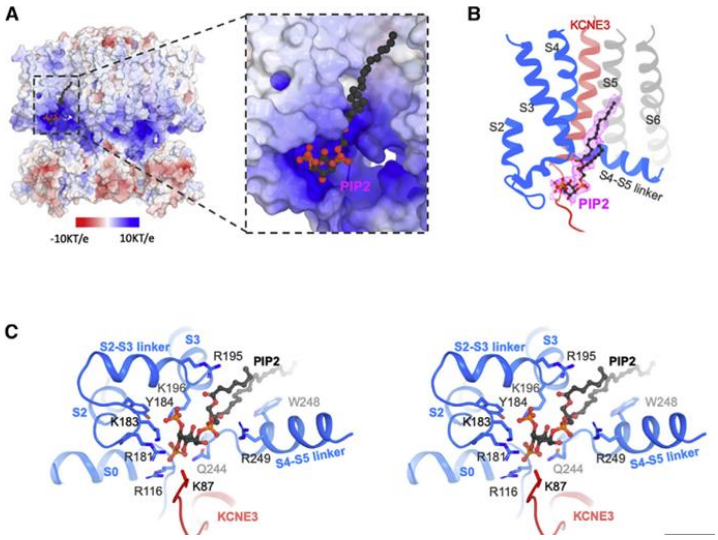

Figure 7.2. PIP_2 Binding site of the hKCNQ1EM-KCNE3-CaM Channel Complex. (A) Surface potential representation (-10KT/e to 10KT/e, in vacuum) of the PIP_2 binding site. PIP_2 binding site is zoomed in on the right. PIP_2 molecule is shown as balls and sticks. (B) Cryo-EM density of PIP_2 in the complex. Only the surrounding region of the PIP_2 binding site are shown in cartoon for clarity. KCNE3 is colored in red, and two neighboring KCNQ1 subunits are colored in gray and blue, respectively. (C) Stereo view of the PIP_2 binding site. The side chains of residues within 4 Å of PIP2 are shown as sticks. PIP_2 is shown as balls and sticks. (From Sun & MacKinnon, 2019).

The physiological relevance of this interaction is unknown, but it suggests a mechanism by which CaM regulates voltage dependence. It is important to remember that the union of Ca^{2+} to the E-F hand 3 is essential in the transmission of the calcium signal in these channels, as we have shown in the previous chapter.

7.1.2. Conserved sequence S2/S3

Sequence alignment of the voltage-gated potassium channels (K_V1-9) families shows that the nine-amino acid S2-S3 loop in KCNQ1EM (and other K_V7s) is conserved in length and sequence among both KCNQ1 orthologues and paralogs, but is absent in the other voltage-gated potassium channels (Sun and MacKinnon, 2017) (Figure 7.3).

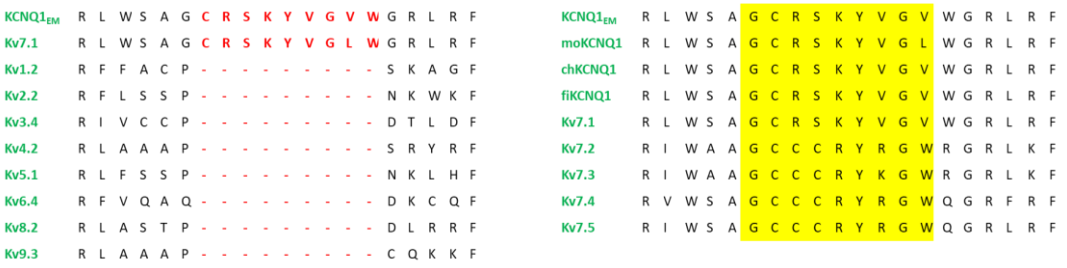

Figure 7.3. Sequence alignment of the S2-S3 loop region among K_V1-9 family and KCNQ1 orthologs and paralogs. Protein accession codes are as follows, K_V1.2: NP_004965.1, K_V2.2: NP_004761.2, K_V3.4: NP_004969.2, K_V4.2: NP_036413.1, K_V5.1: NP_002227.2, K_V6.4: NP_758857.1, K_V8.2: NP_598004.1, K_V9.3: NP_002243.3, K_V7.1: NP_000209.2, K_V7.2: NP_742105.1, K_V7.3: NP_004510.1, K_V7.4: NP_004691.2 and K_V7.5: NP_062816.2. All the above sequences are from *Homo sapiens*. moKCNQ1: NP_032460.2 (*Mus musculus*), chKCNQ1: XP_421022.3 (*Gallus gallus*) and fiKCNQ1: NP_001116714.1 (*Danio rerio*). Adapted from Sun & MacKinnon, 2017.

This loop, **unique to the K_V7s,** forms the second contact surface, specifically with the 3rd EF hand of CaM. No density was observed here, even at the high Ca^{2+} concentration (0.5 mM) under which the structure was determined, suggesting that the E-F (3) site was not occupied by this cation (Sun and MacKinnon, 2017).

7.2. OBJECTIVES

Here, we aim to address the functional significance of S2/S3 insertion, which extends into the cytoplasm and interacts with CaM and analyse its role on Ca^{2+} signal transduction.

7.3. RESULTS

7.3.1. EFFECT OF S2/S3 ON D-CaM

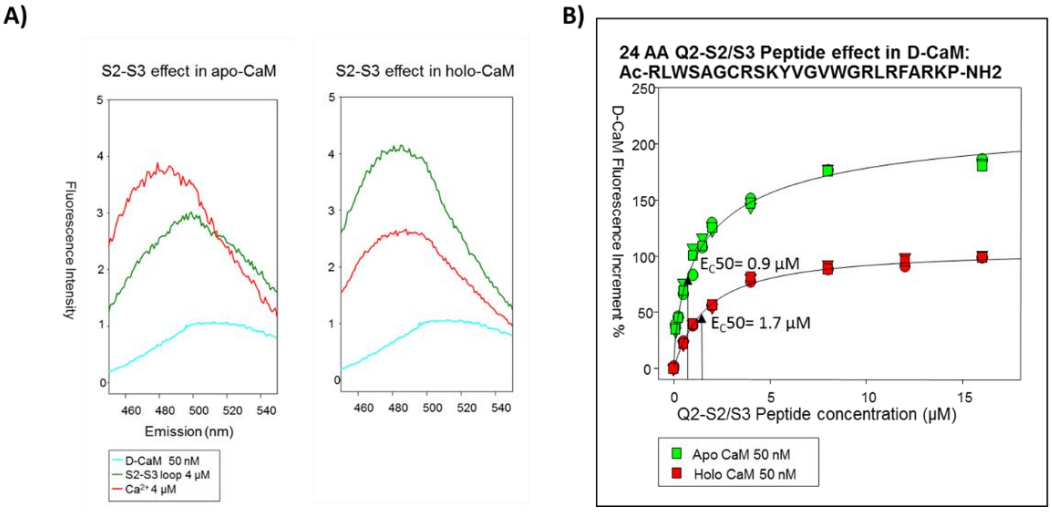

Figure 7.4. Effect of Q2-S2/S3 effect on D-CaM. **(A)** Emission spectra of D-CaM excited a 340 nm. Cyan line show the emission of Apo-D-CaM. Graphic on the left show the peptide titration (green lines) followed by a Ca^{2+} titration (red lines). The spectra on the right show the opposite, first Ca^{2+} titration succeeding peptide titration. **(B)** Graphic shows D-CaM fluorescence intensity increment (490-500 nm) vs. Q2-S2/S3 peptide concentration. Green plots correspond to Apo-D-CaM (5 mM EGTA) and red-plots to Holo-D-CaM (1 mM Ca^{2+}). The lines are the result of fitting the Hill-equation to the data.

We began analysing the interaction between CaM and S2/S3 loop, titrating Q2-S2/S3 peptide (Ac-RLWSAGCRSKYVGVWGRLRFARKP-NH2) on D-CaM fluorescence emission. We observed an increment in the fluorescence intensity of Apo-D-CaM almost 200% (199 ± 13, n = xx). The apparent affinity of the peptide is close to 1 µM (0.9 ± 0.2 µM for Apo-D-CaM). In addition, as also observed when calcium concentration is increased, two different effects of the peptide can be detected in D-CaM based assay. On the one hand, the binding of the peptide produces an **increase in the intensity** of D-CaM fluorescence until it almost triples (with Ca^{2+} it only doubles). Additionally, there is also a **shift to the left** in the maximum emission peak of the fluorescence emission, moving from 500 to 495 nm, whereas with Ca^{2+} it moves up to 490 nm. Therefore, the peptide effect partially recapitulates the effect of Ca^{2+}. To get further insights, the effect of the peptide was also analysed in the presence of Ca^{2+}. In this case, D-CaM was saturated with Ca^{2+} (Figure 7.4., A. right, red line) before peptide titration. Once the maximum effect of Ca2+ on emission spectrum was reached (it is known that from 2 µM of Ca^{2+} all EF hands are occupied), S2/S3 peptide was added, which causes a new increase in D-CaM fluorescence by duplicating the fluorescence reached by Ca^{2+}-D-CaM. An additional shift in the peak emission to the left was observed. Upon peptide addition D-CaM fluorescence duplicates (by 106 ± 2%) (Figure 7.4.). In this case, the apparent affinity was lower, being the EC50 1.7 ± 0.1 µM. Thus, peptide and Ca^{2+} apparently have an **additive effect**, the presence of one does not occlude the effect of the other, which is an indication that both ligands have different mechanisms of action. The presence of both, Ca^{2+} and peptide, have similar effects on D-CaM, achieving maximum intensity quadrupling and maximum peak emission displacement at 485-6 nm, regardless of what order they have been added to D-CaM (Figure 7.4.).

7.3.2. ^{15}N-HSQC SPECTRUM OF Q2-*h*AB:CaM LABELLED IN COMPLEX WITH UNLABELLED Q1-S2/S3

Data from D-CaM experiments suggest that there is an interaction between CaM and S2/S3 independent of Ca^{2+}, but we cannot discern where the peptide binds. Furthermore, the cryo-EM structure in absence of PIP_2 reveals an interaction with the E-F (3) hand, but we do not know if this interaction is specific to the E-F (3), or if it is capable of interacting with any E-F hand.

In order to identify the interaction site between S2/S3 and CaM in solution, NMR data was collected. As we mentioned before the ^{1}H-^{15}N HSQC signals of Q2*h*AB:CaM complex were assigned to resolve the structure. Once assignments are obtained, the ^{1}H-^{15}N HSQC spectra of a ^{15}N-labeled protein, which shows one peak for every backbone amide group in the protein, can be used to monitor its interaction with any unlabelled ligand that is added to the labelled protein

solution. Thus, ^{15}N-HSQC spectra labelled Q2-*h*AB:CaM (75 µM) was collected with 1 mM unlabelled Q1-S2/S3, in apo- and in holo-configuration (2 mM Ca^{2+}).

The ^{15}N-HSQC spectra without peptide and with peptide are superimposed (Figure 7.5 and 7.6).

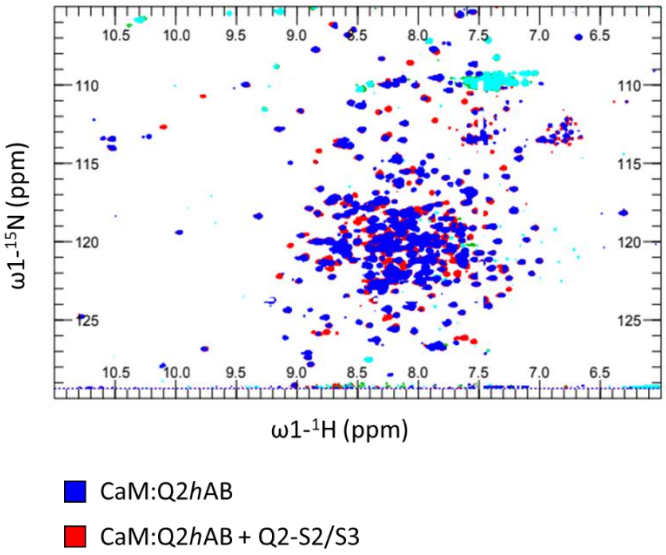

Figure 7.5. ^{15}N-HSQC of Q2*h*AB:CaM titrated with unlabeled Q2-S2/S3. ^{15}N-HSQC of Q2*h*AB:CaM complex at 75 µM (blue) and with Q1-S2/S3peptide at 1 mM (red). Signal overlap demonstrates that peptide tritation does not alter the structure of the complex.

It is noted that the chemical shifts of several residues are changed. Chemical shift perturbations (peak displacement or broadening) arise from changes in the environment of the NMR nucleus and can be caused by direct protein–protein interactions or conformational changes induced by the binding event. These perturbations can then be mapped onto a protein structure to reveal potential interaction sites.

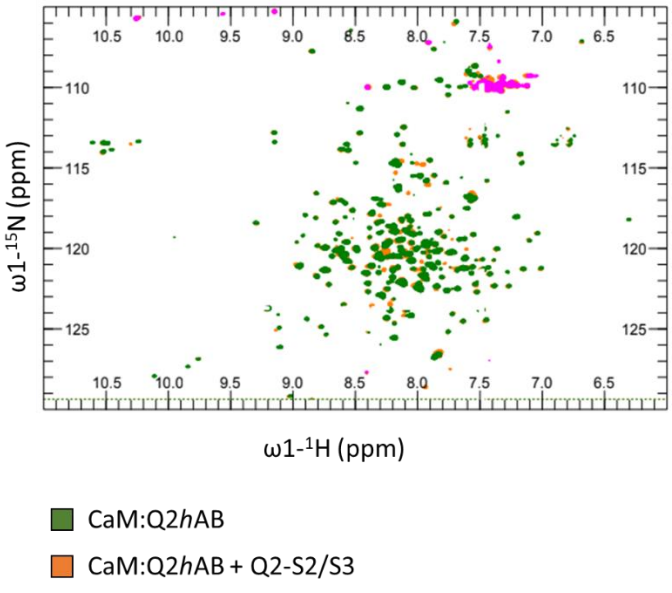

Figure 7.6. Holo-CaM:*h*AB overlay with and without peptide. Green spectra corresponds to the complex CaM:Q2*h*AB with 1 mM Ca^{2+}, and orange to CaM:Q2*h*AB 1 mM Ca^{2+} and 1 mM Q1-S2/S3.

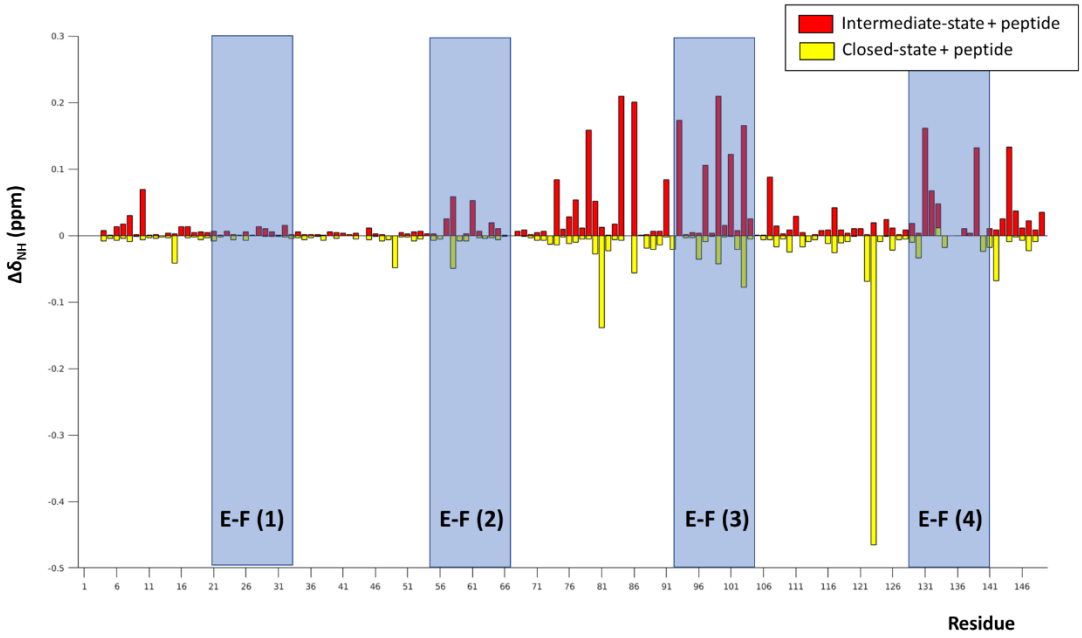

Figure 7.7. ^{1}H-^{15}N Chemical shift comparison of Q2*h*AB complex and peptide in presence and absence of calcium. More differences were shown for the Apo-CaM C-lobe suggesting that the peptide interact with more affinity with E-F (3) and E-F (4) in CaM/K_V7.2_AB complex. E-F (1) (20-31), E-F (2) (56-67), E-F (3) (93-104) and E-F (4) (129-140) were defined as blue boxes. There are not negative values.

As we can observe in figure 7.7., upon peptide binding, larger chemical shifts are observed in residues located in the **C-lobe** of CaM.

The overall displacement magnitude is greater for E-F (3), followed by E-F (4). We cannot differentiate whether the chemical shift is caused directly or indirectly by the peptide.

Analysing the chemical shift displacement on each residue the residues that are interacting with the peptide are especially those located in the C-lobe of the CaM, specially those located in the E-F (3) such as**, D94, N98, Y100, I102 and A104** (Figure 7.7) in the apo-conformation of the complex. In presence of Ca^{2+}, the overall chemial shifts are smaller, concordant with the observations from D-CaM experiments. However, S2/S3 is capable to interact with E-F (3) also in presence of Ca^{2+} (Figure 7.7). This coincides with cryoEM structure (Sun & MacKinnon, 2017), were the interaction was observed although it was resolved with 2 mM free Ca^{2+}. There also displaced residues located in E-F (4), specially I131 and E139. We cannot tell if this is a direct effect of the peptide or an allosteric effect. Also, there are displaced few signals which are not been assigned before. Noteworthy, **N98** and **Y100**, make contacts in the Cryo-EM structure, and agree with the proposed essential role (Sun & MacKinnon). They put special attention to N98, since CaM_N98S mutation is associated with prolonged QT intervals and sudden death in young patients (Jiménez-Jáimez et al., 2016; Makita et al., 2014). This mutation maps directly onto the interface between CaM and the voltage sensor, and clearly interacts with S2/S3 peptide. However, other mutations at E-F (3), or even at E-F (4), lead to the same electrophysiological profile, so the inferences on the N98S specificity can be regarded as an overstatement.

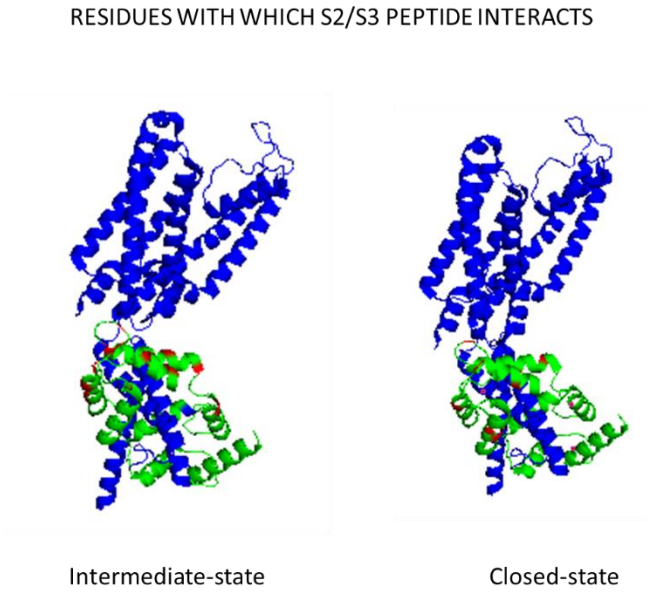

Figure 7.8. Residues with which S2/S3 peptide interact. Subunit of KCNQ1:CaM tetramer resolved by Cryo-EM. K_V7.1 channel is represented in blue and CaM in green. Residues with high chemical displacement ($\Delta\delta_{NH}$>0.1 ppm) upon S2/S3 peptide titration are highlighted in red. On the left it is shown the complex with Ca^{2+} only in the N-lobe. The complex on the right shows the complex in presence of 2 mM free Ca^{2+}.

7.3.3 PEPTIDE EFFECT ANALYSED BY FRET-SENSOR

We analysed the effect of S2/S3 loop on Ca^{2+} signalling by FRET. As it is described in 2nd chapter, Ca^{2+} binding to Q2*h*AB:CaM provokes a conformational change that can be monitored by FRET, using mTFP1-*h*AB-Venus:CaM complex. We titrated Ca^{2+} on the FRET-sensor in presence of different concentrations of Q2-S2/S3 peptide.

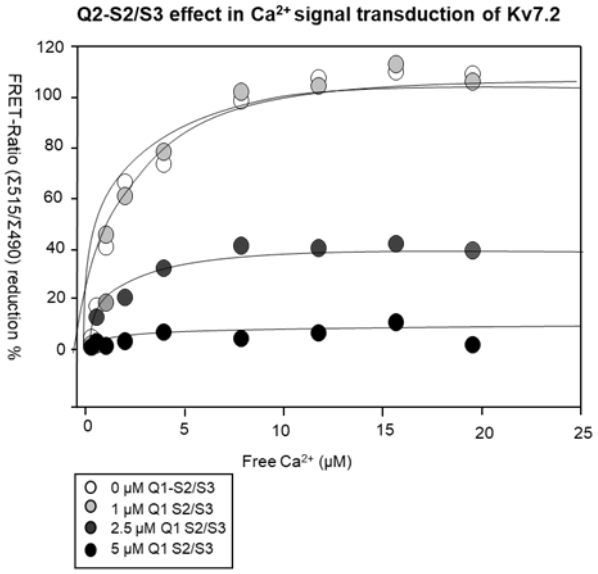

[Peptide]	Max.expec.	Ec50 (µM)	RSQR
0 µM	109 ± 12.3	0.9 ± 0.2	0.97
1 µM	116 ± 17.3	0.8 ± 0.1	0.91
2.5 µM	44 ± 5.6	1.1 ± 0.3	0.98
5 µM	5 ± 1.4	1.8 ± 0.4	0.90

Figure 7.9. Q2-S2/S3 effect on Ca^{2+} signal transduction. The graphic shows the % of FRET-Index reduction vs. Ca^{2+} concentration. Titration of 500 nM mTFP1-*h*AB-Venus:CaM is represented in white spheres. Light gray is in presence of 1 µM Q2-S2/S3. The spheres are darker as the concentration of the peptide in the sample increases, passing through 2, 5 and 10 µM. The lines are the result of fitting the Hill-equation to the data. Beside the parameters of these fittings are shown. Each plot represents the average of at least 3 independent experiments.

Calcium titration was done first without peptide, to test the quality of the sample. As it was expected, FRET-Index was reduced from 1.61 ± 0.05 to 1.17 ± 0.04 (Figure 7.9). These results were taken as reference to estimate the effect of S2/S2 loop. At 2.5 µM peptide a reduction on the Ca^{2+} effect was observed. Upon Ca^{2+} binding the FRET-index reaches 1.42 ± 0.05, which is 40 % than that observed with 0 or 1 µM peptide. In the same way, when we tested the effect of **S2/S3 peptide at 5 µM** the Ca^{2+} driven conformational change was undetectable, the FRET-index upon Ca^{2+} did not suffer any reduction, maintaining at very close values that **FRET-Index in apo-configuration**, at 1.6 ± 0.09. At that time we thought that the interaction between the S2/S3 and the E-F (3) prevented the union to Ca^{2+} in that E-F hand, which as we have seen in the previous chapter, could be in charge of transmitting the Ca^{2+} signal to the channel.

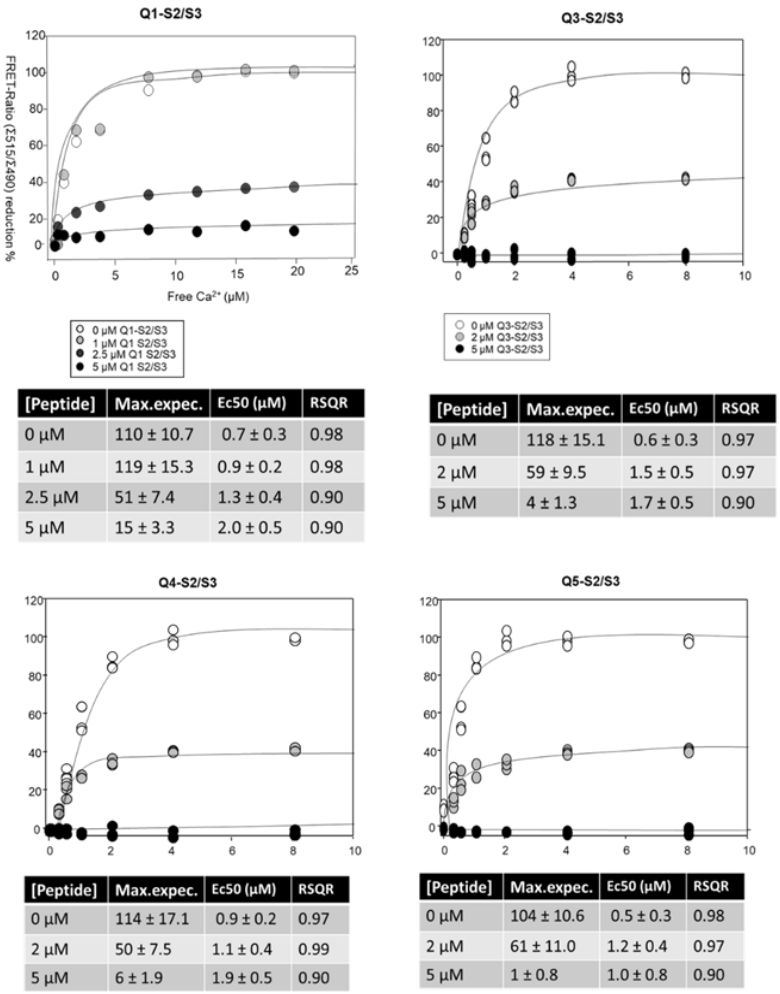

[Peptide]	Max.expec.	Ec50 (µM)	RSQR
0 µM	110 ± 10.7	0.7 ± 0.3	0.98
1 µM	119 ± 15.3	0.9 ± 0.2	0.98
2.5 µM	51 ± 7.4	1.3 ± 0.4	0.90
5 µM	15 ± 3.3	2.0 ± 0.5	0.90

[Peptide]	Max.expec.	Ec50 (µM)	RSQR
0 µM	118 ± 15.1	0.6 ± 0.3	0.97
2 µM	59 ± 9.5	1.5 ± 0.5	0.97
5 µM	4 ± 1.3	1.7 ± 0.5	0.90

[Peptide]	Max.expec.	Ec50 (µM)	RSQR
0 µM	114 ± 17.1	0.9 ± 0.2	0.97
2 µM	50 ± 7.5	1.1 ± 0.4	0.99
5 µM	6 ± 1.9	1.9 ± 0.5	0.90

[Peptide]	Max.expec.	Ec50 (µM)	RSQR
0 µM	104 ± 10.6	0.5 ± 0.3	0.98
2 µM	61 ± 11.0	1.2 ± 0.4	0.97
5 µM	1 ± 0.8	1.0 ± 0.8	0.90

Figure 7.10. S2/S3 peptide interaction with Q2*h*AB:CaM. The effect of the S2/S3 loops of different isoforms of K_V7 family. Each graphic show the FRET-index (FRET/CFP) of 500 nM mTFP-Q2*h*AB-Venus, mixed with different concentrations of S2/S3 peptide, and titrated with Ca^{2+}. The lines are the result of fitting the Hill-equation to the data. Beside the parameters of these fittings are shown. Each plot represents the average of at least 3 independent experiments.

Afterwards, the effect of the S2/S3 loops of the different isoforms of K_V7 channel family were tested in our FRET-Biosensor. The effect was similar for all the isoforms. In presence of 2 µM peptide, the effect of Ca^{2+} is reduced by half. That is, the reduction in the FRET-index as a result of the union with Ca^{2+}, seen in chapter 1, remains at 40%, which would translate as the conformational change caused by Ca^{2+}, **is not fully completed** (Figure 7.10).

Similarly, at 5 µM peptide, the Ca^{2+} effect is **abolished**, that is, the FRET-Index, after Ca^{2+} binding, remains the same as in the apo-configuration. This effect is observed when there is a competition of both ligands for binding to the protein complex.

Additionally, Q1-S2/S3, Q2-S2/S3, Q3-S2/S3 were tested at 10 µM, and interestingly, **the FRET-Index upon Ca^{2+} binding, far from being reduced, was increased, and almost to triplicate (200%).** This means that the protein complex is acquiring a **new configuration**, where helices A and B could be approaching each other, increasing the energy transfer between two fluorophores (Figure 7.11).

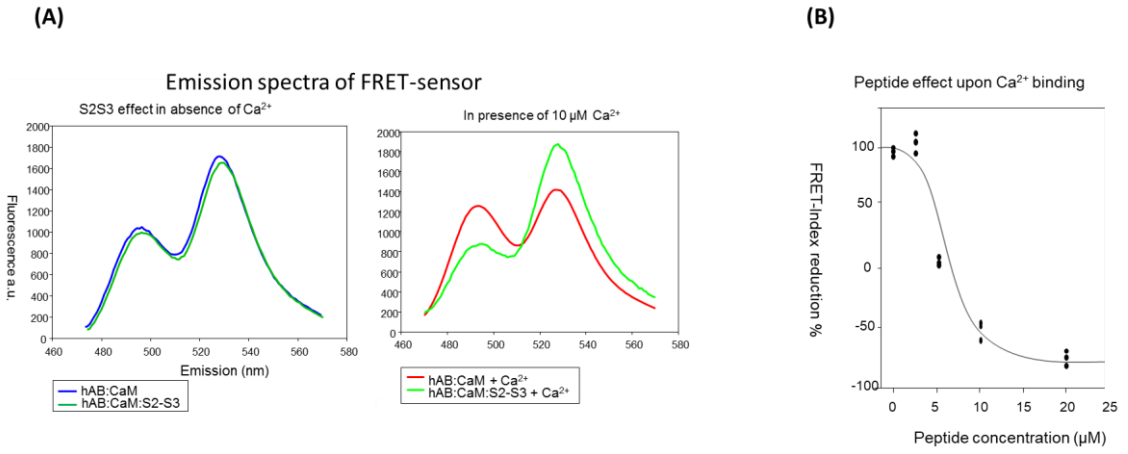

Figure 7.11. FRET-Index upon S2/S3 peptide titration. **(A)** Emission spectra of 500 nM mTFP1-Q2*h*AB-Venus:CaM, excited at 458 nm, of 500 nM mTFP1-Q*h*AB-Venus in complex with S2-S3, in absence and in presence of Ca^{2+} (100 µM). **(B)** FRET-index reduction (%) upon Ca^{2+} (100 µM) binding vs. peptide concentration in the sample. The line is the result of fitting the Hill-equation to the data.

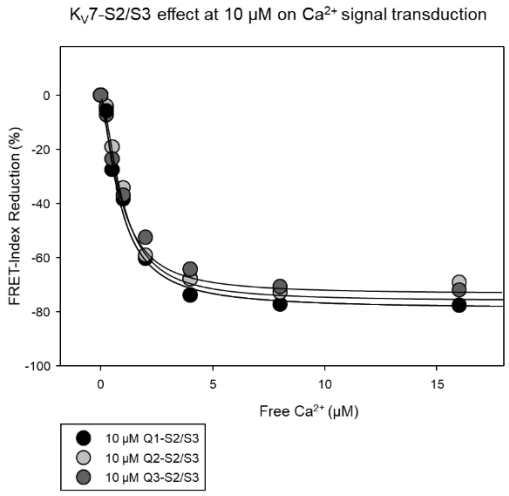

[Peptide] (µM)	Max.expected	Ec50 (µM)	RSQR
Q1-S2/S3	-88 ± 3.05	1.6 ± 0.08	0.97
Q2-S2/S3	-91 ± 2.06	2.1 ± 0.22	0.99
Q3-S2/S3	-80.5 ± 5.2	1.9 ± 0.26	0.96

Figure 7.12. Calcium titration of 500 nM mTFP-*h*AB-Venus mixed with 10 µM S2/S3 peptide of K_V7.1, K_V7.2 and K_V7.3 isoforms. Yellow plots correspond to S2/S3 linker of K_V7.1 isoform, green for K_V7.2 and red for K_V7.3. The result shown is the percentage of the FRET reduction, having as reference the complex without peptide, or calcium. The lines are the result of fitting the Hill-equation to the data. Beside the parameters of these fittings are shown. Each plot represents the average of at least 3 independent experiments.

The affinity for Ca^{2+} in this new configuration is similar for all S2/S3 isoforms proved: 1.16 µM ± 0.16 for Q1-S2/S3, 1.73 µM ± 0.9 for Q2-S2/S3 and 1.55 nM ± 0.5 for Q3-S2/S3 (Figure 7.12). Additionally, The Hill coefficient was determined as 0.83, 0.35 and 0.76 for each isoform.

7.3.4. PEPTIDE SPECIFICITY ON EF-HANDS

As we saw in the previous chapter, the signalling by Ca^{2+} on the K_V7 channels is mostly mediated by the E-F (3) hand, and to a lesser extent by the E-F (4). In the cryo-EM structure of the K_V7.1 in complex with CaM, the interaction between the E-F hand (3) and the linker between the S2/S3 is described. The objective was to analyze whether this interaction was specific to E-F (3) or, on the contrary, the S2/S3 loop was able to interact with the E-F hands in a non-specific way. For this purpose, the complex was purified with CaM3 and with CaM124 and titration by Ca^{2+} was carried out in the presence of peptide Q2-S2/S3 as described above.

The effect of peptide Q2-S2/S3 on the mTFP1-*h*AB-Venus complex with CaM124 closely approximates that observed with the WT CaM. At 5 µM peptide, the reduction in FRET caused by Ca^{2+} is annul, and at 10 µM the increase in FRET observed also with WT is observed. The maximum expected FRET will be 80% and the affinity for Ca^{2+} under these conditions is 1.4 µM, higher than the 0.62 µM observed in the absence of peptide.

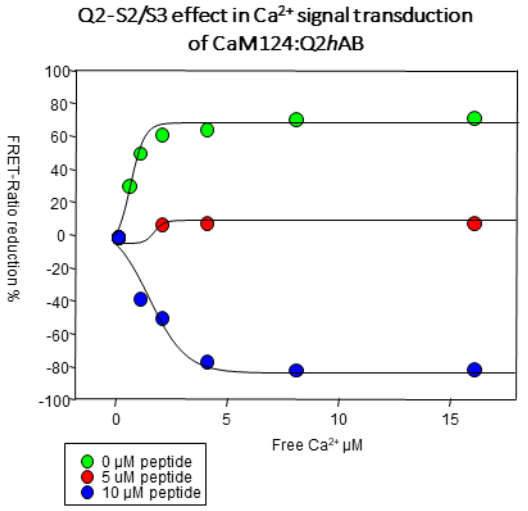

[Peptide] (µM)	Max.expected	Ec50 (µM)	RSQR
0	68 ± 3.05	0.6 ± 0.08	0.97
5	8.8 ± 2.06	1.6 ± 0.22	0.99
10	-80.5 ± 5.2	1.4 ± 0.26	0.96

Figure 7.13. Calcium titration of 500 nM CaM124:mTFP-*h*AB-Venus: mixed with Q2-S2/S3 peptides. Green circles correspond to control titration without Q2-S2/S3 peptide. Red circles to 5µM and blue circles to 10 µM. The result shown is the percentage of the FRET reduction, having as reference the complex without peptide, or calcium. The lines are the result of fitting the Hill-equation to the data. Beside the parameters of these fittings are shown. Each plot represents the average of at least 3 independent experiments.

However, when the complex is formed with CaM3, the same effect is not observed. In this case, when we add the Q2-S2/S3 peptide at 10 µM the increase in the FRET-Index when adding Ca^{2+} is 40.4% and the affinity for Ca^{2+} amounts to 2.8 µM, almost three times higher than the estimated without peptide (0.9 µM).

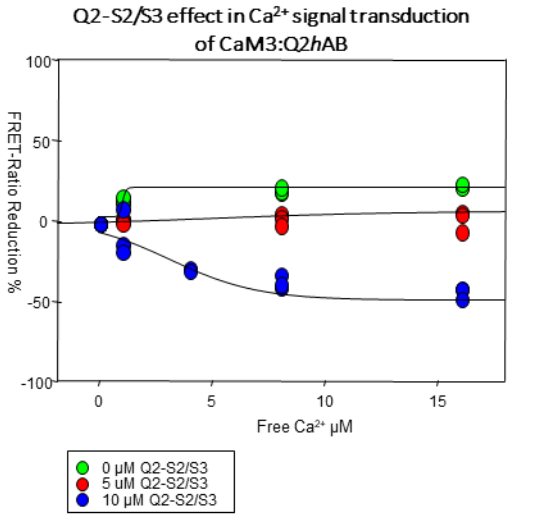

[Peptide] (µM)	Max.expected	Ec50 (µM)	RSQR
0	24 ± 1.08	0.9 ± 0.35	0.99
5	6 ± 1.92	3.4 ± 0.28	0.90
10	-40.4 ± 3.52	1.4 ± 0.44	0.97

Figure 7.14. Calcium titration of 500 nM CaM3:mTFP-*h*AB-Venus: mixed with Q2-S2/S3 peptides. Green circles correspond to control titration without Q2-S2/S3 peptide. Red circles to 5µM and blue circles to 10 µM. The result shown is the percentage of the FRET reduction, having as reference the complex without peptide, or calcium. The lines are the result of fitting the Hill-equation to the data. Beside the parameters of these fittings are shown. Each plot represents the average of at least 3 independent experiments.

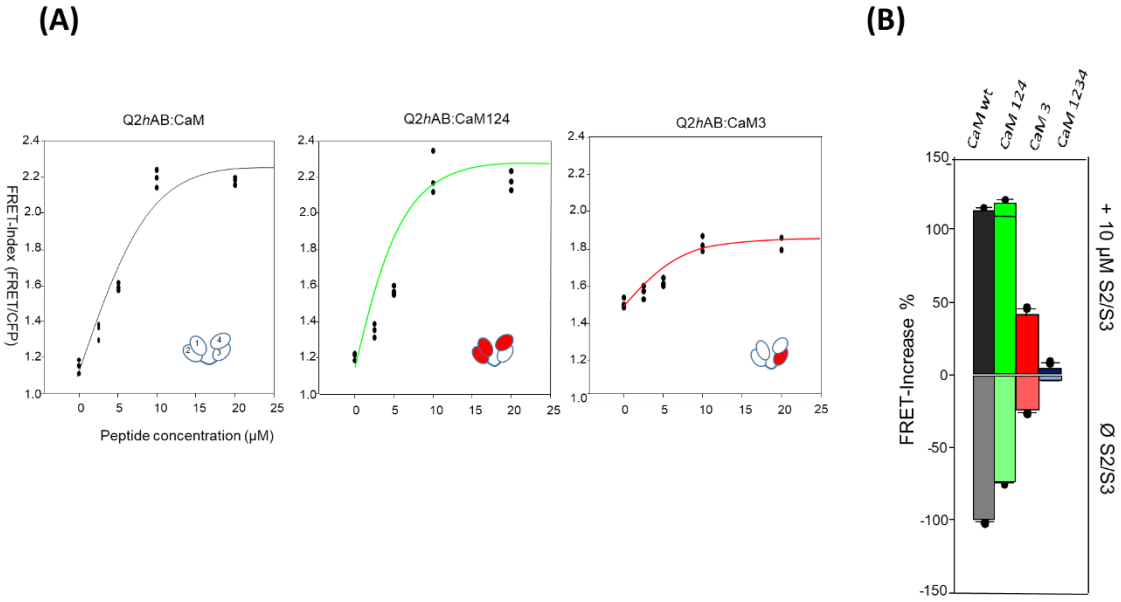

Figure 7.15. Q2-S2/S3 effect on Ca^{2+} signaling monitored by FRET-Sensor in complex with mutant CaMs. (A) Q2-S2/S3 peptide titration in presence of saturating concentration of Ca2+ (100 µM free Ca2+) of Q2hAB in complex with wt CaM (black line), CaM124 (green line) and CaM3 (red lines). **(B)** The graphic shows the Ca^{2+} effect on FRET-index, in both, absence and presence of 10 µM Q2-S2/S3. FRET-Increase % represents FRET-Index increase upon Ca^{2+} binding.

7.4. DISCUSSION

In this chapter we analyze the interaction of the S2/S3 loop within the Q2*h*AB:CaM complex, which was previously identified in the cryoEM structure of the K_V7.1:CaM. The interaction of the peptide was first analysed with D-CaM. This assay discriminates binding to a target to the groove between the lobes (which leads to an increase in fluorescence), and occupation by Ca^{2+} (which in addition to an increase in signal, leads to and a left-shift in the peak emission).

We observe that the **S2/S3 peptide is capable of interacting with CaM, both in the absence and in the presence of Ca^{2+},** causing an increase in fluorescence intensity larger than that previously observed with peptides of helix A and helix B of K_V7.2/3 (Alaimo et al., 2014). Furthermore, the signature response differs in more aspects from the responses observed with other targets. The titration of **D-CaM with S2/S3 peptide, together with the increase in fluorescence, shows a shift to the left**, clearly observed in the maximum peak of the emission spectrum after exciting at 320 nm. This effect had been observed previously, after the addition of Ca^{2+} (Alaimo et al., 2014) and was related to the union of Ca^{2+} to the E-F hands. Furthermore, in the presence of Ca^{2+}, the increase in the intensity of the D-CaM signal when adding the peptide, reaches half of that observed in the absence of Ca^{2+}.

In none of the previously tested peptides have we observed a differential increase in fluorescence depending on the calcium concentration.

Therefore, we can assume that the S2/S3 loop interacts with CaM alone in two different ways. First, CaM could be embracing this loop, just as it does with the A and B helices of K_V7 channels, and this would be responsible of some increment in emission intensity. Second, the peptide could be binding to the EF hands, as it is observed in the cryoEM structure (Sun & MacKinnon, 2017). Through D-CaM analysis we cannot discern if the peptide discriminates between E-F hands.

It is important to note that Ca^{2+} and the peptide have an additive effect on D-CaM, that is, the effect of one does not nullify that of the other. Thus, when they are together, they achieve higher intensity in the D-CaM fluorescence, than that obtained separately. There are also changes in affinity, usually in the presence of peptide the EC_{50} of the CaM for calcium doubles. It can be suggested that Ca^{2+} and peptide S2/S3 share binding sites, and the decrease in affinity is a consequence of competition between the two for binding to CaM.

The next step was to analyze with which residues of the Q2*h*AB:CaM complex was interacting with the peptide. As this complex was completely resolved before by NMR, all the signals are already assigned (except those that from the TW helix). Thus, by means of a titration with unlabelled peptide, in a ^{15}N labelled complex, it is easy to observe where the peptide is interacting, generally due to changes in chemical signals displacements of CaM:Q2*h*AB complex. We observed that ^{15}N-HSQC spectra with Q1-S2/S3 peptide shows slightly lower signal intensity comparing with the spectra without peptide. This could be due to a increment in the volume of the protein-complex, since the peptide is binding to Q2-*h*AB:CaM. Once the size is bigger, the transverse relaxation time constant (T_2) become relatively short, due to the slow tumbling of the molecules. However, the spectra show good quality in purity and dispersity.

The clearest changes in the chemical shifts occur in C-lobe of CaM. In the cryoEM structure, the peptide interaction occurred in the E-F (3) hand, the main responsible of Ca^{2+} signal transmission in K_V7 channels, as we have seen in the previous chapter. We have demonstrated that this peptide interacts with the E-F (3) of the CaM in complex with Q2*h*AB, both, in presence and in absence of calcium, however we cannot analyse by these methods how the peptide affects the calcium signal transmission.

To analyze the effect of the S2/S3 peptide in Ca^{2+} signalling we monitored FRET from the mTFP1-hAB-Venus sensor. Titrations were performed by Ca^{2+} as described in the first chapter, but in presence of different concentrations of S2/S3 peptide. We observed that the S2/S3 loop of the different isoforms of K_V7 has a very similar effect on the Q2*h*AB:CaM complex. We remind that the conformational change of the complex as a function of calcium provokes a reduction of FRET, however, in presence of 2.5 µM S2-S3 peptide, this reduction decreases by half. Looking at the results it was logical to think that the binding of the S2/S3 peptide to the E-F (3), prevented the binding of Ca^{2+} to it, and therefore, blocked the calcium signal transmission in the complex. Actually, when the concentration of the S2/S3 peptide was raised to 5 µM no differences in FRET are observed in the presence and absence of Ca^{2+}, suggesting that the signal transmission was precluded by the peptide. Surprisingly at 10 µM S2/S3 peptide, the FRET increased, but only after adding Ca^{2+}, being even higher that the observed in absence of Ca^{2+} (FRET-INDEX 2.2>1.7). The increment on FRET-Index is a consequence of an approximation between the fluorophores,

provoked, presumably, by an approach between helix A and B. **We can suggest that the peptide causes a different structure that those previously resolved by NMR (Bernardo-Seisdedos et al., 2018).**

We hypothesize that the differences observed at different S2/S3 peptide concentrations are due to the presence of two different conformations: 1. when Ca^{2+} binds the E-F hands of the CaM:K_V7 the C-lobe of CaM rotates and this causes a separation between helices A and B, which translates as a decrease in FRET. 2. In presence of peptide, however, the complex acquires a new conformation, where helices A and B are closer, causing an increase in energy transmission between donor and acceptor fluorophores. At 2.5 µM peptide, the complex is barely bound to the peptide, thus E-F (3) is free to bind Ca^{2+}, and transmits the calcium signal, which reduces the FRET-index. At 5 µM of S2/S3 peptide we will get close to a balance between both conformations, and that is why we do not observe increase or decrease in the FRET after the addition of Ca^{2+}. Finally, at 10 µM peptide most E-F (3) are occupied by S2/S3 peptide, in this case, after Ca^{2+} addition the complex adopts a new orientation, where helix A and B are closer one from each other.

Finally, to confirm that the effect of the peptide is transmitted by the E-F (3), we performed a test using FRET with Q2*h*AB in complex with mutated CaM preventing its binding to calcium in specific E-F hands. For this, the effect of S2/S3 was tested in Q2*h*AB in complex with CaM WT, CaM124, and CaM3. Similar effects are observed between CaM124 and CaM WT, likewise, with CaM3, although an increase in the FRET-Index is observed, it does not reach the values obtained with the other CaM.

We have demonstrated that the binding of Ca^{2+} to E-F (3) drives the conformational changes. However, this configuration could be then stabilized by a new interaction established between the S2/S3 and E-F (3). Actually, has been proposed that this interaction may facilitate the movement of the voltage sensor or set the voltage-sensor in a pre-activated position, such that the channel could open at lower voltages (easier to activate with voltage) (Sun & MacKinnon, 2017). Our data demonstrates that **this contact has two additional consequences: it drives the movement of helix A in the opposite direction**, shortening the distance between helices A and B (as suggested by preliminary FRET studies using our AB/CaM biosensor). The second consequence is that **binding to Ca^{2+} is weaker when E-F (3) is touching the S2-S3 linker, so exit of Ca^{2+} became from E-F (3) becomes faster on returning to basal conditions**. Thus, our preliminary data is consistent with E-F (3) being the central hub for Ca^{2+} signalling, which is a novel concept (signalling by just one out of the four EF hand of CaM) for CaM physiology.

7.5. MATERIALS AND METHODS

7.5.1. PEPTIDE DESSIGN AND SOLUBILIZATION

The solubility of a peptide is determined mainly by its polarity. Acidic peptides can be reconstituted in basic buffers, whereas basic peptides can be dissolved in acidic solutions. Hydrophobic peptides and neutral peptides that contain large numbers of hydrophobic or polar

uncharged amino acids should be dissolved in small amounts of organic solvent such as DMSO, DMF, acetic acid, acetonitrile, methanol, propanol, or isopropanol, and then diluted using water. DMSO should not be used with peptides that methionine or free cysteine because it might oxidize the side-chain.

Test a portion of the synthesized peptide before dissolving the rest of the sample. Lyophilized peptides should be centrifuged briefly to pellet all the material. You might need to test several different solvents until you find the appropriate one. Sonication can be used to enhance solubility.

1. First, assign a value of −1 to each acidic residue (Asp [D], Glu [E], and the C-terminal –COOH). Next, assign a value of +1 to each basic residue (Arg [R], Lys [K], His [H], and the N-terminal -NH2), and then calculate the overall charge of the peptide.

2. If the overall charge of the peptide is positive, the peptide is basic. Try to dissolve the peptide in distilled water if possible. If it fails to dissolve in water, then try to dissolve the peptide in a small amount of 10–25% acetic acid. If this fails, add TFA (10–50 µl) to solubilize the peptide, and then dilute it to your desired concentration.

3. If the overall charge of the peptide is negative, the peptide is acidic. Acidic peptides might be soluble in PBS (pH 7.4). If this fails, add a small amount of basic solvent such as 0.1 M ammonium bicarbonate to dissolve the peptide, and then add water to the desired concentration. Peptides that contain free cysteines should be dissolved in degassed acidic buffers because thiol moieties will be oxidized rapidly to disulfides at pH >7.

4. If the overall charge of the peptide is 0, the peptide is neutral. Neutral peptides usually dissolve in organic solvents. First, try to add a small amount of acetonitrile, methanol, or isopropanol. For very hydrophobic peptides, try to dissolve the peptide in a small amount of DMSO, and then dilute the solution with water to the desired concentration. For Cys-containing peptides, use DMF instead of DMSO. For peptides that tend to aggregate, add 6 M guanidine, HCl, or 8 M urea, and then proceed with the necessary dilutions.

5. Tips: If none of the solvents worked, please try the Trifluoroethanol (TFE). Trifluoroethanol may form a solvent matrix for assisted hydrophobic interactions between peptide side chains (https://doi.org/10.1093/protein/13.11.739). TFE has been shown to induce and stabilize α-helices and to induce β-turns, β-hairpins and also β-strands.TFE disrupts tertiary interactions in proteins by weakening non-polar interactions while preserving secondary structures. TFE is frequently used as a co-solvent in protein folding studies with NMR spectroscopy. A mixture of trifluoroethanol (TFE) or hexafluoroisopropanol (HFIP) and trichloromethane (TCM) or dichloromethane (DCM) was found to be very powerful for dissolving peptides as well. TFE and HFIP have been shown to form clathrate structures starting from 10% HFIP or around 20% TFE.

To prevent or minimize degradation, store the peptide in lyophilized form at −20°C, or preferably −80°C. If the peptide is in solution, freeze-thaw cycles should be avoided by freezing individual aliquots.

Positively charged residues: K, R, H, and the N-terminus

Negatively charged residues: D, E, and the C-terminus

Hydrophobic uncharged residues: F, I, L, M, V, W, and Y

Uncharged residues: G, A, S, T, C, N, Q, P, acetyl, and amide

Most of the materials and methods in this chapter were equivalent to the ones described in Chapter 2 and Chapter 3. Here, we underscore only the differences with the reported protocols.

SOLUBILIZATION OF PEPTIDES

All linear peptides were bought from Proteogenix while, cyclic peptides were bought in Peptide Synthetics. Both were purified by reverse phase HPLC chromatography giving a purity greater than 95%. The peptides are stored at -20 °C in the form of lyophilized. Peptides were solubilized first in DMSO, to get 10 mM concentration. Then, was done a second dilution 1:100 in Fluorescence Buffer with 1 mM DTT, to obtain 100 µM Q2-S2/S3 solution.

7.5.2. PEPTIDE BINDING CHARACTERIZATION FLUORESCENCE SPECTROSCOPY

FRET experiments were done as described before, with the sensor that contains the complete linker.

To calculate the dissociation constant EC50 for the peptides, the FRET efficiency change (B) was plotted against the peptide concentration [P]. Data were fitted using the Hill equation, 3 parameter:

$$y = \frac{ax^b}{c^b + x^b}$$

Where a is the maximum, b is the Hill-coefficient and c is the EC_{50}.

- Dansyl-CaM production was done as described in chapter 4th.

Titration experiments were performed by adding increasing concentrations S2/S3 peptides to a cuvette containing D-CaM (50 nM) in Fluorescence buffer. Experiments were also performed in the presence of an excess of free Ca^{2+} (4 µM) by adding 4.34 mM Ca^{2+} to the Fluorescence buffer. The free Ca^{2+} concentration was determined using Fura-2 (Invitrogen), following the manufacturer's instructions.

Fluorescence enhancement was plotted against the protein concentration to generate the concentration-response curves, or in the case of the time course experiments, it was plotted against time (min) to obtain the time-response curves. The parameters of the Hill equation were fitted to the data by curvilinear regression, enabling the apparent affinity (EC_{50} or concentration that gives half-maximal change in the intensity of the fluorescence emission) or the t_{50} (half-time or time that gives half-maximal change in the intensity of fluorescence emission). The data are shown as the average of 3 or more independent experiments.

7.5.3. PEPTIDE INTERACTION ON ^{15}N-CaM:Q2*h*AB COMPLEX

NMR experiment was performed to analyse the interaction between the peptide Q1-S2/S3 (24 AA) and Q2*h*AB:CaM complex.

^{15}N- HSQC experiments constitute the fingerprint in protein NMR. Each residue of a protein (except proline) contains a proton amide bound to nitrogen in the peptide bond. If the protein is folded, the signals usually have a pattern dispersed in the spectrum, and many signals can be distinguished that do not show overlap. The protons of the amide groups of the side chains also produce a signal. Since the chemical shift of each nucleus is very sensitive to changes in its environment, HSQC experiments are also useful in detecting the interaction of a protein with ligands, such as other peptides, nucleic acids or drugs.

In the most common scenario, only one one of the interacting partners is isotopically labelled (usually by ^{15}N). Usually, a series of ^{15}N-HSQC spectra is collected with increasing concentration of the other interacting partner. However, due to the instability of S2/S3 peptide and its tendency to aggregate, we collected a unique spectrum in saturating concentration of S2/S3 peptide (1 mM), in semi-loaded and holo-configurations (2 mM Ca^{2+}). Simultaneously, spectra of the complex without the peptide were also collected in order to validate the quality of the sample.

5.3.1 Preparation of HSQC samples and experiments

K_V7.2.*h*AB:CaM uniformly ^{15}N-labeled was obtained from BL21-DE3 bacteria. A 5 ml aliquot of bacterial pre-culture in LB with ampicillin (100 µg / ml), grown for 8 hours at 37°C, was used to inoculate 200 ml of rich LB medium that was grown O/N. The culture was centrifuged and the cells were resuspended in 1 L of minimum medium supplemented with ampicillin (100 µg / ml) and $^{15}NH_4Cl$ (1 g/L) as a nitrogen source. The sample was purified as described in Chapter 1 and concentrated up to 75 µM.

The ^{1}H-^{15}N HSQC 2D experiments were performed dissolving the 24 aa Q1-S2/S3 to get 1 mM in 500 µL of a buffer formed by 50 mM MES pH 6, 120 mM KCl, 10% D_2O and in the case of holo-complex 2 mM $CaCl_2$. All experiments were recorded on a Bruker Advance III 800 MHz spectrometer at 303 ° K. The ^{1}H-^{15}N HSQC 2D spectra, on samples containing the labeled K_V7.2*h*AB:CaM, were obtained with spectral widths of 30 ppm (in ^{15}N) and 16 ppm (in ^{1}H). DSP combined with the electronic spectrometer reference was used as the internal reference. Visual inspection of the HSQC spectra of apo and Ca^{2+} K_V7.2*h*AB:CaM confirmed the stability and homogeneity of the samples and made it possible to carry out the experiments described below.

In the experiments of chemical shift perturbation, 13 equivalents of the 24 AA Q1-S2/S3 peptide (1 mM), previously solubilized in DMSO and 1 mM DTT, were added to the apo and Ca^{2+} samples of 75 µM K_V7.2*h*AB:CaM, respectively, using the buffers described above.

8. CONCLUSIONS

1. The *h*A-*h*B Linker plays a role in Ca^{2+} signal transduction. Linker length and composition favors conformational changes as a function of Ca^{2+}.

2. Calmodulin confers calcium sensitivity to the stability of the distal intracellular helix D assembly domain of $K_V7.2$ channels. Formation of distal helix D-dependent tetrameric assemblies influences CaM binding and CaM-dependent $K_V7.2$ properties. Reciprocally, CaM and Ca^{2+} influence the dynamic behavior of the helix D coiled coil.

3. In the absence of metabolic activity, calmodulin remains stably bound to helices A and B within the CRD for at least 180 minutes.

4. Conformational changes driven by Ca^{2+} in the Calcium Responsive Domain (CRD) of Kv7.2 channels involves a rotation of the CaM C-lobe, and a separation of helices A and B. No influence of helix-D dependent tetramerization are revealed by HS-AFM, FRET or NMR.

5. The conformation changes driven by Ca^{2+} in the CRD are funneled by the direct interaction of this cation with the E-F (3) hand, while Ca^{2+} binding to the E-F (4) has a small, but significant, influence.

6. K_V7 S2/S3 peptides interact with the CaM C-lobe in solution, mainly via the E-F (3) hand and reverse the Ca^{2+} -dependent conformational changes on the CRD.

9.SUPPLEMENTAL MATERIAL

Supplemental 1. The Use of Fura 2 for Measurement of Free Calcium Concentration

S1.1. INTRODUCTION

S1.1.1. Calcium Indicators

As mentioned above intracellular Ca^{2+} is essential for many physiological processes from neuronal signaling and exocytosis to muscle contraction and bone formation. Irregularities in Ca^{2+} signaling have critical pathological consequences that can result in heart disease, disorders of the central nervous system, neurodegeneration, skeletal muscle defects, and skin disorders, among others. An important advance to analyze the role of Ca^{2+} in different cellular process has been the development of fluorescent Ca^{2+} indicators. Generally, these indicators have altered fluorescent properties when bound with Ca^{2+}. There are mainly two types of Ca^{2+} indicators, genetically encoded fluorescent proteins and chemically engineered fluorophores.

Ca^{2+} indicators bind and interact only with free Ca^{2+} ions. In this sense, it is important to remind that most of Ca^{2+} within cells is not free to diffuse because it is bound to various cellular buffers. The ratio of bound/free Ca^{2+} fluctuates depending on the cell, even the compartment of the cell. Broadly speaking, cytosolic Ca^{2+} is buffered 100 to 1, this means that for every 100 Ca^{2+} ions in the cytosol, only 1 ion is free to diffuse. However, within the endoplasmic reticulum, the bound/free ratio of Ca^{2+} is of the order of 10 to 1 (Li & Camacho, 2004). Furthermore, the chemical Ca^{2+} indicators also act as Ca^{2+} buffers and can therefore affect both the levels and most notably, the kinetics of Ca^{2+} signaling within cells. That is why not only the spectral characteristics of a chemical indicator, but also pay close attention to its binding properties must be considered.

S1.1.1.1. Chemical vs. genetically encoded Ca^{2+} indicators

The advantage of using chemical indicators over fluorescent proteins is the wide range of Ca^{2+} affinities that are commercially available. Also, these dyes are easy of introduce and employ for experiments. Besides, chemical Ca^{2+} indicators do not have to be transfected or expressed in cells. However, the major disadvantage is that it is difficult to control cellular localization of Ca^{2+} indicators or specifically target to a particular organelle. In addition, chemical indicators used to compartmentalize and are finally expeled from the cell during long recording experiments (Rehberg et al., 2008). To alleviate the compartmentalization problem, indicators with a large dextran tag have been designed (Rogers et al., 2006). This approach allows to record Ca^{2+} levels for long extended periods, up to days (Prilloff et at., 2007). However, the dextran tagged dyes are more difficult to load and, in general, have to be directly injected into cells.

S1.1.2. Selection Criteria of chemical Ca^{2+} indicators

Many factors must be taken into account when selecting a Ca^{2+} indicator. If they are accurately calibrated, different indicators should give similar results for the same experiment. However, as mentioned above, Ca^{2+} indicators are, by themselves, Ca^{2+} buffers that can notably influence physiological signalling. The user must find a balance between increasing the signal and assuming the problems associated with the indicator. Sometimes, it is reasonable to work with an indicator with a lower Ca^{2+} affinity. Thus, the impact of buffering can be reduced but, in turn, the signal

strength is reduced. If we work with multiple fluorophores or with autofluorescence, it is fundamental to select an indicator based principally on its spectral properties. In addition, the system shall be limited by the availability of various excitation wavelengths from which to choose. In the following section, the most important factors that should be considered when choosing the most appropriate Ca^{2+} indicator are discussed.

S1.1.3. Ca^{2+} Affinities of Indicator Dyes

The association constant (K_a) (Jezek et al., 1996) measures the propensity of an indicator dye to bind Ca^{2+} ions. Disassociation constant K_d, is the inverse of K_a, and measures the propensity to separate. The K_d is measured in moles and corresponds to the concentration of Ca^{2+} at which half the indicator molecules are bound with Ca^{2+} at equilibrium. If it is possible, indicators should be used to measure Ca^{2+} concentrations between 0.1 and 10 times their K_d. This is the span over which Ca^{2+} dependent changes in fluorescence are the largest. The indicator dyes that are now commercially available, allows to measure intracellular Ca^{2+} in compartments with levels under 50 nM to more than 50 µM. It is noteworthy that the K_d depends also on pH, temperature, viscosity, ionic strength, protein binding and the amount of Mg^{2+} and other ions present. Hence, the K_d of specific indicator dye *in vitro* may not have the same value as the K_d *in vivo*. To calibrate correctly Ca^{2+} levels, it is required to empirically measure the K_d *in situ*, not only for a specific cell type, but also for each subcellular compartment.

Another factor when choosing indicator dyes is that Ca^{2+} signals are usually transient and in consequence, are measured under non-equilibrium conditions. Therefore, occasionally it is necessary to be conscius of the velocity with which an indicator dye binds Ca^{2+}. The K_a (as opposed to its inverse, the K_d) describes these binding characteristics. The K_a is defined as the ratio of the Ca^{2+} binding rate (k_{on} in units of $M^{-1}s^{-1}$) over the Ca^{2+} dissociation rate (k_{off}, in units of s^{-1}). A time constant (τ) for equilibrium binding to occur can also be defined as:

$1/\tau = k_{on}[Buffer_{total}]$,
assuming a 1 mM Buffer concentration and a 1:1 reaction:

[Ca] + [Buffer] < = = > [CaBuffer]

Equilibrium Affinities and Binding Rate Constants for some commonly used Ca^{2+} indicator dyes are presented in Table 4.

The time constant (τ) for Buffer/Calcium equilibrium is defined as: $1/\tau = k_{on}\{Buffer_{total}\}$ assuming a 1mM Buffer concentration and a 1:1 reaction as described in the text. When available, in situ cytoplasmic values are reported with the corresponding in vitro estimates given in parenthesis. Note that the k_{on} values greater than 10×10^7 M-1s-1 are diffusion limited (Hollingworth et al, 1996).

Ca^{2+} dye	K_{on}, Ca^{2+} ($X10^7$ M-1s-1)	K_{off}, Ca^{2+} (s-1)	τequilibrium (μs)	K_d, Ca^{2+} (μM)	K_d, Mg^{2+} (mM)	Reference
Fura-2	15	23	6.7	0.23, (0.14)	-	(Baylor & Hollingworth, 1988)
Magnesium Green NTA	9	1750	11	19,(6)	2.4, (1.0)	Hollingworth et al, 1996).
Furaptra	5.0	5000	20	100, (17)	5.3, (2.5)	Hollingworth et al, 1996).
Mag-fura-red	2.1	5000	-	17	2.5	Hollingworth et al, 1996).

Table S1.1. Equilibrium affinities and binding-rate constants of Ca^{2+} indicator dies.

S1.1.4. Ca^{2+} Dye Indicator types

Ca^{2+} indicator dyes are commercially available in three chemical forms: salts, dextran conjugates or acetoxymethyl (AM) esters. Even if salts are the simplest form of Ca^{2+} indicators, their need invasive procedures to enter the cell, because they are impermeable for the membrane, due their hydrophilic nature. There are different strategies to introduce these indicators into cells, including microinjection, diffusion from patch clamp pipettes, electroporation and lipotransfer using liposomes. The mayor disadvantage is that once introduced into the cell, the salt start to compartmentalize into bound vacuoles. This, usually, is not a problem for short-term experiments, performed within an hour.

To alleviate the compartmentalization problem dextran conjugates where designed and allows long-term recording experiments, up to days. Dextran conjugates are available for all of the most common and popular Ca^{2+} indicators including, Fluo-4, Rhod-2, Fura-2, and Oregon Green 488 BAPTA-1. The disadvantage of using dextran conjugated Ca^{2+} dyes is that there are also hydrophilic, thus membrane impermeable and requires to be introduced into the cell. A new technique for loading dextran conjugates is to utilise pinocytic cell-loading reagent, created by Molecular Probes that enables the indicator to be absorbed by the cell into pinocytic vesicles that can be lysed by putting the cells into hypotonic medium (Okada & Rechsteiner, 1982).

Finally, there are the acetoxymethyl (AM) esters Ca^{2+} indicator dyes, which were designed to offer a suitable method for loading Ca^{2+} indicators into cells. AM dyes are enough hydrophobic to be permeable for the membrane and can be passively loaded into cells. Then, intracellular esterases cleave the AM group and let the dye in the cells. Other benefit of the use of this type of indicators is that subcellular compartments can be labeled. For instance, low affinity Ca^{2+} indicators are useful to detectr Ca^{2+} levels in the endoplasmic reticulum. Dyes should be dissolved first, usually in organic solvents. Usually, AM-linked Ca^{2+} dyes at first are dissolved in dimethylsulfoxide (DMSO) followed by serial dilutions in the proper extracellular media. A benefit of using DMSO is that impede or slows down the hydrolysis of esters in humid environments. This preserves the activity of the indicator prior to be in the cytosol. Pluronic-F127 is also used to help dissolve the AM-

linked indicator dyes into medium taking into account that AM groups have low solubility in aqueous solutions (Takahashi et al., 1999).

There are diverse commercial companies were researchers commonly buy Ca^{2+} indicator dyes, such as Molecular Probes http://probes.invitrogen.com/handbook/tables/0355.html, Teflabs http://www.teflabs.com/, ALEXIS Biochemical's (http://www.alexis-biochemicals.com) part of AXXORA (http://www.axxora.com) and Anaspec (http://www.anaspec.com/).

S1.1.5. High Affinity Ca^{2+} Indicators

The high affinity indicators are the most used to measure Ca2+ concentration. Generally, there are well characterized, and they have wide variety of spectral properties and binding affinities to adapt to the requirements of different experiments. The main characteristics of each dye are displayed in S1.2. Below, there are described the specific advices of each dye.

High Affinity Calcium Indicators:

Indicator	Kd for Ca^{2+} (nM)	Excitation (nm), emission (nm)	Notes	Reference
Calcium Green-1	190	490ex 531 em	single wavelength	Hurley et al., 1992.
Fluo-3	325	506 ex 526 em	single wavelength	Wahl et al., 1990.
Fluo-4	345	494 ex 516 em	single wavelength	Gee et al., 2000.
Fura-2	145	363/335 ex 512 em	dual excitation/ single emission	Etter et al., 1996.
Indo-1	230	488 ex 405/485 em	single excitation/dual emission	Grynkiewicz et al., 1985.
Oregon Green 488 Bapta-1	170	488 ex 520 em	single long wavelength	Brain & Bennett, 1997.
Fura-4F	0.77	336/366 ex, 511em	Ratiometric Exitation / Single emission	Wokosin et al., 2004.
Fura-5F	0.40	336/363 ex, 512em	Ratiometric Exitation / Single emission	Mercer et al., 2006.
Calcium Crimson	185	590ex 615 em	single long wavelength	Eberhard et al., 1991.
X-rhod-1	0.7	580 ex,602 em	Single excitation/emission	Micu et al., 2007.

Table S1.2. Main characteristics of High Affinity Calcium Indicators dyes. Data is based on product manuals by Molecular Probes and other published papers. Modified from Paredes et al., 2008.

S1.1.5.1. Fluo-3

This dye has been one of the most used Ca^{2+} indicators. It is permeable for the cell and it has fluoroscein-like spectral characteristics. It can easily be excited with an argon laser (488 nm) for confocal microscopy, flow cytometry and in epi-fluorescent microscopes with fluorescein filter (Kao et al., 1989). As it has lower Ca^{2+} affinity (K_d ~390 nM) there are less problems with buffering at resting Ca^{2+} levels (~100 nM) if we compare with Calcium Green-1. At rest and in the Ca^{2+} -free form, fluorescence is insignificant but its fluorescence multiply over 100 times when it binds Ca^{2+}. As occurs with other dyes, the K_d depends also to pH, protein binding, and to changes in temperature and should be measured *in vivo* for a precise Ca^{2+} calibrations (Thomas et al., 2000).

S1.1.5.2. Calcium Green-1

As its peak excitation (~490 nm) and peak emission (~ 530 nm) are similar to standard fluoroscein dyes it can be imaged in almost all fluorescent microscopes. This Ca^{2+} indicator has a high quantum yield, low photo toxicity. Its Ca^{2+} affinity (Jezek et al., 1996) is ~190 nM and in this case its fluorescence emission increases ~100 fold upon binding Ca^{+2}. Although Calcium Green-1 is structurally similar to fluo-3, it is more fluorescent at low calcium concentrations, allowing the estimation of baseline Ca^{2+} levels and facilitates the identification of resting cells.

S1.1.5.3. Fluo-4

Fluo-4 is derived from fluo-3 but it is more photostable. The Ca^{2+} affinity is lower (K_d ~345 nM). The absorption maximum is 494 nm, which is more appropriate for 488 excitation using an argon laser (Gee et al., 2000). That is why fluo-4 is brighter at a lower concentration and hence, less phototoxic. Lower concentrations of dye can duplicate the fluorescence, which is an advantage in cell lines that are plated at small densities. In addition, fluo-4 has very low background absorbance and need shorter incubation times to reach the maximum.

S1.1.5.4. Fura-2

This ratiometric and sensitive dye is probably the most successful and common Ca^{2+} indicator, and it is generally considered as reference point for intracellular Ca^{2+} measurements. Its peak absorbance shifts from 340 nm in the Ca^{2+} bound state to 380 nm in the Ca^{2+} free state. Fluorescence occurs at a peak wavelength of 500 nm for excitation in both cases. This ratiometric readout minimizes the effects of photobleaching, leakage, uneven loading, and varying cell thicknesses in mixed populations, delivering more robust and reproducible results. However, the primary disadvantage is that it is not suitable for confocal microscopy because it is a dual excitation dye. Fura-2 has a Ca^{2+} affinity (K_d ~145 nM) which is eqivalent to endogenous resting Ca^{2+} levels (Pesco et al., 2001) and has wide sensitivity ranging from ~100 nM to ~100 µM. (Gee et al., 2000)

S1.1.5.5. Indo-1

This dye is also a well-known and widely used ratiometric Ca^{2+} indicator. It is similar to Fura-2 but in this case, it is single excitation and has dual emission peak. The main absorption occurs in the UV at ~350 nm and main emission peak shift from ~485 nm in free state, to ~405 nm in the Ca^{2+} bound state. As it is single excitation, it is well appropriated for laser scanning microscopy. The main disadvantage of Indo-1 is photo-instability (Wahl et al., 1990). Photobleaching occur very fast, making it unable for confocal microscopy. Nevertheless, it is still widely used for flow cytometry, where photo stability is less important.

S1.1.5.6. Oregon Green 488 BAPTA

This dye is similar to Fluo-3/4 and Calcium Green indicators. They are single excitation/emission dyes that are easily excited by an argon laser at 488 nm. The absorption peak is at 490 nm and like Calcium Green, the dye can be used at lower concentrations than Fluo-3/4, reducing the photoxicity (Svoboda et al., 1997). Its Ca^{2+} affinity is reasonably high (Kd ~170 nm), which is advantageous to detect small changes in Ca^{2+} close to resting levels.

S1.1.5.7. Ca^{2+} crimson

This single wavelength indicator is generated from tetramethylrhodamine and Texas Red dyes thus it has similar absorption/emission spectra. Ca^{2+} affinity is high (Kd ~170-185 nM) having a very high excitation maximum, making it a good candidate for tissue with a lot of autoflourescence (Duffy et al., 1996). However, it tends to compartmentalize (Del Nido et al.,1998).

S1.1.5.8. X-Rhod

This single wavelength Ca^{2+} dye also comes from tetramethylrhodamine, with similar absorption / emission spectra. Peak absorption / emission wavelengths are ~580 / 600 nm. In this case, the Ca^{2+} affinities are relatively low with Kdof 700 nM. An advantage is that the AM esters of this dye has a net positive charge, facilitating sequestration into mitochondria in many cells.

S1.1.6. Low Affinity Ca^{2+} Indicators

The low affinity indicators are specially used to measure Ca^{2+} when very little buffering can be tolerated or in subcellular compartments with high levels of intracellular Ca^{2+}. For example, in the case of the endoplasmatic reticulum (ER), the appropriate K_d for measuring Ca^{2+} is in the range of 22 µM to 250 µM because the relative ER concentration in most cells is between 100 to 1000 µM (Park et al., 2002). In this case the procedure is different First, cells are incubated with AM-linked dyes as usual. Afterwards, the cytosol dye is removed by plasma membrane permeabilization or by diffusion into a patch-clamp pipette, to reveal the ER accumulated dye (Park et al., 2002). Many of these dyes were firstly designed with the aim of detecting and measuring magnesium (Mag) dynamics. Intracellular Mag concentrations use to be constant and close around 1 mM. However, normally, these reagents are also able to bind Ca^{2+} at ~four-fold higher affinity comparing to Mag binding. The most common ones are the following: Mag-Fura-2, Mag-Fluo-4, Mag-indo-1, Mag-

Fura-5, Mag-Fura-Red, Fura-2-ff, Fluo-5N, Oregon Green BAPTA-5 N, Rhod-5N, Rhod-FF and X-rhod-5F, X-rhod-FF.

S1.2. Calibrating the fluorescence of Chemical Ca^{2+} Indicators

S1.2.1. In vitro calibration of Fura-2

In vitro calibration constants are acquired from samples of solutions of Fura-2 and a background solution that does not contain Fura-2. The calibration solutions are generally used to mimic the intracellular condition. The following recipes serve as examples: Several procedures are used to either normalize or calibrate the fluorescence signals of Ca^{2+} dyes. The following solutions were used to calibration.

Solution A: 120 mM KCl, 50 mM K-HEPES, 5 mM NaCl, 5 mm EGTA.
Solution B: 120 mM KCl, 50 mM K-HEPES, 5 mM NaCl, 5 mm EGTA, 20 mM CaCl2.
The pH of these solutions were adjusted to 7.4 and the assay was done at 20ºC.
The measurements were also taken with calmodulin at 0.5 uM, in order to mimic the conditions used in FRET.
Fura 2 pentasodium salt and other reagents were purchased from Sigma.

S1.2.2 Preparation of solutions with various Ca^{2+} concentrations

The free Ca^{2+} concentration in solutions used in biochemical studies were controlled by mixing two solutions (Solution A and B) in appropriate proportions, progressively increasing free calcium concentration in the final solution as indicated in Table 1 below. **Free Ca^{2+} calculations were done with the software MAXC** (www.maxchelator.stanford.edu) with $CaCl_2$.

SOLUTION A	SOLUTION B (uL)	TOTAL Volume uL	TOTAL Ca^{2+} (mM)	Free Ca^{2+} (nM)
100	0	100	0.00	0
100	10	110	2.27	106.4
100	12	112	2.68	147.3
100	14	114	3.07	203.1
100	16	116	3.45	283.7
100	18	118	3.81	410.4
100	19	120	3.99	505.4
100	20	122	4.17	638.2
100	21	124	4.34	837.4
100	22	126	4,51	1.160
100	23	128	4.67	1.820

100	24	129	4.84	3.750
100	25	131	5.00	25.540
100	26	133	5.16	163.120
100	27	135	5.32	317.420
100	28	145	5.47	470.560
100	29	155	5.62	621.600
100	30	165	5.77	770.430
100	31	175	5.92	917.010

Table S1.3. Calcium Buffering System.

S1.2.3. Studies of the characteristics of the fluorescent Ca^{2+} indicator Fura 2

Two µl of Fura-2 (non-AM form dissolved in distilled water, stock concentration 0.5 mg/ml) were added to 2 ml of the solutions prepared in the previous section. After vortex, the solution was scanned in a Spectronic SLM-Aminco Model 8100, using quartz cuvettes.

S1.3. RESULTS

S1.3.1. Shift in the wavelength of maximum excitation on binding calcium

For determining the emission intensity of Fura-2 the sample is excited at 340 and 380 nm with a maximal fluorescence emission at 510 nm. The ratio of the emitted light intensity (when excited at 340 and 380 nm, respectively) is proportional to the amount of bound calcium.

S1.3.2. Ratioing technique for the calcium concentration measurement

To determine the free Ca^{2+} concentration of a solution the following equation is used:

$$[Ca]_{free} = K_d[F - F_{min}]/F_{max} - F]$$

Where the K_d of a single-wavelength calcium indicator is 140 nM, F is the fluorescence of the indicator at experimental calcium levels, F_{min} is the fluorescence in the absence of calcium and F_{max} is the fluorescence of the calcium-saturated probe.

The emission intensities at excitation wavelength 340 nm and 380 nm were measured and plotted against Ca^{2+}- concentration (Figure S1.1 and S1.2).

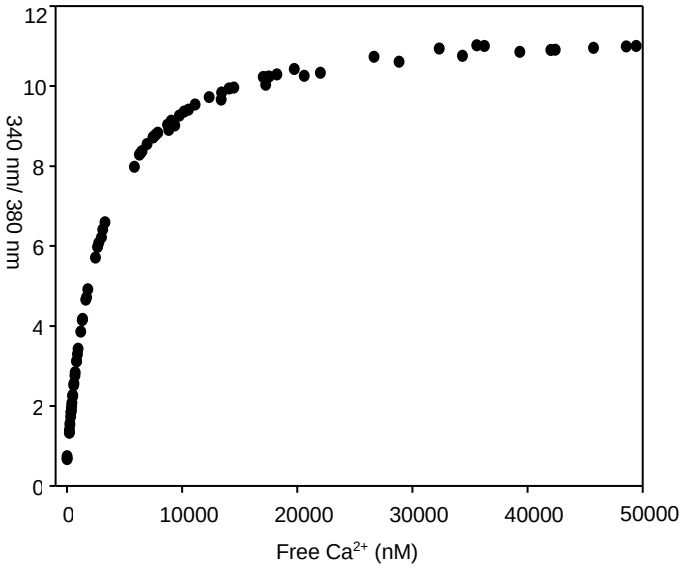

Figure S1.1. Relationship between the ratio of fluorescence intensities of Fura-2 at 340/380 nm and free Ca^{2+} concentrations using the solutions of Table S1.3.

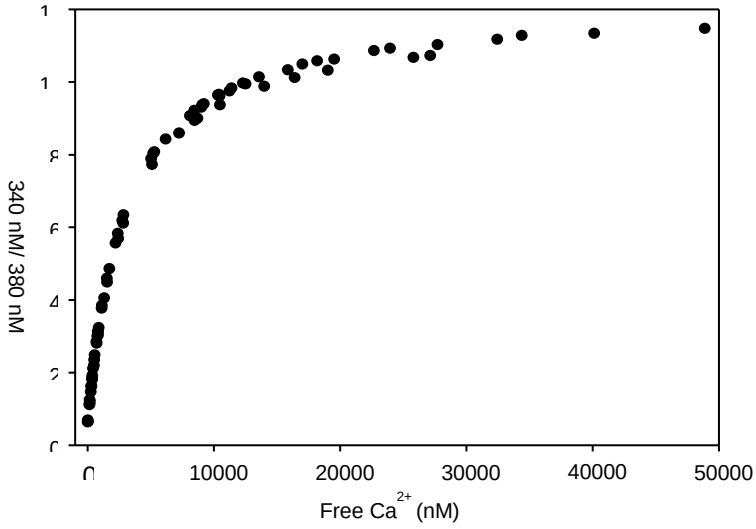

Figure S1.2. Relationship between the ratio of fluorescence intensities of Fura-2 at 340/380 nm and free Ca^{2+} concentrations using the solutions of Table S1.3. and adding CaM at 500 nM.

Then we corrected the data of free Ca^{2+} concentrations previously calculated by Maxchelator. For this, we calculated the relationship between both (Fura-2 estimations against Maxchelator) that was 1.45 higher in the case of Fura-2 (Figure S1.3) and 1.32 higher with CaM 500 nM in the buffer (Figure S1.4).

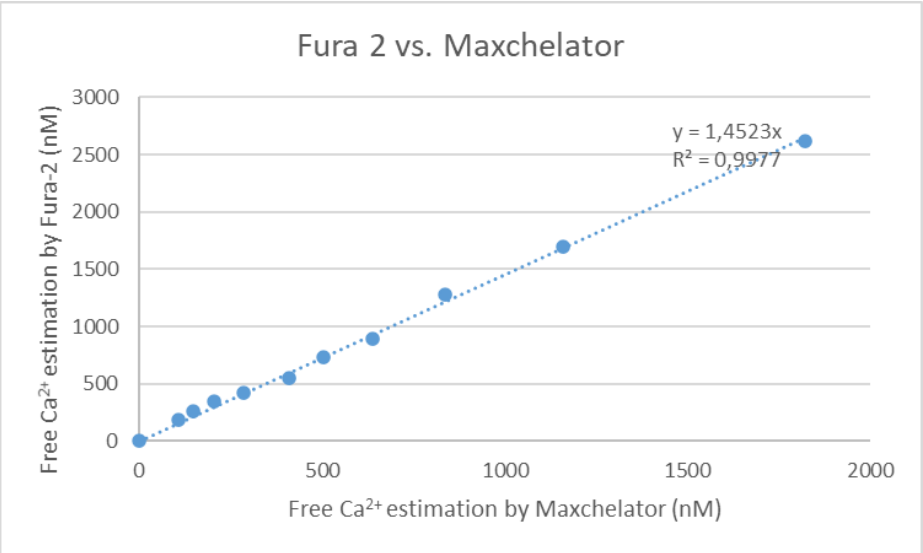

Figure S1.3. Fura-2 Ca^{2+} estimation against Maxchelator´s estimations. The relation between them is 1,423 higher the estimations made by Fura-2.

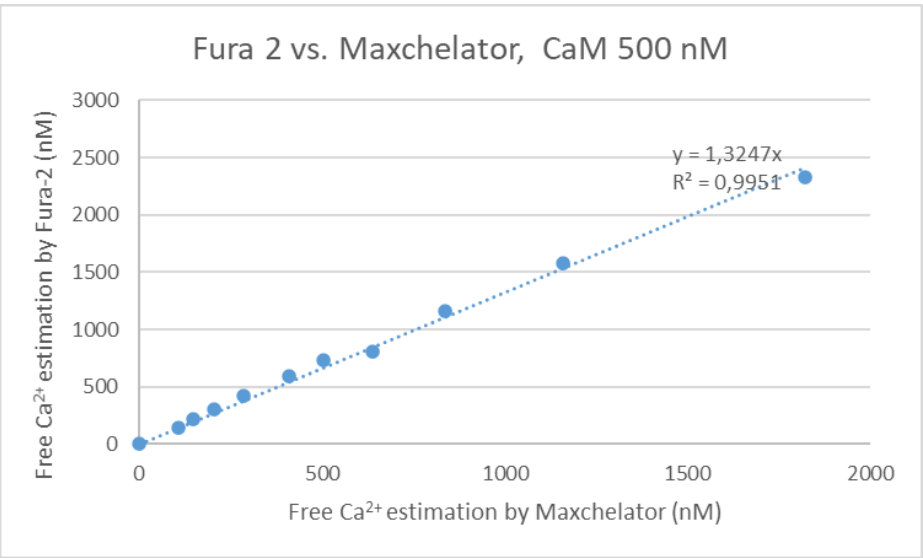

Figure S1.4. Fura-2 Ca^{2+} estimation with CaM 500 nM against Maxchelator´s estimations. The relation between them is 1,325 higher the estimations made by Fura-2.

Therefore, the Kd calculated in the titration by FRET (Figure S1.5), would go from 889.3 nM to 1177.8 nM.

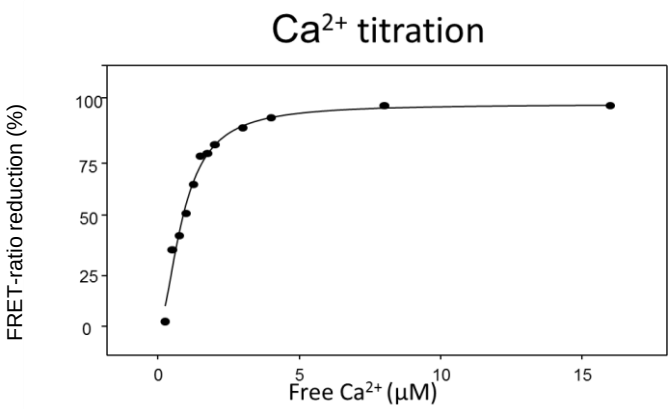

Max expected	Ec50	RSQR
97.1 ± 2.85	0.89 ± 0.05	0.98

Figure S1.5. Ca^{2+} titration by FRET. Ca^{2+} titration curves for Q2hADel Y372-T501-hB- construct. The Ec50 was estimated to be 0.889 ± 0.052 µM, while the amplitude was 97 ± 2.85 and the Hill coefficient was 1.828 ±1.909.

S1.3.3. Free Ca^{2+} Concentration Determination

The free Ca^{2+} concentration in solutions used were controlled by mixing two solutions A and B. (Solution A: 120 mM KCl, 50 mM K-HEPES, 5 mM NaCl, 5 mm EGTA. Solution B: 120 mM KCl, 50 mM K-HEPES, 5 mM NaCl, 5 mm EGTA, 20 mM CaCl2). The pH of these solutions were adjusted to 7.4 and the assay was done at 20 °C. The measurements were also taken with calmodulin at 0.5 µM, in order to mimic the conditions used in FRET.
The range of free [Ca^{2+}] was achieved by adding Ca^{2+} into solution A to reach final [Ca^{2+}] total values of 0 106.4, 147.3, 203.1, 283.7, 410.4, 505.4, 638.2, 837.4, 1.160, 1.820, 3.750, 25.540, 163.120, 317.420, 470.560, 621.600, 770.430, 917.010 nM. Free Ca^{2+} concentrations were determined using the software MAXC (www.maxchelator.stanford.edu) with $CaCl_2$. Experiments were carried using a Spectronic SLM-Aminco Model 8100, using quartz cuvettes (light width 3 mm, 0.1 mL volume).

For determining the emission intensity of Fura-2 the sample is excited at 340 and 380 and the ratio of the emitted light intensity at 510 nm (when excited at 340 and 380 nm, respectively) is proportional to the amount of bound calcium. To determine the free Ca^{2+} concentration of a solution the following equation is used:

$$[Ca]_{free} = K_d[F - F_{min}]/F_{max} - F]$$

Where the K_d of a single-wavelength calcium indicator is 140 nM, F is the fluorescence of the indicator at experimental calcium levels, F_{min} is the fluorescence in the absence of calcium and F_{max} is the fluorescence of the calcium-saturated probe. Data are shown as average of 3 or more independent experiments.

Supplemental 2. CONFERING FLEXIBILITY TO *h*A-*h*B LINKER TO ANALYZE Ca^{2+} DRIVEN CONFORMATIONAL CHANGE

S2.1. OBJECTIVE

We thought that since the linker sequence is poorly conserved in the different isoforms and no relevant function had been described for it, perhaps the reduction in the separation between the helices A and B was because the short linker limited the movement between them.

To analyse if the reduction in the conformational change of *Del1* was **due to a limitation in the motion caused by a linker that was too short and not very flexible**, we introduced into the *Del1* construction sequences that encode very flexible linkers: GGSSG and PolyQ (Figure S2.1). In these experiments, FRET was analysed only in the absence and presence of Ca^{2+}.

S2.2. RESULTS

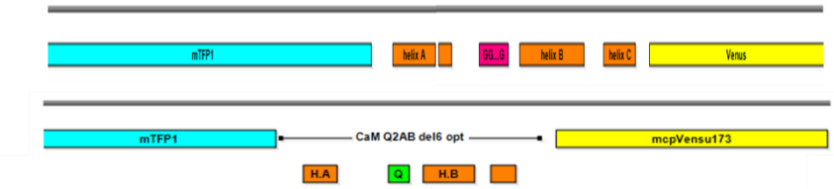

Figure S2.1. Schematic representation of flexible linkers inserted in mTFP1*h*Adel1*h*B-Venus. Above, GGSSG linker (pink) abd below the polyQ (green).

The polyQ linker gave us many aggregation problems, as it has been shown previously (Yushchenko et al., 2018). The results showed great variability and although there is a reduction in the FRET upon adding Ca^{2+} binding, which means a predicted separation of 11.17 Å (from 66.57 Å to 77.74 Å upon Ca^{2+} binding), we cannot really confirm that this change in the FRET ratio is not due to problems with aggregation or protein instability.

Poly-Gly and Gly-rich linkers can be considered as independent units and do not affect the function of the individual proteins to which they attach. The fused proteins behave independently, such that the single chained proteins can perform the combined function of fused partners (Regan, 1997). Flexible Gly linkers have been used to improve the folding and function of epitope-tagged proteins. Flexible polypeptide linkers of 5, 8, or 10 Gly residues have been placed between an epitope and a tagged protein to increase epitope sensitivity and accessibility without interfering in protein folding and function (Sabourin et al., 2007). Even if has been described that these kind of linkers are flexible, connecting various domains in a single protein without interfering with the function of each domain (Mishra et al., 2002), the GGSSG linker did not rescue the effect of the natural linker, showing only a 10.1% of the reduction in the FRET-Ratio. In distance between fluorophores it means a separation of 1.5 Å (from 58.62 Å in apo-state, to 60.12 in holo-state).

A third strategy was tested towards confers flexibility to the complex, and it was to work without the linker. For this purpose, mTFP1-*h*A + CaM and CaM-*h*B-mcpVenus were expressed separately.

Both proteins were incubated at equimolar concentrations (5 µM) O / N at 4°C and the next day the entire complex was isolated by gel filtration, with a Superdex 200 26/60.

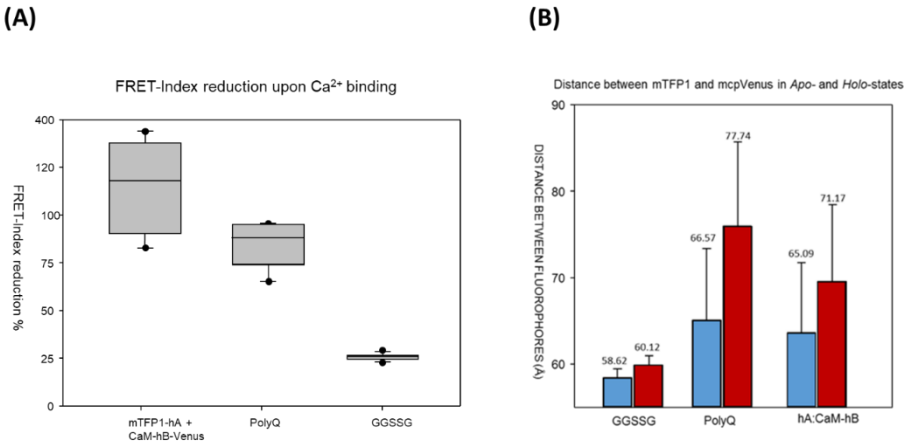

Figure S2.2. Increasing flexibility of the construction (A) The graphic shows FRET-index reduction upon Ca^{2+} binding in different constructions: light gray box for complementation assay, white for polyQ linker and dark gray for GGSSG linker. **(B)** Distance between fluorophores of different construction in absence (blue column) and in presence of Ca^{2+} (red column). Above of each columns the statistical average is shown. Each plot represents the average of at least 6 independent experiments.

The helix A alone tends to aggregate; thus, it was coexpressed with CaM. However, only a scant binds to the CaM:*h*B-mcpVenus complex. Additionally, the complex formed showed great instability and high variability in the FRET-ratio, even at apo-state. On the other hand, we could not discern the orientation in which the helix A binds to the CaM, and there could be an amalgam of different orientations (Fig 3.14). It is also known that both, the C-lobe and the N-lobe, has the capacity to bind to helix B indiscriminately. We cannot discern whether in the construction of CaM-*h*B-Venus, which of the two lobes is bound to helix B, nor if they are both bound, and if it is so, in what proportion they are. Thus, although a reduction in the FRET ratio is observed by adding Ca^{2+} (32%), which means a estimated separation of 6.08 Å between fluorophores (from 65.09 Å to 71.17 Å after Ca^{2+} binding), it cannot be concluded that it is due to a conformational change and not due to other problems with the complex.

S2.3. DISCUSSION

The flexibility conferred by the linker is not responsible for the separation between fluorophores.

At first glance, we thought that *Del1* has too short linker (30 aa) to allow reorientation, while the linker of the *Del1* and *Del2* were long enough to allow conformational change. Suggesting that shorter linkers introduce more strain to the structure, preventing the free movement of helices A and B.

To examine if *Del1* linker was limiting movement between the helices we replaced the linker by two different ones, which have been described to confer high flexibility.

The "GGSSG" was introduced by PCR in *Del1* construction. Gly-rich linkers can be considered as independent units since it has been demonstrated that do not affect the function of the individual proteins to which they attach (Deane et al., 2004). The fused proteins act properly independently, such that the single chained proteins can perform the combined function of fused partners. **The Gly-rich linker was chosen because it was described that provided maximum conformational freedom** (Deane et al., 2004), however it failed to ensure optimal stability (Robinson et al., 1998). In our case, the protein remains stable and soluble in complex with CaM. The FRET ratio in apo-state is 1.67, very similar to those previously observed, suggesting that the introduction of GGSSG does not alter the structural conformation. However, the **increment in flexibility do not replicate the Ca^{2+} effect seen with the complete linker,** causing a separation between the helices of only 1.50 Å, almost the same at that observed with *Del1*, which is 1.61 Å.

The polyQ linker was ordered to ShineGene in such a way that through digestion with restriction enzymes, the linker between helices A and B can be shortened.

The long poyQ was composed by 81 aa (GTQQQQQQ E FQQQ NQQQQ NQQQTSQQQ NQQQQ NQQQ NQQQQ NEFTSQLQQ NQQQQ NQQQ NSQQQ NQQQQ NQQQ NQQQQ NQL), where glutamine repeats were interspersed with other polar amino acids such as aspargines, serines, threonines...

The long polyQ linker leads to aggregation even if it was partially soluble. After purification with Superdex 200 26/60 we saw that all the protein remained in aggregates. As it has been reported that proteins containing glutamine repeats (polyQ) are structurally unstable, the troubles that we faced may be a consequence of this property. Actually, anomalous expansion of polyQ in some proteins exceeding a specific threshold leads to neurodegenerative disease, where the aggregation of proteins is a habitual symptom (Schaefer et al., 2012), such as Huntington´s disease (HD), spinocerebellar ataxia (SCA) and dentatorubral pallidolusyan (DRPLA) (Orr & Zoghbi, 2007). Apaprently polyQ tract undergo a conformational transition from the native conformer to the β-sheet rich structure in a monomeric state, which assembles into oligomers and insoluble aggregates with amyloid fibrillary structure, potentially leading to accumulation as intracellular inclusions (Takeuchi & Nagai, 2017).

Although it is described that polyQ proteins are often unstructured, this is not only due to the presence of polyQ, but also to the place where it is inserted (Totzeck et al., 2017). In addition, PolyQ proteins can adopt a number of biophysical forms including monomers, oligomers, and aggregates depending if it is exceeding the threshold length (Kim et al. 2016). Thus, to avoid aggregation we shortened the linker 71 aminoacids after digestion with MunI and EcoRI, obtaining a linker with just 11 amino acids: GTQ QQQQQ E LA.

However, once we analysed the FRET it shows large variability, in both, with and without Ca^{2+}. Thus, we cannot discard that the observed change is due to protein aggregation or instability.

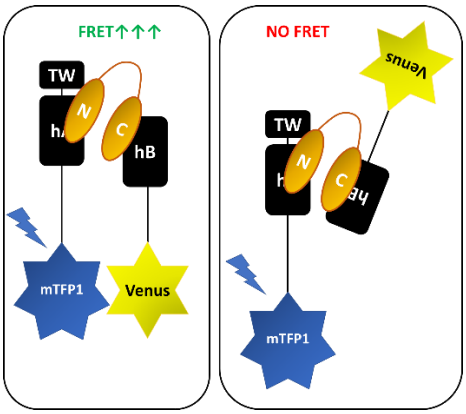

Figure S2.3. Schematic representation of at least two different conformations that the complex could take after the complementation assay.

Similarly, when **we reconstituted the complex from helices A and B expressed separately**, we also obtained great variability. In this case we could not ensure that the complex was being created in the correct orientation, nor in the correct stoichiometry (*h*A:*h*B:CaM) (Figure S2.3).

SUPPLEMENTAL 3. HS-AFM Imaging and Problems

S3.1. Sample preparation
1. Glue a cleaned glass-rod on the Z-piezo by using nail polish and let it dry for at least 20 min. It is possible to accelerate the process by using a fast-drying nails polish oil. Glass-rods can be cleaned by sonication (f ~ 35 kHz) in acetone and stored in a plastic box until use.
2. Glue a mica disk on the glass-rod with cyanoacrylate glue and let it dry for 10 min. It is important to do not add too much glue to fix the Mica as flat as is possible.
3. Cleave the mica disk with adhesive tape to obtain a clean, atomically flat surface. To facilitate the cleavage, mica can be previously cleaned with acetone. Check that the mica is complete using the loupe.
4. Deposit a 1.2–2 µL drop of the sample solution on the mica surface immediately after cleavage. Cover the sample with a humid hood to avoid drying.
5. Fill a cap of a microfuge tube of 1 mL with the working buffer solution (~300 µL). Immerse the sample to wash it; this will remove the excess of molecules that have not adsorbed on the surface. Repeat the procedure at least five times without the need to replace the buffer between rinses.
6. Keep the sample wet with the working buffer solution under the humid hood until it is mounted on the HS-AFM.

S3.2. Sample mounting
1. Wash abundantly the cantilever holder with 2% anionic detergent, tap water, acetone, 70% ethanol, and ultrapure water. Dry it gently with air.
2. Set a small cantilever on the cantilever holder: position the cantilever on the trench of the cantilever holder and fix it with the cantilever holding screws.
3. Mount the cantilever holder on its base by placing the two magnets of the cantilever holder in contact with the micrometer screws of the base.
4. Wash the pool with 110 µL ultrapure water for ten times.
5. Fill the pool with 110 µL of the working buffer.
6. Switch on the laser controller, select the “I mode” and adjust the intensity taking into account the SUM signal and the cantilever thermal fluctuation. This means that the chosen value should allow reaching a high SUM signal (in the range of 0.5–1.2 V) when the intensity of the reflected laser spot from the cantilever on the photodetector is maximized, while the thermal fluctuation of the cantilever is kept lower (in the range of 10–20 mV).
7. Focus the cantilever on the camera screen and find the infrared laser spot (λ ¼ 808 nm).

8. Align the laser on the cantilever and adjust the photodiode parameters: use the micrometer screws of the cantilever holder base to adjust both the lateral and vertical positions of the holder until the intensity of the reflected laser spot from the cantilever on the photodetector is maximized. This corresponds to a maximum value of the SUM parameter on the photodetector controller. Set the DIFF parameter of the photodetector controller as close as possible to zero by using the YFig photodetector micrometer screw. In general, the SUM value should be around 0.5–1.2 V for new cantilevers. ***Troubleshooting the laser alignment: If the SUM is too low, then check the position of the cantilever and try to adjust it. If the cantilever is not in focus point of the laser beam, modify its vertical position by using the Z-cantilever holder micrometer screw. The SUM will increase as the cantilever reaches the focus point of the laser beam. If the laser spot is not well centered, use the XY-cantilever holder micrometer screws to adjust the lateral position of the cantilever. If the back of the cantilever is dirty or is an already-used cantilever the the SUM signal could be lower, in that case replace the cantilever.
9. Place the scanner holder. The scanner holder presents on the backside one linear and one circular grooves. The grooves have to be placed in correspondence with the support screws of the stage that determine the distance between the cantilever holder and the scanner. Ensure that the scanner holder is well positioned and does not move. Check the position of the screws of the scanner holder and ensure that they are retracted.
10. Carefully mount the sample scanner (Fig. 4) on its holder by first accommodating the back (cable) side, putting the magnets in contact with the screws of the scanner holder and then placing the front side of the scanner. During this step, the sample will be plunged in the pool. Pay constant attention to the distance between the scanner and the cantilever while plunging in the sample, always looking at the video monitor. If they are too close to each other, then use the handy controller (“UP”) to move the step motors and lift up the scanner.
11. Check the alignment of the glass-rod and the cantilever by looking if the glass-rod is in the same vertical plane of the cantilever.
12. Connect the scanner to the break-out box.

S3.3. Tip-Sample Approach in Amplitude Modulation Mode
1. Before approaching the sample surface and the tip, check in the video monitor (video camera or CCD) that there are no bubbles around the surface or the AFM chip (that would cause abnormal cantilever deflection). Likewise, ensure that in the camera display there are no particles or dust diffusing around in the liquid, due to contamination. The edges of both the sample support (mica, glass, etc.) and the cantilever should look clean.
2. The tip is placed relative to the sample stage around a millimetre away in the Z-axis. In the camera display, the surface edge must be blurred or unfocused, ensuring that there is enough distance between the substrate surface and the cantilever. Bring the sample close to the cantilever using the micrometer screws in XY-plane.

3. In the Z-axis, bring the sample close to the cantilever performing a coarse approach with the Z-step motor. For approaching, the tip is exactly positioned in the vicinity of the edge of the surface.
4. To find the first (or fundamental) resonance frequency of the cantilever, measure the thermal fluctuation of the HS-AFM probe cantilever performing a power spectrum of the photodiode signal.
5. Using the Fourier Analyzer, apply an AC sinusoidal voltage to the excitation piezo located on the cantilever holder, to excite the cantilever at the measured resonance frequency in point 3.4.
6. Select the cantilever free amplitude between 0.1 and 0.5 V. This typically corresponds to amplitudes between 1 and 5 nm.
7. The amplitude set point of the cantilever should be lower than
the free amplitude. In general, for the approach the amplitude set point is set around 20–40% lower than the free amplitude.
8. Ensure that everything is plugged, Z-scanner, isolation table (if used), X-, Y- and Z-drivers and PID are on.
9. Set parameters to start approaching: center the offset for the output voltage of the X-, Y-, and Z-drivers. In the PID controller: the integral gain is set typically at 20–40% of the maximum, the proportional and derivative gains are set to minimum. The tilt for the X- and Y-axes is also centered. If there are two-time constants in the controller (slow and fast), switch to slow.
10. Approach automatically, selecting the velocity of the step motor and the percentage of amplitude reduction that will halt the automatic approach.
11. When the tip is very close to the surface, the free oscillation amplitude may vary significantly—usually increasing—due to unspecific interactions. If the oscillation amplitude varies, stop the automatic approach, and readjust the set point amplitude 20–40% lower than the free amplitude. Proceed again to approach automatically.
12. If the software detects a tip–sample contact (when the set point amplitude approximates the free amplitude, detected thanks to the readout of the amplitude and the PID output), the automatic approach stops automatically. In case of a manual approach, stop approaching when the Z-piezo starts to retract.
13. After the automatic approach stopped, offset the voltage of the piezo-driver until the output voltage in the PID is close to 0 V.
14. Troubleshooting the approach step: several situations may lead to an anomalous engage or a complete approach failure. It can be observed that the Z-piezo does not hold the voltage value (it moves slowly to fully expanded or contracted position, or back and forth):
(a) Mica is not tightly attached to the glass-rod or the glassrod is not firmly attached to the piezo stage. Sometimes mica partially exfoliates allowing some fluid leakage between the

different layers. All these situations lead to oscillations of the surface while scanning that may prevent a successful approach.
(b) Due to a bad cleavage, or an excess of glue between the mica and the glass, the substrate plane is too inclined respect to the tip, hence the contact is not stable.
(c) The cantilever is tip-less. In this case, decreasing the amplitude set point also changes the SUM value in the photodetector (negative deflection values).
(d) There are big aggregates loosely adsorbed on the surface with strong and unspecific tip–sample interactions that vary the oscillation amplitude. Try to approach with lower amplitude set point, higher free oscillation amplitude or a different area; eventually reconsider the sample preparation.
(e) The solution is dusty or there is material adsorbing on the cantilever, which may lead to false engaging in the surface. Exchange the buffer solution in the pool or eventually increase the free oscillation amplitude. Eventually reconsider the sample preparation.

At this point the clearance distance between the sample stage and the HS-AFM probe is sufficiently small for the Z-piezo range to bring sample and the tip in and out of contact.

S3.4. Image adquisition
1. Out of contact, turn off the cantilever excitation, with the AFM probe, observe in the oscilloscope the width of the thermal vibration of the cantilever AThermal.
2. Turn on the excitation of the cantilever oscillation and set an out of contact oscillation A0 ¼ 10·AThermal.
3. Set a limited pixel number (~100 _ 100 pixels), a set point amplitude A > A0 so the tip is separated from sample, a small scan size (~50 _ 50 nm), and a scan rate of 1 frame/s.
4. Start scanning, then slowly decrease the A; when it is below A0, the highest features on the sample are visualized. In the case of observing very high objects of hundreds of nanometer height that could damage the probe, move away to another region. If the area is appropriate for the HS-AFM tip to scan, decrease A a little more, so most of the area scanned is under slight tip contact.
5. Increase of the feedback speed: First, set the proportional (P) and the derivative (D) gains at their slowest possible reaction speed, next localize the integral (I) gain feedback speed saturation, for this increase the I gain slowly until strips of feedback resonance appear in the image, next reduce the I gain to a close to saturation position. If needed, the A can be slightly further decreased below A0 to obtain an optimal surface profile. Typical A values range from 0.90·A0 to 0.5·A0. In the case of having several time constants in the controller it is possible that you may have to switch to the fastest reaction speed one to achieve the I gain saturation.

Specific P I D values are not given as they will depend on the gain adjustments of the rest of the feedback loop.
6. Localization of “area of interest”: Increase the scan area progressively to several hundred nanometers and increase the number of pixels accordingly. It is recommended to have between 1 and 2 pixels per nanometer. Look for the area of interest where to perform the imaging, displacing on the sample using the sample stage. Use always minimal force (maximal possible set point amplitude A) for imaging to reduce the risk of tip damage. In the case that it is not found an area of sufficient interest in the available scan area, withdraw the sample from the tip, displace macroscopically using the screws and approach on other area.
7. In the case you localize an area of interest, zoom in to frame your experiment, the frame should show clearly all the areas that are important for posterior data analysis.
8. Optimization of oscillation amplitude: Reduce the amplitude excitation signal, the probe will go out of contact, reduce the set point amplitude A to regain tip–sample contact, further reduce the excitation signal, further reduce A. repeat this procedure until you arrive to a cantilever oscillation that is A0 ~5·AThermal.
9. Check again the feedback saturation limit position by increasing the feedback speed of the I gain, next slow down slightly the I gain to avoid feedback resonance, and next increase the feedback speed of the P gain parameter to increase contrast on fine topographic details.
10. Speed increase: progressively increase the imaging speed, evaluate the loss of quality on the image relative to speed increase. Select the speed that provides a fair compromise between image quality and maximum possible speed.
11. If the sample presents height jumps over a few nanometers, the standard PID feedback speed of reaction may be too slow to correctly contour the sample during downhill scanning (so-called parachuting), in this case the HS-AFM dynamic PID should be turned on.
12. Dynamic PID tuning: set all values to 0 (the upper threshold, the lower threshold, and their corresponding gains). Slow down the imaging rate to its lowest speed where parachuting is observed. Next, increase the gain of the upper threshold until the parachuting disappears. Next, increase the imaging speed until parachuting reappears and again increase the gain of the upper threshold until the parachuting disappears. Repeat this action until resonances start appearing in the imaging, then reduce slightly. The gain of the lower threshold is usually set to 0 unless the sample shows very sharp uphill slopes (for example, trenches).

13. The shape of the tip apex is the most important parameter regarding the resolution. If the resolution obtained is not satisfactory, tip sharpening of the amorphous carbon tip deposited by electron beam deposited (EBD) on the end of the small cantilever is advised, for this use the gas plasma chamber.

In a piece of clean glass or Teflon, place on the border a strip of double-sided carbon tape. Position the HS-AFM probe in a way that only the cantilever chip is in contact with the carbon tape, hence the cantilever and its tip are poked out in the air. (b) Introduce the HS-AFM cantilever probe with its support in the plasma chamber of the plasma. Select the gas to fill in the chamber. Run the plasma chamber for a few tens of seconds, inert gases require longer times. Typical parameters we use are pressure ~1 mbar, power ~20 W. (c) Image the sample with the sharpened tip. If resolution is not good enough further repeat steps.

S3.5. PROBLEMS REGARDING HS-AFM IMAGING

S3.5.1. Aggregation due to tetramerization-domain

The insertion of the tetramerization-domains in the N-terminal of the protein favours the formation of multimers. In the elution-profile of the Superdex Increase 10/300 GL the peak corresponding to a tetramer is not symmetric. Actually, although we chose the fraction corresponding to a tetramer, when we visualize by the HS-AFM we appreciate plots corresponding, by size, to an octamer (Figure S3.1).

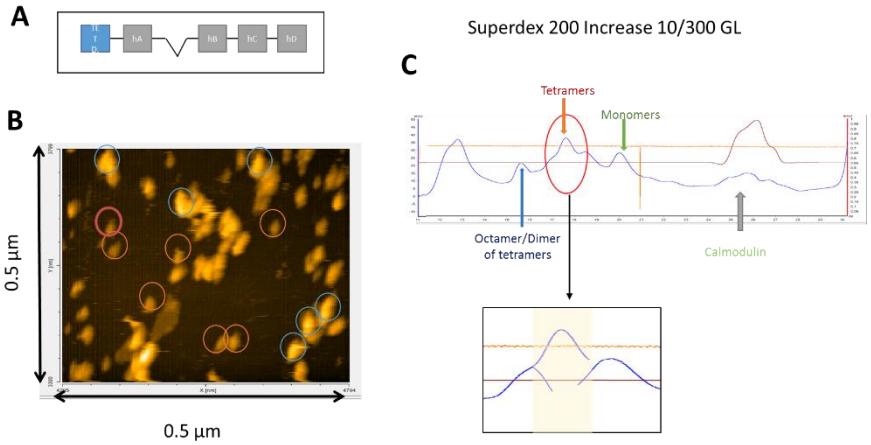

Figure S3.1. Results with double tetramerization domain. A) Cartoon representing the construction used for the experiment, with an artificial tetramerization-domain in the N-terminal, followed by the C-terminal of $K_V7.2$ (ΔR374-K493). B) Image of the tetramers acquired by HS-AFM. The red circles are, by size, tetramers, while blue circles octamers. (C) Elution profile of Superdex Increase 10/30.

During the image recording, the creation of new octamers was observed once two tetramers enter into contact. Given the complications associated with the tetramerization-domain, we decided to work with the construction without that domain.

S3.5.2. Fix the protein in the Mica surface

We have problems to fix our protein-complex to the Mica-surface. **Freshly cleaved mica is negatively charged when exposed to water**.

Our complex pI is 5.1, thus at pH 7.4 has also negative charge and can not fix to the Mica by electrostatic interaction, even less when we try to do the calcium titration (Figure S3.2)

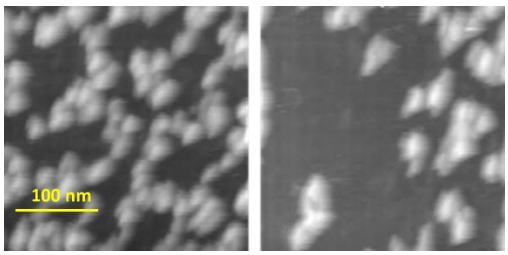

Figure S3.2. Tetramers directly attached to Mica surface visualized by HS-AFM, before (left) and after Ca^{2+} addition (right).

In buffers with high ionic strength, an extensive accumulation of cations near the interface will take place. This in turn can, in principle induce the dissociation of biomolecular assemblies, definitely, if they are stabilized by electrostatic interactions. We rose the concentration of KCl until 200 mM but it did not work. As divalent cations are commonly used to confer positive charge to the surface, we also add to the protein $MgCl_2$ at 5 mM, incubate in the Mica and washed then with a buffer without $MgCl_2$ but it does not work neither.

To avoid this problem and achieve a firm attachment we used the Biotin-Streptavidin two-dimension crystals as substrate. For this aim, we add the strep-tag in the N-terminal of the C-terminal of $K_V7.2$. In the 2D crystals, the two biotin binding sites face the free solution, and therefore, can bind to biotinylated samples to be imaged.

This strategy was used before to analyse Ca^{2+} induces conformational changes in CaM (Yamomoto et al., 2009).

S4. LOOKING FOR INTERACTION RESIDUES BETWEEN E-F (3) AND S2/S3

S4.1. INTRODUCTION

We have demonstrated that E-F (3) is necessary and sufficient to translate the Ca^{2+} signal in KCNQ channels, which results in reorientation of the AB hairpin. However, the direction of this movement of the AB fork is reversed upon protein-protein interactions between S2S3 peptides composed by 24 amino acids (Chapter 7). In this work, **we analyze this interaction at atomic level, identifying the residues that are essential to understand the molecular mechanisms of calcium signaling.** First, shortening the peptide, retaining its effect almost unaltered, to limit the sequence to analyze. Second, modifications of amino acidic composition to also identify those amino acids in the lead sequence that are essential to binding, as well as the amino acids that result in affinity improvement.

S4.2. RESULTS

S4.2.1. Shortening S2/S3 peptide

Based in the 3D cryo-EM structure (Sun & MacKinnon, 2017, PDB:5VMS) and multiple KCNQ S2-S3 linker sequence alignment (Figure S4.1), we postulated that the tryple cysteine sequence, at the center of the linkers, was a good candidate to mediate the interaction between CaM and the peptides analyzed. This triple cysteine is conserved among all K_V7 isoforms, except in $K_V7.1$, where they have been replaced by CRS (Figure S4.1).

Kv7.1	R	L	W	S	A	G	C	R	S	K	Y	V	G	V	W	G	R	L	R	F
Kv7.2	R	I	W	A	A	G	C	C	C	R	Y	R	G	W	R	G	R	L	K	F
Kv7.3	R	I	W	A	A	G	C	C	C	R	Y	K	G	W	R	G	R	L	K	F
Kv7.4	R	V	W	S	A	G	C	C	C	R	Y	R	G	W	Q	G	R	F	R	F
Kv7.5	R	I	W	S	A	G	C	C	C	R	Y	R	G	W	Q	G	R	L	R	F

Figure S4.1. Sequence alignment of S2/S3 loop among different members of K_V7 family.

We began designing peptides of different lengths, shortening the peptide of Q2-S2/S3 at both ends, and keeping the triple cysteine nucleus intact (Figure S4.2). Peptides of 18, 14, 10, 6 and 5 aa were ordered to ProteoGenix. In addition, cyclic peptides of 5 and 6 aa were also designed and ordered to PeptideSynthetics, so as to mimic the secondary structure of the loop. Linear peptides, due to their high conformational flexibility, are possibly not very active. We propose cyclic peptides to try to restrict the conformational freedom of the linear and that they may resemble the original loop, but that cannot be guaranteed either with the small cycle or with the large cycle, since we cannot know a priori what type of conformations preferred are going to adopt each one and if they closely or slightly resemble the loop, but at least they are organized and will not have all possible degrees of freedom. A model of the structures of the different peptides were predicted using the PEP-FOLD server, de novo peptide structure prediction (https://bioserv.rpbs.univ-paris-diderot.fr/services/PEP-FOLD/) and are shown in Figure S4.3.

24 AA	Ac-	R	I	W	S	A	G	C	R	S	K	Y	V	G	L	W	G	R	L	K	F	A	R	K	P	$-NH_2$
18 AA	Ac-	R	I	W	S	A	G	C	R	S	K	Y	V	G	L	W	G	R	L	$-NH_2$						
14 AA		Ac-	W	S	A	G	C	R	S	K	Y	V	G	L	W	G	$-NH_2$									
10 AA			Ac-	A	G	C	R	S	K	Y	V	G	L	$-NH_2$												
6 AA L				Ac-	G	C	R	S	K	Y	$-NH_2$															
5 AA L				Ac-	G	C	R	S	K	$-NH_2$																
6 AA C				Ac-cyclo	E	C	R	S	K	K	$-NH_2$															
5 AA C				Ac-cyclo	E	C	R	S	K	$-NH_2$																

Figure S4.2. Amino acid sequence of the peptides used in the assays. On green de number of amino acids, L means linear peptide and C, cyclic, which is obtained after cyclation process.

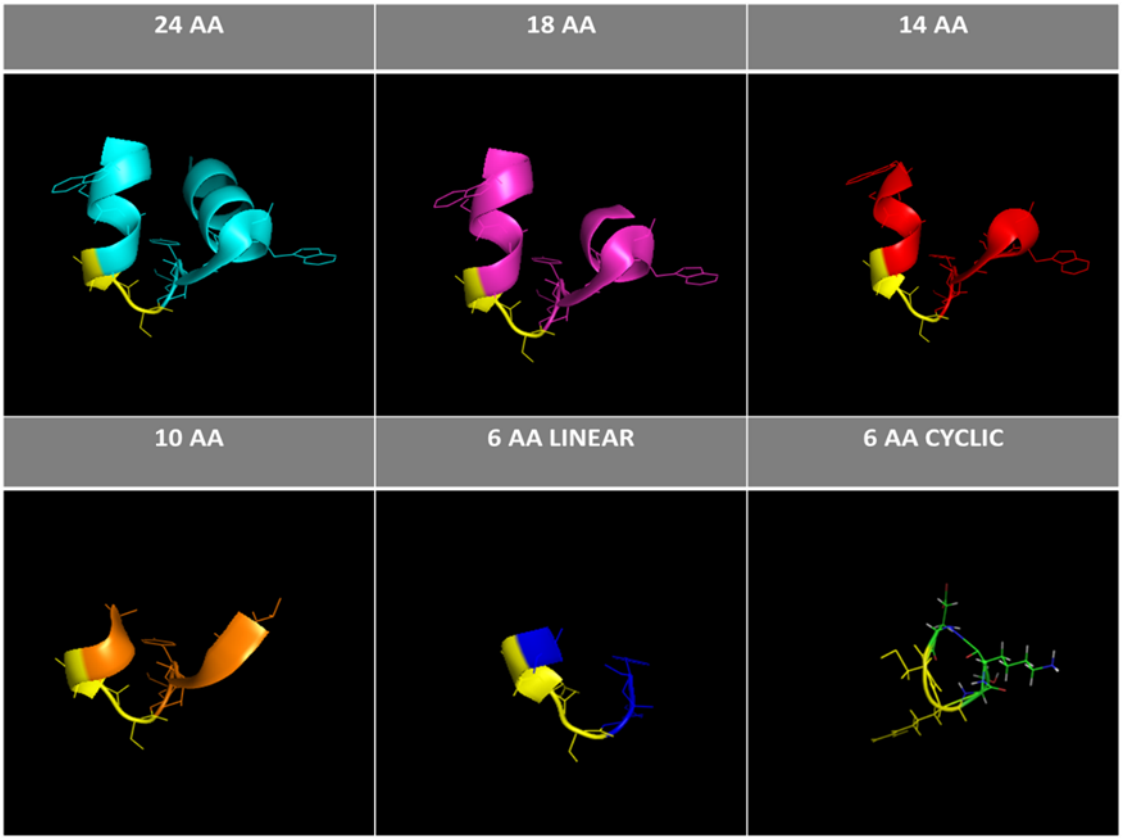

Figure S4.3. Schematic representation of different lenght peptides that mimic S2/S3 loop of KCNQ1. The prediction of the structure has been done by PEP-FOLD, which is the novo structure predictor based on the sequence. 6 aa Cyclic peptide has been done by Pymol using the PDB: 5VMS. In yellow the triple cysteine nucleus is highlighted.

S4.2.2.1. Effect on D-CaM

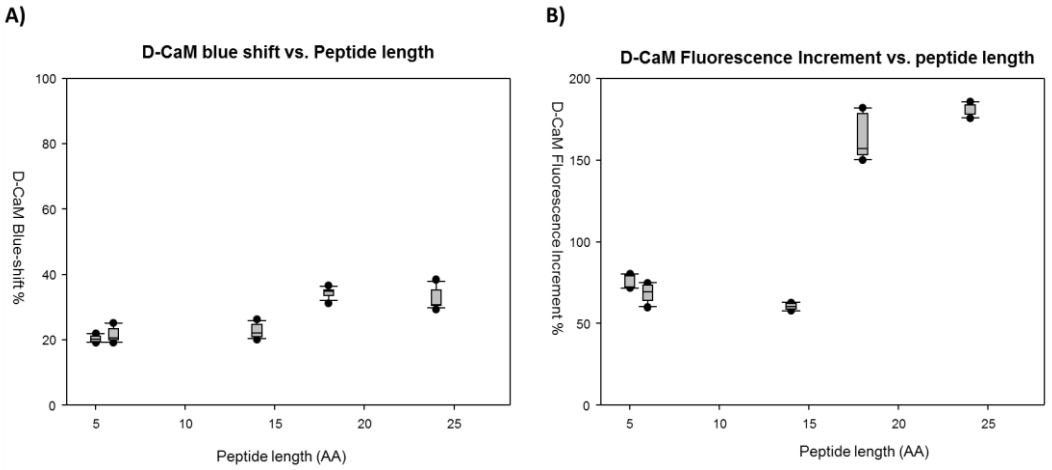

Figure S4.4. S2/S3 peptide deletions. On the right, peak displacement is shown. "Peak displacement" is defined as the movement to the left on the peak of maximum emission of D-CaM with saturating concentration of different peptides. On the right, the increment of fluorescence intensity of D-CaM as a function of the length of the peptides tested. Each plot represents the average of at least 3 independent experiments.

Between the two effects observed using the 24 aa peptide (chapter 7), only the shift to the left of the maximum emission peak is maintained in shorter peptides, while the magnitude of the increase in intensity decreases as the length of the peptide became shorter. Interestingly, **peptides of 18 aa and 24 aa cause similar effects, but by removing two aa more from each end (resulting in a 14 aa peptide) the effect is markedly reduced,** both with regard to the maximum peak displacement as well as in regard to the increase in the intensity. These parameters were similar between the 14 aa peptide and the cyclic peptides of 5 and 6 aa. Importantly, the linear peptides of 5 and 6 aa did not produce any effect on D-CaM, presumably because they are not able to acquire the adequate structure (Figure S4.4). This is a very promising results, because the cyclic structure provides resistance to hydrolysis by exopeptidases due to the lack of both amino and carboxyl termini. Cyclic peptides can be resistant even to endopeptidases, as the structure is less flexible than linear peptides (Joo, 2012).

Additionally, the **shorter the peptide length, the higher the concentration was necessary to obtain half the effect (EC_{50}) in D-CaM intensity** (Figure S4.5). Probably, the shorter the peptide the more flexible is the loop, and a smaller population will be adopting the proper configuration. Furthermore, in every peptide tested the Ec50 was clearly larger for Holo-D-CaM. This is consistent with the hypothesis of a competition between peptide and Ca^{2+} by binding to CaM. Since in such a case, a higher concentration of peptide would be necessary to be able to displace Ca^{2+} previously bound to the CaM.

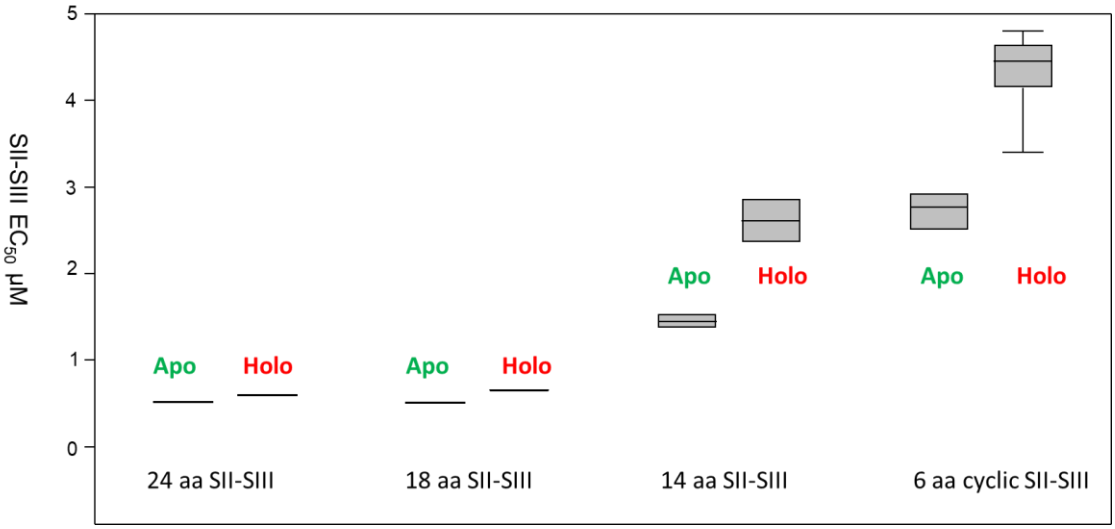

Figure S4.5. S2/S3 peptide affinity. The EC_{50} of different length peptides with apo-D-CaM (green) and holo-D-CaM (red). Each plot represents the average of at least 3 independent experiments.

S4.2.2.2. Effect on Ca^{2+} signal transduction of Q2-*h*AB:CaM complex

Changes on FRET index in response to Ca^{2+} in the presence of S2/S3 peptides were monitored using the K_v7.2 CRD with donor and acceptor fluorophores at the N- and C-termini, as described previously (Nuñez et al., 2020). We shown that the Ca^{2+}-dependent reduction in FRET index was mitigated as the concentration of 24 aa peptide was increased. At higher peptide concentrations (≥ 10 µM), the FRET index increased, suggesting that the distance/orientation of AB helices was even more favorable than in the absence of Ca^{2+}.

First, 14 and 18 aa peptides were tested on Q2*h*AB:CaM complex. These peptides were added at 5 and 10 µM to 0.5 µM mTFP1-*h*AB-Venus:CaM, and a Ca^{2+} titration was done. While 18 aa peptide replicates the effect observed with 24 aa peptide, 14 AA-S2/S3 at 10 µM decreases the Ca^{2+} effect, reduces the FRET-Index by only the ~18%, than that observed without peptide, but in no case the increase in the FRET-Index observed with those of 18 and 24 aa. The affinity for Ca^{2+} remains similar than that observed with the *h*AB:CaM complex bound to peptides of 24 aa, being 0.8 µM for the complex with 18 aa peptide at 10 µM; and 1 µM for peptide of 14 aa (Figure S4.5).

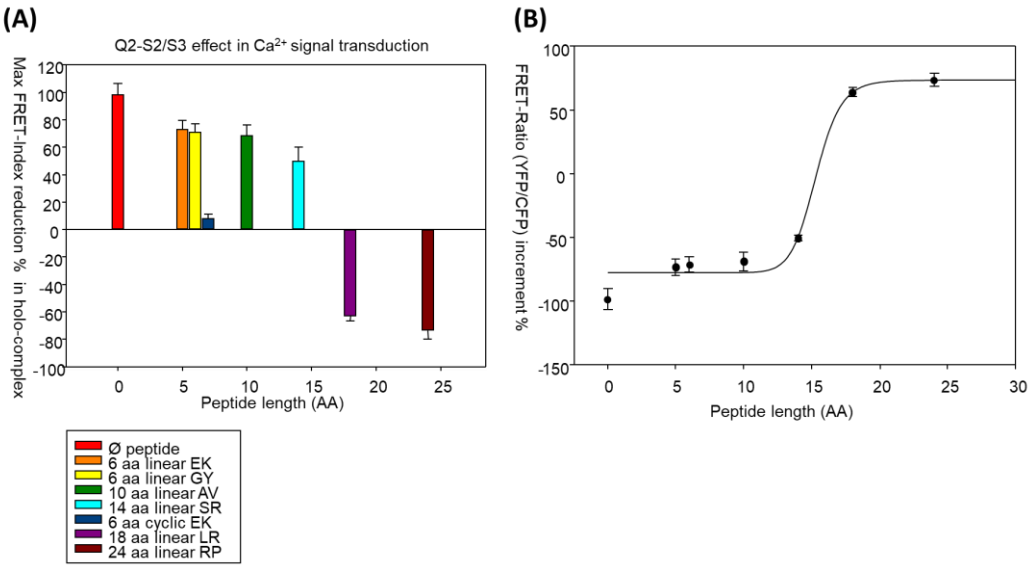

Figure S4.6. Q2-S2/S3 peptides effect in Ca^{2+} signalling. A) FRET-Index reduction in 500 nM mTFP-*h*AB-Venus mixed with 10 µM of different S2/S3 peptides, with 100 µM Ca^{2+}. The result shown is the percentage of FRET reduction, having as reference the complex without peptide, or calcium. B) Maximum FRET plotted against peptide length. The line is the result of fitting the Hill-equation to the data. Above the parameters of this fitting is shown. Each plot represents the average of at least 3 independent experiments.

Figure S4.6 shows effect in Ca^{2+} signalling of the different length peptides in complex with the FRET-Biosensor (mTFP1-*h*AB-Venus:CaM). Peptides 14 and 18 aa not only do not eliminate the reduction in FRET caused by Ca^{2+}, but also cause an increase in FRET. It seems that those peptides are somehow able to provoke the new conformation, where helices A and B far from separating, would be approaching (Figure S4.6.A). Linear peptides of 6 aa do not provoke any effect, while the circularized 6 aa peptide eliminates the reduction in FRET caused by Ca^{2+}. adopting a conformation that can interact with the CaM. The linear peptide, although it has the same sequence, it does not produce any effect, presumably because, due to the adopted conformation, it is not capable of interacting with the CaM. **Generally, the shorter the peptide, the lower the effect it causes on Ca^{2+} signalling,** where finally the 5 and 6 aa linear peptides have no effect (Figure S4.6).

Also, we have plotted the length of the peptide against its maximum effect on the signalling by Ca^{2+} observed by FRET to find out the minimum length of the peptide to obtain half the effect. Our results suggest that the peptide should measure 15.3 aa to observe the half of the effect (Figure S4.6.B).

S4.2.2. Looking for the interaction residues (Testing mutants)

To identify the residues that interact with the *h*AB:CaM complex, different mutants were designed where the triple cysteine nucleus was exchanged for Alanine, Serine and Arginine residues. In this way, it was also intended to find a negative control, that is, a peptide that did not interact with the complex. (Figure S4.7).

WT (CRS)	Ac-	R	I	W	S	A	G	C	R	S	K	Y	V	G	L	W	G	R	L	K	F	A	R	K	P	-NH_2
ARS	Ac-	R	I	W	S	A	G	A	R	S	K	Y	V	G	L	W	G	R	L	K	F	A	R	K	P	-NH_2
ARA	Ac-	R	I	W	S	A	G	A	R	A	K	Y	V	G	L	W	G	R	L	K	F	A	R	K	P	-NH_2
AAA	Ac-	R	I	W	S	A	G	A	A	A	K	Y	V	G	L	W	G	R	L	K	F	A	R	K	P	-NH_2
SRS	Ac-	R	I	W	S	A	G	S	R	S	K	Y	V	G	L	W	G	R	L	K	F	A	R	K	P	-NH_2
SSS	Ac-	R	I	W	S	A	G	S	S	S	K	Y	V	G	L	W	G	R	L	K	F	A	R	K	P	-NH_2
CCC	Ac-	R	I	W	S	A	G	C	C	C	K	Y	V	G	L	W	G	R	L	K	F	A	R	K	P	-NH_2

Figure S4.7. Peptide sequence of mutants tested in the assays. Mutations are highlighted in blue.

S4.2.2.1. Effect on D-CaM

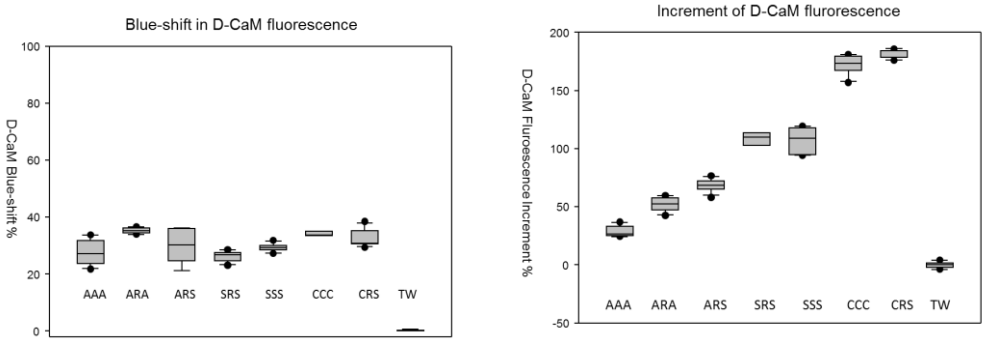

Figure S4.8. Interaction of 4 µM Q1-S2/S3 mutant peptides with 50 nM apo-D-CaM. On the left, peak displacement is represented. On the right, the increment of fluorescence intensity is plotted. The result shown is the percentage of increment, having as reference D-CaM without either peptide, or calcium. Each plot represents the average of at least 3 independent experiments.

Those peptides were first tested on D-CaM. Again, 50 nM D-CaM was mixed with 4 µM peptide to reach saturation, and emission spectra were collected (Figure S4.8). **The shift to the left at the peak of maximum emission did not correlate with the emission intensity.** Therefore, we conclude that the mechanisms that lead to a shift and the mechanism that cause increase in intensity emission are independent. All the mutant peptides show the same extent of displacement to the left, while the increment on fluorescence intensity show important differences. **Apparently, the cysteine at the first position is important for the mechanism that underlies increases in intensity values (188% increment).** This Cys is conserved in all the members of K_V7 family. Replacing it with a serine produces the same effect as a Cys. The S2/S3 of $K_V7.1$ contains CRS instead of the CCC observed in the rest of isoforms and produces the same increase in fluorescence intensity of D-CaM (191%). However, when this last Cys (or Ser in the case of KCNQ1) is replaced by an Alanine, a reduction in its effect is observed. As we have said before and ARS causes a 68% increase in D-CaM fluorescence, the ARA only increases by 50.5%. The role of Cys in 2nd position is more complicated to analyse. Just as its substitution by an Arginine does not seem to reduce its sensitivity to the CaM, when replacing it with Ala (AAA), the increase is only 27%.

The effect of some these peptides were also tested on D-CaM in Holo-configuration (Figure S4.19). The affinity of the D-CaM for the peptide, is always superior in the Holo-configuration although it is also in the µM order. The increase in fluorescence intensity is proportionally higher

in Apo-configuration: 150-200%, for Apo-, 50-70% for Holo-configuration, depending on the peptide sequence, as we observed also in 24 aa S2/S3 peptide (chapter 7).

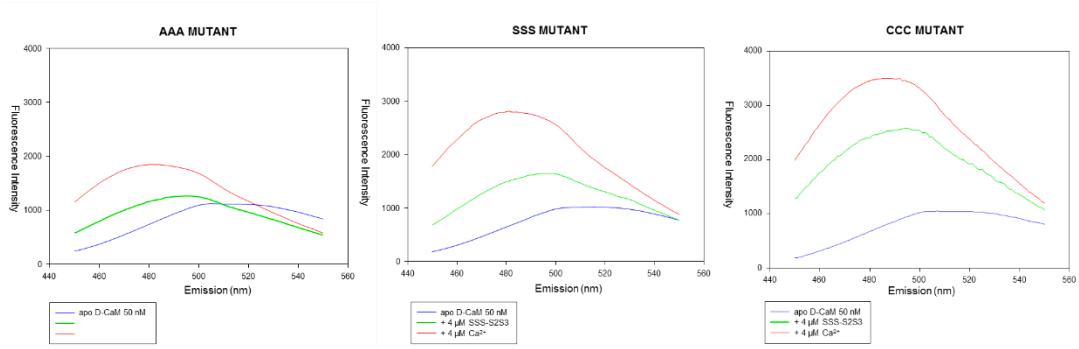

Figure S4.9. Additive effect of Ca^{2+} and peptide. Emission spectra of D-CaM upon adding mutant S2/S3 peptide followed by 4 µM Ca^{2+}. Emission spectra of D-CaM excited a 340 nm. Blue line, show the emission of Apo-D-CaM 50 nM, green lines upon adding 4 µM peptide, and finally red lines, after adding 4 µM Ca^{2+} to D-CaM/Peptide sample.

We demonstrated that the additive effect between the peptide and Ca^{2+} on D-CaM is also present with mutant peptides. Figure S4.9 shows the emission spectra of D-CaM (blue line) upon the addition of 4 µM different Q1-S2/S3 mutants (green line), followed by a saturation with Ca^{2+} (4 µM, red line). **As we mentioned before, AAA mutants shows very modest increment on D-CaM intensity, but a clear displacement of the peak of maximum emission to the left.** The subsequent addition of calcium doubles the intensity and displaces the maximum emission peak by a few nm more. The SSS peptide even if produce a larger effect incrementing the intensity of the fluorescence of D-CaM, is not able to reproduce that observed with the CCC or CRS. The subsequent Ca^{2+} addition increases the intensity and shifts the peak of maximum emission. Finally, the CCC reaches the greatest increase in the intensity observed among the different peptides, maintaining a similar displacement to the left. As occurs with the rest, the subsequent addition of calcium has an additive effect in both intensity and shift.

S4.2.2.2. Effect on Ca^{2+} signal transduction of Q2-*h*AB:CaM complex

After verifying that the mutant peptides had, to a greater or lesser extent, an effect on CaM, we wanted to analyse their effect on the complex formed by Q2-*h*AB:CaM. For this we perform Ca^{2+} titrations in complexes formed with 500 nm of the FRET sensor and different concentrations of the respective peptide (0, 2.5, 5 and 10 µM).

Figure S4.10.A shows peptide Q1-CCC replicates the effects observed with WT. In this case, no changes in affinity for Ca^{2+} was observed, and the maximum expected FRET-Index, at 10 µM peptide was estimated at 66%. Figure S4.10.B shows the Ca^{2+} titration in complexes with SSS-Q1 mutant. As with the WT peptide (CRS), the peptide at a 1: 5 ratio with the complex produces a decrease in the reduction of FRET caused by Ca^{2+}. At 1:10 the changes in FRET are not observed after the addition of Ca^{2+}. Finally, at 1:20 the Ca^{2+} titration causes an increase in the FRET, doubling the FRET/CFP index. The affinity for Ca^{2+} goes from 0.6 ± 0.1 µM in the absence of peptide to 1.14 ± 0.1 µM in the presence of 10 µM SSS-Q1.

Hill equation expects a maximum FRET-Index increment of %73.8 in complex with the peptide at 10 µM.

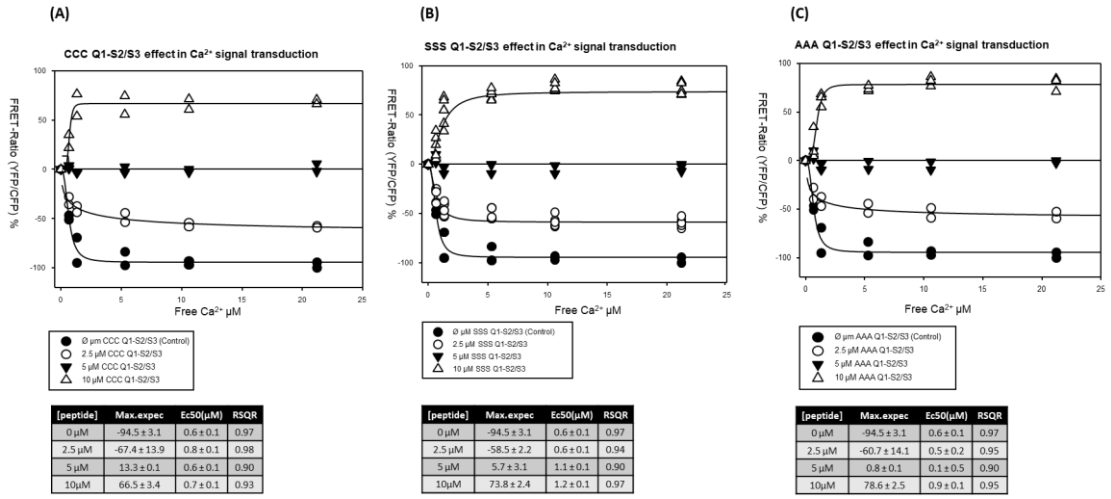

[peptide]	Max.expec	Ec50(µM)	RSQR
0 µM	-94.5 ± 3.1	0.6 ± 0.1	0.97
2.5 µM	-67.4 ± 13.9	0.8 ± 0.1	0.98
5 µM	13.3 ± 0.1	0.6 ± 0.1	0.90
10µM	66.5 ± 3.4	0.7 ± 0.1	0.93

[peptide]	Max.expec	Ec50(µM)	RSQR
0 µM	-94.5 ± 3.1	0.6 ± 0.1	0.97
2.5 µM	-58.5 ± 2.2	0.6 ± 0.1	0.94
5 µM	5.7 ± 3.1	1.1 ± 0.1	0.90
10µM	73.8 ± 2.4	1.2 ± 0.1	0.97

[peptide]	Max.expec	Ec50(µM)	RSQR
0 µM	-94.5 ± 3.1	0.6 ± 0.1	0.97
2.5 µM	-60.7 ± 14.1	0.5 ± 0.2	0.95
5 µM	0.8 ± 0.1	0.1 ± 0.5	0.90
10µM	78.6 ± 2.5	0.9 ± 0.1	0.95

Figure S4.10. Calcium titration of 500 nM mTFP-*h*AB-Venus mixed with Q1-S2/S3 mutant peptides. Black circles correspond to control titration without SSS Q1-S2/S3 peptide. White circles to 2.5 µM, black triangles belong to 5 µM SSS Q1-S2/S3 peptide, and white triangles to 10 µM. The result shown is the percentage of the FRET reduction, having as reference the complex without peptide, or calcium. The lines are the result of fitting the Hill-equation to the data. Beside the parameters of these fittings are shown. Each plot represents the average of at least 3 independent experiments.

Surprisingly, **the Q1-AAA peptide, which has a minor effect on increment of fluorescence intensity of D-CaM, causes the same effect on the Q2-*h*AB complex:CaM.** In this case, we also observed a lower affinity for Ca^{2+} in the presence of 10 µM of peptide Q1-AAA (931 ± 62 nM), though, keeping in all cases about 1 µM. The maximum FRET-Index expected at 10 µM Q1-AAA is 78%, the highest among all analysed (Figure S4.10.C).

Therefore, probably, **the effect we observe in the *h*AB:CaM complex is related to the shift to the left of the peak of maximum emission of D-CaM, rather than to the increase in intensity.**

Likewise, one could say that the effect of the peptide is proportional to the effect of calcium. We tried to find out if the effect of the peptide was related more to the structure than to the sequence, for this we analysed the helicity, by circular dichroism, of the Q1-S3, of the AAA-Q1 mutant and finally, with the negative peptide of 15 aa, in which we do not observe any effect, either on the D-CaM, nor with the mTFP-*h*AB-Venus complex: CaM (Figure S4.20).

S4.2.3. Secondary structure of S2/S3 peptide

(A)

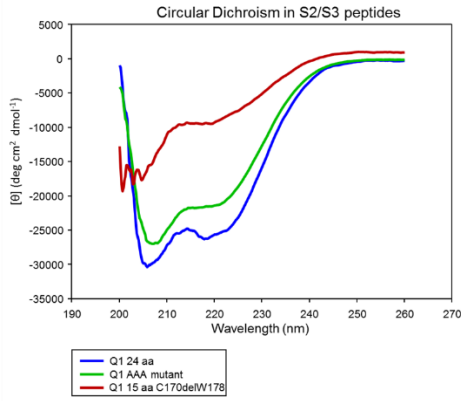

(B)

DPC	H	S+T	U
wt 24 aa Q1	75.6	11.4	13.4
AAA Q1 24 aa	63.6	15.2	21.7
15 aa sin loop	23.2	47.1	28.7

Figure S4.11. Circular Dichroism in wt and negative peptides. (A) Superimposition of CD spectra recorded at a fixed incubation time of the peptides (50 nM). **(B)** Secondary structure of peptides shows as %. H represents the helicity, S+T antiparallel β-sheet conformations, and U for disordered structures. Blue line corresponds to wt Q1-S2/S3 peptide composed by 24 aa, green line to AAA mutant also composed by 24 aa, and red to Q1-S2/S2 C170delW178. Each peptide has been measured at least 3 times.

Circular dichroism measures the difference between the absorbance of left- and right-handed circularly polarized light, and can be used to monitor the secondary structure of peptides (far UV) and the tertiary structure of larger polypeptides (near UV). This technique is especially useful for helix-coil transitions and other aspects of structural alterations. Data from several low-resolution spectroscopic techniques, including CD, can be combined to generate an overall picture of peptide structure.

As we expected peptides that have an effect on both D-CaM and the *h*AB + CaM complex. Just as the 15 AA Negative Control (NC15S2/S3) resulted in a messy structure.

(A)

Kv7.2*h*A	Ac-	F	E	K	R	R	N	P	A	A	G	L	I	Q	S	A	W	R	F	Y	A	T	N	L	S	R	T	D	L	H	S	T	W	-NH_2
Kv7.2*h*B	Ac-	T	E	D	L	T	P	G	L	K	V	S	I	R	A	V	C	V	M	R	F	L	V	S	K	R	K	F	-NH_2				

(B)

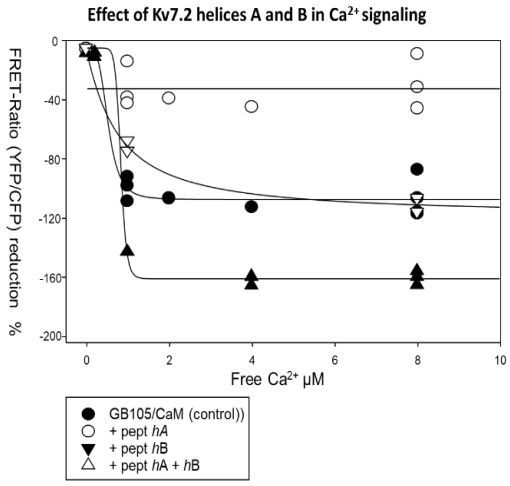

Peptide	Max.expect	Ec50 (µM)	RSQR
Ø	-103 ± 4.8	0.6 ± 0.2	0.97
Q2*h*A	-27.2 ± 12.1	0.2 ± 0.05	0.90
Q2*h*B	-155.1 ± 20.3	0.8 ± 0.4	0.99
Q2*h*A+Q2*h*B	-113.6 ± 10.6	0.7 ± 0.4	0.99

Figure S4.12. Calcium titration of 500 nM mTFP-*h*AB-Venus mixed with 10 µM of Q2*h*A and Q2*h*B separately and together (Q2*h*A+Q2*h*B). (A) Peptidic sequence of the alpha helices tested. **(B)** Graphic of FRET-index reduction during a calcium titration of mtFP-*h*AB-Venus:CaM in presence of *h*A and *h*B peptides. Black circles correspond to control Ca^{2+} titration without peptides. White circles in presence of 10 µM Q2*h*A peptide, black triangles belong to 10 µM Q2*h*B peptide, and white triangles to 10 µM of each peptide added together. The result shown is the percentage of the FRET reduction, having as reference the complex without peptide, or calcium. The lines are the result of fitting the Hill-equation to the data. On the side the parameters of these fittings are shown. Each plot represents the average of at least 3 independent experiments.

Is the CaM binding with S2/S3 since it is an helix? Could any helix replicate the same effect? Saturating the complex with helices A and B

It was analyzed at that time, if any helix with an alpha helix structure could produce the same effect. Peptides of helices A and B of $K_V7.2$ were used, at 10 µM, and a titration by Ca^{2+} was performed as described above. Has been shown previously that these peptides are capable to interact with D-CaM (Alaimo et al., 2014), duplicating its fluorescence intensity. We analyse their effect on Ca^{2+} signalling of $K_V7.2$ channels, because it is known that they form alpha helix structure. Ca^{2+} response show lower effect in presence of saturating concentration of *h*A (10 µM). However, in presence of *h*B, at the same concentration, the FRET-index of mTFP1-*h*AB-Venus reduces even more after Ca^{2+} binding. **When we add both helices together, the FRET-index does not show difference comparing with the sample without peptide**. This could be because two main reasons: 1) they do not

have any effect, or 2) the decrease caused by *h*B is complemented with the low effect shown with *h*A.

Note that neither of the two helices, nor both together, cause an increase in the FRET index observed with the S2/S3 peptides (>70 %) after the addition of Ca^{2+}. Therefore, **we assume that any alpha helix is not capable of producing such an effect, and it is specific to S2/S3 loop.**

S4.3. DISCUSSION

Trying to optimize the peptide and look for interacting residues, we observe that **in a length less than 18 AA, its effect was significantly lost.** Although with 18 AA it maintains> 95% of its effect with 14 AA its effect is reduced to approximately half. With a length of 10 AA, its effect was practically invaluable. Interestingly, by circulating the 5 and 6 aa peptides, part of the effect is recovered (approximately 50%, though, with an affinity much lower than that observed with the 18 and 24 AA peptides). We understand that for the peptide to have an effect it is essential that it maintain the structure of alpha helix. By circulating the 5 and 6 aa peptides we force the peptide to take the necessary curvature to interact with the CaM and recover part of the effect. It is important to note that having so many cysteines in the sequence, these tend to dimerize and complicate the purification and analysis of the results, especially in terms of affinity.

As for the specific residues of the S2/S3 loop that interact with the CaM, the triple cysteine nucleus present in all isoforms was proposed as the main candidate in previous works, except in K_V7.1 where there it is CRS.

We performed the same fluorometric assays previously described with peptides where **that triple cysteine was replaced by a triple serine and a triple alanine**, in S2/S3 sequences of K_V7.1 and K_V7.4. **Differences in the increase in fluorescence intensity are observed in the D-CaM assays, but not in the maximum emission peak displacement.** Once this first Cys is replaced by a Ser reside (compare columns SRS and CRS), the increment on intensity of D-CaM decreases from 200 to 120%. Additionally, when this residue is replaced by Ala (see ARS column), there is a 70% increase in the fluorescence intensity of D-CaM, markedly lower than that observed with Cys. In the same way, the Cys in 3rd position seem not to be so relevant, although it has an effect.

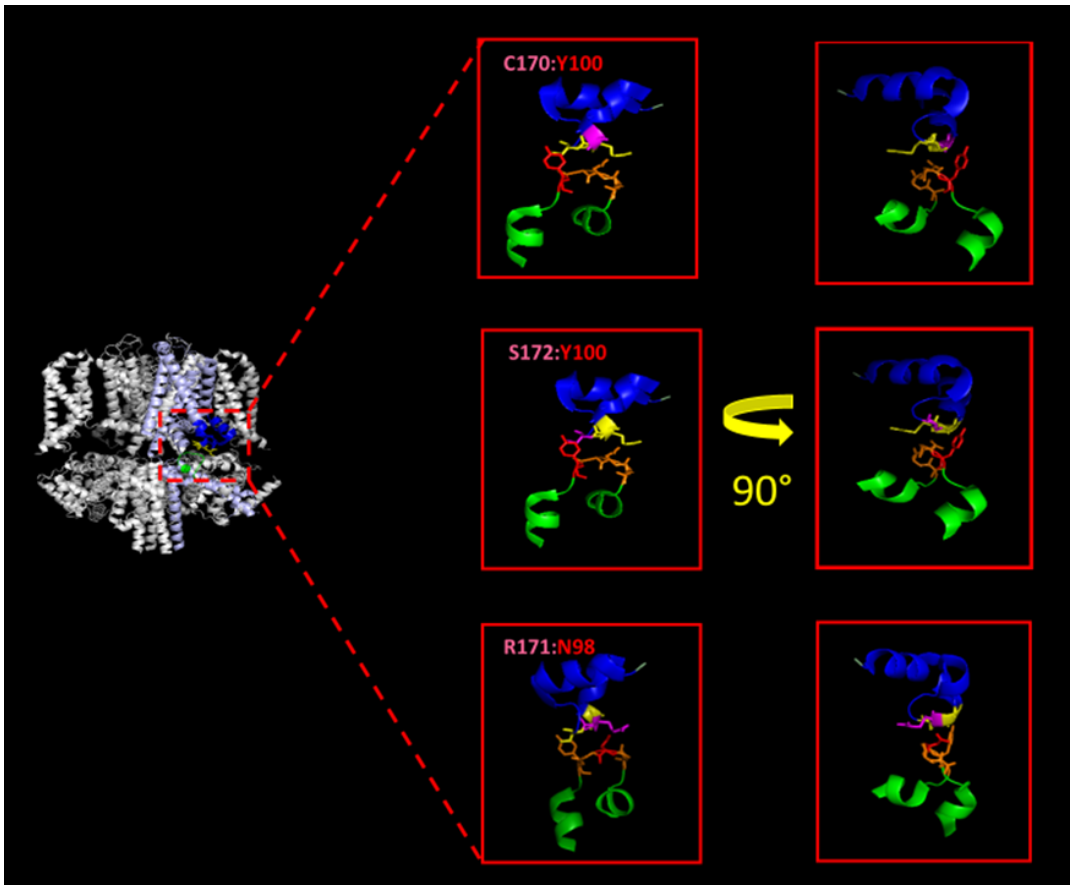

Figure S4.13. Magnified view of the interface between KCNQ1EM and CaM and the possible interactions. C-lobe of CaM is presented in green, the E-F (3) is in orange. The S2/S3 in blue has highlighted the CRS in yellow. The images above show the possible interactions between amino acids, those for S2/S4 are represented in pink, and those for the CaM in red: C170(pink):Y100(red), S172(pink):Y100(red), and R171(pink):N98(red). Based on Sun & MacKinnon, 2017.

Some pathogenic mutations related with longQT syndrome have been located in S2/S3 loop (Figure 20): **p.E170G** (Stattin et al., 2012), **p.R192Cfs91** (Tyson et al., 1997), **p.I198V** (Kapplinger et al., 2009), **p.L191fs** (Kapplinger et al., 2009), **p.R190Q** (Vyas et al., 2016), **p.G168R** (Vyas et al., 2016), **p.G186D** (Vyas et al., 2016), **p.G179S** (Vyas et al., 2016) and **p.G179Sfs*267** (Vyas et al., 2016). However, **none of these are located in the CRS.** According with this and taking in account our results, the residues of S2/S3 that are interacting with E-F (3) could be out of the triple Cys.

With respect to CaM N98 has been related with longQT syndrome (Figure S4.14).

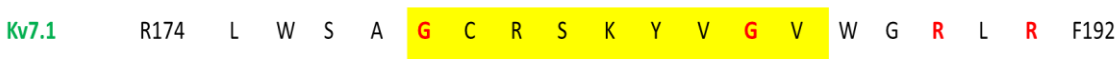

Figure S4.14. Described mutation associated with long QT syndrome localized in the S2/S3 loop.

Looking the cryoEM structure of K_V7.1, CRS seems to interaction site with E-F (3): S172:Y100 and C170:Y100 are apparently the most favourable interaction (Figure S4.13). This could explain why

the substitution by Ala at these positions (ARS and ARA) shows low effects in D-CaM fluorescence increase. Nevertheless, mutations in these sites have not been described yet.

On the other hand, also, the **R171:N98** seems to interact. The S2/S3 the CaM_N98S has been analysed before and demonstrated that did not affect channel assembly or complex formation but it did affect gating (Sun & MacKinnon, 2017).

However, if, at first, based on the structure and previously performed experiments, we postulate triple Cys residues (or CRS in the case of $K_V7.1$) as those that interact with the E-F hand (3), our results show that they are not, or at least not exclusively. It is necessary to continue analyzing different mutations until finding one that maintains a sequence and the secondary structure almost unchanged but where the observed effect is lost.

S4.4. MATERIALS AND METHODS

The methods used are already described previously, except circular dichroism.

S4.4.1. ANALYSING THE HELICITY OF PEPTIDES BY CIRCULAR DICHROISM

Dicrograph J-810 equipped with single/multi-position Peltier-controlled cell holder and a xenon lamp (Jasco, OLIS, Applied Photophysics, AVIV, etc.) and temperature control.

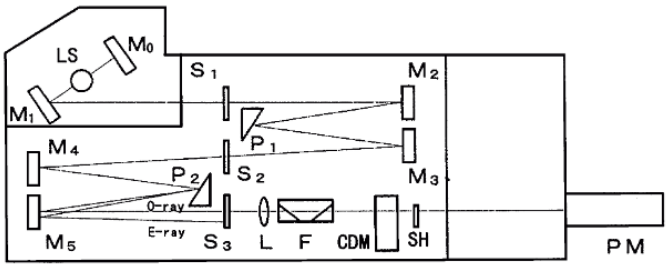

Figure S4.15. Block diagram of a spectropolarimeter (Jasco J-810). Plane polarized radiation is produced by passage of light from the source (LS) through 2 prisms (P1 and P2) and a series of mirrors (M0 to M5) and slits (S1 to S3). The ordinary ray (O) is focused by a lens (L), and passed through a filter (F) to the modulator (CDM). The circularly polarized components are then passed through the shutter (SH) to the sample compartment, before detection by the photomultiplier (PM).

1. 0.1 mm quartz cuvettes (Starna, Hellma) and adapter.
2. Dedicated software for CD data acquisition and processing and Excel and/or Origin software for data analysis.

S4.4.1.1. Instrument Preparation

- Switch on: The CD instrument is purged with pure nitrogen at the manufacturer's indicated flow rate for at least 5 min prior to starting the xenon lamp. Nitrogen flow must be continued until the end of the experiment. Water circulation and Peltier

control are started to maintain a constant temperature while data are being collected.

Initial wavelength scans for far-UV (200S–260 nm) and near-UV (250–340 nm) CD are usually performed at room temperature (or lower temperatures such as 10 °C) in quartz cuvettes with appropriate path lengths. The run parameters are optimized to obtain good signal-to-noise statistics by adjusting the following experimental parameters according to the desired signal levels: scan rate (10–30 nm/min), integration time (time constant) (1–3 s), bandwidth (<2 nm), and number of spectral acquisitions [2, 3, 4, 5]. Examples of typical far-UV CD spectra from the three model peptides are shown in Fig. 1, and representative near-UV CD spectra of the same three model peptides are shown in Fig. 2. In these examples, the three different peptides differ in their content of aromatic amino acid residues (angiotensin I contains one Tyr and Phe, α-melanocyte-stimulating hormone peptide contains one Trp, Tyr, and Phe, while substance P contains two Phe residues) and display some minor differences in their far-UV and near-UV CD spectra.

- Switch off: Purge instrument with N2 before usage (O2 will be converted by the UV to the aggressive O3). After switching on allow for 30 min to warm up. Check stability of the instrument by the drift of the baseline. Lifetime of the light source is approx. 1000 h of usage, after which output will be poorer

S4.4.1.2. Buffer Preparation

Buffers for CD spectroscopy must not contain any materials that are optically active and should be as transparent as possible. The total absorbance of the sample, including the buffer and cell, should be below one for high quality data. Samples where the protein is dissolved in water alone have the highest transparency, but some proteins and peptides are more unstable in the absence of salt. The low wavelength cut offs of several buffers commonly used for CD measurements (buffer + 0.1 mg/ml protein in 0.1 cm cuvettes) are given in Table S4.1. Oxygen absorbs light below 200 nm; for optimum transparency, buffers were prepared with glass-distilled water and the buffer was degassed before use and filtered through filter 0.2 micron sold by Millipore (http://www.millipore.com).

Components	Absorbance (50 mM solution in 0.02 cm pathlength cell)			
	180	190	200	210
NaCl	>0.5	>0.5	0.02	0
NaF	0	0	0	0
$NaClO_4$	0	0	0	0
Boric acid	0	0	0	0
Na borate pH 9.1	0.3	0.09	0	0
Na_2HPO_4	>0.5	0.3	0.05	0
NaH_2PO_4	0.15	0.01	0	0
Na acetate	>0.5	>0.5	0.17	0.03
Tris/H_2SO_4 pH 8.0	>0.5	0.24	0.13	0.02
HEPES/Na^+ pH 7.5	>0.5	>0.5	0.5	0.37
MES/Na^+ pH 6.0.	>0.5	0.29	0.29	0.07

Table S4.1. Absorption properties of selected buffer components in the far UV.

To avoid signal from the buffer we reduced the HEPES concentration to 5 mM from our Fluorescence Buffer. The other components remained as usual (120 mM KCl, 5 mM NaCl, 5 mM EGTA).

Peptides were dissolved in HFIP 25:75 Fluorescence Buffer.

1,1,1,3,3,3-Hexafluoro-propan-2-ol (HFIP) is one of the most effective cosolvents for the structural stabilization of secondary structure forming peptides. It has been shown that HFIP has several effects: First, it removes alternative hydrogen-bonding partners and, second, it provides a low dielectric environment. Together, these factors favor the formation of intrapeptide hydrogen bonds (Roccatano et al., 2005).

S4.4.1.3. Sample Preparation

1. Peptides were bought to Peptide Synthetics at 90% purity in aliquots of 3 mg. First, were resuspended in DMSO to a final concentration of 10 mM. Then we placed 1 µL in different Eppendorf and were lyophilized O/N to remove DMSO.
2. Lyophilized peptides were resuspended in 200 µL DC-Buffer (25% HIPF and 75% 120 mM KCl, 5 mM HEPES pH 7.4, 5 mM NaCl, 5 mM EGTA), to obtain a final concentration of 50 µM.

S4.4.1.4. Cuvette cleaning

• Quartz cuvettes should be handled with care, do not scratch with pipette.

• Quartz cell should be washed after using. We wash with commercial Hellmanex (special cleaning concentrate) for 1 min, in bad case for 1 h, followed by extensive washing with distilled water, then ethanol, followed by drying with N2 gas. Do not use pressurized air since it contains traces of oil.

S4.5. Appendix figures

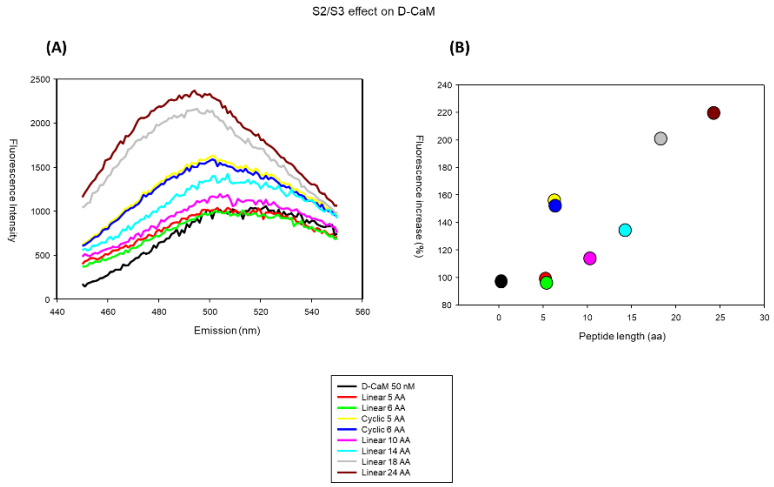

Figure S4.16. Interaction between CaM and S2/S3 peptides of different length. A) Sequences of different peptides tested. A) Emission spectra of D-CaM (black) and after saturation with S2/S3 peptides of different length (colours). B) Increase in fluorescence versus peptides of different length.

Figure S4.17. Calcium titration of 500 nM mTFP-*h*AB-Venus mixed with 5 and 10 µM of 14 and 18 AA S2/S3 peptides. Black circles correspond to 10 µM 18AA-S2/S3 peptide and white circles to 5µM. White triangles belong to 10 µM 14AA-S2/S3 peptide, and black triangles to 5 µM. The result shown is the percentage of the FRET reduction, having as reference the complex without peptide, or calcium. The lines are the result of fitting the Hill-equation to the data. Beside the parameters of these fittings are shown. Each plot represents the average of at least 3 independent experiments.

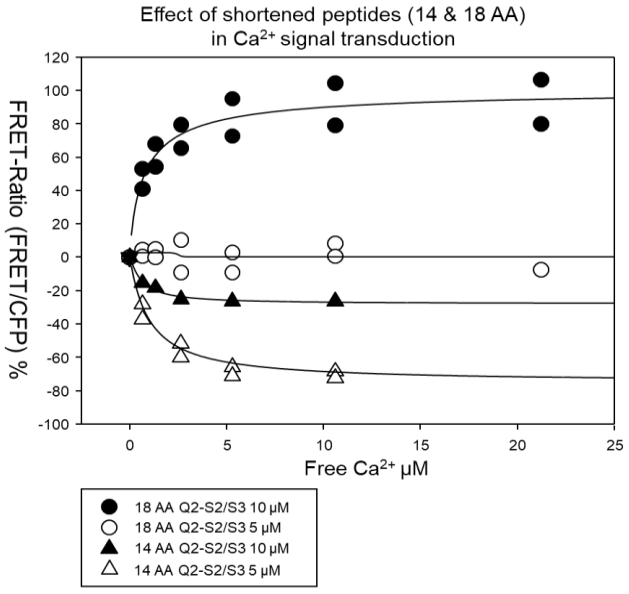

Pept. length (AA)	[peptide]	Max.expec	Ec50(µM)	RSQR
14	5 µM	-28.2 ± 2.2	0.6 ± 0.1	0.99
14	10 µM	-18.2 ± 0.2	1.0 ± 0.2	0.99
18	5 µM	2.5 ± 5.1	2.5 ± 0.5	0.90
18	10µM	100.6 ± 15.5	0.8 ± 0.32	0.91

A)

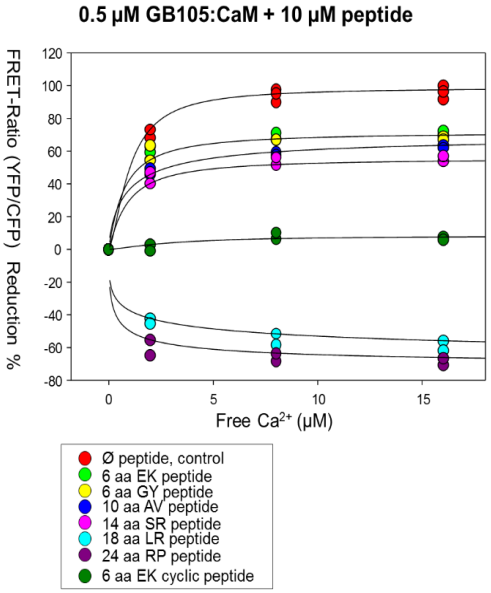

B)

Peptide length	FRET-Increase %	Ec50 (µM)	RSQR
Ø	-100.9	1.36	99.9
6 aa GY Linear	-73.24	0.71	99.9
6 aa EK Linear	-105.4	1.07	99.9
6 aa EK Cyclic	-8.3	3.18	99.9
10 aa AV	-69.9	0.89	99.9
14 aa SR	-55.2	0.88	99.9
18 aa LR	67.0	0.82	99.9
24 aa LR	80.1	1.2	99.9

Figure S4.18. Ca^{2+} titration of 500 nM mTFP-*h*AB-Venus:CaM mixed with 10 µM S2/S3 peptides. The result shown is the percentage of the FRET reduction, having as reference the complex without peptide, or calcium. The lines are the result of fitting the Hill-equation to the data. Above the parameters of these fittings are shown. Each plot represents the average of at least 3 independent experiments.

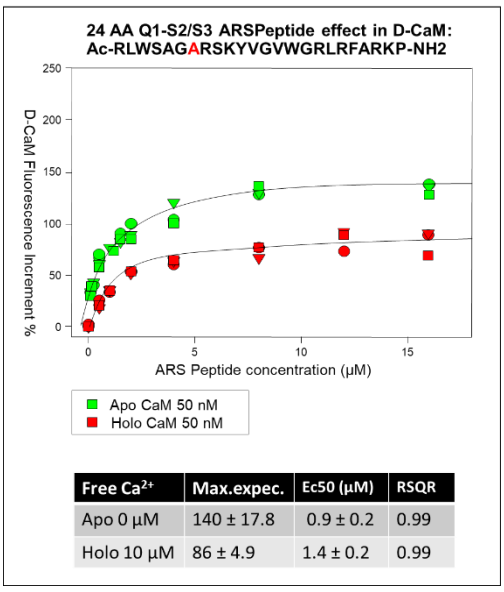

Free Ca^{2+}	Max.expec.	Ec50 (µM)	RSQR
Apo 0 µM	140 ± 17.8	0.9 ± 0.2	0.99
Holo 10 µM	86 ± 4.9	1.4 ± 0.2	0.99

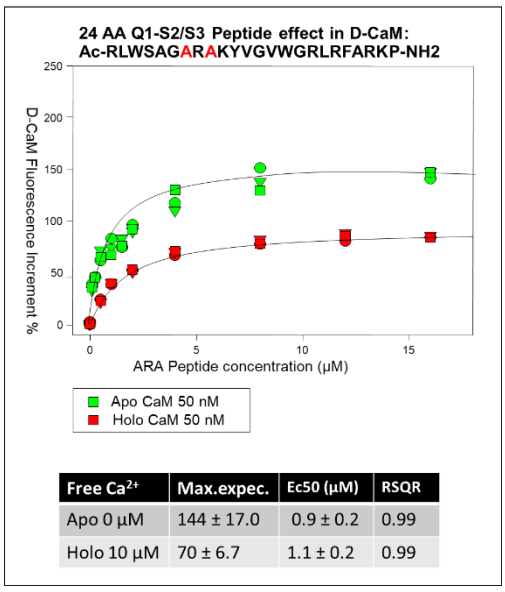

Free Ca^{2+}	Max.expec.	Ec50 (µM)	RSQR
Apo 0 µM	144 ± 17.0	0.9 ± 0.2	0.99
Holo 10 µM	70 ± 6.7	1.1 ± 0.2	0.99

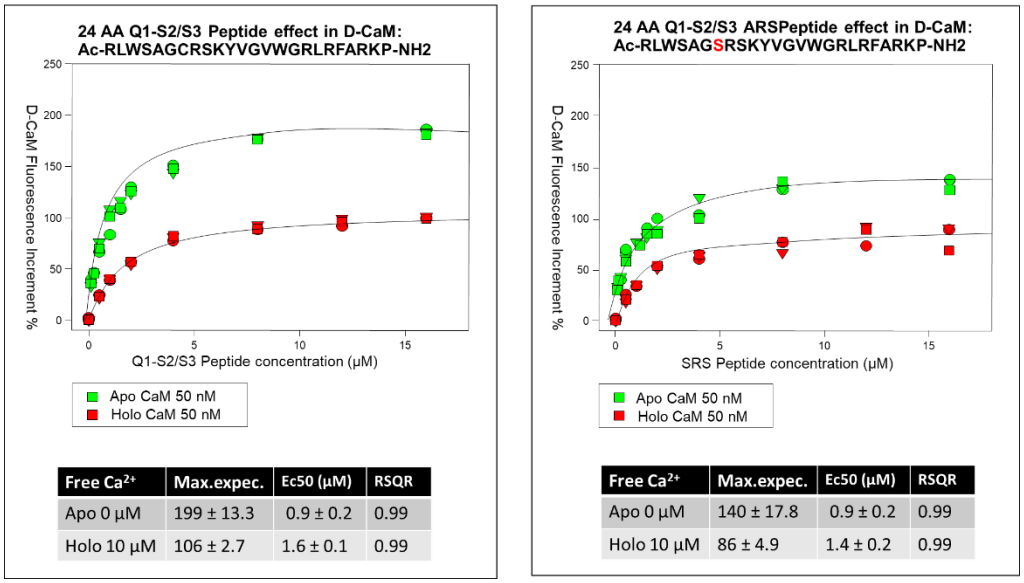

Free Ca^{2+}	Max.expec.	Ec50 (μM)	RSQR
Apo 0 μM	199 ± 13.3	0.9 ± 0.2	0.99
Holo 10 μM	106 ± 2.7	1.6 ± 0.1	0.99

Free Ca^{2+}	Max.expec.	Ec50 (μM)	RSQR
Apo 0 μM	140 ± 17.8	0.9 ± 0.2	0.99
Holo 10 μM	86 ± 4.9	1.4 ± 0.2	0.99

Figure S4.19. Interaction between D-CaM and S2/S3 mutants. Graphic shows D-CaM fluorescence intensity increment (490-500 nm) vs. Q1-S2/S3, SRS, ARS and ARA peptide concentration. Green plots correspond to Apo-D-CaM (5 mM EGTA) and red-plots to Holo-D-CaM (10 μM Ca^{2+}). The lines are the result of fitting the Hill-equation to the data. Each plot represents the average of at least 3 independent experiments.

(A)

24 AA	Ac-	R	I	W	S	A	G	C	R	S	K	Y	V	G	L	W	G	R	L	K	F	A	R	K	P	$-NH_2$
NC18 AA	Ac-	R	I	W	S	A	-	-	-	-	-	-	V	G	L	W	G	R	L	K	F	A	R	K	P	$-NH_2$
NC15 AA	Ac-	R	I	W	S	A	-	-	-	-	-	-	-	-	-	W	G	R	L	K	F	A	R	K	P	$-NH_2$

(B)

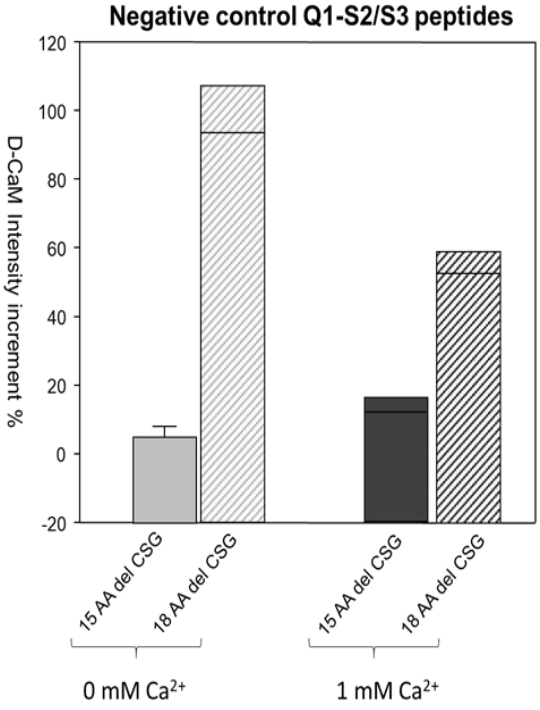

Figure S4.20. Looking for S2/S3 interaction site. (A) Peptidic sequence of the peptides tested as negative control. **(B)** D-CaM intensity increment upon saturation with respective peptides (4 μM), in absence and in presence of Ca^{2+} (10 μM). Each column represents the average of at least 6 independent experiments.

Supplemental 5. Role of S2/S3 loop on cytoprotection

S5.1 INTRODUCTION

Many neuronal ion channels and receptors can be modulated by oxidative modifications. Thus, BK channels (Tang et al, 2004), heteromeric I_{Ks}-like Kþ channels (Busch et al, 1995), ASIC channels (Andrey et al, 2005) and NMDA receptors (Aizenman et al, 1989) are inhibited by millimolar concentrations of oxidizing agents, and GIRK Kþ channels are activated by reducing agents (Zeidner et al, 2001). Effects of oxidation/reduction on the kinetics of some Kv channels (Liu and Gutterman, 2002; Caouette et al, 2003) and HERG channels (Berube et al, 2001) have also been reported.

Also been demonstrated by molecular, electrophysiological and cell biology methods that physiological concentrations of the ROS H_2O_2 induce a strong enhancement of M-channel activity (Gamper et al., 2006). Oxidative modification was induced by physiological concentrations of hydrogen peroxide. They postulated that the triple cysteine pocket in the channel S2–S3 linker is critical for this effect. It has been shown that oxidative treatements of cysteines induced a voltage-independent increase in channel maximal Po and a left-shift in channel voltage dependence. Additionally, replacement of these triple Cys by Ala, supresses the oxidative response. Thus, the S2/S3 linker represents an important mechanism to protect neurons against ROS-induced damage (Gamper et al., 2016).

They find that the current of K_V7.2, 7.4 and 7.5 are notably increased by H_2O_2, whereas K_V7.1 and 7.3 are not. The most pronounced effect of H_2O_2 on Kv7 channels is the enhancement of channel maximal P_O. K_V7 channels have very different tonic maximal P_O values; thus, K_V7.2, 7.4 and K_V7.5 have a rather low P_O (in the range of 0.1–0.2), whereas Kv7.3 has a maximal P_O near unity (Selyanko et al, 2001; Li et al, 2004). As H_2O_2 increases channel P_O, it is, therefore, not surprising that currents of K_V7.3 are not increased, even though Kv7.3 has the required triplet of cysteines (Gamper et al., 2006). K_V7.1 has only one cysteine in the 'triple C' region. Reconstitution of the complete CCC sequence in K_V7.1 by substitution of R86 and S87 by cysteines conferred further H_2O_2 sensitivity to this mutant, promoting our conclusion that this triplet of cysteines mediates the H_2O_2 sensitivity of K_V7 channels. As was expected the effect of oxidation on the K_V7.1 mutant is weaker than on the K_V7.2, 7.4 and 7.5 because K_V7.1 has high maximal P_O (Gamper et al, 2006).

S5.2. OBJECTIVE

We have analysed how the oxidation affects the effect on S2/S3 loop on the binding with CaM and on the Ca^{2+} signal transduction of Q2-*h*AB:CaM complex.

S5.3. RESULTS

S5.3.1. OXIDIZED S2/S3 INTERACTION WITH D-CaM

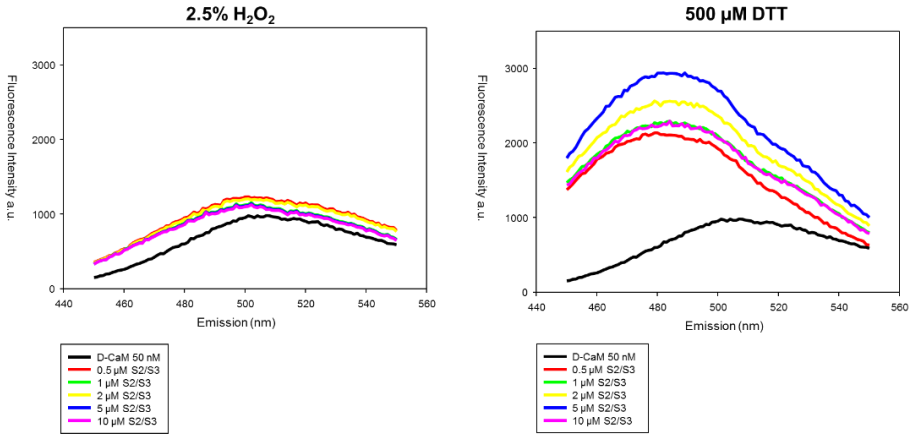

Figure S5.1. Comparison between the effect of oxidized and reduced S2/S3 peptide on D-CaM. On the left, titration on 50 nM D-CaM of oxidized peptide with 2.5 % H_2O_2. On the right the same titration in presence of 500 µM DTT. Each line represents the average of at least 3 independent experiments.

D-CaM was titrated with oxidized and with reduced S2/S3 peptide, in order to analyse how the binding properties to CaM were affected after oxidation. Oxidized peptide does not provoke an increment in the fluorescence intensity as reduced does.

S5.3.2. EFFECT ON Ca^{2+} SIGNAL TRANSDUCTION OF Q2*h*AB:CaM

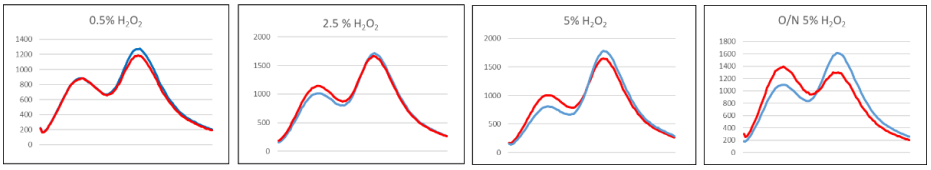

Figure S5.2. Emission spectra of mTFP1-*h*AB-Venus:CaM in presence of Q2-S2/S3 peptide at different levels of oxidation. First graphic in presence of 0.5% H_2O_2, second with 2.5% H_2O_2, third with 5% H_2O_2, and fourth in presence of 5% H_2O_2 and after O/N incubation. Blue line corresponds to the emission spectra in absence of Ca^{2+} (5 mM EGTA) and red line in presence of 100 µM free Ca^{2+}. Each line represents the average of at least 3 independent experiments.

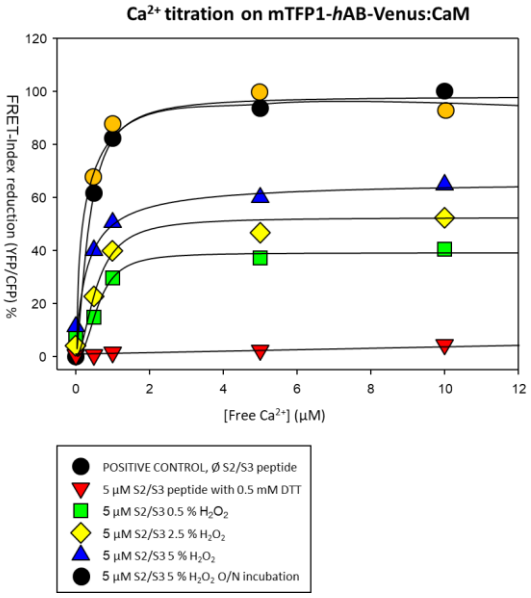

S2/S3 oxid.	Max.expect	Ec50 (µM)	RSQR
Ø no peptide	103 ± 4.8	0.6 ± 0.2	0.97
0.5 mM DTT	7.3 ± 12.1	4.2 ± 0.5	0.90
0.5% H_2O_2	38.1 ± 8.3	1.3 ± 0.4	0.99
2.5% H_2O_2	54.6 ± 10.9	0.8 ± 0.2	0.99
5% H_2O_2	76.8 ± 7.5	0.7 ± 0.2	0.98
5% H_2O_2 O/N	100 ± 5.6	0.5 ± 0.2	0.97

Figure S5.3. Oxidized Q2-S2/S3 effect on Ca^{2+} signal transduction. The graphic shows the % of FRET-Index reduction vs. Ca^{2+} concentration. Titration of 500 nM mTFP1-*h*AB-Venus:CaM is represented in black spheres. Red triangles shows the results of the titration in presence of reduced is 5 µM Q2-S2/S3. Green square with 0.5 µM S2/S3 in presence of 2.5% H_2O_2, yellow rhombus with 2.5 µM S2/S3 in presence of 2.5% H_2O_2 and blue triangles 5 µM S2/S3 in presence of 2.5% H_2O_2. Each plot represents the average of at least 3 independent experiments. The lines are the result of fitting the Hill-equation to the data. Beside the parameters of these fittings are shown.

The addition of H_2O_2 in the sample causes a recovery of the effect of Ca^{2+}. The higher the concentration of H_2O_2 added, the greater the recovery of the conformational change. Actually, at 5% H_2O_2 after O/N incubation at 4°C does not produce any effect, suggesting that its binding capacity to CaM is completely annulled.

S5.4. DISCUSSION

The H_2O_2 could be oxidizing the peptide from its cysteines, complicating its binding to CaM, in both, D-CaM or in complex with Q2-*h*AB.

Has been suggested that the H_2O_2 action is to make the opening conformation more favourable (Gamper et al, 2006). We cannot confirm this conclusion since, we previously observed that Ca^{2+} binding to C-lobe provokes a conformational change that is allosterically transmitted up to the pre-*h*A element and likely to the transmembrane region, ultimately resulting in the closing of the channel. Even if we have demonstrated that S2/S3 produces the opposite movement that the Ca^{2+} does, this is annulled upon H_2O_2 addition.

S5.5. MATERIALS AND METHODS

H_2O_2 (30% w/w H_2O_2, from Sigma-Aldrich 7722-84-1) was used at 2.5 % to oxidize S2/S3 peptide.

BIBLIOGRAPHY

- Abzhanov A, Kuo W, Hartmann C *et al.* The calmodulin pathway and evolution of elongated beak morphology in Darwin's finches. *Nature* 2006; 442, 563–567. https://doi.org/10.1038/nature04843
- Adaixo R, Harley CA, Castro-Rodrigues AF, Morais-Cabral JH. Structural properties of PAS domains from the KCNH potassium channels. *PLoS One*. 2013;8(3):e59265. doi:10.1371/journal.pone.0059265
- Aggarwal SK & MacKinnon R. Contribution of the S4 segment to gating charge in the Shaker K^+ channel. *Neuron* 1996;16, 1169–1177
- Aivar P, Fernández-Orth J, Gomis-Perez C, Alberdi A, Alaimo A, Rodríguez MS, Giraldez T, Miranda P, Areso P and Villarroel A. Surface expression and subunit specific control of steady protein levels by the Kv7.2 helix A-B linker. *PLoS ONE* 2012; 7, e47263. doi:10.1371/journal.pone.0047263CrossRefPubMedGoogle
- Alaimo A, Alberdi A, Gomis-Perez C, Fernandez-Orth J, Bernardo-Seisdedos G, Malo C, Millet O, Areso P, Villarroel A. Pivoting between Calmodulin Lobes Triggered by Calcium in the Kv7.2/Calmodulin Complex. *PLoS ONE*. 2014;9:e86711. doi: 10.1371/journal.pone.0086711
- Alaimo A, Gomez-Posada JC, Aivar P, Etxeberria A, Rodriguez-Alfaro JA, Areso P, Villarroel A. Calmodulin activation limits the rate of KCNQ2 K+ channel exit from the endoplasmic reticulum. *J. Biol. Chem.* 2009;284:20668–20675. doi: 10.1074/jbc.M109.019539.
- Alaimo A, Alberdi A, Gomis-Perez C, Fernandez-Orth J, Gomez-Posada JC, Areso P, Villarroel A. Cooperativity between calmodulin-binding sites in Kv7.2 channels. *J. Cell Sci.* 2013;126:244–253. doi: 10.1242/jcs.114082.
- Alaimo A, Nuñez E, Aivar P, Fernández-Orth J, Gomis-Perez C, Bernardo-Seisdedos G, Malo C, Villarroel A. Calmodulin confers calcium sensitivity to the stability of the distal intracellular assembly domain of Kv7.2 channels. *Sci. Rep.* 2017;7:13425. doi: 10.1038/s41598-017-13811-4.
- Alaimo A, Rubert J. The Pivotal Role of TRP Channels in Homeostasis and Diseases throughout the Gastrointestinal Tract. *Int J Mol Sci*. 2019;20(21):5277. Published 2019 Oct 24. doi:10.3390/ijms20215277
- Alberdi A, Gomis-Perez C, Bernardo-Seisdedos G, Alaimo A, Malo C, Aldaregia J, Lopez-Robles C, Areso P, Butz E, Wahl-Schott C, et al. Uncoupling PIP2-calmodulin regulation of Kv7.2 channels by an assembly de-stabilizing epileptogenic mutation. *J. Cell Sci.* 2015;128:4014–4023. doi: 10.1242/jcs.176420.

- Albert JA, Nerbonne JM. Calcium-independent depolarization-activated potassium currents in superior colliculus-projecting rat visual cortical neurons. J Neurophysiol. 1995;73:2163–2178.
- Amey JS, O'Reilly AO, Burton MJ, Puinean AM, Mellor IR, Duce IR, Field LM, Wallace BA, Williamson MS, Davies TGE. An evolutionarily-unique heterodimeric voltage-gated cation channel found in aphids. *FEBS Letts.* 2015;589:598–607. doi: 10.1016/j.febslet.2015.01.020.
- Ansbacher T, Srivastava HK, Stein T, Baer R, Merkx M, Shurki. A Calculation of transition dipole moment in fluorescent proteins—towards efficient energy transfer. *Phys Chem Chem Phys.* 2012. s 14(12):4109–4117
- Antz, C., Geyer, M., Fakler, B. *et al.* NMR structure of inactivation gates from mammalian voltage-dependent potassium channels. *Nature* 385, 272–275 (1997). https://doi.org/10.1038/385272a0
- Archer CR, Enslow BT, Taylor AB, De la Rosa V, Bhattacharya A, Shapiro MS. A mutually induced conformational fit underlies Ca^{2+}-directed interactions between calmodulin and the proximal C terminus of KCNQ4 K^+ channels. *J Biol Chem*. 2019;294(15):6094-6112. doi:10.1074/jbc.RA118.006857
- Babu YS, Bugg CE, Cook WJ. Structure of calmodulin refined at 2.2 Å resolution. *J. Mol. Biol.* 1988;204:191–204. doi: 10.1016/0022-2836(88)90608-0.
- Banerjee A, Lee A, Campbell E, Mackinnon R. Structure of a pore-blocking toxin in complex with a eukaryotic voltage-dependent K(+) channel. *Elife*. 2013;2:e00594. doi:10.7554/eLife.00594
- Barhanin J, Lesage F, Guillemare E, Fink M, Lazdunski M, Romey G. K(V)LQT1 and lsK (minK) proteins associate to form the I(Ks) cardiac potassium current. *Nature.* 1996 Nov 7;384(6604):78-80.
- Sanguinetti M, Curran M, Zou A *et al.* Coassembly of K_VLQT1 and minK (IsK) proteins to form cardiac I_{KS} potassium channel. *Nature* 1996; 384, 80–83.
- https://doi.org/10.1038/384080a0
- Barros F., Domínguez P., de la Peña P. Cytoplasmic domains and voltage-dependent potassium channel gating. *Front. Pharmacol* 2012;3:49.10.3389 fphar.2012.00049
- Batulan Z, Haddad GA, Blunck R. An intersubunit interaction between S4-S5 linker and S6 is responsible for the slow off-gating component in Shaker K+ channels. *J. Biol. Chem*. 2010;285, 14005–1401910.1074/jbc.M109.097717
- Bauer CK, Schwarz JR. Ether-a-go-go K(+) channels: effective modulators of neuronal excitability. *J. Physiol.,* 2018; 596 pp. 769-783
- Bernardo-Seisdedos, G., Nunez E., Gomis C., Malo C., Villarroel A., Millet O. Structural basis and energy landscape for the Ca^{2+} gating and calmodulation of the Kv7.2 K^+ channel. *Proc. Natl. Acad. Sci. U. S. A*. 2018; 115, 2395-2400.

- Bezanilla F. The voltage sensor in voltage-dependent ion channels. *Physiol. Rev.,* 2000; 80, pp. 555-592
- Biervert C, Schroeder BC, Kubisch C, Berkovic SF, Propping P, Jentsch TJ, et al. A potassium channel mutation in neonatal human epilepsy. *Science.* 1998;279:403–6
- Bonache MA, Alaimo A, Malo C, Millet O, Villarroel A, González-Muñiz R. Clicked bis-PEG-Peptide Conjugated for Studying Calmodulin-Kv7.2 Channel Binding. Org. *Biomol. Chem.* 2014;12:8877–8887. doi: 10.1039/C4OB01338G.
- Bradding P, Wulff H. Ion channels. *Thorax* 2013;68:974-977.
- Brehm P, Eckert R. Calcium entry leads to inactivation of calcium channel in Paramecium. *Science.* 1978;202:1203–1206. doi: 10.1126/science.103199.
- Brown DA, Adams PR. Muscarinic suppression of a novel voltage-sensitive K+ current in a vertebrate neurone. *Nature.* 1980;283:673–676. doi: 10.1038/283673a0.
- Catterall WA. From ionic currents to molecular mechanisms: the structure and function of voltage-gated sodium channels. *Neuron,* 2000;26, pp. 13-25
- Catteral WA. Na+ channel mutations and epilepsy. *Epilepsia,* 2010; 51: 59-59. doi:10.1111/j.1528-1167.2010.02845.x
- Chanda B, Kwame Asamoah O, Blunck R. *et al.* Gating charge displacement in voltage-gated ion channels involves limited transmembrane movement. *Nature,* 2005;436**,** 852–856. https://doi.org/10.1038/nature03888
- Chang A, Abderemane-Ali F, Hura GL, Rossen ND, Gate RE, Minor DL Jr. A Calmodulin C-Lobe Ca^{2+}-Dependent Switch Governs Kv7 Channel Function. *Neuron*. 2018;97(4):836-852.e6. doi:10.1016/j.neuron.2018.01.035
- Chin D, Means AR. Calmodulin: a prototypical calcium sensor. *Trends in cell biology*. 2010; 10, 8, P322-328, https://doi.org/10.1016/S0962-8924(00)01800-6
- Choveau FS, Abderemane-Ali F, Coyan FC, Es-Salah-Lamoureux Z, Baró I, Loussouarn G. Opposite effects of the S4–S5 linker and PIP2 on voltage-gated channel function: KCNQ1/KCNE1 and other channels. *Front. Pharmacol.* 2012;3:125.10.3389/fphar.2012.00125
- Connor JA, Stevens CF. Voltage clamp studies of a transient outward membrane current in gastropod neural somata. *J Physiol*. 1971;213(1):21-30. doi:10.1113/jphysiol.1971.sp009365
- Cooper EC, Aldape KD, Abosch A, Barbaro NM, Berger MS, Peacock WS, Jan YN, Jan LY. Colocalization and coassembly of two human brain M-type potassium channel subunits that are mutated in epilepsy. *Proc Natl Acad Sci USA* 2000;97: 4914–4919.
- Crotti L, Spazzolini C, Tester DJ, Ghidoni A, Baruteau AE, Beckmann BM, et al. Calmodulin mutations and life-threatening cardiac arrhythmias: insights from the

International Calmodulinopathy Registry. *Eur Heart J.* 2019;40:2964–75. 10.1093/eurheartj/ehz311

- Cruzblanca H, Koh DS & Hille B. Bradykinin inhibits M current via phospholipase C and Ca^{2+} release from IP_3-sensitive Ca^{2+} stores in rat sympathetic neurons. *Proc Natl Acad Sci USA* 1998;95, 7151– 7156.
- Davydov DR, Davydova NY, Halpert JR Allosteric transitions in cytochrome P450eryF explored with pressure-perturbation spectroscopy, lifetime FRET, and a novel fluorescent substrate, Fluorol-7GA. *Biochemistry.* 2008; 47(43):11348–11359
- Day RN, Booker CF, Periasamy A. Characterization of an improved donor fluorescent protein for Forster resonance energy transfer microscopy. *J Biomed Opt*. 2008;13(3):031203. doi:10.1117/1.2939094
- de la Peña P, Domínguez P, Barros F. Functional characterization of Kv11.1 (hERG) potassium channels split in the voltage-sensing domain. *Pflugers Arch*. 2018;470(7):1069-1085. doi:10.1007/s00424-018-2135-y
- Delaglio F, Grzesiek S, Vuister GW, Zhu G, Pfeifer J, Bax A. NMRPipe: a multidimensional spectral processing system based on UNIX pipes. *J Biomol NMR.* 1995 Nov;6(3):277-93.
- Delmas P., Brown D.A. Pathways modulating neural KCNQ/M (Kv7) potassium channels. *Nat. Rev. Neurosci.* 2005;6:850–862. doi: 10.1038/nrn1785.
- Delmas P, Coste B, Gamper N, Shapiro MS.Phosphoinositide Lipid Second Messengers: New Paradigms for Calcium Channel Modulation. *Neuron*, 2005;47:2 pp.179-182 ISSN 0896-6273,
- https://doi.org/10.1016/j.neuron.2005.07.001.
- DeMaria C, Soong T, Alseikhan B. *et al.* Calmodulin bifurcates the local Ca^{2+} signal that modulates P/Q-type Ca^{2+} channels. *Nature*. 2001;411, 484–489. https://doi.org/10.1038/35078091
- Dedek K, Kunath B, Kananura C, Reuner U, Jentsch TJ, et al. Myokymia and neonatal epilepsy caused by a mutation in the voltage sensor of the KCNQ2 K+ channel. Proc Natl Acad Sci U S A. 2001;98:12272–12277.
- Doyle DA1, Morais Cabral J, Pfuetzner RA, Kuo A, Gulbis JM, Cohen SL, Chait BT, MacKinnon R. The structure of the potassium channel: molecular basis of K+ conduction and selectivity. *Science.* 1998 Apr 3;280(5360):69-77.
- Durell SR, Shrivastava IH, Guy HR. Models of the Structure and Voltage-Gating Mechanism of the Shaker K+ Channel, *Biophysical Journal,* 2004; 87, 4, 2004, 2116-2130, ISSN0006-3495, https://doi.org/10.1529/biophysj.104.040618
- Eckey K, Wrobel E, Strutz-Seebohm N, Pott L, Schmitt N, Seebohm G. Novel Kv7.1-phosphatidylinositol 4,5-bisphosphate interaction sites uncovered by charge

neutralization scanning. *J Biol Chem*. 2014;289(33):22749-22758. doi:10.1074/jbc.M114.589796

- Ehlers MD, Zhang S, Bernhardt JP, Huganir RL. Inactivation of NMDA receptors by direct interaction of calmodulin with the NR1 subunit. *Cell.* 1996;84:745–755. doi: 10.1016/S0092-8674(00)81052-1.
- Etxeberria A, Aivar P, Rodriguez-Alfaro JA, Alaimo A, Villace P, Gomez-Posada JC, Areso P, Villarroel A. Calmodulin regulates the trafficking of KCNQ2 potassium channels. *FASEB J*. 2008;22:1135–1143. doi: 10.1096/fj.07-9712com.
- Falkenburger BH, Jensen JB, Hille B. Kinetics of M_1 muscarinic receptor and G protein signaling to phospholipase C in living cells. *J. Gen. Physiol*. 2010;135:81–97 10.1085/jgp.200910344
- Falkenburger BH, Jensen JB, Hille B. Kinetics of PIP_2 metabolism and KCNQ2/3 channel regulation studied with a voltage-sensitive phosphatase in living cells. *J. Gen. Physiol*. 2010; 135:99–114 10.1085/jgp.200910345
- Falkenburger BH, Dickson EJ, Hille B. Quantitative properties and receptor reserve of the DAG and PKC branch of G_q-coupled receptor signaling. *J. Gen. Physiol.* 2013;141:537–555
- Ferguson KM, Kavran JM, Sankaran VG, Fournier E., Isakoff S.J., Skolnik E.Y., Lemmon M.A. Structural basis for discrimination of 3-phosphoinositides by pleckstrin homology domains. *Mol. Cell.* 2000;6:373–384.
- Fernando H, Halpert JR, Davydov DR Resolution of multiple substrate binding sites in cytochrome P450 3A4: the stoichiometry of the enzyme-substrate complexes probed by FRET and Job's titration. *Biochemistry* 2006; 45:4199–4209
- Fesik SW, Gampe RT, Zuiderweg ERP. Heteronuclear three-dimensional NMR spectroscopy. Natural abundance carbon-13 chemical shift editing of 1H-1H COSY spectra. *J. Am. Chem. Soc.* 1989, 111, 2, 770-772 https://doi.org/10.1021/ja00184a077
- Feske S, Wulff H, Skolnik EY. Ion channels in innate and adaptive immunity. *Annu Rev 2015*
- Filippov AK, Webb TE, Barnard EA, Town DA. P2Y2 nucleotide receptors expressed heterologously in rat sympathetic neurons inhibit both N-Type Ca2+ and M-Type K+ currents. *J. Neurosci.* 1998;18:5170-5179.
- Gamper N, Li Y, Shapiro MS. Structural requirements for differential sensitivity of KCNQ K+ channels to modulation by Ca^{2+}/calmodulin. *Mol. Biol. Cell.* 2005;16:3538–3551. doi: 10.1091/mbc.e04-09-0849.
- Gamper N, Shapiro MS. Calmodulin mediates Ca^{2+}-dependent modulation of M-type K+ channels. *J. Gen. Physiol.* 2003;122:17–31. doi: 10.1085/jgp.200208783.

- Gamper N, Shapiro M. Regulation of ion transport proteins by membrane phosphoinositides. *Nat Rev Neurosci* 2007;8, 921–934. https://doi.org/10.1038/nrn2257
- Garrett DS, Seok YJ, Peterkofsky A, Clore GM, Gronenborn AM. Identification by NMR of the Binding Surface for the Histidine-Containing Phosphocarrier Protein HPr on the N-Terminal Domain of Enzyme I of the Escherichia coli Phosphotransferase System. *Biochemistry* 1997;36, 4393-4398
- Geiger JR, Alle H.Combined analog and action potential coding in hippocampal mossy fibers. Science. 2006 Mar 3;311(5765):1290-3.
- Gestrelius S, Grampp W. Impulse firing in the slowly adapting stretch receptor neurone of lobster and its numerical simulation. *Acta Physiol Scand.* 1983 Jul;118(3):253-61.
- Giepmans BN, Adams SR, Ellisman MH, Tsien RY. The fluorescent toolbox for assessing protein location and function. *Science.* 2006;312:217–224.
- Gilling M, Rasmussen HB, Calloe K, Sequeira AF, Baretto M, Oliveira G, Almeida J, Lauritsen MB, Ullmann R, Boonen SE, Brondum-Nielsen K, Kalscheuer VM, Tümer Z, Vicente AM, Schmitt N, Tommerup N. Dysfunction of the heteromeric KV7.3/KV7.5 potassium channel is associated with autism spectrum disorders. *Front. Genet.,* 2003
- https://doi.org/10.3389/fgene.2013.00054
- Goedhart J, van Weeren L, Adjobo-Hermans MJ, Elzenaar I, Hink MA, Gadella TW Jr. Quantitative co-expression of proteins at the single cell level--application to a multimeric FRET sensor. *PLoS One*. 2011;6(11):e27321. doi:10.1371/journal.pone.0027321
- Gomez-Posada JC, Aivar P, Alberdi A, Alaimo A, Etxeberria A, Fernandez-Orth J, Zamalloa T, Roura-Ferrer M, Villace P, Areso P, et al. Kv7 Channels Can Function without Constitutive Calmodulin Tethering. *PLoS ONE*. 2011;6:e25508. doi: 10.1371/journal.pone.0025508
- Gomis-Perez C, Alaimo A, Fernandez-Orth J, Alberdi A, Paloma Aivar-Mateo P, Bernardo-Seisdedos G, Malo C, Areso P, Felipe A, Villarroel A. An unconventional calmodulin-anchoring site within the AB module of Kv7.2 channels. *Journal of Cell Science* 2015; 128: 3155-3163; doi: 10.1242/jcs.174128
- Gomis-Perez C, Soldovieri MV, Malo C, Ambrosino P, Taglialatela M, Areso P, Villarroel A. Differential Regulation of PI(4,5)P2 Sensitivity of Kv7.2 and Kv7.3 Channels by Calmodulin. *Front. Mol. Neurosci*. 2017;10:117. doi: 10.3389/fnmol.2017.00117
- Gourgy-Hacohen O, Kornilov P, Pittel I, Peretz A, Attali B, Paas Y. Capturing distinct KCNQ2 channel resting states by metal ion bridges in the voltage-sensor domain. *J Gen Physiol*. 2014;144(6):513-527. doi:10.1085/jgp.201411221
- Grabarek Z. Structural Basis for Diversity of the EF-hand Calcium-binding Proteins. *J Mol Biol.* 2006;359(3):509-25. Epub 2006 Apr 21.

- Grizel AV, Glukhov GS, Sokolova OS. Mechanisms of activation of voltage-gated potassium channels. *Acta Naturae*. 2014;6(4):10-26.
- Gutman GA, Chandy KG, Grissmer S, Lazdunski M, McKinnon D, Pardo LA, Robertson GA, Rudy B, Sanguinetti MC, Stühmer W, Wang X. International Union of Pharmacology. LIII. Nomenclature and molecular relationships of voltage-gated potassium channels. *Pharmacol. Rev*. 2005;57:473–508.
- Ha T, Enderle T, Ogletree DF, Chemla DS, Selvin PR, Weiss S. Probing the interaction between two single molecules: fluorescence resonance energy transfer between a single donor and a single acceptor. *Proc Natl Acad Sci U S A*. 1996;93(13):6264-6268. doi:10.1073/pnas.93.13.6264
- Hadley JK, Noda M, Selyanko AA, Wood IC, Abogadie FC, Brown DA. Differential tetraethylammonium sensitivity of KCNQ1–4 potassium channels. *Br J Pharmacol* 2000;129: 413–415.
- HAGIWARA S, HAYASHI H, and TAKAHAsHI K. Calcium and potassium currents of the membrane of a barnacle muscle fibre in relation to the calcium spike. *J. Physiol. (Lond.).* 1969;205:115
- Haitin Y, Attali B. The C-terminus of Kv7 channels: A multifunctional module. *J. Physiol.* 2008;586:1803–1810. doi: 10.1113/jphysiol.2007.149187.
- Hernandez CC, Zaika O, Tolstykh GP, Shapiro MS. Regulation of neural KCNQ channels: signalling pathways, structural motifs and functional implications. *J Physiol* 2008; 586.7 pp 1811–1821 1811
- Higashida*, Streat, Werner Klee, and Marshall Nirenberg. Bradykinin-activated transmembrane signals are coupled via N. or Ni to production of inositol 1,4,5-trisphosphate, a second messenger in NG108-15 neuroblastoma-glioma hybrid cells. *Proc. Natl. Acad. Sci. USA* 1986; 83, pp. 942-946
- Hille B, Dickson EJ, Kruse M, Vivas O, Suh BC. Phosphoinositides regulate ion channels. *Biochim Biophys Acta*. 2015;1851(6):844-856. doi:10.1016/j.bbalip.2014.09.010
- Hille B. G protein-coupled mechanisms and nervous signaling. *Neuron*, 1992;9:2, pp. 187-195, ISSN 0896-6273,
- https://doi.org/10.1016/0896-6273(92)90158-A.
- Hille B. Ionic channels of excitable membranes. *Sinauer Associates, Inc.*, Sunderland, MA. 2001.
- Hirschberg B, Maylie J, Adelman JP, Marrion NV. Gating of recombinant small-conductance Ca-activated K+ channels by calcium. *J Gen Physiol.* 1998;111(4):565-581. doi:10.1085/jgp.111.4.565

- Hodgkin AL, Huxley AF. A quantitative description of membrane current and its application to conduction and excitation in nerve. *J Physiol*. 1952;117(4):500-544. doi:10.1113/jphysiol.1952.sp004764
- Hoppe A, Christensen K, Swanson JA Fluorescence resonance energy transfer-based stoichiometry in living cells. *Biophys.* 2002; J 83:3652–3664
- Hoshi N, Zhang JS, Omaki M, Takeuchi T, Yokoyama S, Wanaverbecq N, Langeberg LK, Yoneda Y, Scott JD, Brown DA, *et al.* AKAP150 signaling complex promotes suppression of the M-current by muscarinic agonists *Nat. Neurosci.,* 2003;6, pp. 564-571
- Hoshi N, Negishi H, Okada S, Nonami T, Kimoto K. Response of human fibroblasts to implant surface coated with titanium dioxide photocatalytic films. *J Prosthodont Res.* 2010 Oct;54(4): 85-91. doi: 10.1016/j.jpor.2010.04.005. Epub 2010 May 15. PMID:20472524
- Howard RJ, Clark KA, Holton JM, Minor DL Jr. Structural insight into KCNQ (Kv7) channel assembly and channelopathy. *Neuron*. 2007;53(5):663-675. doi:10.1016/j.neuron.2007.02.010
- Huang, S. Feng, D.W. Hilgemann. Direct activation of inward rectifier potassium channels by PIP_2 and its stabilization by Gβγ. *Nature,* 1998;391, pp. 803-806
- McCormick DA, Huguenard JR. A model of the electrophysiological properties of thalamocortical relay neurons. *J Neurophysiol.* 1992 Oct;68(4):1384-400.
- Ishida H, Vogel HJ. Protein-peptide interaction studies demonstrate the versatility of calmodulin target protein binding. *Protein Pept Lett.* 2006;13(5):455-65.
- Janin J, Miller S, and Chothia C. Surface, subunit interfaces and interior of oligomeric proteins. *J. Mol. Biol.* 1988;204, 155–164.
- Jares-Erijman EA, Jovin TM. FRET imaging. *Nat Biotechnol*. 2003;21:1387–1395. doi:10.1038/nbt896
- Jares-Erijman EA, Jovin TM. FRET imaging. *Nat Biotechnol.* 2003 Nov;21(11):1387-95.
- Jenke M, Sánchez A, Monje F, Stühmer W, Weseloh RM, Pardo LA. C-terminal domains implicated in the functional surface expression of potassium channels. *EMBO J*. 2003;22(3):395-403. doi:10.1093/emboj/cdg035
- Jentsch JD, Roth RH, Taylor JR. Object retrieval/detour deficits in monkeys produced by prior subchronic phencyclidine administration: evidence for cognitive impulsivity. *Biol. Psychiatry* 2000;48, 415e424
- Jiang YH, Armstrong D, Albrecht U, Atkins CM, Noebels JL, Eichele G, Sweatt JD, Beaudet AL. Mutation of the Angelman ubiquitin ligase in mice causes increased cytoplasmic p53 and deficits of contextual learning and long-term potentiation. Neuron 1998;21: 799-811.

- Johnston D, Wu SM. Foundations of Cellular Neurophysiology. *Cambridge, MA, USA: MIT Press;* 1995.
- Joiner, William & Khanna, Rajesh & Schlichter, Lyanne & Kaczmarek, Leonard. Calmodulin Regulates Assembly and Trafficking of SK4/IK1 Ca 2+-activated K+ Channels. *The Journal of biological chemistry*. 2001;276. 37980-5. 10.1074/jbc.M104965200.
- Joo C, Ha T, Selvin P. Single-molecule FRET with total internal reflection microscopy. *Single Mol Tech Lab*. 2007; Man 3–36
- Joo SH. Cyclic peptides as therapeutic agents and biochemical tools. *Biomol Ther (Seoul)*. 2012;20(1):19–26. doi:10.4062/biomolther.2012.20.1.019
- Kajihara D, Abe R, Iijima I, Komiyama C, Sisido M, Hohsaka T. FRET analysis of protein conformational change throughposition-specific incorporation of fluorescent amino acids. *NatMethods*. 2006; 3(11):923–929
- Kapanidis AN, Weiss S. Fluorescent probes and bioconjugation chemistries for single-molecule fluorescence analysis of biomolecules. J Chem Phys. 2002;117:10953–10964.
- Kasai H, Aosaki T. Modulation of Ca-channel current by an adenosine analog mediated by a GTP-binding protein in chick sensory neurons. *Pflugers Arch.* 1989 Jun;414(2):145-9.
- Kawasaki H, Kretsinger RH. Calcium-binding proteins. 1: EF-hands. *Protein Profile.* 1994;1(4):343-517.
- Kedziora KM, Jalink K. Fluorescence resonance energy transfer microscopy (FRET). *Methods Mol Biol.* 2015;1251:67-82. doi: 10.1007/978-1-4939-2080-8_5.
- Keen JE, Khawaled R, Farrens DL, Neelands T, Rivard A, Bond CT, Janowsky A, Fakler B, Adelman JP, Maylie J. Domains responsible for constitutive and Ca^{2+}-dependent interactions between calmodulin and small conductance Ca^{2+}-activated potassium channels. *J Neurosci* 1999; 19:8830-8; PMID:10516302
- Keselman I, Fribourg M, Felsenfeld DP, Logothetis DE. Mechanism of PLC-mediated Kir3 current inhibition. *Channels* (Austin). 2007;1(2):113-23. Epub 2007 Apr 23.
- Kharkovets T, Hardelin JP, Safieddine S, et al. KCNQ4, a K+ channel mutated in a form of dominant deafness, is expressed in the inner ear and the central auditory pathway. *Proc Natl Acad Sci U S A*. 2000;97(8):4333-4338. doi:10.1073/pnas.97.8.4333
- Kink JA, Maley ME, Preston RR, Ling KY, Wallen-Friedman MA, Saimi Y, Kung C. Mutations in paramecium calmodulin indicate functional differences between the C-terminal and N-terminal lobes in vivo. *Cell.* 1990;62:165–174. doi: 10.1016/0092-8674(90)90250-I

- Kolb, B. (1990). Prefrontal cortex. In B. Kolb & R. C. Tees (Eds.), *The cerebral cortex of the rat* (p. 437–458). The MIT Press.
- Komatsu N. *et al*. Development of an optimized backbone of FRET biosensors for kinases and GTPases. *Mol. Biol. Cell.2011;* 22, 4647–56.
- Kosenko A, Kang S, Smith IM, et al. Coordinated signal integration at the M-type potassium channel upon muscarinic stimulation. *EMBO J*. 2012;31(14):3147-3156. Published 2012 May 29. doi:10.1038/emboj.2012.156
- Kramer J, Obejero-Paz C, Myatt G. *et al.* MICE Models: Superior to the HERG Model in Predicting Torsade de Pointes. *Sci Rep* 2013; 3, 2100. https://doi.org/10.1038/srep02100
- Kreusch A, Pfaffinger P, Stevens C. *et al.* Crystal structure of the tetramerization domain of the *Shaker* potassium channel. *Nature* 1998; 392**,** 945–948. https://doi.org/10.1038/31978
- Kruse AC, Hu J, Pan AC, et al. Structure and dynamics of the M3 muscarinic acetylcholine receptor. *Nature*. 2012;482(7386):552-556. doi:10.1038/nature10867
- Kubisch C, Schroeder BC, Friedrich T, Lutjohann B, El-Amraoui A, Marlin S, Petit C, Jentsch TJ. KCNQ4, a novel potassium channel expressed in sensory outer hair cells, is mutated in dominant deafness. *Cell.* 1999; 96: 437-446
- Kwak CK, Kim DM, Lee CS, Lee M, Lee TS. Aldehyde-functionalized, water-soluble poly(para-phenylene): synthesisand streptavidin assay using FRET. *J Nanosci Nanotechnol* 2010;10(10):6920–6924
- Lakowicz JR. Principles of Fluorescence Spectroscopy. *Principles of Fluorescence Spectroscopy, 3rd edition; 2006*
- Lambers TT, Weidema AF, Nilius B, Hoenderop JG, Bindels RJ.Regulation of the mouse epithelial Ca2(+) channel TRPV6 by the Ca(2+)-sensor calmodulin. *J Biol Chem* 2004;279:28855–28861
- Lange A, Giller K, Hornig S. *et al.* Toxin-induced conformational changes in a potassium channel revealed by solid-state NMR. *Nature* 2006;440**,** 959–962.
- https://doi.org/10.1038/nature04649
- Lee H, and MacKinnon R. Activation mechanism of a human SK-calmodulin channel complex elucidated by cryo-EM structures. *Science.* 2018;360, 508–513 10.1126/science.aas9466
- Lee H, Norris A, Weiss J. *et al.* Jelly belly protein activates the receptor tyrosine kinase Alk to specify visceral muscle pioneers. *Nature* 2003;425, 507–512. https://doi.org/10.1038/nature01916

- Lehman A, Thouta S, Mancini GMS, et al. Loss-of-Function and Gain-of-Function Mutations in KCNQ5 Cause Intellectual Disability or Epileptic Encephalopathy. *Am J Hum Genet.* 2017;101(1):65-74. doi:10.1016/j.ajhg.2017.05.016
- Lemmon, M.A. Phosphoinositide recognition domains. *Traffic.* 2003;4:201–213
- Lerche H, Biervert C, Alekov AK, Schleithoff L, Lindner M, Klinger W, Bretschneider F, Mitrovic N, Jurkat-Rott K, Bode H, Lehmann-Horn F, Steinlein OK. A reduced K+ current due to a novel mutation in KCNQ2 causes neonatal convulsions. *Ann Neurol* 1999; 46 (3): 305-12.
- Lerche C, Scherer CR, Seebohm G, Derst C, Wei AD, Busch AE, Steinmeyer K. Molecular cloning and functional expression of KCNQ5, a potassium channel subunit that may contribute to neuronal M-current diversity. *J Biol Chem.* 2000 Jul 21;275(29):22395-400.
- Li Y, Gamper N, Hilgemann DW, Shapiro MS. Regulation of Kv7 (KCNQ) K+ channel open probability by phosphatidylinositol 4,5-bisphosphate. *J Neurosci*. 2005;25(43):9825-9835. doi:10.1523/JNEUROSCI.2597-05.2005
- Liang D, Li X, Clark JD. Increased expression of Ca^{2+}/calmodulin-dependent protein kinase IIα during chronic morphine exposure. *j.neursocience* 2003; https://doi.org/10.1016/j.neuroscience.2003.10.007
- Liu X, Sun K, Chen H. *et al.* Curcumin inhibits proliferation of gastric cancer cells by impairing ATP-sensitive potassium channel opening. *World J Surg Onc* 2014;12, 389. https://doi.org/10.1186/1477-7819-12-389
- Liu M, Chen TY, Ahamed B, Li J, Yau KW. Calcium-calmodulin modulation of the olfactory cyclic nucleotide-gated cation channel. Science. 1994;266:1348–1354.
- doi: 10.1126/science.266.5189.1348.
- Locke RE, Nerbonne JM. Role of voltage-gated K+ currents in mediating the regular-spiking phenotype of callosal-projecting rat visual cortical neurons. *J Neurophysiol.* 1997 Nov;78(5):2321-35.
- Long SB, Campbell EB & MacKinnon R. Voltage sensor of Kv1.2: structural basis of electromechanical coupling. *Science* 2005;309, 903–908
- Long S, Tao X, Campbell E. *et al.* Atomic structure of a voltage-dependent K^+ channel in a lipid membrane-like environment. *Nature* 2007;450, 376–382.
- https://doi.org/10.1038/nature06265
- Long F, Gu C, Gu§ AZ, Shi H Quantum dot/carrier–protein/ haptens conjugate as a detection nanobioprobe for FRET-based immunoassay of small analytes with all-fiber microfluidic bio-sensing platform. *Anal Chem* 2012;84(8):3646–3653

- Lőrincz P, Lakatos Z, Varga Á, Maruzs T, Simon-Vecsei Z, Darula Z, Benkő P, Csordás G, Lippai M, Andó I, Hegedűs K, Medzihradszky KF, Takáts S, Juhász G. MiniCORVET is a Vps8-containing early endosomal tether in Drosophila. *eLife* 2016;5(): e14226.
- Lörinczi É, Gómez-Posada J, de la Peña P. *et al.* Voltage-dependent gating of KCNH potassium channels lacking a covalent link between voltage-sensing and pore domains. *Nat Commun* 2015;**6,** 6672. https://doi.org/10.1038/ncomms7672
- Lovell JF, Chen J, Jarvi MT, Cao WG, Allen AD, Liu Y, Tidwell TT, Wilson BC, Zheng FRET quenching of photosensitizer singlet oxygen generation. *J Phys Chem B G*. 2009;113(10):3203–3211
- MacKinnon R. Determination of the subunit stoichiometry of a voltage-activated potassium channel. *Nature* 1991;350, 232–235. https://doi.org/10.1038/350232a0
- MacKinnon R. Potassium channels. *FEBS Lett*. 2003;27;555(1):62-5.
- Maljevic S, Lerche C, Seebohm G, Alekov AK, Busch AE, Lerche H. C-terminal interaction of KCNQ2 and KCNQ3 K+ channels. *J Physiol*. 2003;548(Pt 2):353-360. doi:10.1113/jphysiol.2003.040980
- Maljevic S, Wuttke TV, Lerche H. Nervous system K_V7 disorders: breakdown of a subthreshold brake. The Journal of Physiology, 2008;586: 1791-1801. doi:10.1113/jphysiol.2008.150656
- Maljevic, S., Wuttke, T.V., Seebohm, G. *et al.* K_V7 channelopathies. *Pflugers Arch - Eur J Physiol* 2010;460, 277–288. https://doi.org/10.1007/s00424-010-0831-3
- Marrion NV, Zucker RS, Marsh SJ, Adams PR. Modulation of M-current by intracellular Ca2+. *Neuron*, 1991;6:4, pp 533-545, ISSN 0896-6273, https://doi.org/10.1016/0896-6273(91)90056-6.
- Marrion NV. CONTROL OF M-CURRENT. *Annual Review of Physiology* 1997;59:1, 483-504
- Maylie J, Bond CT, Herson PS, Lee WS, Adelman JP. Small conductance Ca2+-activated K+ channels and calmodulin. *J Physiol,* 2004;554 (Pt 2), pp. 255-261,
- doi10.1113/jphysiol.2003.049072
- Meador WE, Means AR, Quiocho FA. Target enzyme recognition by calmodulin: 2.4 A structure of a calmodulin-peptide complex. Science. 1992;28;257(5074):1251-5.
- Mehta S. and Jin Zhang J. Reporting from the Field: Genetically Encoded Fluorescent Reporters Uncover Signaling Dynamics in Living Biological Systems. *Annual Review of Biochemistry*. 2011; 80:375-401 https://doi.org/10.1146/annurev-biochem-060409-093259
- Merchant KA, Best RB, Louis JM, Gopich IV, Eaton WA. Characterizing the unfolded states of proteins using single-molecule FRET spectroscopy and molecular simulations. *Proc Natl Acad Sci U S A.* 2007;104:1528–1533.

- Meyer T, Teruel MN. Fluorescence imaging of signaling networks. *Trends Cell Biol* 2003; 13:101–106
- Minor DL, Lin YF, Mobley BC, Avelar A, Jan YN, Jan LY, Berger JM. The polar T1 interface is linked to conformational changes that open the voltage-gated potassium channel. *Cell.* 2000;102:657–670.
- Miranda P, Contreras JE, Plested AJ, Sigworth FJ, Holmgren M, Giraldez T. State-dependent FRET reports calcium- and voltage-dependent gating-ring motions in BK channels. *Proc Natl Acad Sci U S A*. 2013;110(13):5217-5222. doi:10.1073/pnas.1219611110
- Miyawaki A. Visualization of the spatial and temporal dynamics of intracellular signaling. *Dev Cell.* 2003 Mar;4(3):295-305.
- Miyawaki, A. Development of probes for cellular functions using fluorescent proteins and fluorescence resonance energy transfer. *Annu. Rev. Biochem.* 2011;80, 357–73.
- Moerner WE, Fromm DP. Methods of single-molecule fluorescence spectroscopy and microscopy. *Rev Sci Inst.* 2003;74:3597–3619.
- Morais Cabral JH, Lee A, Cohen SL, Chait BT, Li M, Mackinnon R. Crystal structure and functional analysis of the HERG potassium channel N terminus: a eukaryotic PAS domain. *Cell.* 1998; 25;95(5):649-55.
- Mori M, Konno T, Ozawa T, Murata M, Imoto K, Nagayama K. Novel interaction of the voltage-dependent sodium channel (VDSC) with calmodulin: Does VDSC acquire calmodulin-mediated Ca^{2+}-sensitivity? *Biochemistry*. 2000;39:1316–1323. doi: 10.1021/bi9912600.
- Murata Y, Okamura Y. Depolarization activates the phosphoinositide phosphatase Ci-VSP, as detected in Xenopus oocytes coexpressing sensors of PIP2. *J Physiol*. 2007;583(Pt 3):875-889. doi:10.1113/jphysiol.2007.134775
- Nagai T, Ibata K, Park ES, Kubota M, Mikoshiba K, Miyawaki A. A variant of yellow fluorescent protein with fast and efficient maturation for cell-biological applications. *Nat. Biotechnol*. 2002;20:87–90.
- Nakayama S, Kretsinger RH. Evolution of the EF-hand family of proteins. *Annu Rev Biophys Biomol Struct.* 1994;23:473-507.
- NEHER, E. Two fast transient current components during voltage clamp on snail neurons. *J. Gen. Physiol.* 1971;58:36
- Neher J. Vesicle Pools and Ca^{2+} Microdomains: Review New Tools for Understanding Their Roles in Neurotransmitter Release. Neuron, 1998;Vol. 20, 389–399, March, 1998,1998 by Cell Press

- Ray D. Nelson, Grace Kuan, Milton H. Saier, Mauricio Montal. Modular assembly of voltage-gated channel proteins: a sequence analysis and phylogenetic study. Journal of molecular microbiology and biotechnology, 1999; Corpus ID: 14207808
- Neubauer BA, Waldegger S, Heinzinger J, Hahn A, Kurlemann G, Fiedler B, Eberhard F, Muhle H, Stephani U, Garkisch S, Eeg-Olofsson O, Müller U, Sander T. *KCNQ2* and *KCNQ3* mutations contribute to different idiopathic epilepsy syndromes. *Neurology* 2008; 71 (3) 177 183; DOI: 10.1212/01.wnl.0000317090.92185.ec
- Nguyen AW, Daugherty PS. Evolutionary optimization of fluorescent proteins for intracellular FRET. *Nat. Biotechnol.* 2002;23(3):355–360.
- Nijenhuis T., Vallon V., Annemiete W.C.M., van der Kemp, Hoenderop J.G.J., Bindels R.J.M. Enhanced passive Ca^{2+} reabsorption and reduced Mg^{2+} channel abundance explains thiazide-induced hypocalciuria and hypomagnesemia. *J Clin Invest*. 2005;115(6):1651-1658. https://doi.org/10.1172/JCI24134.
- Nilius B. Chloride channels go cell cycling. *J Physiol.* 2001 May 1;532(Pt 3):581.
- Noda M, Ikeda T, Suzuki H. *et al.* Expression of functional sodium channels from cloned cDNA. *Nature* 1986;**322,** 826–828. https://doi.org/10.1038/322826a0
- Ohashi T, Galiacy SD, Briscoe G, Erickson HP. An experimental study of GFP-based FRET, with application to intrinsically unstructured proteins. *Protein Sci.* 2007;16(7):1429–1438.
- Okada M, Takezawa D, Tachibanaki S, Kawamura S, Tokumitsu H, Kobayashi R. Neuronal calcium sensor proteins are direct targets of the insulinotropic agent repaglinide. *Biochem J.* 2003;1:375 pp. 87-97.
- Pardo LA, del Camino D, Sánchez A, Alves F, Brüggemann A, Beckh S, Stühmer W. Oncogenic potential of EAG K^+ channels. *EMBO J.* 1999;18: 5540–5547
- Pardo LA, Stühmer W. The roles of K(+) channels in cancer. *Nat Rev Cancer.* 2014;14(1):39-48. doi: 10.1038/nrc3635.
- Pathak MM, Yarov-Yarovoy V, Agarwal G, Roux B, Barth P, Kohout S, Tombola F, Isacoff EY. Closing in on the resting state of the Shaker K(+) channel. *Neuron.* 2007;4;56(1):124-40.
- Penner, R., Petersen, M., Pierau, F.-. *et al.* Dendrotoxin: a selective blocker of a non-inactivating potassium current in guinea-pig dorsal root ganglion neurones. *Pflugers Arch.* 1986;407, 365–369. https://doi.org/10.1007/BF00652619
- Periasamy A, Day RN. Molecular Imaging: FRET Microscopy and Spectroscopy. *Oxford University Press; New York:* 2005
- Periasamy A. Methods in Cellular Imaging. *Oxford University Press, New York.* 2001;434 pp.

- Peterson BZ, DeMaria CD, Adelman JP, Yue DT. Calmodulin is the Ca^{2+} sensor for Ca^{2+}-dependent inactivation of L-type calcium channels. *Neuron.* 1999;22:549–558. doi: 10.1016/S0896-6273(00)80709-6.
- Phillips AM, Bull A, Kelly LE. Identification of a Drosophila gene encoding a calmodulin-binding protein with homology to the *trp* phototransduction gene. *Neuron*. 1992;8:631–642. doi: 10.1016/0896-6273(92)90085-R.
- Pioletti M, Findeisen F, Hura GL, Minor DL Jr. Three-dimensional structure of the KChIP1-Kv4.3 T1 complex reveals a cross-shaped octamer. *Nat Struct Mol Biol*. 2006;13(11):987-995. doi:10.1038/nsmb1164
- Purves D, Augustine GJ, Fitzpatrick D, et al., Voltage-Gated Ion Channels*. Neuroscience. 2nd edition. Sunderland (MA): Sinauer Associates*; 2001. https://www.ncbi.nlm.nih.gov/books/NBK10883/
- Quandt FN. Three kinetically distinct potassium channels in mouse neuroblastoma cells.. *The Journal of Physiology*, 1988;395 doi: 10.1113/jphysiol.1988.sp016926.
- Radivojac P, Vucetic S, O'Connor TR, Uversky VN, Obradovic Z, Dunker AK. Calmodulin signaling: analysis and prediction of a disorder-dependent molecular recognition. *Proteins.* 2006;1:63(2):398-410.PMID: 16493654
- Rett A R, Teubel R. Neugeborenenkrämpfe im Rahmen einer epileptisch belasten Familie*. Wien Klin Wschr* 1964;76:609–613. Richards MC, Heron SE, .
- Rizzo MA, Springer GH, Granada B, Piston DW. An improved cyan fluorescent protein variant useful for FRET. *Nat. Biotechnol.* 2004;22:445–449.
- Roura-Ferrer M, Pérez-Verdaguer M, Oliveras A, Calvo M, Fernández-Fernández JM et al. KCNE4 suppresses Kv1.3 currents by modulating trafficking, surface expression and channel gating. *Journal of cell science.* 2009; 122(Pt 20): 3738-3748. DOI 10.1242/jcs.056689
- Roy R, Hohng S, Ha T. A practical guide to single-molecule FRET. *Nat Methods*. 2008;5(6):507-516. doi:10.1038/nmeth.1208
- Rudy B. Diversity and ubiquity of K channels. *Neuroscience.* 1988 Jun;25(3):729-49. PMID:2457185 DOI: 10.1016/0306-4522(88)90033-4
- Sachyani DM, Strulovich R, Tria G, Tobelaim W, Peretz A, Pongs O, Svergun D, Attali B and Hirsch JA. Structural basis of a Kv7.1 potassium channel gating module: studies of the intracellular C-terminal domain in complex with calmodulin. *Structure*. 2014;22, 1582-1594. doi:10.1016/j.str.2014.07.016
- Saimi Y, Kung C. Calmodulin as an ion channel subunit. *Annu Rev Physiol.* 2002;64:289-311.
- Saimi Y., Kung C. Ion channel regulation by calmodulin binding. FEBS Lett. 1994;350:155–158. doi: 10.1016/0014-5793(94)00782-9.

- Sansom et al., 2002 Potassium channels: structures, models, simulations.
- Sansom MS, Shrivastava IH, Bright JN, Tate J, Capener CE, Biggin PC. *Biochim Biophys Acta.* 2002 Oct 11;1565(2):294-307. Review. PMID: 12409202
- Santagata S, Boggon TJ, Baird CL, Gomez CA, Zhao J, Shan WS, Myszka DG, Shapiro L. G-protein signaling through tubby proteins. *Science.* 2001 Jun 15;292(5524):2041-50. Epub 2001 May 24.
- Saotome K, Murthy SE, Kefauver JM, Whitwam T, Patapoutian A, Ward AB. Structure of the mechanically activated ion channel Piezo1. *Nature*. 2018;554(7693):481-486. doi:10.1038/nature25453
- Scannevin RH, Wang K, Jow F, Megules J, Kopsco DC, Edris W, Carroll KC, Lü Q, Xu W, Xu Z, Katz AH, Olland S, Lin L, Taylor M, Stahl M, Malakian K, Somers W, Mosyak L, Bowlby MR, Chanda P, Rhodes KJ. Two N-terminal domains of Kv4 K(+) channels regulate binding to and modulation by KChIP1. *Neuron.* 2004 Feb 19;41(4):587-98.
- Schmitt N, Schwarz M, Peretz A, Abitbol A, Attali B, Pongs O. A recessive C-terminal Jervell and Lange-Nielsen mutation of the KCNQ1 channel impairs subunit assembly. *EMBO J.* 2000;19:332–340.
- Schroeder BC, Kubisch C, Stein V, Jentsch TJ. Moderate loss of function of cyclic-AMP-modulated KCNQ2/KCNQ3 K+ channels causes epilepsy. *Nature.* 1998;396:687–690.
- Schroeder BC, Hechenberger M, Weinriech F, Kubisch C, Jentsch TJ. KCNQ5, novel potassium channel broadly expressed in brain, mediates M-type currents. *J Biol Chem.* 2000;275:24089–24095.
- Schumacher MA, Rivard AF, Bächinger HP, Adelman JP. Structure of the gating domain of a Ca2+-activated K+ channel complexed with Ca2+/calmodulin. *Nature.* 2001; 26;410(6832):1120-4.
- Schwake M, Pusch M, Kharkovets T, Jentsch TJ. Surface expression and single channel properties of KCNQ2/KCNQ3, M-type K^+ channels invovled in epilepsy. J Biol Chem. 2000;275:13343–13348.
- Schwake M, Jentsch TJ, Friedrich T. A carboxy-terminal domain determines the subunit specificity of KCNQ K+ channel assembly. EMBO Rep. 2003;4:76–81.
- Schwarz E.C. et al. TRP Channels in Lymphocytes. In: Flockerzi V., Nilius B. (eds) Transient Receptor Potential (TRP) Channels. *Handbook of Experimental Pharmacology,* 2007; vo
- Schwindt PC, Spain WJ, Foehring RC, Stafstrom CE, Chubb MC, and Crill WE. Multiple potassium conductances and their functions in neurons from cat sensorimotor cortex in vitro. *Journal of Neurophysiology* 1988;59:2, 424-449

- Scott B, Hoppe A. Optimizing fluorescent protein trios for 3-Way FRET imaging of protein interactions in living cells. *Sci Rep* 2015;5, 10270. https://doi.org/10.1038/srep10270
- Selyanko AA, Brown DA. Intracellular calcium directly inhibits potassium M channels in excised membrane patches from rat sympathetic neurons. *Neuron.* 1996 Jan;16(1):151-62..
- Selyanko AA, Brown DA. Regulation of M-type potassium channels in mammalian sympathetic neurons: action of intracellular calcium on single channel currents. Neuropharmacology. 1996;35(7):933-47. PMID: 8938724
- Selyanko AA, Hadley JK, Brown DA. Properties of single M-type KCNQ2/KCNQ3 potassium channels expressed in mammalian cells. *J Physiol*. 2001;534(Pt 1):15-24. doi:10.1111/j.1469-7793.2001.00015.x
- Shahidullah M, Santarelli LC, Wen H, Levitan IB. Expression of a calmodulin-binding KCNQ2 potassium channel fragment modulates neuronal M-current and membrane excitability. *Proc Natl Acad Sci U S A*. 2005;102(45):16454-16459. doi:10.1073/pnas.0503966102
- Shamgar, L., Ma, L., Schmitt, N., Haitin, Y., Peretz, A., Wiener, R., Hirsch, J., Pongs, O. and Attali, B. Calmodulin is essential for cardiac IKS channel gating and assembly: impaired function in long-QT mutations. *Circ. Res.* 2006;98, 1055–1063. doi:10.1161/01.RES.0000218979.40770.69
- Shaner NC, Steinbach PA, Tsien RY. A guide to choosing fluorescent proteins. *Nat. Methods.* 2005;2:905–909.
- Shapiro MS, Roche JP, Kaftan EJ, Cruzblanca H, Mackie K, Hille B. Reconstitution of muscarinic modulation of the KCNQ2/KCNQ3 K(+) channels that underlie the neuronal M current. *J Neurosci.* 2000 Mar 1;20(5):1710-21. PMID: 10684873
- Sherman AS, Keizer JE, Rinzel. Domain model for Ca^{2+}-inactivation of Ca^{2+} channels at low channel density. *Biophysical journal.* 1990, Medicine, Chemistry DOI:10.1016/S0006-3495(90)82443-7Corpus ID: 35959398
- Shrestha, S., Park, J., Ahn, S.-J. and Kim, Y. PGE_2 MEDIATES OENOCYTOID CELL LYSIS VIA A SODIUM-POTASSIUM-CHLORIDE COTRANSPORTER. *Arch. Insect Biochem. Physiol*., 2015;89: 218-229. doi:10.1002/arch.21238
- Solaro CR, Prakriya M, Ding JP, and Lingle CJ. Inactivating and Noninactivating Ca*+- and Voltage-Dependent K+ Current in Rat Adrenal Chromaffin Cells. *The Journal of Neuroscience*, 1995, E(9): 61 lo-6123
- Soldovieri MV, Boutry-Kryza N, Milh M, Doummar D, et al. Novel KCNQ2 and KCNQ3 mutations in a large cohort of families with benign neonatal epilepsy: first evidence for an altered channel regulation by syntaxin-1A. *Hum. Mutat.* 2014;35, 356–367.

- Spain WJ, Schwindt PC and Crill WE. Two transient potassium currents in layer V pyramidal neurons from cat sensorimotor cortex. *Journal of Physiology.* 1991;434, pp. 591-607 591
- Spratt DE, Taiakina V, Palmer M, Guillemette JG. Differential binding of calmodulin domains to constitutive and inducible nitric oxide synthase enzymes. *Biochemistry* 2007;46 (28), 8288-8300
- Stansfeld CE, Marsh SJ, Halliwell JV, Brown DA. 4-Aminopyridine and dendrotoxin induce repetitive firing in rat visceral sensory neurones by blocking a slowly inactivating outward current. *Neuroscience Letters*, 1986;64:3 pp. 299-304, ISSN 0304-3940,
- https://doi.org/10.1016/0304-3940(86)90345-9.
- Steinlein OK, Conrad C, Weidner B. Benign familial neonatal convulsions: Always benign?. *Epilepsy Research*, 2007;73:3, pp. 245-249,ISSN 0920-1211,
- https://doi.org/10.1016/j.eplepsyres.2006.10.010.
- Storm J.F. Intracellular injection of a Ca^{2+} chelator inhibits spike repolarization in hippocampal neurons. *Brain Res.* 1987;435:387–392.
- Strong PN. Potassium channel toxins. *Pharmacology & Therapeutics,* 1990;46:1 pp. 137-162 ISSN 0163-7258, https://doi.org/10.1016/0163-7258(90)90040-9.
- Strong M, Chandy KG, Gutman GA. Molecular evolution of voltage-sensitive ion channel genes: on the origins of electrical excitability. *Mol Biol Evol*. 1993 Jan;10(1):221-42.
- Strulovich R, Tobelaim WS, Attali B, and Hirsch JA. Structural insights into the M channel proximal C-terminus/calmodulin complex. *Biochemistry* 2016;55, 5353–5365 10.1021/acs.biochem.6b00477
- Sturmey RG, O'Toole PJ, Leese HJ Fluorescence resonance energy transfer analysis of mitochondrial:lipid association in the porcine oocyte. *Reproduction.* 2006; 132(6):829–837
- Suh BC, Inoue T, Meyer T & Hille B. Rapid chemically induced changes of PtdIns(4,5)P_2 gate KCNQ ion channels. *Science* 2006;314, 1454– 1457.
- Sun J, MacKinnon R. Cryo-EM Structure of a KCNQ1/CaM Complex Reveals Insights into Congenital Long QT Syndrome. *Cell.* 2017; 169: 1042-1050
- Sun J, MacKinnon R. Structural Basis of Human KCNQ1 Modulation and Gating. *Cell.* 2019;180, 2, P340-347.E9.
- Tadross MR, Dick IE, Yue DT. Mechanism of Local and Global Ca^{2+} Sensing by Calmodulin in Complex with a Ca^{2+} Channel. *J.cell* 2008; 133:7 pp. 1228-1240.
- https://doi.org/10.1016/j.cell.2008.05.025

- Tempel BL, Papazian DM, Schwarz TL, Jan YN, Jan LY. Sequence of a probable potassium channel component encoded at Shaker locus of Drosophila. *Science.* 1987 Aug 14;237(4816):770-5.
- Thomas GM, Hayashi T, Chiu SL, Chen CM, Huganir RL. Palmitoylation by DHHC5/8 targets GRIP1 to dendritic endosomes to regulate AMPA-R trafficking. *Neuron.* 2012;73:482–496 10.1016/j.neuron.
- Thompson AN, Kim I, Panosian TD, Iverson TM, Allen TW, Nimigean CM. Mechanism of potassium-channel selectivity revealed by Na^+ and Li^+ binding sites within the KcsA pore. Nat Struct Mol Biol 2009;16: 1317–1324.
- Tobelaim WS, Beaurivage C, Champagne A, Pomerleau V, Simoneau A, Chababi W, Yeganeh M, Thibault P, Klinck R, Carrier JC, Ferbeyre G, Ilangumaran S, Saucier C. Tumour-promoting role of SOCS1 in colorectal cancer cells. *Sci Rep.* 2015 Sep 22;5:14301. doi: 10.1038/srep14301. PMID: 26391193
- Tobelaim WS, Dvir M, Lebel G, Cui M, Buki T, Peretz A, Marom M, Haitin Y, Logothetis DE, Hirsch JA, and Attali B. Competition of calcified calmodulin N lobe and PIP_2 to an LQT mutation site in Kv7.1 channel. *Proc. Natl. Acad. Sci. U.S.A.* 2017; 114, E869–E878 10.1073/pnas.1612622114
- Tomczak AP, Fernández-Trillo J, Bharill S, Papp F, Panyi G, Stühmer W, Isacoff EY, Pardo LA. A new mechanism of voltage-dependent gating exposed by $K_V10.1$ channels interrupted between voltage sensor and pore. *J Gen Physiol.* 2017 May 1;149(5):577-593. doi: 10.1085/jgp.201611742
- Tugarinov V, Hwang PM, Ollerenshaw JE, Kay LE. Cross-correlated relaxation enhanced 1H[bond]13C NMR spectroscopy of methyl groups in very high molecular weight proteins and protein complexes. *J Am Chem Soc*. 2003;125(34):10420-8. PMID:12926967
- Tugarinov V, Kay LE, Ibraghimov I, Orekhov VY. High-resolution four-dimensional 1H-13C NOE spectroscopy using methyl-TROSY, sparse data acquisition, and multidimensional decomposition. *J Am Chem Soc.* 2005;127(8):2767-75. PMID:15725035
- Upson, C, Jr T F, Kamins D, Laidlaw D, Schlegel D, Vroom J, Gurwitz R & van Dam A. The Application Visualisation System: A Computational Environment for Scientific Visualisation. *IEEE Computer Graphics and Applications,* 1989;9(4), 30-42.
- Urrutia J, Aguado A, Muguruza-Montero A, Núñez E, Malo C, Casis O, Villarroel A. The Crossroad of Ion Channels and Calmodulin in Disease. *International journal of molecular sciences*, 2019;*20*(2), 400. https://doi.org/10.3390/ijms20020400
- Vargas E, Bezanilla F, Roux B. In search of a consensus model of the resting state of a voltage-sensing domain. *Neuron.* 2011;72(5):713-720. doi:10.1016/j.neuron.2011.09.024

- Villarroel A, Taglialatela M, Bernardo-Seisdedos G, Alaimo A, Agirre J, Alberdi A, Gomis-Perez C, Soldovieri MV, Ambrosino P, Malo C, et al. The ever changing moods of calmodulin: How structural plasticity entails transductional adaptability. *J. Mol. Biol.* 2014;426:2717–2735. doi: 10.1016/j.jmb.2014.05.016.
- Villarroel A, Maurizio T, Bernardo-Seisdedos G, Alaimo A, Agirre J, Alberdi A, Gomis-Perez, C, Soldovieri M, Ambrosino P, Malo C, Areso P. The Ever Changing Moods of Calmodulin: How Structural Plasticity Entails Transductional Adaptability. *Journal of molecular biology.* 2014;426. 10.1016/j.jmb.2014.05.016.
- Wall ME, Clarage JB, Phillips GN. Motions of calmodulin characterized using both Bragg and diffuse X-ray scattering. *Structure.* 1997 Dec 15;5(12):1599-612.
- Wang HS, McKinnon D. Modulation of inwardly rectifying currents in rat sympathetic neurones by muscarinic receptors. *J Physiol.* 1996 Apr 15;492 (Pt 2):467-78. PMID: 9019543
- Wang HS, Pan Z, Shi W, Brown BS, Wymore RS, Cohen IS, Dixon JE, McKinnon D. KCNQ2 and KCNQ3 potassium channel subunits: molecular correlates of the M-channel. *Science.* 1998 Dec 4;282(5395):1890-3.
- Wang HS, Brown BS, McKinnon D, Cohen IS. Molecular basis for differential sensitivity of KCNQ and I(Ks) channels to the cognitive enhancer XE991. *Mol Pharmacol.* 2000 Jun;57(6):1218-23. PMID: 10825393
- Weber YG, Geiger J, Kämpchen K, Landwehrmeyer B, Sommer C, Lerche H. Immunohistochemical analysis of KCNQ2 potassium channels in adult and developing mouse brain. *Brain Res.* 2006 Mar 10;1077(1):1-6. Epub 2006 Feb 28. PMID: 16500630
- Wen H, Levitan IB. Calmodulin is an auxiliary subunit of KCNQ2/3 potassium channels. *J. Neurosci.* 2002;22:7991–8001. doi: 10.1523/JNEUROSCI.22-18-07991.2002
- Whicher JR, MacKinnon R. Regulation of Eag1 gating by its intracellular domains. *Elife*. 20198. PMID 31490124 DOI: 10.7554/eLife.49188
- Wiedenmann J, Oswald F, Nienhaus GU. Fluorescent proteins for live cell imaging: opportunities, limitations, and challenges. *IUBMB Life*;2009 61(11):1029–1042
- Wiener R, Haitin Y, Shamgar L, Fernández-Alonso MC, Martos A, Chomsky-Hecht O, Rivas G, Attali B, Hirsch JA. The KCNQ1 (Kv7.1) COOH terminus, a multitiered scaffold for subunit assembly and protein interaction. *J Biol Chem.* 2008 Feb 29;283(9):5815-30. doi: 10.1074/jbc.M707541200. Epub 2007 Dec 29.PMID: 18165683
- Wiesner S, Sprangers R. Methyl groups as NMR probes for biomolecular interactions. *Curr Opin Struct Biol.* 2015 Dec;35:60-7. doi: 10.1016/j.sbi.2015.08.010. Epub 2015 Nov 9.
- Winks JS, Hughes S, Filippov AK, et al. Relationship between membrane phosphatidylinositol-4,5-bisphosphate and receptor-mediated inhibition of native

neuronal M channels. *J Neurosci*. 2005;25(13):3400-3413. doi:10.1523/JNEUROSCI.3231-04.2005

- Wissmann R, Bildl W, Neumann H, Rivard AF, Klocker N, Weitz D, Schulte U, Adelman JP, Bentrop D, Fakler B. A helical region in the C terminus of small-conductance Ca^{2+}-activated K^+ channels controls assembly with apo-calmodulin. *J. Biol. Chem*.,2002;277, pp. 4558-4564

- Wulff H, Köhler R. Endothelial small-conductance and intermediate-conductance KCa channels: an update on their pharmacology and usefulness as cardiovascular targets. *J Cardiovasc Pharmacol*. 2013 Feb;61(2):102-12. doi: 10.1097/FJC.0b013e318279ba20. Review. PMID: 23107876

- Xia XM, Fakler B, Rivard A, Wayman G, Johanson-Pais T, Keen JE, Ishii T, Hirschber B, Bond CT, Lutsenko S, et al. Mechanism of calcium gating in small-conductance calcium-activated potassium channels. *Nature.* 1998;395:503–507. doi: 10.1038/26758.

- Xu J, Koni PA, Wang P, Li G, Kaczmarek LK, Wu Y, et al. The voltage-gated potassium channel Kv1.3 regulates energy homeostasis and body weight. *Hum. Mol. Genet.* 2003;12 551–559. 10.1093/hmg/ddg049

- Yang T, Yao WX, Jiang MX. Ionic channel pathies. *Sheng Li Ke Xue Jin Zhan*. 1998 Jul;29(3):239-42. Review. PMID: 12501643

- Yu H, Wu M, Hopkins C, Engers J, Townsend S, Lindsley C, McManus OB & Li M.A small molecule activator of KCNQ2 and KCNQ4 channels 2010–2011, Mar 29

- Yus-Nájera E, Santana-Castro I, Villarroel A. The identification and characterization of a noncontinuous calmodulin-binding site in noninactivating voltage-dependent KCNQ potassium channels. *J. Biol. Chem.* 2002;277:28545–28553. doi: 10.1074/jbc.M204130200.

- Zacharias DA, Violin JD, Newton AC, Tsien RY. Partitioning of lipid-modified monomeric GFPs into membrane micro-domains of live cells. *Science.* 2002;296:913–916.

- Zaika O, Lara LS, Gamper N, Hilgemann DW, Jaffe DB, Shapiro MS. Angiotensin II regulates neuronal excitability via phosphatidylinositol 4,5-bisphosphate-dependent modulation of Kv7 (M-type) K+ channels. *J Physiol*. 2006;575(Pt 1):49-67. doi:10.1113/jphysiol.2006.114074

- Zaydman MA, Cui J. PIP2 regulation of KCNQ channels: biophysical and molecular mechanisms for lipid modulation of voltage-dependent gating. *Front Physiol*. 2014;5:195. Published 2014 May 27. doi:10.3389/fphys.2014.00195

- Zaydman MA, Silva JR, Delaloye K, Li Y, Liang H, Larsson HP, Shi J, Cui J. Kv7.1 ion channels require a lipid to couple voltage sensing to pore opening. *Proc Natl Acad Sci USA.* 2013;110:13180–13185.

- Zerangue N, Jan YN, Jan LY. An artificial tetramerization domain restores efficient assembly of functional Shaker channels lacking T1. *Proc Natl Acad Sci U S A*. 2000;97(7):3591-3595. doi:10.1073/pnas.060016797
- Zhang H, Zeng X, Li Q *et al.* Fluorescent tumour imaging of type I IGF receptor *in vivo*: comparison of antibody-conjugated quantum dots and small-molecule fluorophore. *Br J Cancer* 101, 71–79 (2009). https://doi.org/10.1038/sj.bjc.6605103
- Zhang J, Campbell JRE, Ting AY, Tsien RY. Creating new fluorescent probes for cell biology. *Nat. Rev. Mol. Cell Biol.* 2002;3:906–918.
- Zhou Y, Dong Q, Louahed J, Dragwa C, Savio D, Huang M, Weiss C, Tomer Y, McLane MP, Nicolaides NC, et al. Characterization of a calcium-activated chloride channel as a shared target of Th2 cytokine pathways and its potential involvement in asthma. *Am J Respir Cell Mol Biol,* 2001;25:486–491
- Zühlke RD, Pitt GS, Deisseroth K, Tsien RW, Reuter H. Calmodulin supports both inactivation and facilitation of L-type calcium channels. *Nature.* 1999;399:159–162. doi: 10.1038/20200.
- Zuttion F, Redondo-Morata L, Marchesi A, Casuso I. High-Resolution and High-Speed Atomic Force Microscope Imaging. *Methods Mol Biol*. 2018;1814:181-200. doi: 10.1007/978-1-4939-8591-3_11.

Abbreviations

- ºC: Celsius degrees (Temperature unit)
- Å: Ångström (Length unit, equivalent to 0.1 nm)
- AA Amino acid
- AKAP A-kinase anchor proteins
- Amp Ampicillin
- ANOVA: Analysis of Variances
- AP Action Potential
- APS: Ammonium PerSulphate
- ApoCaM Apo-calmodulin
- ATP Adenosine 5'-triphosphate
- BFNC Benign familial neonatal convulsions
- BSA: Bovine Serum Albumin
- CaMBD Calmodulin binding domain
- CaM Calmodulin
- cAMP cyclic adenosine 5’-monophosphate
- cDNA Complementary DNA
- cm / mm / µm / nm: centimetre / millimetre / micrometre / nanometre (Length units)
- Ct: Carboxy-terminus (Cter or C-terminus)
- CVs Colum volumes
- CFP: Cyan Fluorescent Protein
- DAG Diacylglicerol
- D-CaM Dansyl-calmodulin
- DMSO Dimethyl sulfoxide
- DNA Deoxyribonucleic acid
- DTT Dithiothreitol
- EC50: Half maximal effective concentration.
- EDTA: Ethylenediaminetetraacetic acid
- EGTA: Ethylene glycol tetraacetic acid
- FBS: Foetal Bovine Serum
- Fiji: Fiji Is Just Imagej
- g: Gravitational constant (6.674 · 10-11 N · kg-2· m-2). Used for centrifugation
- G: Conductance
- GΩ / MΩ: GigaOhm / MegaOhm (Resistance unit)
- GFP: Green Fluorescent Protein
- GST Glutathione S-transferase
- h Hour
- HEK 293 cells: Human Embryonic Kidney 293 cells
- HFIP: Hexafluoroisopropanol
- HoloCaM holo-calmodulin
- HS-AFM High Speed Atomic Force Microscopy
- HSQC Heteronuclear Single-Quantum Correlation
- Ic50 Half maximal inhibitory concentration
- IP3 Inositol tri-phosphate

- IPTG Isopropyl-beta-thio galactopyranoside
- IQ Calmodulin binding domain motive
- Kan Kanamycin
- Kv Voltage-dependent potassium channel
- Kb: Kilobases (equivalent to 1000 base pairs)
- KDa: KiloDaltons (Molecular weigth unit)
- KHz: KiloHertz (1000/sec) (Frequency unit)
- Kv: Voltage-gated potassium channels (VGKC)
- KCa: Calcium-dependent potassium channels
- LB Luria Bertani BrothI: Intensity (Current)
- LPS: LipoPolySaccharide
- LQTS: Long QT Syndrome
- MBP Maltose-Binding Protein
- mut: mutated
- mM / nM: millimolar / nanomolar (Molarity unit)
- mL / µL: millilitre / microlitre (Volume unit)
- mVenus monomeric circularly permutated venus
- min Minutes
- mRNA Messenger RNA
- µg / ng: microgram / nanogram (Mass unit)
- NMR Nuclear Magnetic Resonance
- NOE Nuclear Overhauser Effect
- N-terminus: Amino-terminal
- Osm: Osmol (Osmolality unit, equivalent to 1 mol of osmotic-active solute)
- pA: picoampere (Intensity unit)
- pA/pF: picoampere/picofarad (Current density unit)
- O/N over nightPBS: Phosphate Buffer Solution
- PD: Pull-down
- PCR Polymerase chain reaction
- PDB: Protein DataBase (https://www.rcsb.org/)
- PIC Protease Inhibitor Cocktail
- PIP2 Phosphatidylinositol 4,5-bisphosphate
- PMSF phenylmethanesulfonylfluoride
- RMSD Root Mean Square Deviation
- RPMI: Roswell Park Memorial Institute
- S1-S6: Transmembrane domains in Kv channels
- SDS: Sodium Dodecyl Sulphate
- SDS-PAGE: Sodium Dodecyl Sulphate PolyAcrylamide Gel Electrophoresis
- sec / ms: second / millisecond (Time unit)
- SM: Starting Material
- SN: Supernatant
- SNP: Single Nucleotide Polymorphism
- T cells: T lymphocytes
- TD: Tetramerization domain in Kv7
- TBS: Tris Buffer Solution

- TEA: TetraEthylAmmonium
- TEMED: Tetramethylethylenediamine
- YFP: Yellow Fluorescent Protein
- V / mV: Volt / millivolt (Voltage unit)
- Q2ABc Kv7.2_ABc
- RNA Ribonucleic acid
- RPM Revolutions per minute
- RT Room temperature
- s seconds

FIGURE LIST

Table list

eman ta zabal zazu

Universidad del País Vasco

Euskal Herriko Unibertsitatea

KALTZIOAREN EFEKTUA KV7.2 KANALAREN DINAMIKA ETA EGONKORTASUNEAN

DOKTORETZA-TESIA LEIOA, 2020

EIDER NUÑEZ VIADERO

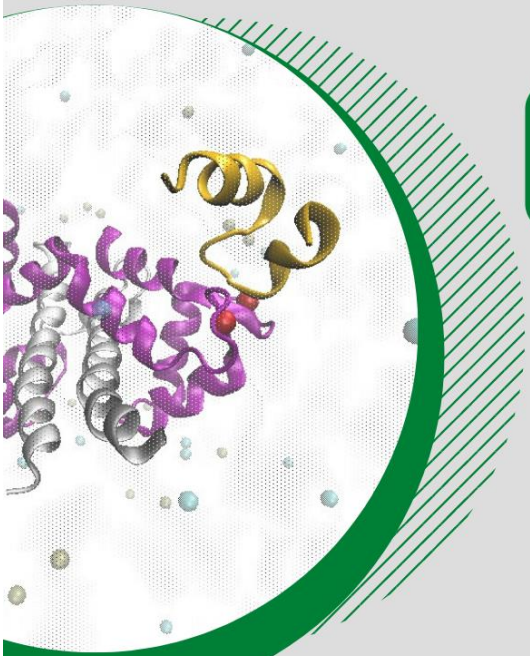

Dr. Alvaro Villarroel
Dr. Oscar Millet

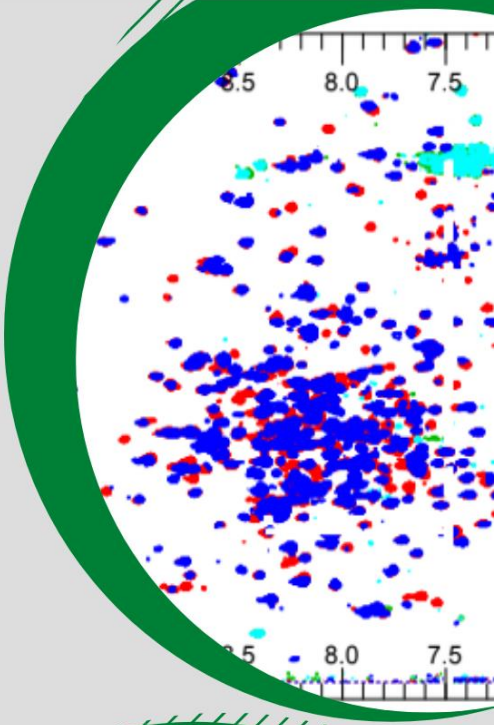

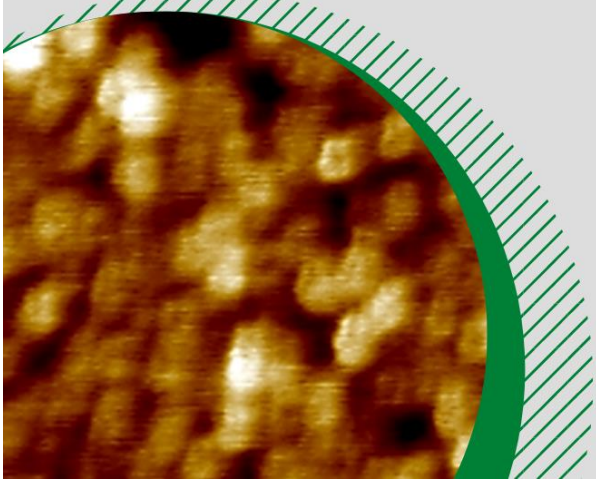

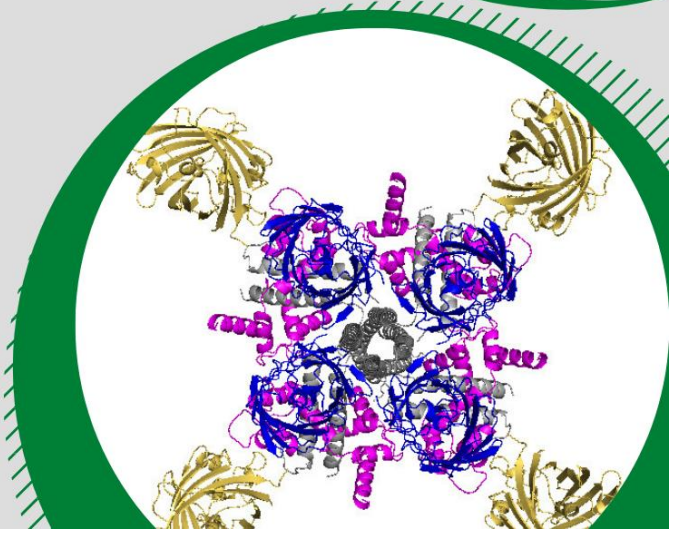

AURKIBIDEA

1. SARRERA

1.1. Kanal ionikoak

Zelula bakoitza mintz plasmatiko batez inguratuta dago, bigeruza fosfolipidiko batez osatuta dagoena. Mintz honek, zelularen osagai esentzialak bateratu eta ingurune extrazelularretik banatuta mantetzen ditu. Lipidoen enpaketatze hertsiari esker, bigeruza lipidikoa hidrofoboa da, horrela, kargatutako molekula txikien eta ioien (hala nola, Na^+, K^+, Ca^{2+} edo Cl) difusioa eragozten du.

Kanal ionikoek, mintz-zeharreko proteina mota bat dira eta ioien fluxua ahalbidetzen duten poroak sortzen dituzte mintz zelularretan, bai plasmatikoan, baita organuluen mintzetan ere (nukleoan, mitokondrioan, erretikulu endoplasmatikoan, Golgi aparatuan, etab.).

Egunerarte, 200 kanal ioniko ezberdin baino gehiago deskribatu dira (Purves et al., 2001). Dibertsitate hau mekanismo ezberdinen bidez lortu da: poroa osatzen duten α azpinunitatea kodetzen duten hainbat generen presentziagatik, transkribatutako RNA mezulariaren lotura alternatiboagatik (*alternative splicing*), α azpiunitate ezberdinez osatutako hetero-tetrameroak sortuz eta beste azpiunitate osagarrien bidezko propietateen modulazioari esker.

Aldaketa estruktural txikien bidez, kanal hauek, itxi egotetik ireki egotera pasatzen dira, 10 milioi ioi/segundu-ko fluxua ahalbidetuz, zelula barnera zein kanpora, kanalaren arabera. Orokorrean, kanal ionikoak, hauek zeharkatzen duten ioi espezifikoaren arabera sailkatzen dira, hala ere, batzuk ez dira oso selektiboak.

Bestalde, potasio kanalen barruan, bigarren sailkapen bat egiten da: boltai menpekoak, kaltzio-menpekoak, sodio-menpekoak, bi-porodunak eta K^+ barne aztergailua (Kir, K^+ *inward rectifier*).

Susperraldian dagoen ebidentziak iradokitzen duenez, gaixotasun asko kanal ionikoekin erlazionatuta daude (Levitan et al., 2015).

Kanal ionikoek ioien difusio pasiboa ahalbidetzen dute, gradiente elektrokimikoaren alde. ATP-menpeko ioi garraiatzaileek gradiente elektrokimikoa ezartzen eta mantentzen dute, ioiak modu aktiboan ponpatuz. Kanal ioniko bat irekitzean, ioiak berehala pasatzen dira mintzaren alde batetik bestera, korronte-fluxu bat sortuz eta mintzaren potentziala aldatuz. Kanal ionikoak, zelulen mintzean kokatzen dira, non zenbait oinarrizko funtzio betetzen duten, hala nola,

atsedeneko mintz potentziala kontrolatu, zelula kitzikatzaileetan seinale elektrikoak sortu, eta Ca^{2+} ioi mezulariaren fluxua ireki (Hille, 2001).

Kanal ioniko askok (esaterako K, Na, Ca, HCN eta TRP kanalak) antzekotasun estruktural asko partekatzen dituzte. Kanal hauek, arbaso amankomuna izan zutela uste da, eta elkarrekin sailkatzen dira, boltai menpeko kanal ionikoen familian (*voltage-gated-like, VGL*) (Yu *et al*., 2005). Alabaina, beste kanal ioniko batzuk, esaterako Cl kanalak, akuaporinak eta konexinak, estrukturalki oso ezberdinak dira, beste bide ebolutibo bat jarraitu dutela adieraziz.

1.2 Mintz potentziala

Mintz potentziala zelula baten mintzaren kanpo eta barnealdearen arteko boltai aldaketa da. Zelula guztietan ematen da, bereziki kitzikagarrietan. Atseden egoeran, gizaki zelula gehienetan, mintz-potenziala -70 eta -90 mV tartean egoten da, non zelularen barnealdea, kanpoaldea baino negatiboa den. Neuronetan, honen balioa -70 mV da. Mintz potentziala mintz plasmatikoa zeharkatzen duten proteinei esker ematen da. Hau da, proteina hauetatik igaroz, mintza zeharkatu dezaketen ioien kontzentrazio ezberdintasunek sortzen dute, eta ezinbestekoa da zelulen aktibitate egokirako. Mintz potentzialaren funtzio nagusia ekintza potentziala burutzea da, honen bidez, besteak beste, nerbio garraioa edo muskuluaren uzkurketa gertatzen baita.

Mintzean kokatuta dauden ioi-ponpa, transportatzaile eta ioi-trukatzaileen arabera (nabarmenki Na^+/K^+ ponpa), zelula bakoitzak atsedeneko potentzial espezifiko bat dauka. Hauen artean, Na^+/K^+ ponpak dira garrantzitsuenak, ATP energia erabiliz, Na^+ kanporatu eta K^+ barneratzen dutenak, hauen gradienteen kontra. Mintzaren alde bakoitzeko kontzentrazio diferentziek sortzen dute gradientea.

Zitoplasman batez ere, K+ ioiak eta negatiboki kargatutako proteinen kontzentrazio altua dago, mintz plasmatikoa zeharkatu ezin dutenak. Zelularen kanpoaldean, ostera, Na^+, Cl^- eta Ca^{2+} ioiak daude.

Mintz potentziala, oreka elektrokimikoa lortzen duenean ioi zehatz batentzako, ioi honen mugimendu-netoa eten egiten da. Egoera honetan, **Nernst ekuazioa** aplikatu daiteke, ioi baten atseden potentziala kalkulatzeko. Ekuazioa honek boltaia eta ioiaren kontzentrazio gradientea mintzean zehar kontuan dauka. Gogoan badaukagu mintz potentzialak ioi bat baino gehiagoren influentzia jasotzen duela, aproposagoa liteke **Goldman-Hogkin-Katz** ekuazioa erabiltzea, egoera

multi-ionikoa aurreikusten duelako. Izan ere, ekuazio hau erabiltzen da zelula mota baten atseden-potentzial teorikoa kalkulatzeko.

Zelula kitzikagarrien mintz-potentziala ez da konstante mantentzen. Zelula hauek, mintz plasmatikoan, boltai-menpeko kanal ionikoak dituzte, ekintza-potentziala (AP, ingelesez *action potential*) hasteaz arduratzen direnak (1.1 irudia).

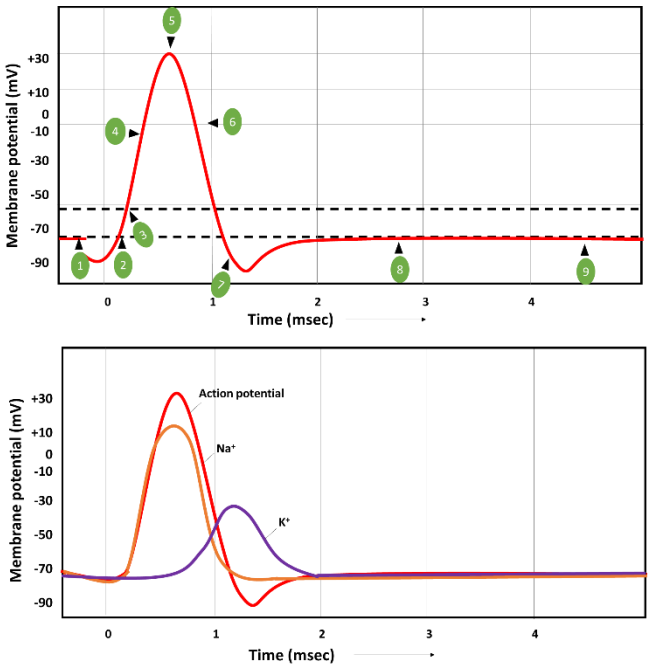

1.1 irudia. Ekintza-potentzialaren irudikapena, fase ezberdinekin. **(1)** Atsedeneko mintz potentziala (inolako estimulurik gabe). **(2)** Zelulak estimulu despolarizatzailea jasotzen du. **(3)** Sartzen den estimuluak atalasea gainditzen badu, boltai-menpeko Na^+ kanalak irekitzen dira. **(4)** Na^+-ren barne-fluxuak zelularen despolarizazioa eragiten du. **(5)** Na^+ azkar sartzeak mintz plasmatikoaren polaritatea itzultzea eragiten du. Beraz, Na^+-ren kanalak azkar aktibatzen dira, eta K^+ kanalak motelagoko. **(6)** Na^+ ioiak jada ezin dira neuronara sartu eta sodio eta potasio ponpa aktiboek zelulatik kanpora garraiatzen dituzte. **(7)** K^+ kanalak aktibatuta daude. K^+ ioien kanpo-fluxu bat dago. Kasu honetan, mintz plasmatikoak hiperpolarizazioa jasaten du, eta horrek estimulu despolarizatzaile berria balaztatzen du. **(8)** K_V kanalak itxi egiten dira. **(9)** Denbora baten ondoren, gradiente elektrokimikoa atseden-egoerara itzultzen da. Human Physiologytik egokitua (hirugarren edizioa).

1.2.1. Ekintza potentziala

Mintzaren Na^+ eta K^+-arekiko iragazkortasun aldaketek ekintza potentzialak sortzen dituzte. Ekintza potentzialak, **dena ala ezer ez** motatako erantzuna izaten du, atalase bat dauka hasteko, normalean -50 mV-tan kokazten dena. Seinale bat heltzean, zelula depolarizatu daiteke, eta

depolarizazio honek atalasea gaindituz gero, ekintza potentziala hasten da, boltai menpeko Na^+ kanalen irekitzea eraginez.

Ekarpenik ez badago, neuronek potentzial egonkorra dute mintz osoan zehar, orokorrean -70 mV-tan kokatzen dena. Baina, ekarpen kitzikagarri edo inhibitzaile bat dagoenean, normalean dendritetan ematen dena, aldaketak sortarazten dira potentzialetan eta hauei **potentzial lokal** deritze. Kitzikagarri edo inhibitzaile esaten zaie, aldaketak sortzen dituztelako mintz potenzialean, potentzial atalaseari hurbilduz edo aldenduz. Potentzial lokalak denboran eta espazioan zehar ahulduz joaten dira, hortaz, sarrera kitzikagarri batek sortzen duen polarizazioa indargabetzen doa mintzean hedatu ahala. Berdina gertatzen da sarrera inhibitzaile batek sortzen duen hiperpolarizazioarekin. Hala ere, distantzia luzeetan garraiatu daiteke, metro batera edo gehiagora helduz.

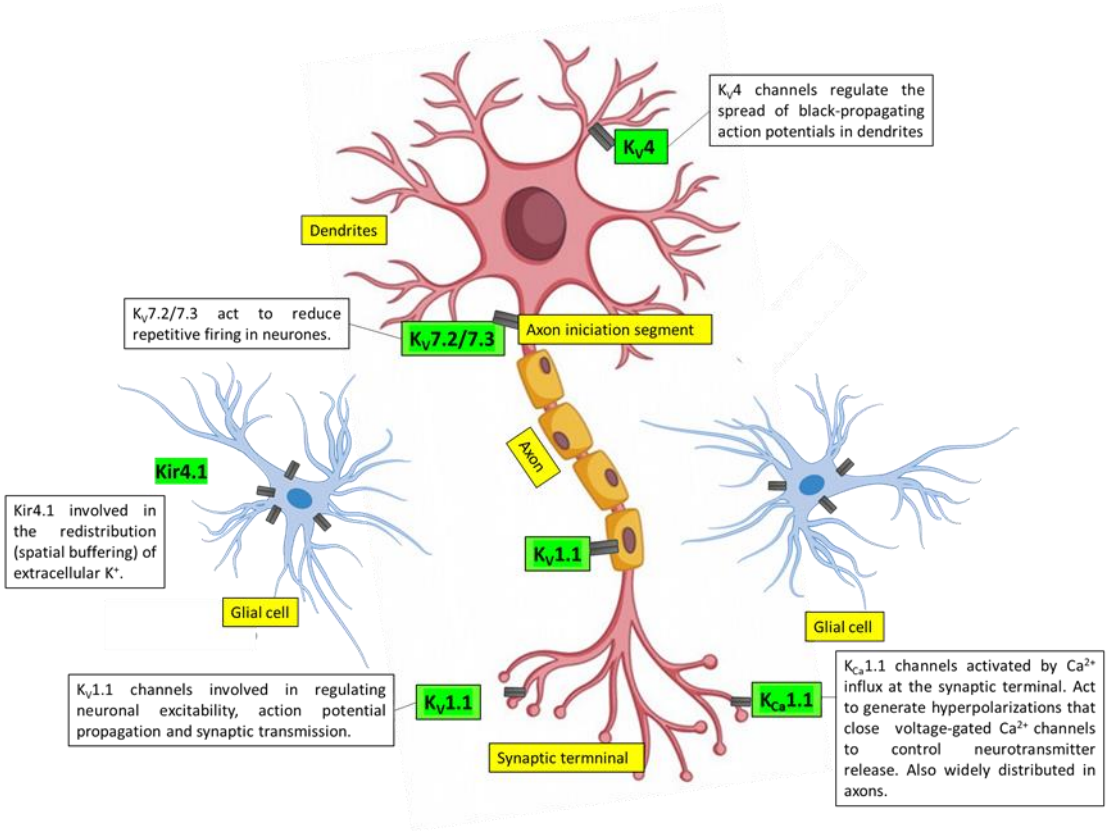

1.2 irudia. K^+ kanalen azpimoten kokapen diferentziala neuronetan. $K_V1.1$ kanalak axoian eta mutur presinaptikoan adierazten dira, non kitzikagarritasun neuronala, akzio-potentzialaren hedapena eta transmisio sinaptikoa erregulatzen diren. $K_V4.3$ kanalek dendritetan adierazten dira, eta zuhaitz dendritikoan alderantzizko hedapen-ekintzaren potentzialen hedapenaren erregulazioan parte hartzen dute. M-korrontea osatzen duten $K_V7.2/7.3$ kanalak axoiaren hastapen-segmentuan adierazten dira, eta boltai bidez aktibatutako K^+ kanal gehienak itxita daude ekintza potentzialaren atalasearen azpitik. Neuronen kitzikagarritasuna eta tiro errepikakorrak moteltzeko balio dute. KCa1.1 kanalak mutur presinaptikoan adierazten dira, eta boltai menpeko Ca^{2+} kanalekin kokatzen dira. Ca^{2+} sartzean aktibatzen dira, ekintza-potentzialak eragindako despolarizazioari erantzunez gertatzen dena, eta ekintza-potentzialaren amaitzeko Ca^{2+} kanalak ixten dituzten eta kitzikagarritasun neuronala murrizten duten post-hiperpolarizazioak sortzeko jarduten dute. Kir4.1 duten kanalak zelula glialetan adierazten dira, non K^+-ren birbanaketan parte har dezaketen. Humphries & Dart, 2015-tik egokitua.

Neuronek, K^+ kanal mota askoren presentziari esker, hainbat patroi ezberdin sortzeko gai dira, frekuentzia tarte zabal batetan hedatzen direnak.

Nola lan egiten dute kanal motek elkarrekin, neurona baten ekintza-potentzialaren propietateak zehazteko?

Gai hau, lehendabiziz, modulazio konputazionalaren bidez landu zen, **Hodgkin-Huxley ekuazioa** erabiliz. Gainera, ioiaren araberako konduktantzia ezberdinak gehitu zizkioten, modu

experimentalean lortutako ekuazioekin, boltaian eta denboran oinarrituta zeudenak (Connor eta Stevens, 1971; Huguenard eta McCormick, 1992; Johnston eta Wu, 1995; Locke eta Nerbonne, 1997).

1.2 irudian ikus daitekeenez, boltai menpeko potasio kanalek funtsezko eginkizun bat betetzen dute neuronen ekintza potentzialean, birpolarizazioan eta ekintza errepikakorretan (Connor and Stevens, 1971; Hille, 1992;Hodgkin and Huxley, 1952; Kolb, 1990; Rudy, 1988; Schwindt et al., 1988). Atzeratutako arteztailu K^+-korrontea (I_K) Hodgkinek eta Huxleyk deskribatu zuten lehen aldiz, 1952an, eta ekintza potentzialaren birpolarizazioaren arduraduna zelaz jabetu ziren, txibiaren axoi erraldoiak ikertzen zebiltzatela. Hala ere, korronte honen aktibazio eta inaktibazio geldoaren propietateak direla eta, korronte honen funtzioa ekintza potentzial arinagoak dituzten ugaztunetan zein ote zen galdetu ziren. K^+ korronte iragankor batek (I_A) neuronen birpolarizazioan eta ekintza errepikakorretan laguntzen zuela proposatu zuten, I_A korrontea hain zuzen ere (Connor eta Stevens 1971; Hagiwara et al. 1961; Neher 1971; Schwindt et al. 1988; Storm 1987). I_A korrontearen kanal arduradunak (K_A kanalak) aktibatu egiten dira atalasea gainditu aurretik eta oso arin inaktibatzen dira.

Urte batzuk geroago, neuronetan, boltai menpeko aktibazio eta inaktibazio tarte zabalak dituzten K^+ korronte iragankor anitz daudela proposatu egin zen (Albert and Nerbonne 1995; Gestrelius and Grampp 1983; Kasai et al. 1986; Quandt 1988; Penner et al. 1986; Rudy 1988; Solaro et al. 1995; Spain et al. 1991; Stansfeld et al. 1986).

1.3. Boltai-menpeko kanal ionikoak

Gizakietan, 200 gene baino gehiago daude kanal ionikoak kodifikatzen dituztenak, eta hauen erdia baino gehiago, boltaiaren bidez erregulatzen dira, aktibatuz zein inaktibatuz. Batzuk, arbaso beretik eboluzionatu zuten, eta sekuentziaren eraldaketek, funtzio eraginkor zehatz batetan espezializatzea ahalbidetu dute. Izan ere, boltai menpeko potasio (K_V), kaltzio (Ca_V) eta sodio (Na_V) kanalak superfamilia berdinaren kide dira (Gutman et al., 2005). Proposatu egin da, boltai-menpeko kanalen arbaso amankomuna mintza zeharkatzen duten 2 helizez (2 TM) osatutako K_V bat izan zela, estruktura sinpleena duelako. Honetatik kanal ioniko talde gehienek dibergitu omen zuten (1.3 irudia).

Boltai-menpeko kanal ioniko klasikoak multimeroetan egituratzen dira, 4 (edo gehiago) α-azpiunitateen mihiztaduraz osatuta, azpiunitate hauek elkarren artean berdinak edo ezberdinak izan daitezkeelarik. Ioi zehatz batentzat poro selektibo bat sortzeko antolatzen dira. Monomero bakoitzak, gutxienez, 2 TM ditu, poroa osatzen duen domeinua sortzen dutenak. Gainerako

mintz-zeharreko domeinuak eta N- eta C-muturrak domeinu erregulatzaileak dira, eta kanal motaren araberako ezberdintasunak izan ditzakete.

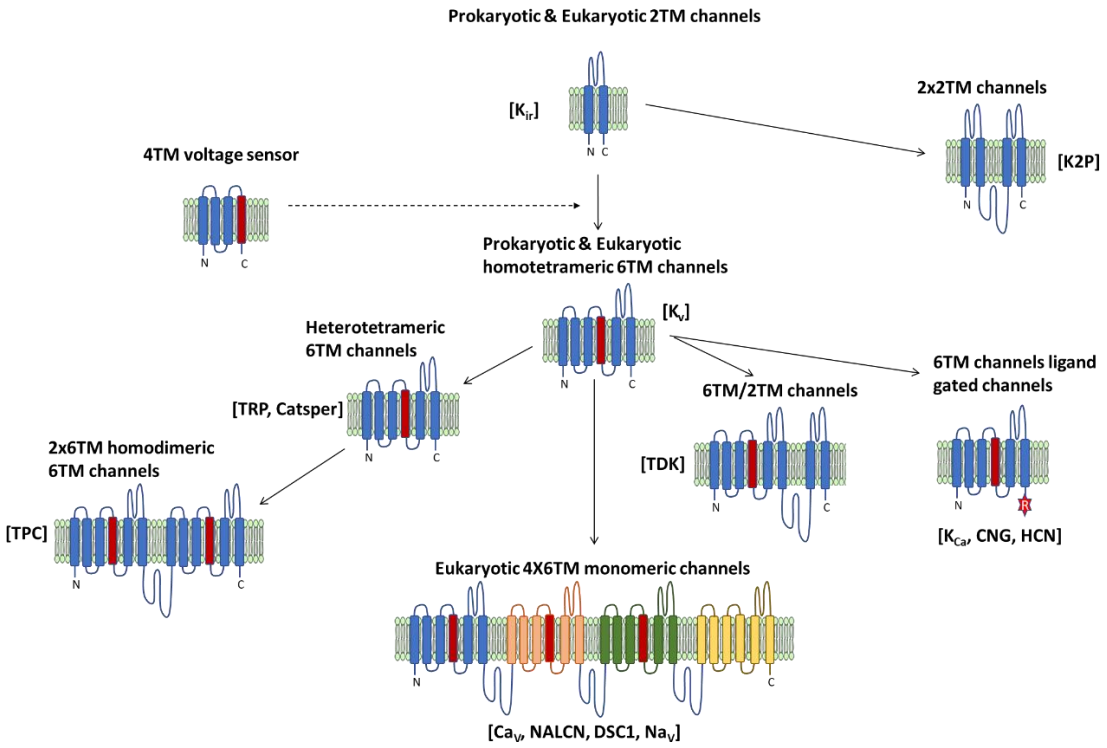

1.3 irudia. Boltai bidez aktibatutako kanal ionikoen familiako kideen artean proposatutako harreman ebolutiboen eskema. K^+-barne artezgailuak (Kir) egitura-motibo sinpleena du zelula eukariotoetako kanal ionikoen superfamilian; 2 TM egitura, berriz, antzinako kanal prokarioto eta eukarioto askotan dagoen poro domeinuaren oso adierazgarria da. Kanal eukarioto gehienetan, 2 TM motiboa, 4 TM segmentu bat gehituz handitu dira, boltaia detektatzeko domeinu bat hartzen dutenak (Hv1 protoien kanalaren antzekoa). Beraz, K_V kanalak (eta Na_V prokariotikoak) 6 TM azpiunitateen multzo homo-tetramerikoak dira. Gaur egun, domeinu bakarreko K_V 6 TM kanalek, gene bikoizketaren ondoren, Na_V eta Ca_V-kanalak sortu zituela uste da, kanalen aktibazio, inaktibazio eta berreskurapenaren zinetika eta modulazio handiagoa emanez. Bi kanal homodiko 6 TM errepikatuak daude, bitartekari ebolutibo bat izan daitezkeenak bi poroko kanalen familian (TPC), Ca^{2+}-ra iragazkorrak direnak (Amey et al., 2015).

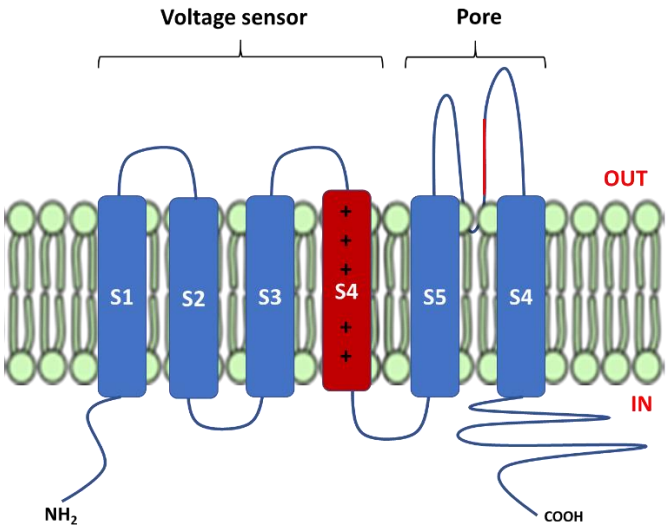

1.4 irudia. Boltai-menpeko kanal ioniko baten arkitektura orokorra. Azpikunitate bakoitza sei mintz-zeharreko segmentuz (S1-S6) osatuta dago, N- eta C-muturrekin. S1-S4 kanaleko boltai sentsorearen zatia da eta S5-S6 segmentuek poro selektiboa osatzen dute. S5 eta S6-ren arteko aminoazidoak (marra gorria) selektibitatearen arduradunak dira.

Boltai-menpeko kanal klasikoek arkitektura berdina aurkezten dute. Azpiunitate bakoitzak sei segmentu hidrofobiko ditu, mintz plasmatikoan txertatuta (6 TM) (1.4 irudia). S5 eta S6 segmentuek poroa osatzen dute eta S1-S4 boltaia sentitzen dute, bereziki, 4. segmentuak, positiboki kargaturiko zenbait aminoazidoz osatuta dagoena (Long et al., 2005). Karboxil eta amino motibo intrazelularrak dituzte, kanalaren erregulaziorako funtzio garrantzitsuak izaten direnak, estekatzaileen interakzio tokiak baitira. Izan ere, mota hauetako kanalak beste azpiunitate laguntzaile batekin expresatzen ei dira, kanalaren propietate funtzioanalak modulatu edo areagotzen dituztenak.

1.3.1. Boltai-Menpeko Potasio Kanalak (*Voltage gated K^+ channels*, VGKC)

80ko hamarkadan lehengo Shaker potasio kanala deskribatu zenetik, *Drosophila melanogaster*-ean, K^+ kanalak kodifikatzen duten 90 gene baino gehiago aurkitu dira, Na^+ edo Ca^{2+} kanalentzako aurkitutakoak baino hamar aldiz gehiago. Gainera, hauen % 50-a boltai-menpekoak dira (Bradding & Wulff, 2013).

IUPHAR-en (International Union of Basic and Clinical Pharmacology, www.iuphar.org) arabera, boltai menpeko K^+ kanalak 12 familiatan sailkatzen dira (K_V1-12) (1.5 Irudia), bi multzo nagusitan bereiztuta: lehenengoan K_V1-K_V9 familiak barneratzen dira eta bigarren multzoa K_V10-K_V12 familiek osatzen dute.

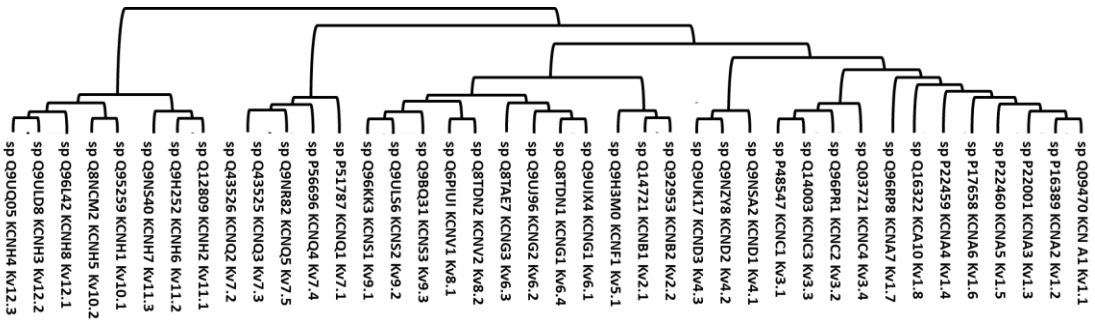

1.5 irudia. Gizakiaren K_V kanalen zuhaitz filogenetikoa. Kanal bakoitzaren aminoazidoen sekuentzia lortzeko, izenaren ondoan agertzen den sarbide-zenbakia erabili zen, www.uniprot.org datu-basean.

K^+ kanalen irekidurak, mintz potentziala orekatik gertu mantentzen laguntzen du, ekintza potentziala sortzeko atalasetik aldenduz. Horrela, zelula kitzikagarrietan, K^+ kanalek atseden potentziala finkatzen dute, ekintza potentziala laburtu, aktibitate altuko denboraldiak amaitu, ekintza errepikakorren arteko tarteak erregulatu eta sarrera kitzikakorren efizientzia murrizten dute (Hille, 2001).

Geroago eztabaidatuko dugunez, K_V kanalak, 4 alfa azpiunitate ezberdinez osatutako tetrameroak dira, eraztun moduan mihiztatuta daudenak (MacKinnon, 1991). Na^+ eta Ca^{2+} kanalak, ordea, proteina bakar batez osatuta daude, patroi berdinaren 4 errepikapenez sortuta daudenak (Catteral, 2000). Na_V, Ca_V eta K_V kanalak sei mintz-zeharreko domeinutako topologia aurkezten dute. Hortaz, K_V kanalen lau kopia tetramerizatzean, Na^+ eta Ca^{2+} kanaleen estruktura analogoa lortzen da.

1.3.1.1. Alfa azpiunitateen sailkapena

K_V kanalen alfa azpiunitateak printzipio ezberdinetan oinarrituta sailkatu badaitezke ere, normalean, funtzioaren arabera taldekatzen dira (Hille, 2001; Gutman et al., 2005).

- **Atzeratutako artezgailu-K^+ korrontea (K^+ delayed rectifier, I_K):** K^+ fluxu etengabea ahaldidetzen duten kanalak dira, mintzaren depolarizazioaren ostean aktibatzen direnak. K^+ ioien kanporatzeak, mintza azkar birpolarizatu egiten du. Na^+ ioien barneratzeak mintz potentziala handitzen du, eta kanal hauek irekitzea eragiten du, mintza birpolarizatzen dutenak. Birpolarizazio honek, nerbio-bulkadaren luzapena galgatu egiten du, baita neuronaren ekintza potentzial errepikakorrak erregulatu ere. Gainera, astiro inaktibatzen dira, edo ez dira guztiz inaktibatzen. Talde honen barruan

daude K_V1 (KCNA, *Shakers*), K_V2 (KCNB, *Shabs*), K_V3 (KCNC, *Shaws*), K_V7 (KCNQ) eta $K_V10.1$ (KCNH1, eag1) familiak.

- **A-motatakoak (IA):** kanal hauek ere kanporanzko K^+ korronteak sortzen dituzte mintzaren depolarizazioaren ondoren. IDR kanalak ez bezala, depolarizazioaren osteko hiperpolarizazioaren ondoren irekitzen dira. Hiperpolarizazio honek ekintza potentzialen arteko tarteak handitzen ditu. Talde honek K_V1 ($K_V1.4$), K_V3 ($K_V3.3$ and $K_V3.4$) K_V4 (KCND, *Shals*) familiaren kide guztiak barneratzen ditu.
- **Eraldatzaileak/Isiltzaileak:** proteina hauek, beste kategorietako kanalen antzeko sekuentzia eta estruktura badute ere, ez dira kapazak, bere kabuz, ioi korronterik sortzeko. K_V2-ko kanalekin heterotetramerizatzen dute, euren aktibitatea eraldatuz edo inhibituz. Kategoria honen barruan K_V5 (KCNF), K_V66 (KCNG), K_V8 (KCNV) eta K_V9 (KCNS) aurkitzen dira.
- **Bestelakoak:** Beste kanal ioniko batzuk ez dira sartzen aurretik aipatutako kategorietan, ez baitira nahiko ikertu kategoria baten barruan sailkatu ahal izateko. Hau da $K_V10.2$, $K_V11.1$, $K_V11.2$, $K_V11.3$ eta K_V12-ren kasua.

1.3.1.2. Boltai-menpeko K^+ kanalen mintz-zeharreko domeinuak

Poroa osatzen duen domeinua, potasio kanalek partekatzen duten ezaugarri nagusiena da. Poroa sortzen duten lau domeinu elkarrekin mihiztatu behar dira poro funtzional bat sortzeko. Ezaugarri hori K^+-kanal guztiek dute, eta KcsA-ren mintz zeharreko bi domeinuek ederki irudikatu dezakete. Izan ere, KcsA kanalak ikertzen ari zenean aurkitu zituen Roderick MacKinnon-ek poroaren estrukturaren ezaugarri nagusiak (Doyle et al., 1998) (PDB: 1K4C).

Informazio estruktural hau ezinbestekoa izan da zenbait aspektu ulertu ahal izateko, hala nola, zergatik diren K^+ ioiarekiko selektiboak (10000:1 K^+ ioi, Na^+ ioiekiko), nola garraiatu dezakete horrenbeste ioi hain denbora laburrean (10^7 ioi kanalekiko s^{-1}) edota nola gertatzen den kanalaren irekidura (Sansom et al., 2002).

1.3.1.2.1. Iragazki selektiboa eta konduktantzia

Iragazki selektiboaren mekanismoa 1.6 irudian erakusten da. K^+ ioi bat, porotik gertu dagoenean, ur molekuletara elektrostatikoki lotzen da. Lotura intermolekular hauek ioiak poroa zeharkatzen duenean apurtu daitezke, eta hau energetikoki desegokia da (75 kcal/mol inguru) (Thompson et al., 2009). Hala ere, badude aminoazido batzuk poroaren inguran, euren talde karboxiloa kanpora begira dutenak, urarekin loturak desplazatzeko gai direnak, ioien desolbatazioa kausatuz. Ioia, berriro hidratatuko da mintza zeharkatzen duenean.

KcsA **kanalari selektibotasuna** ematen dion sekuentzia P-begiztan kokatzen da eta TVGYG sekuentzia peptidikoa dauka. GYG tripletea oso kontserbatuta dago potasio kanaletan. Hauen talde-karboniloen oxigeno atomoak, poroaren barrualdera begira kokatuta dituzte (1.6. irudia). Iragazki selektibo honek, K^+ ioi hidratatuentzat lau interakzio toki ditu, hauetatik bi urarekin interakzionatzeko kokatuta daude, beste biak, bi ioiekin interakzionatzen dutelarik. Hirugarren ioi bat poroan barneratzean, interakzio elektrostatikoak sortzen ditu, aurretiko ioia ezegonkortuz, eta mintzean zehar honen igarotzea utziz.Izan ere, talde karboniloen karga negatiboak, anioiak aldaratzen ditu, porotik pasatzea galaraziz. Bestalde, K^+ ez diren beste katioi batzuk, porotik pasatu daitezke, K^+ egiten duen bezala. Hala ere, tamaina diferentziak direla eta, talde karboniloak ez dira hain ondo ahokatzen beste katioiekin.

Nola gertatu daiteke ioien konduktantzia prozesua hain azkar? MacKinnon eta bere kideek adierazi zutenez, 2 K^+ ioi bakarrik pasa daitezke elkarrekin iragazkian zehar. Lehenengotik bigarrenera desplazatzea energetikoki onuragarria da, gaineko ioi deshidratatuaren hidratazioak azpiko ioiaren deshidratazioa faboratzen duelako. Gainera, K^+ ioiek, iragazki selektiboaren irekidura-konformazioa egonkortzen dute, K^+ ioien kondukzioa lagunduz.

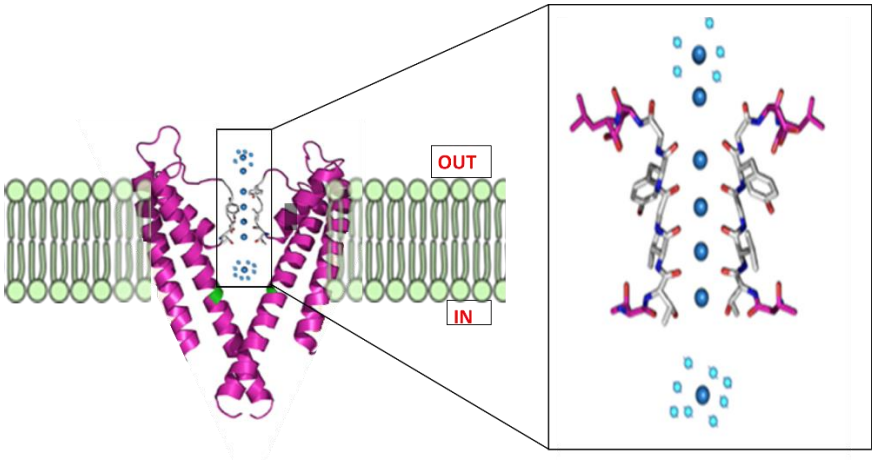

1.6 irudia. Kcsaren egitura. (Eskuinean) Kanala osatzen duten lau monomeroetatik biren irudikapena. Berdez nabarmendu da 99. glizina, irekitze-giltzarri funtzioa hartzen duena. Zuriz, TVGYG iragazki selektiboa koloreztatuta dago. Esfera urdin ilunak K^+ ioiak dira, eta zian esferak H_2O molekulak dira, ioien hidratazioan dihardutenak. **(Ezkerrean)** Kanalaren iragazki selektiboa. P begiztaren TVGYG motiboa zuriz agertzen da. Aminoazido horien alboko kateek kontaktu polarrak sor ditzakete ur-molekulekin eta K^+ ioiekin. (PDB: 1K4C)

1.3.1.2.2. Boltai-sentsore domeinua

Nerbio-zelulek sortutako ekintza potentzialak boltai-menpeko kanal ionikoen menpe daude. Boltai-sentsore domeinua (ingelesez voltage-sensor domain, VSD) mintzean txertatzen diren 4 alfa helizez osatzen da, S1-S4 izendatutakoak, oso kontserbatuta daudenak. Boltai-sentsoreak, mintz-potentzialaren aldaketei erantzuten dio, mintzaren potentzial elektrikoan gertatzen diren aldaketak akoplatuz eta kanalaren ioi-konduktantzia erregulatuz. Orokorrean, S4 segmentua, 4-8 aminoazido basikoz osatuta dago (argininaz, batez ere), boltai-sentsorearen eskakizunak konplituz.

S4-an ematen diren aldaketa estrukturalen eta elektrikoen oinarria ulertzea funtsezkoa da, boltai-menpeko kanal ionikoak mintz potentzialari ematen dioten erantzuna ulertzeko. Datu estrukturaletan oinarrituta, proposatu da, S4-ko aminoazidoek, errotatu eta desplazatu egiten direla, S6-aren konformazioa aldatuz , eta ondorioz, kanala irekiz (Bezanilla et al., 2000; Aggarwal & MacKinnon 1996).

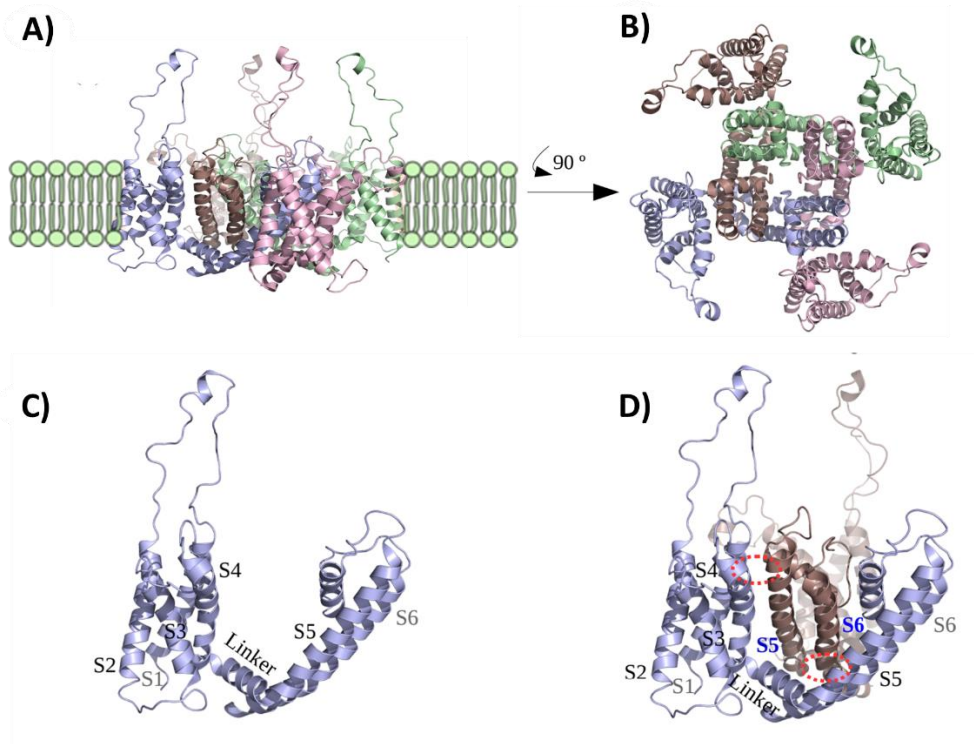

1.7 irudia. K_V7.2-ren estruktura. **(A)** K_V7.2 tetrameroaren bista laterala. Azpiunitate bakoitza kolore ezberdin batez irudikatuta dago. Mintz-zeharreko domeinuak baino ez dira erakusten. **(B)** Kanalaren goiko bista, erdiko poroa ikusteko. Iragazki selektibo guztiek poroaren barrualdera begiratzen dute. **(C)** Azpiunitate bakar baten egitura (S1-S4) eta poroa eratzen duen domeinua (S5 eta S6). **(D)** Molekulen arteko kontaktu-eskualdeak, zirkulu gorriz inguratuak. Kontaktu horien bidez, boltaiaren menpeko aktibazioa gertatzen da (PDB: 3LUT).

1.3.1.2.3. Domeinu intrazelularrak

Boltai-menpeko potasio kanal baten domeinu intrazelularren lehendabiziko bereizmen handiko estruktura berriki ebatzi zen (Sun & MacKinnon, 2017), non $KCNQ1_{EM}$/CaM konplexuaren estruktura 3.7 Å ebazpenarekin eta C4 simetria ezarriarekin ebatzi zen. Eskuragarri dagoen informazio guztia kontuan izanda, K_V familia bi talde nagusitan sailkatu daiteke (Barros et al., 2012):

1) Tetramerizazio domeinua N-muturrean duten K_V kanalak (K_V1-K_V4)

2) Tetramerizazio domeinua C-muturrean duten K_V kanalak (K_V7 and K_V10-K_V12).

N-muturraren zenbait domeinu ebatzi egin dira: Shaker kanalen T1 domeinua (PDB: 1A68) (Kreusch et al., 1998), K_V1.2 (PDB: 1QDW) (Minor et al., 2000), K_V4.3 (PDB:1S1G) (Scannevin et al., 2004), K_V4.3 KchIp1-rekin (PDB: 2I2R) (Pioletti et al., 2006), K_V1.3 (PDB: 4BGC) (Kremer et al., 2013). Baita N-mutur distalaren aktibazio estrukturak ere: K_V3.4 (PDB: 1ZTO) (Antz et al., 1997), K_V1.4 (PDB: 1KN7) (Wissmann et al., 2003). Azkenik, K_V11.1-ren PAS domeinua (PDB: 1BYW) (Morais Cabral et al., 1998), (PDB: 2LOW) (Ng et al., 2011), (PDB: 4HQA &4HP9) (Adaixo et al., 2013).

C-mutur batzuk ebatzi egin dira ere: zenbait kanalen helize superkiribildua, hala nola, K_V7.4 (PDB: 2OVC) (Howard et al., 2007), K_V7.1 (PDB: 3BJ4) (Wiener et al., 2008). K_V7.1 kanalaren B helizea holo-Kalmodunirekin (holo-CaM) konplexuan (PDB: 4GOW) (Q. Xu et al., 2013), K_V7.1 kanalaren A eta B helizeak Kalmodulinarekin (CaM) konplexuan (PDB: 4UMO & 4V0C) (Sachyani et al., 2014) eta berriki, $KCNQ1_{EM}$ estruktura 4 helize intrazelularrekin (*h*A-*h*D) (Sun & MacKinnon, 2017).

A eta B helize zitosolikoak, S6 tranmintz helizeari konektatuta daude eta CaM-ren lotura guneak dira. C eta D helizeak, bi helize luze dira, tetramerizazioa ahalbidetzen dutenak. Aurretik egindako SAXS ikerketa batean, mintz-zeharreko domeinurik gabe egin zena, malgutasuna aurkitu zuten C helizearen alde proximalean (Sachyani et al., 2014). Hala ere, mikoroskopia elektronikoz ebatzi den estruktura berri honetan, C helizearen alde distalean aurkitu zuten malgutasuna (Sun eta MacKinnon, 2017). Malgutasun honek desordena eragiten du D helizean, horregatik, ebazpen handiagoko estruktura lortu zuten estrukturaren berreraiketan D helizea ezkutatu zutenean.

Gogoan hartzen badugu domeinu intrazelularren artean dagoen dibergentzia txikia, K_V kanalen estrukturaren eredu bat irudikatu daiteke K_V7.1-ren estrukturan oinarrituta (1.8 irudia).

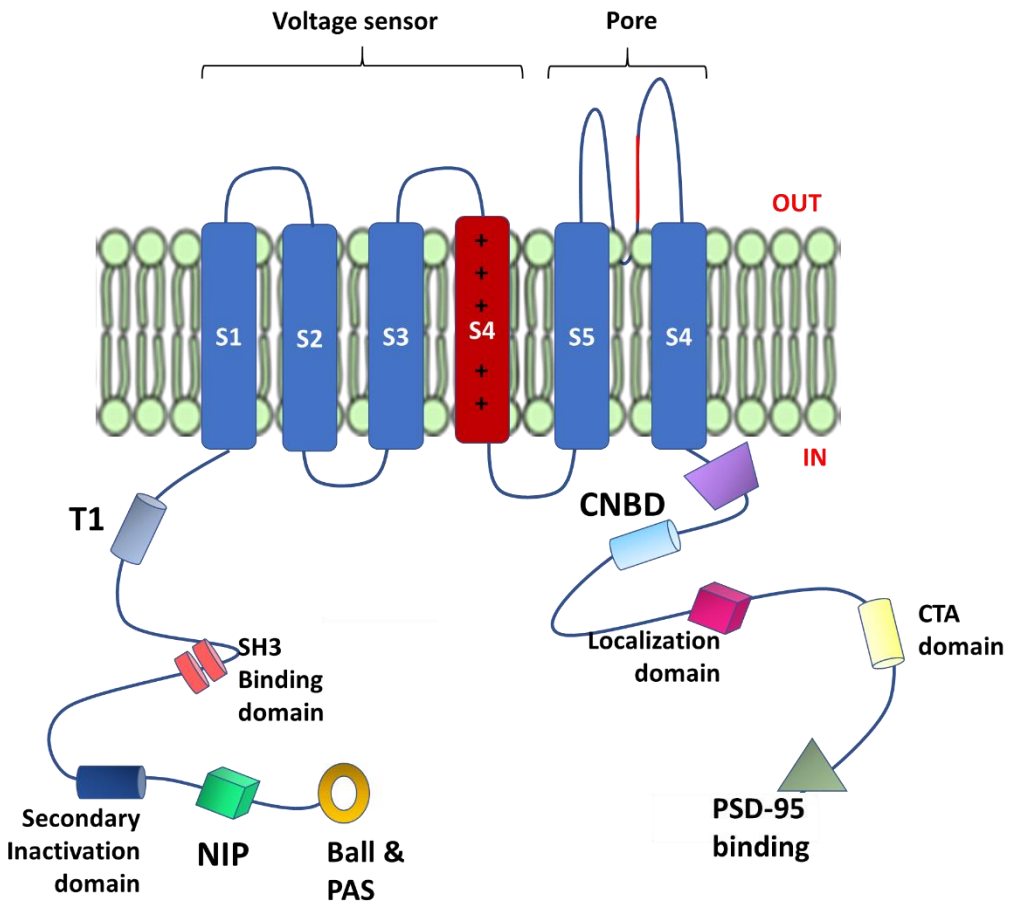

1.8 irudia. K_V kanalen zelula barneko domeinuen irudikapen eskematikoa. Hainbat eskualde eta eremu nabarmendu dira. N-muturrean, T1, K_V1-K_V4 kanalen tetramerizazio-domeinua, K_V1.5-ren SH3 lotura-domeinua; K_V1.4-ren bigarren inaktibazio-domeinua; K_V1.6ko Nip, N-motako inaktibazio-prebentzioko domeinua; Eag kanalen bola formako egitura eta PAS domeinua. C-muturrean, HCN eta CNG kanalen, C-lotailu/cNBD eskualdeetan; K_V2.1 kokapen-domeinua eta CTA domeina (C-mutur aktibatzailea); eta K_V1 kanal batzuen dentsitate post-sinaptikoko proteinekin lotzeko domeinua, PSD-95.

K_V1-K_V4 kanalen T1 tetramerizazio domeinua, NAB bezala ere ezagutzen dena, N-muturrean kokatuta dago. Gainera, K_V1.5 kanalek, SH3 proteinaren bi lotune dituzte, tandemean kokatuta, eta K_V1.4 kanalek inaktibazio domeinu sekundario bat. K_V1.6 kanalek, N-motatako inaktibazio-prebentzio domeinua (NIP) dute, K^+ kanalak inaktibazio azkarretik babesten duena. Azkenik, N-muturraren hasieran pilota-antzeko estruktura kokatzen da, N-motatako inaktibazioaren arduraduna, eag-kanalen PAS domeinuarekin erlazionatuta dagoena. C-muturrean, K_V2.1 familiaren C-muturraren aktibazio domeinua (CTA) kokatzen da, baita proteina post-sinaptiko

dentsoaren lotura domeinua (PSD-95), K_V1 kanalen C-muturraren zati distalean kokatuta dagoena.

1.3.1.3. Irekidura

Boltai-menpeko kanal ionikoen irekidura mekanismoa asko eztabaidatu da, Hodgkin eta Huxley, ioi-fluxua, neuronetan aurkitu zutenetik (Hodgkin & Huxley, 1952). Hiru hamarkada geroago, boltai-sentsore domeinuak (*voltage sensor domain*, VSD) identifikatu ziren K^+, Na^+ eta Ca^{2+} kanalen aktibazioa kontrolatzen zutenak (Noda et al., 1985; Tempel et al., 1987; Nelson et al., 1999). Domeinu hauek mintzaren boltai aldaketei erantzuten diete, kanalak aktibatuz edo inaktibatuz (Bezanilla et al., 2000).

Ordutik, kanal ionikoak irekitzeko eredu mekanistiko ezberdinak proposatu dira, S4-ko arginina eta lisinen kargak eremu elektrikoarekin erlazionatzen dituztenak, (Aggarwal & MacKinnon, 1996; Long et al., 2007).

Hauek dira boltai-menpeko kanal ionikoen irekidurarentzako proporasatu diren bi mekanismo nagusiak:

- KcsA-ren kasuan, hiru aminoazido hidrofobiko aurkitu dira bigarren mintz-zeharreko domeinuaren amaieran: V, T eta A. Hauen motibo hidrofoboak poroaren sarreran kokatuta daude, eta ioien igarotzea blokeatzen dute. Poroa irekitzen denean, aminoazido hauek euren konfigurazioa aldatzen dute, “banda” moduan aritzen den glizina bati esker (1.6. irudia). Hala ere, glizina ez da kanal guztietan aurkitzen, baina kontserbatutako beste aminoazido batzuk ere “banda” moduan aritu daitezke, esaterako PxP, non P prolina da eta x beste edozein aminoazido. K_V kanaletan, mekanismo honek, poroaren S6 eta boltai-sentsore domeinuaren arteko interakzioa ahalbidetzen du. Boltai-sentsore domeinuak seinalea alosterikoki transferitzen dio poro domeinuari (Long et al., 2005).
- N-inaktibazioa: ”baloi-eta-kate” mekanismoaz ezagutzen da ere. N-muturraren zati espezifiko bat poroan txertatzeko gai da kanala irekita dagoenean, hau blokeatuz. Kanal batek “baloirik” ez duenean, kanalaren beste azpiunitate erregulatzaile batzuk, K_V β esaterako, “baloiaren” funtzioa mimetizatu dezake. N-inaktibazioa, KcsA-ren inaktibazioa baino geldoagoa da (Batulan et al., 2010). Uste da, metodo hau K^+ kontzentrazio extrazelularrarekiko sentikorra dela, beraz, K^+ ioien gehiegikeria erregulatu dezakete.

K_V kanalen funtsezko aktibazio ereduak

K_V kanal guztiek antzeko aktibazio mekanismoak dituzte. Hauek azaltzeko, kanalak hiru egoera funtzionaletan egoten direla gogoratu behar dugu: egoera geldia (konformazio itxia) ↔ egoera aktiboa (konformazio irekia) ↔ egoera inaktiboa.

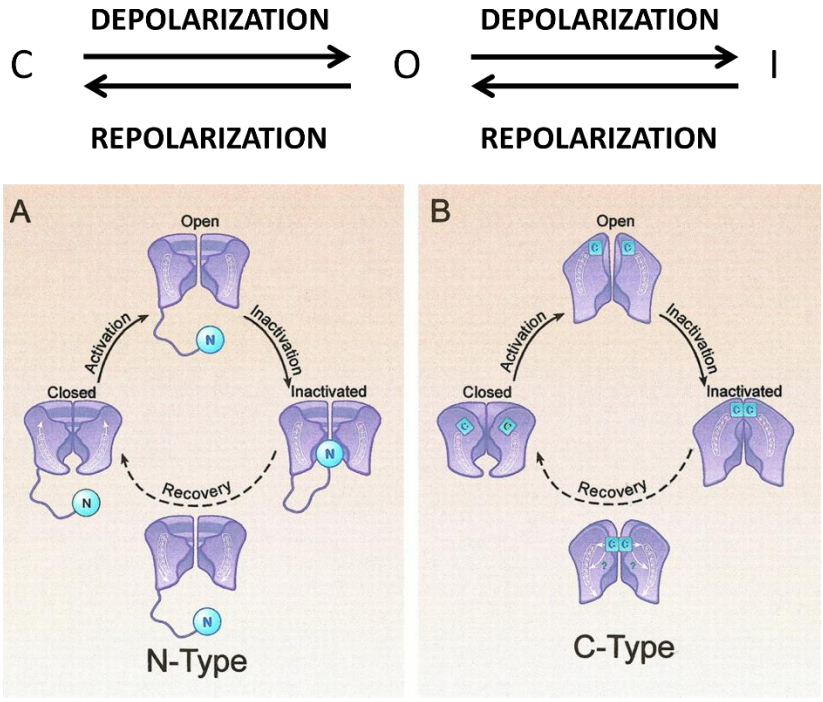

1.9 irudia. Konformazio-trantsizioen eskema K_V kanaletan: C-Kanal itxia; O-Kanal irekia; I-Kanal inaktibatua. **A)** N -motako inaktibazioa. Inaktibazio-peptidoa porora sartzen da eta ioien transferentzia fisikoki blokeatzen du. **B)** C-motako inaktibazioa. Selektibitate-iragazkiak bigarren ate bezala jokatzen du, eta itxi egiten da, ioiak sartzea saihestuz. Kanalak konformazio itxira itzultzen dira. (Grizel et al., 2014)

- **Helize irristakorraren eredua (A sliding-helix model, SHM)** *(Cattetall, 2010)*

  Mekanismo hau lotura elektromekaniko batean oinarritzen da, non S4 segmentuaren mugimenduak, S4-S5 konektorea bultzatzen du, eta honek, S6 inklinatu egiten du, poroa irekiz (Catterall, 2010).

  S4 segmentuan dauden aminoazido positiboak, mintz potentzialaren indar elektrostatiko negatiboagatik erakarriak izaten dira. Despolarizazioaren ondoren, indar elektrostatiko hori leundu egiten da, eta S4 segmentua kanporantz mugitzen da espiralean egindako ibilbide bat eginez; bertan, S4 segmentuan positiboki kargatutako aminoazido bakoitzak karga negatiboak dituzten aminoazidoekin ioi-pareak eratzen dituzte (Catterall, 2010).

- Pala eredua (A paddle model) (*Jiang et al., 2003)*

  Aktibazio-eredu hau K_VAP bakterio-kanalaren egitura kristalinoa ebatzi ondoren deskribatu zen (Jiang et al., 2003). Hemen, S3-S4 helizeak mintzaren zelula barneko azaleraren ondoan daude eta poroen ardatzarekiko perpendikularrak dira.

  S3 begiztaren bidez konektatuta dauden bi segmentuk (S3a eta S3b) S3 helizea osatzen dute. S3b segmentua eta S4 helizearen N-muturra elkarren artean hertsiki kontrajarriak daude, antiparaleloan orientatuta eta helize-begizta-helize egitura hidrofobikoa osatzen dute. S3 helizearen begizta malgua eta S4-S5 lotailua poroaren domeinuari lotuta daude. S3b-S4 eskualdeari "pala" deitu zioten (Jiang et al., 2003).

  Kanala itxita dagoenean, kanaletik positiboki kargatutako “palak” mintzaren zelula barruko azaleratik gertu kokatzen dira, eremu elektriko handi bati esker; mintzaren atseden potentziala, berriz, negatiboa da. Despolarizazioaren ondoren, palak elkarrekin mugitzen dira kanpoalderantz, S4-S5 lotailutik tiraka, honek, aldi berean, poroaren ardatzetik S5 helizea urruntzen duelarik, poroa irekiz (Jiang et al., 2003).

- Helize irristakorraren eredu aurreratua (Advanced SHM model) *(Durell et al., 2004)*

  Shaker kanalaren sekuentziako datuetan eta K_VAP kanalaren egitura kristalinoan oinarrituta proposatu zen (Jiang et al., 2003). Kasu honetan lehenengo S4a ~ 13,5 Å mugitzen da ardatzean zehar eta 180°-tako bira egiten du.

- Garraio eredua (Transport model, TM) *(Chanda et al., 2005)*

  Eredu honek, S4-a, kanala aktibatzen den bitartean mugitzen dela iradoki zuen, 45°-tako inklinazioarekin, baina, aldi berean, mintzaren azalerarekiko perpendikularki mugituz. S4-ko arginina, zelula barneko aldean kokatuta, barrunbera mugitzen da, mintzaren kanpoko aldean kokatuta. S4 helizearen mugimendu honek errotazioa eta inklinazioa konbinatzen ditu, helizea beti inguru polarrean dagoelarik. Mekanismo horri esker, karga kantitate handi bat transferitzen da eremu elektrikoaren bidez, S4-a mintzean zehar mugitu gabe.

- Helizeen mugimendu koordinatuaren eredua (Model of coordinated movement of helices, CMH) *(Pathak et al., 2007)*

  Eredu honek iradokitzen duenez, despolarizazioan zehar, S4-ak ~ 180°- ko mugimendua du, erlojuaren orratzen noranzkoan (zelula kanpoko aldera). Ondorioz, 6-8 Å altxatzen da eta bere inklinazioa 65°-tik 35°-ra aldatzen da. S4 helizearen inklinazioak, S5-aren

inklinazioa sustatzen du. Mugimendu hau erlojuaren orratzen kontrako noranzkoan ematen da, S4-S5 konektoreak eta S6 helizeak (azpiunitate guztietan) elkarrekin mugituz eta zelula barneko atea irekitzea ahalbidetuz.

- Adostasun-eredua (consensus model, CM) *(Vargas et al., 2011)*

  Vargas et al. (2011) CMH ereduari (Pathak et al., 2007), zenbait zehaztapen gehitu zizkioten. Kanala itxita zegoenean, boltai sentsore domeinuko helizeen (S1-S4) aminoazidoen arteko oinarrizko interakzioei buruzko datuak erabili zituzten eredu hau proposatzeko.

- Kargen transferentziaren eredua (A model of charge transfer, MCT)

  Era berean, konposatu edo toxina ezberdinek kanalen aktibazio-propietateak modulatu ditzakete. Denbora luzez jakin izan da animalia batzuek, armiarmak, sugeak eta eskorpioia kasu, toxina barietate handia dutela, gizakiak barne hartzen dituen beste animalia batzuen sistema neuralari eragiten diotenak (Strong et al., 1990). Jatorrian, pentsatzen zen, toxina horietako batzuek, kanal ionikoetan espezifikoki eragiten zutela. Ideia hori ikerketa fisiologikoek babestu zuten. Hala ere, ikerketa berriago batetan, erresonantzia magnetiko nuklearrez (EMN) egina, KcsA aztertu zen kaliotoxinaren (eskorpioi-toxina) presentzian, eta kanalaren blokeoa azal dezaketen egiturazko berrantolaketa batzuk erakutsi zituzten (Lange et al., 2006). 2013an, MacKinnonen taldeak, K_V1.2-2.1 kimerako egitura bat argitaratu zuen eskorpioiaren toxinarekin konplexuan (PDB: 4JTA) (Banerjee et al., 2013). Bigarren kasu honetan, toxinak, ioiak porotik pasatzea oztopatzen du, kanalaren egitura aldatu beharrean. EMN datuekin bat etorri ez arren, ez dago toxinek kanaletan eragiten ez dutelaren ebidentzia zuzenik, eta, beraz, bi mekanismoak onargarriak dira.

1.3.1. Boltai-menpeko beste kanal ionikoak

Doktoretza tesi hau K_V kanaletan enfokatzen bada ere, beste boltai-menpeko kanal ionikoak birpasatuko ditugu, irudi orokorrago bat lortzeko.

1.3.2.1. Ca_V kanalak: Boltai bidez aktibatutako kanal ionikoen talde bat da, zelula kitzikagarrien (adibidez, muskulua, zelula glialak, neuronak, etab.) mintzean aurkitzen direnak, kaltzio ioiarekiko selektibitatearekin. Kanal hauetatik sodio ioi gutxi batzuk pasa daitezke ere. Prozesu fisiologiko askotan hartzen dute parte, hala nola, muskuluen uzkurduran eta erlaxazioan, zelula barneko seinalizazioan, bihotzeko taupaden kontrolean eta neurotransmisoreen eta hormonen jariaketan. Ca^{2+} kanal ezagun guztietan, poroak sortzen dituen unitatea, lau domeinu errepikatuz osatutako

proteina bakar gisa adierazten da. Proteina horiek banan-banan adierazi eta ondoren mihiztatu egiten dira. Boltai-menpeko kaltzio kanalak hainbat azpi-unitate dituen multzo bat bezala eratzen dira: α1, α2δ, β1-4, eta γ. α1 azpiunitateak poroa eta boltai-sentsorea eratzen ditu. Lau motibo homologotan antolatuta daude (I-IV), horietako bakoitzak sei mintz-zeharreko segmentu dituelarik. Ca^{2+} kanalek aniztasun estruktural eta funtzional handia erakusten dute, agerikoa dena bihotzaren uzkurduraren kasuan, non prozesuan 3 azpifamilia parte hartzen duten: Ca_V1 (L mota), Ca_V2 (p/Q, n eta R mota) eta Ca_V3 (t mota).

1.3.2.2. Na_V kanalak: Boltai-menpeko sodio kanalek, zelula kitzikagarrietan ekintza-potentziala hasteko eta zabaltzeko ardura dute, nerbio-zelulak, zelula muskularrak eta neuroendokrinoak barne. Kanal hauek Na^+-erako oso selektiboak badira ere, Ca^{2+} kanalekin antzekotasun estrukturala dute. Gizakietan, 11 gene ezberdinek Na^+ kanalen α-azpiunitateak kodetzen dituzte. Gainera, prozesu fisiologiko askoren erantzule ere badira; horietan ikertuena ekintza potentziala sortzea eta hedatzea da.

Hurrengo kanalak ez dira zehazki boltai-menpekoak, baina boltai bidez aktibatutako ioi-kanalekin homologia handia erakusten dute.

1.3.2.3. Nukleotido-ziklikoez aktibatutako kanalak (Channels activated by cyclic-nucleotides, CNG): CNG familiak boltai bidez aktibatutako beste kanal ioniko batzuen ezaugarri estruktural berberak ditu. Nukleotido ziklikoak, cAMP eta cGMP zuzenean lotuz irekitzen dira. Katioi ez selektiboen kanalak dira, hainbat ehun eta zelula motaren mintzetan daudenak, eta transdukzio sentsorialean eta zelulen garapenean garrantzitsuak dira. Usaimena eta ikusmena hautemateko ezinbestekoak dira. Bere jarduerak boltaiarekiko mendekotasun txikia erakusten duen arren, GNC kanalak boltai bidez aktibatutako ioi kanalen superfamiliakoak dira. Hala ere, bere ligandoak zelula barneko karboxilo muturrari (cAMP edo cGMP) lotuta daudenean bakarrik aktibatzen dira. Bere lehengusuak bezala, boltai menpekoak diren K^+ kanalak, GNC kanalek konplexu heterotetramerikoak eratzen dituzte, bi edo hiru azpiunitate mota ezberdinez osatuak.

- 1.3.2.4. SK kanalak: SK kanalek ekintza-potentzial baten ondorengo hiperpolarizazioan laguntzen dute, eta zelula kitzikagarri askoren berezko kitzikagarritasuna neurtzen dute (Adelman et al., 2012), erantzun immunearen aktibazioa modulatzen dute (Feske, 2015) eta tonu baskularra erregulatzen laguntzen dute. (Wulff, 2013). 6TM-tako kanal hauek sekuentziaren ~ % 40 partekatzen dute boltai bidez aktibatutako K^+ kanalekin. S4 segmentuak positiboki kargatutako hiru Arginina dituen arren, SK kanalen irekiera ez da sentikorra boltaiarekiko (Hirschberg, 1998). CaM-ren C lobulua, S6 mintz-zeharreko segmentuaren ondoren dagoen helizearen zati distalarekin elkartzen da. Elkarrekintza honek C-lobuluaren E-F eskuen geometria aldatzen du,

honela, bata edo biak Ca^{2+}-a batzeko gai ez direlarik (Lee eta MacKinnon, 2018; Schumacher et al., 2001). CaM-k, Ca^{2+} seinalizazioan duen paperaz gain, kritikoa da ere azaleko adierazpenerako eta tetramerizaziorako (Joiner et al., 2001; Lee et al., 2003).

1.3.2.5. EAG kanalak: EAG1 potasio-kanala, KCNH edo ether-a-go-go familiakoa da, eta funtzio nagusienak bihotz-birpolarizazioan, kitzikagarritasun neuronalean (Bauer eta Schwarz, 2018; Pardo eta Stuhmer, 2014) eta tumorogenesian (Pardo et al., 1999) ditu. Kanal familia honek S2 eta S3 segmentuak elkartzen dituen konektore luze bat du. N- eta C- muturretara konektatutako eskualde zitoplasmatikoek aminoazidoen sekuentziaren % 70-a baino gehiago hartzen dute. PAS (Per-ARNT-Sim) domeinu bat du N muturrean, aurretik 25-27 aminoazidoko sekuentzia bat duena, PAS-cap bezala ezagutzen dena. C-muturrak, nukleotido ziklikoekin lotzen diren domeinuekin homologia duen eskualde bat dauka (*cyclic nucleotide binding homology domain*, CNBHD), baina nukleotido ziklikoekin lotzen ez dena. Ondoren, C-muturraren tetramerizazio-domeinu bat, helize superkiribilduak sortzen dituena (Jenke et al., 2003). Kanal hauek funtzionalak dira ere eskualde zitoplasmatikoa ezabatzen denean, C-muturreko tetramerizazio-domeinua mantentzen bada (Whicher eta MacKinnon, 2019), edo azpiunitate zatituak konbinatzen direnean, N-muturra/VSD alde batean + PD/C-muturra beste aldean (Lorinczi et al., 2015). Gainera, kanal funtzionalak sortzen dira dibisio-puntua S2-S3 zelula barneko begiztan edo S3-S4 zelulaz kanpoko konektorean dagoenean (de la Pena et al., 2018). Poro domeinua, berez, ez da funtzionala. Badirudi poro-domeinua, boltai-sentikor domeinuarekin lotu behar dela ioien iragazketarekin bateragarria den konfigurazio bat hartzeko (Tomczak et al., 2017).

1.3.2.6. Potentzial iragankorreko kanalak (Transient Receptor Potential, TRP): TRPV5 eta TRPV6 homologoak dira (~% 75eko sekuentzia-identitatea dute), hartzaile iragankorraren kanal ionikoen familiakoak (TRP), baina familiako beste kide batzuk ez bezala, ez dira termosentikorrak, ezta ligandoen bidez aktibatuak ere. Biak zelula epitelialetan adierazten dira, TRPV5 giltzurrunean eta plazentan batez ere, eta TRPV6 hesteetan. Ca^{2+}-rako selektibitate altua dute, beste katioi monobalenteekiko 100 aldiz altuagoa eta Ca^{2+}-aren homeostasian paper kritikoa jokatzen dute (Alaimo eta Rubert, 2019; Nijenhuis et al., 2005; Nilius et al., 2001). TRPV5/6 kanalak lau azpiunitatez osatuta daude, horietako bakoitzak 4TM dituelarik. S1/S4-a boltai-sentikor domeinuari gogorarazten badu ere, boltaiarekiko sentigaitza da (Voltage Insensitive Domain, ViSD). Poro domeinua (PD) eta amino- eta karboxilo-mutur intrazelularrak, 6TM-tako potasio kanalen antzekoak dira. Kanal honen ezaugarri karakteristiko bat, N-muturrean, helize-begizta-helize kanonikoaren tolesdura duten ankirina errepikakorren eremu bat da. Ca^{2+}-arekiko selektibitatea aspartato erresiduo bakar batek zehazten du (TRPV5-D542, TRPV6-D541) poroan sartzen den begiztan kokatuta dagoena (Saotome et al., 2018). Kanal hauek hertsiki erregulatuta

daude PIP_2 eta CaM-ren bidez, hauen jarduerek kanala estimulatzen eta inhibitzen dute, hurrenez hurren. CaM-k kanalaren jarduera inhibitzen duen atzeraelikadura negatiboko mekanismo batean parte hartzen du, Ca^{2+}-aren gehiegizko sarrera saihestuz (De et al., 2011; Lambers et al., 2004). Ca^{2+} intrazelularraren kontzentrazio aldaketek eragin handia dute kanal hauen bidezko Ca^{2+} sarreran, 90 nM inguruan kanalaren inhibizioaren erdia ikusten delarik (Nilius et al., 2001).

1.4. K_V7 kanalak eta M-korrontea

M-kanalen bidez sortutako korrontea, M edo I_M korrontea, Brown eta Adamsek deskribatu zuten lehen aldiz, 1980an, igel zezenaren neurona gonglionar sinpatikoetan (Brown et al., 1980). M-korrontea izena hartu zuen, muskarina bidez inhibitzen zela ikusi zutelako (1.9 irudia). K^+ korronte bat da, boltaiaren eta denboraren menpe dagoena, ez inaktibatzailea, mintz-potentziala, ekintza potentziala sortzeko atalasetik gertu dagoenean aktibatzen dena. M-korrontearen aktibazioa motela da, ez du zelularen birpolarizazioan parte hartzen, baina moteltze efektu sakona eragin dezake aktibazio errepikakorrean eta neuronen kitzikagarritasun orokorrean. Horregatik, M-korrontea ezabatzen denean, kitzikagarritasun neuronala handitu egiten da.

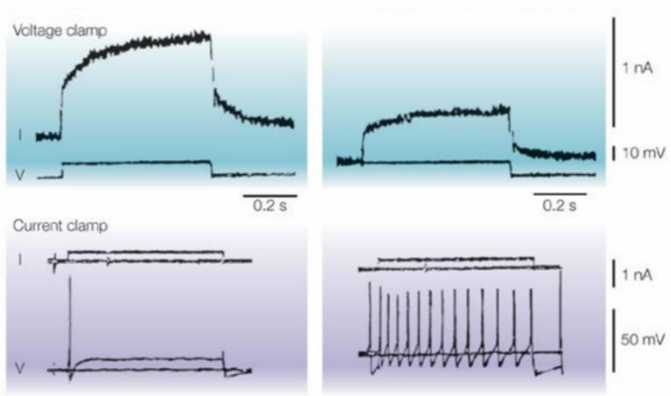

1.10 irudia. Estimulu baten erantzun neuronala, muskarinaren presentzian eta gabezian. Ezkerra: -40 mV-ko atseden-potentzialean neurona despolarizatu ondoren, M-korrontea aktibatzen du, non balio maximo bakar bat agertzen den. **Eskuina:** $K_V7.2$ eta $K_V7.3$ efektu muskarinikoaren ondorioz itxita daudenean, M-korrontea ezabatu egiten da eta, beraz, estimulu despolarizatzaile batek ekintza potentzial errepikakorrak sor dezake. Delmas & Brownetik hartuta, 2005).

Izan ere, M-korrontea, zelula askorentzat, mintz potentzialaren atalasearen azpitik dagoen potasio korronte nagusia da, kitzikagarritasuna eta ekintza errepikakorrak saihesten dituena. Gainera, korronte hori ez da inoiz inaktibatzen, beraz, eragina du ekintza potentzial errepikakorretan (1.10 irudia).

1998ra arte $K_V7.2$ eta $K_V7.3$ heterotetrameroak korronteaz arduratzen diren osagai molekularrak zirela baieztatzeko froga nahikorik ez zegoen (Wang et al., 1998), ezta azpiunitate horien

mutazioek jaioberriaren konbultsio onbera familiarra (ingelesezko BFNC) gaixotasunaren erantzuleak zirela ere (Biervert et al., 1998; Cooper et al., 2000; Delmas & Brown, 2005). Gainera, bi kanal horiek hipokanpoan, neokortexean eta azal zerebelosoan adierazten dira batez ere.

Neuronaren barnean, K_V7.2 eta K_V7.3 kanalak (KCNQ2 eta KCNQ3 geneek kodetuak, hurrenez hurren) soman, dendritetan, axoiaren hasierako segmentuan eta, azkenik, Ranvier nodoetan adierazten dira.

Eskualde horietan, KCNQ2 eta KCNQ3 elkarrekin adierazten eta mihiztatzen dira (Cooper et al., 2000), eta, beraz, uste da, bi azpiunitateek heterotetramero gisa mihiztatzen direnean erabat funtzionatzen dutela, KCNQ2/KCNQ3 kanal heteromerikoek kanal homomerikoek baino 15 aldiz korronte handiagoa sortzen dutelako (Wang et al., 2000;

Bi kanal hauek neuronetan duten presentzia handiak, M-korronteak kitzikagarritasun neuronalaren erregulazioan duen funtsezko eginkizuna nabarmentzen du. Hala ere, frogatu da M-korronteak nagusiki K_V7.2 eta K_V7.3 korronteek ekoizten dituzten arren, K_V7.2 eta K_V7.5-ren heteromeroek ere M-korrontea sor dezaketela *in vivo* (Schwarz et al., 2006), eta HEK293T eta CHO bezalako kultibo zelularretan, berriz, edozein K_V7-k sor dezakeela (Shapiro et al., 2000).

1.4.1. Estruktura

K_V7 familiako kideek 6TM kanalen estruktura tipikoa partekatzen dute. S1-S4 segmentuek boltaia detektatzeko eremua osatzen dute, batez ere argininan aberatsa den eta, beraz, positiboki kargatuta dagoen S4-ak.

S5, S6 eta euren arteko begiztak poroa osatzen dute, potasioari selektibotasuna ematen dion GYG ezaugarri tipikoarekin. Bi mutur amino (N-) eta karboxiloak (C-) zelularen barnean daude. Beste kanal ioniko askotan bezala, poro funtzionala osatzeko, lau azpiunitate mihiztatu behar dira tetramero bat sortuz.

K_V kanal gehienak N-muturrean tetramerizatzen dira, T1 izeneko tetramerizazio-domeinu bati esker. K_V7 kanalek ez dute domeinu hori, baina C-muturraren D-helizean tetramerizazio domeinua dute, helize superkiribilduak sortzen dituena (Maljevic et al., 2003). Esan beharra dago K_V7 kanalen C-muturra bereziki luzea dela eta kanalaren mihiztadura, trafikoa eta irekidura erregulatzen dituela (Haitin et al., 2008; Barros et al., 2012).

1.4.2. K_V7 FAMILIA KIDEAK

1.4.2.1. K_V7.1

K_V7.1 proteina kodetzen duen genea, KCNQ1, klonatu zen familiako lehen kidea izan zen eta 11p15.5 kromosoman identifikatu zen 1 motako QT luzeko sindromea zuten familietan posizio-klonazioko ikuspegi bat erabiliz (Wang et al., 1996). K_V7.1-a, K_V7-ko beste kideekin heterotetrameroak osatu ezin dituen familiako kide bakarra da. Hala ere, KCNE1 azpiunitate osagarriarekin batera lotzen da, *mink* edo IK bezala ere ezagutzen dena. KCNE1, IK_S korronte kardiakoa sortzeko funtsezko osagaia da (Barhanin et al., 1996; Sanguinetti et al., 1996). K_V7.1/KCNE1 konplexua barneko belarrian, tiroide-guruinan, birikan, traktu gastrointestinalan, heste meharran, eta pankrean ere adierazten da.

QT luzearen sindromea (inglelesezko siglengatik LQTS) bihotzeko aktibitate elektrikoaren nahasmendu bat da, zelulen birpolarizazioak eragiten duena. Sarritan, IK_S korronteen ezabatze gogor bat eragiten du eta pazienteak arritmietara eta bat-bateko heriotzara eramaten ditu bihotzeko baten ondorioz (Maljevic et al., 2010).

Gainera, beste bi sindrome ezberdin KCNQ1-en mutazioekin erlazionatu dira: Romano-Ward autosomiko dominantea eta Jervell eta Lange-Nielsen sindrome errezesiboa. Azkenekoan, gizabanakoak, bihotz-urritasunaz gain, jaiotzetiko gorreria pairatzen du ere (Wang et al., 1996).

1.4.2.2. K_V7.2 and K_V7.3

K_V7.2 eta K_Vv7.3, KCNQ2 eta KCNQ3 kanalak kodetzen dituzten geneak bi ikuspegi ezberdin erabiliz identifikatu ziren. Lehenik eta behin, giza garunaren DNAc liburutegia, KCNQ1-etik eratorritako sekuentzia batean oinarrituta bahetu zen (Yang et al., 1998) eta, bigarrenik, BFNC duten familietan posizio-klonazioa aztertu zen (Biervert et al., 1998; Schroeder et al., 1998). M-korrontearen atalean aipatu dugun bezala, K_V7.2 eta K_V7.3 garuneko hainbat eskualdetan daude eta homo zein heterotetrameroak era ditzakete. M-korronte neuronala sortzen dute, eta proteina horien mutazioak hainbat gaixotasunekin lotu da, hala nola konbultsio neonatalarekin, epilepsia errolandikoarekin (Neubauer et al., 2008), entzefalopatia epileptikoarekin (Weckzure et al., 2012) eta autismoarekin (Gilling et al., 2013).

1.4.2.3. K_V7.4

Giza erretinako DNAc liburutegian, KCNQ3 DNAc partzialean oinarritutako baheketa bat egin zen eta KCNQ4 genea identifikatu zen. DFNA2, entzumen-galera ez-sindromiko batekin (DFNA2), erlazioatu zen (Jentsch et al., 2000). Adierazpen-maila txikia aurkitu zen burmuinean, batez ere

entzumen-bide zentraleko nukleoetan eta ibilbideetan (Kharkovets et al., 2000), baina koklean asko adierazten da, barne-belarriaren zati dena (Kubisch et al., 1999). DFNA2-ren mutazioek funtzio-galera erakusten dute, dela haplourritasun-mekanismo batengatik, dela eragin negatibo nagusi batengatik (Maljevic et al., 2010). Azkenik, K_V7.4-k, heterotetrameroak sor ditzake K_V7.3-rekin, M-motako korronteak sortuz (Kubisch et al., 1999).

1.4.2.4. K_V7.5

KCNQ5 klonatua izan zen azken kidea da, eta ez dago besteak bezain ikertua *KCNQ3*-arekin homologia nabarmena duen arren (Schroeder et al., 2000). Nagusiki garunean eta muskulu eskeletikoan adierazten da, eta mioblastoen ugaritzean zehar erregulatzen da (Lerche et al., 2000). K_V7.5 adierazpen-maila baxuagoak aurkitu dira kolonean, biriketan eta umetokian. Hartzaile muskarinikoek inhibitu dezaketenez, eta nagusiki nerbio-sistema zentralean adierazten denez, M-kanalen familian sar daiteke. Berez, nerbio-sistema zentralean eta gongoil periferikoetan adierazitako K_V7.2 eta K_V7.3 kanalekin heteromultimeroak ere osa ditzakete. K_V7.3 bidezko mihiztadurarekin korrontea anplifikatzen du eta aldaketa txikiak eragiten ditu aktibazio zinetikan. K_V7.5-ak KCNE (KCNE1, KCNE3) peptidoekin elkarreragin dezakeela ere frogatu da, K^+ korronteen aniztasuna areagotuz (Roura-Ferrer et al., 2009). Funtzio galera edo irabazia eragiten duten *KCNQ5* mutazioek fisiopatologiara eramaten dute (Lehman et al., 2017). Mutazio hauek kitzikagarritasuna handitzearekin eta birpolarizazio-erreserba gutxitzearekin erlazionatuta daude.

1.4.3. M-korrontearen erregulazioa K_V7.2 and K_V7.3 kanaletan

K_V7 kanalek karboxilo mutur luzea dute (320-560 aminoazidoz osatuta), bere luzera, kideen artean, honela aldatuz: K_V7.5> K_V7.2> K_V7.3> K_V7.4> K_V7.1. Horrek, kontrastea egiten du kanal hauek duten N-mutur laburrarekin (~ 100 aminoazidotakoa). Nahiz eta oraindik ez den lortu C-mutur osoko egitura kristalinorik, 4 α-helizez osatuta daudela (A, B, C eta D) iradoki dute bigarren mailako egitura iragartzeko programek. C-muturrak, trafikoa, kanalen mihiztadura eta beste molekula batzuen interakzioa modulatzen du, horregatik "domeinu multimodularra" deritzogu (Sachyani et al., 2014).

Helizeak, luzera ezberdineko aminoazido-kate batzuen bidez bananduta daude (1.11 irudia).

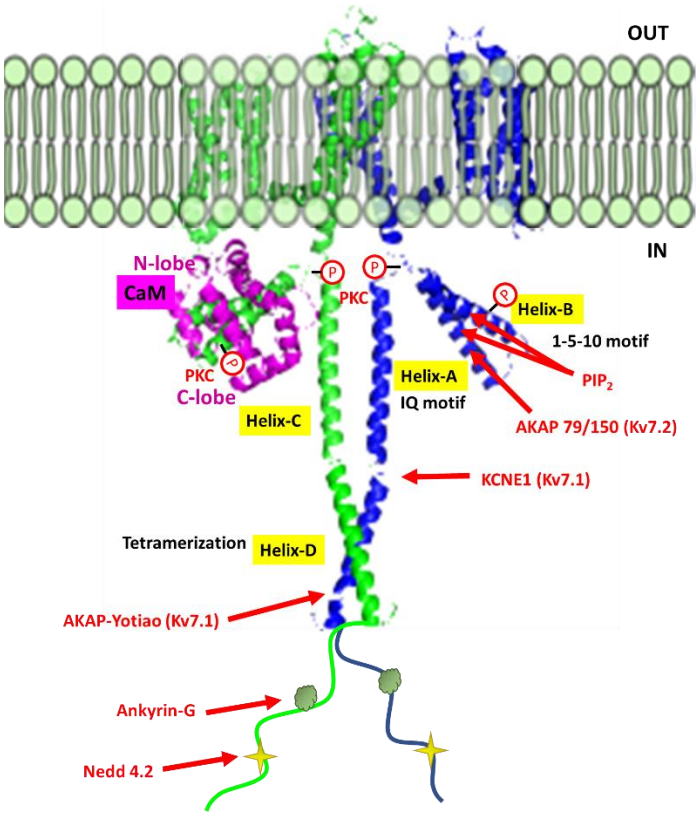

1.11 irudia. K_V7 kanaletako C-muturraren eskema. Lau azpiunitateetatik bi irudikatuta daude (berdez eta urdinez). A eta B helizeek elkarrekintza domeinua mantendu dute CaM-rekin (Magentan). Helize horietan PIP_2 interakzio-guneak ere egon daitezke. AKAP-yotiao-rekin $K_V7.1$ kanalean, AKAP79/150-rekin $K_V7.2$ kanalean, Ankyrin-G-rekin $K_V7.2/3$ kanalean eta Nedd 4.2 $K_V7.1$-3 kanalean ere elkarri eragiten diote K_V kanalekin. Hainbat fosforilazio leku daude ere. C helizeak dimerizazioa jasan dezake, D-helizeak, berriz, estruktura espiral bat eratzen du, estruktura kristalinoetan ikusi den bezala.

1.4.3.1. A eta B helizeak

A helizea, mintz-zeharreko seigarren segmentuaren ondoren dago, $K_V7.2$-ren kasuan, V320-tik Y372-ra bitarteko aminoazidoei dagokiena. Helize honi jarraituz, ia 130 aminoazidoko konektore bat dago, bigarren B helizetik banatzen duena. B helizeak, T551-etik E529-ra aminoazidoak hartzen ditu. Berriki, $K_V7.2$ kanaletan, eskualde honen egitura ebatzi zen, erresonantzia magnetiko nuklearrarren bidez (Bernardo-Seisdedos et al., 2018).

2002an CaM-, K_V7 familiako kide guztiekin elkartzen dela frogatu zen. Bi lotura-guen ezberdin deskribatu dira: 1) A helizean, IQ motiboa (IQxxxRxxxxR) eta 2) B helizean, 1-5-10 bi motibo (LxxxIxxxxV eta MxxxVxxxxF) (1.2 taula). $K_V7.2$ egitura ebatzian ikusi da A helizea CaM-ren C-lobuluari lotuta dagoela, B helizea N-lobuluarekin kontaktuan dagoen bitartean, emaitza hau bat dator CaM/$K_V7.1$-*h*AB eta CaM/$K_V7.3$-*h*A/$K_V7.2$-*h*B konplexuen egitura kristalografikoekin.

Hirschek eta laguntzaileek jakinarazitakoak. Baita, K_V7.1:CaM konplexuaren krio-mikospokia elektronikoz ebatzitako estrukturarekin (Sun eta MacKinnon, 2017).

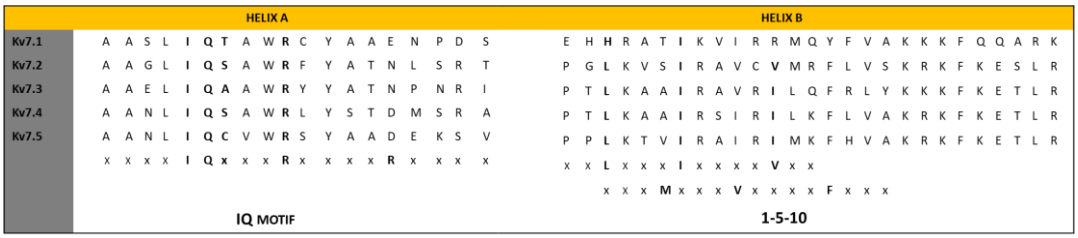

3.1 taula. K_V7 kanaletako A eta B kanalen sekuentzia-lerrokadura. Letra lodiz, CaM lotzeko motiboak osatzen dituzten aminoazido kontserbatuak nabarmentzen dira.

CaM, Ca^{2+}-a modulatzen duen proteina bat da, organismoarentzako kaltzio sentsore bezala jokatzen duena. Egia esan, kaltzioak prozesu askotan parte hartzen du, hala nola muskulu-uzkurketan, nerbio-seinalizazioan, ugalketan eta zelula-banaketan. CaM, 148 aminoazidoko (16,7 kDa) proteina txiki bat da, disolbagarria, termoegonkorra eta azidoa (pI ~ 4). Haltera formako egitura du eta bi domeinu globularrek osatzen dute, N-lobuloa (1-77 aa) eta C- lobuloa (82-148 aa), konektore malgu batez (77-81 aa) konektatuta daudela. Lobulu bakoitzak Ca^{2+}-a lotzeko bi E-F esku motibo ditu, hau da, Ca^{2+}-rako lau lotune guztira. E-F (1) eta E-F (2) N-lobuluan, eta E-F (3) eta E-F (4), berriz, C-lobuluan.

Apo-egoeran (Ca^{2+}-rik gabe), CaM-ek "konformazio itxia" du, non erresiduo hidrofobikoak ezkutatuta dauden (Babu et al., 1988) (PDB: 3CLN), baina zelulan Ca^{2+} sarrera bat dagoenean, E-F esku bakoitza ioi bati batuko zaio, CaM egitura egoera "itxitik", egoera "irekira" aldatuz eta aminoazido hidrofoboak agerian utziz.

Normalean, CaM- beste proteinekin lotzen da, bere bi domeinu globularren bidez itu-proteinaren lotura espezifikoetan. Bere plastikotasun estruktural zabalak, proteina ezberdin asko ezagutu eta erregulatzeko gaitasuna ahalbidetzen du. Izan ere, CaM konformazio ezberdinak har ditzake [Ca^{2+}]-aren arabera, E-F esku bakoitzak afinitate ezberdina duelako ioi honengatik. Gainera, bi globuluen arteko konektorea oso malgua da, eta horrek are plastikotasun konformazional handiagoa ematen dio. Izan ere, CaM 300 proteina baino gehiago antzemateko gai dela argitaratu da (Maylie et al., 2004).

Oraindik ez da ondo ulertzen nola erregulatzen duen CaM:Ca^{2+}-ak K_V7 kanala. Oro har, uste da, kalmodulina, K_V7-z eratutako azpiunitate osagarri bat dela, eta funtsezkoa dela bere funtziorako. Badirudi kaltzioaren presentzia ez dela beharrezkoa kanalen C-muturrera lotzeko. Egia esan,

kaltzioaren presentziak CaM eta kanalaren arteko lotura areagotu (Hernández et al., 2008) edo murriztu (Yus-Najera et al., 2002) dezakeela iradoki da. Kanal horien jardueraren erregulazioari dagokionez, Ca^{2+}-ak inhibitu egiten ditu $K_V7.2$, $K_V7.4$ eta $K_V7.5$ korronteak, baina ez $K_V7.1$ eta $K_V7.3$ (Delmas et al., 2005). Hala ere, CaM funtsezkoa da ere $K_V7.1$ eta $K_V7.3$ kanaletarako, beharrezkoa baita tetrameroetan mihiztatzeko eta mintzera garraiatzeko (Etxeberria et al., 2008; Spratt et al., 2006). CaM eta Ca^{2+}-ari buruzko informazio gehiago emango da aurrerago.

1.4.3.2. PIP_2

K_V kanalen artean, KCNQ1-5 kanalen ($K_V7.1$-7.5) seinalizazioa zelula barneko zenbait molekulak erregulatzen dute, horien artean 4,5-bisfosfatidilinositola (PIP_2), zelularen mintz plasmatikoaren barneko aldean kokatzen dena, ugaritasun apal batekin.

Mintzaren fosfatidilinositolaren 3, 4 eta/edo 5 posizioetako inositol taldea fosforilatzean, zazpi fosfoinositida ezberdin sor daitezke. Guztiak lipido minoritario bezala sailkatzen dira, eta bakoitza organulu baten mintzean adierazten dela uste da, zelulan zehar disposizio asimetrikoa mantenduz (Hille et al., 2014). Mintz plasmatikoan dagoen fosfoinositidarik garrantzitsuena fosfatidilinositol-4,5-bifosfatoa da.

Fosfatidilinositol-4,5-bisfosfatoa beharrezkoa da K_V7 kanalaren egoera irekia egonkortzeko. Boltai-sentsore domeinuaren eta poro eskualdearen arteko akoplamendua handitzen du, horrela korrontea murriztea saihestuz (Gamper eta Shapiro, 2007). $K_V7.2$-4 kanaletako PIP_2 interakzio-gunea A eta B helizeak konektatzen dituen lotailuan kokatu da (Hernández et al., 2008). Hala ere, beste ikerketa batek adierazi zuen lotailu hori ez dela beharrezkoa $K_V7.2$-aren PIP_2 bidezko erregulaziorako (Aivar et al., 2012). $K_V7.1$ kanaletan, non PIP_2-a beharrezkoa den jarduerari eusteko, PIP_2-aren interakzio-guneak osa ditzaketen oinarrizko erresiduo-taldeak identifikatu dira, bereziki S2-S3 eta S4-S5 zelula barneko konektoreetan, baita C-muturrean ere (Choveau et al., 2012; Eckey et al., 2014; Thomas et al., 2011).

Duela gutxi, PIP_2-ren eta CaM-ren N-lobuluaren arteko konpetizio bat deskribatu da, B-helizeari lotzeko (Tobelaim et al., 2017). $K_V7.1$ B-helizeko K526 eta K527 erresiduoek toki kritiko bat osatzen dutela ikusi da, non CaM PIP_2-rekin lehiatzen den IK_S kanalaren egoera irekia egonkortzeko. Itxuraz, PIP_2 eta Ca^{2+}-CaM funtzio bera betetzen dute IK_S kanalen aktibazioan, aktibazioaren boltai-menpekotasunean ezkerrerako desplazamendua eragiten baitute. Gainera, aminoazido horiek $K_V7.2$ eta $K_V7.3$ azpiunitateetako B helizean kontserbatu dira, eta horrek, B helizean gertatzen diren PIP_2-CaM interakzioak kanalaren jarduera modulatzeko oso garrantzitsuak izan daitezkeela iradokitzen du (Tobelaim et al., 2017).

1.4.3.3. Azetilkolinaren M_1 hartzaile muskarinikoak eta Angiotensina 2-ren AT_1 hartzailearen bidezko erregulazioa

M1 hartzaile muskarinikoen azetilkolina aktibatu ondoren, Gq/11rekin akoplatuta dagoena, C-fosfolipasak (PLC), PIP_2-a, aktibatu eta apurtu egiten du, diazilglizerola (DAG) eta inositol-3-fosfatoa (IP_3) sortuz. Ondoren, DAGek C-proteina kinasa (PKC) aktibatzen du eta IP_3k Ca^{2+}-a askatzen du zelula barneko erreseborioetatik. Bi bide horiek denbora luzez aztertu dira, muskarinaren inhibizioaz arduratzen den bigarren mezularia identifikatzeko. Azkenean, frogatu zen PIP_2-aren agortze bera dela inhibizioaren erantzulea. Lehenik eta behin, PLC-ren aktibazioak PIP_2-ren K_V7 inhibitzaileak hidrolizatzen ditu, eta PIP_2-ren analogo disolbagarrien administrazioek funtzioa berrezartzen dute (Zhang et al., 2003; Li et al., 2005; Hernandez et al., 2008). Bigarrenik, PIP_2-ren desfosforilizazioak, boltai-sentsore baten bidez edo lipido-5-fosfatasa baten bidez, K_V7 kanalen inhibizioa eragiten du (Suh et al., 2006b; Murata et al., 2007; Kruse et al., 2012). Azkenik, PIP_2 agortzearen ondoren, PIP_2-ren birsintesiaren denbora-bilakaera mintz plasmatikoan K_V7 korrontearen berreskurapenaren proportzionala da (Falkenburger et al., 2013).

Gainera, frogatu da estimulazio muskarinikoak 30-60 segundotan, neuroblastoma-zeluletan dagoen PIP_2-aren % 75 baino gehiago agortu dezakeela (Xu et al., 2003). Aldi berean, zitosoleko PIP_2-a agortzeak, inhibizio muskarinikoarekin korrelazio ona erakusten du (Winks et al., 2005). Angiotensina II AT1 aktibatzeak, PIP_2-a agortzen du ere (Zaika et al., 2006).

K_V7 kanalek afinitate ezberdina dute PIP_2-arekiko, $K_V7.1$>$K_V7.3$> $K_V7.2$> $K_V7.4$>$K_V7.5$ ordenan. EC50 balioak 3 µM eta ehunka mikromolar artekoak dira. $K_V7.2/3$ kanalek tarteko balioak dituzte, $K_V7.3$ afinitate handiagoa duelarik. Horrek azaltzen du zergatik, atseden-baldintzetan, $K_V7.3$-ren probabilitate irekia (Po), ia 1 den; eta $K_V7.2$-rentzat, 0,15-0,17. Kontuan hartuta hainbat *loci* neuronaletan M-korronteko kanalak hainbat azpiunitatez osatuta daudela (homomerikoak edo heteromerikoak), PIP_2-arekiko afinitatean dauden ezberdintasun horiek inhibizio-maila ezberdinak erakuts ditzakete (Delmas et al., 2005).

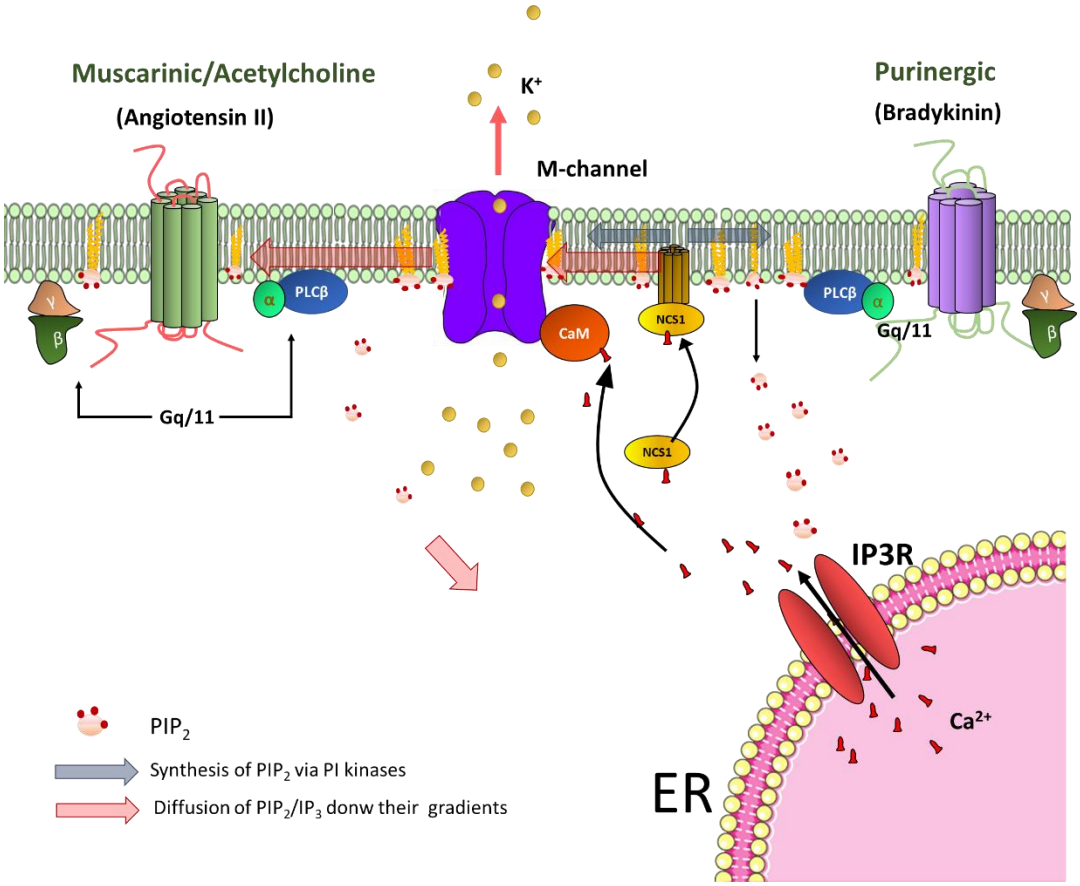

1.12 irudia. Irudia. M-korrontearen inhibizio-mekanismoak neurona sinpatikoetan. Azetilkolinaren edo angiotensinaren hartzailearen (M_1/AT_1 hartzailea) estimulazioak PIP_2-aren agorpena eragiten du, M-kanala inhibituz. Bradikinaren hartzailea edo hartzaile purinergikoa (B_2/P_{2Y} hartzailea) aktibatzean ordea, PIP_2-aren hidrolisiaren ondorioz IP_3-ak eragiten duen [Ca2+] igoerak M-kanala inhibitzen du CaM eta NCS-1-ren bidez. Hernández et al., 2008-tik modifikatua.

1.4.3.4. Kaltzio eta Bradikinika bidezko inhibizioa

Atseden egoeran [Ca^{2+}] ~ 0,1 µM-tan mantentzen da. PIP_2-ren hidrolisiaren ondoren, IP_3 zitoplasmara lekualdatzen da eta Ca^{2+}-a zelula barneko erreserbetatik askatzen du. Hainbat esperimentuk, Ca^{2+}-a K_V7 korronteetan efektu zuzena duela erakusten dute. Neurona sinpatikoetan egindako esperimentu elektrofisiologikoetan, Ca^{2+}-k ~ 100 nM-ko IC50 (korrontearen % 50aren inhibizioa) erakusten du, Ca^{2+}-ren kontzentrazioa baino zertxobait handiagoa (atsedenean, Ca^{2+} kontzentrazioa 70-80 nM-koa baita) (Selyanko et al., 1996). M1 hartzaileak, bradikinaren hartzaileak eta P2Y purinergikoak (Filippov et al., 1998) Gq/11 proteinetara lotzen dira ere, eta horrek PLC-ren aktibazioa ahalbidetzen du, PIP_2 hidrolisitik

abiatuta DAG eta IP_3 sortzen dituena. Erregulazio muskarinikoan ez bezala, bradikininaren inhibizioa, zelula barneko Ca^{2+}-a indargetuz prebenitu daiteke (Cruzblanca et al., 1998).

Bai inhibizioa muskarinikoan, bai bradikina bidezko inhibizioan, PLC aktibatzen da, baina bitartekaria ezberdina da. Bradikinina gehitu ondoren, Ca^{2+}-ren kontzetrazio igoera azkarrak, PIP_2-ren bersintesia aktiba dezake, NCS1 kaltzio sentsoriala den proteina neuronala aktibatuz, zeinek PI4K aktibatuko duen (Santagata et al., 2001), mintzean PIP_2-ren agorpena saihestuz. Hala ere, muskarinen inhibizioak ezin du Ca^{2+} kontzentrazioaren hazkunderik eragin mintz-azpiko eskualdean, eta, beraz, ezin ditu mintzaren PIP_2 mailak azkar berreskuratu.

1.4.3.5. AKAP79/150 eta PKC

PIP_2-ren hidrolisiak sortutako bigarren produktua diazilglizerola (DAG) da. Bigarren mezulari honek C-kinasa proteinaren (PKC) fosforilazio ibilbidea aktibatzen du inhibizo muskarinikoan (Hoshi et al., 2010). AKAP79/150-k, K_V7.2 kanalari, 321 eta 499 aminoazidoen artean lotzen zaio (Cooper et al., 2000; Hoshi et al., 2003) eta PKC-k urkabe gisa erabiltzen du, bertatik B edo C helizean hainbat leku fosforilatu ditzakeelarik.

Hasiera batean, PKC M-kanalen modulatzaile bezala deskribatu zen arren (Higashida et al., 1986), bere eragina oso eztabaidatua izan da. PCK, Phorbol-esterrekin aktibatu zen esperimentuetan ez zen M-korrontearen ezabaketarik ikusi (Marrion, 1997). Iradoki da, AKAP79 kinasari ainguratutako proteina bati PKC ainguratzeak, PKC-ren suszeptibilitateari eragin diezaiokeela, estaurosporina bezalako modulatzaileetan (Hoshi et al., 2010). Horrek azal lezake zergatik PKC modulatzaile batzuek ez duten inolako efekturik erakusten K_V7 kanaletan.

Frogatu da ere, Kir2.3 kanalek, PKC bidezko fosforilazioari ematen dioten erantzuna, eskuragarri dagoen PIP_2 mailen araberakoa dela (Keselman et al., 2007). Era berean, frogatu zen K_V7.2 kanaletan, PKC-ren fosforilazioak M-korrontea ezabatzen duela, PIP_2-ren kontzentrazio endogenoen arabera (Kosenko et al., 2012). Ikerketa berean, PKC-ren fosforilazioak PIP_2-ren afinitatea murrizten duela eta PIP_2-ren agortzeak eta afinitatearen murrizteak modu sinergikoan jokatzen dutela adierazi zuten.

1.4.3.6. C eta D helizeak

A eta B helizeek CaM-rekiko lotura domeinua eta beste proteina osagarri batzuetarako lotuneak mantentzen dituzten arren, ezin dira berez tetramerizatu. C eta D helizeetan, azpiunitateen interakzio-domeinu bat (SID, Sununit Interaction Domain) identifikatu da, hainbat K_V7 azpiunitateren mihiztatze esklusiboarekin lotuta dagoena. Xehetasunez aztertu den arren, K_V7

azpiunitatearen mihiztadura zehazten duten mekanismo molekularrak oraindik ez dira ongi ezagutzen.

C helizea, D helizea baino kontserbatuago dago K_V7 kanal guztietan. Eskualde honek, M537-V561 aminoazidoak biltzen ditu K_V7.2 kanalean, eta beharrezkoa da homomeroak eta heteomeroak sortzeko. D helize distala (R594-R619), eskualde aldakorrago bat da, K_V7 azpiunitate guztien arteko elkartze mugatua azal dezakeena. D helizearen egitura kristalinoak (K_V7.1 eta K_V7.4 kanaletarako eskuragarri) helize superkiribildua erakusten du (Howard et al., 2007; Sun & MacKinnon, 2017). Aurretik aipatu dugunez, aurreko SAXS ikerketa batean ez bezala (Sachyani et al., 2014), non C helizearen alde proximalean malgutasuna identifikatu zuten, krio-EM egituran C helizearekiko alde distalean malgutasuna ikusi da (Sun eta MacKinnon, 2017). Malgutasun honek D helizearen posizioan desordena eragin zuenez, erresoluzio handiagoko mapa bat lortu zuten D helizea maskaratzean. Merezi du aipatzeak D helizea K_V7.2 eta K_V7.3 arteko mihiztaduran garrantzitsua izateaz gain, adierazpenaren handikuntza ere bermatzen duela (Wiener et al., 2008).

1.4.3.7. Mutur distala

K_V7.2/3 kanalek eskualde honetan G-ankirina proteinari lotzeko motibo bat dutela deskribatu da (C3 motiboa, ~ 10 aminoazidotakoa). Kanalaren eta adaptatzaile handi honen arteko elkarreraginaren ondorioz, K_V7 kanalek axoiaren hasierako segmentuetan eta Ranvierren nodoetan mantentzen dira, G-ankirina, zitoeskeletoaren aktinarekin elkartzen delako. Beraz, uste da G-ankirina beharrezkoa dela M-kanalen kontzentrazioa erregulatzeko neuronetan. K_V7.1-3-rako, Nedd4-2 ubikuitina ligasarekin ere elkarreragiten dutela deskribatu da. Elkarreragin honek, ioien fluxua murrizten du KCNQ1/KCNE1, KCNQ2/KCNQ3 eta KCNQ3/KCNQ5 konplexuetan (Miranda et al., 2013).

1.5. Kanalopatiak

Kanal ionikoek jokatzen duten funtsezko paperen eta ehunetan duten banaketa orokorra dela eta, ez da harritzekoa kanal ionikoen azpiunitateak kodifikatzen dituzten geneetako mutazioek, edo eragiten dioten proteinek, heredatutako kanalopatia ionikoak eragitea. Gaixotasun horiek ohikoak izan daitezke edo oso arraroak, eta haien larritasuna arina, ezgaitzailea edo hilgarria izan daiteke. Hala eta guztiz ere, droga komertzialen % 5-aren helburu nagusia kanal ionikoak dira, eta horrek drogen aurkikuntzan duten potentziala iradokitzen du.

K_V kanalak kodifikatzen dituzten geneetan zentzurik gabeko mutazioak aurkitu izanak, funtzio anitzeko kanalak direla azpimarratzen du. Mutazioek, proteinen adierazpenari, trafikoari,

tolesteari edo proteinen erregulazioari eragin diezaiokete, baina askotan ez dute eragiten kanal ionikoaren funtzioan. Boltai-menpeko kanalek, zelulatik kanpo karga positiboak ponpatzen dituztenez, funtzionamendu txarrak hiperkitzikagarritasun zelularra eragiten du askotan. 1.2 taulan kanalopatien adibide batzuk agertzen dira.

Protein	Gene	Disease
Kv1.1	KCNA1	Episodic ataxia myokymia
Kv7.1	KCNQ1	Autosomal-dominant long -QT-syndrome with deafness
		Autosomal-dominant long-QT-syndrome
Kv7.2	KCNQ2	Benign familial neonatal convulsions (BFNC), also with myokymia
Kv7.3	KCNQ3	Benign familial neonatal convulsions (BFNC)
Kv7.4	KCNQ4	Autosomal-dominant deafness
KCNH2	KCNH2	Long-QT syndrome
Kir1.1	KCNJ1	Batter syndrome
Kir2.1	KCNJ2	Long-QT syndrome with dysmorphic features
Kir6.2	KCNJ11	Persistent hyperinsulinaemic hypoglycaemia of infancy diabetes mellitus
SUR1	SUR1	Persistent hyperinsulinamic hypoglycaemia of infancy
SUR2	SUR2	Dilated cardiomyopathy
KCNE1	KCNE1	Autosomal-dominant long-QT syndrome with deafness
		Autosomal-dominant long-QT-syndrome
KCNE2	KCNE2	Long-QT syndrome
KCNE3	KCNE3	Hypokalaemic periodic paralysis

1.2 taula. Potasio kanalak eta giza-gaixotasunak. Gaixotasuna eragiten duen proteinen taula: genea, kodetzen duen proteina, eta azkenik, eragindako gaixotasuna.

Garrantzitsua da nabarmentzea, boltai-menpeko kanal ioniko familia guztien artean, ohikoena K_V7 familia dela. Izan ere, K_V7 familiako kide guztiak, gutxienez gaixotasun batekin lotuta daude. KCNQ2 eta KCNQ3-ri dagokionez, Konbultsio neonatal onbera familiarraren (Benign Familial Neonatal Convulsions, BFNC) fenotipo klinikoarekin lotu ziren (Maljevic et al., 2008). Denboraren poderioz, beste fenotipo ezberdin batzurekin lotu dira, hala nola nerbio periferikoaren hiperkitzikagarritasunarekin (Peripheral Nerve Hyperexcitability, PNH), miokimiarekin edo epilepsia errolandikoarekin. Azkenik, KCNQ2-ren mutazioak, Ohtahara sindromearekin ere erlazionatu dira, haurren entzefalopatia epileptiko goiztiar bat, haurren entzefalopatia epileptikoa (early infantile epileptic encephalopathy, EIEE) ere deitua.

1.5.1. Konbultsio Neonatal Onberaren ezaugarri kliniko eta patologikoak

Gaixotasun hau bizitzaren bosgarren eguna baino lehen azaltzen da normalean (Rett et al., 1964) eta adierazpen iragankorra duten eraso fokal orokortuak dira. Konbultsioak berez desagertzen dira, asteak eta hilabeteak igaro ondoren. Herentzia autosomiko dominantea du, % 85 inguruko sarkortasunarekin. Pazienteen % 15-ak konbultsio errepikariak izan ditzakete bizitzan zehar (Maljevic et al., 2008).

Batzuetan, atzerapen mentala eta tratatzeko zailak diren epilepsiak dituzten pazienteak deskribatu dira. Gaixotasun hau duten familiekin egindako ikerketa batek, pertsona batzuek ezaugarri kliniko larriagoak izaten dituztela adierazi zuen (Soldovieri et al., 2014). Familiako beste kide batzuek eraso neonatal onberak baino ez zituzten jasan, baina beste batzuek atzerapena erakusten dute garapen psikomotorrean, desgaitasun intelektualean edo beste ezaugarri neurologiko batzuetan. Paziente horien fenotipoa KCNQ2-rekin lotutako entzefalopatia gisa deskribatzen da orain.

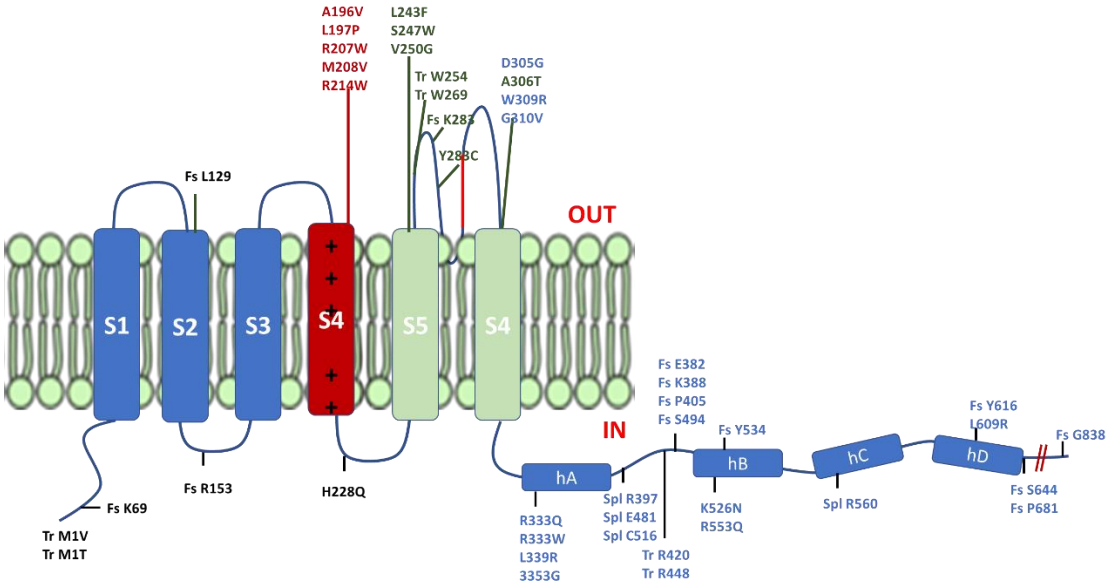

Figure 1.13. Konbultsio Neonatal Onbera sortzen duten mutazioen kokapena. *Fs* (frame shift) irakurketarauaren aldaketa eragiten duten mutazioak; *Spl*, lotura alternatiboaren barianteak; *Tr*, trunkazioa.

K_V7.2 eta K_V7.3 mutazio gehienak sistema heterologoetan ikertu dira, eta emaitzarik arruntena K^+ korrontean murrizketa bat da, batzuetan funtzioaren erabateko galera dagoen arren (Jentsch et al., 2000; Lerche et al., 1999; Maljevic et al., 2010). K_V7.2 edo K_V7.3 WT azpiunitateekin batera alelo mutatu bat adieraztean (2:1:1 proportzioan) paziente gaixoaren fenotipoa agertzen da, eta

horrek agerian uzten du korronteren % 20-25eko murrizketak nahikoa dela konbultsioak eragiteko (Schroeder et al., 1998). Fenotipo larriagoa duten familiek ere K_V7.2/3 korrontearen murrizketa arina erakusten dute, hortaz, beste faktore batzuk inplikatuta egon daitezke (Steinlein et al., 2007).

K_V7.2 sisteman konbultsio neonatal onbera familiarrean eragiten duten 130 mutazio baino gehiago deskribatutako dira, proteinaren zati ezberdinetan: C-mutur zitoplasmatikoan, poroen eskualdean (S5-S6), boltai-sentsorean (S4) eta S1-S2 eskualdeaan. K_V7.3-an, aldiz, soilik sei mutazio jakinarazi dira, horietatik bost poroan, eta azkena S6-an aurkitu zen (Soldovieri et al., 2014).

Aurretik adierazi den bezala, C-mutur domeinuak eskualde ezberdinak ditu proteina erregulatzaileak batzeko, baita tetramerizazio domeinua ere. Hemen gertatzen diren mutazioek kanalaren funtzionaltasunari eragin diezaiokete, tetramerizazioari eta/edo adierazpenari eragiten baitiote (Etxebarria et al., 2008; Schwake et al., 2000). Poroan emandako mutazioek ziurrenik kanalaren eroankortasuna aldatuko dute, haplo-urritasun mekanismo baten bidez. S1-S2 eta S4 emandako mutazioak kanalen aktibazioan izandako aldaketekin erlazionatu dira.

Egundaino, ordea, ez dago konbultsioak berez desagertzearen alde egiteko azalpen molekularrik. Zenbait zientzialarik, jaioberriaren lehen asteetan karraskarien garunean aurkitutako erregulazio positiboan oinarrituta, K_V7.2/3-ren adierazpena jaioberriaren garapenean zehar aldatzen dela iradoki dute (Geiger et al., 2006; Maljevic et al., 2008; Weber en al., 2006). Ondorioz, azpiunitate mutante bat adierazteak korrontea murriztea ekarriko luke, eta hori ez da nahikoa zelulen funtzio normalerako garapenaren lehen etapan. Hala ere, helduaroan, K^+-ko beste kanal batzuk ere aktibatuta daudenez, K^+-ren konduktantzia osoa handituz, K_V7.2/K_V7.3-ren mutazioa konpentsatu dezakete. GABAk, jaioberriaren garunean iradokitako ekintza kitzikatzaileak efektu hori okertu dezake, GABAren sistema inhibitzailea behar bezala garatzen den neurrian (Okada et al., 2003).

1.5.2. Ohtahara sindromearen ezaugarri kliniko eta patologikoak

Kasu honetan, konbultsioak 3 hilabete bete baino lehen hasten dira. Haurrek, oro har, erronka larriak izaten dituzte garapenean eta azterketa neurologiko anormala izaten dute, baita konbultsioak hasi aurretik ere. Berez, arazo motor eta kognitiboek okerrera egin dezakete pixkanaka, konbultsioak areagotu ahala. Ohtahararen sindromeak mutilei zein neskei eragin diezaieke.

Konbultsio mota asko gerta daitezke, baina konbultsio tonikoak (besoen edo hanken zurruntasuna) maizago antzematen dira.

Konbultsio horiek segundo batzuk baino ez dute irauten eta haurra esnatuta zein lotan dagoenean gertatzen dira. Ohtahararen sindromean gerta daitezkeen beste konbultsio mota batzuk konbultsio fokalak (garunaren eremu batean hasten direnak), atonikoak, mioklonikoak edo toniko-kloniko orokortuak dira. Ohtahara sindromea duten haurrek ere espasmoak garatu ditzakete.

Ohtahara sindromearen kasu gehienak garuneko malformazioak edo mutazio genetiko jakin batzuek eragindakoak dira. Kausa metabolikoak ez dira hain probableak. Kasu batzuetan, ez da kausa argirik aurkitzen.

Garuneko malformazioak lausoak (garunaren bi aldeei eragiten dietenak) edo fokalak (eremu edo alde bati bakarrik eragiten diotenak) izan daitezke.

Ohtahararen sindromearekin lotu diren gene batzuen artean KCNQ2, Arx, CDKL5, 23SLC25A22, STXBP1... daude besteak beste.

1.5.3. KCNQ3 eta Autismoa

KCNQ3ko mutazioak, M-korrontearen beste arduraduna, espektro autistarekin lotuta daude (Gilling et al., 2013). Duela gutxi, fenotipo elektrokliniko berria deskribatu da konbultsiorik ez duten KCNQ3-n mutazio heterozigotoak dituzten 11 pazienterengan. Aldiz, bizitzako lehen 2 urteen barruan, NDD globala eta espektro autistaren nahasmendua (ASD) edo ezaugarri autistak erakusten dituzte. 1,5 eta 6 urte bitartean erregistratutako 9 pertsonetatik 6tan (% 67), loaldian zehar espasmoak eman ziren ia etengabe, eta horrek entzefalopatia epileptikoarekiko kezka sortu zuen (Tristan et al., 2019).

KCNQ2 duten pazienteetan, ia guztiei eragiten dieten desgaitasun kognitiboez gain, haur askok mugimendu errepikakorrak, ikusmen-kontaktu txarra, autolesioak edo autismoarekin lotutako beste sintoma batzuk ere erakusten dituzte.

1.6. Kaltzioaren garrantzia

Kaltzio ioia zelula barneko mezulari garrantzitsuenetako bat da. Prokariotoetan edo eukariotoetan, ioi honen bidez hainbat jarduera erregulatzen dira, hala nola adierazpen genikoa, hazkunde zelularra, garapena, migrazioa, biziraupena eta heriotza. Egia esan, Ca^{2+}-k bizitza zelularraren alderdi ia guztietan du eragina. Horren arrazoia da, ingurune aldakorretara egokitzeko, zelulek seinalizazio-prozesuak egin behar dituztela eta seinalizazioa egiteko mezulariak behar dituztela.

Calcium effect on dynamics and stability of Kv7.2 channel

Mezulari hauen kontzentrazioa aldatu egiten da. Kinada extrazelular bati erantzuteko, kaltzio ioiaren kontzentrazio zitosolikoa handitu egiten, atseden-egoeran 100 nM inguru egotetik, 1 µM-ra. Fenomeno hau, boltai menpeko, hartzaile menpeko eta kaltzioaren menpeko TRP kanalen bidez ematen da, euren poroak irekitzen dituztenak, Ca^{2+} sarrera ahalbidetuz. Gainera, erretikulu endoplasmatikoak eta sarkoplasmatikoak kaltzioa askatzen dute ere, IP_3 edo rianodina bezalako bigarren mezulariek estimulatzen dituztenean.

Zelulek beren energiaren zati handi bat inbertitzen dute Ca^{2+}-en kontzentrazioan aldaketak sortarazteko. Molekula konplexuak ez bezala, Ca^{2+} ezin da kimikoki aldatu. Beraz, Ca^{2+} kontrolatzeko, zelula kelatzailetan mantendu, konpartimentalizatu edo zelulatik askatu behar dute. Ehunka proteina Ca^{2+}-rekin lotzeko egokitu dira, afinitate-tarte zabal bat erakusten dutelarik (nM-tik mM-ra), kasu batzuetan Ca^{2+}-ren kontzentrazioa murrizteko soilik, eta beste batzuetan prozesu zelularrak abiarazteko. Ca^{2+} seinaleztapenaean duen garrantzia estuki lotuta dago afinitate-tarte zabal horrekin.

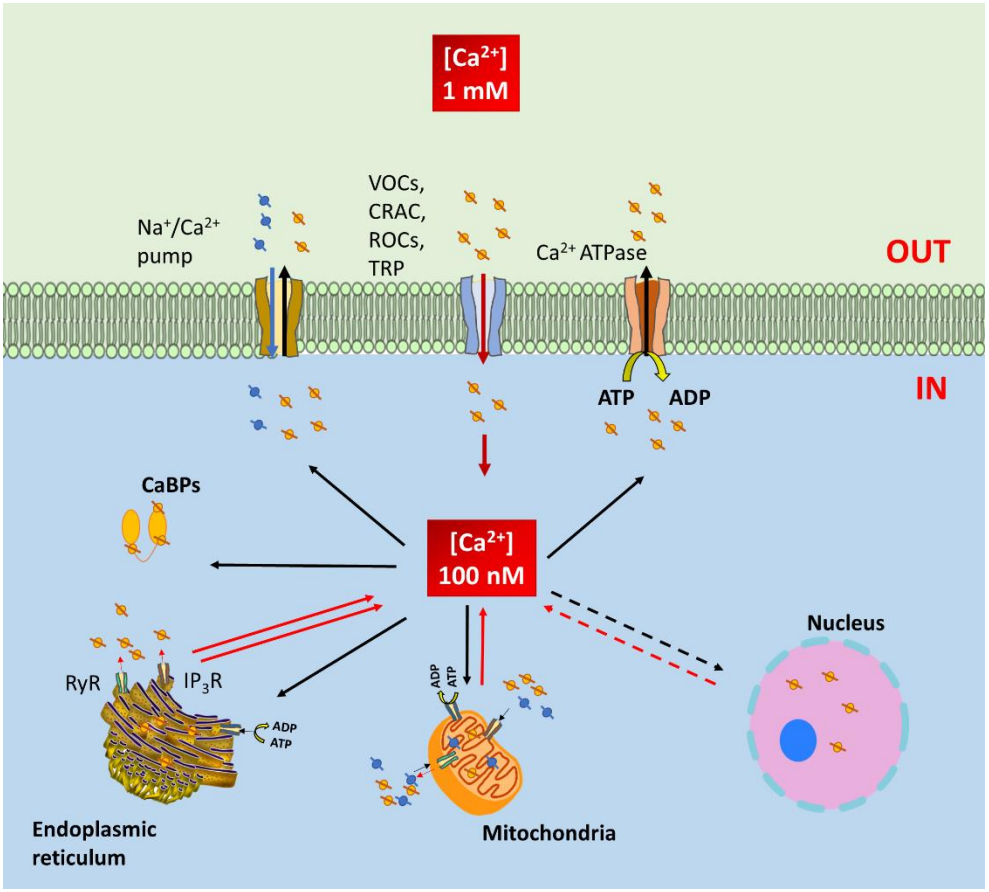

1.14 irudia. Kaltzioaren homeostasia zeluletan. Estimulu baten ondoren, Ca^{2+}-ren kontzentrazioa azkar handitzen da, boltai menpeko Ca^{2+} kanalaen, hartzaileak operatutako kanalen (Receptor Operated channels, ROC), kaltzioren askapenagatik aktibatutako kanalen (Calcium Release-Activated Channels, CRAC) edo potentzial iragankorreko kanalen (Transient Receptor Potential Channels, TRP) bidez. Gainera, Ca^{2+} gehiago aska daiteke zitoplasmara inositol 1,4,5-trifosfatoaren (IP_3P) edo Rianodinaren (RyR) hartzaileak aktibatuz. Atsedenean, Ca^{2+}-aren mailak < µM mailetan mantentzen dira, mintz plasmatikoan, erretikulu endo/sarkoplasmatikoan eta mitokondrietan dauden Ca^{2+} -ATPasak eta Na^+/Ca^{2+} trukatzaileei esker. Poro nuklearrak aldiro irekitzen dira eta Ca^{2+} mailak moteltzen lagun dezakete.

1.6.1. Kalmodulina eta Kalmodulina lotzeko domeinuen estruktura

Ca^{2+} proteina-kelatzaile nagusienetako bat E-F esku domeinua da (horrela deitzen zaie parbalbuminaren E eta F eskualdetan aurkitu zirelako) (Nakayama eta Kretsinger, 1994), ehunka proteinatan agertzen dena. Helize-giro-helize-motiboak ohikoak dira proteina askotan, boltai-menpeko sentsoreetatik, DNA lotzeko proteinetara. E-F eskuko helize-giro-helize motiboetan, negatiboki kargatutako oxigeno atomoek Ca^{2+} lotzen dute ~ 12 aminoazidoko eremu baten barruan, bi α-helize ortogonalen artean.

E-F esku bakar batek, N-muturrean helize bat (E helizea) dauka, ondoren bobina txiki bat eta C-muturrean beste helize bat (F helizea). Egitura honek antzekotasun berezia du esku batekin, non hatz erakusleak F helizea irudikatzen duen, hatz lodiak E helizea eta gainerako hatzek Ca^{2+}-a lotzeko begizta (1.17 irudia).

E-F-dun proteina guztiak kaltzioa lotu badezakete ere, mekanismo ezberdinak erakusten dituzte. E-F eskuen Ca^{2+}-rako afinitateak ~ 100,000 aldiz aldatzen dira, hainbat faktoreren arabera. Kaltzioa lotzeko proteina (CaBP, Calcium Binding Protein) batzuek (parbalbumina, karetikulina, kalbindina, etab.) Ca^{2+} lotu ondoren ez dute konformazio-aldaketarik jasaten, eta garrantzia nagusiagoa dute indargetzaile funtzio batekin seinaleztatze funtzioarekin baino. Beste batzuek, ordea, "kaltzio sentsore errealtzat" hartzen direnak, Ca^{2+} loturaren ondoren aldaketa estrukturala pairatzen dute, kaltzio seinaleztapena dekodetzen duena: lehenik, Ca^{2+} CaBPrekin elkartzen da bere egitura irekiz, itu-proteina batentzako interakzio gune bat erakutsiz, eta, bigarrenik, CaBP itu-proteinarekin lotzen da bere egitura aldatuz. Hala ere, ikusiko dugunez, CaBP proteina guztiek ez dute Ca^{2+}-rik behar euren itu-proteinekin elkarreragiteko.

CaM ez ezik, CaBPs horien guztien artean, bi talde nagusi dira garrantzitsuak funtzio neuronalerako.

- Sinaptotagminak: Mintz-plasmatikoan kokatuta dauden proteina hauek besikula sinaptiko eta jariatzailearekin lotuta daude. Bi C2 domeinuz osatuta daude, eta 3 Ca^{2+} ioi lotu ditzakete afinitate

nahiko baxuarekin (Kd> 10 µM). Lotura-prozesu horrek mintzaren proteina eta lipidoak elkarrekin koordinatzea eskatzen du.

- Kaltzio-sentsore neuronalak (NCS): CaM-rekin erlazionatuta daude. Lau E-F esku dituzte, baina guztiak ez dira funtzionalak. CaM ez bezala, konformazio trinkoa dute Ca^{2+}-arekin lotzen direnean, eta konformazio irekia, kaltziorik ez dutenean. Beste motibo batzuk ere badituzte, mintzera lotzea ahalbidetzen dutenak.

CaM gehien ikertutako Ca^{2+} sentsore proteina da, ziurrenik Ca^{2+}-aren seinaleztapenean duen garrantzi ebolutiboagatik. 1.500 milioi urteko eboluzioan oso gutxi aldatu da eta, gainera, gizakiengan hiru kromosoma ezberdinetatik abiatuta transkribatzen da (Abzhanov et al., 2006). Proteina azido oso disolbagarria, termoegonkorra eta txikia da (pI ~ 4), 148 hondakinetakoa (lehen metionina ez dago zenbakituta), eta zelula guztietan adierazten da.

CaM, Ca^{2+} detektatzeko erabiltzen duen mekanismoa, E-F eskuen bidezkoa da (Grabarek, 2006; Kawasaki & Kretsinger, 1994). Lau E-F esku motibo ditu, Ca^{2+}-rekin lotzeko: E-F (1) eta E-F (2), N-lobuluari lotuak, eta E-F (3) eta E-F (4), C lobuluari lotuak. Bi domeinuak tarteko sekuentzia malgu baten bidez lotuta daude, lotailu bezala ezagutzen dena (Babu et al. 1988). Horregatik CaM-k pisu baten forma du (Meador et al., 1992).

CaM-ren E-F eskuek Ca^{2+}-arekiko afinitate ezberdinak dituzte, eta haien lotura-afinitateak aldatu egiten dira sarritan, itu-proteinekiko elkarrekintzaren ondorioz. Ca^{2+}-arekin lotura erlazionatuta dago azalera hidrofoboaren osaera eta esposizioarekin. Hondakin hidrofobikoak, oro har metionina dutenak, itu-proteinen eskualde anfipatikoen inguruan biltzen dira.

1.6.2. Kalmodulinaren papera Kaltzioaren seinalizazioan

CaM-k prozesu zelular askotan parte hartzen du, non zelularen barruko kaltzio mailak detektatzen dituen eta bere helburuetan kaltzio seinaleak transmititzen dituen. Eginkizun horien guztien artean, frogatu da CaM-k prozesu inflamatorioetan, erantzun immunean, muskulu lauaren uzkurduran, zelulen zatiketan eta ugaritzean, adierazpen genikoan, hormonen jariaketan, neurotransmisoreen jariaketan, memorian eta epe labur eta luzeko apoptosian parte hartzen duela.

Ca^{2+}-a CaM-rekin elkartzen denean, kalmodulina domeinuen forma aldatu egiten da, proteinen autoinhibizioa arintzeko, toki aktiboak birmoldatzeko eta proteinen dimerizatzeko gaitasuna handituz. Ehunka proteinek dituzte CaM lotzeko domeinuak. Lotune hauetan oinarrizko aminoazido hidrofobikoak aminoazido aromatikoen artean nahastuta egoten dira.

1.6.2.1. K_V7:CaM Konplexua

2002an, CaM- K_V7 kanalen proteina osagarri bat zela frogatu zen (Yus-Nájera et al., 2002). K_V7 kanalek CaM-rekin lotzeko bi eremu ezberdin dituzte: bata A helizean dago eta bestea B helizean (Yus-Nájera et al., 2002), eta 135 aminoazidoz osatutako lotailu baten bidez konektatuta daude (1.15 irudia). Lotailu horren barruan beste helize bat deskribatu da, TW helizea.Helize hau, CaM-rekin lotu daitekeela iradoki bada ere (Gomis-Perez et al., 2015), oraindik ez da esperimentalki frogatu.

CaM- funtsezkoa da M-korronte funtzionala sortzeko (K_V7.2/K_V7.3) zelula heterologoetan (Gamper eta Shapiro, 2003) eta neuronetan (Shahidullah et al., 2005). Uste da, halaber, neurona sinpatikoetan, K_V7.2/7.3 heterotetrameroen Ca^{2+} menpeko inhibizioa ematen dela, bradikinina edo UTP bidez (Selyanko eta Brown, 1996) (Gamper eta Shapiro, 2003). Frogatu da, halaber, CaM-k, K_V7 kanalen irekitzean eragina duela, K_V7.2, K_V7.4 eta K_V7.5 korronteak ezabatuz, baina K_V7.1 eta IK_S (K_V7.1 + KCNE1) kanalen jarduera estimulatuz (Gamper eta Shapiro, 2003). CaM- eta K_V7.1 kanala elkartzea beharrezkoa da ere C-muturra behar bezala tolesteko, eta, halaber, kanalak mintz plasmatikora garraiatzeko (Shamgar et al., 2005).

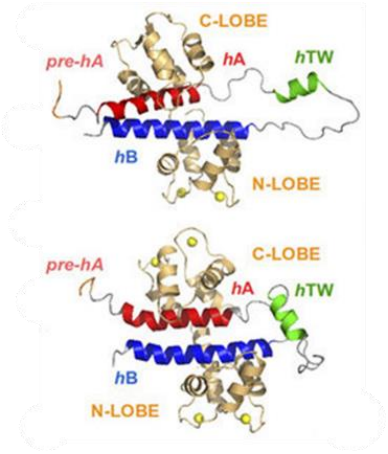

1.15 irudia. CaM/K_V7.2-*h*AB edo holoCaM/K_V7.2*h*AB konplexuaren irudikapena. CaM proteina (laranja); A prehelizea (pre-*h*A) (purpura), K_V7.2 kanaleko poroaren 6. segmentua C-mutur intrazelularrarekin lotzen duena; A helizea (gorria); Ca^{2+} ioiak esfera gisa irudikatzen dira. Kolore kode bera erabiltzen da holoCaM/KV7.2-*h*AB konplexuaren irudikapenetarako. Bernardo-Seisdedos et al., 2018.

CaM-rekin lotzeko gaitasuna galdu duten mutanteetan ezin izan zuten korronterik neurtu (Saimi eta Kung, 2002), Ca^{2+} konduktantzia txikiko Ca^{2+} bidez aktibatutako K^+ kanaletan (SK) gertatzen den bezala (Xia et al., 1999). Horregatik, CaM- K_V7.2/3 kanalen C-muturrari lotutako azpiunitate integral gisa definitu zen. Hala ere, eredu hori zalantzan jarri da azken urteotan; izan ere, K_V7.2 (Gomez-Posada et al., 2011) edo K_V7.4 kanal mutatuak (Sihn et al., 2016), CaM-rekin lotzeko gai ez direnak, mintz plasmatikora heldu eta funtzionalak zirela frogatu zuten. Laburbilduz, itxuraz, CaM-ri ainguratzea M-kanalaren funtziorako baldintza absolutua ez bada ere, 2007an, gure laborategiak lehen aldiz erakutsi zuen CaM-k funtsezko papera jokatu behar duela K_V7.2 kanalen

trafikoan. Izan ere, Konbultsio Neonatal Onbere Familiarrean (BFNC), A eta B helizeetan emandako mutazioek, CaM-rekin elkarketa ahultzen dutela ikusi zen, eta horrek korronte murriztuak sortzen dituela, K_V7.2 azpiunitateak erretikulu endoplasmikora (ER) atxikitzearen ondorioz. Dena dela, kanal kopuru txiki batek mintz plasmatikora heltzea lortzen zutela frogatu zen (Etxeberria et al., 2008).

Gainera, CaM-ren paper kritikoa frogatu zen K_V7.2 proteinen zelula barneko garraioan. Proposatu egin da CaM-k, egitura "aktiboa" behar duela, K_V7.2-ren azpiunitateak erretikulu endoplasmatikotik irtetea sustatzeko (Alaimo et al., 2009). Ondoren, hipokanpoko neuronetan ere ikusi zen hori, non CaM-k K_V7.2/K_V7.3 kanalen trafikoa eta aberastea erregulatzen duen axonetan (Liu et al., 2014). CaM-ren lotura kanal tetramerikoaren azpiunitate berean edo ezberdinetan gerta daiteke (Sachyani et al., 2014). CaM- kanalari lot dakioke, bai Ca^{2+}-a dagoenean, bai ez dagoenean ere (Alaimo et al., 2013). Gure taldeak deskubritu zuen K_V7.2-ren A helizeak CaM-ren C-lobuluarekiko preferentzia nabarmena duela, eta B helizeak CaM-ren N-lobuluarekiko (Alaimo et al., 2014) (1.15 irudia). Gainera, antolamendu hori konplexu kristalografikoetan ere ikusten da, K_V7.1 (Sachyani et al., 2014), K_V7.4, K_V7.5 (Chang et al., 2018) eta K_V7.2/K_V7.3 kimera batean (Strulovich et al., 2016). Antolamendu hori agerikoa da ere K_V7.2*h*AB-CaM erresonantzia magnetiko nuklearreko konplexuan (Bernardo-Seisdedos et al., 2018) eta K_V7.1eko (Sun eta MacKinnon, 2017) crio-EM teknikaz ebatzitako estrukturan ere.

1.6.3. Kaltzioa lotzen duten E-F eskudun proteina familia

Proteina familia hau Ca^{2+}-ari modu itzulgarrian eta espezifikoki lotzeko gai diren proteinek osatzen dute. E-F eskuaren motiboa proteinetan aurkitzen den kaltzioa biltzeko motiborik arruntena da, 3. kapituluan xehetasun handiagoz eztabaidatuko dugun bezala.

Kaltzioarekin biltzeko proteinak (Calcium Binding Protein, CaBP) normalean zitoplasman edo erretikulu endoplasmikoaren barruan egoten dira. Kasu batzuetan, Ca^{2+} kapaza da zuzenean CaBP baten funtzioa erregulatzeko, hala nola PKC, PI3K, PLC, kalpaina edo kaltzineurina. Hala ere, CaBPek bitartekari baten papera izaten dute maiz, non Ca^{2+}-aren kontzentrazioa senti dezaketen eta seinalea euren itu-proteinei jakinarazi.

CaBP delakoek Ca^{2+} detektatzen dute E-F eskua izeneko helize-giro-helizezko egitura-elementu oso hedatu batengatik (Grabarek, 2006; Kawasaki eta Kretsinger, 1994).

Neurona bakar batek jasan ditzakeen kaltzio fluktuazio guztiak kontuan hartuta, E-F eskuko proteinen familiak eboluzionatu egin du kaltzio kontzentrazio tarte zabal bat detektatzeko, 10^{-9} eta 10^{-5} M arteko afinitateak deskribatu direlarik. Gainera, E-F eskuen kopurua ere aldatu egiten

da proteina batetik bestera (lau ditu CaM-k, bost kalpainak eta sei kalbindinak), baita E eta F helizeen luzera ere.

1.6.4. Kalmodulina

Kalmodulina E-F eskuak dituen gehien ikertu den proteina da. CaM proteina azido oso disolbagarria da, termoegonkorra eta txikia (pI ~ 4), 148 hondakin eta 16,8 kDa dituena. Ez da asko aldatu eboluzioan zehar. Izan ere, CaM-ren aminoazidoen sekuentzia berdina da ornodun guztientzat. Zelulek, sarri, ~ 10 µM-tako CaM kontzentrazio zitosilikoa izaten dute. Neuronetan, ordea, kontzentrazio hori 100 µM-raino iristen da. Zelula gehienetan, kalmodulinaren itu-proteina kopuruak CaM berarena gainditzen du, eta CaM-en gehiengoak konplexu batean parte izaten dira (Villarroel et al., 2014).

Aurretik esan dugun bezala, CaM-k prozesu zelular askotan parte hartzen du. Prozesu horietan, zelularen barruko kaltzio-mailak detektatzen ditu eta itu-proteinei kaltzio-seinaleak transmititzen die, hala nola, hantura-prozesuetan, erantzun immunean, muskulu lauaren uzkurduran, zelula-zatiketan eta -ugaritzean, adierazpen genikoan, hormonen jariaketan, neurotransmisoreen jariaketan, epe labur eta luzerako memorian eta apoptosian. Gainera, CaM-k proteina asko (entzimak, zitoeskeletoko proteinak, garraiatzaileak, hartzaileak eta kanal ionikoak) zuzenean aktibatzen eta erregulatzen ditu (1.16 irudia) (1.3 taula). Hainbat kanal ionikoren modulazioan parte hartzen du ere, zuzenean nahiz zeharka, boltai-menpeko Na^+, K^+ eta Ca^{2+} kanalak, L motakoak eta RyR2 kanalak barne.

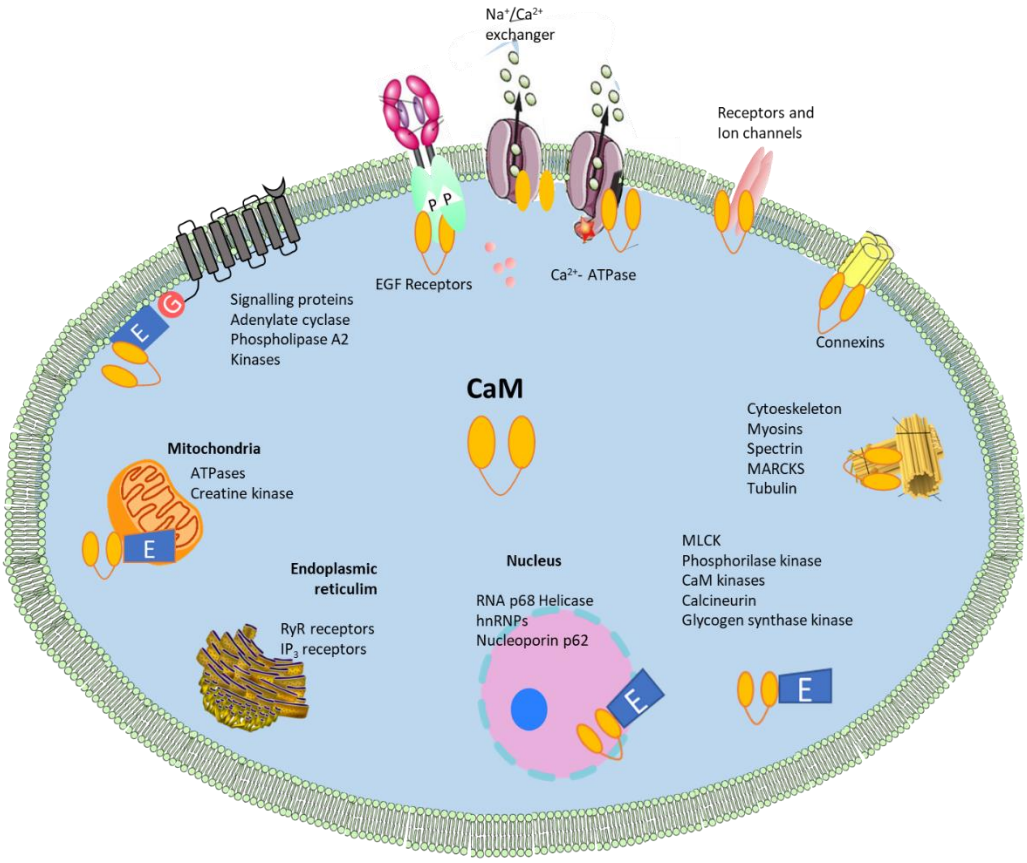

1.16 irudia. CaM-k erregulatutako proteinen sarea. CaM-k hainbat prozesu zelular erregulatzen ditu.

Type	Proteins
Kinases	Myosin light-chain kinases (MLCKs)
	Ca^{2+}-CaM dependent protein kinases (CaMKs)
	Phosphorylase kinases
	Phosphofructokinases
	G-protein coupled receptor kinases s(GRKs)
	NAD+ kinases
	Glycogen synthase kinases
Other enzymes	Calcineurins
	Adenylate cyclases
	Glutamate descarboxylases
	Nitric oxide synthases (NOS)
	Phosphodiesterase
Transporters	Ca^{2+}-ATPases
	Na^{+}/Ca^{2+} exchangers
Reticular receptors	Inositol 1,4,5-triphosphate receptors (IP_3P)
	Ryanodine receptors (RyR)
Ion channels and receptors	Small conductance calcium-activated potassium channels (SK, IK)
	Cyclic nucleotide gated channels (CNGs)
	Transient receptor potential channels (TRPs)
	NMDA receptors
	Ca_V channels (L, P/Q, R)
	Na_V channels
	K_V channels
	Epidermal growth factor receptor (EGFR)
	Connexins (GAP junctions)
CaM reservoir proteins	Neuromodulin
	Neurogranin
	Regulator of calmodulin signalling (RCS)
Genes expression systems	RNA helicase p68
	Heterogeneous nuclear ribonucleoproteins (hnRNPs)
	Nucleoporin p62
	Caldesmon, Spectrin. Syntrophin, Dystrophin, PEP-19
Cytoeskeleton and other proteins	MAP2, Adducin, Marck, Tubulin, Myosin, Actinin, etc.

1.3 taula. CaM-ren bidez erregulatutako proteinen adibideak.

Ikusi dugunez, CaM- gai da proteina kopuru handi batekin elkarreragiteko, baina, nola da posible proteina bakar batek proteina mota horiek guztiak ezagutu eta horiekin elkarreragiteko? Aurrerago ikusiko den bezala, bere egituraren moldakortasuna da giltzarria.

1.6.4.1. Arkitektura

CaM- bi domeinu globularrez osatuta dago, ziur asko gene bikoizketa gertaera baten ondorioz sortu direnak. Domeinu bakoitzak (N- eta C-muturrak; N-lobulua eta C-lobulua ere deitua) Ca^{2+}-rekin lotzeko bi E-F esku motibo ditu. Bi lobuluak konektore oso malgu batez lotuta daude, eta horrek plastikotasun estrukturala ematen dio CaM-ri. Gainera, konektore honek lobulu bakoitzari autonomia ia osoa ematen dio tolesteko, Ca^{2+}-arekin bat egiteko edo itu-proteinekin elkarreragiteko. Plastikotasun honek, beste proteina kopuru handi batekin elkarreragiteko gaitasuna ematen dio. Iradoki denez, CaM-ren egiturazko plastikotasun hori, itu-eskualde asko berez desordenatuta egotearen emaitza da, CaM-rekin bat egitean tolesten direnak (Radivojac et al., 2006; Wall et al., 1997).

Gainera, bi lobuluen egiturak apur bat ezberdinak dira: N-lobuluak konformazio oso trinkoa du, C lobuluak, berriz, konformazio erdi irekia du, non hondakin hidrofobo batzuk disolbatzailearen eraginpean dauden. Horri esker, kaltziorik ez dagoenean, CaM- itu-proteinari lotzen lagun dezake SK2, neurogranina, boltai-menpeko Ca^{2+} eta Na^{+} kanaletan gertatzen den bezala. Ca^{2+}-ari lotzean, apo-CaM-k egitura-berrantolaketa handia jasaten du, bere konformazioa itxia izatetik irekia izatera aldatuz (Holo-CaM). Ondorioz, aldez aurretik ezkutuan zeuden hondakin hidrofobikoak erabat agerian geratuko dira. Gainera, lehen desordenatuta zegoen lobuluen arteko lotailuak, E-F (2) eta E-F (3) eskuak konektatzen dituena, α helize handi bat osatuko du (1.17 irudia).

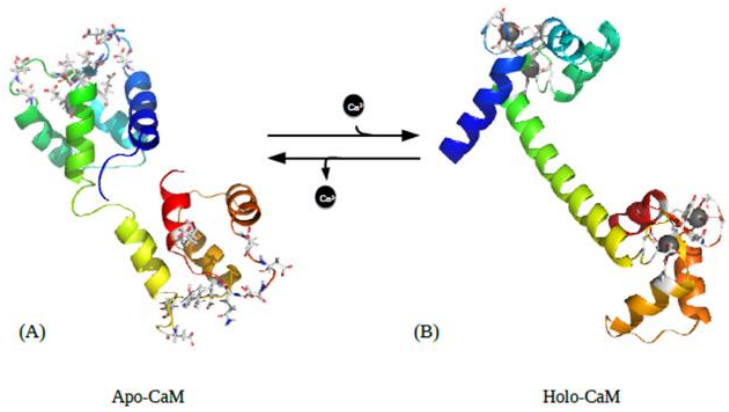

1.17 irudia. CaM egituraren berrantolaketa, Ca^{2+}-n oinarrituta. (A) Apo-CaM (B) Holo-CaM. CaM-ren N-lobulua eta C-lobulua konektore malgu batez lotuta daude. Konektore hori ez dago egituratuta Ca^{2+}-rik ez dagoenean, eta haren presentzian egituratuta dago. Alboko kate grisean, E-F eskuak osatzen dituzten erresiduoen atomoak nabarmendu dira.

1.6.4.2. Kalmodulina-helburuen aintzatespena

Lehen aipatu dugun bezala, CaM-k kaltzio sentsore bat bezala jokatzen du itu-proteina askorentzat, Ca^{2+} seinalea zelula-prozesu batean itzultzen dutenak. Oro har, itu-proteinen CaM-ren lotura domeinuak, oinarrizko aminoazidoz eta aminoazido hidrofoboz osatutako 16-30 aminoazidoetako sekuentziak dira (1.18 irudia). Orokorrean, egitura helikoidal anfipatikoa hartzen dute, baina horietako batzuek egitura desordenatua dute. Hala ere, behin CaM-rekin elkarreragiten dutenean, sarri, α konfigurazio helikoidala hartzen dute ere. Gainera, CaM-k bere ituak identifikatzen ditu "puntu bero" izeneko aminoazido batzuengatik, sarritan Van der Waals eta beste interakzio mota batzuk gertatzen diren gune hidrofobikoetan agertzen direnak (1.19 irudia).

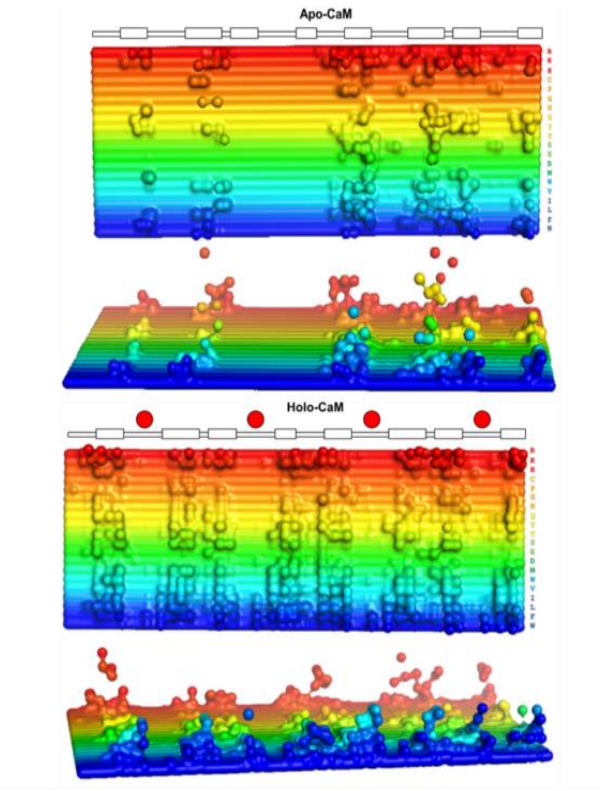

1.18 irudia. CaM-ren aminoazido bakoitzaren interakzio-lehentasuna, itu-peptidoen aminoazidoekin. Ukipen-azaleraren eremuaren airetiko eta alboko bista (z ardatza). 3D grafikoak, itu-aminoazidoak (y ardatza), apo-CaM edo holo-CaM ornodunen erresiduo bakoitzarekin kontaktuan (x ardatza). Ca^{2+}-ren lotura-begiztak esfera gorriek adierazten dituzte, eta CaM -ren α-helizeak grafikoaren goiko aldean kokatuta daude. Villarroel et al., 2014.

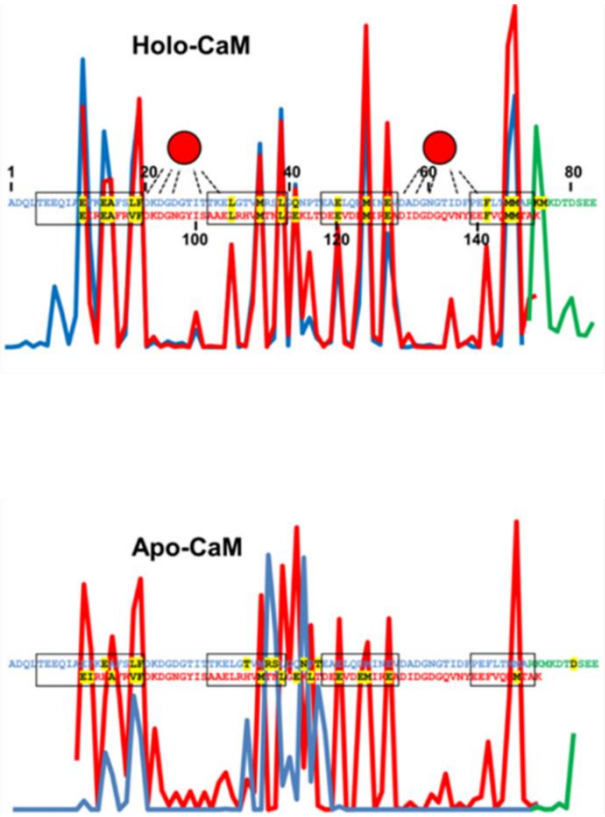

1.19 irudia. CaM azaleraren batez besteko kontaktua itu-proteinekin. Zortzi "puntu bero" definitzen dira, CaM-ren α-helizeak koadro gisa irudikatzen dira. Grafikoek holo-CaM eta apo-CaM-ren itu-proteina batekin batez besteko ukipen azalera unitatea erakusten dute. Gorriz: C-lobuluko aminoazidoak, urdinez: N-lobulukoak. Ca^{2+}-a esfera gorriz irudikatzen da, eta hauen lotura-aminoazidoak lerro etenen bidez adierazten dira. Itu-proteinarekin elkarreragiten duten aminoazido nagusiak grisez adierazita daude. Lerro berdeak lobuluen arteko lotailu malguaren bi hondakin adierazten ditu (Lys75 eta Met76), itu-proteinarekin loturan ekarpen esanguratsuak egiten dituztenak. E-F eskuen arteko bi lotailuek ere ekarpen esanguratsua egiten dute, Gln41 (N-lobuluan) eta Glu114 (C-lobuluan).

CaM-k bere itu-proteinaren inhibitzaile edo aktibatzaile gisa jardun dezake. Frogatu da bere kontrako funtzioak dituzten proteinak erregulatzen dituela ere (adibidez, kinasak eta fosfatasak). CaM-rentzat lotesle motibo ezberdin ugari daudenez, ez da erraza erabat sailkatzea. Hala ere, gehienak bi taldetan bana daitezke: holo-konfigurazioan lotzen direnak eta apo-konfigurazioan lotzen direnak:

1.6.4.2.1. Ca^{2+}-aren menpeko lotura

CaM-k ezagutzen dituen motiboak, oro har, 20 hondakineko helize txikiak dira, gutxi gorabehera, non oinarrizko aminoazidoak eta hidrofoboak nagusitzen diren. Askotan, "ainguraketa" izeneko bi erresiduo hidrofobiko behar dira CaM- ezagutu eta lotu ahal izateko. Ainguraketa-erresiduo bi horiek elkarri eragiten diote CaM-ren bi lobuluetako bati. Motibo hauek, erresiduo hidrofobiko horien artean aminoazidoak zenbakituz sailkatu dira. Adibide batzuk 1.4 taulan ikus daitezke.

Salbuespenak egon arren, Ca^{2+}-aren menpeko itu-proteinen CaM-ri lotzeko prozesuak bi konformazio-aldaketa ditu (1.20 irudia). Lehenik, apo-CaM kaltzio ioiekin batzen da, eta horrek aldaketa konformazionala eragiten du apo-CaM konfiguraziotik holo-CaM-era. Gero, CaM-k hondakin hidrofoboak azaleratu ahala, itu-proteinari lotzeko motiboak ezagutzeko gai da.

Ondoren, CaM-k itu-proteinarekin interakzionatzen du eta "besarkatu" egiten du. Gainera, proteina mota batzuetan, efektu bilgarri honek, itu-proteinak, α-helize baten konformazioa hartzea eragin dezake.

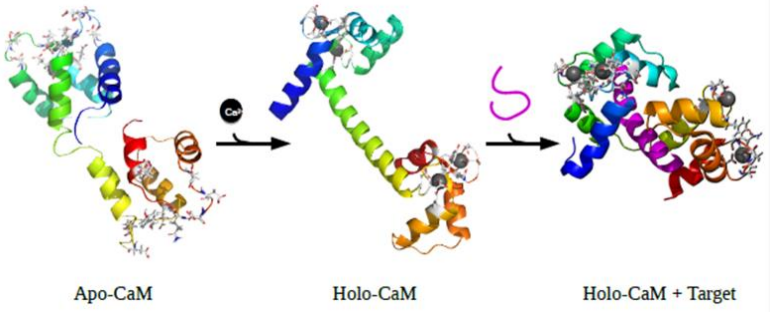

1.20 irudia. CaM-ren konplexuen eraketa kaltzioaren menpe. Apo-CaM (PDB: 1CFC) Ca^{2+} ioiekin batzen da, eta horrek aldaketa konformazionala eragiten du (PDB: 3CLN). Aminoazdido hidrofobikoak esposiziopean daude eta itu-proteinarekin lotura gertatzen da (PDB: 2JZI).

1.6.4.2.2. Ca^{2+} ez-menpeko lotura

Ca^{2+}-aren menpekotasunik gabe CaM-rekin lotzen diren itu-proteina askok IQ motiboa dute. Aurreko taldean ez bezala, IQ motiboa kontserbatu egin da ebaluzioan zehar, eta sekuentzia hau du: IQxxxBGxxxBxxX, non B oinarrizko aminoazidoa (Lys edo Arg) den eta x aminoazido hidrofoboa (Phe, Ile, Leu, Val, Trp edo Tyr) (1.4 taula). IQ motiboa duten itu-proteinek apo -CaM konfigurazioarekin elkarreragiteko joera dute, nahiz eta kasu batzuetan holo-konfigurazioan ere elkartu daitezkeen.

Informazio gutxiago dago apo-CaM-rekin lotzen diren konplexuei buruz. Hipotesi onartuena 1.21 irudian azaltzen da. Itu-proteina CaM-rekin lotu ondoren, C-lobuluak Ca^{2+}-arekiko duen afinitatea handitu egiten da, eta ondorioz, Ca^{2+}-a lotzen zaio, proteina-proteina konplexua egonkortuz. Gainera, N-lobulua, oraindik libre dago Ca^{2+}-ari edo beste motibo bati lotzeko.

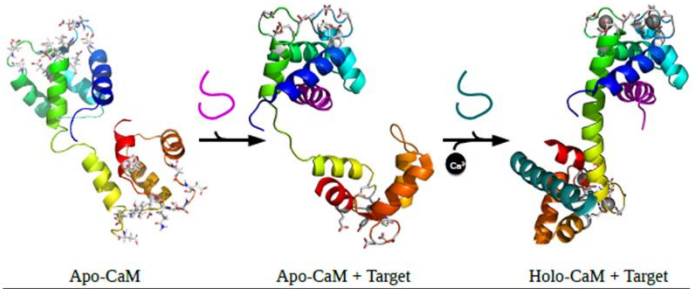

1.21 irudia. CaM eta itu-proteinaren konplexuen eraketa kaltziorik ez dagoenean. Apo-CaM-k (PDB: 1CFC) konformazio-aldaketa txikiagoa izaten du itu-proteina bati (SK2) lotzen zaionean (PDB: 1G4Y). Hala ere, Ca^{2+}-a batu ondoren, aldaketa konformazional drastiko bat gertatzen da, honen bidez bigarren helburura batu daitekeelarik (PDB: 3SJQ). Azken egitura honetan, irudikatu ez den dimero bat eratzen da.

Motif name	Motif sequence	Known targets
1-5-8-14	(FILVW)xxx(FAILVW)xx(FAILVW)xxxxx(FILVW)	Sodium calcium exchanger
1-8-14	(FILVW)xxxxxx(FAILVW)xxxxx(FILVW)	Neuronal nitric oxide synthase
1-8-14 basic	(RK)(RK)(RK)(FILVW)xxxxxx(FAILVW)xxxxx(FILVW)	Myosin light chain kinase
1-14	(FILVW)xxxxxxxxxxxx(FILVW)	Ryanodine receptor 1
1-5-10	xxx(FILVW)xxxx(FAILVW)xxxx(FILVW)	Heat shock protein 90
1-5-10 basic	(RK)(RK)(RK)(FAILVW)xxxx(FILV)xxxx(FILVW)	CaM dependent kinase II
1-10	(FILVW)xxxxxxxx(FILVW)	Inositol triphosphate 3 kinase
1-16	(FILVW)xxxxxxxxxxxxxx(FILVW)	CaM dependent kinase kinase
IQ	(FILV)Qxxx(RK)Gxxx(RK)xx(FILVWY)	L-type calcium channel
IQ-like	(FILV)Qxxx(RK)xxxxxxxx	Voltage-gated sodium channel

1.4 taula. CaM- ezagutzen duten proteina-motibo ezberdinak (Ishida & Vogel, 2006-tik eraldatuta).

1.6.5. CaM eta gaixotasuna

Ornodunetan, hiru CaM gene daude genoman (CALM1-3), CaM proteina berdinak kodifikatzen dituztenak. Kontuan hartuta eboluzioan zehar aminoazidoen sekuentzia ez dela aldatu ornodunen CaM-rentzat, pentsa genezake CaM-ren mutazioek zelulen funtzionamendu okerra ekarriko luketela eta, ziurrenik, zelulen heriotza. Hala ere, azken urteotan, hamar CaM mutazio gaixotasun arritmogenikoekin lotu dira (Urrutia et al., 2019) (1.22 irudia), Kalmodulinopatia izenekoak. Ikerketa batean, 74 subjektu gaixoren sekuentzia aztertu da, CALM1 (n = 36), CALM2 (n = 23) edo CALM3 (n = 15) geneetan (Crotti et al., 2019). Ikertutako kasuen % 86,5-a (n = 68) sintomatikoak izan ziren, eta 10 urtera metatutako hilkortasuna % 27-koa izan zen. Bi fenotipo

nagusiak hauek dira: QT luzearen sindromea (LQTS; CALM-LQTS, n=36,49) eta takikardia bentrorular polimorfiko katekologaminergikoa (CPVT; CALM-CPVT, n=21,28%). CALM-LQTS duten pazienteek QTc tarte oso luzeak dituzte (594 ± 73 m), prebalentzia handia (% 78), gaixotasuna hasteko batez besteko adina 1,5 urtetakoa, hilgarriak izan daitezkeen arritmien prebalentzia handia (% 78) eta terapiei erantzun txarra erakusten dute. CaM-rekin lotutako beste fenotipo batzuk fibrilazio bentrikular idiopatikoa (FIV, n = 7), azaldu gabeko bat-bateko heriotza (n = 4), LQTS-ren ezaugarri berdinak (n = 3) eta fenotipo neurologiko nagusia (n = 1) dira (Crotti et al., 2019).

Nabarmentzekoa da mutazioen % 80-a C-lobuluan daudela, zehazki E-F (3) eta E-F (4) eskuetan (1.22. irudia).

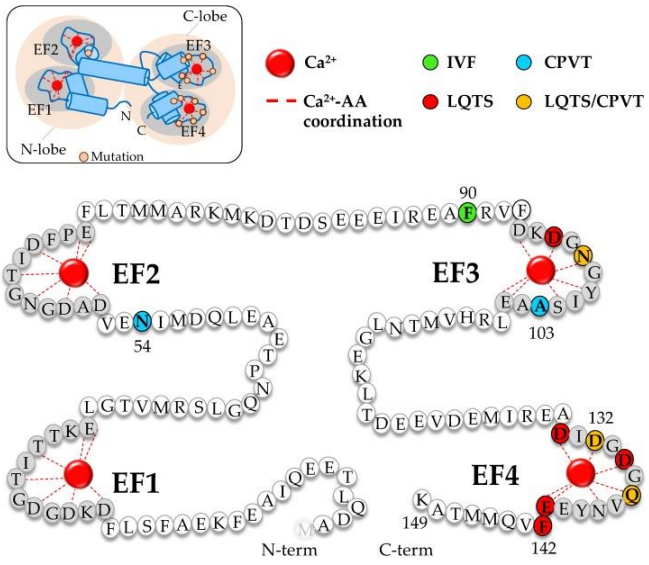

1.22 irudia. Kalmodulinopatiak sortzen dituzten mutazioen kokapena. Goiko ezkerreko panela: CaM egituraren irudikapen eskematikoa, kalmodulinopatietan aurkitutako mutazioak erakusten dituena, gaixotasunaren arabera kolore kode bat erabiliz. Panel nagusian eremu grisek E-F eskuak nabarmentzen dituzte. Gaixotasunarekin lotutako mutazioak hauek dira: berdea (FIV: fibrilazio bentrikular idiopatikoa), urdina (TVPC: takikardia bentrikular polimorfikoa katekolaminergikoa), gorria (LQTS: QT luzeko sindromea) eta laranja (biak: LQTS/BrS). Urrutia et al., 2019.

2. HELBURUAK

Doktorego tesi honen helburuak honako hauek dira:

1. CaM/Kaltzioaren erregulazioan, K_V7 kanaletako C-muturreko A eta B helizeen arteko lotailuaren papera ebaztea.
2. Tetramero batean azpiunitateen arteko trukea eta D helizearen ekarpena CaM-ren lotura-konfigurazioan (zuzena eta zeharkakoa) aztertzea. Gainera, Ca^{2+}-ak tetrameroen egonkortasunean duen eragina ebaluatzea.
3. Kaltzioak K_V7 kanalen tetrameroetan (A, B, C eta D helizez osatuta, CaM-rekin konplexuan) bultzatutako konformazio-aldaketa aztertzea FRET, EMN eta HS-AFM bidez.
4. Konplexuko kaltzio-estekiometria zehaztea eta E-F esku bakoitzak kaltzio-seinaleen transmisioan egiten duen ekarpena ikertzea.
5. Zitoplasmarantz hedatzen den eta CaM-rekin elkarreragiten duen S2/S3 lotailuaren garrantzi funtzionala eta Ca^{2+} seinaleen transmisioan duen eginkizuna aztertzea.

3. K_V7 KANALEN C-TERMINALEKO A ETA B HELIZEEN ARTEKO LOTAILUAREN PAPERA Ca^{2+}-AREN SEINALEZTAPENEAN

3.1 SARRERA

3.1.1. TW helizea

Gomis-Perezek eta bere lankideek, $K_V7.2$ kanalaren A eta B helizeen artean beste eskualde helikoidal bat zegoela frogatu zuten, CaM-ren menpeko erregulazioan eragina duena. Gehienezko D-CaM fluoreszentziaren eta ageriko lotura-afinitatearen arteko erlazioaren analisiak iradoki zuen leku horretako mutazioek CaM-$K_V7.2$. konplexuaren berrantolaketei eragiten dietela. Zelula osoen azterketa funtzionalak, gune hau, funtziorako funtsezkoa ez dela erakutsi zuen. Aitzitik, gune hau lagungarria da CaM-ren konfigurazio aktibo baten egonkortasuna mantentzeko (Gomis-Perez et al., 2015). TW gunearen barruan, B helizean edo A helizean CaM-rekin elkartzea eragozten duten mutazioek, kanal funtzionalak sortzen dituzte, baina ez zen funtziorik ikusi TW eta A helizea, edo TW eta B helizea aldi berean mutatu zirenean (Gomis-Perez et al., 2015).

Gainera, TW guneak SK2 kanalen C-lobuluaren TRS-arekin antza handia du. SK2-CaM konplexuan, C-lobulua TW motiboa besarkatzen ari da, IQ motiboa duten beste konplexu batzuetan ikusitakoaren oso antzeko antolamendua (Villarroel et al., 2014). Bitxia bada ere, SK2-ren CaM-ren lotura-domeinuaren egitura, CaM-ri lotuta ez dagoenean, eskualde helikoidal distortsionatu bat da, TWLIY sekuentzia zentrala barne hartzen duena. Gainontzeko molekulek, tolestura global egonkorrik ez duten bitartean (Wissmann et al., 2002).

$K_V7.2$ kanalen TW eskualdea baztergarria denez, ez dirudi paper garrantzitsu bat jokatuko duenik $K_V7.2$ CaM-ri lotzeko hasierako urratsetan.

$K_V7.1$:CaM egiturak IQ-motibo-apoCaM lotura tipikoa aurkezten du C-lobuluarekin, N-lobulua B helizea ainguratzen ari den bitartean (Sachyani et al., 2014) (Sun & MacKinnon, 2017).

3.1.2. *h*A eta *h*B helizeen arteko konektorea

Zoritxarrez, K_V7 familian ebatzitako egitura guztiak ez dira C-terminaleko A eta B helizeen arteko konektorearekin ebatzi, delezionatu egiten da proteinaren egonkortasuna handitzeko (Sachyani et al., 2014; Sun & MacKinnon, 2017; Bernardo-Seisdedos et al., 2018).

3.1.2.1. PIP_2 lotzeko domeinua

Fosfatidilinositol 4,5-bisfosfatoak (PIP_2) mintz plasmatikoan kanal ioniko askoren funtzioa erregulatzen du, M-motako K^+ kanalak barne (KCNQ, K_V7); hala ere, inplikatutako mekanismo molekularrak oraindik ez dira oso ezagunak.

A-B helizeen konektorea PIP_2 interakzionatzeko gune gisa identifikatu da, bai KCNQ2-rentzat, bai KCNQ3-rentzat (Hernández et al., 2008). Bereziki, "talde kationiko" bat (K452, R459 eta R461 KCNQ2n), KCNQ2 eta KCNQ3 A eta B helizeen arteko konektorean kokatua. Iradoki zen lotura elektrostatikoak eratzen zituela PIP_2 molekulen fosfato taldeekin (Hernández et al., 2008).

Bitxia bada ere, PIP_2-rekin lotutako domeinu guztien arteko konparazio batek sekuentzia-homologia oso mugatua erakusten du (% 10-30), baina funtsezko ezaugarri bat partekatzen dute: mintzaren barne-azalerara orientatutako oinarrizko aminoazido multzo batek elektrostatikoki polarizatutako egitura proteiko bat sortzen du, fosfoinositidekiko interakzioak ahalbideratu ditzakeena (Hernández et al., 2008).

Analisiak PIP_2 eta pH domeinuak lotzeko kontserbatutako sekuentzia motibo bat erakusten du, hau da, [R/k] - X - [R/k] -, non x edozein aminoazido den (Harlan et al., 1994). K_V7 kanalen AB helize-lotailuak ere antzeko motiboa du, [K452] - [S/p] -X4- [d/n] - [R459/k] -X- [R461] - [F/a] - [R463] ($K_V7.2$ sistemaren oinarrizko hondakinak zenbakituta daude), eta horrek egitura-mekanismo kontserbatuak iradokitzen ditu. Ondorio hori oinarri hartuta, fosfoinositidarekin lotzeko moduluen egitura ebatziak bat datoz zazpi harizpietako β- upel estruktura batekin, α-helize batez itxita daudenak (Ferguson et al., 2000; Lemmon, 2003) non barrilaren "muturra" lipidoarekin interakzioan diharduen (Hernández et al., 2008).

$K_V7.2$ egitura-ereduan, PIP_2-rekiko lotura-domeinua ere zazpi kateko A eta B helizeek mugatzen duten barril bat da. Begizta horretan oinarrizko hiru hondakinez osatutako nukleoak (R459, R461 eta R463) PIP_2 talde nagusiko fosfatoekin hidrogenozko loturak osatzen dituela uste da. Ereduak aurreikusten du erresiduo horien mutazioek biziki aldatzen dituztela egitura.

3.1.3. Försterren erresonantzia-energiaren transferentzian (Fluorescence resonance energy transfer, FRET) oinarritutako bio-sentsoreak

1992an lehen proteina-fluoreszentea aurkitu zenetik, fluoreszentzian oinarritutako biosentsoreak funtsezko bihurtu dira fisiologia zelularra, dinamika molekularra eta interakzio molekularrak monitorizatu eta identifikatzeko (Periasamy 2001). Förster Erresonantzia energiaren transferentzia (FRET), fluoroforo "emaile" batetik fluoroforo "hartzaile" batera erradiaziorik gabeko energia transferentzian oinarritzen den prozesu bat da. FRET saiakuntzek eremu hurbileko interakzio bat eremu urruneko seinale batean itzul dezakete, fenomeno biologikoak ikertzeko tresna paregabea, orain arte erabilitako mikroskopia optiko estandarrak baino erresoluzio handiagoa duena (Roy et al. 2008; Moerner eta Fromm, 2003). FRET-ak

aldaketa konformazional mikroskopikoak anplifikatzen ditu argi igorpenaren bidez, sentsore batekin neur daitekeena (Han et al. 1996).

Hurbiltasun molekularraren fisikan oinarrituta, FRET-ak energia transferitzeko aukera ematen du bakarrik fluoroforoen arteko distantzia 1 eta 10 nanometro (nm) artean dagoenean. Fluoroforo emailea kitzikatu ondoren, fotoi birtual bat igortzen du, fluoroforo hartzaile batek xurgatzen duena dipolo-dipolo ez-erradioaktiboaren akoplamenduaren bidez (Merchant et al. 2007; Kapanidis eta Weiss 2002).

FRET biomolekulen arteko elkarrekintza aztertzeko erabil daiteke eta biosentsoreen oinarria da. Biosentsoreak egoera kimikoen berri emateko diseinatuta daude, eta ioien edo molekula txikien kontzentrazioak, peptidoen fosforilazioa edo proteina baten nukleotidoen karga neurtzeko erabil daitezke (Mehta eta Zhang, 2011). FRET-en oinarritutako biosentsoreen erabilpena bere distira eta maila dinamikoaren araberakoa da. Atributu horiek erabilitako proteina fluoreszenteen ezaugarrien menpe daude (Goedhart et al., 2007). FRET-en eraginkortasuna distira iraungitze-koefizientearen eta errendimendu kuantikoaren bidez zehazten dira; beraz, gomendio orokor bat eskuragarri dauden proteina fluoreszente distiratsuenak erabiltzea da (Scott eta Hoppe, 2015). Zelula bizietan FRET irudiak lortzeko, beste parametro batzuk hartu behar dira kontuan, heltzea, fotoegonkortasuna, egoera oligomerikoa eta ingurumen-aldaketekiko sentikortasuna barne (Scott eta Hoppe, 2015).

Fluoroforo emaileak eta hartzaileak hainbat modutan jar daitezke. Adibidez, fluoroforo bat substratu bati lotu dakioke, eta bestea, berriz, bere lotuneari, eta behin lotuta daudenean, fluoroforoak energia transferitzeko bezain hurbil egongo dira (Joo et al. 2007). Bestela, gure kasuan bezala, bi fluoroforoak proteina berarekin lotuta daude eta, giroaren aldaketa baten ondorioz, proteinak bere osaera aldatzen du eta FRET gertatzen da (Kajihara et al. 2006).

3.1.3.1. FRET distantziak neurtzeko

FRET eraginkortasuna emailearen eta hartzailearen espektroen gainjartzearen, une dipolarren orientazioaren eta R_0 distantziaren araberakoa da (Ansbacher et al. 2012). FRET eta R_0-ren eraginkortasunaren arteko erlazioa honako ekuazio honen bidez argitzen da:

$$E = \frac{1}{[1+\frac{R}{R_0}]}$$

Non R_0 Försterren erradioa den.

Oro har, fluoroforo emaileek eta hartzaileek ezaugarri ezberdinak izan behar dituzte, batez ere emisioari dagokionez. Kitzikapenaren ondoren, fluoroforo emailearen elektroiek beren funtsezko egoeratik energia maila altuago batera salto egiten dute. Oinarrizko egoerara itzultzen direnean, fotoi izeneko argi partikula bat igortzen dute. FRET saiakuntzetan, fotoia, igorri beharrean, hartzaileak xurgatzen du, bere elektroiak kitzikatuz eta hartzaileak fotoi bat igortzea eraginez (Meyer eta Teruel, 2003).

3.1.3.2. FRET Biosentsoreak diseinatzeko kontuan hartu beharrekoak

g. Fluoroforo emailearen emisio-tartea

Kontuan hartu beharreko lehen faktorea emailearen emisio-tartea da, hau da, zenbat energia igortzen duen kitzikatutako emaile batek eta zenbat energia behar den hartzaile bat kitzikatzeko. Gutxienez, % 30-ekoa izan behar du (Lovell et al. 2009). Beraz, fluoroforo bikote kopuru mugatua dago.

Zelula bizietan gehien erabili den FRET parea zian proteina fluoreszentea (CFP) eta proteina fluoreszente horia (YFP) izan dira. Hala ere, beste FRET pare batzuk, CFP eta dsRED, BFP eta GFP, GFP (edo YFP) eta dsRED, Cy3 eta Cy5, Alexa488 eta Alexa555, Alexa488 eta Cy3, eta FITC eta rodamina ere asko erabili dira (Wiedenmann et al., 2009).

h. Auto-fluoreszentzia

Autofluoreszentzia izeneko fenomenoa ere hartu behar da kontuan, FRETen datuak oztopatu baititzake. Autofluoreszentzia substantzia naturalen fluoreszentzia da, eta argi-fotoiek kitzikatzen dituztenean, fotoiak askatzen dituzte (Sturmey et al., 2006). Erradiazio honek FRET bikotearen fluoreszentzia espezifikoa maskaratzen du, sentsoreek, beraiek sortutako erradiazioaz gain, autofluoreszentia hau sentituko dutelako. Beraz, errore bat sortuko du zelula-jarduera monitorizatzen saiatzean. Egitura biologiko autofluoreszenteenak mitokondriak eta lisosomak dira; molekula ohikoenak NADPH eta flabinak dira; eta, oro har, triptofano, tirosina eta fenilalanina aminoazido asko dituzten proteinek nolabaiteko autofluoreszentzia maila erakusten dute ere.

i. Fluoreszentziaren balio-bizitza

Fluoroforoen erabileraren beste eragozpen bat fluoreszentziaren balio-bizitza laburra da. Kitzikatuta daudenean, oso denbora laburrez egoten dira kitzikatuta. Gainera, fluoroforo emisioak neurtzeko denbora gutxi dagoenez, auto-fluoreszentziak denboran zehar erregistratutako emisioen ehuneko handiagoa hartuko du (Davydov et al., 2008; Fernando et al., 2006).

j. Estruktura aldaketa

Garrantzitsua da kontuan hartzea FRET fluoroforoek kitzikapen- eta emisio-espektro egokiak izan behar dituztela, baina, gainera, ez dute eraginik izan behar lotuta dauden molekulen hiru dimentsioko egituran.

k. Analito kontzentrazioa

FRET detektatzeko beste faktore garrantzitsu bat analitoaren kontzentrazioa da (Long et al., 2012). Elkarri eragiten dioten molekulek bakarrik izango dute energia transferentzia. Molekula emaileen eta hartzaileen kontzentrazio handia badago, baina elkarrekintzarik gabe, FRET baxua izango litzateke. Kasu honetan, fluoroforo emaileak eta hartzaileak detektatzen errazak dira; FRET aktibitate efektiboa, berriz, ez da izango detektatzeko bezainbestekoa (Kwak et al., 2010).

l. Heltzea

Heltzea ezinbesteko faktorea da proteina fluoreszente baten benetako distirarako eta FRET eraginkor baterako (Miyawaki, 2011). Heltze-eraginkortasuna, kromoforo fluoreszente funtzional batekin zuzen tolestutako proteina bat sortzen duen proteina frakzioa da. Teorikoki, proteina fluoreszentearen heltzea % 100 ingurukoa da. Proteina bat ez bada behar bezala tolesten edo kromoforo okerra osatzen badu, FRET pareak ez du emaile edo hartzaile funtzionalik izango, eta horrek FRET-a galarazten du, FRET pare funtzionalen kopurua gutxituz eta tarte dinamikoa murriztuz (Scott & Hoppe, 2015).

Ikusi dugunez, FRET esperimentuen diseinuak mugak ditu. Gaur egungo FRET ereduen mugarik nabarmenena emaileen eta hartzaileen arteko hurbiltasun fisikoaren beharra da. Gainera, emaile eta hartzaile pare egokiek espektro gainjartze nahikoa izan behar dute energia transferentzia efiziente bat gerta dadin edo espektroetan euren artean bisualki bereizgarriak izateko diferentzia nahikoa izan dezaten. Uhin fluoreszentearen luzera hautatzeko iragazkiak hautatzea ere kritikoa da; izan ere, emailearentzako kitzikapen-iragazkiak emailea kitzikatzeko gai izan behar du, hartzailearen kitzikapena minimizatzen den bitartean. Gainera, biosentsoreak zelula bizietan sartzea % 20-30 inguruko eraginkortasuna duela estimatu izan da (Komatsua et al., 2011).

3.1.3.3. mTFP1 eta mcpVenus FRET-parea

FRET-ren funtsezko baldintza da emailearen igorpenaren eta hartzailearen xurgatze-espektroaren arteko espektro gainjartzea (Periasamy & Day, 2005). Baldintza hori betetzen duten fluoroforo pare ezberdin asko dauden arren, gaur egun FRET parerik ohikoena *Aequorean* oinarritautako zian (CFP) eta proteina fluoreszente horia (YFP) konbinatzea da (Zhang et al., 2003). Fluoroforo hauek aldaketa asko izan dituzte, FRET-en oinarritutako saiakuntzetan erabilgarritasuna hobetzeko. Adibidez, Nagaik eta bere lankideek Venus izeneko YFP distiratsuago bat garatu zuten, heldutasun eraginkorragoa duena eta pH eta haluroekiko sentikortasuna murrizten duena (Nagai et al., 2002). Gainera, Rizzo et kideek frogatu zuten CFP-ren gainazalean disolbentearen eraginpean zeuden aminoazidoen ordezkapenek bere egoera kitzikatua egonkortzen zutela eta Zerulean izeneko errendimendu kuantiko altuagoa zuen proteina bat sortu zuten (Rizzo et al., 2004). Zenbait ikerketak frogatu dutenez, Zerulean eta Venus-en bariante hauek eskuragarri dauden FRET-pare eraginkorrenen artean daude (Koushik et al., 2006). Hala ere, oraindik mikroskopian erabiltzeko hainbat muga ditu, eskaneatze laser mikroskopio sistemeak direla eta (LSM) (Day & Booker, 2008).

Day eta Booker, duela hamarkada bat, muga horietako batzuk gainditzeko fluoroforo-proteina berrien ezaugarriak aztertu zituzten (Day & Booker, 2008). mTFPAak, Venuserako FRET emaile bezala abantailak dituela deskubritu zuten. Zerulean-rekin alderatuta, distira handiagoa dauka, proteinen adierazpen baxuak dituzten zeluletan detekzioa hobetuz, edo zeluletan maila baxuetan ekoitzi behar diren proteinen detekzioa hobetuz. Gainera, fotoegonkortasun handiagoa eta proteina hartzaileekin (Venus edo belaunaldi berriko FP laranjak) hobetutako espektro gainjarriak ditu (Shaner et al., 2005). Gainera, dimeroak sortzeko probabilitatea murriztu egiten dela frogatu zen (Zacharias et al., 2002).

Proteina fluoreszenteen arteko interakzioak FRET esperimentuetan nahi ez diren efektuak badira ere, abantaila izan daitezke FRETn oinarritutako biosentsoreak erabiltzen dituzten saiakuntzetan. Zunda horiek sentsore-domeinu bat dute, fluoroforo emailea eta hartzailea zuzenean lotzen dituena. Horri esker, sentsorearen domeinuan konfigurazio-aldaketak hauteman daitezke, igorpen-erlazioan aldaketak eginez (Giepmans et al., 2006). Beste ikerketa batek CFP eta YFP-ren tarte dinamikoa hobetu zuen baina hauen errendimendu kuantikoa apur bat baxuagoa zen, jatorrizko proteina fluoreszenteekin alderatuta (Nguyen eta Daugherty, 2002). Geroago, FRET seinale hobetuak zituzten fluoroforo berri hauek

barneko konplexu baten egonkortzea sustatzen zuten mutazioen emaitza zirela frogatu zen (Ohashi et al., 2007).

FP	Peak Absorption	Peak Emission	Quantum Yield	Extinction Coefficient [a]	Intrinsic Brightness [b]
mTFP1	462	492	0.85	64	54
Venus	515	528	0.57	92.2	53

a. (x 10^{-3}) (M^{-1} cm^{-1})

3.1 taula. mTFP1 and Venus-ren ezaugarri espektralak.

3.2. HELBURUA

Kapitulu honen helburua CaM/Kaltzioaren erregulazioan K_V7 kanalen C-terminalaren A eta B helizeen arteko lotailuaren zeregina ebaztea da, FRET sentsoreak erabiliz.

3.3. EMAITZAK

3.3.1. $K_V7.1$ and $K_V7.2$-ren Ca^{2+}-arekiko erantzun ezberdinak

Behin FRET-a, Ca^{2+}-k eragindako aldaketa konformazionalak neurtzeko teknika egokia zela frogatuta, $K_V7.1$ eta $K_V7.2$-ren arteko aldaketa konparatu genuen. Ca^{2+}-rako sentikortasun ezberdina ikusten dugu $K_V7.1$ kasuan, non FRET-ratioa (YFP/CFP) $K_V7.2$ -rako baino hiru aldiz gehiago murriztu (%28,1 eta %9,7-ko murrizketa hurrenez hurren) biak Ca^{2+} kontzentrazio asetzaileetan zeudelarik ([500 µM]) (3.1 irudia). Horrek esan nahi du Ca^{2+}-ak eragindako konformazio berrantolaketa ezberdina izan litekeela isoforma bakoitzerako. Hala ere, hasierako FRET-ratioa, apo egoeran dagoena, antzekoa izan zen bi isoformentzat, 1,68 eta 1,71 $K_V7.1$ eta $K_V7.2$-rentzat, hurrenez hurren, eta horren arabera, apo konplexuaren egitura antzekoa izan litekeela pentsa genezake.

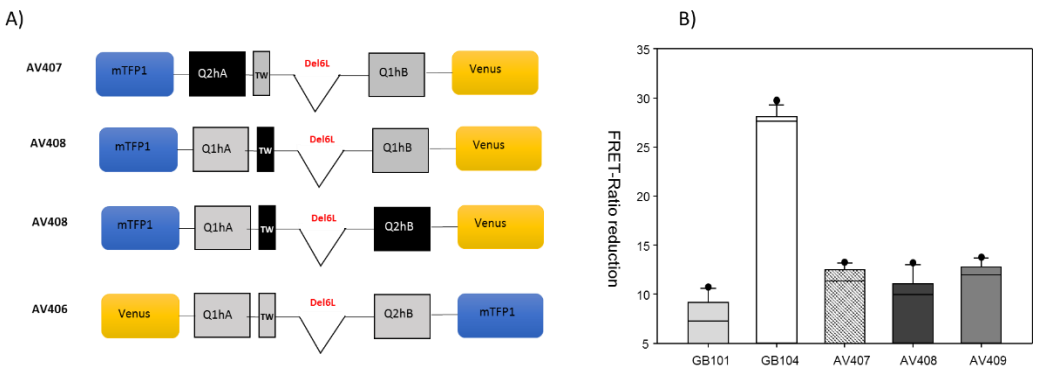

3.1 irudia. Ca^{2+}-ren efektua $K_V7.1$, $K_V7.2$ eta kimeretan. A) Kimera bakotzaren irudi eskematikoa. B) FRET-indizearen murrizpena %-tan, Ca^{2+}-aren gehikuntzaren ondoren (500 µM Ca^{2+} librea) Q2*h*AB Del Y372-T501 (GB101), Q1hAhB (GB104), eta hiru kimera ezberdin AV407 mTFP1-Q2hA-Q1TWhB-pVenus, Q1 hAdelQ2hB AV408-mTFP1-Q1hA-Q2TW-Q1hB-pVenus, AV409 mTFP1-Q1hA-TW-Q2hB-pVenus.

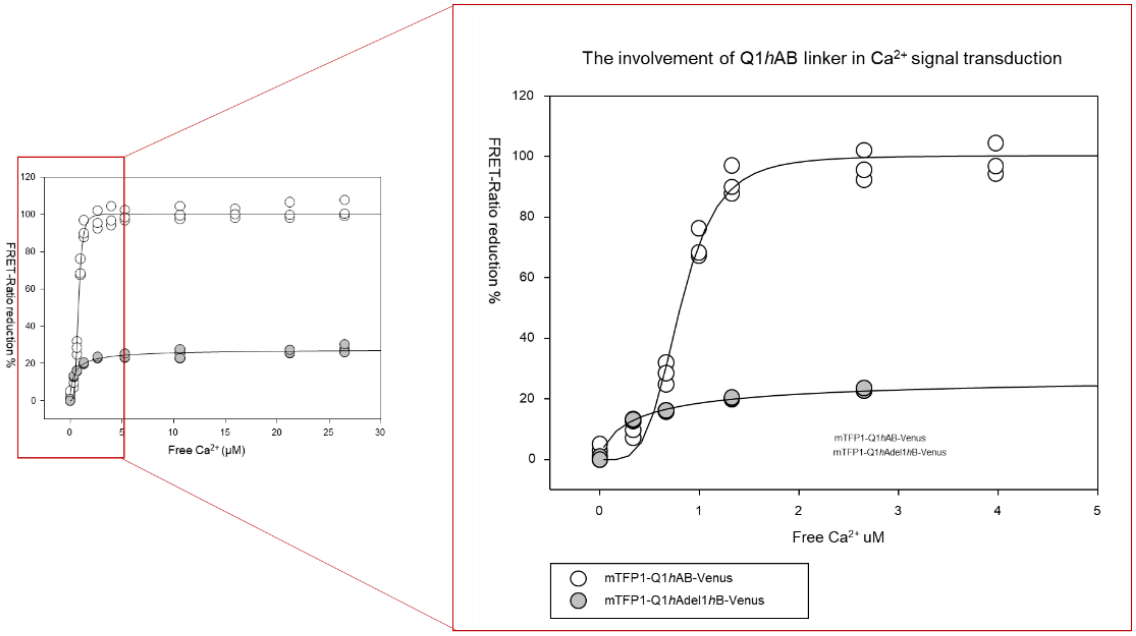

Construction	Max.expected	Ec50 (µM)	RSQR
Q1*h*AB	100.3 ± 9.8	0.81 ± 0.02	0.99
Q1*h*Adel1*h*B	27.8 ± 7.7	0.41 ± 0.04	0.98

3.2 irudia. Q1hAB Linkerrek Ca^{2+} seinaleen transmisioan duen papera. Ezkerreko grafikoak FRET indizearen murrizketa ehunekotan erakusten du, Ca^{2+} kontzentrazioaren aldean. Ezkerreko grafikoak 0-30 µM Ca^{2+} kontzentrazio tartea erakusten du: mTFP1-Q1hAB-Venus:CaM esfera zurietan irudikatzen da eta grisean mTFP1-Q1hAdel1hB-Venus:CaM, bi konplexuak 500 nM-tan daudelarik. Eskuinean, grafiko beraren anplifikazioa, Ca^{2+}-aren 1-5 µM arteko tartean. Lerroak Hillen ekuazioa datuetara doitzearen emaitza dira. Azpian, osagarri horien parametroak agertzen dira. Balio bakoitzak gutxienez 3 esperimentu independenteren batezbestekoa adierazten du.

Ca^{2+}-arekiko sentikortasun handiagoa emateko ardura $K_V7.1$-ren zein eskualderi zegokion deskubritzeko, kimera ezberdinak sortu ziren, non bi isoformetako eskualde ezberdinak konbinatu ziren. Kimera hauek CaM-pOKD4-rekin batera kotransformatu ziren eta His-Trap eta gel iragazketaz purifikatu ziren. Ondoren, Ca^{2+}-aren efektua FRET bidez aztertu genuen, aurretik egin genuen bezala. Hala ere, kimeretako bat ere ez zuen $K_V7.1$-an ikusitako efektua erakutsi, eta FRET-indizearen murrizketa txikia izan zuten Ca^{2+}-aren gehikuntzaren ondoren, $K_V7.2$-an

ikusitakoaren antzekoa (3.1 irudia). Q1en TW eta B helizeak dituen kimerak (Q2hA-Q1TW-hB, AV407) FRET-indize murrizketarik handiena erakutsi zuen, baina K_V7.1-ak aurkeztutakoatik oso urrun dago), honen efektuaren erdia lortuz (% 12,9 eta % 28,1-eko murrizketa hurrenez hurren). Ondoren Q1hA-Q2TW-hB (AV409) % 12,5-eko murrizketa erakutsi zuen eta azkenik Q1hA-Q2TW-Q1hB (AV408) % 10,2-a.

Ondoren, A eta B helizeen arteko konektorearen papera frogatu zen, Q1-ekin egindako senstoreak konektora zeramalako, eta Q2-koa (baita kimera guztiek ere) Del1 (Y372delT501) zeramatelako, A eta B helizeen arteko konektorea ezabatzen zelarik. Lotailuaren papera jorratzeko, bi sentsore probatu ziren: K_V7.2, lotailu osoarekin, eta K_V7.1, lotailuarik gabe (Δ Y347-H478) (3.2 eta 3.3 irudiak). Emaitzek erakusten dutenez, K_V7.2 an A eta B helizeen arteko lotailua berrezartzean, K_V7.1-ean ikusitako Ca^{2+}-ren efektua erreplikatu egiten da (FRET-indizea % 30,5-eko murrizketa erakutsiz) (3.3 irudia), eta K_V7.1-n konektore bera ezabatzeak FRET-ean % 9,4-ko murrizketa ikusi zen Ca^{2+}-ren gehikuntzaren ondoren (3.2 irudia).

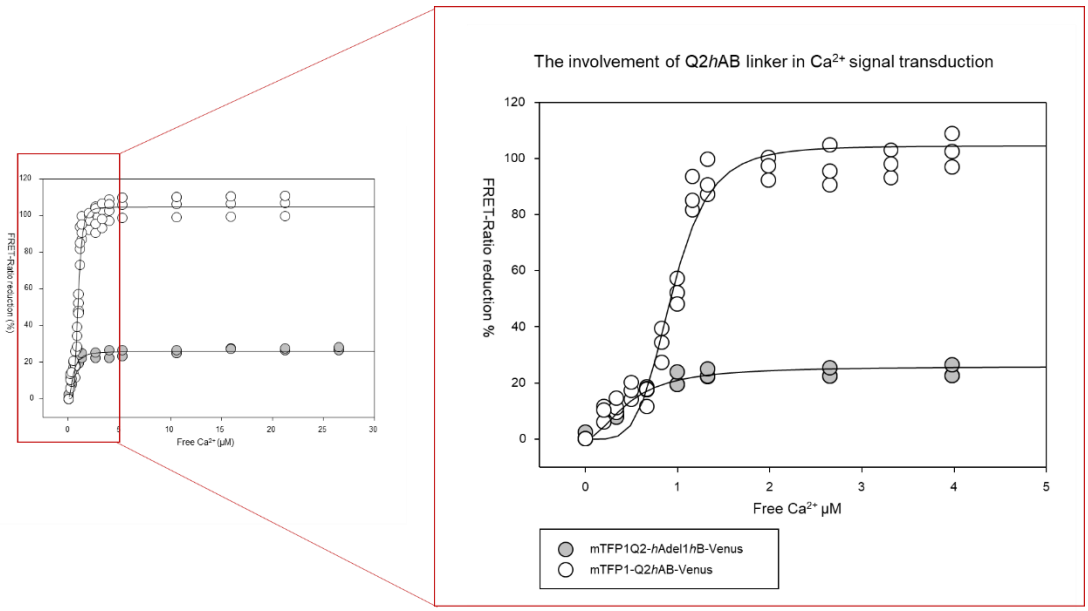

Construction	Max.expected	Ec50 (µM)	RSQR
Q2*h*AB	104.5 ± 5.9	0.94 ± 0.02	0.97
Q2*h*Adel1*h*B	25.9 ± 4.2	0.47 ± 0.03	0.96

3.3 irudia. Q2hAB Linkerrek Ca^{2+} seinaleen transmisioan duen papera. Ezkerreko grafikoak FRET indizearen murrizketa ehunekotan erakusten du, Ca^{2+} kontzentrazioaren aldean. Ezkerreko grafikoak 0-30 µM Ca^{2+} kontzentrazio tartea erakusten du: mTFP1-Q2hAB-Venus:CaM esfera zurietan irudikatzen da eta grisean mTFP1-Q2hAdel1hB-Venus:CaM, bi konplexuak 500 nM-tan daudelarik. Eskuinean, grafiko beraren anplifikazioa, Ca^{2+}-aren 1-5 µM arteko tartean. Lerroak Hillen ekuazioa datuetara doitzearen emaitza dira. Azpian, osagarri horien parametroak agertzen dira. Balio bakoitzak gutxienez 3 esperimentu independenteren batezbestekoa adierazten du.

Balio-absolutuetan, apo-egoeran dagoen FRET-indizea antzekoa da, estekagailua dagoenean eta ez dagoenean, hortaz, kaltziorik gabe duten estruktura oso antzekoa izan behar da kasi bietan. Hala ere, konplexua (500 nM) kaltzioarekin (500 µM) asetzen dugunean, FRET-indizea askoz txikiagoa da konektorearen presentzian (1,55 Del1erako eta 1,19 konektorearen presentzian) (3.3 irudia).

Ca^{2+} ren sentikortasuna handitu egin zen Kd ~ 0,5 nm (~ 0,9 nm) duen lotailuaren presentzian, bai K_V7.1 bai K_V7.2 (3.4 irudia).

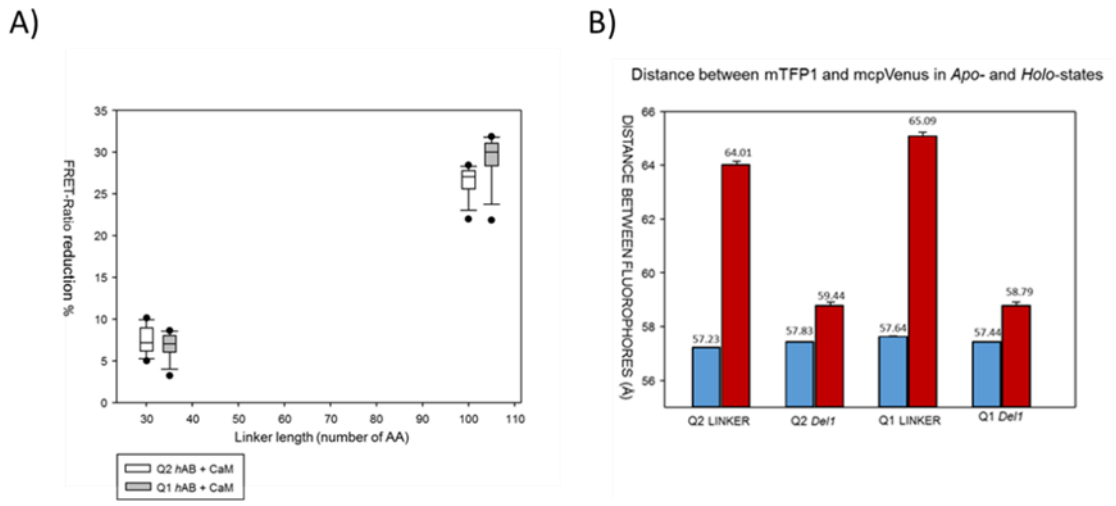

3.4 irudia. Q2hAB Linkerrek Ca^{2+} seinaleen transmisioan parte hartzea. Ezkerreko grafikoak FRET indizearen murrizketa ehunekotan erakusten du, lotailuaren luzeraren aldean. Eskuinean, KV7.1 eta KV7.2 sentsoreen fluoroforen arteko distantzia erakusten du, kaltziorik ez dagoenean (urdinez) eta kaltzioarekin (gorriz). LINKER lotailu osoa daramatenak dira, eta Del1 Y372-T501 tardeko delezioa daramatenak.Datuek, 6 esperimentuen batez besteko balioak erakuste dute.

Kaltzioak bultzatutako aldaketa konformazionalean ezberdintasun hori azal lezakeen arrazoietako bat, lotailuaren faltak A eta B helizeen mugimendu erlatiboa murrizten duela da. Ideia hau

frogatzeko, bi helizeen arteko malgutasuna hiru estrategia ezberdinekin handitzen saiatu ginen.: 1.- Lotailuaren ordez poli-Q sekuentzia bat jarriz, 2.- konektorea, GSG konektore malgu batez ordezkatuz, 3.-A helizea eta B helizea banan-banan expresatuz, CaM-rekin batera, lotailurik gabe. 1. eta 3. metodoek bariabilitate handia erakutsi zuten, eraikuntzak ezegonkorrak eta agregatzeko joera zutelako. GSG-rekin ez zen FRET-indizearen murrizketa handirik ikusi, % 12 ingurukoa, Del1 ikusitakoaren oso antzekoa (2. osagarrian esperimentuaren emaitzak daude). Beraz, malgutasunaren falta ez zen Ca^{2+}-aren erantzun ezberdinaren arrazoia.

3.3.2. Konektorean delezioak

K_V7 kanalen C-terminal domeinuaren A eta B helizeen arteko konektorea oso luzea denez eta gutxi aztertua dagoenez, hurrengo urratsa Ca^{2+} bidezko seinaleztapenean inplikatutako eskualde zehatza identifikatzen saiatzea izan zen. Horretarako, hainbat delezio egin ziren konektorean, eta FRET bidez, Ca^{2+}-ak eragindako egitura-aldaketa aztertu zen, aurreko esperimentuetan bezala:

3.3.2.1. Konektorearen N-muturrean egindako delezioak

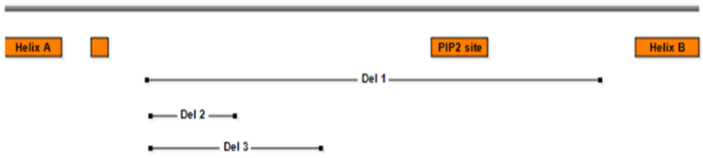

3.5 irudia. *h*AB lotailuko Del1, Del2 and Del3 delezioen irudi eskematikoa.

Lotailua zeraman FRET-Biosentrsoretik abiatuta, lehenengo delezioak, A eta B helizeen arteko lotailuaren N-muturrean egin ziren, TW helizearen atzean. Kasu honetan, Ca^{2+} titulazioak ere egin ziren, konplexuaren Ca^{2+}-arekiko afinitatea aztertzeko (3.6 irudia). Del2-ak (I375-P400) 25 aa-tako delezioa du, eta Del3-ak, berriz, 50 aa-takoa (I375-A424). Bi kasuetan, kaltzio efektuak konektore osoko konplexuan behatutakoa erreplikatzen du (% 109 ± 1,91 Del2-rako eta% 97,07 ± 1,15 Del3-rako). Ez zen kaltzioarekiko afinitate ezberdintasun handirik ikusi: 980 nM konektore osoa duen konplexurako, 494 nM Del2-rako eta 341 Del3-rako. Onartzen dugu ezberdintasun horiek gerta daitezkeela pipeteatzean egindako errore baten ondorioz edota disoluzio indorgetzailearen konposizio, tenperatura edo pH-aren ezberdintasunen ondorioz, esperimentuak hainbat egunetan egin baitziren.

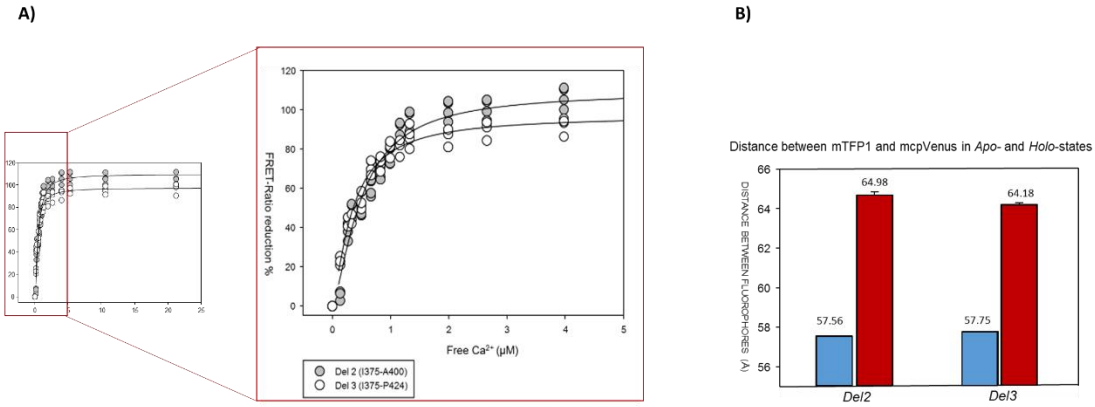

Construction	Max.expected	Ec50 (µM)	RSQR
Del2 (I375ΔA400)	109.4 ± 7.3	0.5 ± 0.02	0.97
Del3 (I375ΔP424)	97.18 ± 9.2	0.34 ± 0.03	0.98

3.6 irudia. Q2hAB Linkerrek Ca^{2+} seinaleen transmisioan parte hartzea. Ezkerreko grafikoak FRET indizearen murrizketa ehunekotan erakusten du, Ca^{2+} kontzentrazioaren aldean. Ezkerreko grafikoak 0-30 µM Ca^{2+} kontzentrazio tartea erakusten du: mTFP1-Q2hAdel2hB-Venus:CaM esfera grisetan irudikatzen da eta zurietan mTFP1-Q2hAdel3hB-Venus:CaM, bi konplexuak 500 nM-tan daudelarik. Eskuinean, grafiko beraren anplifikazioa, Ca^{2+}-aren 1-5 µM arteko tartean. Lerroak Hillen ekuazioa datuetara doitzearen emaitza dira. Azpian, osagarri horien parametroak agertzen dira. Partzela bakoitzak gutxienez 3 esperimentu independenteren batezbestekoa adierazten du.

Ezabatutako konektorearen sekuentzia, TW helizearen atzean dagoena, K_V7 familiako kideen artean gutxi kontserbatuta dagoela ikusten dugu (3.7 irudia). Gainera, K_V7-ren isoforma batzuek, $K_V7.1$, $K_V7.3$ eta $K_V7.5$ kasu, badute naturalki, konektorearen zati hau delezionatuta, eta horrek kanalaren erregulazioan funtzio garrantzitsurik ez duela iradokitzera garamatza.

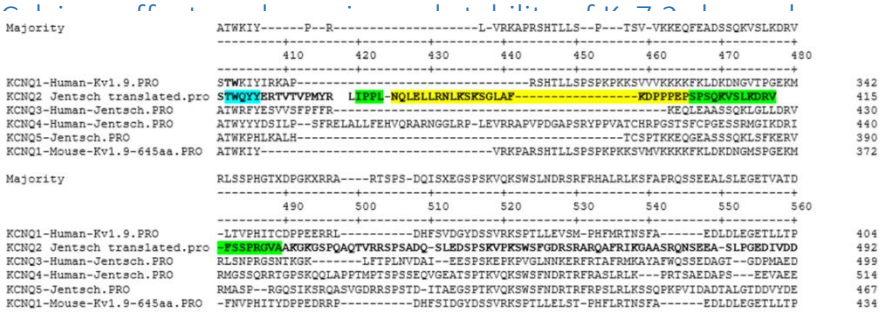

3.7 irudia. K_V7 isoformen a eta B helizeen arteko loturaren sekuentzien lerrokatzea. Del2-n ezabatutako frakzioa (I375-P400) horian nabarmentzen da, eta Del3-n ezabatutako frakzioa (I375-A424) berdean, Del2-ren frakzioaz gain, hori ere ezabatzen baita Del3-an.

3.3.2.2. Konektorearen C-terminaleko delezioak: Del 4, Del 5 and Del 6

.Datuen arabera, ezberdintasunen arrazoia ez zen konektorearen luzeran, baizik eta Ca^{2+} seinaleztapenean diharduen domeinu baten ezabaketan, konektorean dagoena eta Del1ean ezabatzen dena. A eta B helizeen lotailuaren sekuentzian gehien kontserbatu ziren eskualdeei erreparatuz, PIP_2-rekiko loturaren domeinua CaM bidezko kaltzio seinaleztapenean parte hartzen duen hautagai potentzial moduan proposatu zen, beste eskualde batzuen balizko lankidetza baztertu gabe. Honek zentzua du, Del2 eta Del3 delezioek eskualde hau mantentzen baitute, Del1ek erabat ezabatzen duen bitartean. Gainera, horrek azalduko luke kaltzioa elkartu ondoren fluoroforoen arteko urruntzean dagoen aldea, eta lotailu artifizialekin lotailu naturalarekin behatutako efektua erreplikatzeko ezintasuna.

Holo-konplexuan A eta B helizeen arteko aldentze handiago baten erantzule den domeinu hau sakonago ikertzeko, lotailuaren C-terminalaren muturrean delezio ezberdinak zituzten hiru konektore berri diseinatu ziren, non PIP_2-ren lotunea dagoen (3.8 irudia). Del3-a, parental bezala erabili zen, aurretik, lotura osoarekin gertatzen den Ca^{2+}-aren efektua, erreplikatzeko gai delako, baina egonkorragoa da eta agregatzeko joera txikiagoa du.

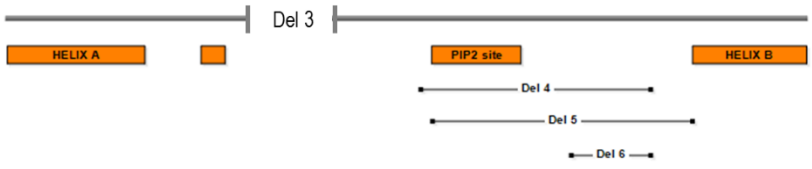

3.8 irudia. Del4, Del5 and Del6 delezioen irudi eskematikoa, non *h*ADel3*h*B parental bezala erbabili zen.

Del4 eta Del5 delezioetan, proposatutako PIP_2-rekin lotzeko lekua ezabatzen da. Del6-an (I375-P424) (3.8 irudia) PIP_2 eta B helizearen lotunearen artean kokatutako 18 aminoazido baino ez dira ezabatzen.

Delezio berrietako bakar batek ere ezin izan zuen bere parentalaren eragina erreplikatu (Del3), kasu guztietan FRET erlazioan Del1-ean ikusitako antzerako murrizketa lortuz (% 11,6, % 14,15 eta % 12,52 Del4, Del5 eta Del6ren kasuan, hurrenez hurren) (3.9 irudia). Berriz ere, apo-egoeran dauden fluoroforoen arteko distantzia konektore osoarekin behatutakoaren antzekoa da, ziurrenik, estruktura bera hartzen duelako. Hala ere, CaM- Ca^{2+}-arekin lotzen denean, fluoroforoen arteko banaketa estimatua 2 Å ingurukoa da kasu guztietan, Del2 eta Del3-rekin behatutakoa baino 3 aldiz txikiagoa.

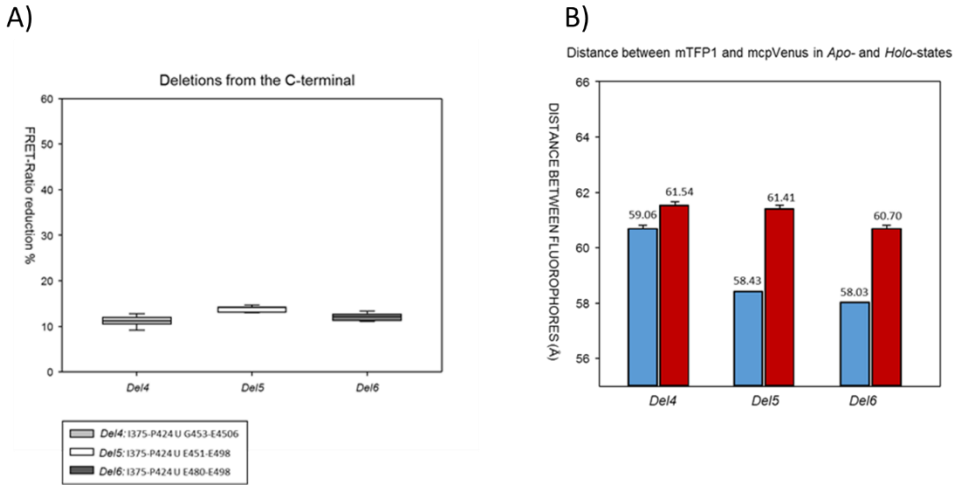

3.9.irudia. C-muturrean egindako delezioak (A) Grafikoan ikus daitekeenez, Ca^{2+} loturaren ondoren FRET indizeak izan duen murrizketa Del4, Del5 eta Del6 lotailuetan . **(B)** Eraikuntza ezberdineko fluoroforoen arteko distantzia, Ca^{2+}-rik ez dagoenean (zutabe urdina) eta Ca^{2+}-a dagoenean (zutabe gorria). Zutabe bakoitzaren gainean, batez besteko estatistikoa erakusten da. Partzela bakoitzak gutxienez 6 esperimentu independenteren batezbestekoa adierazten du.

3.4. EZTABAIDA

K_V7.2 potasio-kanalaren kaltzio eta CaM bidezko erregulazioa prozesu konplexua da, hainbat faktorek parte hartzen dute eta hainbat galdera daude argitzeke. Jakina da Ca^{2+}-a CaM:K_V7.2 konplexuan elkartzeak N eta C lobuluen konformazio-aldaketa dakarrela, eta horrek, aldi berean, K_V7.2-ren A eta B helizeak birorientatzea eragiten duela. Iradoki da aldaketa hori mintzaren zeharkako domeinura transmititzen dela, kanala itxiz eta M-korrontea inhibituz (Bernardo-Seisdedos et al.2018). Prozesu hori fluoreszentziaren erresonantzia-energiaren

transferentzian (FRET) izandako aldaketen bidez kuantifika daiteke, fluoroforo emaileen eta hartzaileen arteko distantzia kalkulatzea ahalbidetzen baitigute. Beraz, A helizearen aurretik fluoroforo emaile bat eta B helizearen ondoren fluoroforo hartzaile bat jartzean, Ca^{2+}-ak eragindako konformazio aldaketa neurtu dezakegu. Lehenik, A eta B helizeen berbideratze bat dagoela frogatu dugu, helizeen arteko distantzia handitzen duena. Ondoren, Ca^{2+}-a lotuz gero, fluoroforoen arteko distantzia handiagoa zela lotailu osoa duen biosentsorearen kasuan ikusi genuen. Beraz, Ca^{2+}-ak eragindako egitura-aldaketa, Bernardo-Seisdedos deskribatutakoa (Bernardo-Seisdedos et al., 2018) baino handiagoa dela pentsa dezakegu. Lan horretan, egiturazko berrantolaketa bat deskribatu zen, baina lotailurik gabeko proteina konplexuan (Del1), non N-lobulu/ B-Helizeak ia aldaketarik gabe jarraitzen duen, A helizearen hasierako zatia, C-lobuluaren bihurdura batekin konkomitsuki bikoizten den bitartean.

FRET emaitzak kontuan hartuta, konektore osoa duen holo-CaM egiturak ezberdina izan beharko luke. FRET murrizketa A eta B helizeen arteko aldentze batekin erlazionatuta dago eta nahiz eta lotailuarekin, aldentze hori handiagoa den, esperimentu gehiago egin beharko genituzke holo-konplexuaren azken egitura hori nolakoa den zehazteko.

Lotailuak kaltzioaren seinaleztapenean paper bat duela jakinik, argitzeke daukagu lotailuaren zein eskualdek parte hartzen duen kaltzioaren bitarteko konformazio-aldaketan.

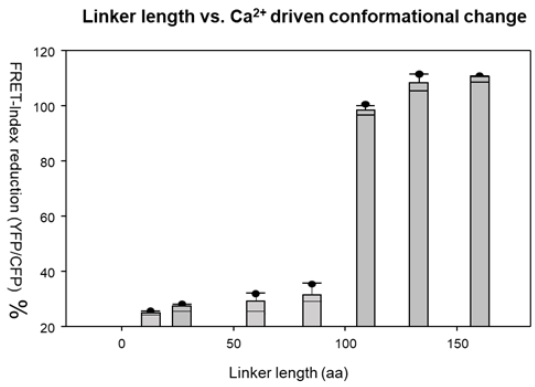

3.10 irudia. FRET murriztu egiten da lotailuaren aminoazido kopuruaren arabera. Grafikoak kaltzioaren gehikuntzaren ondoren FRET-indizearen murrizketa adierazten du, A eta B helizeen arteko lotailuak osatzen duen aa kopuruaren arabera.

Erregulazio honetan, A eta B helizeen arteko 157 aminoazidotako lotailuak funtzio ezezagun bat duela ikusi dugu. Lotailu naturalarekin (157 aa) eta 30 aminoazidotako lotailuarekin (Del1) egindako probetan, lotailuaren luzera murriztean, birorientazioa erasaten zela ikusi zen, bai K_V7.2hAB eta K_V7.1hAB isoformetan. Hala ere, efektu hau ez zen nabarmena izan 25 aminoazido delezionatzean (Del2), ezta 50 aminoazido kentzean ere ez (Del3). Beraz, pentsatu genuen, lotailuaren eskualde espezifiko batek Ca^{2+}-aren seinaleztapenean parte hartzen zebilela. Horren arabera, PIP_2-ren lotura-gunea prozesuan parte hartzen duen hautagai potentzial gisa proposatu zen. Horretarako, PIP_2-ren lotura gunea kendu genuen

(K449-K469) (Hernández et al., 2008) Del4 eta Del5 delezioetan, bai eta gune hori mantendu eta ondoren dagoen beste sekzio bat delezionatu ere, hau da, B helizetik gertuen dagoen segmentua (Del6), kontrol gisa diseinatu genuena. Hala ere, A eta B helizeen birorientazioa, Ca^{2+} eta CaM-ren bidez, Del6-an ere murrizten dela ikusten dugu, non PIP_2-ren lotunea mantentzen den. Beraz, egiturazko aldaketak murriztu zituen frogatutako deleziorik txikiena Del6-a izan zen, eta horrek kaltzifikazioaren ondoren A/B helizearen mugimendu erlatiboaren adierazpen osoa ahalbidetzeko determinatzaile molekularra E481-E498 aminoazidoen artean dagoela adierazten du, familiako K_V7 kideen artean gaizki kontserbatuta dagoena. Homologiarik handiena $K_V7.4$ak du, % 39-koa, eta txikiena $K_V7.3$ak, %17-koa (3.11 irudia).

(A)

KCNQ1	E D L D L E G E T L L T P I T H - - -
KCNQ2	E A - S L P G E D I V D D K S C P C E
KCNQ3	D A G T - - G D P M A E D R G Y G N D
KCNQ4	D A P S - - - E E V A E E K S Y Q C E
KCNQ5	A D T A L G T D D V Y D E K G C Q C D

(B)

ISOFORM	HOMOLOGY WITH Q2	HOMO. OTHER ISOFORMS
KCNQ1	(4/18) 22%	(1/18) 6%
KCNQ3	(3/18) 17%	(7/18) 39%
KCNQ4	(7/18) 39%	(7/18) 39%
KCNQ5	(6/18) 33%	(7/18) 39%

3.11 irudia. K_V7 isoformen a eta B helizeen arteko lotailuaren lerrokatze-sekuentzia. (A) Del6 sekuentziaren lerrokadura erakusten da, KCNQ2rekiko kointzidentzia gorrian adierazita eta beste isoforma batzuekiko kointzidentzia berdean. **(B)** KCNQ isoformen arteko homologia laburbiltzen duen taula.

Etorkizuneko azterketetan, eskualde honen azterketa sakonagoa egin behar da, analisi elektrofisiologikoarekin konbinatuta. Beste teknika batzuk erabil litezke, hala nola erresonantzia magnetiko nuklearra, eskualde honek ligando potentzialekin izan ditzakeen elkarreragin molekularrak aztertzeko, konplexuaren tamaina handiak teknika hau aplikatzeko erronka handia den arren. Konektorea 20 aa-ko peptidoetan zatitu daiteke, non lehen 10 aa-k aurreko peptidoaren azken 10 aa-ekin gainjartzen diren. HSQC esperimentu soil baten bidez, hAB:CAM markatutako konplexuarekin, eta peptido bakoitza banan-banan gehituz, seinaleztapenean parte hartzen duen eskualde loteslea aldaketa kimikoen bidez identifika liteke, 10 aa-ra arte murriztuz.

4. TETRAMEROEN EGONKORTASUNA ETA KALTZIOAREN EFEKTUA

4.1. SARRERA

4.1.1. K_V7-en helize superkiribilduak

Helize-superkiribilduak α helize sorta elkarlotuak dira, naturan dauden proteina-proteina elkarreragin hedatuenetako eta aldakorrenetako konformazio bat da. Egitura hauek zenbait kanal-ioniko tetramerikotan daude, eta multimerizazioaren egonkortasuna eta selektibitatea zehazten dutela pentsatzeko ebidentzia asko dago. I_K korrontearen kanal arduraduna, K_V7.1 (KCNQ1), ez da beste K_V7 azpiunitateekin mihiztatzen. K_V7.3-k (KCNQ3), ordea, heterotetrameroak osa ditzake azpiunitate guztiekin, K_V7.1ekin izan ezik (Schwake et al., 2000). Familiako beste kideek, K_V7.2 (KCNQ2), K_V7.4 (KCNQ4) eta K_V7.5 (KCNQ5), homotetramero edota heterotetramero funtzionalak osa ditzakete K_V7.3-rekin. K_V7 azpiunitateen konbinazio ezberdinek propietate biofisiko ezberdinak erakusten dituzte (Hadley et al., 2000; Kubisch et al., 1999; Schwake et al., 2000; Selyanko et al., 2000; Wang et al., 1998).

K_V7 potasio kanalek ez dute T1 domeinurik, K_V1 kanalen tetramerizazioaren arduraduna dena, baina helize superkiribilduak sortzeko C-terminalean bi domeinu dituzte C eta D helizeak (Jenke et al., 2003; Schwake et al., 2006). Izan ere, D-helizearen ezabaketak kanalaren tetramerizazioa eta altamerizazioa saihesten duela frogatu da. K_V7.2/3-ren kasuan, D-helizea ezabatzeak ez du funtzioa erabat ezabatzen, baina korrontearen murrizketa handia dago. Beste K_V7 kanal batzuetan bezala, K_V7.2-ren D helizea domeinu tetrameriko artifizial bategatik ordezka daiteke ere (Schwake et al., 2006).

Izan ere, D-helizeak K_V7 kanalen isoformen arteko sekuentzia-diferentzia esanguratsua erakusten duenez, domeinu hau mihiztaduraren espezifikotasunaren determinatzaile nagusia izan liteke (Maljevic et al. 2003; Schwake et al. 2003, 2006).

4.1.2. CaM eta Helize Superkiribilduak

Helize superkiribilduen domeinuez gain, kanal askok kalmodulinarekin (CaM) lotzeko domeinu bananduak dituzte, SK, IK, TRP, K_V7 (KCNQ) eta CNG kanalak barne. SK kanalen antzera, KCNQ kanalek mintzaren trafikorako CaM behar du (Etxebarria et al., 2008), eta CaM-ren erabilgarritasunak korronte-dentsitateari eragiten dio: CaM-ren gehiegizko adierazpenak korrontearen handipena, murrizpena edo inolako efekturik ez duela jakinarazi da (Gamper et al., 2005; Shamgar et al., 2006; Etxebarria et al., 2008). CaM-ri lotzeko domeinuek, CaM-rik ez

dagoenean, agregazio joera nabarmena dute bakterioetan. Horregatik CaM KCNQ kanalen azpiunitate osagarri bat dela uste da. Hala ere, CaM batzea eragotzita duten kanal mutante batzuk erabat funtzionalak dira, eta horrek iradokitzen du CaM-rekin elkartzea ez dela funtziorako betekizun hertsia (Gomez-Posada et al., 2011; Sihn et al., 2016), edota CaM kanaletik askatu eta kanalera itzul daitekeela zenbait egoeratan.

K_V7 kanalen beste ezaugarri bat PIP_2-rekiko menpekotasuna da, honen lotura ezinbestekoa baita kanala funtzionala izateko (Delmas eta Brown, 2005; Li et al., 2005; Suh et al., 2006). Gainera gero eta nabariagoa da PIP_2-rekiko sentikortasuna CaM-ren loturak modulatzen duela (Gomis-Perez et al., 2017). Duela gutxiko aurkikuntzek, D helizearen funtzioa, kanalak mihiztatzeko plataforma fisiko bat eskaintzetik haratago doala adierazten dute. Helize superkiribilduaren eta CaM-ren lotura-domeinuen arteko erlazioa duela gutxi aztertu da $K_V7.2$ kanaletan, eta helize superkiribilduaren egonkortasunak CaM-ren batasunari eragiten diola iradokitzen du. Ondorioz, PIP_2-rekiko sentikortasuna aldatutako da (Alberdi et al., 2015).

CaM-ren loturak $K_V7.2$ azpiunitatearen mihiztadura/tetramerizazio domeinuan (CD modulua) duen eragina aurretik gure taldean aztertu zen. Helburu horrekin, proteina kimerikoak eraiki genituen Tac mintzaren zeharkako proteina monomerikoa, $K_V7.2$*h*AB-rekin lotuta, eta HEK293T zeluletan expresatu genituen (Etxebarria et al., 2008). GFPren etiketa gehitu zen C-terminalean, konplexuak GFP-ren aurkako antigorputzak erabiliz detektatzea ahalbidetu zuena. Gainera, hirugarren kimera batean, CD modulua sekuentzia artifizial batekin ordeztu zen, Tet izenekoa, proteina tetramero baten konfigurazioa hartzen laguntzen duena (Zerangue et al., 2000). CaM seinalearen gorakada dramatikoa ikusi genuen tetramerizazio naturalaren edo artifizialaren seinalea zuten kimerak adierazi zirenean (4.1. irudia). Beraz, helize superkiribilduak CaM-ren lotura errazten duela ondorioztatu zen.

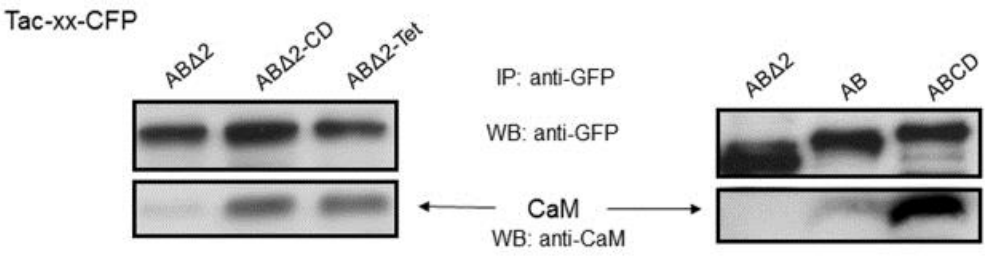

4.1 irudia. Tetramerizazio-domeinu bat egoteak kalmodulina mintz proteina batekin lotzea errazten du. HEK293T zeluletatik ateratako Tac-K_V7.2-CFP kimerak anti-GFP antigorputzak erabiliz immunoprezipitatu ziren, SDS-PAGE bidez banandu ziren, mintz batera transferitu ziren (WB) eta anti-GFP eta anti-CaM antigorputzekin zundatu ziren.

Aldi berean, Sachayinik eta bere kolaboratzaileek, SAXS esperimentuetan oinarrituak, C eta D helizeen deskribapena egin zuten, gutxi gora-behera koaxialak diruditen modulu bezala deskribatzen dituzte, euren konektorea malgua eta flexibilitate nahiko mugatua duelarik (Sachyani et al., 2014). krio-EM irudiek, ordea, C helizearen eskualdea distala malgua dela erakutsi zuten (Sun and MacKinnon, 2017).

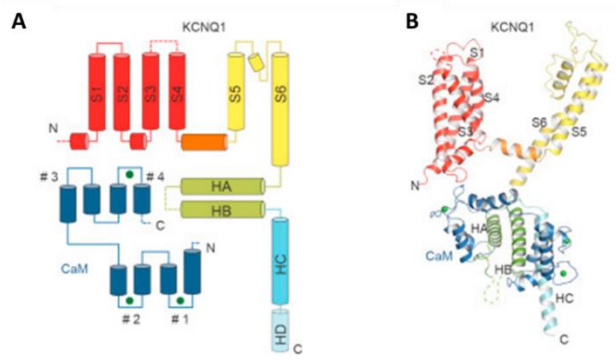

4.2. irudia. K_V7.1ren estruktura Krio-EM bidez ebatzita. (A) Azpiunitate baten domeinuen antolaketa. D helizea, 3D berreraikuntzan maskaratuta dagoena, inguru etenak dituen zilindro baten bidez adierazten da. CaM-ren E-F eskuak #1-#4 gisa etiketatuta daude N-terminaleko muturretik C-terminaleko muturrera. E-F eskuaren lehen bi eskualdeek lobulua osatzen dute, eta beste biek C-lobulua, esfera berdeek kaltzio ioiak irudikatzen dituzte. **(B)** (A)-n bezalako domeinu koloreztatuak dituen azpiunitatearen eredua. (Sun eta MacKinnon, 2017) PDB: 5VMS.

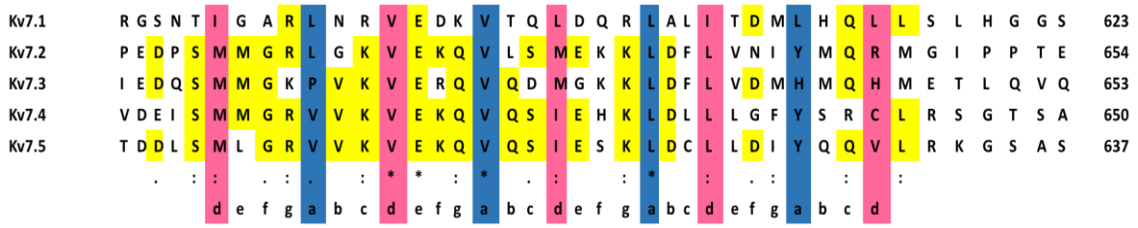

4.3. irudia. 1-9 K_V7en D helizearen sekuentzia-lerrokadura. Nabarmenketa horiak eta lerrokaduren azpiko ikurrek sekuentziaren kontserbazioa adierazten dute (izartxoek, hondakin berdin-berdinak; bi puntuek, ordezko kontserbatzailea; puntu bat, kontserbazio aula. Azpian, helize superkiribiludaren zazpi aminoazidoen errepikapenen posizioak (abcdefg) adierazten dira. "a" eta "d" posizio hidrofobikoek betetzen dituzten aminoazidoak urdinez eta arrosaz adierazten dira, hurrenez hurren. Howard et al., 2007-tik egokitua.

4.1.3. Lotura-zuzena eta zeharkakoa

Duela urte batzuk, CaM-k azpiunitate bereko (lotura zuzena) edo ondoko bi azpiunitatetako (zeharkako lotura) har zitzakeela iradoki zen (Alaimo et al., 2013). Itxuraz, alboko azpiunitateetako AB moduluak biltzen dituenez, mihiztadura distalaren domeinuak zeharkako lotura errazten du. Aitzitik, adierazgarri funtzionalak daude zeharkako lotura K_V7.2 kanaletan ematen dela pentsatzeko. A edo B helizean mutazio bat daramaten K_V7.2 kanalak konbinatzean, mutazio bakoitzak CaM-rekin elkartzea eragozten duelarik, kanal funtzionalak sortu zituzten, zeharkako CaM loturaren garrantzia nabarmenduz (Alaimo et al, 2013).

4.2. HELBURUA

Kapitulu honen helburu nagusia tetramero bateko azpiunitateen arteko trukea eta CaM loturaren konfigurazioan (zuzena eta zeharkakoa) D helizearen ekarpena aztertzea da. Gainera, Ca^{2+}-ak tetrameroen egonkortasunari nola eragiten dion aztertuko dugu. Horretarako fluoreszentzian oinarritutako experimentuak egingo dira.

4.3. EMAITZAK

4.3.1. Osagarritasuna frogatzeko analisia: D-helizeak sortzen duen helize superkiribildua, CaM-ren zeharkako-konfigurazioko loturan eragiten du.

Lehenik, D-CaM-, mutaziorik gabeko proteinekin lotzeko propietateak ebaluatu genituen. D-CaM deribatu dansilatua erabiliz, proteina honek CaM konformazio aldaketen berri ematen du, fluoreszentzia emisioaren gehikuntza kasu, itu-proteina batekin elkartuz (Alaimo et al., 2013). 4.4.

(A) irudiak D-CaM fluoreszentzia handipenaren denborazko ibilbidea erakusten du, CaM lotzeko AB eta ABCD modulua gehitu ondoren. Bi minutu baino gutxiago igaro ondoren, seinalea erantzun maximora hurbildu zen bi kasuetan.

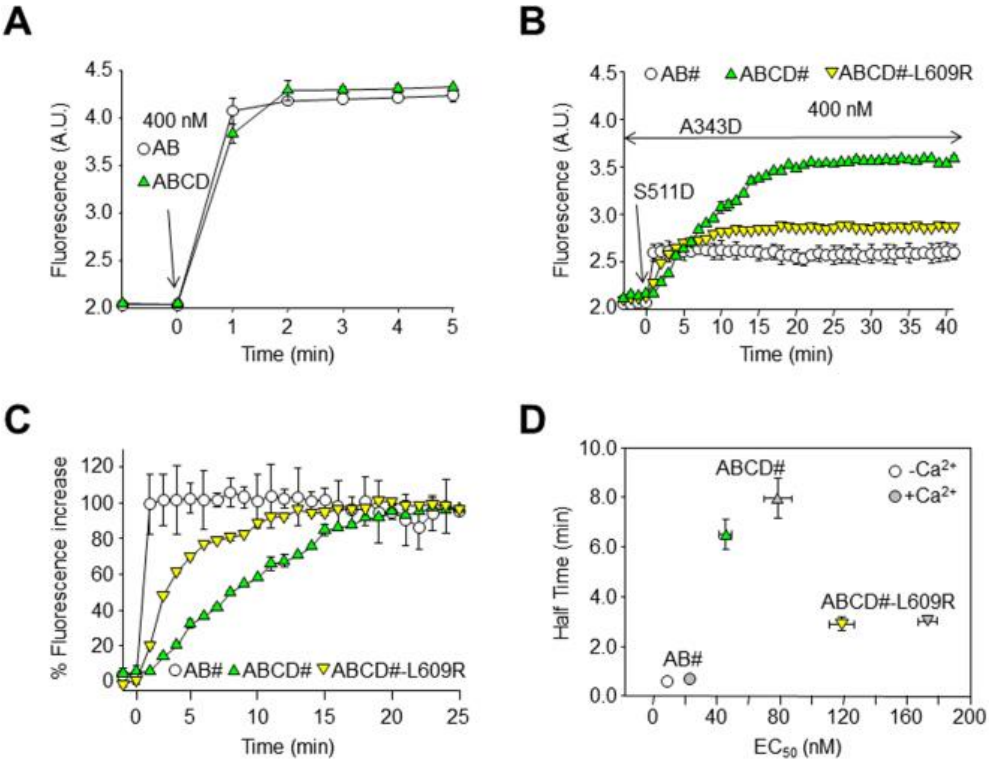

4.4. irudia. Zeharkako loturaren konfigurazioari D-helizeak sortzen duen helize superkiribilduak eragiten dio. (A) AB-ra eta ABCD-ra (400 nM) batu ondoren D-CaM-ren (12,5 nM) fluoreszentzia handitzen da. Puntu bakoitzak 4 esperimenturen batezbestekoa adierazten du. Fluoreszentziaren gehieneko igoera 2 minutu baino gutxiagotan heldu zen. **(B)** A343D (400 nM) helizearen mutantearen presentzian D-CaM fluoreszentziaren igoera, B helizeko mutantea, S511D, (400 nM) gehitu ondoren, CD (AB#, zirkulu irekiak), ABCD# (triangelu berdeak gorantz) eta AB#CD modulurik gabeko proteinentzat. Traolak (#) A helizearen eta B helizearen mutanteen nahasketa berdina adierazten du. Traza bakoitzak 3 esperimenturen batezbestekoa adierazten du. **(C)** Fluoreszentzia igoera denboran zehar, normalizatua, (B) -n erakusten diren datuetatik abiatuta. **(D)** AB #, ABCD #eta ABCD # -L609R bidez D-CaM fluoreszentziaren gehienezko emisiora iristeko batez besteko denboraren grafikoa.

Ondoren, konplementazio-saiakuntza baten bidez, zeharkako loturaren konfigurazioaren jabekuntza aztertzen dugu, CaM-rekin lotu ezin diren mutanteak erabiliz: A helizean (A343D) eta B helizean (S511D). K_V7.2 lotura-domeinuen mutante horiek konbinatuz, zeharkako lotura-mota *in vitro* hartzeko saiakera bat diseinatu genuen, D-CaM-ren fluoreszentzia monitorizatuz, proteina mutanteak sekuentzialki gehitzen diren bitartean. Sinplifikatzeko, AB-A343D (A helizearen mutantea) eta AB-S511D (B helizearen mutantea) nahasketa ekimolarrari AB# deitzen zaio, eta ABCD≠, ABCD-A343D eta ABCD-S511D-ren nahasketa ekimolarrari. Kontzentrazioak mutatutako

proteina bakoitzari dagozkio, eta, beraz, AB-343D-ren 100 nM eta AB-S511D-ren beste 100 nM nahastearen emaitza dela.

Beraz, D-CaM-ren fluoreszentzia handitzea gerta daiteke A343D B helizeko mutantea eta S343D A helizeko mutantea elkartzen direnean. Lehenik, A343D mutantea D-CaM-ri gehitu zitzaion, eta fluoreszentziaren emisioan ez zen aldaketa esanguratsurik egon (4.4. AB#). B helizearen mutantearen, S511D, ondorengo gehikuntzak, ordea, fluoreszentzia minutu batean handitzea ekarri zuen. Beraz, disoluzioan zeharkako konfigurazioa eskuratzeko minutu bat baino gutxiago behar izan zen mihiztadura domeinurik (D-helizea) ez zegoenean (4.4.B, C, zirkuluak).

Ondoren, C eta D helizeen eragina frogatu genuen zeharkako lotura eskuratzeko, tetramerizazioa eragozten duen mutazio bat erabiliz. 4.4. irudian B eta C grafikoek erakusten dute CD helizeen presentziak (goranzko triangeluak) hainbat aldaketa eragin zituela erantzunaren profilean. Lehenik, fluoreszentziaren gehikuntzaren magnitudea handiagoa izan zen, eta, bigarrenik, zeharkako-loturara eskuratzeko denbora gehiago behar izan zen. Fluoreszentziaren maximoa berdina izan zen 25 ° C eta 37 ° C-tan, baina maximo hori 37 °C-tan azkarrago lortu zen, batez besteko seinalera iristeko denbora 9,2 ± 0,3 eta 12,0 ± 0,4 minutu izan ziren 37°C eta 25°C-tan hurrenez hurren, frogatutako kontzentrazioa 400 nM-koa izan zenean.

Ca^{2+}-aren inpaktua ABCD proteina mutanteekin egindako konplementazio-saiakuntza batean ere aztertu zen, eta kasu honetan, Ca^{2+}-aren presentziak nabarmen murriztu zuen D-CaM fluoreszentziaren igoera-tasa (4.4. irudia B eta C). Ca^{2+}-aren eta zeharkako lotura-abiaduraren arteko mendekotasuna argia zen probatutako proteina kontzentrazio guztietian. Gainera, itxurazko lotura-afinitaeta txikiagoa izan zen Ca^{2+}-aren presentzian, frogatutako konplexu guztietarako ere (Yus-Najera et al., 2002; Bonache et al., 2014; Alaimo et al., 2017).

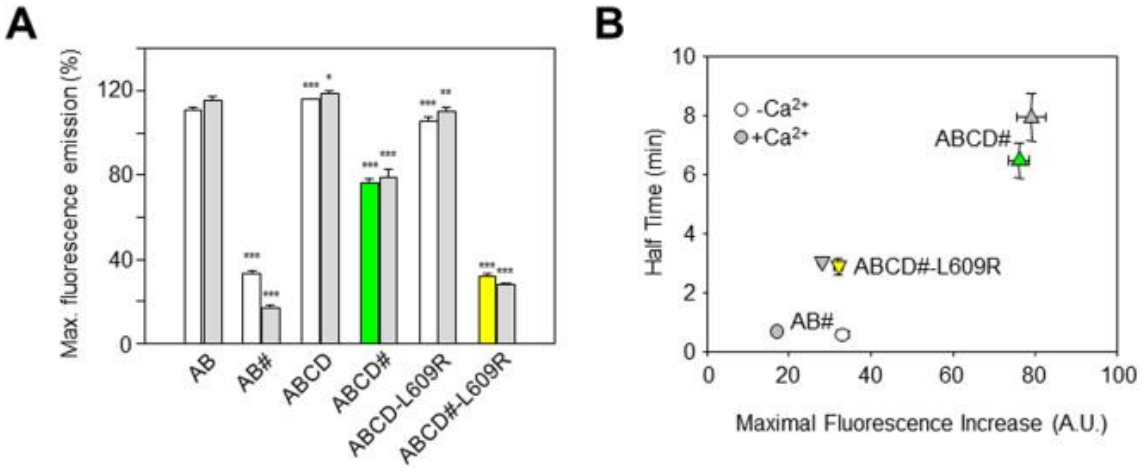

4.5. irudia. D-CaM fluoreszentzia-ren emisio maximoaren laburpena. (A) Adierazitako proteinen kontzentrazio aseek eragindako D-CaM fluoreszentziaren emisioaren gehieneko igoerak. Datuak Ca^{2+}-aren presentzian (barra grisak) edo Ca^{2+}-rik gabe (zuria; eta barra hori eta berdeetan ABCD eta ABCD -L609R, emaitzak nabarmentzeko) adierazten dira (n>3). Izartxoek balio nabarmen ezberdinak adierazten dituzte AB-rekin konparatuz: *p< 0,05;** p<0,01;*** p<0,001. **(B)** Fluoreszentzia maximoa lortzeko denbora (D-CaM-ren balio maximoaren erdia versus fluoreszentziaren gehikuntza maximoa). # ikurrak A343D eta S511D mutanteen nahasketa ekimolarra adierazten du.

Azkenik, fluoreszentziaren gehieneko igoera murriztu egin zen konplementazio-saiakuntzan (4.5 irudia, A grafikoan, AB vs AB #, ABCD vs ABCD#, ABCD-L609R vs ABCD#-L609R), D-CaM fluoreszentziaren igoeraren zinetikarekin partzialki lotuta zegoena (4.5. irudia, B). Lotura-zuzena eragozteak %25 inguruko murrizketa eragin zuen D-CaM fluoreszentzia maximoan, (ABCD eta ABCD# 4.5. irudia). AB# izan ezik, murrizketa horren magnitudeak ez zuen Ca^{2+}-aren eraginik izan, eta handiagoa izan zen (>%65-eko murrizketa) tetramerizazio domeinua falta zenean (AB vs #) edo helize superkiribildua eragotziko zuen mutazio bat zegoenean (ABCD vs ABCD#-L609R).

4.3.2. FP-ABCD/CaM konplexu tetramerikoen arteko azpiunitateen trukea Ca^{2+}-aren eraginpean dago.

GST-AB sistemarekin lortutako emaitzek eta A eta B helizeen mutanteen osagarri funtzionalak zeharkako konfigurazio baten eraketa adierazten dute. D helizearen bidezko tetramerizazioak trukeari nola eragiten dion ebaluatzeko eta CaM eta wt ABCD domeinuaren tetramerizazioaren arteko loturari buruzko informazio gehiago lortzeko, FRETren bidez mihiztadura tetramerikoen arteko trukea monitorizatu zen. ABCD domeinuaren bi bertsio etiketatu ziren N muturrean CaM-rekin konplexuan, bat zian proteina fluoreszentearekin etiketatua (CFP turquoise2) eta bestea

fluoroforo hori batekin etiketatua (YFP zitrina) (4.7. irudia). Frogatu genuen proteina hauek ABCD/CaM 4:4 estekiometria dutela eta tetramero gisa konfiguratzen direla.

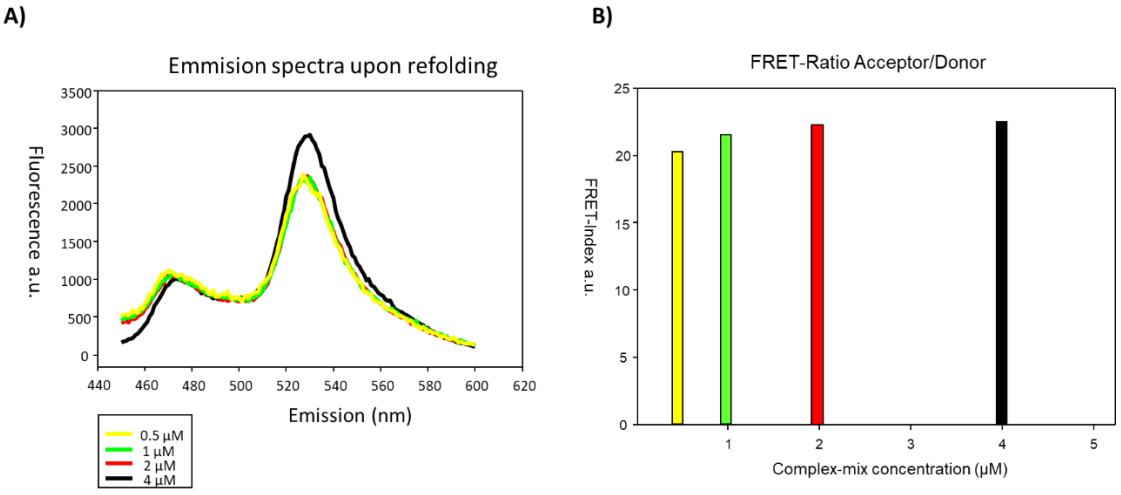

4.6. irudia. Urearekin hedatzea eta atzera tolestea. (A) CFP-hABCD eta YFP-hABCD tetrameroak kontzentrazio ekimolarrekin nahastu ziren (0,5, 1, 2 eta 4 µM) eta urea 6 M gehituz destolestu ziren. Fluoreszentzia-tanpoian dializatu eta gel-iragazketaren bidez garbitu ondoren, laginak 500 nM-tan diluitu edo kontzentratu ziren, eta lagin bakoitzaren emisio-espektroak 433 nm-tan kitzikatu ondoren neurtu ziren. **(B)** Lagin-kontzentrazio ezberdinen FRET indizea, birtolestearen ondoren.

Lehenik, FRET-indize maximoa zein zen kalkulatzeko, 6 M urearekin desnaturalizatu ziren proteinak eta kontzentrazio ekimolarretan nahastu ziren bi tetrameroak. Ondorean, dialisiz, urea ezabatu zen eta tetrameroak ausaz mihiztatuko dira. Proteina nahasketen kontzentrazio ezberdinetara egin genuen esperimentua: 0,5, 1, 2 eta 4 µM, laginaren kontzentrazioak lortutako FRET maximoari nola eragin ziezaiokeen aztertzeko. FRET indizea neurtu zen, lehen deskribatu bezala. FRET indizea (YFP/CFP) antzekoa izan zen frogatutako kontzentrazio guztietan: 2,1 ± 0,02 0,5 µM-tan, 2,1 ± 0,05 1 µM-tan, 2,2 ± 0,08 2,5 µM-tan eta 2,2 ± 0,1 4 µM-tan. Beraz, laginaren kontzentrazioak lortutako FRET-maximoan duen eragina hutsaren hurrengoa da, frogatutako kontzentrazio tartean. Kontuan izan, banaketa binomialaren arabera, ausaz mihiztatutako tetrameroak hainbat konposiziotan osatzea espero dela: (1) 3/8 bi CFP-hABCD azpiunitatek eta bi YFP-hABCD azpiunitatek osatua, (2) ¼ hiru YFP eta beste CFP-hABCD batek osatua, (3) ¼ gehienez hiru CFPk eta YFP- batek osatua (4) $1/16$ YFP-hABCDren tetramero osoak izango dira eta (5) 1/16 CFP-hABCDren tetrameroak.

%100-eko trukearen ondoren lor dezakegun FRETren balio bat lortu ondoren, esperimentua egin genuen tetrameroak 0,5, 1, 2,5 eta 4 µM kontzentrazioetan inkubatuz (4.6. irudia).

Beraz, bi tetrameroak nahastu egin ziren eta emisioa 45 minutuz neurtu zen. Denboraren araberako igoera bat egon zen hartzailearen 530 nm-ko emisioan 436 nm-tan eszitatu ondoren, konplexu tetramerikoen azpiunitateen arteko elkartrukea gertatzen ari zela iradokitzen zuena. CFP-ABCD/CaM konplexuaren (emailea) eta YFP-ABCD/CaM konplexuaren (hartzailea) nahasketa ekimolar batean denboran zeharreko FRET garapena 4.8 irudian erakusten da. Bere FRET-maximoaren erdia lortzeko denbora 1,2 ± 1,6 minutukoa izan zen 500 nM nahasketa baterako.

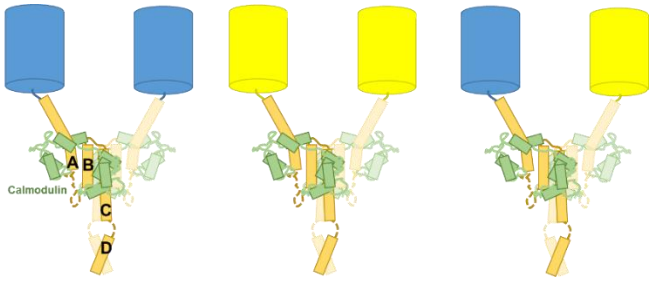

4.7. irudia. Esperimentua irudikatzen duen eskema: CFP-ABCD/CaM konplexua YFP-ABCD/CaM delakoarekin nahastu zen, FRET garatzera eraman zuen proteina truke baten ondorioz. Konplexu tetramerikoen bi azpiunitate bakarrik marraztu dira argitasun gehiagorako.

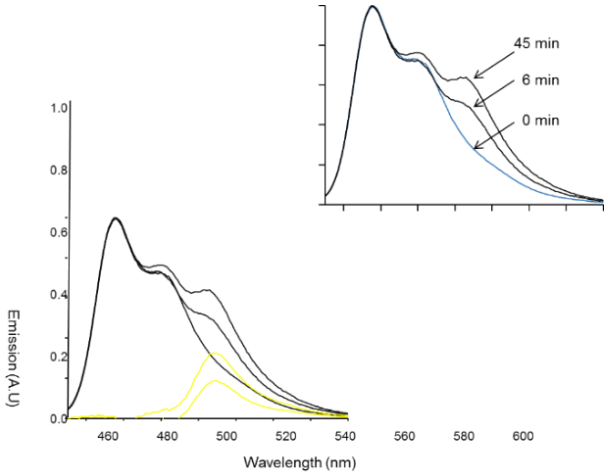

4.8. irudia. Nahaste ekimolar baten emisio-espektroak 2,5 µM-tan. 2,5 µM CFP-ABCD/CaM eta 2,5 µM YFP-ABCD/CaM nahasketaren emisio espektro normalizatuak denbora ezberdinetan. Trazadura horiak CFP normalizatuaren (urdina kentzearen) emaitza dira.

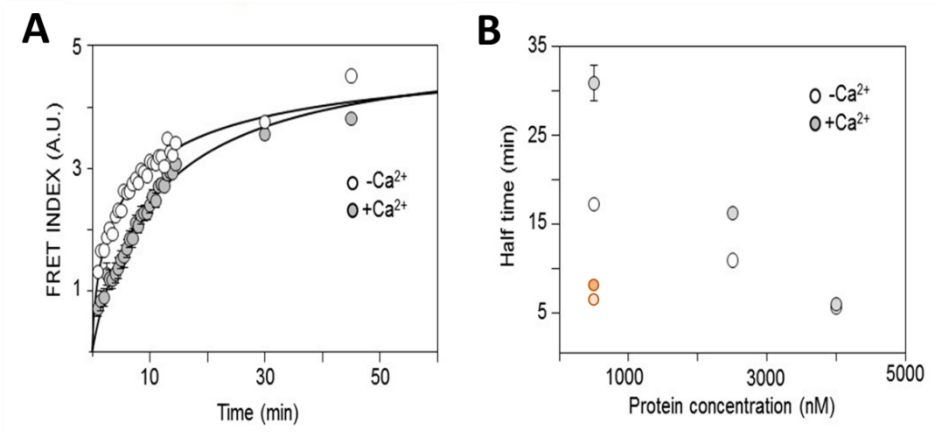

4.9. irudia. (A) 2,5 µM CFP-ABCD/CaM eta 2,5 µM YFP-ABCD/CaM nahasketa baten FRET indizearen igoera denboran zehar, Ca^{2+}-ren presentzian (zirkulu grisak) eta gabezian (zirkulu zuriak). Traza bakoitzak 3 esperimenturen batezbestekoa adierazten du. **(B)** FRET indizearen batez besteko igoera maximoa lortzeko denboraren eta proteinen kontzentrazioaren (zirkulu grisak) eta Ca^{2+} gabeziaren (zirkulu zuriak) arteko erlazioa. Laranjaz, osatze-saiakuntzaren balioak adierazten dira (4.4 irudia). Puntu bakoitzak 3 esperimentu edo gehiagoren batezbestekoa adierazten du.

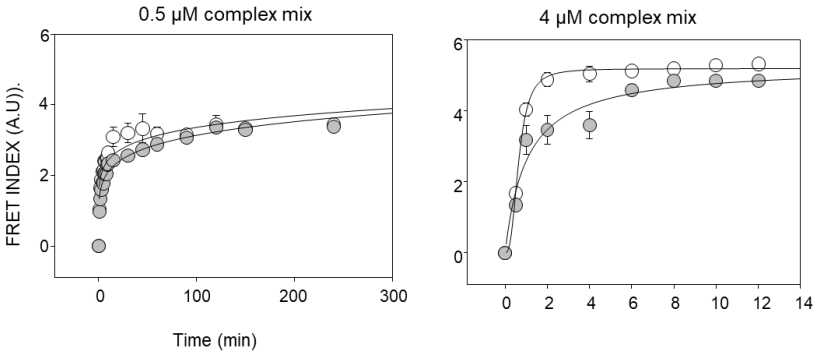

4.10. irudia. FRET indizearen gorakada denboran zehar. 0,5 µM-tako nahastea ezkerrean eta 4 µM-ren nahasketa eskuman, Ca^{2+}-aren presentzian (zirkulu grisak) eta gabezian (zirkulu zuriak). Emaitzak, 4 esperimenturen batezbestekoa da.

FRET garapenaren denbora-ibilbidea Ca^{2+}-arekiko sentikorra izan zen. Katioi horren aurrean, EC50 beranduago lortzen da kaltzio gabeko laginarekin alderatuta: 17,2 ± 0,8 minutu kaltziorik gabe eta 30,8 ± 2,1 minutu Ca^{2+}-aren presentzian (4.9. irudian, denbora erdia Ca^{2+}-arekin eta Ca^{2+}-rik gabe). Beraz, azpiunitateen arteko trukea motelagoa izan zen katioi honen aurrean, tetrameroak egonkorragoak direla iradokituz. Hau zeharkako lotura aztertzeko osatze-saiakuntzan lortutako

emaitzen antzekoa da (4.5. irudia), non frogatu zen ABCD/CaM konplexuak egonkorragoak zirela fisiologikoki esanguratsua zen Ca^{2+} kontzentrazio baten presentzian.

Hala ere, 45 minutuko inkubazioaren ondoren lortutako FRET balioak oso baxuak izan ziren. 4 µM-tan egindako esperimentuan, 45 minutuko inkubazioaren ondoren, 0,8 ± 0,04-ko FRET-indizea lortu zen Ca^{2+}-rik ez zegoenean eta 0,7 ± 0,05 Ca^{2+}-aren presentzian. Balio hauek, ausaz sortutako tetrameroetan kalkulatutako maximoa baino askoz baxuagoa da, non FRET indizea 2,2-ra heltzen zen (4.6. irudia), horrek esan nahi du azpiunitateen arteko trukea motela dela, eta 45 minutuko inkubazioaren ondoren, azpiunitate gutxi batzuk bakarrik trukatu zirela.

Ca^{2+}-ak tetrameroen egonkortasunean duen eragina bereziki nabarmena da, kontuan hartuta D helizea CaM lotura-domeinutik 20 Å-tara dagoela, krio-EM irudien arabera eta D helize eta CaM edo AB domeinuaren arteko zuzeneko interakzio fisikoaren ebidentziarik ez dagoela (Sun eta MacKinnon, 2017).

4.3.3. FP-AB/CaM-FP konplexuen arteko CaM-en trukerik ez da gertatzen.

Nolabaiteko eztabaida dago CaM-ren loturaren dinamikari dagokionez. Alde batetik, CaM Kv7.2 kanalaren egitura-elementutzat hartzen da, eta, bestalde, CaM. $K_V7.2$ kanalen funtziorako ezinbestekoa ez dela uste da. CaM loturaren arteko erlazioa hobeto ulertzeko, FRETren bidez CaM-en arteko trukea monitorizatu zen. AB domeinua zian fluoroforoarekin (mTFP1 aldaera) markatu zen N-terminalean, eta AB konplexuaren bi bertsio sortu eta purifikatu ziren: lehenengoa wt CaM-rekin (etiketarik gabe) eta bigarrena CaM-YFP (mcpVenus) proteina fluoreszentearekin (4.11 eta 4.12 irudia).

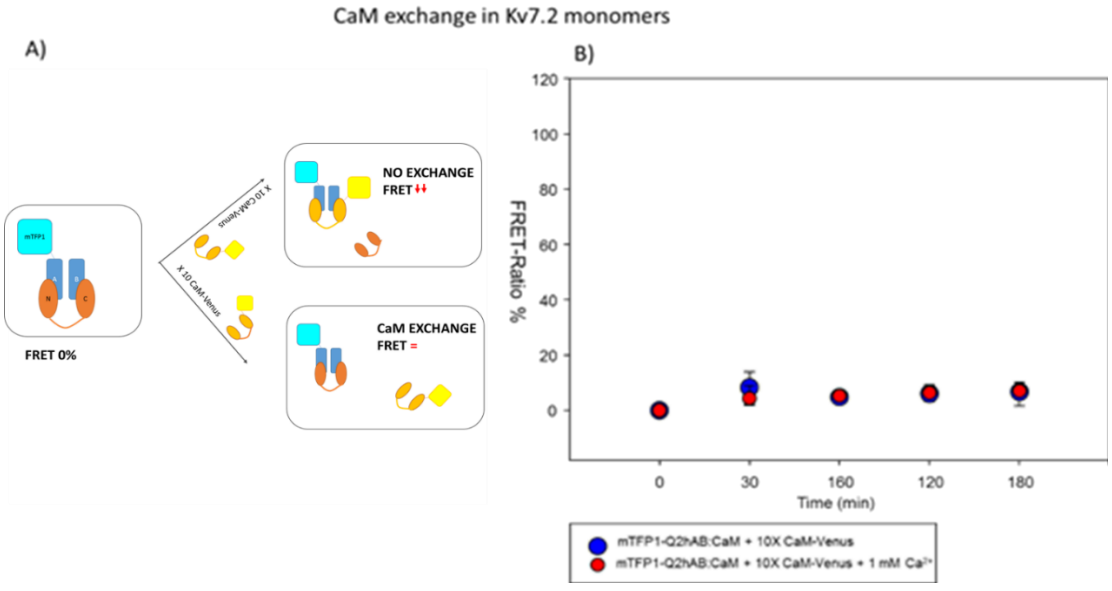

4.11. irudia. CaM trukea monomeroetan K_V7.2. (A) Esperimentua irudikatzen duen eskema: CFP-*h*AB/CaM konplexua CaM-YFPrekin nahastu zen, FRET garatzera eraman lukeen proteina trukea dagoen aztertzeko. **(B)** FRET indizea ehunekotan denboran zehar adierazten da mTFP-Q2*h*AB:CaM (500 nM) konplexuan, CaM-Venus 5 µM-tan gehitu ondoren. Zirkulu urdinek Ca^{2+}-rik gabeko lagina irudikatzen dute, eta gorriek Ca^{2+} librea 1 mM-tan dagoenean. Datuek 4 esperimentu independenteren batezbestekoak adierazten dituzte.

mTFP-hAB:CaM konplexua CaM-Venusekin nahastu zen 10 aldiz handiagoa zen kontzentrazioan, 500 nM eta 5 µM, hurrenez hurren. Bi proteinak nahastu ondoren, elkarren arteko energiaren transferentzia kuantifikatzen dugu, mTFP1 (458 nm) kitzikatuz eta 470 eta 570 nm arteko emisioa neurtuz. CaM-en arteko trukea badago, FRETren garapena ikusiko genuke. CFP-hAB/CaM konplexuaren (emailea) eta CaM-YFP (hartzailea) nahasketaren FRETren garapena denboran zehar neurtu genuen (3 orduz) (4.11 irudia). FRET-indizea ez zen aldatu inkubazio tarte horretan, CaM-en artean trukerik ez dagoela erakutsiz, ez Ca^{2+}-aren presentzian, ez gabezian. Modu bertsuan, mTFP1-Q2hAB:CaM-YFP konplexua 10 aldiz CaM konplexuarekin nahastu genuenean, ez genuen FRETen murrizketarik ikusi 3 orduko inkubazioaren ondoren, CaM-en arteko trukea balego espero zen bezala (4.12. irudia). Kasu honetan, FRET-indizea txikiagoa da Ca^{2+}-aren presentzian, baina kaltzioaren presentzian konplexuak duen konfigurazioari zor zaio, eta ez CaM-en arteko truke bati.

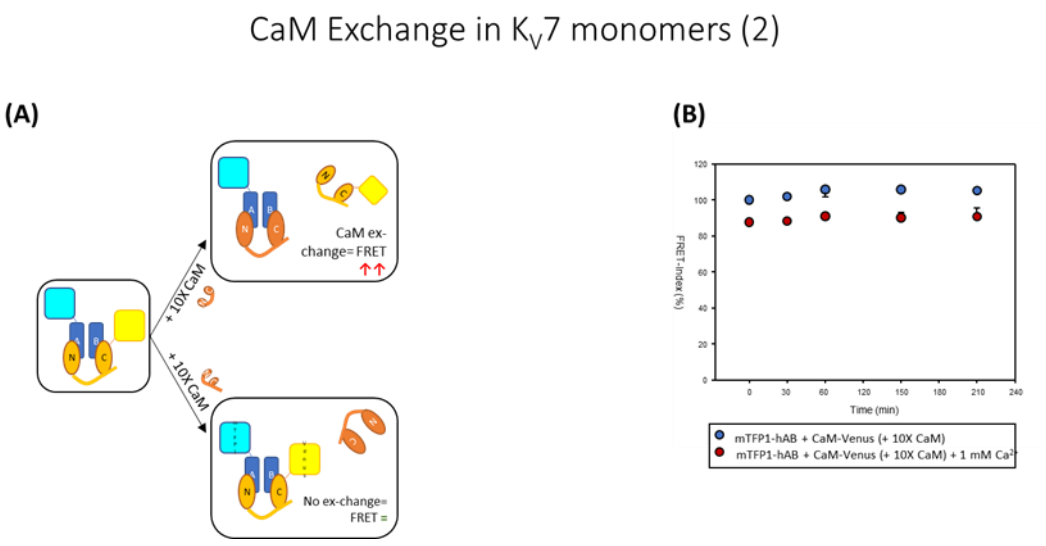

4.12. irudia. CaM trukea K_V7.2 monomeroetan (2). (A) Esperimentua irudikatzen duen eskema: CFP-ABCD/CaM-YFP konplexua CaM-rekin nahastu zen, FRET murrizketa ekarriko lukeen proteina trukea dagoen aztertzeko. **(B)** FRET harremanaren denbora-ikastaroa mTFP-Q2*h*AB:CaM-Venus (500 nM) konplexuan CaM 5 µM-tan gehitu ondoren. Zirkulu urdinek Ca^{2+}-rik gabeko lagina irudikatzen dute, eta gorriek Ca^{2+} librea 1 mM-tan dagoenean. Datuek 4 esperimentu independenteren batezbestekoak adierazten dituzte.

4.4. EZTABAIDA

Hemen, D helizeak CaM elkarteari egiten dion ekarpena ikertzen dugu. Aurretik, D helizearen presentziak CaM K_V7.2 kanaletan elkartzea sustatzen zuela frogatu zen, ziuraski helize superkiribilduaren eraginez (4.1. irudia). Hau, bereziki deigarria da, D helizea eta AB CaM-ren lotura domeinua, krio-EM irudien arabera 20 Å baino gehiagok banatzen dituztela kontuan hartuta, D eta CaM helizearen edo AB domeinuaren arteko zuzeneko elkarreragin fisikoen ebidentziarik gabe (Sun eta MacKinnon, 2017).

Kapitulu honetan, D helizeak sortzen duen helize superkiribilduak AB/CaM arteko zeharkako lotura errazten duela eta aldiberean, CaM loturak tetrameroen mihiztadura egonkortzen duela dioen hipotesia babesten duen ebidentzia aurkezten dugu. Harrigarria bada ere, badirudi konfigurazio tetramerikoa Ca^{2+}-arekiko sentikorra dela nolabait, katioi honen aurrean egonkorragoa bihurtuz. Beraz, gure datuek erakusten dute elkarrekiko komunikazio garrantzitsu bat egon daitekeela CaM eta K_V7 kanalen D-helizearen artean.

L609R mutazioa, helize superkiribilduen disruptiboa dena, D-CaM loturaren bidez aztertu genuen. Bitxia bada ere, wt ABCDrekin alderatuta, fluoreszentzia maximoaren balioa eta maximo hori lortzeko denbora murriztu egin zen. Gainera, lotura-afinitatea txikiagoa izan zen ABCD#-rekin (A helizeko mutantea eta B helizeko mutantearen nahasketa ekimolarra) alderatuta (Ec50 = 45,5 ± 3,8 nM). Beraz, afinitatearen aldaketek ezin izan zituzten zinetikaren ezberdintasunak azaldu. Ez zen aldaketa esanguratsurik egon D-CaM-ren fluoreszentziaren emisioan, B helize mutantea (S511D) gehitu ondoren (Alaimo et al., 2013).

ABCD eta ABCD#-rekin lortutako datuak alderatzean, ABCD#-k ABCD-ren CaM lotura guneen kopuru bera edo soilik lotura guneen erdia erakusten duen konfigurazio bat har lezakeela pentsatu behar da. Bi lotura-moduak proportzio berdinetan baleude, ABCD#-ren fluoreszentzia maximoak %75 ingurukoa izan beharko luke, benetan behatutako baliotik ez oso urrun. Azalpenik sinpleena da D helizerik ez egoteak edo L609R mutazioaren ondorioz helize superkiribilaren sorpena eteteak AB-CaM*-ren zeharkako-loturen egonkortasuna murriztu zuela.

CaM loturaren eta wt ABCD-ren tetramerizazioaren arteko harremanari buruzko informazio gehiago lortzeko, mihiztadura tetramerikoen arteko trukea FRETren bidez monitorizatu zen. ABCD domeinuaren bi bertsio, N-terminalean etiketatuta, zian proteina fluoreszentearekin (CFP turquoise2) edo hori batekin (YFP zitrina) kontzentrazio ekimolarretan nahastu ziren. Baldintza hauek ez dute CaM-ren lotzeko modua bereizten, eta, izatez, CaM- konfigurazio-zuzenean zein zeharkako-konfigurazioan egon daiteke. Bi proteinak nahastu ondoren, denboraren araberako handipen bat egon zen hartzailearen 530 nm-ko igorpenean, 436 nm-tan kitzikatu ondoren,

konplexu tetramerikoen azpiunitateen arteko elkartrukea gertatzen ari zela iradokitzen duena. Batez besteko gehieneko FRET-indizea lortzeko denbora 12,2 ± 1,6 minutukoa izan zen 500 nM-ko nahasketa baterako. ABCD domeinuen arteko trukea abiaduraren mugatzailea dela suposatuz, bai osagarritasun-saikuntzerako, bai FRET saiakuntzetarako, bi paradigmen bidez lortutako tasak alderatzeko modukoak dirudite. Batez besteko FRET-maximoa lortzeko denbora (500 nM) ABCD# 400 nM proteinen bikoitza izan zen gutxi gorabehera. Hala ere, emailearen eta hartzailearen kontzentrazioa 5 aldiz handitu zenean (2,5 µM), gehieneko FRETren erdia lortzeko denbora 6.9 ± 0,2 minutura murriztu zen, 400 nM-tan osagarritasun-saiakuntzan ikusitakoren batez besteko denboratik hurbil (4.5. irudia). Beraz, CaM-ren lotura-gunean mutazioak sartzeak truke azkarragoa ekarri zuen (osagarritasun-saiakuntzan), beraz, mutazio horiek aldatu egin zuten mihiztadura tetramerikoaren egonkortasuna.

Hemen ere, tetrameroen azpiunitateen arteko trukea Ca^{2+}-arekiko sentikorra izan zen, eta denbora gehiago behar izan zen batez besteko balio maximora iristeko katioi honen presentzian (4.9. irudia). Hori zeharkako-lotura kontrolatzeko diseinatutako baldintzetan ematen den erantzunaren antzekoa da (4.5. irudia). Hortaz, pentsa genezake ABCD/CaM konplexuak egonkorragoak zirela Ca^{2+}-aren presentzian.

Gure datuek erakusten dutenez, ABCD domeinuen azpiunitateen arteko trukea gertatzen da, baina oraindik ez dago argi kanalaren mintz zeharreko domeinuek, nola eragiten duen mihiztatze-domeinuaren trukakean eta malgutasunean.

Azkenik, $K_V7.2$ azpiunitatearen eta CaM-ren arteko trukea nola gertatzen den aztertzeko, beste FRET esperimentu bat egin genuen. Konplexuaren egonkortasuna aztertzeko CaM librea gehitu zen. Giro-tenperaturan inkubatu, eta fluoreszentzia-emisioa 30 minuturo erregistratu zen. Ez zen aldaketarik ikusi FRET-indizean, Ca^{2+}-rik gabe zein Ca^{2+}-aren presentzian (1 mM), eta horrek iradokitzen du ez dagoela CaM-ren arteko trukerik denbora-tarte horretan.

Nola azal dezakegu tetrameroko azpiunitateen trukea eta, aldi berean, CaM-ren trukaketarik ez egoteak?

Kontuan hartu beharko genuke tetrameroko lotura zuzena eta zeharkakoaren arteko aldaketak ez dakarrela nahitaez CaM molekulen trukea. Litekeena da CaM lobulu bat helize bati lotua egotea konstitutiboki, segur aski, B helizera N-lobuluaren bidez, afinitate handiagoarekin lotzen baitira (Alaimo et al., 2014). Beste lobulua, ordea, C-lobulua, azpiunitate ezberdinen A helizetara txandaka lotzen zaion bitartean.

Gainera, gure datuek erakusten dutenez, D helizearen menpeko helize superkiribilduaren eraketak CaM eta A eta B helizeen arteko elkarrekintza egonkortzen du (4.5. irudia). Sun eta

MacKinnonek ebatzitako K_V7.1-ren egitura tetramerikoak, C helizearen eta CaM-ren C-lobuluaren arteko elkarrekintzak erakusten ditu (Sun eta MacKinnon, 2017), egitura sendoago bat sortzen lagundu dezakeena. Egonkortze hau, neurri batean, konfigurazio geometrikoaren bidez sor daiteke, D helizearen bidez, poroaren azpian trinkoagoa den AB/CaM eraztun baten eraketa sustatzen duelako. Honek, aldi berean, CaM-ren lotura A eta B helizeetara, modu ezberdinetan aktibatzea ahalbidetuko lukeelarik, zeharkako-konfigurazioan kasu. Emaitzak bat datoz A-B moduluaren eta D helizeak, CaM-k eta Ca^{2+}-ak osatutako tetrameroaren arteko elkarrekiko akoplamendu aktiboa barne hartzen duen ereduarekin, eta horrek iradokitzen du D helize superkiribilduak portaera dinamikoa duela.

Hemen aurkeztutako emaitzek CaM-ren funtzioa eta K_V7.2 kanalen Ca^{2+} menpeko aktibazioa mekanismoa azal ditzakete. Lehen aipatu dugun bezala, K_V7.2-*h*AB konplexuar ez da disolbagarria CaM-rik ez dagoenean, agregatu egiten da. Gainera, CaM-k kanalarekiko duen afinitatea hain da handia, non frogatu ditugun *in vitro* baldintzetan ezin izan dugula konplexutik banatu. Ziur asko, hau ere *in vivo* gertatzen da, CaM-ren zelula barneko kontzentrazio altua (10^{-6} - 10^{-5} M) dela eta (Ching eta Mean, 2000).

Egoera hau K_V7.1 kanal homologoaren antzekoa da, non CaM-ren lotura konstitutiboa proposatu zen (Sachyani et al., 2014), eta beste proteina batzuetan ere, fosforilasa kinasa kasu (Ching eta Mean, 2000). Hala ere, eredu hau zalantzan jarri da K_V7.2 kanalak, B helizean mutazio baten eramaileak, S511D, CaM elkartzea eragozten dutenak, funtzionalak zirela frogatu zenetik (Gomez-Posada et al., 2011). Ikusi dugunez, funtzioaren kontserbazioa CaM-ren zeharkako-loturaren konfigurazioagatik izan liteke. Gainera, kontuan izan behar dugu S511D mutazioa fosfomimetikoa dela. Toki honen fosforilazioak, nolabait, CaM-ren batasuna ahuldu lezake, zeharkako lotura erraztuz.

5. KALTZIOAK ERAGINDAKO ALDAKETA KONFORMAZIONALA K_V7.2 TETRAMEROETAN

5.1. SARRERA

Sarreran aipatzen dugun bezala, M-korronteak bere izena hartzen du hartzaile muskarinikoen aktibazioak K^+-ren konduktantzia ezabatzen duelako neurona sinpatikoetan, neuronaren kitzikagarritasuna areagotuz. Laster jakin zen bigarren mezulariak C fosfolipasa aktibatzen zuela, IP_3-ren lotutako ekoizpenarekin eta Ca^{2+}-a zelula barneko biltegietatik askatuz. Beraz, Ca^{2+}-a susmagarri bihurtu zen, eta hasierako lan batzuek bigarren mezulari hau inhibizioaren arduradun nagusitzat jo zuten. Hala ere, M-korrontea aurkitu eta 20 urtera, "bigarren mezulari misteriotsu" hura aurkitu zen (Suh eta Hille, 2002). PIP_2 zen, KCNQ kanalaren funtziorako behar-beharrezkoa den kofaktorea. PIP_2 mailak jaisten direnean, boltai sentsorearen domeinua, poro domeinutik deskonektatzen da eta kanala ezin da ireki boltai-aldaketei erantzuteko (Zaydman eta Cui, 2014).

Ca^{2+}-ren efektua M-korrontean, ordea, konplexuagoa da. Igoera moderatuek neurona sinpatikoen korrontea hobetzen dute, eta kontzentrazio altuagoan korrontearen ezabatzea ikusten da (Marrion et al., 1991). Ca^{2+}-ak, neurona sinpatikoetan, M-kanalaren aktibitatea erreprimitzen du modu itzulgarrian; beraz, ezin liteke izan kinasen edo fosfatasen efektuaren bitartekaria (Selyanko eta Brown, 1996).

Ca^{2+} eta CaM zelula barneko estimulazioa handitzeak, C-fosfolipasaren bide metabolikoak aktibatzearen ondorioz M-korrontea hobetzea eragiten du, KCNQ2/3 heteomeroak adierazten dituzten Xenopusen obozitoetan, Eag1 korronteak erabat ezabatzen diren bitartean (Gomez-Posada et al., 2011). Beraz, Ca^{2+}-ak, KCNQ-ren korronte neuronalen inhibizioa eta indartzea eragin dezake. Aitzitik, I_K edo KCNQ1-n bihotz-korronteen sustapena bakarrik deskribatu da (Tobelaim et al., 2017). Oro har, suposatzen da CaM zuzenean inplikatuta dagoela KCNQ kanalen Ca^{2+}-aren menpeko erregulazioan, nahiz eta zeharkako ebidentziak baino ez dauden eskuragarri.

Sarreran esan dugun bezala, KCNQ kanalen boltai sentsore domeinuak 6TM arkitektura permutatu bat dute, bost alfa helize dituen C-terminal zitoplasmatiko luze batekin (Sun eta MacKinnon, 2017). Urkila antiparaleloaren konfigurazioa hartzen dute eta boltai-sentsore domeinuaren pean egoteko joera dute. A/B helizeak KCNQ1 kanaletan mintzatik 45°-tara kokatuta daude, gutxi gora-behera, CaM-ri tokia utziz, AB helizeen eta boltai-sentsore domeinuaren artean jarri ahal izateko (5.1. irudia). TW helizea (edo post-A-helizea), horrela

izendatua SK2 C-lobuluaren akoplamendu-helizearekin duen sekuentzia antzekotasunagatik, A helizearen ondoren kokatuta dago, gutxi kontserbatutako konektore luze baten erdian (Gomis-Perez et al., 2015). B helizearen ondoren kurba itxi bat dago, eta, beraz, C helizea, mintzarekiko perpendikularki kokatuta dago. *In vitro* dimero ahulak eratzeko joera duela deskribatu da (Wiener et al., 2008). B helizearen atzetik kontserbatu gabeko sekuentzia malgu bat dator eta azkenik D-helizea, beste azpiunitateekin helize superkiribilduak osatzen dituena, tetrameroak sortuz, Eag1 eta SK kanaletan ere ikus daitekeen ezaugarri bat (Jenke at al., 2003). Arkitektura globala SK kanalen oso antzekoa da, CaM-ren C lobulua ere ia orientazio berdinarekin A-helizeari lotzen baitzaio (Zhou et al., 2001). Hala ere, C-lobulua poroaren atetik gertu kokatzen da KCNQ kanaletan, A/B urkila helikoidala askoz laburragoa da eta A eta B helizeak askoz luzeagoa den begizta malgu batez konektatuta daude.

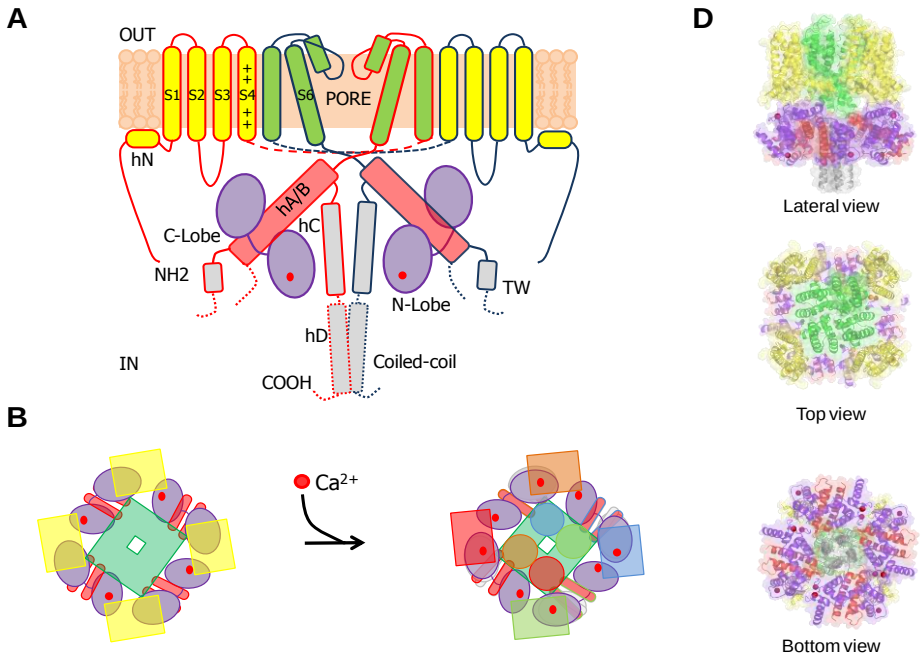

5.1. irudia. KCNQ kanal baten irudikapena. (A) mintz zeharreko segmentuak horiz daude boltai-senstsore domeinurako, berdez poro-domeinurako eta CaM purpuraz dago. S1 baino lehen mintzaren pareko helize zitosolikoa hN bezala etiketatzen da. A eta B helizeak, gorriz koloreztatuak, boltai-sentsore domeinuaren azpiko mintzaren ~ 45°-tara. Ertzak kolore gorria edo urdina du azpiunitate bakoitza identifikatzeko. Trukea kontuan hartzeko, bi azpiunitateren boltai sentsore domeinua eta poro domeinua lerro etenekin irudikatzen dira. D-helizearen helize superkiribildua tetrameroan duen ustezko posizioa lerro etenen bidez adierazten da. **(B)** Kanalaren bistaren irudikapena goialdetik, A irudiko kolore-eskema bera erabiliz. Eskuinean, Ca^{2+} kargatzean (puntu gorriak) A helizearen mugimendu txiki bat dago. (D) PDB (5VMS) koordenatuak erabiliz bistaratutako egiturak, Pymol 1.30ekin errenderizatuak A irudiko kolore-eskema bera erabiliz. (Nuñez et al., 2019).

CaM eta Ca^{2+}-a duen kanal osoaren egitura, 2017an krio-EM bidez ebatzi zena, S4 (boltai-sentsorea) goiko posizioan dagoen konfigurazio batekin ebatzi zen, baina poro domeinutik

deskonektatua. Konfigurazio ez-funtzional hori mintz plasmatikoaren PIP_2 mailak jaisten direnean hartutako konfigurazioa dela onartu da (Sun eta MacKinnon, 2017). Krio-EM bidez eratorritako egituretan, lau domeinu trinko identifika daitezke: boltai-sentsore domeinua, poro-domeinua, CaM lotzeko domeinua eta D helize helikoidala, helize superkiribilduaren konfigurazioarekin. Hala ere, A eta B helizeen arteko lotaiulu luzea ez da eredu atomistikoan ikusten, eta, beraz, ez dakigu A eta B helizeak azpiunitate beretik edo ezberdinetatik datozen. Poro domeinua konfigurazio itxian dago, beste potasio kanal batzuen egitura itxia duelarik.

5.1.1. Kalmodulinak KCNQ kanaletako S6 poro domeinuarekin eragin dezake zuzenean.

KCNQ-ren CaMBD isolatuaren zenbait egitura ebatzi dira (PDB: KCNQ1: 4V0C, 4UMO; KCNQ2: 6FEG, 6FEH; KCNQ2/3 kimera: 5J03; KCNQ4: 6B8L, 6B8M, 6B8N, 6B8N, 6B8N) Guztiek, antzeko arkitektura orokor bat erakusten dute, non A-helizea C-lobuluari lotzen zaion eta B-helizea C-lobuluari, *in vitro* saiakeretan deskribatutako lotura lehentasunekin bat datorrena (Alaimo et al., 2014). Lehenengo konplexua Ca^{2+}-rik gabe kristalizatu zen, baina N-lobuluko E-F eskuak Ca^{2+}-arekin okupatuta zeuden, honek N-lobuluko Ca^{2+}-rako afinitatea handiagoa dela iradokitzen du (Sachyani et al., 2014). Geroago ideia hau *in vitro* saiakeretan berretsi zen (Bernardo-Sesidedos et al., 2018).

5.1.2. Ca^{2+}-ren efektua azaltzen duten egungo ereduak

Kanalen estruktura osoa kaltzioarekin ebatzi ondoren (Sun eta MacKinnon, 2017; 2019) Ca^{2+}-ak eragindako konformazio-aldaketari buruzko eztabaida berpiztu zen K_V7 kanaletan.

E. Bernardo-Seisdedos et al., 2018. Lan honetan, CaM-rekin konplexuan dauden $K_V7.2$-ren A eta B helizeak Ca^{2+}-rik gabe eta Ca^{2+}-aren presentzian ebatzi ziren, Erresonantzia Magnetiko Nuklearraren (EMN) bidez. Ca^{2+}-ak sortutako KCNQ2 kanaletako CaM lotzeko domeinuaren egiturazko berrantolaketek, N-lobulu/B-helize konplexuak ia aldaketarik gabe jarraitzen duela erakusten dute, A helizearen hasierako zatia, C-lobuluaren bihurdura batekin konkomitatzen den bitartean. A helizearen segmentu proximal hau S6-rekin lotua dago (5.2. irudia). Ematen du Ca^{2+}-ak eragindako mugimenduak S6-ari eragiten diola, aurretik KCNQ2-ren egoera aktibatuko eredu batean ikusi zen bezala (Gourgy-Hacohen et al., 2014).

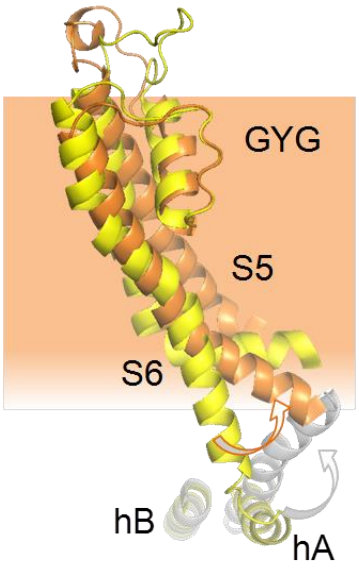

5.2. irudia. A-helizetik S6ra transmititutako mugimendua aktibazio zuzena eragin dezake KCNQ2 kanaletan. KCNQ2 irekierako eredu bat, S5 eta S6 segmentuen mugimendua, C-lobuluan Ca^{2+}-ak lotzean eragiten duen mugimenduaren eraginez. Grisa, kaltziorik gabe (PDB 6FEH) eta laranja, kaltzioarekin (Gourgy-Hacohen et al., 2014) (Nuñez et al., 2019)

F. Tobelaim et al., 2017. Proteinen erauzketak, akoplamendu molekularrak, dinamika molekularreko simulazioek eta erregistro elektrofisiologikoek adierazten dute CaM-ren A eta B helizeetara lotzen dela C-lobulu eta N-lobuluekin, hurrenez hurren. Atseden egoeran, N-lobulua kaltzifikatuta dagoela iradokitzen dute, eta CaM-ren C-lobulua K_V7.1.-ren A helizearekin interakzioa izan dezake. Baina Ca^{2+}-aren gorakada baten ondoren, CaM-ren C-lobulua kaltzifikatu egiten da, A helizetik disoziatuz. CaM kanalari lotuta mantenduko da N-lobuluaren bidez, zeinak B helizeari lotuta jarraituko duen.

G. Chang et al., 2018 and Xu et al., 2013 (Daniel Minor lab.). K_V7.4 eta K_V7.5 X-izpien analisi kristalografikoak, analisi biokimiko eta funtzionalekin konbinatuta, K_V7-en modulaziorako mekanismo erregulatzaile bat proposatzen dute. Attalik eta Hirschek lehen aldiz egindako hipotesia berretsi zuten: *in vitro* Ca^{2+}-ak eragindako konplexuaren bolumenaren gehikuntza orokorra, C-lobulua A helizetik banatzearen edo A helizearen destolestearen ondorio izan zitekeela proposatu zuten (5.3. irudia). Beraz, hau Attaliren ereduaren bertsio bat da, C-lobulua desakoplatzeko proposamenean oinarrituta.

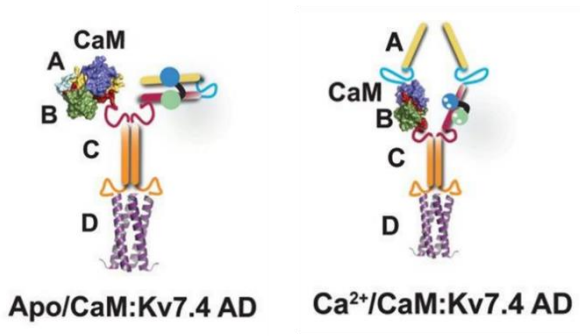

5.3. irudia K_V7 kanalen kaltzioak bultzatutako konformazio-aldaketa, 2018ko Chang et al. Ezkerrean, $K_V7.4$ Ca^{2+}-rik ez dagoenean, egitura trinkoagoa erakusten du. Eskuinean, Ca^{2+} loturaren ondoren, non A helizea CaM-tik askatzen den. (Chang et al., 2018)

H. Archer et al., 2019. (Shapiro lab): "Lobulua trukatzeko eredua" proposatu zuten. ITC, EMN eta X-izpien kristalografia tekniketan oinarrituta, CaM eta $K_V7.4$ren A eta B helizeen arteko elkarreraginak ikertu zituzten. Ca^{2+}-aren igoerari erantzunez, CaM-k lobulu-aldaketa bat jasaten duela iradokitzen dute, eta horrek konposizio-doikuntza eskatzen duela, bai KCNQ4 kanalen C-terminalean, bai CaM-n. Proposatzen dute Ca^{2+}-aren menpeko erregulazio bat dela, zeina KCNQaren aktibazioaren menpekoa baita (5.4. irudia).

Hala ere, lan honetan badira ebidentzia zientifikorik ez duten premisa batzuk, eta zaila da CaM-ren lotura domeinuen propietateekin bateratzea. Aurreko lanek erakutsi dutenez, CaM-rik ez dagoenean, C-muturrak agregatzeko joera du, beraz, ez da azaltzen nola tolestu daitekeen C-muturra CaM-ren elkareraginik gabe.

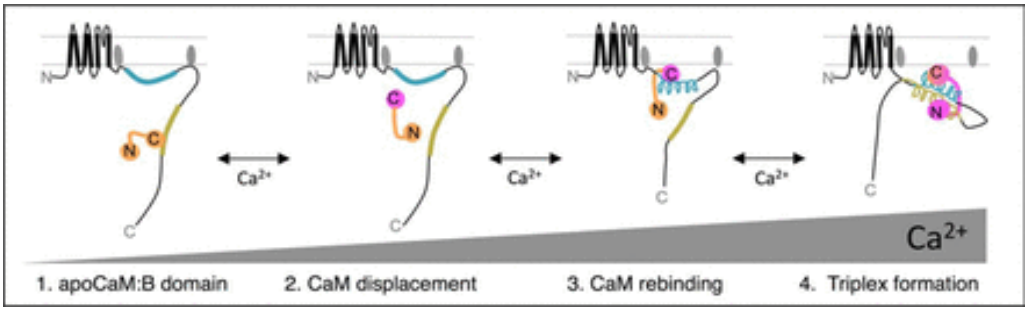

5.4. irudia. Lobulua aldatzeko ereduaren proposamena, KCNQ kanal neuronalen CaM arautzeko. 1. [Ca^{2+}] zitosolikoa oso baxua denean (<10 nM) (zehaztu ezin dugun egoera fisiologikoa), apoCaM B domeinuaren aurretik dago, A eta B domeinuak ziur asko desordenatuta daude, eta ez konformazio helikoidal batean. **2.** atsedenean dauden neuronetan [Ca^{2+}] zitoplasman <100 nM da Ca^{2+}-a C lobuluaren E-F eskuekin batzen da lehenik eta B-domeinutik banatzen da. **3.** [Ca^{2+}] gehiago igoz gero, C-lobulua 400 nM-ko Kd batekin lotzen zaio A-domeinuari, honek konformazio helikoidala eragiten duelarik. 4. Amaitzeko, [Ca^{2+}] seinale indartsu baten ondoren (Gq/11ri akoplatutako hartzaile batzuen estimulazio indartsu bat bezala), N-lobuluaren E-F eskuak Ca^{2+} ioiez okupatzen dira, honek B domeinuarekiko afinitatea handitzen duelarik, honen tolestura helikoidala induzituz, C-lobulua A-helizeari atxikituta jarraitzen duelarik (Archer et al., 2019)

5.2. HELBURUA

Hainbat teknika erabili dira CaM-k erregulatutako K_V7 kanaletarako erabiltzen duen seinale-transmisioaren mekanismoa ikertzeko. Teknika bakoitzak bere mugak ditu, bereziki, egitura-teknika gehienek huts egin dezakete eskualde malguak hautemateko.

Gainera, aurreko kapituluan frogatu dugun bezala, D helizeak paper garrantzitsu bat beteko luke CaM-ren loturan.

Hori kontuan hartuta, Ca^{2+}-ak bultzatutako egiturazko berrantolaketa aztertu zen tetramerotan, horretarako, C-terminalaren C eta D helizeak gehitu zitzaizkien proteina errekonbinanteei, horiek arduratzen baitira kanal horietan tetramerizazioa bitartekotzeaz. FRET eta EMN esperimentuak erabiltzeaz gain, HS-AFM ere erabili dugu, informazio dinamikoa denbora errealean lortzeko aukera ematen digulako, zelularen barnealdea simulatzen duten soluzioetan.

5.3. EMAITZAK

5.3.1. HS-AFM tetrameroen dinamika aztertzeko

Ca^{2+} titulazioak egin ziren $K_V7.2$-ren C-terminal zitoplasmatikoan, (*h*ABCD:CaM) Estreptabidina-Biotina 2D-tako kristalei lotuta zegoela.

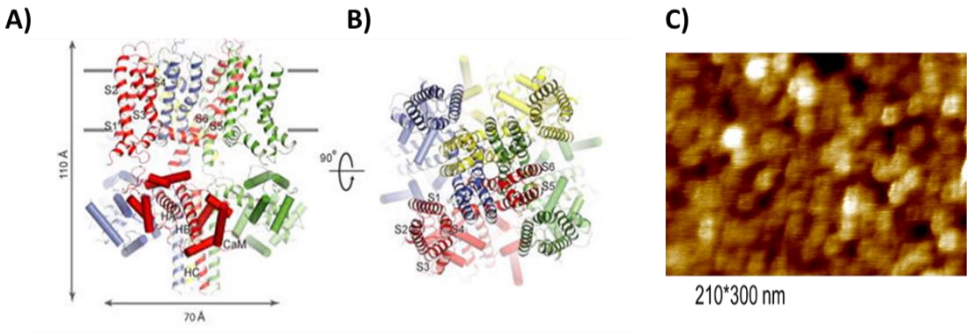

5.5. irudia. Holo-CaM/$K_V7.2$ tetrameroaren konplexua, HS-AFM-z bistaratua. (A-B) KCNQ1EM/CaM konplexuaren alboko bista eta goiko bista. Protomero bakoitza kolore ezberdin batean agertzen da, eta CaM zilindro bezala irudikatzen da. S1-S6 eta hA-hC helize moduan daude etiketatuta (Sun & MacKinnon, 2017). **(C)** KCNQ2 *h*ABCD/CaM konplexuaren goiko ikuspegia, HS-AFM-ez erregistratua.

Proteina mika-xaflan zuzenean finkatzea zaila denez (interakzio elektrostatikoa galtzen baita, (3. osagarrian informazio gehiago), biotina-estreptabidinaren 2D kristalen estrategia erabili genuen konplexua geldiarazteko.

Proteina (estreptabidina lotzeko domeinu bat gehitu diogula) biotina-estreptabidinazko kristaletan inkubatu zen 15 minutuz, disoluzioak 5 mM EGTA zituela.

Instrumentua hegal txiki batekin hornituta dagoenez (Nanoworld 0.6), uretan 1,5 MHz-ko erresonantzia-maiztasunarekin eta 0,6 n/my-ko erresorte-konstante batekin, eskaner azkar bat erabiliz, 2-3 nm-ko erresoluzioa izango genuke alboko norabidean (proteinentzako bereizmen submolekularra) eta~1,5 nm-takoa norabide bertikalean.

Lehenik, tetrameroak kaltziorik gabe eskaneatu ziren, bi minutuz. Ondoren, Ca^{2+} titulazioa egiteko, kaltzio-soluzioa (KCl 120 mM, HEPES 50 mM, NaCl 5 mM, EGTA 5 mM, $CaCl_2$ 140 mM) gehitu zitzaion laginari poliki-poliki, irudi-prozesua eten ez zedin. Lagin-ganberan 100 µL proteina-tanpoi zeuden (KCl 120 mM, HEPES 50 mM, NaCl 5 mM, EGTA 5 mM). Lagin-ganberak 130 µL-tako edukiera duenez, kaltzio soluzioa 5 µL-ko bi injekziotan gehitu zen. Lehen injekzioarekin, Ca^{2+} askeak 2 mM-tara igotzea lortu zen eta 7 mM-tara bigarrenarekin, Maxchelatorren kalkuluen arabera (https://somapp.ucdmc.ucdavis.edu/pharmacology/bers/maxchelator/CaEGTA-TS.htm).

Irudia esperimentuen hasieratik amaierara arte grabatu zen, Ca^{2+}-aren lehen injekzioa 5 minutu igarota izan zelarik (1. bideoa).

Ez zen aldaketa markaturik ikusi gainazalaren topografian ezta 2D-ko kristalezko enpakean ere, 10 Å-ko erresoluzioan lortu zirenak (5.5. irudia).

5.3.2. Kaltzioak eraginadako aldaketa-konformazionala monomeroan (Q2*h*AB:CaM) eta tetrameroan (Q2*h*ABCD:CaM), FRET bidez aztertuta.

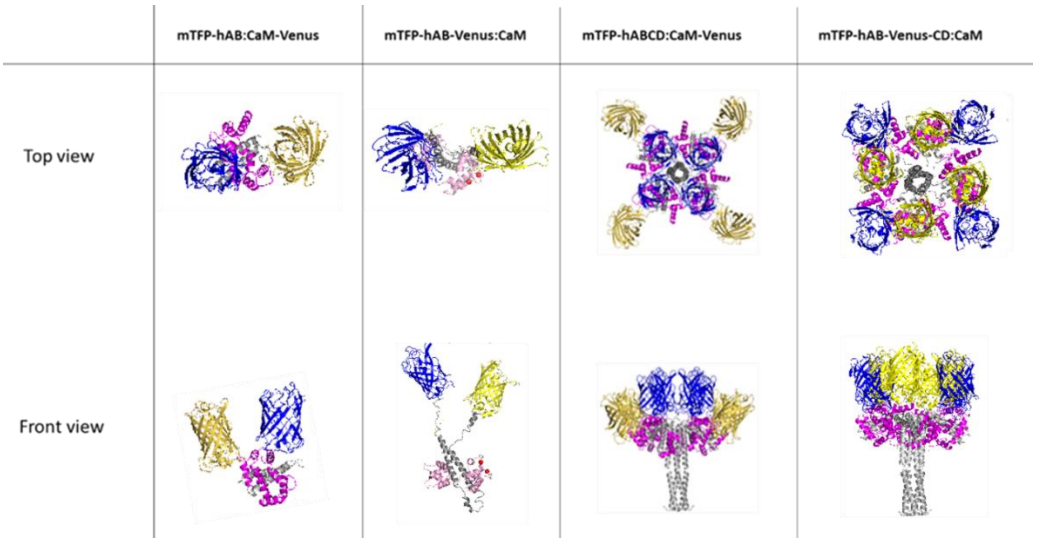

5.6. irudia. Ca^{2+}-aren titulazioetan erabilitako FRET konplexuen irudikapen eskematikoa, goiko eta aurreko ikuspegietatik. mTFP urdinez irudikatzen da, Venus horiz, CaM purpuraz eta C-terminal K_V7.2 grisez. Pymol bidez egina.

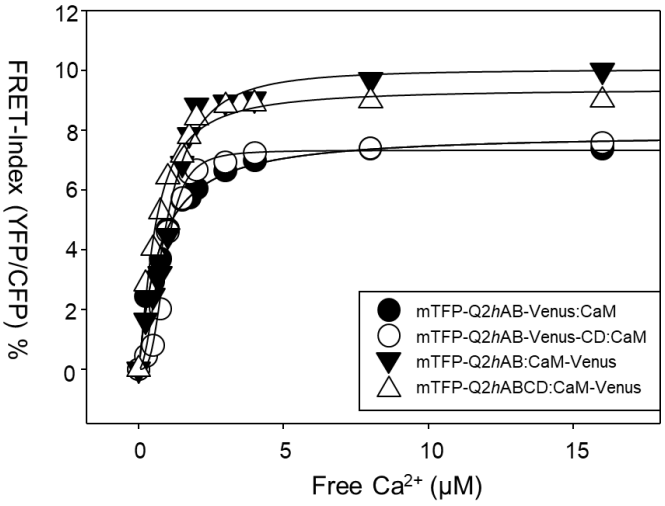

FRET-COMPLEX	Affinity E_C50 (nM)	RSQR
mTFP-Q2hAB-Venus:CaM	989 ± 75	0.98
mTFP-Q2hAB:CaM-Venus	695 ± 64	0.99
mTFP-Q2hAB-Venus:CaM	661 ± 40	0.99
mTFP-Q2hABCD:CaM-Venus	934 ± 34	0.99

5.7. irudia. FRET-Indizearen (YFP/mTFP) aldaketa Ca^{2+}-aren arabera. Kaltzioaren titulazioa FRET sentsoreen hainbat konplexutan egin zen. Ca^{2+} gehitzeak antzeko aldaketa konformazionalak eragiten ditu monomeroan (CaM:K_V7.2-*h*AB) eta tetrameroan (CaM:K_V7.2-*h*ABCD), frogatutako bi estrategietan. Gainera, Ca^{2+}-arekiko afinitatea ere oso hurbileko balioetan mantentzen da. Balio bakoitzak gutxienez 3 esperimentu independenteren batezbestekoa adierazten du. Lerroak Hillen ekuazioa datuetara doitzearen emaitza dira. Azpian, osagarri horien parametroak agertzen dira.

C-lobuluak Ca^{2+}-arekiko duen afinitatea CaM/K_V7.2-*h*AB fluoreszentziaren erresonantzia-energiaren transferentziaren bidez zehaztu da (FRET). K_V7.2-*h*AB-rekin independenteak diren bi

fluoroforo elkartzen direnean, lehen aipatutako Ca^{2+}-arekin lotutako konformazio-berrantolaketak aldaketa bat eragiten du FRETren intentsitatean. FRETren intentsitateak Ca^{2+} librearen kontzentrazioaren arabera (fura-2-ren arabera) (1.eranskina) 0,98 ± 0,07 µM-ko itxurazko afinitate-konstantea ematen du mTFP-*h*AB:CaM-Venus-rentzat eta 0,69 ± 0,06 µM mTFP-*h*AB-Venus:CaM-rentzat (5.7. irudia), beste determinazio batzuekin bat datorrena (Alaimo et al., 2014). Era berean, tetrameroekin egindako saiakuntza berak oso hurbileko afinitate balioak erakusten ditu: 0,66 ± 0,04 µM mTFP-Q2*h*AB-Venus-CD:CaM-ren kasuan eta 0,93 ± 0,03 µM mTFP-*h*ABCD:CaM-Venus-ren kasuan (5.7. irudia). Kontuan izan FRET oso teknika sentikorra dela, eta lortu ditugun datuak oso mugimendu arinekoak direla. Kaltzioak bultzatutako aldaketa konformazionalak FRET erlazioa % 10 inguru murriztea eragiten du bai *h*AB:CaM monomeroetan, bai *h*ABCD:CaM tetrameroetan (5.7. irudia).

mTFP-*h*AB:CaM-Venus eta bere tetramero mTFP-*h*ABCD:CaM-Venus sentsoreen kasuan (5.6. irudia), aurrez ikusitakoaren oso antzekoa den arren, FRETren murrizketa are txikiagoa izan zen, konposizio-aldaketa txikiago batekin erlazionatuta (5.7. irudia). FRET-indizean ikusitako murrizketa C-lobuluaren orientazioan izandako aldaketa txiki baten ondorio izan litekeela iradokitzen dugu.

5.3.3. $^{1}H,^{15}N$-TROSY-HSQC of the CaM/K_V7.2-*h*ABCD

Behatutako aldaketak egitura tetrameriko batean ere gertatzen diren balioztatzeko, Ca^{2+}-aren menpeko konformazio-aldaketa aztertuko dugu, tetramerizazioaren ardura duten eskualdeak barneratuz (K_V7.2 C-terminaleko C eta D helizeak).

EMN-ren esperimentuek Ca^{2+}-aren menpeko konformazio aldaketa konplexu tetramerikoan ere gertatzen dela erakusten dute. CaM/K_V7.2-*h*ABCD-ren ^{1}H, ^{15}N-TROSY-HSQC (5.9. irudia) eskualde malguetako hondakinei dagozkien seinale gutxi batzuk baino ez ditu erakusten, 120 kDa baino gehiagoko egitura tetrameriko bati dagokiona. Aldiz, metilo taldeen metil-TROSY espektroak (Wiesner & Sprangers, 2015) hondakin gehienak erakusten ditu. Kv7.2-*h*ABCD:CaM eta K_V7.2-*h*AB:CaM espektroen gainjartzeak CaM/K_V7.2-*h*ABCD sistemetan *h*AB-ren Ile hondakinak esleitzeko aukera ematen du (5.9. irudia). Nabarmen, K_V7.2-*h*ABCD:Holo-CaM-ren espektroak Ca^{2+}-ak eragindako desplazamendu kimikoaen aldaketa K_V7.2-*h*AB:Holo-CaM-ean ikusitakoak dira (5.9. irudia); horrek esan nahi du Ca^{2+}-aren menpeko egitura-aldaketak konplexu tetramerikoan mantentzen dela.

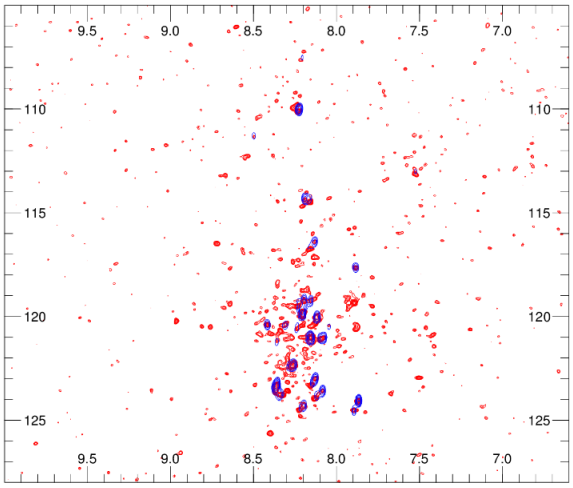

5.8. irudia. Q2*h*ABCD:CaM-ren ^{15}N-HSQC espektroak proteina multzoa. Amida talde guztien ^{1}H-^{15}N korrelazioa erakusten da. Urdinez esperimentuaren hasieran eta gorriz amaieran.

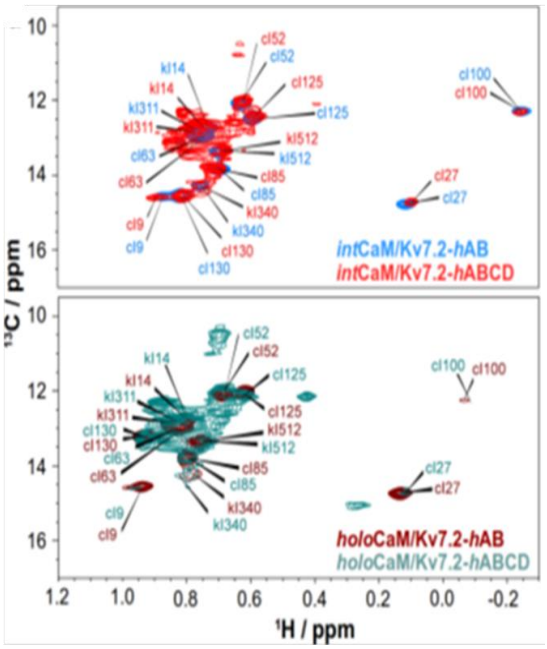

5.9. irudia. Tetrameroan ere egitura-aldaketak ikusten dira. ^{13}C-δ-Ile METIL-TROSY espektroaren gainjarpena. IntCaM:*h*AB (N-lobuluak bakarrik du Ca^{2+} karga), intCaM/K_V7.2-*h*AB (urdina, goian), intCaM/K_V7.2-*h*ABCD (gorria, goian), holoCaM/K_V7.2-*h*AB (marroia, behean) eta holoCaM/K_V7.2-*h*ABCD (berdea, behean). Konplexu monomerikoak (CaM/K_V7.2-*h*AB) eta tetramerikoak (CaM/Kv7.2-*h*ABCD) Ca^{2+}-k eragindako konposizio-aldaketa berberak jasaten dituzte. Metilo-seinaleak apoCaM/K_V7.2-*h*ABen esleitzea 3D-ko esperimentu anitzen konbinazio baten bidez lortu zen, apoCaM/K_V7.2-*h*ABCD-ren seinale berak espektroen gainjartzearen bidez estimatzen diren bitartean.

5.4. EZTABAIDA

Konformazio-aldaketa, kaltzioa batu ondoren, FRET, EMN eta indar atomikoko mikroskopiaren bidez aztertu zen. Horretarako bi FRET sentsore ezberdin diseinatu ziren: mTFP1-*h*AB:CaM-Venus eta mTFP1-*h*ABCD:CaM-Venus. Lehenak monomeroak sortzen dituen bitartean, bigarrenak tetrameroak osatzen ditu, D helizeak, helize superkiribilduaren egitura hartzen baitu. Laginak kaltzio libreko hainbat kontzentraziotan prestatu ziren, 250 nM eta 16 µM tartean, aurrez Fura-ren bidez kalibratuta (ikus gehigarria) eta 500 nM-ko proteina-kontzentrazioan. Horietako bakoitzean FRET aztertu zen, 458 nm-ra kitzikatuz eta emisioa jasoz 470-570 nm-ko tartean.

5.7 irudiak erakusten duen bezala, FRET analisia sentibera da apoCaM/K_V7.2-*h*AB eta holoCaM/K_V7.2-*h*AB arteko trantsizioan gertatzen den konformazio-aldaketari, A eta B helizeen arteko mugimendua aztertzen dugunean. Aldaketa horren magnitudea K_V7.2-*h*ABCD tetrameroan

mantentzen da. Bitxia bada ere, CaM-ren C lobuluaren eta A helizearen arteko mugimendua aztertzen badugu, FRET indizea ia aldaezina izaten da (mTFP-*h*AB:CaM-Venus eta mTFP-*h*ABCD:CaM-Venus). Ca^{2+}-a lotu ondoren, C-lobuluaren eta A helizearen arteko banatzea gertatzen bada, beste autore batzuek iradokitzen duten bezala (Tobelaim et al., 2017; Chang et al., 2018), FRET-indizearen galera ikusiko genuke haien arteko urruntzeagatik. Beraz, gure emaitzek iradokitzen dute C-lobulua eta A helizea lotuta mantentzen direla.

Emaitzak bat datoz Bernardo-Seisdedos et al. (2018) proposatutako ereduarekin, non Ca^{2+}-aren lotura C-lobuluarekiko E-F eskuetan 17.8°-tako errotazioa eragiten duen, CaM-ren segmentu bat desplazatuz (h5 eta h8 helizeak), mugimendu hau gainontzeko kanalera alosterikoki transmititzen da, A eta B helizeen orientazioa aldatuz. Ondoren, aurre-A elementuraino transmititzen da, ziur asko, kanalaren itxiera eraginez.

Honen harira, FRET saiakuntzek oso mugimendu apala erakusten dute mTFP-Q2*h*AB-Venusen, FRET-indizea 1,68tik 1,51ra murrizten delarik. Honek esan nahi du Ca^{2+}-a lotzen denean, egitura aldaketa bat dagoela, non A eta B helizeak elkarrengandik bananduago dauden. FRET teknika oso sentikorra denez, hartzailearen/emailearen arteko erlazioaren murrizketa hori 1,5 ± 0,02 Å-koa dela estimatzen dugu (58,62 Å-tik 60,12 Å-ra). Distantzia-kalkuluak guk diseinatutako simulagailu baten bidez egin ditugu, 3. kapituluan deskribatuta. Era berean, emailea (mTFP) A helizean eta hartzailea (mcpVenus) CaM-ren C-lobuluan kokatuta dagoenean, Ca^{2+}-aren loturak, oso aldaketa txikia eragiten du (FRET-indizea 1,54tik 1,41era murriztuz). Izan ere, EMNz ebatzitako egituran, C-lobulua A helizeari lotua dago holo-CaM/Q2*h*AB-ren egituran ere. CaM-ren C-lobuluak A-helizeari lotuta jarraitzen badu, kaltzioaren presentzian zein gabezian, **nola azaltzen da FRET-indizearen murrizketa bat Ca^{2+} konplexuari elkartu ondoren?** A helizearen eta C-lobuluaren artean banaketarik ez dagoen arren, fluoroforoen orientazioan aldaketa bat gerta daiteke, beharbada, CaM-ren C lobulua biratu delako, EMN-z ikusi genuen bezala.

EMN bidez Ca^{2+}-ak eragindako konformazio-aldaketa tetrameroan aztertzeko, TROSY esperimentu bat egin genuen. Q2*h*ABCD_DelY372-T501/CaM osatzen duen tetramero konplexuak 140 KDa baino gehiago dituenez esperimentu homonuklearrek gainezarpen espektrala jasaten du, eta, beraz, konplexuen ikerketa, bideraezina izaten da. Zeharkako erlaxazioko espektroskopia optimizatua (TROSY) eskualde malguetako aminoazidoei dagozkien seinale gutxi batzuk baino ez ditu erakusten. Metilo taldeen metil-TROSY espektroak hondakin gehienak erakusten ditu eta Ile hondakinak esleitzeko aukera ematen du. Nabarmen, espektroak Ca^{2+}-ak eragindako desplazamendu kimikoko asaldura berberak erakusten ditu monomeroan zein tetrameroan (5.9. irudia).

Esan beharra dago ez FRETren bidez, ezta EMNren bidez, ezin izan dugula detektatu C eta D helizeen orientazioan gertatzen dena. K_V7.2 tetrameroetan kaltzioak bultzatutako konformazio-aldaketa aztertzeko, HS-AFM erabiltzen dugu. Teknika horri esker, aldi berean ebaluatu daitezke proteina indibidualen molekulen egitura eta dinamika. Mintz-proteinen kasuan, garrantzitsua da proteina geruza bikoitz lipidiko batean immobilizatzea, baina proteina guztia ezin izan genuenez purifikatu bere tamaina eta hidrofobikotasun handiagatik, K_V7.2-ren C-terminalarekin lan egin genuen, CaM-rekin konplexuan. Q2*h*ABCD/CaM immobilizatzeko biotina-estreptabidinaren teknika erabili genuen, metodoetan deskribatzen den bezala. Konplexua titulazioan zehar bistaratu zen, 0 mM-tan hasi eta 7 mM Ca^{2+}-ra iritsiz (3. bideo osagarria).

Bereizmen handiko irudi bat lortu genuen, kaltzioa zeramana 5 mM-tan. Irudia zuzendu ostean, bere forma karratua argi ikusten da goiko ikuspegi batetik, eta erdian zulo bat hautematen da, ustez poroa. Irudi hori bat dator holo-CaM/K_V7.2 krio-EM egiturarekin (Sun & MacKinnon, 2017) (5.5. irudia), bai tamainari bai formari dagokienez. Gaienra, titulazioan zehar, ez zen egitura-aldaketarik antzeman. Kontuan hartuta erabilitako HS-AFM-ren bereizmen-muga 10 Å-ekoa dela, tetrameroaren konformazio-aldaketak 10 Å-etik beherakoak izan behar direla ondorioztatzen da, EMN eta FRET esperimentuetan ikusi dugun bezala (Bernardo-Seisdedos et al, 2018).

Lehen esan dugun bezala, K_V7 kanaletan denbora luzez uste izan da Ca^{2+} eta CaM-ren arteko elkarreraginaren ondoriozko konformazio-aldaketak handiak direla. Zenbait ikerketa-lan iradoki dute CaM-ren konposizio-aldaketa izan zitekeela poroa irekitzeko/ixteko behar den etengailu mekanikoa (Tobelaim et al., 2017; Sun & MacKinnon, 2017; Bernardo-Seisdedos et al., 2018; Chang et al, 2018). Tobelaim eta Chang-ren ereduek, Ca^{2+}-a, C-lobulura lotzean A helizetik banatzen dela iradokitzen dute. C-lobulua mugikorra den bitartean, N-lobulua bere tokian mantentzen dela B helizean. Hau ere aurretik proposatu zen (Xu et al., 2013). Era berean, Shapiroren taldeak beste eredu bat iradoki zuen berriki, KCNQ aktibatzeko Ca^{2+}-aren mendeko erregulazioarekin lotuta (Archer et al., 2019). Ca^{2+}-aren gorakadari erantzunez, CaM-k lobulu-aldaketa egiten duela iradokitzen du, eta horrek elkarrekiko doikuntza konformazional dramatikoa eragiten duela. Hala ere, HS-AFM, EMN eta FRETren bidez, ez dugu ikusi Ca^{2+}-ak eragindako egitura-aldaketa garrantzitsurik. Kapitulu honetan ebidentzia esperimental zabala ematen dugu, Ca^{2+}-ak bultzatutako konformazio-aldaketa hori oso leuna dela adierazteko. Izan ere, konposizio-aldaketa hain da sotila, ezin dugula HS-AFM bidez detektatu, HS-AFM teknikaren bereizmen-mugaren azpitik baitago.

6. CaM-ren 3. E-F eskuak kaltzio seinalea transmititzen du K_V7 kanaletan

6.1. Sarrera

1978an, Brehmek eta Eckertek lehen aldiz deskribatu zuten *Paramecium*-en, Ca^{2+}-ak boltai menpeko ioi kanal baten inhibizioa eragiten zuela (Brehm eta Eckert, 1978). Kanal horiek Ca^{2+} delakoarekiko sentikorra den "makineria" berezi batez hornituta daude. Tresna horiek Ca^{2+}-aren sarrera bera modu bikainean manipulatzeko eta, beraz, Ca^{2+}-aren sarreraren ondoren datozen erantzun eraginkor ugariak doitzeko gai dira. Hala ere, kanal ioniko baten Ca^{2+} menpeko erregulazio honen azpian dagoen mekanismo molekularra ilun mantendu zen 90eko hamarkadara arte. Orduan iradoki baitzen Na^+ eta K^+ kanalen Ca^{2+}-aren menpeko erregulazioa CaM-ren bidez egin zitekeela (Kink et al. al., 1990; Saimi eta Kung, 1994). Ordutik, hainbat ikerketek frogatu dute CaM-k funtsezko papera duela zenbait kanal eta hartzaile ionikoren modulazioan, esaterako Ca^{2+}-ak aktibatutako K^+ kanaletan (Xia et al., 1998), N-metil-D-aspartato glutamato-hartzaileetan (NMDA) (Ehlers et al., 1996), nukleotido ziklikoen menpeko kanal ionikoetan (Liu et al., 1994), aldi baterako hartzaile potentzialeko kanaletan (TRP) (Phillips et al., 1992) eta boltai menpeko Ca^{2+}, Na^+ edo K^+ kanaletan (Saimi eta Kung, 2002).

Izenak dioen bezala, kalmodulina kaltziozko proteina modulatzaile bat da. CaM, bi domeinu globularrez osatua dago, N- eta C-lobuluak, oso sekuentzia malgu batez elkartuak. Lobulu bakoitzaK, bi E-F esku osatzen dute, eta guztira, lau Ca^{2+} ioien loturaren arduradunak dira. CaM helburuak, oro har, erresiduo hidrofoboetan eta oinarrizkoetan aberatsak diren eskualde helikoide anfipatikoak dira. CaM lobuluak konfigurazio ireki, erdi-ireki edo itxian egon daitezke, Ca^{2+}-aren okupazioaren arabera (6.1 irudia).

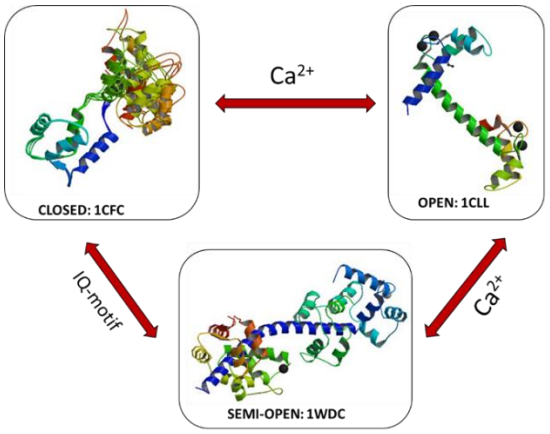

6.1 irudia. E-F esku domeinuen hiru egitura: zinta irudikapenak kalmodulina (apo eta kaltzioz kargatutakoa) eta miosinaren funtsezko kate arinaren C-terminal domeinua E-F eskuko domeinuen hiru egitura ezagun ilustratzeko erabiltzen dira. Goiko aldean, ezkerraldean, apo CaM-N (pdb = 1CFC) konformazio itxian dago. Goiko aldean, eskuinean, kaltzioz kargatutako CaM-N (pdb = 1CLL) konformazio itxian dago. Behealdean, miosinaren C-terminal domeinua (pdb = 1WDC) konformazio erdi-irekian dago. Proteinak zinta bezala prozesatu ziren PDB_Ribbons modulua erabiliz. (Upson et al, 1989).

Gainera, metionina aminoazidoen ugaritasunak plastikotasun handiagoa ematen dio CaM-ri. Ezaugarri hauei esker, CaM 300 itu-proteina baino gehiagotara elkartzen da.

Bi lobuluak konektore malgu batek konektatzen ditu, eta horrek egiturazko malgutasuna eta lotura-azalera moldagarria ematen dio CaM-ri. Beraz, CaM proteina askorekin elkarreragin dezake eta zelula-bide askotan inplikatuta dago. Izan ere, CaM proteina berdina gizakiengan kodetzen duten hiru gene egoteak (CALM1-3) proteina horrek fisiologian duen paper kritikoa nabarmentzen du.

Lehen aipatu bezala, CaM-k lau E-F esku operatibo ditu, bi N-lobuluan kokatzen dira: E-F (1) (20 aa-tik 31-ra) eta E-F (2) (56 aa-tik 67 aa-ra); eta beste biak C-lobuluan E-F (3) (93 aa-tik-104 aa-ra) eta E-F (4) (129 aa-tik 140-ra).(6.2. irudia).

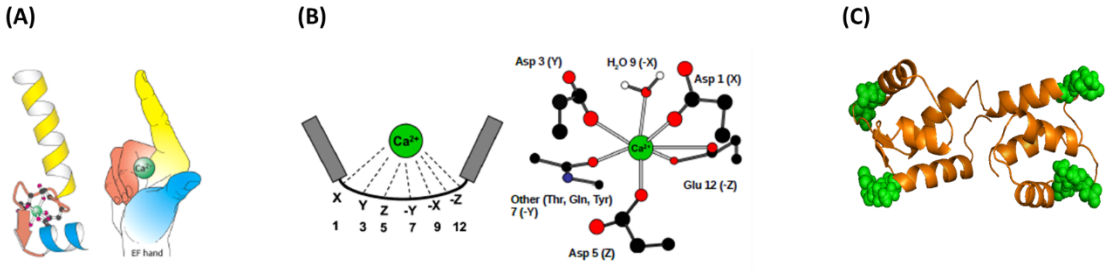

6.2. irudia. (A) "E-F eskua" terminologiaren jatorriaren adierazpena. **(B)** Ca^{2+}-ren lotua globalaren arrazoia, E-F esku bati dagokiona. Karaktereak (x, y, z,...) eta zenbakiak E-F begizpeko posizio erlatiboei dagozkie (Alessandro Alaimo doktoreak emandako argazkiak). **(C)** CaM-en irudikapen eskematikoa, non E-F eskuak esfera berdeetan irudikatuta dauden.

E-F eskuen sekuentzia kanonikoa 12 aminoazidok osatzen dute, Asp hondakin batekin hasi eta Glu hondakin batekin amaitzen direnak. Sekuentzia honen aminoazido erdien oxigeno atomoek (1-3-5-7-9 eta 12 hondakinak) Ca^{2+}-aren loturan parte hartzen dute. Izan ere, aminoazidoen arteko ezberdintasun txikiak direla eta, C-lobuluak Ca^{2+}-arekiko afinitate handiagoa du N-lobuluak baino (Kd ~ 0,2 µM eta ~ 2 µM hurrenez hurren) soluzioan. Kondizio ioniko ezberdinak eta CaM-kontzentrazio ugari egon daitezkeenez, hainbat zenbatespen proposatu dira emaitza gisa Ca^{2+}-ak lotzeko duen afinitatea azaltzeko, jakinarazitako Kd balioek, 0,3 eta 5 µM tartean aldatzen direlarik. Zelula barneko kondizio ioniko ia fisiologikoetan, Kd-a, gutxi gora-behera, 1 µM-koa da, CaM, Ca^{2+}-ren zelula barneko oszilazioei erantzutea ahalbidetzen duen balio bat. Hala ere, afinitate hori aldatu egiten da CaM bere itu-proteinekin lotzen denean.

Oro har, CaM eta Ca^{2+}-aren arteko afinitatea handiagoa da itu-proteina batekin konbinatzen denean, baina kontrako efektua ere deskribatu da. Konplexuan dagoen CaM-ren Ca^{2+} afinitatearen balio batzuk 50 nM-tik beherakoak dira. Honek, atsedenean dauden zelulen baldintzetan, non Ca^{2+}-aren kontzentrazioa 100 nM ingurukoa den, CaM/itu-proteinaren konplexua Ca^{2+}-arekin asetuta egon daitekeela iradokiko luke. Bestalde, itu-proteina askoren CaM-rekiko duten afinitatea handitu egiten da CaM Ca^{2+}-arekin kargatuta dagoenean.
Agerian geratu da E-F (1) edo E-F (2) mutazioak, CaM-ren N-lobuluan, SK kanalen Ca^{2+}-aren itxurazko sentikortasuna murrizten duela, dosi-erantzun kurba eskuinerantz mugituz, E-F (1,2) mutante bikoitzak kanalaren jarduera erabat baliogabetu zuen bitartean (Keen et al., 1999). Aitzitik, C-lobuluraren, E-F (3) edo E-F (4) edo bien E-F (3,4) mutazioak ez zuen inolako eraginik izan Ca^{2+} bidezko aktibazioan (Keen et al., 1999). Esperimentu hauen interpretazioa, N-lobulua Ca^{2+} seinalearen efektorea dela izan zen, erabat bat datorrena SK4-ren mikroskopia elektronikoz ebatzitako estrukturekin, kaltzioarekin eta kaltzio gabe lortutakoak (Lee eta MacKinnon, 2018).

$Ca_V2.1$ kanaletan, CaM lobuluek kontrako efektua sortzen dute: CaM-ren C-lobuluak Ca^{2+}-aren menpeko erraztasun zinetikoki azkarra eragiten du (Ca^{2+}-dependent facilitation CDF), N-lobuluak Ca^{2+}-aren menpeko inaktibazio motelagoa eragiten duen bitartean (Ca^{2+}-dependent inactivation, CDI) (DeMaria et al., 2001; Lee et al., 2003). $Ca_V2.2$ eta $Ca_V2.3$ kanalek CDI adierazten dute, batez ere CaM-ren N-lobuluak eraginda (Liang et al., 2003). Kanal hauek mekanismo ezberdin bat dute baldintza fisiologikoetan Ca^{2+}-aren selektibitate-espazialerako, non Ca^{2+} seinalea bi osagai ezberdinen batura den, kaltzio lokala eta globala. Lehenik, kanala irekitzerakoan Ca^{2+}-a sartzeak "tokiko seinalearen" osagai bat sortzen du, ~ 100 µM-rainoko kontzentrazio gorakada labur baina biziak barne hartzen dituena. Gorakada hauek kanal irekidurekin estuki sinkronizatuta daude eta

nanodomeinutan daude (Neher, 1998; Sherman et al., 1990). Bigarrenik, Ca^{2+}-a urrunago dauden iturrietan metatzeak (adibidez, Ca^{2+} motako beste kanal batzuk) "seinale globalaren" osagaia sortzen du, hau da, askoz ere txikiagoa den idulki global bat (~ 5 µM), espazioan hedatuta dagoena. Ca^{2+}-kanaletako Ca_V1-2 familian, kaltzio lokalak erregulatzen du CaM-ren C-lobuluaren bidezko aktibazioa. Kaltzioaren menpeko inaktibazioak Ca^{2+}-korrontearen beherakada handia eragiten du korronte zuzenaren aktibazioan. Ca^{2+}-kontzentrazio altua buferrean biltegiratzeak kontzentrazio globala jaisten duenez eta tokiko kontzentrazioari ia eragiten ez dionez (Neher, 1998), kaltzioaren menpeko inaktibazioak seinale lokala bakarrik behar du.

Aitzitik, Ca_V2 kanal guztien lobuluen erregulazioak nahiago du kontzentrazio global txikia askoz handiagoak diren tokiko kontzentrazioa baino (Tadross et al., 2008).

Esan beharra dago selektibitate espazial honek zentzua duela kaltzio iturri batentzat, TRP, Ca_V edo Ryonidina kanaletan kasu, baina ez boltaiz aktibatutako potasio kanalentzat (K_V). Egia esan, Ca^{2+} seinalea kanal hauetan CaM-ren zein lobuluk transmititzen duen oso eztabaidatuta dago. K_V7 familiarentzat, bi kasuetarako datuak argitaratu dira, batzuek iradokitzen dute Ca^{2+} seinalea N-lobuluak transmititzen duela (Archer et al., 2019), eta beste batzuek C-lobuluaren bidez transmititzen dela argudiatzen dute (Tobelaim et al., 2015; Bernardo-Seisdedos et al., 2018; Chang et al., 2018). Hau argitzeko, oso erabilgarria izango litzateke isoforma berdineko egiturak kaltziorik gabe eta kaltzioaren presentzian lortuko balira. K_V7.1 kanalaren egiturak Ca^{2+}-aren presentzian baino ez dira ebatzi (Sachyani et al., 2014; Sun & MacKinnon, 2017); K_V7.2 kanala, kaltzioaren presentzian eta absentzian ebatzi dugu, baina kaltzioarekiko sentikorra den domeinua baino ez (C terminaleko hAB) (Bernardo-Seisdedos et al., 2018). Azkenik, K_V7.4rako ebatzitako egitura bakarra kaltziorik gabekoa da.

Egia esan, K_V7 familiako egitura ebatzi horietan, K_V7.3/7.2, K_V7.4 eta K_V7.1 konplexuen arteko ezberdintasunik bereizgarrienak, E-F esku ezberdinen Ca^{2+} okupazioan gertatzen dira. Apo/CaM konplexuan: K_V7.4:*h*AB konplexua Ca^{2+}-z hutsik dago (Chang et al., 2018), baina N-lobuluak Ca^{2+}-z kargatutako konfigurazioa hartzen du. CaM:K_V7.1*h*AB konplexuaren egitura kristalinoan, N-lobuluaren E-F eskuek kaltzio ioiak dituzte, C-lobuluaren E-F eskuek, berriz, ez dute ioi dibalenterik (Sachyani et al., 2014). CaM:Q3*h*A/Q2hB kimera konplexuaren egiturak kaltzio ioiak ditu kalmodulinaren lau E-F eskuetan (Strulovich et al., 2016). Hala ere, lobuluaren egitura orokorrak bat datoz N-lobuluaren egitura "irekiaren" eta C lobulu "erdi-irekiarekin". Cryo-EM egituran, E-F-n (3) ez dago Ca^{2+} ioi batek sortuko lukeen dentsitaterik, Ca^{2+} kontzentrazio altuan ebatzi zen arren (5 mM Ca^{2} -pean ebatzi zen). Argitaratutako azken egituran ere (Archer, 2019), K_V7.4-ren A eta B helizeak CaM-rekin konplexuan X-izpien kristalografiaren bidez ebatzia, E-F (3) eta E-F (4)

eskuak hutsik daude, konplexuak 2 mM kaltzio duen soluzioan zegoen arren (Chang et al., 2018). Ikerketa funtzionalek K_V7.1: CaM-ren E-F (3)-rako paper kritikoa iradoki zuten (Chang et al., 2018).

6.2. HELBURUAK

Hemen, gure helburua CaM-ren E-F esku bakoitzak K_V7 kanalen kaltzio seinalearen transmisioan duen paper diferentzialari buruzko informazioa lortzea da. Helburu horretarako, E-F eskuen ekarpenak ezaugarritzen ditugu Ca^{2+} seinaleztapenean. Aurretik erabilitako K_V7.2 FRET-biosentsorea CaM mutante ezberdinekin (CaM wt, CaM 4, CaM124, CaM3, CaM123 eta CaM1234) adierazi zen, Ca^{2+}-a, E-F esku ezberdinekin elkartzeak eragozten dutenak.

6.3. EMAITZAK

6.3.1 E-F (3)-k, Ca^{2+} transdukzio-seinalearen bitartekotza egiten du K_V7.2 kanaletan

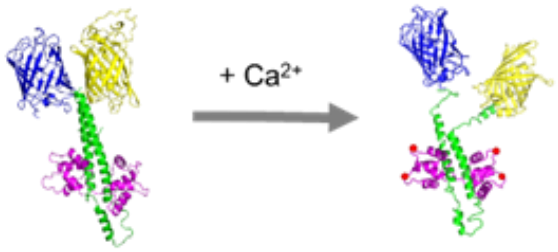

6.3 irudia. A helizearekin fusionatutako mTFP1 (urdina) eta Venusek (horia) B helizera fusionatuta duen biosentsorearen irudikapen eskematilkoa. C-lobuluaren kaltzifikazioaren (zirkulu gorriak) ondoren, A eta B helizeen orientazio erlatiboa aldatu egiten da, mTFP1 eta Venus bananduz, FRET (YFP/CFP) erredukzio batera garamatzana.

Aurretik deskribatutako FRET biosentsorea erabiliko dugu (lotailu osoa daramana, 3. kapituluan deskribatuta); bertan, K_V7 kanalaren A eta B helizeak (kaltzioarekiko sentikorra den eremua) fluoroforo emaile eta hartzaile bat (mTFP1-hAB-Venus) ditu alboetan. Proteina hau CaM ezberdinekin adierazi zen (CaM3, CaM4, CaM123, CaM124, CaM1234), E-F-ren esku espezifikoetan mutatuta daudenak, Ca^{2+}-aren lotura eragotziz. Proteinak His-Trap eta Gel filtrazio bidez purifikatu ziren, metodoetan deskribatzen den bezala. Ondoren, 500 nM proteina, bi soluzioren nahasketa ezberdinetan disolbatu zen, batek EGTA 5 mM-rekin eta besteak 20 mM-Ca^{2+} librearekin, amaierako Ca^{2+} kontzentrazio ezberdinak lortzeko. Laginak 458 nm-ko uhin-luzeran kitzikatzen dira, eta emisioa 470 nm-tik 570 nm-ra irakurtzen da. Hemen, FRET biosentsorearen "tarte dinamikoa" YFP/CFP-ren tarte teorikoa da.

FRET seinalearen "irabazia" edo “galera” YFP/CFP-ren gehikuntza edo gutxitze erlatibo bezala adieratzen da.

FRET-indizea (YFP/CFP) 1,75etik 1,25era jaitsi da CaM WT-rekin osatutako konplexuan, Ca^{2+} librea 20 µM-tan gehitu ostean (6.4. irudia); CaM WT hau kontrol gisa erabili zen CaM mutanteekin alderatzeko, eta % 100 gisa irudikatzen da. FRET indizea 1,71tik 1,27ra jaitsi da, hau da, % 90 CaM4ren kasuan, ia % 80 (1,75etik 1,31ra) CaM124ren kasuan. CaM3ren kasuan, Ca^{2+}-a gehitu ondoren, FRET indizeak, ez du aldaketa handirik izaten, 1,68tik 1,55era (% 32), eta 1,74tik 1,66ra CaM123ren kasuan. CaM1234rekin, FRET indizea egonkor mantentzen da, espero genuen bezala.

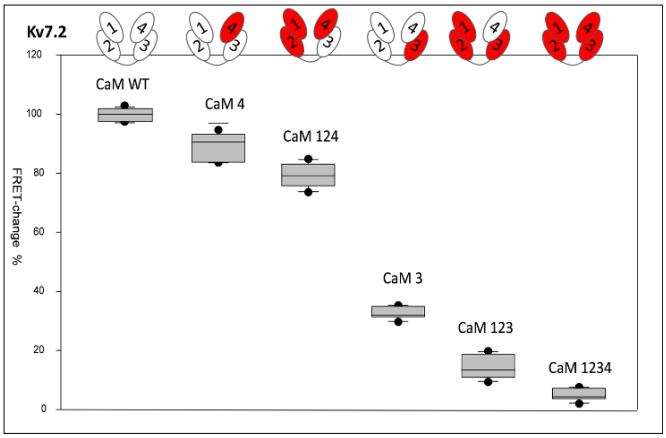

6.4. irudia. CaM, CaM4, CaM124, CaM3 eta CaM123rekin batera adierazitako K_V7.2 konplexu purifikatuaren FRET indizearen murrizketa (%), Ca^{2+}-ren eraginez. FRET-en murrizketa %90ean mantentzen da CaM4rekin, %79an CaM124rekin, %32an CaM3rekin, %13an CaM123rekin eta ia erabat ezabatzen da CaM1234rekin (% 4). Partzela bakoitzak gutxienez 6 esperimentu independenteren batezbestekoa adierazten du.

6.3.2 Kaltzio-seinaleztapenerako makineria K_V7 isoforma guztietan mantentzen da

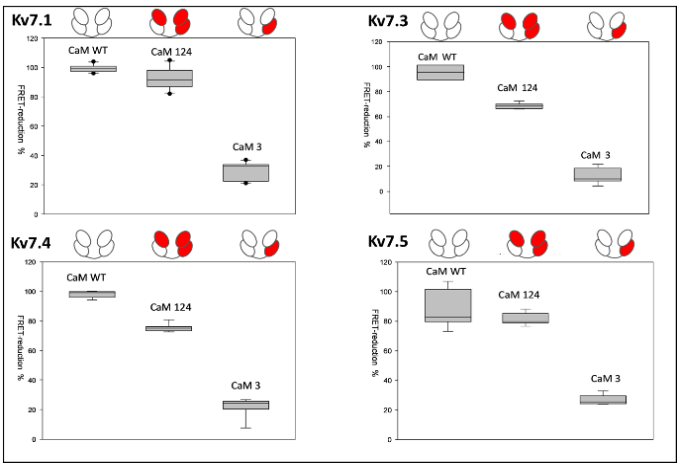

6.5. irudia. E-F (3)-k Ca^{2+} seinalearen transdukzioa K_V7 familiako beste kide batzuengan ere egiten du. CaM, CaM124 eta CaM3rekin sortutako K_V7 isoformen konplexu purifikatuen FRET indizearen murrizketa (%)-tan, Ca^{2+} (Ca^{2+} 1 mM libre) gehitu ondoren. Partzela bakoitzak gutxienez 6 esperimentu independenteren

K_V7 familiako beste kideek portaera antzekoa dute. Frogatu dugu Ca^{2+}-a, E-F (3)-ri lotzea eragozteak aldaketa konformazionala gelditzea eragiten duela (6.5. irudia), baina, nolabait, E-F

(4)-k ere Ca^{2+} seinaleztapena modulatzen du, proportzio txiki batean, CaM-ren N-lobuluaren (E-F (1) eta E-F (2)) E-F eskuetako mutazioek inolako eraginik ez duten bitartean.

K_V7.1-aren kasuan, FRETen murrizketa %91-koa da CaM124-rekin, eta %33-ra murrizten da CaM3-ren kasuan. K_V7.3rako, FRET-indizea %65-era murrizten da CaM124-ren kasuan, eta %10-era CaM3-ren kasuan. Era berean, K_V7.4 kanalen CaM124 FRET-indizea %65era jaisten da eta CaM3-rekin % 24ra. K_V7.5-ari dagokionez, CaM124-k Ca^{2+}-aren gehikuntzak FRET-indizea %80-an mantentzen du, eta CaM3-rekin % 25-era murrizten da.

6.4. EZTABAIDA

FRET biosentsorearen eraginkortasuna emailearen eta hartzailearen distantziaren eta orientazio erlatiboaren araberakoa da nagusiki (Miyawaki, 2003).

FRET ratiometria bidez detektatu dugu (Jares-Erijman eta Jovin, 2003): proteinak 458 nm-ko uhin-luzera batera kitzikatu eta mcpVenus kanalaren fluoreszentzia-intentsitatea (YFP), mTFP kanalaren fluoreszentzia-intentsitatearekiko (CFP) estimatu dugu, hau da, YFP/CFP erlazioa.

FRET esperimentuek, kaltzioak eragindako konformazio aldaketak, nagusiki, Ca^{2+} eta CaM E-F (3) arteko loturaren ondorio direla erakusten dute. FRET-indizea nahiko egonkor mantendu da Ca^{2+}-a CaM3:Q2*h*AB konplexuan gehitu ondoren. Badirudi, E-F (4)-k ere nolabaiteko eragina duela Ca^{2+} seinalearen transmisioan, baina ez hain handia, seinalea modulatzen duela esan genezake. Bestalde, ezin da konformazio aldaketarik detektatu Ca^{2+}-arekin lotzeko gai ez den CaM mutante bat erabiltzen denean (CaM [1234]). FRET-indizearen arabera, kaltzio-seinalearen transdukzioa E-F (3) eskuaren menpe dago ~% 70-an; E-F (4)-a, berriz, ~% 30-ren erantzule da. Hala ere, gogoratu behar dugu FRET-indizearen eta distantziaren arteko erlazioa ez dela lineala, esponentziala baizik, eta zenbaki horiek distantzia bihurtzean, E-F esku baten eta bestearen ekarpena ezberdina izan daitekeela.

Gure aurretiazko datuek, erresoluzio handiko egiturekin batera, honako eredu hau iradokitzen dute: lehenik, zelula atseden-egoeran dagoenean (Ca^{2+} 100 nM), N-lobulua B helizearekin akoplatzen da eta Ca^{2+}-arekin kargatzen da; C-lobulua, berriz, B helizeari lotzen zaio, E-F esku hutsekin (6.3. irudia).

Jarduera neuronalaren ondorioz, edo Gq-ra akoplatutako hartzaileak aktibatzearen ondorioz (bradikinina-hartzailea, adibidez), Ca^{2+}-aren zelula barneko mailak kanaletatik 1 µM-tik gora igotzen direnean, E-F (3) zein E-F (4) kargatzen dira, baina E-F (3)-ren okupazioak eragiten du A eta B helizeen birorientazioa eta bereizketa. Garrantzitsua da kontuan hartzea kaltzio lotura ez

dela independentea E-F esku bakoitzarentzat, batez ere lobulu bereko E-F eskuetan. Kaltzioa esku bati lotzeak besteari eragiten dio, eta alderantziz. Ca^{2+} selektibitatearen euskarri diren mekanismoak CaM-z erregulatutako beste K^+ kanal batzuetarako deskribatu dira, esaterako: N-lobuluak zuzentzen dute SK kanaletan Ca^{2+}-aren seinaleztapena (Lee eta MacKinnon, 2018), eta C-lobuluak Eag1 kanaletan (Lorinczi et al.2016).

Nabarmentzekoa da K^+ kanalen kaltzio-seinaleztapenean hemen emandako datuen diskriminazio-maila aurretik inoiz ez dela eman, E-F esku bakoitzaren ekarpena bereiztuz. Aurreko lanak lobulu bakoitzaren ekarpena banaka aztertzera mugatu ziren, lobulu bakoitza osatzen duten E-F eskuen artean bereizi gabe.

Aurretik esan dugun bezala, EMN-aren bidez egindako esperimentuek frogatu zuten Ca^{2+} eta CaM-ren arteko elkarketak C lobuluan dauden E-F eskuen 17.9 graduko errotazio bat eragiten duela, CaM-ren h8 eta h5 helizeetatik ere tira egiten duena eta K_V7.2ren hA helizera transmititzen direnak.

Ikuspegi funtzionaletik, funtsezko urratsa apoCaM/K_V7.2-hAB-tik holoCaM/K_V7.2-hAB-rako trantsizioa da: ioiak E-F (3)-ra elkartzeak CaM-ren segmentu bat lekualdatzen du (h5 eta h8 helizeak), gainontzeko kanalera alosterikoki transmititzen dena, A eta B helizeen orientazioa aldatuz (Bernardo-Seisdedos et al., 2018). Suposatzen da egitura-aldaketa hori mekanikoki transmititzen dela kanalaren mintz barneko eskualdera, poroa ixten duen eta, azkenik, M-korrontea eteten duen pre-hA elementuaren orientazio-aldaketa baten bidez.

Antzera, CaM4-n (% 90) eta CaM124-n (% 79) izandako FRET murrizketek ia imitatu egiten dute K_V7.2: CaM WT konplexuan gertatzen den FRET harremanaren murrizketa (% 100). Hala ere, E-F (3) mutatuta dagoenean, konformazio-aldaketa txikiagoa da eta FRET-indizearen beherakada %32-ra murrizten da K_V7.2:CaM3 eta % 13,4-ra CaM123 konplexuetan. K_V7.3n emaitzak are argiagoak dira. Kasu honetan, K_V7.3:CaM124 konplexuak K_V7.3:CaM WT konplexuak bezainbeste murriztu du FRET indizea kaltzioak eragindako konformazio aldaketaren eraginez (% 97), CaM3 indizeak % 36 baino ez duen bitartean.

Esperimentua K_V7-ren isoforma guztiekin errepikatu zen, CaM WT, CaM3 eta CaM124rekin kaltzioaren efektua aztertuz, eta Ca^{2+} erantzunak kualitatiboki profil bera duela ikusi genuen. Kaltzio sentsoreak modu berean erantzuten du isoforma guztietan, non Ca^{2+}-a E-F (3) eskuari lotzea eragozteak Ca^{2+}-ak eragindako konformazio aldaketa nabarmen murrizten duen. Gainera, CaM124-rekin, non soilik E-F (3) eskua Ca^{2+}-a lotzeko gai den, erantzuna CaM wt-rekin sortutako konplexuan behatutakoaren antzekoa da.

K_V7.1 isoforman, E-F esku bakoitzaren eragina K_V7.3 isoforman bezain argia da. CaM124-k CaM WT efektua imitatzen duen bitartean, K_V7.1: CaM3k efektu osoaren herena baino ez du

erreproduzitzen (% 33,1). Hala ere, aurreko lanetan, Ca^{2+}-arekiko sentikorrak ez ziren CaM mutanteek K_V7.1 erantzuna aldatu zuten despolarizazio norabidean, kanala aktibatzearen aurka agertuz (Chang et al., 2018), K_V7.2-K_V7.5 kanalarekin kontrastean. Hala ere, K_V7.4 isoforman bezala, CaM1234-ren efektua CaM34 mutanteak fenokopiatu zuen, baina ez CaM12-k. Kasu honetan, K_V7.1-ean ez bezala, CaM1234-ren efektuek paper inhibitzaile bat adierazten dute, aktibatu beharrean. Gainera, CaM1234-rekin sortutako konplexuak bakarrik murriztu zuen korronte-dentsitatea (Chan et al., 2018).

Hala ere, emaitza horiek ez datoz bat aurretik lortutako emaitzekin: K_V7.1/KCNE adierazten duten zelulek korronte-dentsitatea ezabatzen zuten (Sachyani et al., 2014) eta BAPTA-ren efektu eza K_V7.1 kanalen aktibazioan (Tobelaim et al., 2017). Diferentzia horiek zelula-erregistroetako teknika esperimental ezberdinen ondorio izan litezke (Chang et al.,2018). Gainera, CaM kanalaren konplexuan sartzeko moduak ezberdintasun horiek eragin ditzake ere.

Gure emaitzak bat datoz Changek eta lankideek egindako azterketa funtzionalekin (Chang et al., 2018). K_V7.4-ko jarduera CaM edo CaM mutanteen aurrean neurtu zuten, hauek C-lobuluaren (CaM12), N-lobuluaren (CaM34) edo bien (CaM1234) kaltzioarekin lotzeko gaitasuna desaktibatu zutelarik (Keen et al., 1999). Erregistro elektrofisiologikoek erakutsi zutenez, CaM1234ren koadierazpenak K_V7.4 kanalaren aktibazioaren osagai azkarra bizkortu zuen, desaktibazioa saihestuz eta ezkerrerantz desplazamendu handia eraginez (> 35 mV) aktibazioaren tentsio-mendekotasunean. Sihnek eta bere lankideek (Sihn et al., 2016) antzeko emaitzak lortu zituzten. CaM1234rekin batera egindako K_V7.2 esperimentuetan, aldaketa txikiago bat gertatu zen, baina boltaian ezkerrerantz desplazatuta baita ere (~ 25 mV) (Gomis-Perez et al., 2017). Hau gure emaitzekin bat dator, non CaM 1234 ez den Ca^{2+}-arekiko sentikorra, titulazioak ez zuen Ca^{2+}-aren araberako konformazio-aldaketarik eragin.

Era berean, CaM34-k, CaM1234ren ondorioak imitatzen dituela erakusten dute, bai aktibazio-tasan, bai boltai menpeko aktibazioan ere (Sihn et al., 2016). Hala ere, CaM12k asaldura apalak baino ez zituen eragin propietate biofisikoetan, aktibazio-tasa arinki azkarragoa azalduz eta aktibatzeko kurba ezkerrerantz pixka bat desplazatuz.

Gainera, CaM3 mutante bakarrak CaM34ren antzeko efektuak eragiten ditu, bai aktibazio-tasan, bai boltai menpeko aktibazioan; CaM4-k, berriz, efektu arinagoa eragin zuen. Era berean, K_V7.4:CaM124 konplexuan, Ca^{2+}-aren gehikuntzak eragiten duen FRET murrizketak (% 67) K_V7.4:CaM WT konplexuan gertatzen denaren gertu dago (% 100). E-F (3) mutatuta dagoenean, konformazio-aldaketa txikiagoa da, eta FRET erlazioa % 22 baino ez da murrizten Ca^{2+} gehiketaren ondoren.

K_V7.5en kasuan, CaM124k CaM WTren konposizio-aldaketa bera simulatzen du baita ere (% 95), CaM3rekin sortutako konplexuak, FRET indizea Ca^{2+}-a gehitzean, ia erdira murrizten delarik (% 46).

Era berean, CaM1234-ren efektuek K_V7.2 (Gomis-Perez et al., 2017), K_V7.3 (Gomis-Perez et al., 2017) Kv7.4 (Chang et al., 2018) eta K_V7.5ean (Chang et al., 2018) kanal horietarako mekanismo bateratu bat erakusten dute, non Apo/CaM sistemak K_V7.2-isoforma neuronalen aktibazioa errazten duen.

Oro har, eskuragarri dauden datuek adierazten dute CaM E-F (3)-k Ca^{2+}-aren menpeko etengailu gisa jarduten duela, eta K_V7 familiako kanalaren jarduera kontrolatzen duela; E-F (4)-k, berriz, paper modulatzailea du. Lobulu bereko E-F eskuen arteko mendekotasun-maila kontuan hartuta, CaM3-rekin lortutako emaitzek harritu egiten gaituzte. **Nola eragin diezaioke kaltzioa esku batekin lotzeak kaltzioaren seinaleztapen orokorrari hain zorrotz?** Gainera, E-F (3) eskua, aldi berean, S2-S3 zehar-mintzaren arteko begiztarekin elkarreragiten duela deskribatu da (Sun eta MacKinnon, 2017). **E-F (3) eskuaren espezifikotasuna eta S2/S3-rekin duen interakzioa kaltzioa seinaleztatzeko kanal horietan garatutako mekanismo ebolutiboa al da?**

Galdera hau hurrengo kapituluan aztertuko dugu.

7. S2/S3 begiztak Kaltzio seinaleztapenean parte hartzen du

7.1. SARRERA

7.1.1 S2-S3 LOTAILUAREN PAPERA

Xenopus-ren KCNQ1-en PIP_2-rik gabeko cryo-EM egitura, giza KCNQ1-rekin %78-ko identitate-sekuentzia partekatzen duena, duela gutxi ebatzi zen 3,7 Å-eko ebazpen orokor batekin (Sun eta MacKinnon, 2017). Egiturak erakutsi zuen CaM bi interfaze ezberdinen bidez jartzen dela harremanetan KCNQ1-rekin. Horietako bat aldez aurretik identifikatu zen ebatzitako eremu zitoplasmatikoetako egitura kristalinoetan (Sachyani et al., 2014). Kontaktu honetan, KCNQ1-ren A-B helizeak CaM-ren N eta C lobuluek osatutako estalki baten antzeko egitura baten erdian txertatzen dira (Sachyani et al., 2014). CaM/*h*AB konplexuaren egitura oso antzekoa da krio-EM eta egitura kristalinoetan. Hala ere, egitura kristalinoan falta zen laugarren E-F eskuaren dentsitatean diferentzia bat ikusi zuten (PDB kodea: 4V0C). Dentsitate hau Ca^{2+} ioi baten presentziarekin bat dator. Ganera, bigarren kontaktu bat deskribatu da, boltai-sentsorearen S2/S3 begizta (mintz zeharreko kanalaren zati bat) eta CaM-ren hirugarren E-F eskuaren (7.1 irudia) artean eratzen dena. Bigarren kontaktu eremu hau ez zen kristal egituretan ikusi, ez baitzuen mintz zeharreko segmenturik.

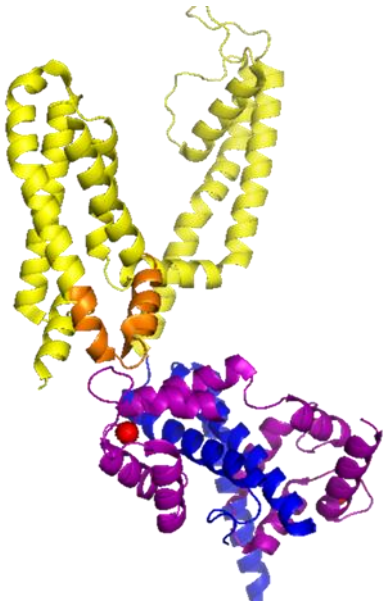

7.1 irudia. K_V7.1 kanalaren azpiunitate baten irudikapen eskematikoa, CaM duen konplexuan. CaM purpuraz irudikatzen da, Ca^{2+} ioiak esfera gorri bezala, C-terminala urdin bezala, mintz zeharkako domeinuak horiz irudikatzen dira eta S2/S3 begizta, esperimentuetarako erabilitako peptido bezala sintetizatu zena, laranjan. PDB: 5VMS.

Aipatzekoa da Sun eta MacKinnonek duela gutxi Kv7.1: CaM-ren bigarren egitura bat ebatzi zutela, PIP_2ren presentzian, non ez den CaM eta S2-S3 begiztaren arteko elkarrekintza ikusten (Sun & MacKinnon, 2019). PIP_2 eta KCNE3-ra konektatzen denean, konformazio-aldaketa handiak daude, baita poroko atearen dilatazioa ere. Jakina da poroaren eroankortasuna PIP_2

seinaleztapen-lipidoak arautzen duela neurri handi batean: lipido horren aurrean bakarrik ireki daiteke pororaren atea. PIP_2-k, ziurrenik, boltai-sentsorearen domeinua KCNQ1 poroen domeinura akoplatzen duenez, PIP_2-rik ez dagoenean, boltai-sentsoreak mugitu egiten dira, baina porotik desakoplatuta daudenez poroa ez da irekitzen (Zaydman et al., 2013). Egitura berri honek erakusten du PIP_2-ren elkarketak CaM-ren elkartze domeinuaren ia 180 graduko errotazioa eragiten duela. Aipatzekoa da PIP_2-ren lotura-guneak S2-S3 begizta, S0 eta S4-S5 lotailua barne hartzen dituela (7.2 irudia), eta horrek S2-S3, CaM-rekin duen interakzioa ekidin dezake. Hala ere, PIP_2-ren beste lotune ezagun batzuetan ez zen lipidorik atzeman, beraz, kontuz ibili behar gara krio-EM irudiak interpretatzean.

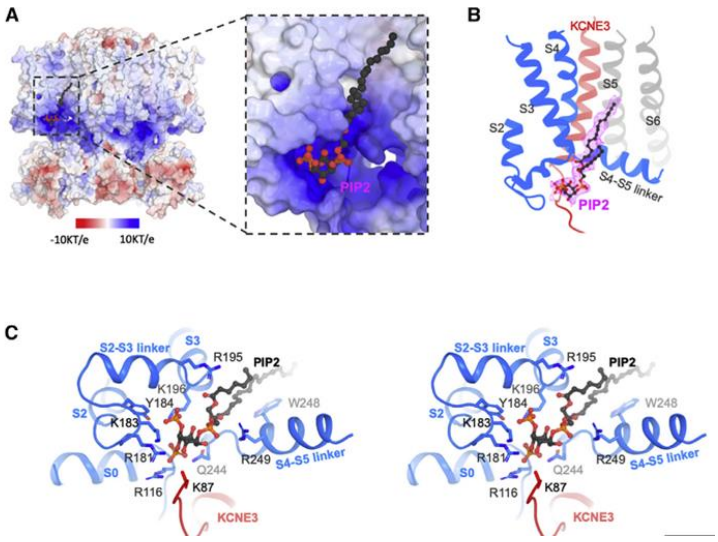

7.2 irudia. $HKCNQ1_{EM}$-KCNE3-CaM kanaleko PIP_2 lotunea. (A) PIP_2-a lotzeko gunearen azalera-potentzialaren irudikapena (-10KT/e 10KT/e, hutsean). PIP_2 lotunea eskuinera zabaltzen da. PIP_2 molekula bola eta makilen bidez irudikatzen da. **(B)** PIP_2ren krio-EM dentsitatea konplexuan. PIP_2-ren lotunearen inguruko eskualdea bakarrik agertzen da argitasun gehiagorako. KCNE3 gorriz koloreztatua dago, eta ondoko bi KCNQ1 azpiunitateak grisez eta urdinez koloreztatuak daude, hurrenez hurren. (C) PIP_2-a lotzeko gunearen ikuspegi estereoa. PIP_2-aren 4 Å -ren barruko aminoazidoen alboko kateak barra gisa agertzen dira. PIP2 bolak eta makilak dira. (De Sun eta MacKinnon, 2019).

Ez da ezagutzen elkarrekintza honen garrantzi fisiologikoa, baina CaM-ek boltaiarekiko menpekotasuna erregulatzeko mekanismo bat iradokitzen du. Garrantzitsua da gogoratzea funtsezkoa dela Ca^{2+}-a E-F (3) eskuari lotzea.

Orain, Ca^{2+}-ez titulatuko dugu FRET sentsorea, S2/S3 peptidoaren kontzentrazio desberdinak daudelarik.

7.1.2. S2-S3-ren sekuentzia kontserbatuta dago K_V7 familian

Boltai-menpeko potasio kanalen familien sekuentzia-lerrokadurak (K_V1-9) erakusten du bederatzi aminoazidoko S2-S3 begizta KCNQ1-en (eta beste K_V7 isoformetan) luzeran eta sekuentzian kontserbatzen dela KCNQ1en ortologo eta paralogoen artean, baina ez dagoela presente boltaiaren menpeko beste potasio-kanaletan (Sun eta MacKinnon, 2017) (7.3 irudia).

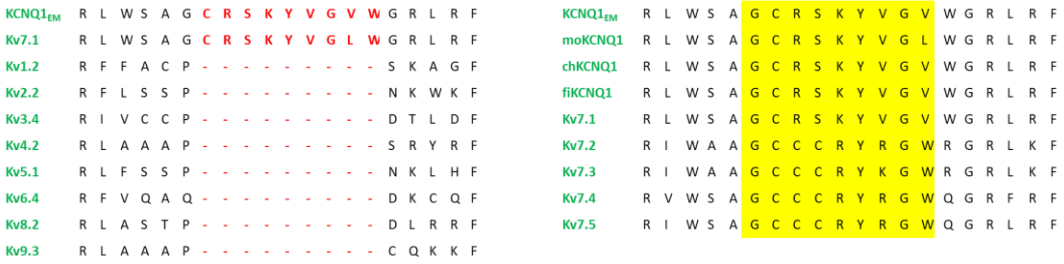

7.3 irudia. S2-S3 begizta eskualdeko sekuentzia lerrokatzea K_V1-9 familiaren eta KCNQ1 ortologo eta parametroen artean. Proteinak eskuratzeko kodeak honako hauek dira: $K_V1.2$: NP_004965.1, $K_V2.2$: NP_004761.2, $K_V3.4$: NP_004969.2, $K_V4.2$: NP_036413.1, $K_V5.1$: NP_002227.2, $K_V6.4$: NP_758857.1, $K_V8.2$: NP_00858.2: Aurreko sekuentzia guztiak Homo sapiens. moKCNQ1: NP_032460.2 (mus musculus), chKCNQ1: XP_421022.3 (Gallus gallus) eta fiKCNQ1: NP_001116714.1 (Danio rerio) dira. Sun eta MacKinnonetik egokitua, 2017.

S2-S3 begizta CaM-ren hirugarren E-F eskuarekin kontaktua egiten duen estrukturan ez zen Ca^{2+} ioiari dagokion dentsitaterik ikusi, nahiz eta estruktura 5 mM-ko Ca^{2+} kontzentrazioan ebatzi zen (Sun eta MacKinnon, 2017).

7.2. HELBURUA

Hemen, gure helburua S2/S3 begiztaren garrantzi funtzionalari heltzea da, zitoplasmara hedatzen dena eta CaM-rekin elkarreragiten duena. Ca^{2+} seinalearen transmisioan duen eginkizuna aztertuko dugu.

7.3. EMAITZAK

7.3.1. S2/S3-REN EFEKTUA D-CaM-N

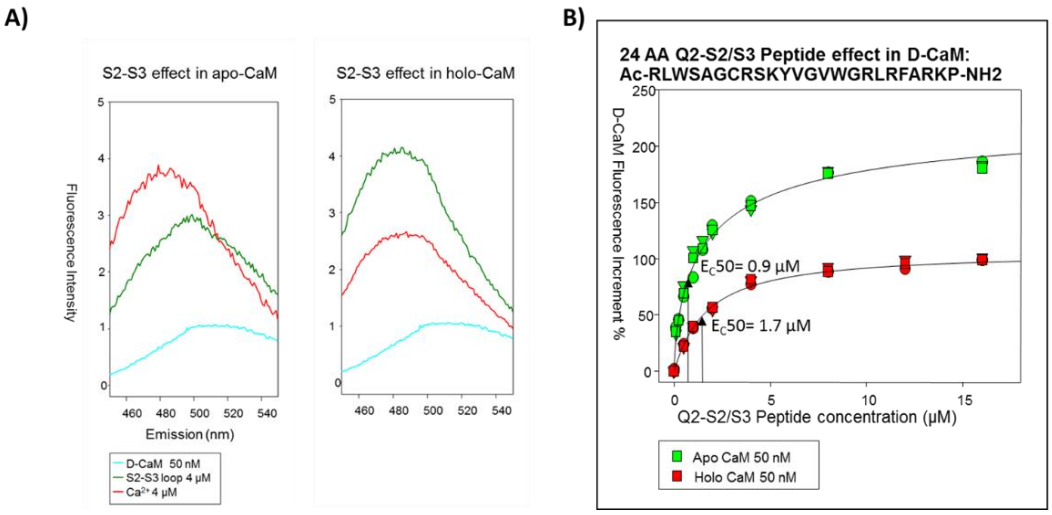

7.4 irudia. Q2-S2/S3 efektuak D-CaM efektuan duen eragina. (A) D-CaM-ren igorpen-espektroak 340 nm-ra kitzikatu ziren. Zian lerroa, Apo-D-CaM-ren igorpena erakusten du. Ezkerreko grafikoak peptidoaren titulazioa erakusten du (lerro berdeak) eta, ondoren, Ca^{2+} titulazioa (marra gorriak). Eskuineko espektroek kontrakoa erakusten dute, lehen Ca^{2+}-aren titulazioa eta ondoren peptidoarena. **(B)** Grafikoan D-CaM (490-500 nm) fluoreszentziaren intentsitatea handitu dela ikus daiteke, Q2-S2/S3 peptido-kontzentrazioaren aldean. Grafiko berdeak Apo-D-CaM-ri dagokio (EGTA 5 mM) eta grafiko gorriak Holo-D-CaM-ri (Ca^{2+} 1 mM). Lerroak Hillen ekuazioa datuetara doitzearen emaitza dira.

CaM eta S2/S3 begiztaren arteko elkarreragina aztertzen hasiko gara, D-CaM fluoreszentziaren emisioan Q2-S2/S3 (Ac-RLWSAGCRSKYVGWGRLRFARKP-NH2) peptidoa titulatuz. Peptidoa gehietzean, Apo-D-CaM fluoreszentziaren intentsitatea ia % 200 igotzen dela ikusten dugu (199 ± 13, n =20). Peptidoaren ageriko afinitatea 1 µM ingurukoa da (0,9 ± 0,2 µM Apo-D-CaM-rako). Gainera, kaltzioa gehitzean gertatzen den bezala, peptidoaren titulazioan bi efektu ezberdin antzeman daitezke D-CaM-ren emisio espektroan. Alde batetik, peptidoaren elkarketak D-CaM fluoreszentziaren intentsitatea handitzea eragiten du, ia hirukoiztu arte (Ca^{2+}-ak soilik bikoizten duelarik). Gainera, fluoreszentziaren balio maximoa ezkerrerantz desplazatzen da, 500 nm-tik 495 nm-ra mugituz, (Ca^{2+}-arekin 490 nm-raino mugitzen da). Beraz, efektu peptidikoak Ca^{2+}-aren efektua partzialki birkapitatzen du.

Informazio gehiago lortzeko, peptidoaren eragina Ca^{2+}-aren aurrean ere aztertu zen. Kasu honetan, D-CaM Ca^{2+}-z asetu zen (7.4 irudia, A. eskuina, marra gorria) peptidoarekin titulatu aurretik. Ca^{2+}-aren gehienezko efektua emisio-espektroan lortu zenean (jakina da E-F esku guztiak Ca^{2+}-z okupatuta daudela 2 µM-tik aurrera), S2-S3 peptidoa gehitu zen, eta horrek beste igoera bat eragin zuen D-CaM-ren fluoreszentzian, Ca^{2+}-D-CaM zuen fluoreszentzia bikoiztuz (106 ±% 2, n=20). Emisio espektroaren maximoan ere aldaketa gehigarri bat antzeman zen, ezkerrerantz 3-4 nm gehiago desplazatuz (7.4 irudia). Kasu honetan, itxurazko afinitatea txikiagoa izan zen, EC50 1,7 ± 0,1 µM-koa. Beraz, peptidoak eta Ca^{2+}-ak, itxuraz, eragin gehigarria dute, baten presentziak ez du bestearen efektua oztopatzen, eta hori bi ligandoek ekintza-mekanismo ezberdinak dituztela adierazten du. Bien presentziak, Ca^{2+} eta peptidoarena, antzeko ondorioak ditu D-CaM-n, intentsitatearen laukoizketa eta emisio balio maximoaren desplazamendua 485-486 nm-raino, D-CaM-ra gehitzeko ordena edozein dela ere (7.4 irudia). Bitxia bada ere, Hillen koefizientea ere 1 ingurukoa da bi kasuetan (0,8 Ca^{2+}-rik gabe eta 1,0 Ca^{2+}-aren presentzian), CaM peptidoarentzat lotune bakarra duela iradokitzen duena.

7.3.2. Q2-*h*AB:CaM -ren ^{15}N-HSQC espektroa Q1-S2-S3rekin

D-CaM esperimentuen bidez, badakigu CaM eta S2-S3 arteko elkarrekintza bat dagoela, Ca^{2+}-arekiko independentea dena, baina ezin dugu bereizi non lotzen den peptidoa. Gainera, krio-EM egiturak, PIP_2-rik ez dagoenean, E-F (3) eskuarekin interakzioa erakusten du, baina ez dakigu interakzio hori E-F (3)-ren espezifikoa den, edo edozein E-F eskurekin interakzioanatzeko gai den.

S2/S3 eta CaM-ren arteko interakzio-gunea identifikatzeko, EMN datuak bildu ziren. Lehen esan bezala, aurretik, Q2*h*AB:CaM konplexuaren ^{1}H-^{15}N HSQC seinaleak esleitu ziren egitura ebazteko. Behin esleipen hori izanda, ^{15}N-rekin markatutako konplexuaren HSQC ^{1}H-^{15}N espektroa, eskeletoaren amida talde bakoitzerako seinale bat erakusten duena, edozein ligandorekin duen interakzioa ikertzeko erabil daiteke. Horrela, Q2-*h*AB:CaM (75 µM) markatutako ^{15}N-HSQC espektroak, markatu gabeko Q1-S2/S3 1 mM-rekin bildu ziren, apo eta holo konfigurazioan (Ca^{2+} 2 mM).

Zenbait aminoazidoren desplazamendu kimikoan aldaketak ikusten dira. Desplazamendu kimikoak eragindako perturbazioak (seinalea mugitzea edo handitzea) EMN nukleoaren inguruko aldaketetatik sortzen dira, eta proteinaren arteko interakzioe zuzenek edo loturek eragindako

konformazio-aldaketek eragin ditzakete. Perturbazio hauek proteina egitura batean mapeatu daitezke, peptidoaren interakzio gune posibleak errebelatzeko.

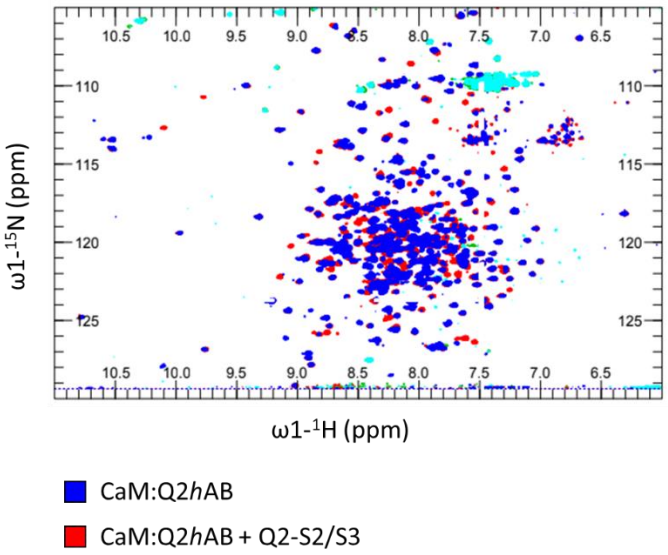

7.5 irudia. Q2*h*AB:CaM-ren ^{15}N-HSQC markatu gabeko Q2-S2/S3rekin. ^{15}N-HSQC Q2*h*AB:CaM konplexua 75 µM-tan (urdina) eta Q1-S2/S3 peptidoarekin 1 mM-tan (gorria). Seinaleen gainjartzeak, peptidoen titulazioak, konplexuaren egitura aldatzen ez duela frogatzen du.

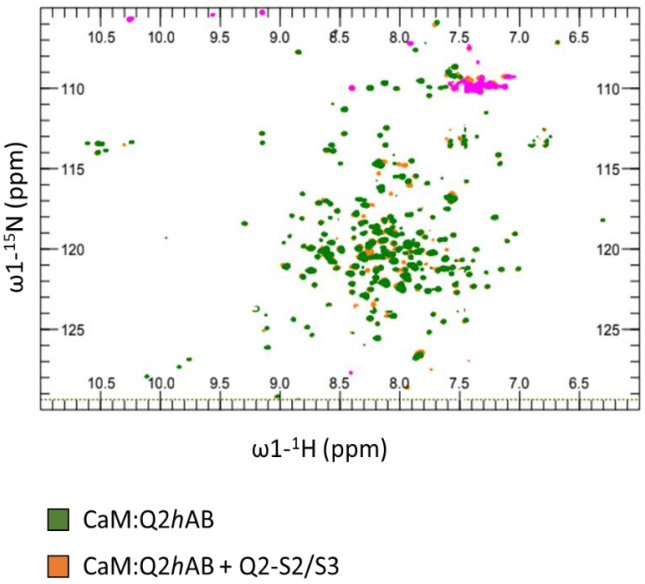

7.6 irudia. Holo-CaM:*h*AB konplexuaren ^{15}N-HSQC peptidoarekin eta peptidorik gabe gainjarrita. Espektro berdeak Q2*h*AB:CaM konplexuari dagokio Ca^{2+} 1 mM-tan, eta laranjaz konplexu berdina Q1-S2/S3 1 mM-rekin.

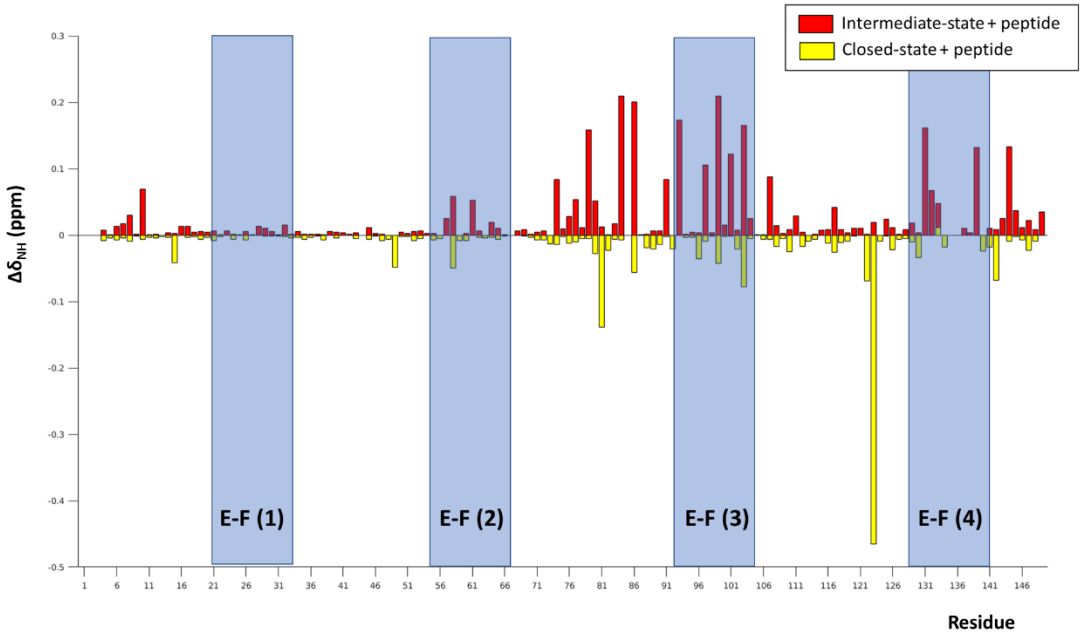

7.7 irudia. ^{1}H-^{15}N Q2*h*AB konplexuaren desplazamendu kimikoaren eta kaltzio presentziaren eta gabeziaren peptidoaren alderaketa. Apo-CaM-en C-lobulurako ezberdintasun gehiago agertu ziren, peptidoak, CaM/K_V7.2_AB konplexuan, E-F (3) eta E-F (4) -rekin antzekotasun gehiagorekin elkarreragiten duela iradokitzen duena. E-F (1) (20-31), E-F (2) (56-67), E-F (3) (93-104) eta E-F (4) (129-140) koadro urdin gisa definitu ziren. Ez dago balio negatiborik.

7.7 irudian ikus dezakegun bezala, peptidoa konplexura batu ondoren, aldaketa kimiko handiagoak ikusten dira CaM-ren C-lobuluan dauden aminoazidoetan. Peptidoarekin elkarreragiten ari diren aminoazidoak bereziki E-F (3)-n daude, hala nola D94, N98, Y100, I102 eta A104 (7.7 irudia) konplexuaren apo-konformazioan. Ca^{2+}-aren presentzian, desplazamendu orokorrak baxuagoak dira. Hala ere, S2/S3 E-F (3)-rekin elkarreragiteko gai da, Ca^{2+}-ren aurrean ere (7.8 irudia). Hau bat dator krioEM egituran ikusitakorekin (Sun eta MacKinnon, 2017), non elkarrekintza E-F (3)-an ikusi zen. Badira E-F (4) eskuan kokatutako hondakin desplazatuak ere, bereziki I131 eta E139. Ezin dugu esan kasu honetan, peptidoaren efektu zuzena edo efektu alosterikoa den. Gainera, aurretik esleitu ez ziren seinale desplazatu gutxi batzuk ere badaude.

Aipatzekoa da N98 eta Y100 krio-EM egituran kontaktuak egin ahal zuten kandidatu nagusiak zirela ere (Sun eta MacKinnon). Arreta berezia jarri zioten N98-ri, CaM_N98S mutazioa epilepsia eta paziente gazteen bat-bateko heriotzarekin lotzen baita (Jiménez-Jáimez et al., 2016; Makita et al., 2014). Mutazio hori zuzenean esleitzen zaio CaM eta boltai-sentsorearen arteko interfazeari, eta argi eta garbi elkarreragiten du S2-S3 peptidoarekin. Hala ere, E-F (3)-n edo E-F

(4)-n dauden beste mutazio batzuek profil elektrofisiologiko berera daramate, eta, beraz, N98Sren espezifikotasunari buruzko inferentziak gehiegikeriatzat jo daitezke.

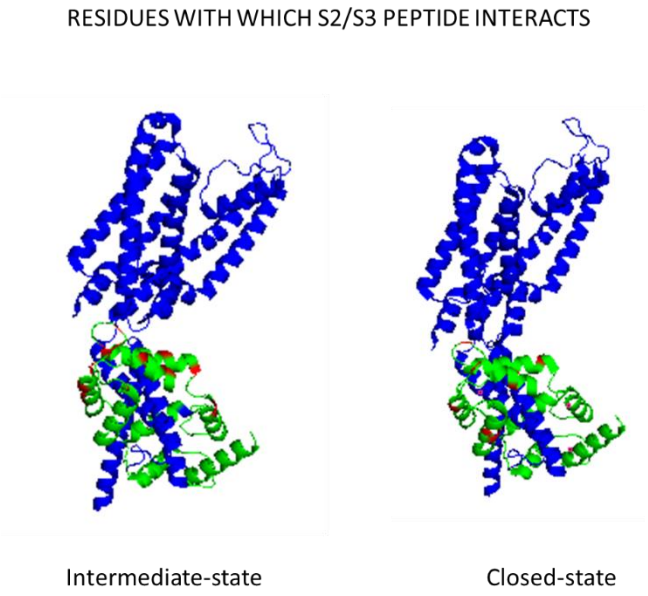

7.8 irudia. S2/S3 peptidoak Q2hAB konplexuari eragiten dion aminoazidoak. KCNQ1:CaM azpiunitatea: krio-EM-ez ebatzitako tetrameroa. K_V7.1 kanala urdinez irudikatzen da eta CaM berdez. Q1-S2/S3 peptidoa gehitu ondoren (1 mM-tan), desplazamendu kimiko handia duten aminoazidoak gorriz nabarmentzen dira, apo-konfigurazioan ezkerrean (Ca^{2+} CaM-ren N-lobuluan bakarrik) eta holo-konfigurazioan (1 mM Ca^{2+}).

7.3.3. PEPTIDOAREN EFEKTUA FRET-SENTSOREAREN BIDEZ AZTERTUTA

S2/S3 begiztak Ca^{2+} seinaleztapenean duen eragina aztertuko dugu FRET bidez. Bigarren kapituluan deskribatzen den bezala, Ca^{2+}-a Q2*h*AB:CaM-ri elkarketzeak konformazio aldaketa bat eragiten du, FRETren bidez monitorizatu daitekeena, mTFP1-*h*AB-Venus:CaM konplexua erabiliz. Orain, Ca^{2+}-z titulatuko dugu FRET sentsorea, S2/S3 peptido kontzentrazio ezberdinen presentzian dagoelarik.

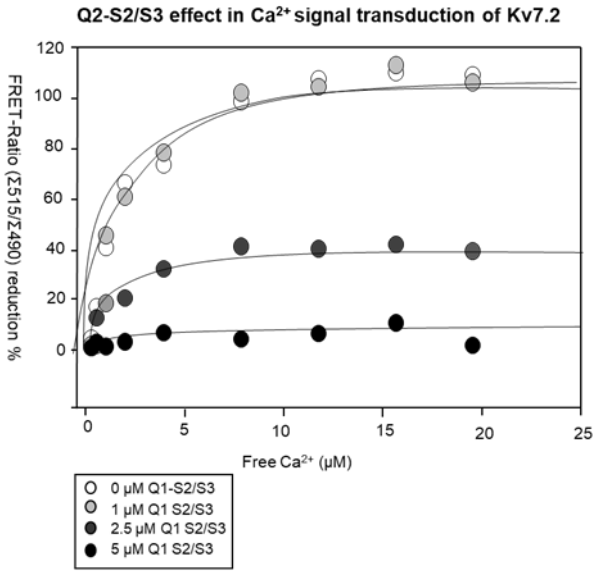

[Peptide]	Max.expec.	Ec50 (µM)	RSQR
0 µM	109 ± 12.3	0.9 ± 0.2	0.97
1 µM	116 ± 17.3	0.8 ± 0.1	0.91
2.5 µM	44 ± 5.6	1.1 ± 0.3	0.98
5 µM	5 ± 1.4	1.8 ± 0.4	0.90

7.9 irudia. Q2-S2/S3 efektua Ca^{2+} seinalearen transmisioan. Grafikoak erakusten du FRET-indizearen murrizketa %-tan, gehitutako Ca^{2+} kontzentrazioaren aldean. 500 nM mTFP1-*h*AB-Venus: CaM esfera zurietan irudikatzen da. Gris argia 1 µM Q2-S2/S3-rekin. Esferak ilunagoak dira laginean peptidoaren kontzentrazioa handitzen den heinean, 2, 5 eta 10 µM-tik igaroz. Lerroak Hillen ekuazioa datuetara doitzearen emaitza dira. Osagarri hauen parametroak azpian erakusten dira: Balio bakoitzak gutxienez 3 esperimentu independenteren batezbestekoa adierazten du.

Lehenik eta behin, peptidorik gabe neurtu zen FRET-indizea, laginaren kalitatea ebaluatzeko. Espero zen bezala, FRET indizea 1,61 ± 0,05etik 1,17 ± 0,04ra jaitsi zen, Ca^{2+} indizeak bultzatutako konformazio-aldaketaren ondorioz (7.8 irudia). Emaitza horiek erreferentziatzat hartu ziren S2/S3 peptidoaren efektua zenbatesteko. S2/S3 1 µM peptidoaren presentzian, FRET indizea peptidorik gabe lortutakoarekin gainjartzen da, kontzentrazio honetan beraz, peptidoaren eragina hutsala da. 2 µM peptidoren presentzian, Ca^{2+}-aren efektua murriztu zen. Ca^{2+} loturaren ondoren, FRET indizea 1,42 ± 0,05-koa da, 0 edo 1 µM peptidoarekin behatutakoa baino % 40 altuagoa. Era berean, S2/S3 peptidoaren eragina 5 µM-tan frogatzen dugunean, Ca^{2+} indizeak bultzatutako konformazio-aldaketa antzemanezina izan zen, Ca^{2+}-aren gaineko FRET indizeak ez zuen murrizketarik jasan, Ca^{2+}-rik gabeko FRET indizearen oso gertuko balioak mantenduz, 1,6 ± 0,09-ra. Une horretan pentsatu genuen S2/S3 eta E-F (3) delakoen arteko elkarrekintzak Ca^{2+}-arekin elkartzea eragozten zuela E-F esku horretan, zeina, aurreko kapituluan ikusi dugun bezala, Ca^{2+} seinalea kanalera transmititzeaz arduratzen den.

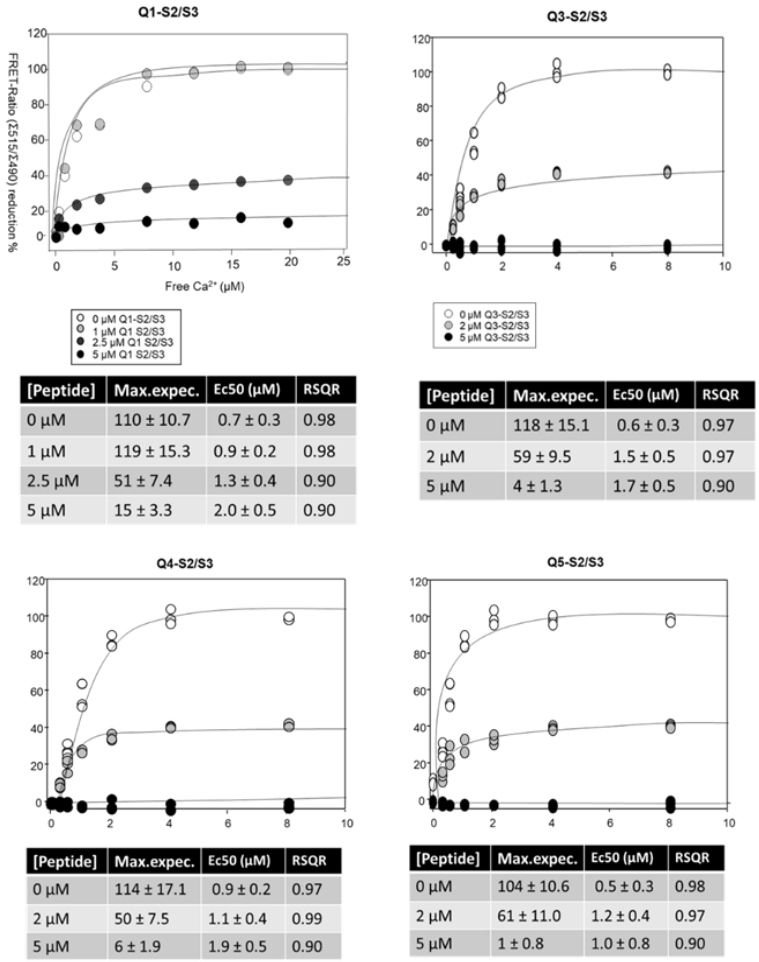

[Peptide]	Max.expec.	Ec50 (µM)	RSQR
0 µM	110 ± 10.7	0.7 ± 0.3	0.98
1 µM	119 ± 15.3	0.9 ± 0.2	0.98
2.5 µM	51 ± 7.4	1.3 ± 0.4	0.90
5 µM	15 ± 3.3	2.0 ± 0.5	0.90

[Peptide]	Max.expec.	Ec50 (µM)	RSQR
0 µM	118 ± 15.1	0.6 ± 0.3	0.97
2 µM	59 ± 9.5	1.5 ± 0.5	0.97
5 µM	4 ± 1.3	1.7 ± 0.5	0.90

[Peptide]	Max.expec.	Ec50 (µM)	RSQR
0 µM	114 ± 17.1	0.9 ± 0.2	0.97
2 µM	50 ± 7.5	1.1 ± 0.4	0.99
5 µM	6 ± 1.9	1.9 ± 0.5	0.90

[Peptide]	Max.expec.	Ec50 (µM)	RSQR
0 µM	104 ± 10.6	0.5 ± 0.3	0.98
2 µM	61 ± 11.0	1.2 ± 0.4	0.97
5 µM	1 ± 0.8	1.0 ± 0.8	0.90

7.10 irudia. S2/S3 peptidoaren interakzioa Q2*h*AB:CaM-rekin K_V7 familiako hainbat isoformen S2/S3 begizten efektua. Grafiko bakoitzak mTFP-Q2*h*AB-Venus 500 nM-ren FRET indizea (YFP/CFP) erakusten du, S2/S3 peptido-kontzentrazio ezberdinekin nahastuta eta Ca^{2+}-arekin titulatuz. Lerroak Hillen ekuazioa datuetara doitzearen emaitza dira. Osagarri horien parametroak azpian erakusten dira. Balio bakoitzak gutxienez 3 esperimentu independenteren batezbestekoa adierazten du.

Ondoren, K_V7 kanalen familiako beste isoformatako S2/S3 begizten eragina gure FRET-biosentsorean probatu zen. Efektua antzekoa izan zen isoforma guztientzat. 2,5 µM-ko peptidoa dagoenean, Ca^{2+} efektua erdira murrizten da. Hau da, Ca^{2+}-aren loturaren ondorioz FRET-indizeak izandako murrizketa % 40-ra jaisten da, eta Ca^{2+}-ak eragindako konformazio-aldaketa ez da erabat osatzen (7.10. irudia).

5 µM-ko peptido baten antzera, Ca^{2+}-aren efektua ezabatzen da, hau da, FRET indizea, Ca^{2+} batu ondoren, apo konfigurazioan bezala mantentzen da. Efektu hori ikusten da bi ligandoek proteina multzoarekin bat egiteko gaitasuna dutenean.

Gainera, Q1-S2/S3, Q2-S2/S3, Q3-S2/S3 10 µM-tan probatu ziren eta, bitxia bada ere, FRET indizea Ca^{2+}-ra batzean, murriztu beharrean, handitu egin zen, FRET-indizea ia bikoiztuz (+ % 78). Horrek esan nahi du proteinen konplexuak konfigurazio berri bat hartzen ari dela, non A eta B helizeak elkarren artean hurbilduko liratekeen (7.12 irudia).

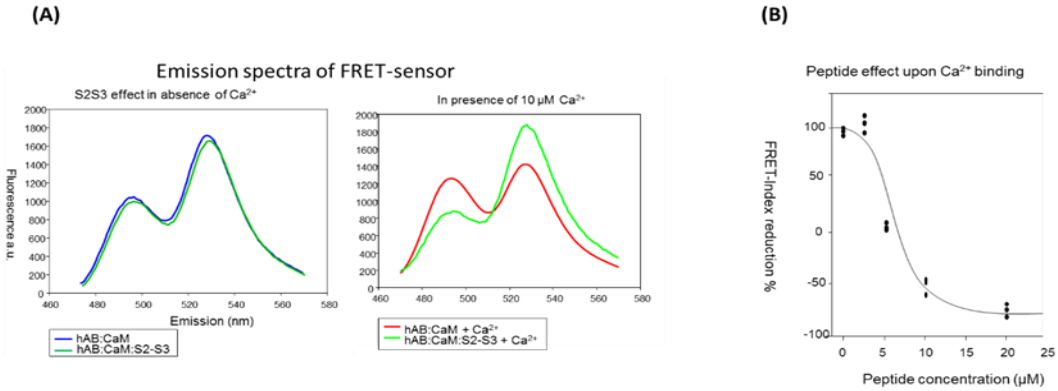

7.11 irudia. FRET indizea, S2/S3 peptidoa gehitu ondoren. (A) mTFP1-Q2*h*AB-Venus:CaM-ren 500 nM emisio espektroa, 458 nm-tan kitzikatua, 500 nM mTFP1-QhAB-Venus eta 10 µM S2-S3 peptidoarekin, Ca^{2+} -aren absentzian eta 10 µM Ca^{2+}-ren presentzian. (B) FRET indizearen murrizketa (%-tan) 10 µM Ca^{2+}-ren presentzian eta Q2-S2/S3 peptido-kontzentrazio ezberdinetan (x abzisa). Lerroa Hillen ekuazioa datuei doitzearen emaitza da.

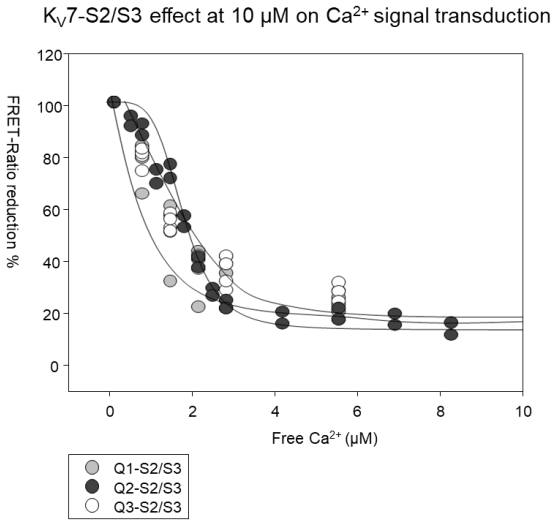

7.12 irudia. 500 nM mTFP-hAB-Venus:CaM kaltzioaren titulazioa, K_V7.1, K_V7.2 eta K_V7.3 isoformen S2/S3 10 µM peptidoarekin nahastuta. Zirkulu grisak K_V7.1 isoformako S2/S3 lotailuari dagozkie, beltzak K_V7.2 sistemarako eta zuriak K_V7.3 sistemarako. Erakutsitako emaitza FRET-en murrizketa ehunekotan adierazten da, erreferentziatzat peptidorik edo kaltziorik gabeko konplexua hartuta. Balio bakoitzak gutxienez 3 esperimentu independenteren batezbestekoa adierazten du.

Konfigurazio berri honetan Ca^{2+}-arekiko afinitatea antzekoa da S2/S3 isoforma guztientzat: 1,16 ± 0,16 µM Q1-S2/S3-rekin, 1,73 ± 0,8 Q2-S2/S3-rekin eta 1,55 ± 0,5 µM Q3-S2/S3-rekin (7.12 irudia). Gainera, Hill-en koefizientea 0,83, 0,35 eta 0,76 izan zen isoforma bakoitzerako.

7.3.4. E-F ESKUEN PEPTIDOAREN ESPEZIFIKOTASUNA

Aurreko kapituluan ikusi dugun bezala, Ca^{2+} seinaleztapena, K_V7 kanaletan, batez ere E-F (3) eskuaren eta, neurri txikiagoan, E-F (4) eskuaren bidez ematen da. K_V7.1-ren cryo-EM egituran,

CaM konplexuan, E-F (3) eskuaren eta S2/S3-aren arteko lotailuaren arteko elkarreragina deskribatzen da. Esperimentu honen helburua interakzio hori E-F (3)-arekiko espezifikoa den edo, aitzitik, S2/S3 begiztak E-F eskuekin modu ez-espezifikoan elkarreragin zezakeen ikertzea zen. Helburu horretarako, FRET-sentsorea CaM3, CaM124 eta CaM1234rekin purifikatu zen, eta Ca^{2+}-arekin titulazioak egin ziren, Q2-S2/S3 peptidoaren presentzian.

Q2-S2/S3 peptidoak mTFP1-*h*AB-Venus konplexuan CaM124rekin duen eragina CaM wt-rekin behatutakotik oso gertu dago. 5 µM peptidotan, Ca^{2+}-ak eragindako FRETren murrizketa baliogabetu egiten da, eta 10 µM-tan, CaM wt-rekin ere behatutako FRET-indizearen handipena ikusten da. Baldintza horietan, espero den FRET-balio maximoa % 80koa izango da, eta Ca^{2+}-arekiko afinitatea 1,4 µM da, peptidorik ez dagoenean ikusitakoa baino txikiagoa.

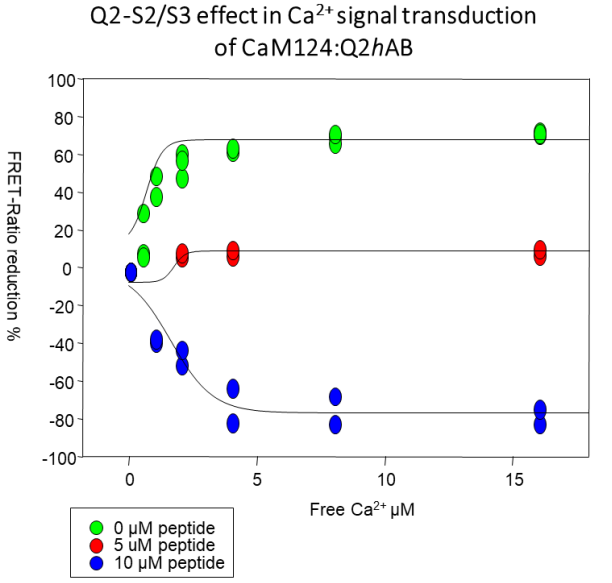

[Peptide] (µM)	Max.expected	Ec50 (µM)	RSQR
0	68 ± 3.05	0.6 ± 0.08	0.97
5	8.8 ± 2.06	1.6 ± 0.22	0.99
10	-80.5 ± 5.2	1.4 ± 0.26	0.96

7.13 irudia mTFP-hAB-Venus:CaM124 500 nM-ren kaltzio-titulazioa: Q2-S2/S3 peptidoarekin nahastuta. Zirkulu berdeak Q2-S2/S3 peptidorik gabeko kontrol-titulazioari dagozkio. Q2-S2/S3 5 µM-rekin zirkulu gorriak eta 10 µM-rekin zirkulu urdinak. Erakutsitako emaitza FRETen murrizketa-ehunekotan adierazten da, erreferentziatzat peptidorik eta kaltziorik gabeko konplexua hartuta. Lerroak Hillen ekuazioa datuetara doitzearen emaitza dira. Ekuazio horren osagaiak azpiko taulan agertzen dira. Balio bakoitzak gutxienez 3 esperimentu independenteren batezbestekoa adierazten du.

Hala ere, konplexua CaM3-rekin adierazten denean, ez da efektu bera ikusten. Kasu honetan, Q2-S2/S3 peptidoa 10 µM-tan gehitzen dugunean, FRET-indizearen igoera, Ca^{2+}

gehitzean, % 40,4koa da, eta Ca^{2+}-arekiko afinitatea 2,8 µM-koa da, peptidorik gabeko estimatua baino ia hiru aldiz txikiagoa (0,9 µM).

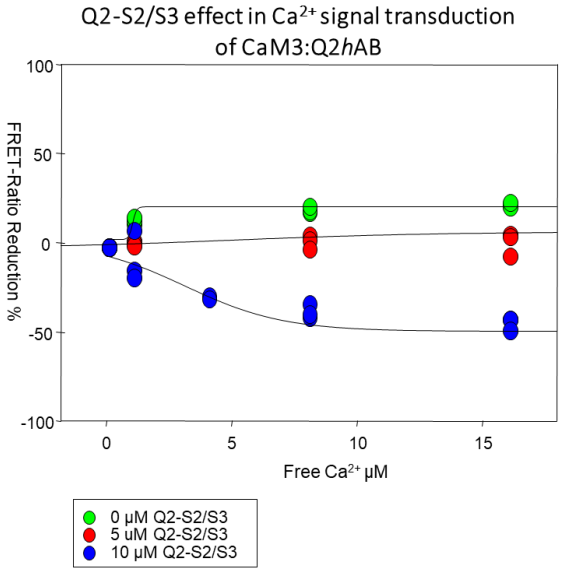

[Peptide] (µM)	Max.expected	Ec50 (µM)	RSQR
0	24 ± 1.08	0.9 ± 0.35	0.99
5	6 ± 1.92	3.4 ± 0.28	0.90
10	-40.4 ± 3.52	1.4 ± 0.44	0.97

7.14 irudia 500 nM mTFP-*h*AB-Venus:CaM3-ren kaltzioko titulazioa Q2-S2/S3 peptidoarekin. Zirkulu berdeak Q2-S2/S3 peptidorik gabeko kontrol-titulazioari dagozkio. S2/S3 5 µM peptidoaren presentzian zirkulu gorriak eta 10 µM-rekin zirkulu urdinak. Erakutsitako emaitzek FRET-en murrizketa-ehunekotan adierazten dute, erreferentziatzat peptidorik edo kaltziorik gabeko konplexua hartuta. Lerroak Hillen ekuazioa datuetara doitzearen emaitza dira. Ekuazio horren osagaiak azpiko taulan agertzen dira. Balio bakoitzak gutxienez 3 esperimentu independenteren batezbestekoa adierazten du.

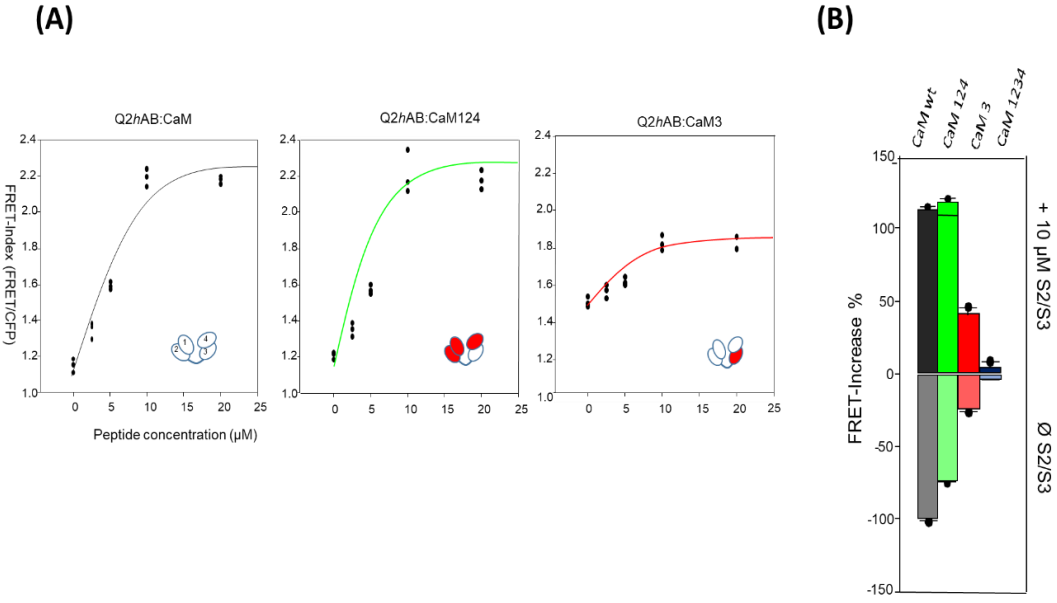

7.15 irudia Q2-S2/S3-ren efektua Ca^{2+} seinaleztapenean FRET-Sentsorearen bidez monitorizatua CaM mutantedun konplexuan. (A) Q2-S2/S3 peptidoaren titulazioa, 500 nM Q2*h*AB-ren Ca^{2+}titulazioa, CaM wt-rekin konplexuan (marra beltza), CaM124-rekin (marra berdea) eta CaM3-rekin (marra gorriak). **(B)** Grafikoak sentsorearen FRET-indizearen handipena erakusten du CaM mutante ezberdinetan, Q2-S2/S3 10 µM-ren presentzian eta absentzian.

7.4. EZTABAIDA

Kapitulu honetan S2/S3 begiztak Q2*h*AB:CaM konplexuaren barruan duen interakzioa aztertuko dugu, aurrez K_V7.1:CaM-ren krioEM egituran identifikatu zena. Peptidoaren interakzioa, lehenik, D-CaM-rekin aztertu zen. Saiakuntza honek lobuluen arteko lotura (fluoreszentzia handitzea eragiten duena) eta E-F eskuetara lotura (seinalea handitzeaz gain, emisio balio maximoaren ezkerrerako desplazamendua eragiten duena) bereizten ditu.

Ikusi dugunez, S2/S3 peptidoa CaM-rekin elkarreragiteko gai da, bai Ca^{2+}-rik ez dagoenean, bai Ca^{2+}-aren presentzian, eta aurrez, K_V7.2/3ko A eta B helizeen peptidoekin ikusitakoa baino fluoreszentzia-intentsitate handiagoa eragiten du (Alaimo et al., 2014). Gainera, S2/S3 peptidoarekin D-CaM-ean egindako titulazioak, fluoreszentzia handitzearekin batera, ezkerrerako desplazamendu bat erakusten du emisio-espektroaren balio maximoan, 320 nm-tan kitzikatu ondoren. Efektu hori aurretik ikusi zen, eta Ca^{2+}-a E-F eskuei lotzearekin erlazionatu zen (Alaimo et al., 2014). Beraz, S2/S3 begiztak CaM-rekin bi modutan elkarreragiten duela suposatu dezakegu. Lehenik eta behin, CaM begizta hori besarkatzen ari da, K_V7 kanaletako A eta B helizeekin egiten duen bezala, eta horrek igorpenaren intentsitatea handitzearen erantzukizuna izango luke. Bigarrenik, peptidoak E-F eskuekin bat egin dezake, cryoEM egituran ikus daitekeenez (Sun & MacKinnon, 2017). D-CaM analisiaren bidez ezin dugu bereizi peptidoak E-F eskuen artean diskriminatzen duen ala ez.

Garrantzitsua da kontuan hartzea Ca^{2+} eta peptidoak D-CaM-n efektu baterragarria dutela, hau da, baten efektuak ez du bestearena deuseztatzen. Beraz, elkarrekin daudenean, D-CaM-ren fluoreszentzian, intentsitate handiagoa lortzen dute, bereizita lortutakoa baino. Afinitatean ere aldaketak daude, ikusi da Ca^{2+}-rik ez dagoenean CaM duen peptidoarekiko afinitatea bikoizten dela. Ca^{2+} eta S2/S3 peptidoak lotura guneak partekatzen dituztela iradoki daiteke, eta afinitatearen murrizketa, biek, CaM-rekin bat egiteko duten lehiaren ondorio bat izan daitekeela.

Elkarrekintza berri horren ezaugarriak hauek dira: intentsitate askoz handiagoa (gutxienez bi aldiz handiagoa) eta ezkerrerako desplazamendua, dosiaren menpekoa, Ca^{2+}-ak eragindakoaren antzeko magnitudean.

Hurrengo urratsa Q2*h*AB:CaM konplexuko zein aminoazidok peptidoarekin elkar eragiten duten aztertzea izan zen. Konplexu hau, lehenago, EMNez erabat ebatzi zenez, seinale guztiak jada esleituta daude (TW helizetik datozenak izan ezik). Beraz, markatu gabeko peptidoarekin egindako titulazio baten bidez, ^{15}N-z markatutako konplexu batean, peptidoa non ari den elkarreragiten ikustea erraza da, CaM:Q2*h*AB konplexuko seinale kimikoen desplazamenduen aldaketen ondorioz. Ikus daitekeenez, ^{15}N-HSQC espektroek, Q1-S2/S3 peptidoarekin, peptidorik gabeko espektroekin baino seinale intentsitate txikiagoa erakusten dute. Hori, proteina konplexuaren bolumena handitzearen ondorio izan liteke, peptidoa Q2-*h*AB:CaM -rekin lotzen denaren seinale. Tamaina handiagoa denean, zeharkako erlaxazio-denboraren konstantea (T2) laburtzen da, molekulen mugimendu geldoaren ondorioz. Hala ere, espektroek kalitate ona erakusten dute purutasunean zein dispertsioan.

Aldaketa kimikoen aldaketa argienak CaM-ren C lobuluan gertatzen dira. KrioEM egituran, interakzio peptidikoa E-F (3) eskuan identifikatu zen, Ca^{2+} seinalea K_V7 kanaletan transmititzearen arduradun nagusia, aurreko kapituluan ikusi dugun bezala. Frogatu dugu peptido honek CaM-ren E-F (3)-rekin interakzioan diharduela Q2*h*AB-rekin konplexuan, bai kaltziorik ez dagoenean, baita kaltzioaren presentzian ere, baina metodo hauen bidez ezin dugu aztertu peptidoak nola eragiten dion kaltzio-seinalearen transmisioari.

S2/S3 peptidoak Ca^{2+} seinaleztapenean duen eragina aztertzeko, mTFP1-*h*AB-Venus sentsorea peptidoaren presentzian FRET bidez monitorizatu dugu. Titulazioak Ca^{2+} bidez egin genituen, hirugarren kapituluan deskribatzen den bezala, baina S2/S3 peptido-kontzentrazio ezberdinen aurrean. K_V7 isoformen S2/S3 begiztak Q2*h*AB:CaM konplexuan oso antzeko eragina duela ikusten dugu. Gogoratu behar dugu konplexuaren konposizio-aldaketak, kaltzioaren arabera, FRET murriztea eragiten duela, baina S2/S3 peptidoa 2,5 µM-tan dagoenean, murrizketa hori erdira jaisten da. Emaitzak ikustean, logikoa zen pentsatzea S2/S3 peptidoa E-F (3)-ra elkartzeak, Ca^{2+}-a elkartzea eragozten zuela eta, beraz, konplexuan kaltzio seinalearen transmisioa blokeatzen zuela. Izan ere, S2/S3 peptidoaren kontzentrazioa 5 µM-ra igo zenean, ez zen alderik ikusi FRET-indizean, eta horrek peptidoak seinalearen transmisioa eragotzi zuela iradokitzen du. Baina S2/S3 peptidoa 10 µM-tan gehitu genuenean, FRET-indizea handitu egin zuen, baina Ca^{2+}-a gehitu ondoren soilik. FRET indizearen gehikuntza fluoroforoen arteko hurbilketa baten ondorioa da, ustez, A eta B helizeen arteko gerturatze batek eragindakoa.

S2/S3 peptidoen kontzentrazio ezberdinei behatutako ezberdintasunak bi konposizio ezberdinen presentziagatik gertatzen direla uste dugu: 1. Ca^{2+}-a CaM-ren E-F eskuekin elkartzen denean: CaM-ren C-lobulua biratzen da eta honek K_V7-ren A eta B helizeen arteko urruntzea eragiten du,

FRETren murrizketa bezala itzultzen dena. 2. Peptidoaren presentzian, konplexuak egitura berri bat hartzen du, S2/S3 E-F (3) eskuari lotzen denean. Honek, A eta B helizeen hurbilketa eragiten du, fluoroforo emaileen eta onarleen artean energiaren transmisioa handituz. Horrela, 2,5 µM-eko peptido-kontzentrazioan, konplexuak ia ez du bat egiten peptidoarekin, eta, beraz, E-F (3) libre dago Ca^{2+}-arekin lotzeko, eta, hala, kaltzio-seinalea transmititzen du. S2/S3ren kontzentrazioa 5 µM denean, bi konformazioen arteko oreka batera iritsiko gara, eta horregatik ez dugu ikusten FRETen ez murrizketarik, ezta gehikuntzarik ere ez. Azkenik, 10 µM-eko kontzentrazioan, E-F (3) gehienak daude S2/S3 peptidoari lotuta. Kasu honetan, Ca^{2+}-a gehitu ondoren, konplexuak beste orientazio bat hartzen du, non A eta B helizeak bata bestetik hurbilago dauden.

Azkenik, peptidoaren efektua E-F (3)-k transmititzen duela baieztatzeko, saiakuntza beri bat egiten dugu FRET erabiliz, Q2*h*AB-rekin, CaM mutatua duten konplexuetan, E-F esku espezifikoetan kaltzioari lotzea saihestuz. Honetarako, S2/S3-ren efektua Q2*h*ABen probatu zen CaM WT, CaM124 eta CaM3rekin konplexuetan. Antzeko efektuak ikusten dira CaM124 eta CaM WT artean, era berean, CaM3-rekin, nahiz eta FRET indizean gorakada ikusten den, ez da iristen CaM WT-rekin lortutako balioetara.

Frogatu dugu Ca^{2+} eta E-F (3) arteko batasunak egitura-aldaketak bultzatzen dituela. Hala ere, konfigurazio hori egonkortu daiteke S2/S3 eta E-F (3) sistemen arteko interakzio berri baten bidez.

Egia esan, interakzio honek boltai-sentsorearen mugimendua erraztu edo boltai-sentsorea posizio aurreaktibatu batean jar dezakeela proposatu da, kanala boltai baxuagoetan ireki ahal izateko (boltaiarekin aktibatzeko errazagoa) (Sun & MacKinnon, 2017). Gure datuek erakusten dute kontaktu honek bi ondorio gehigarri dituela: AB helizeen mugimendua kontrako norabidean bultzatzen du, gure biosentsorea erabiltzen duten aurretiazko azterketek iradokitzen dutenez. Bigarren ondorioa, Ca^{2+}-rako lotura ahulagoa dela E-F (3)-rentzako S2/S3 konektorearekin elkarreragiten duenean, eta, beraz, E-F (3)-tik Ca^{2+}-aren irteera gertatzen da, baldintza basaletara itzuliz. Beraz, gure aurretiazko datuak koherenteak dira E-F (3) eskuarekin Ca^{2+}-a seinaleztatzeko zentro neuralgiko gisa, eta kontzeptu berritzailea da (CaM-ren E-F esku bakar baten bidezko seinalizazioa) CaM fisiologiarako.

8. ONDORIOAK

1. A-B helizeak lotzen dituen lotailuak paper bat betetzen du Ca^{2+} seinalearen transdukzioan. Lotailuaren luzerak eta konposizioak Ca^{2+}-aren araberako konposizio-aldaketak errazten dituzte.

2. Kalmodulinak kaltzioarekiko sentsibilitatea ematen dio K_V7.2 kanalen zelula barneko helize distalaren mihiztatze-domeinuaren egonkortasunari. D helizearen mendeko mihiztadura tetramerikoen eraketak eragina du CaM-ren loturan eta CaM-ren mendeko K_V7.2 propietateetan. Elkarri dagokionez, CaM eta Ca^{2+}-ak D helize superkiribiliduan portaera dinamikoa eragiten dute.

3. Jarduera metabolikorik ez badago, kalmodulina modu egonkorrean lotzen zaio A eta B helizeei, gutxienez 3 orduz.

4. Ca^{2+}-ak K_V7.2 kanalen kaltzioarekiko sentikorra den domeinuan bultzatutako aldaketa konformaziona, CaM-ren C lobuluaren errotazio bat da, A eta B helizeen banaketa bat inplikatzen duena. Aldaketa konformazional honetan, D helizearen mendeko tetramerizazioaren eragina ez da FRET ezta EMN-ez hautematen.

5. Ca^{2+}-ak eragindako konformazio-aldaketak katioi horrek E-F (3) eskuarekin duen zuzeneko interakzioaren bidez bideratzen da; Ca^{2+} eta E-F (4) arteko batasunak, berriz, eragin txikia du, baina esanguratsua.

6. K_V7 S2/S3 peptidoek CaM-ren C lobuluarekin elkarreragiten dute soluzioan, batez ere E-F (3) eskuaren bidez, eta Ca^{2+}-aren mendeko konformazio-aldaketak eraldatzen dituzte.